DOE/PC/88939--T3

DE92 018094

UNIVERSITY OF UTAH
COLLEGE OF MINES AND EARTH SCIENCES
DEPARTMENT OF MINING ENGINEERING

FORMATION AND RETENTION OF METHANE IN COAL

by

V. J. Hucka, Principal Investigator
D. M. Bodily, Co-Principal Investigator
H. Huang, Graduate Assistant

Final Report

prepared for the U.S. Department of Energy

Contract Number: DE-FG22-88PC88939

May 15, 1992

ABSTRACT

The formation and retention of methane in coalbeds was studied for ten Utah coal samples, one Colorado coal sample and eight coal samples from the Argonne Premium Coal Sample Bank. Methane gas content of the Utah and Colorado coals varied from zero to 9 cm^3/g. The Utah coals were all high volatile bituminous coals. The Colorado coal was a gassy medium volatile bituminous coal. The Argonne coals cover a range or rank from lignite to low volatile bituminous coal and were used to determine the effect of rank in laboratory studies.

The methane content of six selected Utah coal seams and the Colorado coal seam was measured in situ using a special sample collection device and a bubble desorbometer. Coal samples were collected at each measurement site for laboratory analysis. The cleat and joint system was evaluated for the coal and surrounding rocks and geological conditions were noted. Permeability measurements were performed on selected samples and all samples were analyzed for proximate and ultimate analysis, petrographic analysis, ^{13}C NMR dipolar-dephasing spectroscopy, and density analysis. The observed methane adsorption behavior was correlated with the chemical structure and physical properties of the coals.

The thermodynamics of gas molecules adsorbed on coal surfaces was studied by gas chromatography. Adsorption coefficients and heats of adsorption were measured. Elemental gases such as oxygen, nitrogen, and argon were found to adsorb by non-specific forces due to dispersion and repulsive forces. Hydrocarbon gases (methane, ethane, and propane) show stronger adsorption than expected due to dispersion forces alone. This is attributed to the similarity between the hydrocarbons and the coal surface. Carbon oxide gases (carbon monoxide and carbon dioxide) and propylene show specific interactions due to permanent or induced dipole or π-electron interactions. Carbon monoxide shows a specific adsorption effect, but no effect of coal rank. The strength of the van der Waals interaction increases with the number of electrons. Methane shows specific adsorption and the effect increases with rank. The order of specific adsorption effects is $C_3H_6 > CO_2 > C_3H_8 > C_2H_6 > CH_4 > CO$. The effect of rank or carbon content on specific adsorption is in the order $C_3H_6 > C_3H_8 > C_2H_6 > CO_2 > CH_4 > CO$. All gases studied, except water, have higher heats of adsorption than heats of vaporization. Only propylene showed a strong correlation with N_2 surface area.

Static adsorption experiments demonstrated that diffusion of methane through coal pores is limited below temperatures < 50 °C. The isosteric heat of adsorption of methane was found to be 14.9 kJ/mol for a high volatile bituminous coal. Water adsorbed on the coal inhibits methane adsorption. The

adsorption capacity for different gases was in the order CO_2 > CH_4 > CO ~ N_2 ~ Ar ~ O_2. A slow depressurization technique was developed to measure continuous adsorption isotherms. A linear adsorption region between 0.2 and 0.6 relative pressure was observed in BET plots and used to calculate surface areas.

The desorption of water was studied by scanning calorimetry and thermal analysis. A first order rate expression was used to model the reaction. The activation energy for desorption varied from 27 to 78 kJ/mol, depending on moisture content. The average value, 49.2 kJ/mol was close to the heat of vaporization of water of 40.63 kJ/mol.

Programmed-temperature pyrolysis was used to investigate gas evolution during pyrolysis. Chemical reaction rates were found to control devolatilization under the experimental conditions. The temperature dependence of gas evolution during pyrolysis parallels that observed during coalification. Pyrolysis methane yields increase with increasing in situ methane content for gassy coal seams, indicating that recent rates of methane formation are important in determining methane content. Methane and hydrogen yields increase and carbon oxide yields decrease with increasing carbon content of the coal. A mechanism is proposed in which carbon and oxygen compete for activated hydrogen during devolatilization.

TABLE OF CONTENTS

	Page
ABSTRACT	i
LIST OF FIGURES	vii
LIST OF TABLES	xvii
LIST OF SYMBOLS	xx
1. INTRODUCTION	1-1
2. FORMATION OF COAL	2-1
2.1 Biochemical and Metamorphic Processes	2-1
2.2 Coalification Processes	2-1
2.3 Influence of Depth of Strata and Tectonic Pressure	2-2
2.4 Coal Structure	2-5
2.5 Porosity and Surface Area	2-5
3. FORMATION AND RETENTION OF METHANE	3-1
3.1 Methane Formation during the Coalification Process	3-1
3.2 Methane Adsorption and Transport	3-3
3.3 Methane Retention in Coal	3-4
3.4 Methane Resources in American Coal Fields	3-5
3.5 Coalbed Methane Recovery Techniques	3-5
3.5.1 Underground Techniques	3-5
3.5.2 Surface Techniques	3-5
3.6 Utilization of Methane	3-7
4. GEOLOGY OF WASATCH PLATEAU, BOOK CLIFFS, AND CARBONDALE COAL FIELDS	4-1
4.1 Environment of Deposit	4-1
4.2 Stratigraphy	4-1
4.3 Wasatch Plateau Field	4-2
4.3.1 Southern Utah Fuel Mine	4-2
4.3.2 Skyline Mines	4-4
4.3.3 Beaver Creek Mine No. 7	4-7
4.4 Book Cliffs Field	4-8
4.4.1 Pinnacle and Apex Mines	4-9
4.4.2 Castlegate No. 3 Mine	4-10
4.4.3 Soldier Creek Canyon Mine	4-12
4.4.4 Sunnyside Mines	4-13
4.5 Carbondale Coal Field in Colorado	4-14
4.5.1 B Seam at the Dutch Creek Mine in Redstone	4-14

Page

5. COALBED METHANE RESOURCES OF BOOK CLIFFS AND CARBONDALE COALFIELDS. 5-1

5.1 Coalbed Methane Determination by the Utah Geological Survey. 5-1
5.2 In Situ Measurements. 5-3
5.3 Drainage Tests. 5-4

6. COAL SAMPLE CHARACTERIZATION 6-1

6.1 Analytical Data 6-1
6.2 Multivariate Analysis 6-5
6.3 Hardness and Grindability 6-8

7. RESULTS OF LABORATORY AND FIELD INVESTIGATIONS . 7-1

7.1 Natural Conditions of Coalbeds in the Wasatch Field 7-1
7.1.1 Castlegate A Seam at the Beaver Creek Mine No. 7 7-1
7.2 Natural Conditions of Coalbeds in the Book Cliff Field. 7-1
7.2.1 Sub 3 Seam at the Castle Gate Coal Mine. 7-6
7.2.2 Rock Canyon Seam at the Soldier Creek Canyon Coal Mine 7-6
7.2.3 Sunnyside Seam at the Soldier Creek Canyon Coal Mine 7-9
7.2.4 Sunnyside Seam at the Soldier Creek Canyon Coal Mine 7-9
7.3 Natural Conditions of Coalbeds at the Mid-Continent Resources Mines in Colorado. 7-13
7.4 Permeability Tests. 7-13
7.5 Field and Laboratory Coalbed Methane Content Determination Tests 7-13

8. CHARACTERIZATION OF THE COAL SURFACES BY GAS CHROMATOGRAPHY. 8-1

8.1 Introduction. 8-1
8.2 Theoretical Basis 8-2
8.2.1 Techniques 8-2
8.2.2 Relationship between Adsorption Coefficient and Retention Variables. 8-3
8.2.3 Determination of the Retention Time. 8-6
8.2.4 Measurement of the Gas Hold-up Time. 8-7
8.2.5 Symmetry of GC Peaks 8-7
8.2.6 Thermodynamic Relationships. 8-7
8.3 Experimental. 8-9
8.3.1 Apparatus. 8-9
8.3.2 Coal Samples 8-11

Page

8.3.3 Gas Samples 8-13
8.4 Results and Discussion 8-13
8.4.1 Determination of the Thermodynamic Constants 8-14
8.4.2 Measurement of the Coefficients of Gas Adsorption 8-23
8.4.3 Multivariate Analysis 8-30
8.4.4 Regression Analysis 8-32
8.4.5 Factor Analysis 8-34
8.5 Conclusions. 8-46

9. A STUDY OF GAS ADSORPTION ON COAL 9-1

9.1 Introduction 9-1
9.2 Experimental 9-1
9.2.1 Adsorption Apparatus. 9-1
9.2.2 Sample Preparation and Characteristics 9-2
9.2.3 Theory of Measurements. 9-3
9.3 Results and Discussion 9-5
9.4 Conclusions. 9-16

10. DETERMINATION OF THE SURFACE AREA OF SUB 3 UTAH COAL BY CONTINUOUS CO_2 DESORPTION AT 298 K. . . . 10-1

10.1 Introduction. 10-1
10.2 Experimental. 10-2
10.2.1 Adsorption Apparatus. 10-2
10.2.2 Sample Preparation and Characteristics 10-3
10.2.3 Principle of Measurement. 10-4
10.3 Results and Discussion. 10-6
10.4 Conclusions 10-14

11. GAS EVOLUTION IN THE PROGRAMMED-TEMPERATURE PYROLYSIS OF COAL 11-1
11.1 Introduction. 11-1
11.2 Experimental. 11-2
11.2.1 Pyrolysis 11-2
11.2.2 Gas Chromatograph 11-2
11.2.3 Coal Preparation and Characteristics 11-4
11.3 Results and Discussion. 11-4
11.3.1 Primary Experimental Results on Coal Pyrolysis. 11-4
11.3.2 Effect of Particle Size 11-5
11.3.3 Gas Evolution in Coal Pyrolysis . . 11-11
11.3.4 Coal Pyrolysis and Coalification. . 11-12
11.3.5 Correlations. 11-28
11.3.6 Redistribution of H, O and C in Coal Pyrolysis Products 11-41
11.4 Conclusions 11-42

Page

12. KINETICS AND THERMODYNAMICS OF WATER DESORPTION FROM COAL 12-1

12.1 Introduction. 12-1
12.2 Experimental. 12-1
12.3 Results and Discussion. 12-2
12.3.1 Interaction of Coal and Water . . . 12-2
12.3.2 Heats of Desorption 12-4
12.3.3 Kinetics of Desorption. 12-10
12.4 Conclusions 12-17

13. CONCLUSIONS 13-1

14. REFERENCES. 14-1

APPENDIX A. AN ASSESSMENT OF METHANE CONTENT BY DETERMINATION IN SITU

APPENDIX B. RESULTS ON FIELD AND LABORATORY TESTS ON METHANE CONTENT

APPENDIX C. CONSERVATION EQUATIONS OF ADSORPTIVE GAS IN A GAS CHROMATOGRAPHIC COLUMN

APPENDIX D. RESULTS ON PERMEABILITY TESTS

APPENDIX E. COMPUTER CODE

APPENDIX F. DIRECTIONAL PERMEABILITY OF SELECTED COALBEDS IN UTAH AND COLORADO

LIST OF FIGURES

Figure		Page
2.1	Classification of coal by rank	2-3
2.2	Coal coalification and classification chart.	2-4
3.1	Gas release during coalification	3-2
3.2	Methane resources of U.S. coal basins. . .	3-6
3.3	Surface techniques for methane recovery. .	3-8
3.4	Directional drainage drilling technique. .	3-9
4.1	Utah coal mines and coal fields.	4-3
4.2	Pinnacle and Apex Mines.	4-9
4.3	Sunnyside Mine	4-13
5.1	Methane demarcation line for Book Cliffs Coal Field.	5-2
6.1	Correlation coefficients of analytical variables with coal rank	6-7
6.2	Scree plot for coal variables.	6-7
6.3	Cumulative percent versus factor number. .	6-8
6.4	Factor loadings for coal variables	6-9
6.5	Factor pattern plots	6-10
7.1	Section map of the Castlegate A seam at the Beaver Creek Mine (Central Utah) . . .	7-5
7.2	Geologic profile of the strata through the Sub 3 seam	7-7
7.3	Section map of the Sub 3 seam.	7-8
7.4	Section map of the Rock Canyon seam. . . .	7-10
7.5	Section map of the Sunnyside seam at the Soldier Creek Canyon mine.	7-11
7.6	Section map of the Lower Sunnyside seam at the Sunnyside mine.	7-12

Figure		Page
7.7	B seam at the Dutch Creek mine	7-14
7.8	Methane content in Utah gassy mines. . . .	7-17
7.9	Methane content in the B seam (Carbondale coal field).	7-18
8.1	Concentration of species A across a chromatographic column	8-4
8.2	Three types of symmetry of elution curves	8-8
8.3	Symmetry of methane elution peak	8-8
8.4	Apparatus for coal surface studies by GC .	8-10
8.5	Methane elution peaks for various injection volumes.	8-14
8.6	Methane adsorption isotherm at low pressures.	8-14
8.7	Symmetry factor as a function of injection volume	8-17
8.8	Plot of $\ln(K_p)$ versus a/T	8-18
8.9	Interactions between coal surfaces and gas molecules.	8-20
8.10	Correlation of K_p with heats of adsorption	8-22
8.11	Correlation of heats of vaporization with heats of adsorption	8-22
8.12	Correlation of heats of vaporization with number of electrons	8-24
8.13	Correlation of heats of adsorption with number of electrons	8-24
8.14	Correlation of specific adsorption ratio with carbon content.	8-32
8.15	Correlation coefficients for K_p with aromaticity, carbon content, and N_2 surface area	8-34
8.16	Scree plots.	8-35

Figure		Page
8.17	Cumulative percent versus factor number. .	8-37
8.18	Factor loadings versus variables for methane adsorption	8-37
8.19	Factor pattern plots	8-38
8.20	First factor loadings versus sample variables	8-39
8.21	Second factor loadings versus sample variables	8-40
8.22	Third factor loadings versus sample variables	8-41
8.23	Fourth factor loading versus sample variables	8-42
8.24	Correlation of K_p for argon with aromaticity and carbon content	8-43
8.25	Correlation of K_p for carbon dioxide with aromaticity and carbon content. . . .	8-44
8.26	Correlation of K_p for methane with aromaticity and carbon content	8-45
9.1	Apparatus for low pressure gas adsorption	9-2
9.2	Schematic example of gas adsorption curves	9-6
9.3	Methane adsorption at four temperatures. .	9-6
9.4	Comparison of equilibrium methane adsorption with continuous adsorption. . .	9-7
9.5	Relative rates of methane adsorption at two temperatures.	9-8
9.6	Particle size effects on gas adsorption at 299 K.	9-8
9.7	Particle size effects on gas adsorption at 352 K	9-10
9.8	Correlation of particle size effect ratio with molecular parameters.	9-12
9.9	Methane adsorption isotherms	9-14

Figure		Page
9.10	Plot of $\ln(K_p)$ versus 1/T.	9-15
9.11	Isoteric heat of adsorption of methane versus surface coverage.	9-15
9.12	Adsorption of gases on Castlegate Sub 3 seam coal.	9-17
9.13	Effect of coal rank on gas adsorption. . .	9-18
9.14	Correlation of gas adsorption with carbon content	9-18
10.1	Schematic of coal surface.	10-1
10.2	High-pressure gas adsorption apparatus . .	10-3
10.3	Carbon dioxide in high-pressure cell during slow depressurization	10-7
10.4	Carbon dioxide adsorbed versus pressure. .	10-7
10.5	Carbon dioxide adsorbed versus time. . . .	10-8
10.6	Carbon dioxide adsorbed at short times . .	10-8
10.7	Comparison of continuous desorption and equilibrium desorption	10-9
10.8	BET plot of CO_2 adsorption	10-11
10.9	BET plot of continuous depressurization data	10-11
11.1	Pyrolysis apparatus.	11-3
11.2	Heating profile for programmed-temperature pyrolysis of coal.	11-6
11.3	Reproducibility of methane formation for triplicate experiments	11-6
11.4	Gas chromatograms: a, helium carrier gas; b, argon carrier gas.	11-7
11.5	Pyrolysis gas yields	11-8
11.6	Gas evolution for Lower Sunnyside coal . .	11-9
11.7	Cumulative gas production for Lower Sunnyside coal	11-9

Figure		Page
11.8	Effect of particle size on methane evolution for Dutch Creek coal	11-10
11.9	Effect of particle size on methane evolution for Lower Sunnyside coal	11-10
11.10	Effect of particle size on methane evolution for Skyline coal	11-11
11.11	Pyrolysis gas yields for Castlegate A seam coal, Aberdeen mine	11-13
11.12	Pyrolysis gas yields for Lower Sunnyside seam coal, Apex mine	11-13
11.13	Pyrolysis gas yields for Lower Sunnyside seam coal, Beaver Creek #8 mine.	11-14
11.14	Pyrolysis gas yields for Sub 3 seam coal, Castlegate mine.	11-14
11.15	Pyrolysis gas yields for Gilson seam coal, Pinnacle mine.	11-15
11.16	Pyrolysis gas yields for Upper O'Connor seam coal, Skyline mine.	11-15
11.17	Pyrolysis gas yields for Rock Canyon seam coal, Soldier Creek mine.	11-16
11.18	Pyrolysis gas yields for Lower Sunnyside seam coal, Soldier Creek mine. .	11-16
11.19	Pyrolysis gas yields for Upper Hiawatha seam coal, SUFCO mine	11-17
11.20	Pyrolysis gas yields for B seam, Dutch Creek mine	11-17
11.21	Pyrolysis gas yields for Upper Freeport coal.	11-21
11.22	Pyrolysis gas yields for Wyodak-Anderson coal.	11-21
11.23	Pyrolysis gas yields for Illinois #6 coal.	11-22
11.24	Pyrolysis gas yields for Pittsburgh #8 coal.	11-22

Figure		Page
11.25	Pyrolysis gas yields for Pocahontas #3 coal.	11-23
11.26	Pyrolysis gas yields for Blind Canyon coal	11-23
11.27	Pyrolysis gas yields for Lewiston-Stockton coal.	11-24
11.28	Pyrolysis gas yields for Beulah-Zap coal	11-24
11.29	van Krevelen plots	11-30
11.30	Pyrolysis methane yield versus carbon content.	11-31
11.31	Pyrolysis hydrogen yield versus carbon content	11-31
11.32	Pyrolysis ethane and ethylene yield versus carbon content.	11-32
11.33	Pyrolysis carbon monoxide yield versus carbon content	11-32
11.34	Pyrolysis carbon dioxide yield versus carbon content	11-33
11.35	Pyrolysis yields versus carbon content . .	11-33
11.36	Pyrolysis methane yield versus aliphatic carbon	11-34
11.37	Pyrolysis methane yield versus pyrolysis hydrogen yield	11-37
11.38	Pyrolysis methane yield versus oxygen content.	11-39
11.39	Pyrolysis hydrogen yield versus oxygen content	11-39
11.40	Pyrolysis methane yield versus hydrogen to oxygen ratio.	11-40
11.41	Pyrolysis hydrogen yield versus hydrogen to oxygen ratio.	11-40
11.42	Pyrolysis methane yield versus coalbed methane content.	11-41

Figure		Page
11.43	Hydrogen content in gaseous products . . .	11-42
11.44	Percent hydrogen content of gaseous products versus carbon content	11-43
11.45	Oxygen content in gaseous products and coals.	11-43
11.46	Percent oxygen content of gaseous products versus carbon content	11-44
11.47	Percent carbon content of gaseous products versus carbon content	11-44
12.1	Correlation of equilibrium moisture with oxygen, nitrogen and sulfur	12-3
12.2	Oxygen, nitrogen and sulfur content of Argonne coal samples	12-3
12.3	Correlation of equilibrium moisture with oxygen content.	12-5
12.4	DSC curves of water desorption for Argonne coal samples	12-5
12.5	DSC baseline for water desorption.	12-6
12.6	DSC curves of water desorption on Blind Canyon coal char	12-6
12.7	Baseline corrected DSC curves for water desorption of Argonne coal samples	12-8
12.8	Heat flow normalized by moisture content for Argonne coals.	12-8
12.9	Correlation of heats of water desorption with oxygen content.	12-10
12.10	Hydrogen bonds in water molecules.	12-11
12.11	Water desorption rates of Argonne coal samples	12-12
12.12	Comparison of water desorption rates from TGA data with modelling results for two samples.	12-14
12.13	Comparison of TGA weight loss with modelling results for Argonne coal samples.	12-14

Figure		Page
12.14	Correlation of activation energy for water desorption with moisture content . .	12-16
12.15	Correlation of pre-exponential factor with moisture content.	12-16
APPENDIX A		
Fig. 1	Manual bubble desorbometer	A-5
Fig. 2	Flow chart of methane content determination.	A-6
Fig. 3a	Slope K_t plotted on log-log paper (power decay function)	A-8
Fig. 3b	Slope K_t plotted on semi-log paper (exponential decay function)	A-8
Fig. 4	Milled gas collection system	A-10
Fig. 5	Regional map of the sampling site in Sunnyside Mine, Utah	A-14
Fig. 6	Desorption rate versus time.	A-17
Fig. 7	Relationship between actual measured and estimated gas content determined by use of the exponential decay function theory.	A-21
Fig. 8	Relationship between actual measured and estimated gas content determined by use of the power decay function theory	A-21
Fig. 9	Relationship between actual and estimated gas content determined by use of the quadratic decay function theory . .	A-22
Fig. 10	Results on desorption flow versus desorption time plotted on semi-log paper using exponential decay function . .	A-23
Fig. 11	Results on desorption flow versus desorption time plotted on log-log paper using power decay function	A-23
Fig. 12	Results on cumulative desorbed volume of gas versus square root of time using quadratic decay function	A-24

Figure		Page
APPENDIX C		
C-1	Pressure gradient (a) and volumetric velocity gradient (b) along a gas chromatographic column	C-6
APPENDIX D		
D-1	Permeability tester.	D-3
D-2	Platens for the permeability tester. . . .	D-4
D-3	Permeability versus axial stress for gas flow parallel and to bedding planes. .	D-19
D-4	Permeability versus axial stress for gas flow perpendicular to bedding planes	D-19
D-5	Permeability versus inlet stress for gas flow parallel to bedding planes. . . .	D-20
D-6	Permeability versus inlet stress for gas flow perpendicular to bedding planes	D-20
D-7	Permeability versus confining stress for gas flow parallel to bedding planes	D-21
D-8	Permeability versus confining stress for gas flow perpendicular to bedding planes	D-21
APPENDIX F		
Fig. 1	Laboratory direct method of methane gas content determination.	F-2
Fig. 2	Bubble desorbometer for in-situ methane gas determination.	F-2
Fig. 3	A special sampling device for collecting fine drill cuttings from the bottom of the borehole	F-3
Fig. 4	Relation between the depth of the borehole and the methane content	F-3
Fig. 5	A plain view of directional permeability due to the cleat orientation	F-3

Figure		Page
Fig. 6	Location of horizontal boreholes at Seam No. 1.	F-4
Fig. 7	Location of horizontal boreholes drilled in Seam No. 2	F-6
Fig. 8	Location of boreholes drilled in Seam No. 3.	F-6

LIST OF TABLES

Table		Page
3.1	Methane resources of U.S. coal basins . . .	3-6
4.1	Cleat and joint orientations in Utah coal mines and outcrop rocks.	4-5
5.1	Coalbed methane in the Book Cliffs Field. .	5-1
6.1	Proximate and ultimate analyses of coals. .	6-2
6.2	Carbon structural distribution of coals . .	6-3
6.3	Maceral analyses, heating values and densities of coals.	6-4
6.4	Correlation coefficients of multi-regression analysis	6-6
6.5	Physical and mechanical properties of coal.	6-11
7.1	Technical parameters of coal seams under investigation	7-2
7.2	Summary of results on methane content determination and permeability.	7-13
8.1	Characteristic data of chromatographic columns	8-12
8.2a	Experimental conditions and primary results of the different methane concentration injections.	8-15
8.2b	Gas adsorption coefficients and pertinent experimental parameters of different methane concentration injections.	8-16
8.3	Dependence of the retention volume on flow-rate at 273.15 K	8-17
8.4	Heats of gas adsorption on Upper Freeport Coal (-150/+200 mesh)	8-19
8.5	Properties of the gases used in the adsorption studies.	8-26

Table		Page
8.6a	Gas adsorption coefficients (Kc) or net gas retention volumes (Vn) at 273.15 K. . .	8-27
8.6b	Gas adsorption coefficients (Kp in m/(STP)/(psia)(g dry coal)) at 273.15 K . .	8-28
8.6c	Gas adsorption coefficients (Kp in m/(STP)/(psia)g daf coal)) at 273.15 K. . .	8-29
8.7	Relationship between Kp and (bVm) of methane adsorption at 273.15 K.	8-30
8.8	Specific adsorption ratios.	8-31
8.9	Correlation coefficients of the variables used in the multivariate analysis.	8-33
9.1	Ranges and sensitivities of the mass flow meter.	9-3
9.2	Particle size effect on gas adsorption. . .	9-10
9.3	Helium densities of different particle sizes.	9-11
9.4	Water effect on methane adsorption.	9-17
10.1	Ranges and sensitivities of the mass flow meter.	10-3
10.2	Surface areas of Castlegate Sub 3 Coal by CO_2 adsorption at 298 K.	10-12
10.3	External surface areas of different particle sizes calculated by spherical particle model.	10-13
11.1	Characteristic parameters of the programmed-temperature pyrolysis of the ten Utah coals and one Colorado coal. . . .	11-18
11.2	Characteristic parameters of the programmed-temperature pyrolysis of the Argonne Premium Coal Bank samples . . .	11-25
11.3	Gas, char and tar yields in coal pyrolysis	11-27
11.4	Proximate and ultimate analyses of chars. .	11-29

Table		Page
11.5	Comparison of yields from pyrolysis and hydropyrolysis at 69 atm pressure	11-36
12.1	Analysis data of the Argonne Premium Coal Bank samples (daf basis)	12-9
12.2	Kinetic and thermodynamic data of water desorption on the Argonne Premium Coal Bank samples	12-15
APPENDIX A		
1.	Sample Field Test Results	A-15
2.	Summary of Field Results.	A-20
3.	Regression Analysis Summary	A-25
APPENDIX B		
B-1	Methane Content of Utah and Colorado Gassy Coalbeds.	B-1
APPENDIX D		
D-1	Results on permeability performed on large diameter specimens	D-2
D-2	Summary of results on permeability tests performed on 2.125 in. diameter specimens.	D-7
D-3	Results on permeability tests.	D-8
APPENDIX F		
I.	Proximate analysis of three gassy Utah coal seams	F-4
II.	Results on Drainage Tests.	F-5

LIST OF SYMBOLS

a_A	adsorption quantity of species A on a unit mass of coal, mol/g
A	Darcy's law area
A_{column}	cross-sectional area of column, cm^2
b	constant in the Langmuir isotherm equation
C	constant in the BET isotherm equation
C	FIck's law concentration
C_A	concentration of adsorbed species A in the mobile phase, mol/cm^3
D	diffusivity
f_a	total fraction of sp^2-hybridized carbon in coal
$f_{a'}$	fraction of carbon in an aromatic ring
f_a^B	fraction of aromatic bridgehead carbon in coal
f_a^C	fraction of carbonyl in coal
f_a^H	fraction of protonated and aromatic carbon in coal
f_{al}	total fraction of the sp^3-hybridized carbon in coal
f_{al}^H	fraction of CH or CH_2 in coal
f_{al}^O	fraction of carbon bonded to oxygen
f_{al}^*	fraction of CH_3 or nonprotonated carbon in coal
f_a^N	fraction of nonprotonated and aromatic carbon in coal
f_a^P	fraction of phenolic or phenolic ether in coal
f_a^S	fraction of alkylated aromatic carbon in coal
F_c	volumetric flow rate across the column, cm^3/s
f_D	dispersion force
f_i	induced dipole interaction force
f_q	quadrapole moment force
f_R	short-range repulsive force
f_μ	permanent dipole interaction force

F_{sym}	symmetric factor of GC peak
h	response of gas chromatography
$J_{p,T}$	pressure and temperature correction factor
k	permeability
k_0	constant in the Freundlich isotherm equation
$K_{c,A}$	adsorption coefficient of concentration of species A, cm^3/g
$K_{p,A}$	adsorption coefficient of pressure of species A, mol/(Pa)(g)
L	column length, cm
L	Darcy's and Fick's law length
m_L	mass of coal in a unit length of the column, g/cm
m_c	moisture content in coal, wt%
n	order in the Freundlich isotherm equation
N_e	number of electrons in molecule
P	Darcy's law pressure
P_i	column inlet pressure, psia
P_o	column outlet pressure, psia
q	flow rate
r_d	water desorption rate, 1/s
S	specific surface area of coal, m_2/g
S_e	external surface area of coal, m_2/g
S_p	GC peak area, (V)(s)
$S_{p,r}$	peak retention area, $(V)(s)^2$
STP	standard pressure and temperature of a gas, i.e., p = 1 atm and T = 0 °C
t	time
T_c	column temperature, K
t_r	retention time, s
t_M	retention time of unsorbed gas (gas hold-up time), s

$t_{r,p}$	peak retention time, s
$t_{r,m}$	weighted arithmetic mean retention time, s
$t_{r,1/2}$	half elution retention time, s
u_A	linear migration velocity of species A at concentration C_A moves along the column in the mobile phase, cm/s
V	total volume of the mobile phase or total free volume in the column, cm^3/cm
V_{ads}	volume of adsorbate, cm^3(STP)/g
$V_{ads,d}$	volume of adsorbate adsorbed on dry coal, cm^3(STP)/g
$V_{ads,e}$	volume of adsorbate at equilibrium, cm^3(STP)/g
$V_{ads,w}$	volume of adsorbate adsorbed on moist coal, cm^3(STP)/g
V_{column}	volume of the column, cm^3
V_{GC}	dead volume in gas chromatography, cm^3
V_L	volume of the mobile phase or free volume in a unit length of the column, cm^3/cm
V_M	retention volume of unsorbed gas (gas holdup volume), cm^3
V_m	volume of adsorbate equivalent to a monolayer
V_N	net unit retention volume, cm^3/g-adsorbent
V_r	retention volume, cm^3
W_c	total mass of coal in the column, g/cm
$W_{e,H2O}$	equilibrium moisture in coal, wt%
x	distance from the inlet to any point of the column, cm
ΔH_a	heat of gas adsorption, kJ/mol
ΔH_{vap}	heat of vaporization, kJ/mol
ΔS_a	change in entropy during adsorption, kJ/(mol)(K)
α_p	relative saturation pressure
α_s	specific adsorption ratio
α_{size}	particle size effect ratio

$\alpha_{\%,w/d}$	percentage of methane adsorption capacity of moist coal with respect to that of dry coal
ϵ	parked-column porosity, cm^3/cm^3
ρ_c	density of coal, g/cm^3
ρ_m	density of mineral matter, g/cm^3
μ	Darcy's law viscosity

1. INTRODUCTION

Coal contains methane gas which during normal mining operations is released into the mine atmosphere and may form an explosive mixture with air resulting in a safety hazard, a lost resource, and an environmental problem. Methane gas is a by-product of the process of coalification. Coal is a highly porous solid having two distinct pore systems, macropores and micropores. The methane gas has a great affinity for coal and is adsorbed on the surfaces of the micropores. When released from the micropores the methane gas exists as a free gas in the macropores from which it can migrate from the coal particles into the mine workings or the outside atmosphere.

Association of methane with coal has always presented a safety problem in mines. Methane concentrations of 5 to 15 % (the explosive limits of methane in air) in the mine atmosphere renders the mines dangerous. To prevent buildup to this concentration range, the methane gas must be diluted by ventilation well below the 5% level or removed prior to mining by separate drainage systems, independent of the mine operations. Both ventilation and methane drainage systems are costly. However, in the second case, methane can be used as a clean source of energy.

Many United States coal seams contain methane. Mroz et al. (1983) estimated the methane reserves of U. S. coalbeds at more than 400 trillion cu ft (tcf) (11.2 Gm^3). Ayers and Kelso (1989) estimated the coalbed resources of 13 U. S. coal basins and arrived at a similar figure. According to Deul and Kim (1975), more than 200 million cu ft (5.6 Mm^3) of methane was released into the atmosphere each day in 1974. This represents a large potential fuel resource. If recovered, the sale of the methane could pay for many of the costs of the recovery system and, in some cases, realize a profit.

The formation and retention of methane depends on a number of factors. The amount of methane formed depends on the starting material and the degree of maturation as represented by maceral content and rank. The thermal history of the coal seam is important in maturation processes. The retention of the methane depends on the temperature and pressure of the coal seam (depth) and physical properties such as porosity and permeability. Geological factors such as the permeability of the roof rock and fracturing in the seam are important. Retention of the methane also depends on the thermodynamics of gas adsorption, which is determined by the chemical nature of the coal surface and of methane.

Methane is a "greenhouse" gas in the atmosphere in that it absorbs infrared radiation from the earth and re-irradiates

concentration of such gases in the atmosphere lead to a change in the thermal balance of the earth and a new equilibrium temperature. Although the concentration of methane is much less than that of carbon dioxide and its lifetime in the atmosphere is much shorter, methane absorbs in a different region of the infrared spectrum. According to Beer's Law, low concentrations are most effective in absorbing light on a per mass basis. Methane is oxidized in the atmosphere by the hydroxyl radical, resulting in the formation of carbon dioxide, another "greenhouse" gas. In the stratosphere, methane reacts with chlorine atoms to reduce ozone depletion, but it also reacts with electronically excited oxygen atoms, reducing the formation of ozone (Hileman, 1992). Methane is a major source of water in the stratosphere and water aids in the destruction of ozone. Atmospheric concentrations of methane are presently about 1.7 ppm, but are increasing at over 1 % per year and have doubled since the beginning of the industrial revolution (Hileman, 1989). Major sources of methane in the atmosphere are from swamps, marshes, rice paddies, and domestic animals. Coal mining is estimated to contribute from 10 to 20 % (Warneck, 1988).

For these reasons, recovery of methane from coalbeds is an important problem. The formation of coal (Chapter 2) and the formation and retention of methane (Chapter 3) are reviewed in this report. The geological conditions and history of the coal fields where measurements were made was determined (Chapter 4) and the methane resources of Utah coal fields are reviewed (Chapter 5). Chapter 6 contains a description of the samples studied in the laboratory. In this project, the methane content of several gassy Utah and Colorado mines was measured by an in situ technique. The results of the studies of methane content, porosity, and permeability are found in Chapter 7. Laboratory measurements of the chemical and physical properties of coals were conducted. A gas chromatic technique was developed to measure the adsorption coefficients and heats of adsorption of methane and other gases on coal surfaces (Chapter 8). These parameters were correlated with coal properties by multivariant analysis. The diffusion of gases into the coal and the accessibility of coal pores to various gases was studied by static adsorption experiments (Chapter 9). A novel technique using slow continuous desorption of adsorbed gas was developed and applied to the determination of surface areas (Chapter 10). The formation of methane was studied by pyrolysis as a measure of the current propensity of coals to produce methane (Chapter 11). Mechanisms for the formation of methane and other gases are proposed based on pyrolysis results and the chemical composition of the coals. The effect of water on adsorption and desorption processes and the kinetics and thermodynamics of water desorption were studied (Chapter 12). The laboratory experiments are summarized and interpreted in Chapter 13, although other chapters contain conclusion sections. The results of this study should be

useful in understanding the processes by which methane is formed in coal and retained by coal seams. The results of the study have already found use in modeling methane transport in coal seams.

2. FORMATION OF COAL

The U.S. Bureau of Mines' definition of coal is as follows: "A solid, brittle, more or less distinctly stratified, combustible carbonaceous rock, formed by partial to complete decomposition of vegetation; varies in color from dark brown to black; not fusible without decomposition and very insoluble" (Thrush, 1968). Another definition is as follows: "Coal is a sedimentary rock accumulated as peat and composed principally of macerals, subordinately of minerals, and containing water and gases in submicroscopic pores" (Neavel, 1981). These definitions indicate the complexity of the physical and chemical properties of coal and the possibility for large differences in these properties between coal samples from different locations. It is beyond the scope of this report to discuss in detail the formation of coal. However, an understanding of the genesis of coal is helpful in the study of the occurrence and properties of methane gas within coal.

2.1 Biochemical and Metamorphic Processes

Coal was created in warm, tropical or subtropical climates where plant life was abundant due to the climate and to large amounts of water. The water allowed for abundant plant growth and rapid decay of the dead plants in lagoons, coastal swamps, slow moving rivers, and deltas. The combination of partial decay of the plant material and the deposition of sediments produced a peat. Diagenetic and metamorphic processes altered the peat mainly through biochemical action of various bacteria present in this environment. The result was an increase of carbon content simultaneous with loss of water due to pressure causing a compression of the peat. With increase in depth, the bacteria ceased to exist and further changes were of a chemical nature. Consequently, the temperature, time and pressure were factors determining the degree of the coalification process as the carbonaceous material progressed through lignite, subbituminous, bituminous, and anthracite coals. The effect of temperature is to increase the rate of chemical reactions. Time allows for these reactions to occur at slower rates and the effects of temperature and time are complementary. Elevated pressure brings the reacting species closer together and prevents the escape of intermediate and final products.

2.2 Coalification Processes

Many descriptions of the coalification process are offered in the literature (Teichmuller and Teichmuller, 1982; Given, 1984; Speight, 1983). Kim and Douglas, 1973, describes coalification as

a series of biochemical and geochemical reactions

which transform plant material into a combustible, carbonaceous solid. Methane is the primary gaseous by-product of this process, but other hydrocarbons, CO_2, and hydrogen are also produced. Coalification begins with a biochemical stage during which plant materials are partially decomposed by anaerobic microorganisms, humic substances are formed, and peat accumulates. During this stage are also produced methane (CH_4), carbon dioxide (CO_2), and traces of ethane, ethylene, propane, propylene, butane, and pentanes. These gases may be retained in the peat by adsorption. Atmospheric nitrogen (N_2) and oxygen (O_2) may also be adsorbed. Atmospheric nitrogen (N_2) and oxygen (O_2) may also be adsorbed on the peat during deposition. Inundation and the deposition of inorganic sediments usually terminates the development of peat and initiates the geochemical phase of coalification. During the geochemical stage of coalification, the time, temperature, and pressure cause physical and chemical changes in the coal.

The classification of coals is shown in Figure 2.1 (Plaizier, 1990), and the coalification process is shown schematically in Figure 2.2 (Francis, 1961). In general, as coalification proceeds, the oxygen content, moisture, volatile matter, and hydrogen content decrease. Calorific value, carbon content, and vitrinite reflectance increase with increasing rank. Pore size distributions also vary with rank. Maceral composition and mineral matter content depend on the starting biomass material, the conditions at the time of initial coalification, and the history of intrusions into the coal bed. The quality of the coal and the physical and chemical properties of the coal depend on rank, maceral composition, and mineral matter content.

2.3 Influence of Depth of Strata and Tectonic Pressure

The amount of methane stored in coal depends on rank and depth of the coal. Higher rank coals have higher content of gas. The effect of depth is to increase temperature and pressure, thus increasing the rate of the coalification process. The capacity of coal to hold gas is decreased with increasing temperature in the range of coalbed temperatures, but increases with pressure. Tectonic pressure may cause folding and faulting of coalbeds thus contributing to the release of gas from the coal matrix. Consequently, some gas may migrate into cavities of surrounding rocks and through cracks and fissures to the surface.

Alpern (1970) studied the distribution of gas in coalbeds with respect to stratigraphy, tectonics, lithology and overburden. He analyzed the distribution of gas in tectonic

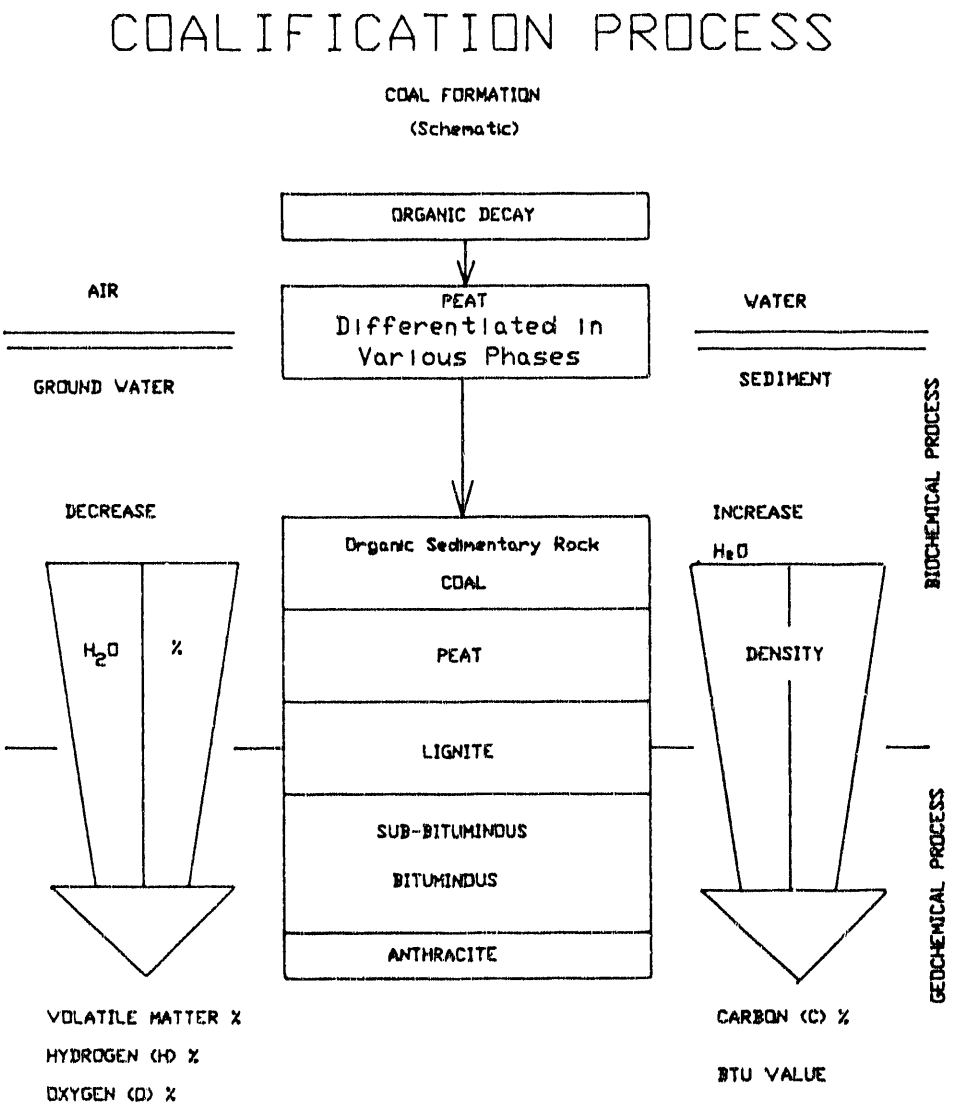

Figure 2.1 Classification of coal by rank (after Plaizier, 1990)

structures such as anticlines and domes and other folded structures, and measured the permeability. The gas was trapped in the crest of anticlines at depths of about 300 ft (100 m) while synclines were free of gas at depths up to about 1,000 ft (300 m). The Wasatch Plateau field contains several faults, which must be considered in this study.

From the point of view of permeability, Alpern (1970), distinguishes the following types of disturbances:

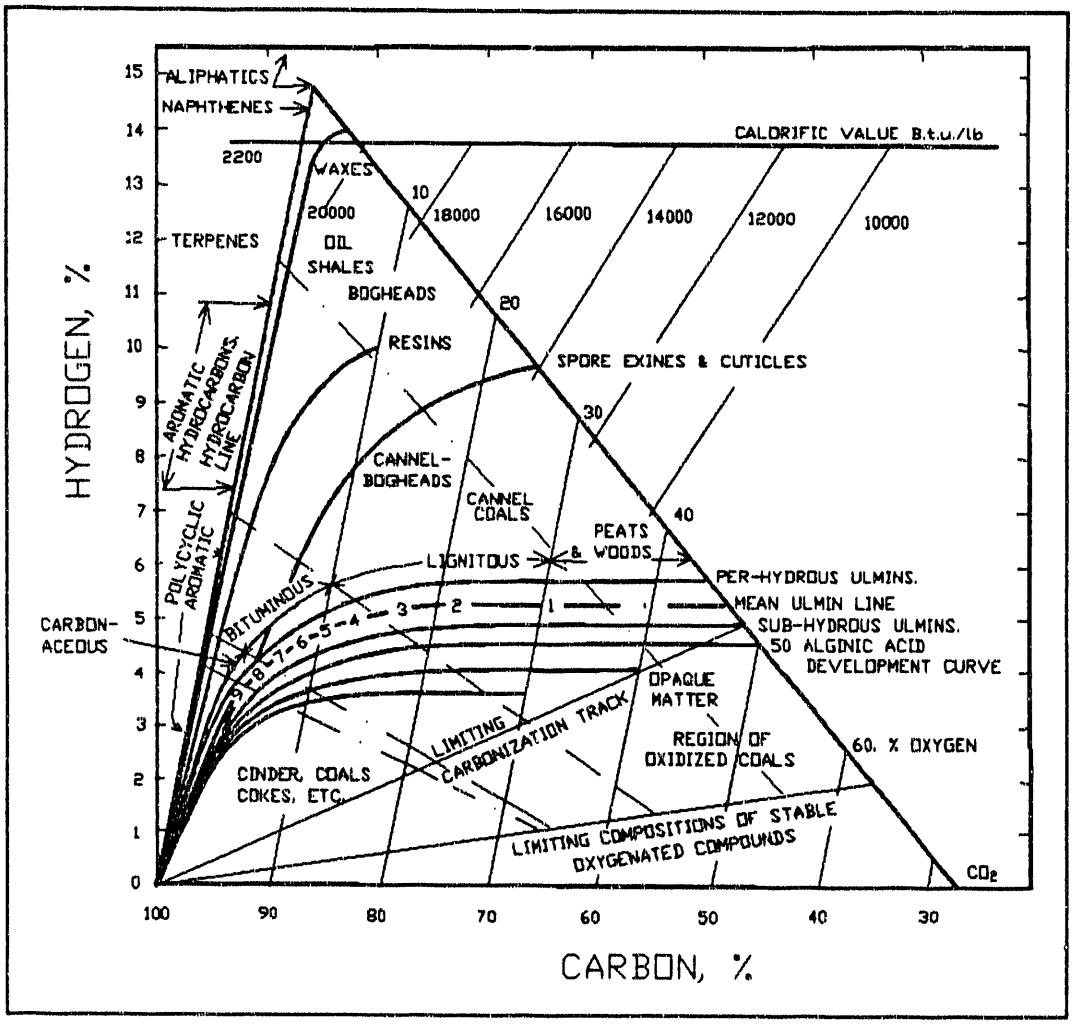

Figure 2.2 Coal coalification and classification chart (after Francis, 1961)

1. Impermeable disturbances, represented by overthrusts and flat faults.

2. Permeable disturbances. Here the permeability varies with the dip. Permeable disturbances are at right angles to the strike of right-angle bed faults. In this case a symmetrical degasification takes place on both sides of the disturbance.

Tectonic pressure can have a great effect on the formation of methane in coals. It can affect the rate of change in rank. This is caused by an increase in temperature and pressure through direct influence of tectonics or by increased depth of burial (Francis, 1961).

2.4 Coal Structure

Coal may be treated as a highly crosslinked macromolecular network (Larson et al., 1985; Brenner, 1983, 1984, 1985; Bodily et al, 1989). Crosslinks include covalent bonds, hydrogen bonds and induced dipole-induced dipole interactions from association of the aromatic ring systems in clusters. The increased size and long-range ordering of the clusters result in anisotropy of many coal properties of high rank coals. While the condensed-ring aromatic units are planar, the hydroaromatic rings and alkyl substituents are not planar and stacking of the clusters results in an extensive pore system. Coal is an amorphous glass at ambient conditions in a coalbed with a glass transition temperature above 300 °C (Lucht et al., 1987; Mahajan, 1982). It may be in a strained conformation as it is removed from the higher pressure and temperature of the coal seam to ambient conditions, without sufficient segmental mobility to undergo rearrangement. Solvents may lower the glass transition temperature, and this may also be true for gases that cause swelling of the coal.

2.5 Porosity and Surface Area

Mahajan (1982) and Mahajan and Walker (1978) have reviewed coal porosity. Pores may be divided into macropores > 50 nm, mesopores between 20 and 50 nm, micropores between 0.8 and 20 nm and submicropores < 0.8 nm in diameter. Pores are reported to be spherical, based on the shapes of molecules that can enter the pores, but in the presence of swelling solvents, cylindrical pores are observed (Gethner, 1986; Winans and Thiyagarajan, 1988; Goslar et al, 1989).

Reucroft and Patel (1983) attributed the steep rise in adsorption at low partial pressure for a variety of adsorbents to an extensive micro- and mesopore system in which the adsorbents condensed. However, surface area measurements with different gases and the time required to reach equilibrium in adsorption measurements indicates that the pores are not readily accessible to all gases. The effect of temperature and pressure changes on pores and access to pores has not been clearly established. The thermal expansion coefficient is of the order of 10^{-5}/°C and the compressibility is of the order of 10^{-10} m^2/N.

The amount of nitrogen gas adsorbed by coal goes through a maximum as the temperature is increased. Since the adsorption process is exothermic, the adsorption should decrease with temperature. However, at low temperatures, the diameter of some pores approach the kinetic diameter of the nitrogen molecule. Repulsive forces increase very rapidly and become the dominant force in the interaction. This effectively prevents the nitrogen from entering much of the pore system, resulting in decreased adsorption at low

temperatures. At higher temperatures, thermal expansion of the coal matrix and the increased kinetic energy of the gas molecules allow the gas to enter the pores, but the thermodynamic equilibrium favors less adsorption. The rate of adsorption therefore has a positive temperature coefficient.

Nandi and Walker (1964) measured the diffusion of N_2 and CO_2 into coals. The activation energy for diffusion of N_2 was greater than that of CO_2 for all coals studied. This was attributed to the difference in the kinetic diameters of nitrogen (3.65Å) and carbon dioxide (3.3Å). Surface areas of coal measured at liquid nitrogen temperatures using the Brunauer-Emmett-Teller (BET) equation are only of the order of a few m^2/g, much less than that measured by other techniques. Walker and Kini (1965) reported that more pores are accessible to CO_2 than to He. This has been reported for a large number of coal maceral fractions and was also found for methane and methanol (Walker et al., 1988). However, He is generally assumed to enter all pores at surface area measurement temperatures. Xenon gave about the same surface area as CO_2. Methane with a large kinetic diameter of 3.8Å is readily adsorbed by coal at room temperature, although the equilibrium time is long. Water with a much smaller kinetic diameter of 2.7Å gave much lower densities than methanol. Experiments in this laboratory have shown that methane, nitrogen, and argon are slowly adsorbed by coal in a pycnometer at about 0.2 MPa, giving unreasonable coal densities compared to that measured with helium.

Marsh and Siemieniewska (1965) used the Dubinin-Polanyi equation to measure surface areas with carbon dioxide at 25 °C. At this temperature, the entire pore system of the coal is accessible to the CO_2. The results were shown to be in agreement with BET measurements using CO_2 at the same temperatures, but higher pressures (Walker and Kini, 1965). Surface areas measured by this method are of the order of 150 to 300 m^2/g.

The validity of surface area measurement is brought to question by recent studies. Coal is known to swell in the presence of solvents. The swelling is dominated by polar hydrogen bonds which act as crosslinks and prevent swelling. Polar solvents which disrupt the hydrogen bonds cause substantial swelling. When hydrogen bond effects are removed from experiments, coals show maximum swelling in solvents with Hildebrand solubility parameters of about 22 $MPa^{1/2}$. The swelling is anisotropic and partially irreversible (Bodily et al., 1989; Cody et al., 1988). Experiments with carbon dioxide indicate that a portion of the surface area measured may be due to creation of new pores by swelling in the carbon dioxide (Reucroft and Sethuraman, 1987; Reucroft and Patel, 1986; Walker, et al., 1988). Harpalani and Schraufnagel (1990) have recently reported on the swelling of coal due to

methane adsorption. These measurements were made with strain gauges and do not provide information on what changes occur in the micropore structure due to swelling. Swelling due to gases appears to not be unusual.

Solubility parameters are calculated for gases by assuming a hypothetical dissolved liquid and are 5.3, 11.6, and 12.3 $MPa^{1/2}$ for nitrogen, methane and carbon dioxide respectively at 25 °C. The effect of pressure is to increase the value of the parameter. For carbon dioxide and methane at higher pressures, the solubility parameter would be in the range of that of liquids that cause coal swelling. The effect of swelling with liquid solvents is to increase the segmental mobility in the coal and increase diffusion rates of other molecules into the coal. It is not clear what happens in the case of gases. Carbon dioxide is non-polar but in the presence of polar groups an induced dipole can be formed. The fact that Xe and CO_2 give comparable surface areas is taken to mean that adsorption is not due to a polar interaction. Methane is also non-polar and it is not clear why it is strongly adsorbed in coal. Adsorption of water has been shown to have a large effect on the amount of methane that can be adsorbed (Joubert et al., 1973, 1974). Beyond a critical moisture content, which is related to the equilibrium moisture of the coal, suppression of methane adsorption no longer occurs. The critical moisture content is correlated with the oxygen content. Walker et al. (1988) concluded that the surfaces of resinite and fusinite were hydrophobic, while the surface of vitrinites was partially hydrophilic.

3. FORMATION AND RETENTION OF METHANE

3.1 Methane Formation during the Coalification Process

Methane is a product of metamorphism of coal substance (Raistrick and Marshall, 1939; Deul and Kim, 1986; Creedy, 1988). Hence, methane is a byproduct of the coalification process. It is formed at all ranks of coal but its formation is accelerated for the bituminous rank above 80% of carbon when the coal substance loses hydrogen very rapidly. In the course of coalification methane is released in amounts depending on rank and type of coal and thermodynamic conditions. Curl, (1978) considers the process of methane retention as a sorption process.

During the coalification process methane and other gases are generated by the thermal alteration of organic material. Chemical changes that occur in the organic material lead to a decrease in both atomic O/C and atomic H/C ratios with increasing maturity. As coal matures, it continues to lose oxygen and moves to the left along the curve of coal maturation shown in Figure 2.2. Oxygen loss occurs more readily than hydrogen loss during the lower temperature, diagenetic portion of the maturation process.

The major by-products of the coalification process are methane, carbon dioxide, nitrogen and water. Methane is generated by two mechanisms during the coalification process: biogenic and thermogenic (Claypool et al., 1980; Fuex, 1977). During the early stages, at temperatures below 50 °C, biogenic methane is formed by microbial decomposition of the organic material. The biogenic methane may comprise up to 10% of the methane generated at less than 200 °C. As temperature increases above 50 °C through increased depth of burial or increasing geothermal gradient, the maturation of coal also increases. The temperature profile during coalification, often referred to as the time-depth of burial, dictates the level of maturity of the coal and controls the volume of methane generated. The principal product gases generated during the processes are CH_4, CO_2, and N_2. A large quantity of methane is generated at temperatures in excess of 50 °C due to thermogenic processes. During coalification, more than twice as much CO_2 as CH_4 is generated, up to a medium volatile bituminous coal. Methane generation increase rapidly after this stage.

The amount of methane formed at any rank can be approximately estimated from the plot of hydrogen versus carbon shown in Figure 2.2 (Francis, 1961). In early stages of coalification, oxygen is lost by formation of carbon dioxide and/or water with lesser amounts of methane. At the bituminous coal stage methane formation begins to dominate, as indicated by the rapid decrease in hydrogen content. The

total amount of released gas at any stage of coalification is illustrated in Figure 3.1 (after Ayres and Kelso., 1989).

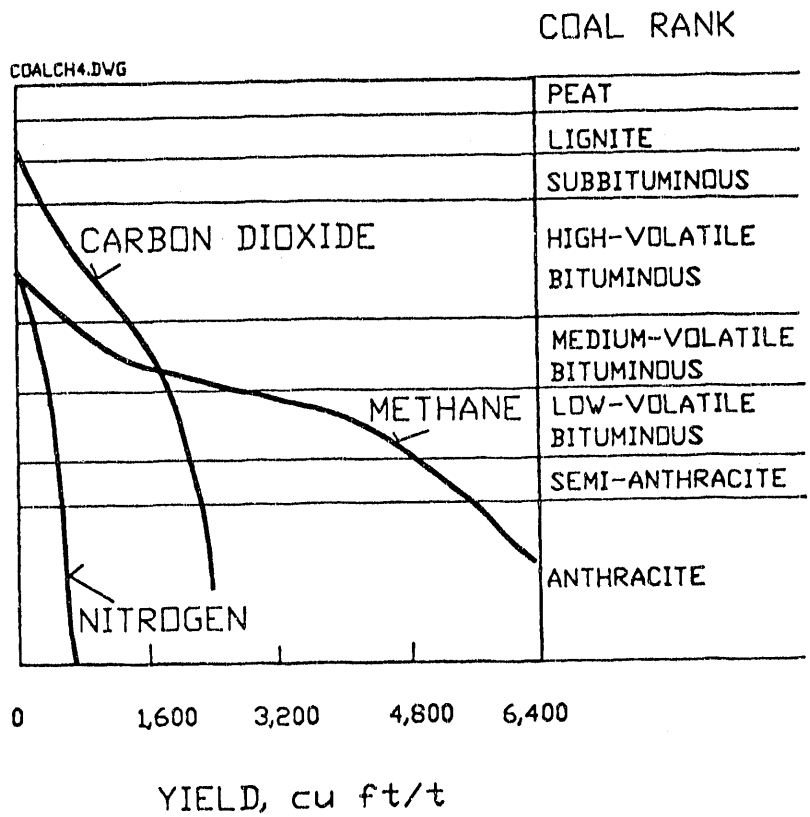

Figure 3.1 Gas release during coalification (after Ayers and Kelso, 1989).

Although the total amount of methane formed in the bituminous rank range is an inverse function of volatile content, the latter is no indicator of gas content capacity or gassiness of coal. Gas content depends on the geological history, lithology of the immediate lower and upper rock strata, tectonic effects, depth of burial, etc. For a shallow coalbed the released methane may escape into the atmosphere. This is more difficult in deep seated beds. If the coal strata are tectonically disturbed there is more chance for the formation of faults, joints and fissures, and other channels which favor migration of methane (as it is the case for the Wasatch Plateau coal field in Utah). On the other hand, any coalbed associated with impermeable roof and floor rocks is likely to retain more gas.

3.2 Methane adsorption and transport

Langmuir (1916) derived an equation for the adsorption of gases on uniform surfaces and this is applied to the adsorption of methane on coal:

$$V_{ads} = \frac{V_m bp}{1 + bp} \qquad (1)$$

where V_{ads} is the quantity of methane adsorbed at pressure p; V_m and b are known as Langmuir constants. The Langmuir constant b is related to the heat of adsorption and decreases with increase in temperature.

The flow of methane in micropores has been represented by Fick's law where the driving force is the concentration gradient (Cervik, 1967; Kim and Douglas, 1973; Fisekci and Barron, 1975):

$$dq/dt = DA\ dC/dL \qquad (2)$$

where q is the flow rate, t is the time, D is the coefficient of diffusion (diffusivity), A is the cross-sectional area, C is the concentration of gas, and L is the length of diffusion path.

Gas transport through the fracture systems in coal depends on the pressure gradient and is considered to obey Darcy's law of fluid flow with some modification. The general Darcy equation is as follows:

$$q = \frac{-kA}{\mu}\ dP/dL \qquad (3)$$

where q, A, and L are defined above, k is the permeability, P is the pressure, and μ is the gas viscosity.

There is more probability therefore, that gas might be retained at a high pressure in bituminous rank if pre-mining natural permeability happened to be low. This natural permeability thus controls whether the released methane may escape into the atmosphere or it may be trapped in some rock layers or in some other coalbed.

The rate of gas emission is influenced by Fick's and Darcy's laws. A coalbed may also receive methane from some other adjacent coalbed. It can be thus stated that gas content of any particular coal seam is a function of coal rank, permeability of coal and associated rocks. In any particular coal measure containing several coalbeds it is very difficult to determine the share of gas from internal and external sources for any particular bed.

3.3 Methane Retention in Coal

When the gas is released from the coal by desorption, it flows into the pores and fissures in the coalbeds or associated strata. Thus, the flow of methane from the coal is considered as a two-step process (Gunther, 1965; Kissell, 1976). In the course of mining this stored methane may be released slowly or in a form of sudden outbursts. Methane gas release as high as 200 times the coal volume can be obtained from coal. It has already been said that methane exists in coal as a free gas within the pores and fractures of the coal mass and in the adsorbed state, and it is also possible that some methane is absorbed by the coal matrix. Methane is also present in adjacent porous strata.

Most of the methane is adsorbed onto the walls of microvoids in coal. It has been estimated that the surface area of one kilogram of coal is between 20 000 m^2 to 200 000 m^2. Surface area measurements depend on the coal and also on the method of measurement. At 20 atmospheres, in some coals, the adsorbed methane is 10 times greater than methane as a free gas. At 100 atmospheres the adsorbed gas can be as densely packed as a liquid.

The volume of methane gas held in coal depends on the volume of gas that exists as a free gas and the adsorbed gas capacity. The volume of free gas in the coal can be calculated from kinetic theory of gases (the methane can be assumed to be an ideal gas as the results would not lead to errors greater than 1 % for normal mining pressures).

Once mining is started the equilibrium of the natural coal system is disturbed and a new stage develops in the phenomenon of methane migration. The effect of mining in relation to methane flow may be described as follows:

- formation of a free face (working face)
- permeability increase due to mining activities
- formation of cavities in the hangingwall during mining
- formation of high and low stress concentration zones which influence changes in permeability.

It is thus apparent, that the method of mining influences methane migration from the coal into mine workings. Fast mining will cause a release of higher volumes of gas. On the other hand, rapid transport of broken coal out of the mine may reduce methane emission by shortening the time of stay underground. The smaller the size of the broken coal the larger the volume of methane that can be expected. From this

point of view a coal plow cutting system is considered more favorable than the drum type cutter-loader mostly in use in U.S. underground coal mines.

3.4 Methane Resources in American Coal Fields

The United States is blessed by tremendous reserves of coal. Most of this coal contains methane. The U.S. Department of Energy estimates that U.S. coalbeds contain more than 400 X 10^{12} cu ft (11.2 Tm^3) of gas in place (Mroz et al., 1983; Schwoebel, 1985). Later, Ayers and Kelso (1989), estimated coalbed methane resources in 13 U.S. coal basins to be about 401 tcf. Reserves are listed in Table 3.1. The important U.S. coalbed methane resources are in the Warrior (Alabama), Piceance (Utah and Colorado), Northern Appalachian (Pittsburgh, Ohio, and West Virginia), Central Appalachian (Kentucky and Tennessee), and San Juan (Colorado and New Mexico) basins. Kuuskraa and Brandenburg (1989) report that there are about 250 tcf of natural gas in these basins. There are eight additional coal basins with an estimate of 150 tcf of gas (Table 3.1).

Coalbed methane gas resource estimates are calculated from the tonnage of coal which is multiplied by known gas content. The composition of the gas is predominantly methane (95-98%). As has been discussed above, the methane gas is stored in coal as a monomolecular layer adsorbed on the large internal surfaces of micropores. Kuuskraa and Brandenburg (1989) claim that gas contents of 500-600 cu ft/ton (15.7-18.5 m^3/tonne) have been measured for the higher rank coals in the U.S.A. Diamond (1984) estimated methane content of about 595 cu ft/ ton (18.5 m^3/tonne) for an anthracite coal from Pennsylvania.

3.5 Coalbed Methane Recovery Techniques

3.5.1 Underground Techniques

Coalbed methane can be recovered from existing mines by drilling horizontal boreholes (3-inch or 76.2 mm diameter) into coal (Uhrin et al., 1980; Schwoebel, 1987). The methane is then collected into an underground pipeline system and directed towards the surface. Vertical boreholes (1-5/8 inch or 41.3 mm diameter) can also be drilled from the surface into a gob behind active longwalls (Maksimovic and Kissell, 1980). The coalbed methane is thus drained through the borehole out of the mine (Figure 3.2).

Vertical boreholes are drilled from mine workings into an overlying coalbed and the collected methane is again piped to the surface.

Table 3.1. Methane resources of U.S. coal basins (modified after Ayres et al., 1989).

Basin	Area, Sq. Mile	Maximum Depth of Coal (feet)	Number of Primary Seams	Coal Thickness (feet)	Coal Rank	Gas Content scf/ton	Gas in Place (tcf)
Western United States							
San Juan Basin	7,500	4,000	14	100	LvB	600	88
Piceance	6,700	12,000	20	100	SA	430	84
Green River	21,000	6,000	30	95	HvaB	544	31
Powder River	25,800	4,000	24	300	SBa	71	30
Raton Mesa	2,200	3,000	40	90	LvB	500	30
Western Washington	6,500	-	-	-	HvbB	75	24
Wind River	8,100	12,000	6	100	SBa	-	2
Uinta	14,400	3,000	-	-	HvaB	352	1
Subtotal							**290**
Eastern United States							
Northern Appalachian	43,000	2,000	6	20	LvB	440	61
Illinois	50,000	3,000	3	16	HvaB	149	21
Black Warrior	6,000	4,000	4	20	LvB	600	20
Central Appalachian	5,000	2,500	6	15	LvB	680	5
Arkoma	13,500	3,000	2	10	LvB	550	4
Subtotal							**111**
Total							**401**

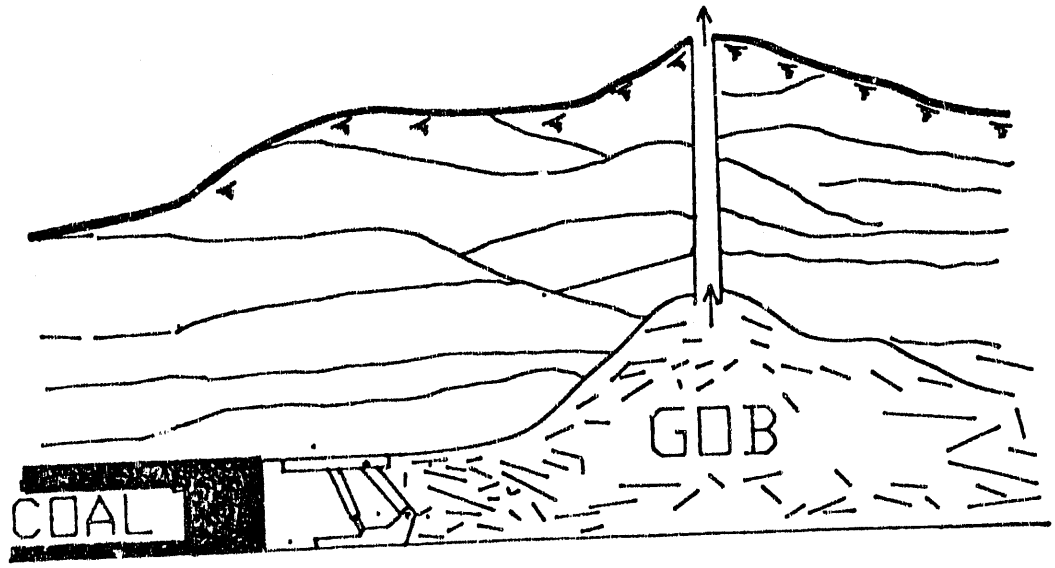

Figure 3.2 Methane drainage from a gob.

3.5.2 Surface Techniques

Pre-mining degasification is done by vertical boreholes (about 8 inch or 203 mm diameter) drilled from the surface into virgin coalbeds (Figure 3.3). The formation pressure and the permeability of coal control the effectiveness of this method. The boreholes are cased. For best results, the coal must be stimulated by injections of water, gels, or foams into the coalbed to induce fractures. Sand is also pumped into the boreholes to prop open the fractures. Vertical or near vertical boreholes are also drilled from the surface into the seam and by using a special technique, the borehole is deviated to continue inside the seam horizontally (Figure 3.4). This technique allows drainage of gas from a larger area (Maurer and Wise, 1979; Steele and McCulloch, 1980; Baker et al., 1984).

3.6 Utilization of Methane

Coalbed methane has the same use as natural gas. The main issues in European coal mining countries such as England, Germany, France, Belgium, Czechoslovakia and Poland are used for underfiring coke ovens, generating steam by firing of boilers, generating electricity, heating, or in use in the

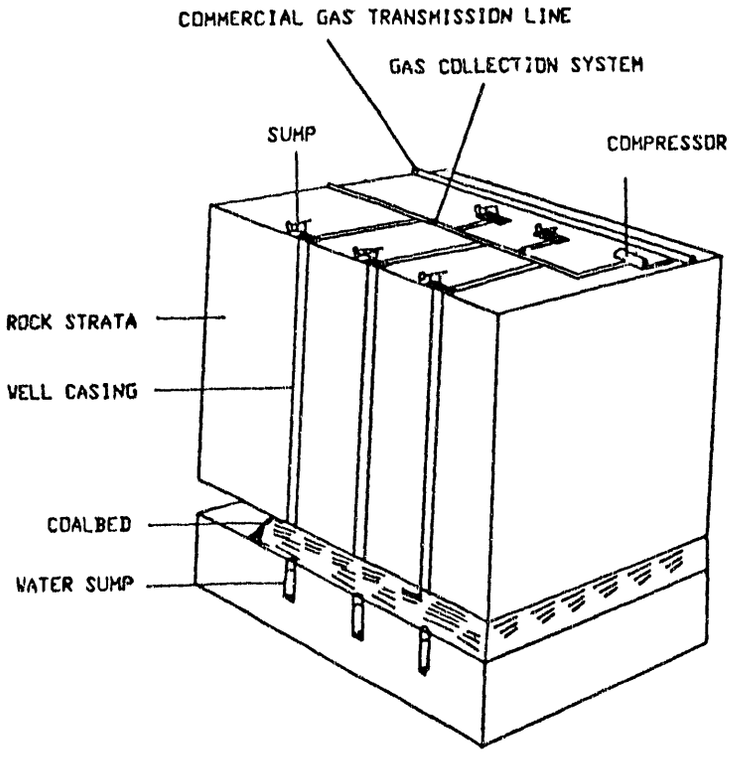

Figure 3.3 Surface techniques for methane recovery.

chemical industry. For example, in Czechoslovakia, in the Ostrava-Karvina coal basin, pipeline networks between the mines and the consumer have been established over distances of 50 miles (80 km).

Dames and Moore Mining Consultants (Stephenson, 1977), report that gas-fired boilers (conversion of a Lancashire Boiler) are common practice in England. The units use 200 cu ft (5.66m^3) of gas per minute giving 6,000 pounds (2,700 kg) per hour of steam. The units costs about $300,000. A gas turbine is also an alternative. The methane consumption is 500 cu ft (14.15 m^3) per minute per 1 MW capacity.

In the U.S.A., Mid-Continent Resources, Inc., in Carbondale, Colorado, uses methane for drying coal, heating water in bathhouses, and for space heating in mine buildings. Scott, 1981, reports that at the Bethlehem mine, methane recovered from the Pittsburgh coalbed supplies about 5% of the mine's total electric power requirements. The methane gas runs the 300-hp ventilation fan and a 100-hp gas compressor motor.

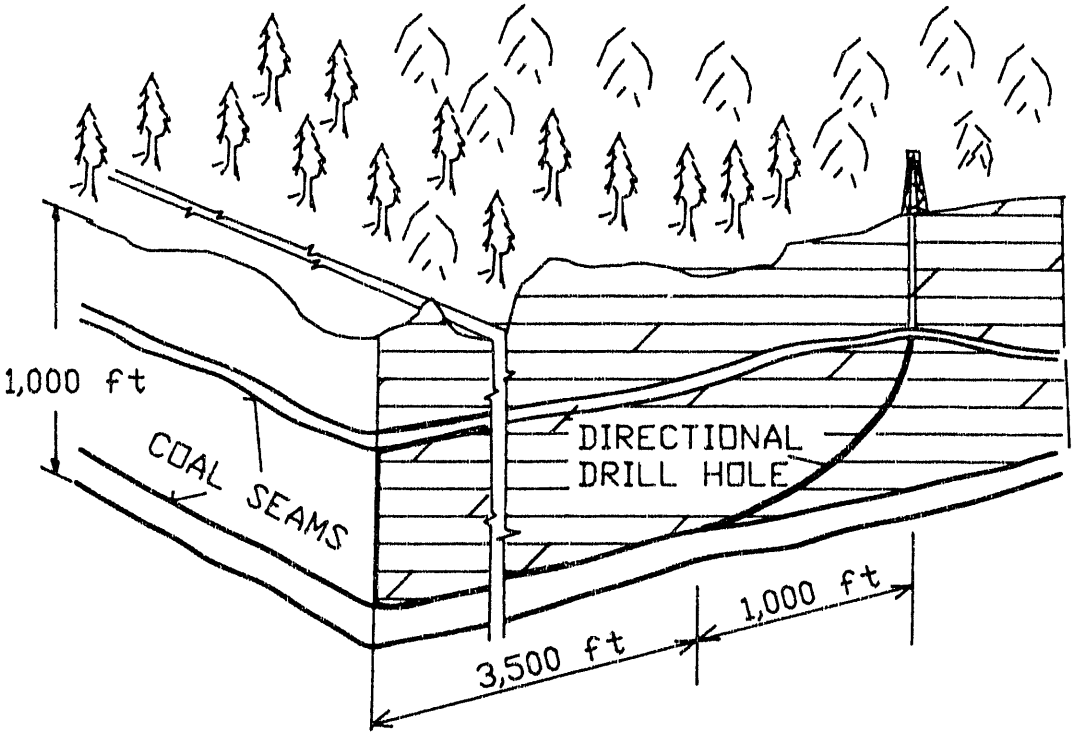

Figure 3.4 Directional drainage drilling technique.

4. GEOLOGY OF WASATCH PLATEAU, BOOK CLIFFS, AND CARBONDALE COAL FIELDS (Adapted from Smith and Keith, 1989).

4.1 Environment of Deposit

During the Triassic and Jurassic periods, the Book Cliffs Coal Field was gradually subsiding and receiving sediments. A thick red sequence suggests tropical conditions and great thicknesses of sand accumulating suggest arid conditions. Short periods of inundation by a shallow inland sea occasionally suspended the arid conditions. During the Jurassic period the area of sediments lay to the west and south (Doelling, 1972).

During the Cretaceous period, a trough developed in the area of the present-day Colorado Rockies and it was subsequently invaded by the sea. Gradually, the sea crept westward as the trough continued to subside and reached the edge of the Colorado Plateau by the beginning of the Upper Cretaceous period. The sea did not transgress westward continuously. The advancement of the sea was probably influenced by distinct pulses of basinal subsidence producing periods of rapid westward movement of the shoreline with longer intermittent periods of relative quiescence (Young, 1966). During these lulls beaches formed at the shoreline and began to grow seaward as thin bodies of sand, grading downward and seaward into nearshore marine mud. Long shore currents added layers to the prograding beaches causing minor regressions of the sea. While these beaches were forming at the shoreline, swamps or marshes formed behind then along the low-lying shore. The carbonaceous sables and coal beds of the Dakota Sandstone originated in these protected wetlands.

4.2 Stratigraphy

Continued basinal subsidence caused rapid advancement to a new beach-forming shoreline. As the shoreline shifted with these landward and seaward movements of the sea, the boundarys between offshore marine and nearshore marine, nearshore marine and littoral, littoral and paludal and floodplain environments were shifted also (Young, 1966).

During the westward transgression of the sea the Dakota Sandstone units extended as far as Sanpete County in central Utah. This occurred during Cenomanian time coincidentally with the deposition of the Tununk Member of the marine Mancos over the present San Rafael Swell. In the Book Cliffs area the sea remained in this westerly position until Campanian time, but the exact shoreline fluctuated as orogenic pulses elevated the lands to the west. Each pulse initiated an increase in the volume of clastic material being eroded from the western highlands and transported to the marine basin in the east. The increase in clastics filled the basin faster

than the basin was subsiding and resulted in the movement of the shoreline eastward. After each pulse, the volume of sediments decreased while the basin continued to subside causing the shoreline to migrate in a westerly direction. With each pulse the boundaries of the depositional environments moved eastward and then returned westward. As the boundaries shifted the sandstone tongues and the associated delta plain/alluvial plain carbonaceous facies - the Ferron, Garley Canyon, and the Emery Members - accumulated as projecting wedge-like facies into the Mancos marine beds.

4.3 Wasatch Plateau Field

This north-south trending field is about 94 miles (150 km) in length and about 18 miles (30 km) in width. In the east the coalbeds outcrop along the cliff faces. In the north the coal-field plunges into the Uinta Basin and in the south the field is buried beneath volcanic. The field is contiguous with the Book Cliff field at its northeast end. However, it is separated from it by the North Gordon fault zone (Figure 4.1). The main fault zones trend almost parallel to the long axis of the field. Many canyons are present in this area indenting the coal outcrops.

Economically important coal beds are found from about 200 to 450 feet (60 to 136 m) in the Blackhawk formation.

4.3.1 Southern Utah Fuel Mine (adapted from Hucka, 1991a)

SUFCO Mine No. 1 is located in the East Spring Canyon of the SE corner of the Acord Lakes quadrangle, approximately 27 miles (43 km) east from the town of Salina, Sevier County (Figure 4.1). The mine is part of the southern portion of the Wasatch Plateau coal field and is owned by the Southern Utah Fuel Company, a subsidiary of the Coastal States Energy Corp. The mine extracts coal from the Upper Hiawatha coal seam. The second seam, the Lower Hiawatha, is more or less a seam of unmineable thickness.

The Upper Hiawatha seam is contained in the lower part of the coal-bearing Blackhawk Formation of Upper Cretaceous age. Overlying this formation is the Castlegate Sandstone of the Price River Formation and the Star Point Sandstone Formation underlies it. Structurally, the only significant deformation in this area is the Acord Lake fault. The strata is inclined 2 degrees to the west and northwest (Doelling, 1972).

The Hiawatha seam attains a thickness of 12.5 ft (3.8 m) within the SUFCO leasehold and otherwise averages 8.9 ft (2.7 m). Faults counted in the mine have a mean strike of N 25.8 W and are mostly graben or half-graben bounding faults. Occasionally, spalling occurs when the thickness of the coal

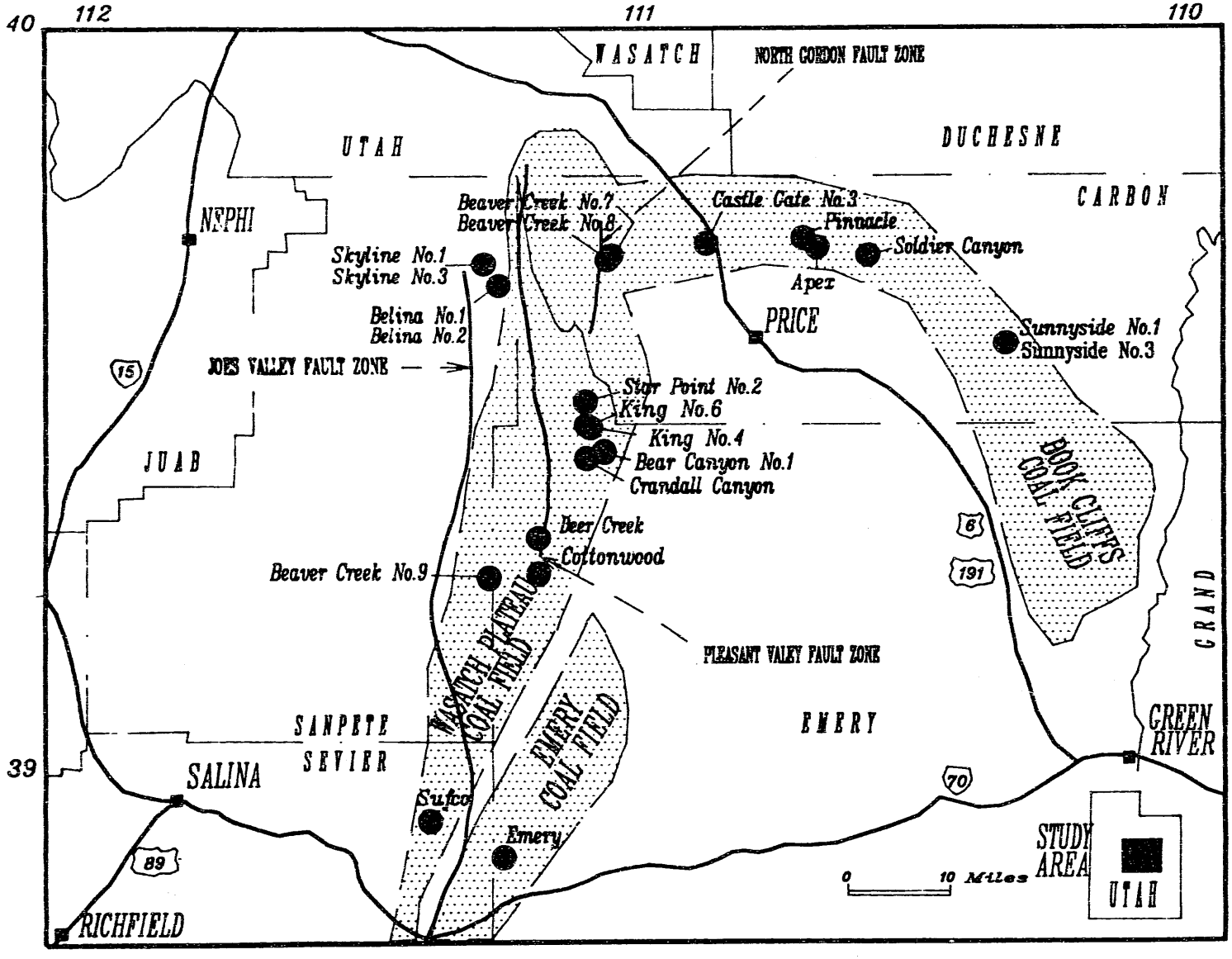

Figure 4.1 Utah coal mines and coal fields.

exceeds 10 feet. The immediate roof consists of 3 ft (0.9 m) of top coal overlain by shale. The lithology of the floor rock varies between siltstone, sandstone and shale.

Megascopically, the Upper Hiawatha seam is composed of indistinctly banded semi-bright, semi-dull and dull coal. The top of the seam is a semi-bright coal with an abundance of clarain. Durain and thin vitrain are present in subordinate amounts. The middle part of the seam consists of semi-dull coal where dull clarain, occasionally bright clarain and durain are the predominant components. In the lower part of the seam, durain is most abundant. Fusain lenses can be detected in varying parts of the seam, though mostly in the lower 2/3 of the seam.

Maceral composition of the samples collected from the top, middle and bottom of the seam (determined microscopically) averages 67.2% vitrinite, 5% exinite and 27.8% inertinite. The amount of inertinite is considerably higher in the middle and lower parts of the seam, and vitrinite decreases from top to bottom. The results of reflectance analyses show average reflectance Ro = 0.48, classifying the coal as high volatile bituminous C in rank.

Fifty cleat observations were made in the Hiawatha seam. The results display a bimodal distribution for the face and butt cleats. The first set, showing considerably stronger development, has a face cleat striking N 15 E and butt cleat striking N 55 W. The face cleat of the second set has a strike of N 15 W and a butt cleat N 85 W. The average angle of dip is about 86.1 degrees.

Butt cleats of both sets are not well represented. The average spacing interval between the face cleats is 0.25 inch (6.3 mm) for the first group and for the face cleats of the second group 0.3 to 0.4 inches (7.6 to 10 mm). The plane surfaces of the face cleats are usually smooth or planar and those of the butt cleats are generally rough.

Thirty-two joint measurements were taken on outcrop rocks. These consisted of yellowish to buff, cross-bedded sandstone, approximately 0.7 mile (1.12 km) from the mine portal. The results show two joint orientations with the main joint orientation striking N15W. and the minor joint N 65 E (Table 4.1).

4.3.2 Skyline Mines (adapted from Hucka, 1991a)

Skyline Mines Nos. 1 and 3, owned by Utah Fuel Company, are located in Eccles Canyon near Scofield, Carbon County and approximately midway between the towns of Fairview and Price. The mines are part of the Wasatch Plateau coal field. The Upper and Lower O'Connor "A" seams are presently being worked.

Table 4.1. Cleat and joint orientations in Utah coal mines and outcrop rocks (modified after Hucka, 1991a).

Mine/Seam	Cleat: Face	Butt	Secondary
Southern Utah Fuel Co. No. 1 Mine/ Hiawatha	1. N 25 E	N 55 W	N 15 W N 85 W
(SUFCO)	2. N 15 W	N 65 E	
Skyline No. 1 and	1. N 15 E	N 85 W	N 25 W
Skyline No. 3 Mines/	1. N 05 E	N 75 W	
Upper and Lower O'Connor	2. N 05 E	N 65 W	
Beaver Creek No. 7	1. N 65 W	N 35 E	
and 8/Castlegate A	2. N 15 E	N 45 W	
Castle Gate No. 3	1. N 55 W	N 35 E	
Mine/ Sub 3	2. N 65 W	N 35 E	
Pinnacle Mine and	1. N 65 W	N 35 E	
Apex Mine/Gilson and	1. N 55 W	N 45 E	
Lower Sunnyside	2. N 85 W	N 35 E	N 45 W
Soldier Creek Canyon	1. N 65 W	N 25 E	
Mine/Rock Canyon	2. N 35 W	N 85 W	N 25 E
Sunnyside No. 3 and	1. N 65 W	N 35 E	N 65 E N 45 E
Sunnyside No. 1	1. N 75 W	N 05 W	
Mines/Sunnyside	2. N 75 W	N 15 W	N 05 E

The O'Connor seams lie in the lower part of the Blackhawk Formation of Upper Cretaceous age. The sequence is composed predominantly of sandstone, shale and coal. The overlying Castlegate Sandstone and Price River Formations, comprised of conglomerate, sandstone and shale, are exposed only in the north and west of the Scofield quadrangle. The underlying strata consist of the sandstone (Storrs member) of the Star Point Sandstone Formation (Doelling, 1972).

The coal thickness of the Lower O'Connor "A" seam where the field tests were performed is 8.4 ft (2.5 m). Carbonaceous siltstone forms the roof and massive sandstone of the Star Point Sandstone Formation forms the floor. In the Upper O'Connor seam, which has a thickness of 6.3 ft (1.9 m), the roof consists of 6 inches (152 mm) of gray carbonaceous siltstone, above which are interbeds of sandstone, shale and siltstone, with sandstone being predominant. The floor consists of mudstone.

The overall appearance of the two seams is follows:

a) Lower O'Connor "A" seam: semi-dull, hard coal.
b) Upper O'Connor seam: bright, very hard coal.

Megascopically, in the Lower O'Connor "A" seam, semi-dull clarain is the most abundant lithotype. The clarain which has a dull appearance is interbedded with numerous variably thick vitrain bands or lenses. Two durain bands of measurable thickness can be observed as well.

The Upper O'Connor seam, classified as bright coal, is composed mostly of bright clarain and vitrain. It has a very high vitrinite content; therefore, clarovitrain would be a more appropriate name. Durain is sparsely distributed throughout the seam, however, the thickness is insufficient to classify it as individual lithotype bands.

It was observed that localized channeling cuts through the seams. Several lamprophyric dikes intrude into the coal, causing its alteration and showing formation of natural coke. Further, microfaults exist in the Upper O'Connor seam, present with small dislocations and powdered coal (gouge zone).

Microscopic analyses of the Lower O'Connor "A" seam collected at the time of field observation average 82.9% vitrinite, 3.3 exinite and 13.8% inertinite. The Upper O'Connor seam averages 93.6% vitrinite, 3.5% exinite and 2.9% inertinite (compare with Table 6.3). Close correlation can be seen in the maceral composition of the Lower and Upper O'Connor seams of the Belina mines with the Lower and Upper O'Connor seams.

The results of the reflectance analyses from measurements taken on vitrinite (Lower O'Connor seam Ro = 0.50 and Upper O'Connor seam Ro = 0.51) classify the O'Connor coals as high volatile bituminous C coals.

The coal of the Lower O'Connor "A" seam shows higher inertinite content, due to a higher percentage of thin durain bands. Their composition consists mostly of semifusinite. The coal of the Upper O'Connor seam is characterized by very high vitrinite content and remarkable consistency in maceral composition throughout the whole seam, reflected in the greater hardness of the coal.

A total of 106 cleat measurements in the Lower O'Connor "A" seam and 104 cleat measurements in the Upper O'Connor seam were obtained. The results show face cleat striking N 05 E. and butt cleat N 75 W for the Lower O'Connor "A" seam, and bimodal face cleat orientation with strikes N 15 E and N 25 W and butt cleat N 75 W for the Upper O'Connor seam.

Both mines show remarkable similarity in the orientation of the face and butt cleats even though more than one seam is

involved. Furthermore, their orientations are almost in agreement with the results obtained in the Belina mines.

Both seams are well cleated. In general, their surfaces are smooth, silky or with slickensides. Occasionally, the cleats extend into the roof rocks. Calcite filling, sometimes thick or coating covers the fracture planes (more easily seen in the Upper O'Connor seam). Resin and pyrite are disseminated mostly in the form of small flakes or films. When oxidized, iron hydroxides in the form of iridescent sulfides can be seen on the surface planes.

A total of 100 joint measurements were collected on the right side of the road less than a mile (1.6 km) from the portal of Skyline No. 3 mine. They were obtained from measurements on buff, fine-grained sandstone. The results obtained (main joint N 05 E and minor joint N 65 W) show similar patterns with the face and butt cleat in both seams (Table 4.1).

4.3.3 Beaver Creek Mine No. 7 (adapted from Hucka, 1991b)

Beaver Creek Mine No. 7 is one of two mines operated by Beaver Creek Coal Company, a subsidiary of Anaconda Minerals. The mine is located west-northwest of the town of Price, Carbon County, in Bryner Canyon (in the vicinity of the old Swisher mine) and is part of the Wasatch Plateau coal field (Figure 4.1).

Coal is being mined in the Castlegate "A" seam, the lowest seam in the Castlegate coal group. The seam rests on the transgressive sandstone of the Aberdeen Sandstone member of the Blackhawk Formation which separates the Castlegate group from the basal group, the Spring Canyon group, a tongue of the Star Point Sandstone Formation. In turn, the Star Point Sandstone Formation is underlain by the Mancos Shale, the oldest unit outcropping within the area. The formations overlying the Blackhawk Formation, in ascending order: Castlegate, Price River, and North Horn.

The area is structurally complex due to the numerous faults of the North Gordon fault zone, causing displacements of the surface and underground rocks. A thickness of 8.2 ft (2.5 m) of coal was measured on the site where cleat measurements and coal samples were collected. The mine roof consists of carbonaceous shale and the floor is shale. Several N-S trending faults (of the Fish Creek Complex) could be observed in the mine. Their offset is at most a few feet.

The results of megascopic observation (in situ and in the laboratory) classify the Castlegate "A" coal as a semi-bright, highly resinous clarain characterized by the absence of any partings. Bright clarain, dull clarain and thin vitrain bands

are the most abundant components. The usual banded texture due to bands of different lithotype components is not very distinct in this coal.

The maceral composition of the Castlegate "A" seam, determined microscopically, averages 83.1% vitrinite, 9% exinite, and 7.9% inertinite. The results reveal a fairly high concentration of exinite in comparison with other coals under study. The rank determined by means of reflectance measurements (Ro = 0.52) classify the coal as high volatile bituminous C.

One hundred and five cleat measurements were made in the Castlegate "A" seam. Two sets of cleats, each approximately at right angles to each other, show greater variations in orientation for the face and butt cleats than in most coal seams under study. The face cleat strikes N 65 W; the butt cleat N 35 E (Table 4.1).

Generally, the cleats in the Castlegate "A" seam are poorly expressed. Two distinct spacing distributions with spacing averaging 1.5 inches (38.1 mm) for the main cleats and average spacing of 0.08 inch (2 mm) for the more densely distributed cleats were measured. The latter, which shows a regular pattern, are filled with calcite, and their surface planes are smooth and lustrous. The former have larger and uneven plane surfaces with pyrite grains or calcite coatings. Resin, occasionally in large amounts in the lower part of the seam, was observed as cleat filling, as well.

One hundred surface measurements of joint orientations on an exposure of sandstone on the right side of the mine portal and across from the office building show two sets of joints with the main set striking N 15 E and minor set striking N 45 W.

4.4 Book Cliffs Field

The Book Cliffs coal field (Figure 4.1) is of Cretaceous age. It consists of about 72 miles (108 km) long and about 12.5 miles (20 km) wide strip. The field's coal-bearing outcrop extends easterly from the North Gordon fault zone to Sunnyside coal mine. The outcrop then continues southeasterly to Green River city. The field is exposed along high cliffs at the south edge of the Uinta Basin.

In the north and northeastward, the overburdens do not exceed a height of 3,125 ft (950 m). The coal-bearing strata is locally cut by high-angled faults. The sea regression occurred in the Cretaceous age with eastward movement. As a consequence, the western seams are older then those mined in the east.

4.4.1 Pinnacle and Apex Mines (adapted from Hucka, 1991a)

The Pinnacle and Apex mines, owned by Andalex Resources Company, are located in Straight Canyon, Carbon County (Figure 4.1). The portals of the mines are located several miles north from the town of Price. The Apex mine operates in the Lower Sunnyside seam and the Pinnacle mine operates in the Gilson seam. Both mines are part of the Book Cliffs coal field. The Lower Sunnyside and Gilson seams occur in the upper part of the Blackhawk Formation of Upper Cretaceous age. The Blackhawk Formation, which consists of alternating beds of sandstone, shale and coal, is overlain by the Castlegate Sandstone Member of the Price River Formation. The Mancos Shale Formation directly underlies it (Figure 4.2).

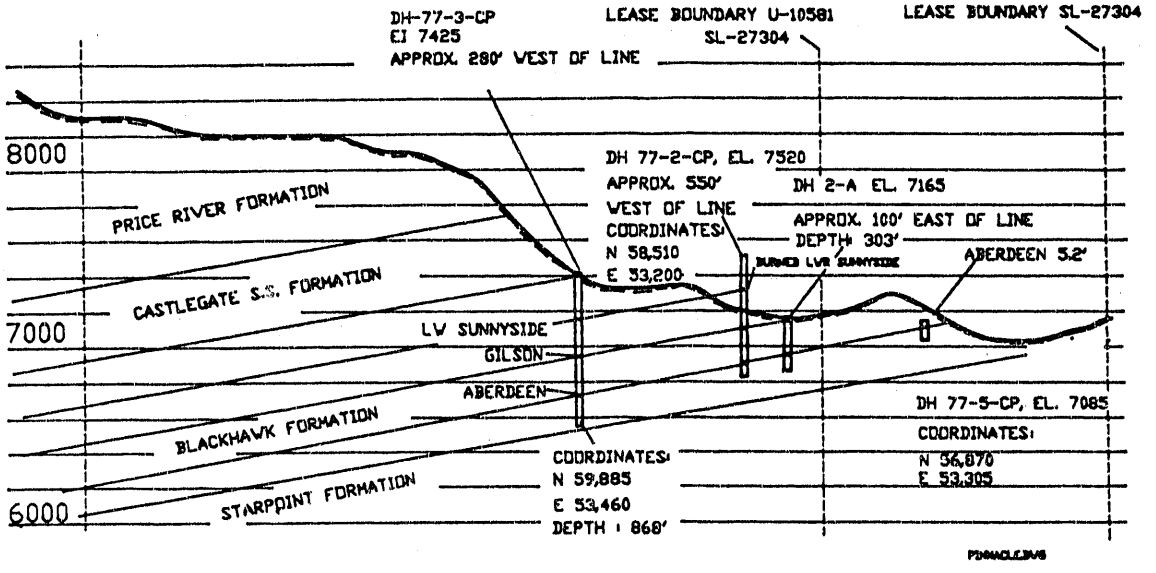

Figure 4.2 Pinnacle and Apex Mines.

Structurally, the Deadman Canyon quadrangle, where the mines are located, is part of the simple northward dipping Book Cliffs monocline which forms the southern rim of the Uinta Basin. The surface rocks dip gently at an average of four degrees (Clark, 1928).

Underground measurements and coal sampling were performed at a location where the coal thickness of the Lower Sunnyside was 4.2 ft (1.28 m) and that of the Gilson seam was 5.6 ft

(1.7 m). The roof and floor lithology of both seams consist of sandstone.

Megascopically, both seams are banded coals. The Lower Sunnyside coal is banded coal composed of bright clarain, thin vitrain bands and occasionally fusain lenses. Durain bands are sparse; three bands of approximately equal thickness occur at different positions within the seam. The Gilson coal is banded coal composed of semi-dull clarain with one moderately thick split in the upper part of the seam. The duller appearance of the Gilson coal is due to the higher percentage of dull clarain and durain.

Microscopically, the Lower Sunnyside seam averages 80.1% vitrinite, 3.9% exinite and 16% inertinite, and the Gilson coal averages 74% of vitrinite, 4.7% exinite and 21.3% of inertinite (compare with Table 6.3). Differences exist in the maceral composition, with the Gilson seam having a fairly high inertinite content. Based on the results of reflectance conducted on vitrinite, both seams are of high volatile bituminous B rank.

A total of 112 cleat measurements from the Gilson seam and 100 cleat measurements from the Lower Sunnyside seam were obtained.

The face cleat in the Gilson seam strikes N 65 W (mean N 57.8 W) and the butt cleat strikes N 35 E (mean N 31.3 E). The face cleat in the Lower Sunnyside seam strikes N 55 W (mean N 53.3 W) and butt cleat N 45 E (mean N 47.2 E). The dip varies between 70-90 degrees in both seams.

While butt cleat in the Gilson seam is not clearly discernible, face cleat is well-developed and generally confined to the clarain and vitrain components of the coals. They lack in durain bands and rock partings. Cleat surfaces are either lustrous or striated. The cleat spacing averages 1/4 inch (6.3 mm) for the Gilson seam and 1/4-1/2 inch (6.3-12.7 mm) for the Lower Sunnyside seam. Calcite fills the cleat fractures, and calcite coating is more frequent on the butt cleat surfaces. Pyrite occasionally occurs as microscopic grains on the cleat surfaces.

A total of 105 joint measurements were collected from a small exposure of sandstone outcropping on both sides of the road, approximately 0.5 mile from the mines. The main joint set has an E-W orientation of N 85 W and is characterized by high dispersion. The minor joint set has a N-S orientation (N 35 E). Possible secondary set strikes N. 45 W (Table 4.1).

4.4.2 Castlegate No. 3 Mine (adapted from Hucka et al., 1991b)

The Castlegate Coal Company, which operates Castlegate No. 3 mine, is located in Hardscrabble Canyon near the town of Price, Carbon County. The mine works the Sub-seam 3, the basal seam of the Spring Canyon group in the Blackhawk Formation of the Upper Cretaceous age. The seam, one of three present in the Spring Canyon group, is considered to be correlative to the Hiawatha coal seam of the Wasatch Plateau.

Part of the Wasatch Plateau, the mine forms the midway between the Book Cliffs and Wasatch Plateau fields studied in the cleat investigation.

The Spring Canyon group has a thickness between 100 and 125 ft (30.4-38 m), and is overlain and underlain by the Aberdeen Sandstone member and Storrs Sandstone Tongue of the Star Point Formation (Young, 1955).

A seam thickness of 5.9 ft (1.8) was measured at the same location as cleat measurements were collected. The immediate roof rock consists of carbonaceous shale; however, the type of roof rock varies within the mine (Bunnell, 1987). The floor rock consists of massive sandstone. Two rock partings, not exceeding one foot, occur within the seam.

Megascopically, the predominant lithotype is bright-banded clarain with minor durain bands showing higher concentrations in the upper parts of the seam. Thin, very bright vitrain bands and fusain lenses are present throughout the seam. Inorganic accessories include calcite and pyrite, mostly as cleat surface coating or filling and as disseminated grains mainly on the clear surfaces or in the durain bands. Resin is present in small amounts.

A characteristic feature of the coal is its hardness, probably due to the overall lithotype uniformity of the seam. The microscopic analyses carried out on the channel sample and additional samples taken from the top, middle and bottom of the seam indicate that the coal has an average of 85% vitrinite, 6.5% exinite, and 8.5% inertinite. The coal is classified as high volatile bituminous B by its average rank of R = 0.57, determined by vitrinite reflectance.

A total of 47 cleat measurements taken from the Sub-3 seam show the face cleat with a strike of N. 55 W. and butt cleat with N. 30 E. A secondary set of cleats strikes N. 75 E. The average dip is 81.9 degrees. Both sets of cleats are abundant and well developed in clarain and vitrain but conspicuously lacking in thin durain bands. Cleat filling consists of calcite and occasionally of resin. The surface of the cleats in clarain and vitrain are smooth and lustrous with an average spacing of 0.8 inches (20mm) (clarain).

On the surface, one hundred joint measurements were taken

on a buff, fine-grained, cross-bedded, calcareous sandstone and gray, fine-grained siltstone in front of the office building and approximately 0.8 mile (1.3 km) from the mine on the right side of the road. Spacing of the joints varies between 1-1.25 ft (0.3-0.38 m), with joints more closely spaced in the thinner gray sandstone bed. Orientations of the main and minor joints are N 65 W and N 45 E; those of the secondary sets of joints N 85 E and N 15 W, respectively.

4.4.3 Soldier Creek Canyon Mine (adapted from Hucka, 1991c)

This mine is operated by the Soldier Creek Coal Company and is located in Soldier Creek canyon, Carbon County, 40 miles (64 km) NE from the town of Price (Figure 4.1). Three coal seams, Gilson, Rock Canyon, and Lower Sunnyside are present within the mine property. However, only the Rock canyon seam is presently mined while the Sunnyside coalbed in under development. The seams belong to the upper part of the coal-bearing Blackhawk Formation of the Book Cliffs coal field. The formation is approximately 225 ft (68.4 m) thick within the Pine Canyon quadrangle and contains as many as six mineable seams. It is overlain by the Castlegate sandstone member of the Price River Formation and underlain by the Mancos Shale Formation (Doelling, 1972).

The thickness of the seam attains a value of 9.2 ft (2.8 m) at the location where a channel sample, as well as samples from the top, middle, and bottom, were collected. The seam contains three rock partings that constitute approximately 0.4% of the total thickness. Roof rock consists of carbonaceous shale and the floor rock is sandstone.

The results of the megascopic description of the Rock Canyon seam indicates that the coal is a semi-bright clarain consisting of fine to medium bands of bright and dull clarain alternating with durain bands. Sparsely distributed vitrain bands are present throughout the whole seam.

Microscopically, the coal macerals average 76% vitrinite, 4% exinite, and 20% inertinite. Average vitrinite reflectance for the above mentioned samples is Ro = 0.63, classifying the coal as high volatile bituminous B in rank (Table 6.3).

The coal is characterized by a uniform maceral composition and a relatively high percentage of inertinite. Inertinite (represented mostly by semifusinite and fusinite) are the predominant macerals in the durain bands.

A total of 49 cleat measurements taken at the mine show two principal orientations with the face cleat striking N65W (mean N63W) and the butt cleat striking N25E (mean N26.6E). Both systems of cleats are well developed. Parting between the cleats is very small, and as a result, secondary calcite

occurs only as a very thin coating on the cleat planes. The surface planes of the cleats are mostly uneven or striated (Table 4.1).

One hundred joint measurements were taken on the surface of two successive beds (approximately 0.4 mile or 0.64 km from the mine). The two beds consisted of gray, fine-grained, laminated, highly calcareous sandstone and dark gray, calcareous siltstone. The joint spacing averages 0.8 inch (20 mm) with more closely spaced joints in the dark gray siltstone.

4.4.4 Sunnyside Mines (adapted from Hucka, 1990)

The Sunnyside mines are located near Whitmore Canyon about 27 miles (43.2 km) southwest from the town of Price, Carbon County, Utah (Figure 4.1). Presently, the mines are inactive. Two mineable coalbeds are present on the property: Upper Sunnyside and Lower Sunnyside. The coalbeds are located

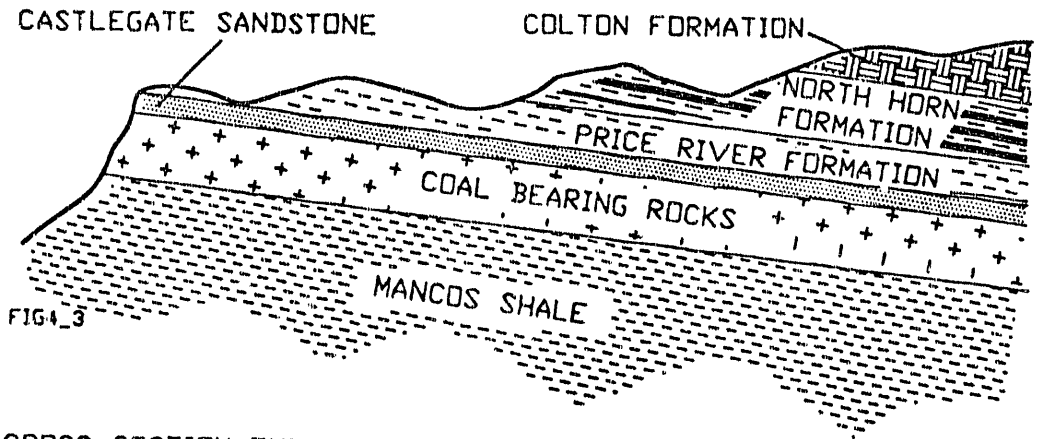

Figure 4.3 Sunnyside Mine.

in the Upper Cretaceous Blackhawk Formation (Figure 4.3). Doelling, 1972, estimates the thickness of the formation of about 700 ft (213 m). Overlying unit is Castlegate Sandstone of the Upper Cretaceous strata. Underlying are thick, massive, cliff forming sandstones or coarse-grained siltstones

(Gray et al., 1966). The thickness of the Lower Sunnyside coalbed is about 7 ft (2.1 m).

The strike of beds is to the northwest with the dip averaging between 6-12 degrees eastward and northeastward. According to Doelling (1972), there is a cluster of northwest trending faults but displacements are not large enough to affect seriously the mining conditions. However, these faults may have contributed to degasification of the south part of the Sunnyside coalbed (Figure 4.1).

4.5 Carbondale Coal Field in Colorado (adapted from Hucka, et al. 1989)

4.5.1 B Seam at the Dutch Creek Mine in Redstone

Dutch Creek mine owned by the Mid-Continent Resources, Inc., is located several miles from the town of Redstone, Pitkin County, Colorado. The B coalbed is opened in the property. The B coalbed is a part of the Carbondale coal field, and outcrops at approximately 10,000 ft (3040 m) elevation. The Mountainous surrounding is providing an overburden reaching 2,500 ft (760 m).

Stratigraphic formations of interest in the Carbondale coal field compose of the Mesaverde Group of Upper Cretaceous age. This strata is divided into the Iles and Williams Fork Formation. According to Collins (1985), the Williams Fork Formation is divided into the Bowie Shale Member, the Paonia Shale Member and the upper "undifferentiated beds". The developed section of the B coalbed occurs in the basal part of the Bowie Shale Member and rests on the Rollins Sandstone Member of the Iles Formation. Two coalbeds are found in the property: A-bed, and B-bed, altogether providing and aggregate thickness of 12 - 53 ft (3.6-16.1 m). The mining conditions are hampered by high methane gas emissions and proneness to sudden coal and gas outbursts. The rank is medium volatile bituminous metallurgical coal (Table 6.1).

5. COALBED METHANE RESOURCES OF BOOK CLIFFS AND CARBONDALE COALFIELDS

The gassy coalbeds in Utah are of interest not only for the mining safety reasons, but also for their potential as a source of energy. The Utah Geological Survey in collaboration with the U.S. Bureau of Mines conducted a thorough investigation of methane content of all Utah coalbeds. The direct method recommended by the U.S. Bureau of Mines was used for methane gas estimates (Kissell et al., 1973; Lama and Bartosiewicz, 1982; Diamond, 1984). The following is an extract of this particular report prepared by A. Smith (1985).

5.1 Coalbed Methane Determination by the Utah Geological Survey

The Book Cliffs field was sampled by Utah Geological Survey geologists for methane over a geographic area of twelve townships. Twelve coalbeds were sampled at a mean depth of 1,325 ft (402.7 m). The average total gas content of the twelve beds is 110 cu ft/ton (3.5 cm^3/gm). This coal field has been classified as moderately gassy (32-160 cu ft/ton or 1-5 cm^3/gm). At specific locations, the field can be classified as gassy (>160 cu ft/ton or 5 cm^3/gm). The average residual gas content is 35 cu ft/ton (1.1 cm^3/gm).

Table 5.1 Coalbed methane in the Book Cliffs Field (after Smith, 1985)

BED	SAMPLES	AVG DEPTH (meters)	AVG TOTAL GAS*	AVG RSDL GAS*
Gilson	6	617.2	4.2	0.9
Sunnyside	9	175.5	2.9	0.9
Castlegate A	14	343.1	3.7	0.8
Castlegate B	8	175.6	1.4	0.9
Castlegate C	8	296.5	2.7	0.5
Castlegate D	8	214.9	2.4	0.9
Rock Canyon	6	516.8	3.0	0.8
Kenilworth	6	624.1	5.8	1.5
Subseam 1	3	581.2	6.0	1.2
Subseam 2	4	429.0	3.5	1.7
Subseam 3	1	537.1	2.3	2.3

*Cubic centimeters/gram

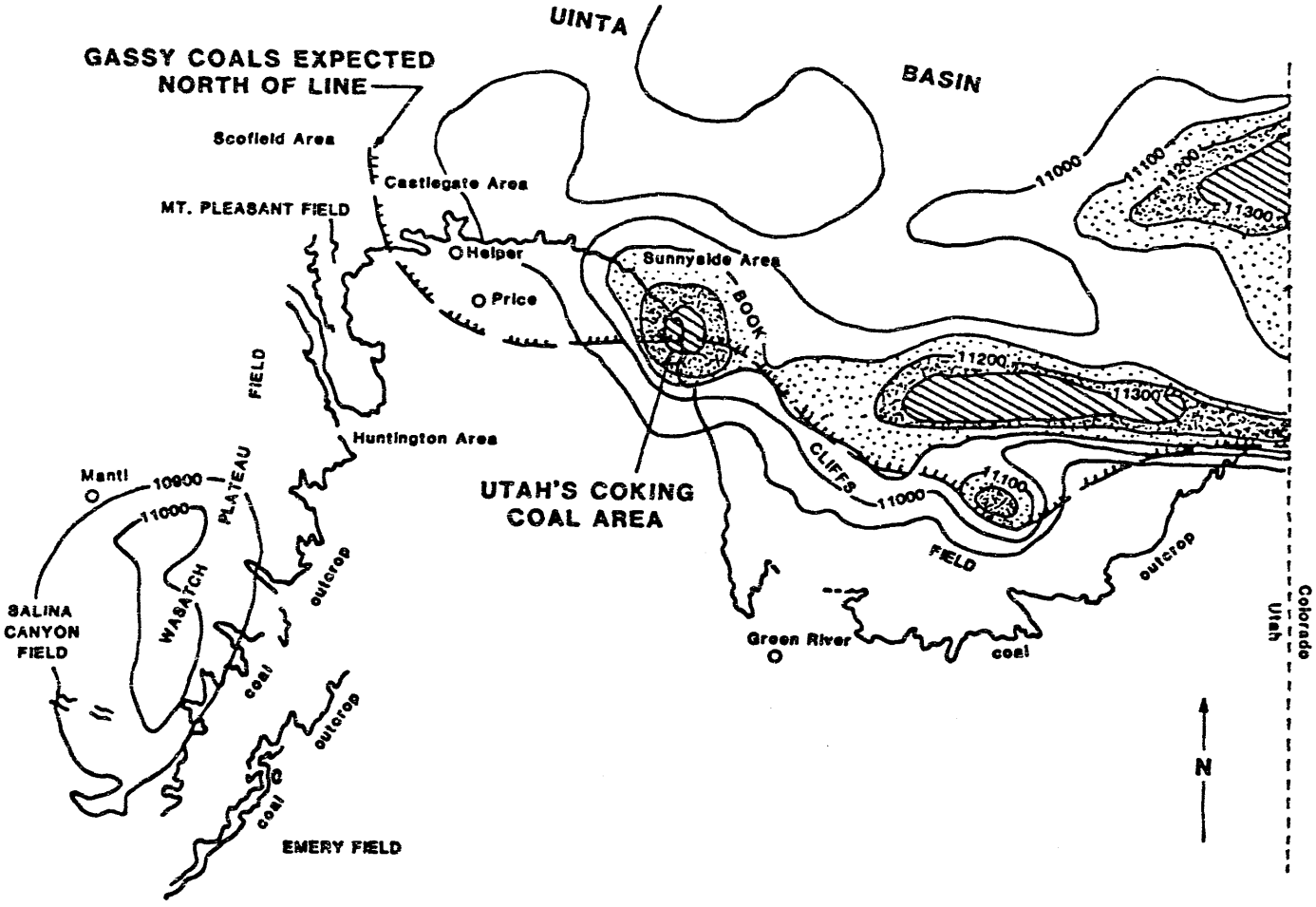

Figure 5.1 Methane demarcation line for Book Cliffs Coal Field.

If a line is drawn east-west at the Sunnyside Mine (Figure 5.1) the north half of the field is moderately gassy and locally can be gassy, whereas the south half is low gassy. This result is supported by mine ventilation readings, as well as the collected coal cores from both sides of the line. Working mines north of Horse Canyon (which is just south of Columbia) can ventilate to the atmosphere each day approximately 3.4 X 10^6 cu ft (98,026.1 m^3) of methane per 24 hours, according to the Mine Safety & Health Administration (MSHA) records (this figure may vary depending on the number of working sections in the mines), whereas the mine at Horse Canyon ventilates no methane for all practical purposes.

No apparent tectonic or stratigraphic reasons explain why gas emissions are so regulated. This gas emission phenomena has been noted by Doelling et al. (1979)

> Although the quality of the coal is the same south of the line (Carbon-Emery County line), it contains much less gas. There are no obvious explanations, but an interesting suggestion comes by superimposing aeromagnetic contours over the area. High magnetic readings coincide with Utah's area of gassy coals. The high magnetic areas supposedly show the emplacement of magnetic materials in the basement may have been responsible for increasing heat or pressure and thereby favor gas formation or the formation of coking coal...,

5.2 In Situ Measurements

In this research work, five coal seams (four in Utah and one in Colorado) have been identified for the initial studies. The Sub 3 seam of the Castle Gate Mine No. 3, Rock Canyon and Sunnyside seams of the Soldier Creek Mine, the Sunnyside seam of the Sunnyside Coal Mine, in Central Utah, were tested for methane content. These Utah coal seams are gassy and belong to the Book Cliffs coal field. The seams belong to the Blackhawk Formation. The B seam of the Dutch Creek mine (Carbondale, about 40 miles (64 km) south of Glenwood Springs, Colorado) was tested as well. The B seam belongs to the William Formation.

The methane content was determined in situ from fine cuttings collected from a bottom of horizontal bore holes drilled into a coal face. Samples are collected from a coal face at a depth of 6.6 feet (2 meters) gradually increasing up to 50 feet (15 meters).

Testing methods used in Germany and France for determining in situ gas content have been studied and modified

for use in western coal seams. The so-called "bubble desorbometer method" was used in this research work. The method is described and the results are compared with results obtained from the direct method.

During the underground testing, the coal seam was evaluated. The natural fracture system consisting of fractures or fissures in the coal and in mine roofs was measured. The coal fractures in coal, called cleats in the mining industry, are reported in Chapter 4, A cleat is a joint or set of joints in coal generally almost perpendicular to each other. Major cleats (or face cleats) may extend to great distances. Minor cleats (butt cleats) usually extend from one face cleat fracture to the next. It has been found that face cleats yield longer fractures and often are more prominent.

The face and butt cleats in the coal provide a directional permeability; the flow of gas is greater in the direction parallel to the dominant face cleat. The Bureau of Mines reports that degasification experiments conducted underground in coal mines have shown that horizontal holes drilled perpendicular to, and therefore intersecting, the largest number of face cleats will yield 2.5 to 10 times as much gas as holes drilled perpendicular to the butt cleats (see Appendix F). The Utah Geological and Mineral Survey undertook an extensive study of cleat and joint systems in all working coal mines in Utah. The cleat system of a coalbed also affects vertical degasification holes drilled from the surface into a coalbed.

5.3 Drainage Tests

As it has been mentioned, utilizing methane from coalbeds has been shown to be of considerable value. Methane drainage tests have been initiated by the Bureau of Mines in 1964. In the Sunnyside seam, a total of 35 x 10^6 MMcf (10^6 m^3) of commercial-quality gas was removed by workers of the Bureau of Mines (Perry, et al., 1978). Resource Enterprises, Inc., Salt Lake City, is successfully engaged in draining methane gas from the Rock Canyon seam (Soldier Creek Canyon mine, Schwoebel,1987). However, drainage tests in the Sub 3 seam (Castle Gate mine) performed by the Occidental Research Corporation were not successful even though the Sub 3 seam is one of the most gassy coalbeds in Utah (Aul, 1983).

We have evaluated results on methane drainage tests performed by the Bureau of Mines in the Sunnyside seam, by Resources Enterprise in the Rock Canyon seam, and by the Oxydental Research Group in the Sub 3 seam. Using the directional permeability ellipse, with its long and short axes

representing maximum and minimum values of drained gas, an attempt was made to calculate the gas for optimum production (Appendix F, Table II). The last column indicates the improvement in gas yield for proper orientation.

6. COAL SAMPLE CHARACTERIZATION

Nineteen coal samples were used in this study. Ten were collected from Utah coal fields, all of similar geological age, but of varying methane content and methane drainage behavior. One was collected from Colorado. It is a higher rank gassy coal. Eight coal samples from the Argonne Premium Coal Sample Bank, which cover a wide range of coal rank from lignite to low volatile bituminous, were used for comparison. These samples were collected, ground, sized, and stored under oxygen-free conditions, and were received in sealed vials.

6.1 Analytical Data

The proximate and ultimate analyses of the nineteen coals are given in Table 6.1. The data of the eight Argonne Premium Coals are from Vorres (1989, 1990). Carbon, hydrogen, and nitrogen content was determined with a LECO CHN 600 analysis system. Proximate analysis was with a LECO MAC 400 automated analysis system. Sulfur was determined with a LECO SC132 sulfur analyzer which uses infrared absorption of combustion gases to determine sulfur oxides. These methods give results which are comparable to the ASTM standard tests for coal analysis, but are much more rapid and allow for analysis of multiple samples to obtain reliable results. The rank number in Table 6.1 is an arbitrary scale in which an integer is assigned to show increasing rank.

Carbon structural parameters were determined by ^{13}C nuclear magnetic resonance (NMR) tests using the procedure described by Solum, et al. (1989). Spectra were recorded at 25.15 MHz using cross polarization and magic angle spinning techniques to determine aromaticities. The carbon types in the carbon skeleton of the coal were determined by dipolar-dephasing techniques. Results for the nineteen coals are given in Table 6.2. The NMR data for the 8 Argonne Premium Coals are from Solum et al. (1989).

Helium densities of each of the coal samples were measured using a pycnometer (AccuPyc 1330 Pycnometer, micromeritics, Inc.). The results are listed in Table 6.3. The measurements are corrected to a mineral matter-free basis using the formula:

$$\frac{x}{\rho_m} + \frac{1-x}{\rho_c} = \frac{1}{\rho} \qquad (1)$$

where x is the weight fraction of the mineral matter, ρ_m the density of the mineral matter, assumed to be 2.85 g/ml, ρ_c the density of the coal, and ρ the measured density. The measured ash content is used for mineral matter. The calculated coal densities are also given in Table 6.3.

Table 6.1 Proximate and ultimate analyses of coals.

Sample No.	Seam	State	Rank	Rank No.*	Proximate analysis (wt%)			Ultimate analysis (wt%, daf)				
					Moisture**	Ash***	V.M.***	C	H	O	N	S
1	Upper Freeport	PA	Med. Vol. Bit.	4	1.13	13.18	27.45	85.50	4.70	7.51	1.55	2.67
2	Wyodak-Anderson	WY	Subbituminous	2	28.09	8.77	44.73	75.01	5.35	18.02	1.12	0.69
3	Illinois #6	IL	High Vol. Bit.	3	7.97	15.48	40.05	77.67	5.00	13.51	1.37	5.72
4	Pittsburgh (#8)	PA	High Vol. Bit.	3	1.65	9.25	37.82	83.20	5.32	8.83	1.64	2.41
5	Pocahontas #3	VA	Low Vol. Bit.	5	0.65	4.77	18.60	91.05	4.44	2.47	1.33	0.69
6	Blind Canyon	UT	High Vol. Bit.	3	4.63	4.71	45.84	80.69	5.76	11.58	1.57	0.65
7	Lewiston-Stockton	WY	High Vol. Bit.	3	2.42	19.84	30.17	82.58	5.25	9.83	1.56	0.89
8	Beulah-Zap	ND	Lignite	1	32.24	9.72	44.94	72.94	4.83	20.34	1.15	0.89
9	Castlegate A, AB	UT	High Vol. Bit.	3	5.61	3.40	45.04	80.18	5.83	11.42	1.84	0.73
10	L. Sunnyside, Apex	UT	High Vol. Bit.	3	6.40	4.83	37.46	80.53	5.17	12.09	1.62	0.60
11	Castlegate A, BC	UT	High Vol. Bit.	3	6.20	2.99	50.01	81.25	6.20	10.15	1.72	0.68
12	Sub-3	UT	High Vol. Bit.	3	3.01	5.76	45.43	82.85	6.12	8.71	1.75	0.56
13	Gilson	UT	High Vol. Bit.	3	5.45	9.12	38.32	81.12	5.18	13.17	1.55	0.35
14	Upper O'Connor	UT	High Vol. Bit.	3	6.78	8.05	52.74	79.22	5.74	13.02	1.53	0.49
15	Rock Canyon	UT	High Vol. Bit.	3	4.44	10.60	38.63	82.37	5.37	10.23	1.67	0.36
16	L. Sunnyside, SC	UT	High Vol. Bit.	3	4.41	6.15	43.30	82.64	5.63	9.55	1.63	0.55
17	Upper Hiawatha	UT	High Vol. Bit.	3	7.83	9.86	43.85	79.59	5.26	13.43	1.44	0.28
18	L. Sunnyside, SY	UT	High Vol. Bit.	3	3.53	4.04	36.79	85.29	5.48	6.98	1.78	0.47
19	B Seam	CO	Med. Vol. Bit.	4	1.31	5.93	23.70	91.24	5.20	0.78	2.25	0.53

Abbreviations: V.M., volatile matter; daf, dry ash free basis; L., Lower; AB, Aberdeen; BC, Beaver Creek #8; SC, Soldier Creek; SY, Sunnyside
** arbitrary integers assigned to coals by their ranks; ** equilibrium or coalbed moisture; *** dry basis*

Table 6.2 Carbon structural distribution of coals*.

No.	Coal	f_a	$f_{a'}$	f_a^C	f_a^H	f_a^N	f_a^P	f_a^S	f_a^B	f_{al}	f_{al}^H	f_{al}^*	f_{al}^O
1	Upper Freeport	0.81	0.81	0.00	0.28	0.53	0.04	0.20	0.29	0.19	0.09	0.10	0.02
2	Wyodak-Anderson	0.63	0.55	0.08	0.17	0.38	0.08	0.14	0.16	0.37	0.27	0.10	0.10
3	Illinois #6	0.72	0.72	0.00	0.26	0.46	0.06	0.18	0.22	0.28	0.19	0.09	0.05
4	Pittsburgh (#8)	0.72	0.72	0.00	0.27	0.45	0.06	0.17	0.22	0.28	0.13	0.15	0.03
5	Pocahontas #3	0.86	0.86	0.00	0.33	0.53	0.02	0.17	0.34	0.14	0.08	0.06	0.01
6	Blind Canyon	0.65	0.64	0.01	0.22	0.42	0.07	0.15	0.20	0.35	0.22	0.13	0.04
7	Lewiston-Stockton	0.75	0.75	0.00	0.27	0.48	0.05	0.21	0.22	0.25	0.14	0.11	0.04
8	Beulah-Zap	0.61	0.54	0.07	0.26	0.28	0.06	0.13	0.09	0.39	0.25	0.14	0.12
9	Castlegate A, AB	0.59	0.58	0.01	0.19	0.39	0.07	0.14	0.18	0.41	0.28	0.13	0.06
10	L. Sunnyside, Apex	0.62	0.57	0.05	0.19	0.38	0.08	0.16	0.14	0.38	0.29	0.09	0.06
11	Castlegate A, BC	0.57	0.55	0.02	0.17	0.38	0.05	0.11	0.22	0.43	0.30	0.13	0.07
12	Sub-3	0.62	0.59	0.03	0.20	0.39	0.05	0.14	0.20	0.38	0.26	0.12	0.08
13	Gilson	0.65	0.62	0.03	0.22	0.40	0.07	0.16	0.17	0.35	0.25	0.10	0.07
14	Upper O'Connor	0.56	0.52	0.04	0.18	0.34	0.07	0.13	0.14	0.44	0.34	0.10	0.06
15	Rock Canyon	0.65	0.64	0.01	0.22	0.42	0.04	0.13	0.25	0.35	0.25	0.10	0.08
16	L. Sunnyside, SC	0.59	0.54	0.05	0.22	0.32	0.07	0.13	0.12	0.41	0.29	0.12	0.09
17	Upper Hiawatha	0.54	0.50	0.04	0.15	0.35	0.06	0.13	0.16	0.46	0.33	0.13	0.06
18	L. Sunnyside, SY	0.68	0.65	0.03	0.23	0.42	0.03	0.14	0.25	0.32	0.20	0.12	0.08
19	B Seam	0.72	0.70	0.02	0.25	0.45	0.03	0.14	0.28	0.28	0.19	0.09	0.08

Abbreviations: L., Lower; AB, Aberdeen; BC, Beaver Creek #8; SC, Soldier Creek; SY, Sunnyside

* Fractions of sp^2-hybridized carbon (error estimate): f_a total carbon (±0.03); $f_{a'}$ in an aromatic ring (±0.04); f_a^C carbonyl, δ > 165 ppm (±0.04); f_a^H protonated and aromatic (±0.03); f_a^N nonprotonated and aromatic (±0.03); f_a^P phenolic or phenolic ether, δ = 150 - 165 ppm (±0.02); f_a^S alkylated aromatic, δ = 135 - 150 ppm (±0.03); f_a^B aromatic bridgehead (±0.04). Fractions of sp^3-hybridized carbon (error estimate): f_{al} total carbon (±0.02); f_{al}^H CH or CH_2 (±0.02); f_{al}^* CH_3 or nonprotonated (±0.03); f_{al}^O bonded to oxygen, δ = 50 - 90 ppm (±0.02)

Table 6.3 Maceral analyses, heating values and densities of coals,

Sample No.	Seam	State	Rank	Maceral analysis			H.V. (daf)	Density, g/ml	
				Vitrinite	Inertinite	Exinite	Btu/lb	measured*	calculated**
1	Upper Freeport	PA	Med. Vol. Bit.	91	8	1	15,510	1.408	1.308
2	Wyodak-Anderson	WY	Subbituminous	89	11	1	12,840	1.411	1.345
3	Illinois #6	IL	High Vol. Bit.	85	10	5	14,140	1.452	1.332
4	Pittsburgh (#8)	PA	High Vol. Bit.	85	8	7	15,020	1.358	1.289
5	Pocahontas #3	VA	Low Vol. Bit.	89	10	1	15,780	1.369	1.334
6	Blind Canyon	UT	High Vol. Bit.	87	8	5	14,610	1.299	1.265
7	Lewiston-Stockton	WY	High Vol. Bit.	73	15	12	14,730	1.458	1.301
8	Beulah-Zap	ND	Lignite	-	-	-	12,180	1.452	1.379
9	Castlegate A, AB	UT	High Vol. Bit.	69	24	7	14,260	1.297	1.285
10	L. Sunnyside, Apex	UT	High Vol. Bit.	83	15	2	13,930	1.344	1.309
11	Castlegate A, BC	UT	High Vol. Bit.	80	8	12	14,500	1.291	1.266
12	Sub-3	UT	High Vol. Bit.	86	9	6	14,800	1.296	1.254
13	Gilson	UT	High Vol. Bit.	76	19	5	14,000	1.352	1.298
14	Upper O'Connor	UT	High Vol. Bit.	94	3	3	13,870	1.328	1.261
15	Rock Canyon	UT	High Vol. Bit.	75	22	3	14,810	1.350	1.271
16	L. Sunnyside, SC	UT	High Vol. Bit.	76	19	5	14,900	1.306	1.261
17	Upper Hiawatha	UT	High Vol. Bit.	64	32	4	13,800	1.355	1.281
18	L. Sunnyside, SY	UT	High Vol. Bit.	85	11	4	14,650	1.310	1.257
19	B Seam	CO	Med. Vol. Bit.	89	9	2	15,330	1.345	1.302

Abbreviations: H.V., heating value; daf, dry ash free basis; L., Lower; AB, Aberdeen; BC, Beaver Creek #8; SC, Soldier Creek; SY, Sunnyside
** dry basis; ** daf basis or coal density*

Maceral analyses of the Utah coal were obtained from Sommer et al. (1991). Maceral analysis of the Colorado coal was from Hucka et al. (1989). The heating value of these coals was determined with a LECO AC300 isothermal calorimeter. Maceral analysis and heating value of the Argonne Premium Coal Sample Bank samples were obtained from Vorres (1989). The results on maceral content and heating value are found in Table 6.3. The coal rank was determined using ASTM procedures.

6.2 Multivariate Analysis

In order to understand the correlation of the analytical variables, such as carbon content, hydrogen content, oxygen content, moisture, heating value and density, with coal rank, multivariate analysis was used to determine interactions between the variables. The statistical analysis results can be used to eliminate variables by examining the translation of one analytical parameter into another and to choose one analytical variable which quantitatively represents the coal rank parameter.

The correlation of analytical data with coal rank, which was represented by an arbitrary integer, were first examined using multi-regression analysis. The correlation coefficients are given in Table 6.4. The correlation coefficients of analytical variables with coal rank are plotted in Figure 6.1. As shown in this figure, coal rank is strongly correlated with carbon content.

Factor analysis was performed to reduce the data matrices to their lowest dimensionality by the use of orthogonal factor space and transformations that yield predictions and/or recognizable factors. The number of significant factors was determined by either a Scree plot or a Cumulative plot. From the Scree plot (Figure 6.2), the slope levels off after factor 4, indicating that the first three factors are most important. The eigenvalues of the three retained factors are greater than one, and those of the rest are much less than one, further supporting this determination. From a plot of cumulative percent versus factor number (Figure 6.3), the retained three factors account for about 90% of the variation.

To explore the physical meaning of the factors, the three retained factor loadings are plotted against the variables in Figure 6.4. Factor 1 has positive correlation with coal rank, carbon content and heating value, and negative correlation with oxygen content, moisture content and volatile matter. These variables all are coal rank dependent, indicating that the physical interpretation of factor 1 is coal rank. Factor 2 has strong contributions from hydrogen, volatile matter and density. This is interpreted as indicating that factor 2 is dependent on the coal density. Factor 3 shows strong

Table 6.4 *Correlation coefficients of multi-regression analysis.*

	Rank	Moisture	Ash	V.M.	C	H	O	N	S	H.V.	Density
Rank	1.000	-0.761	-0.147	-0.723	0.924	-0.245	-0.915	0.534	0.025	0.854	-0.209
Moisture	-0.761	1.000	0.073	0.402	-0.772	-0.127	0.805	-0.657	-0.042	-0.898	0.650
Ash	-0.147	0.073	1.000	-0.219	-0.209	-0.425	0.227	-0.347	0.501	-0.078	0.341
V.M.	-0.723	0.402	-0.219	1.000	-0.759	0.718	0.692	-0.190	-0.119	-0.609	-0.318
C	0.924	-0.772	-0.209	-0.759	1.000	-0.190	-0.985	0.619	-0.133	0.901	-0.296
H	-0.245	-0.127	-0.425	0.718	-0.190	1.000	0.083	0.411	-0.323	-0.047	-0.736
O	-0.915	0.805	0.227	0.692	-0.985	0.083	1.000	-0.687	0.070	-0.921	0.362
N	0.534	-0.657	-0.347	-0.190	0.619	0.411	-0.687	1.000	-0.212	0.571	-0.602
S	0.025	-0.042	0.501	-0.119	-0.133	-0.323	0.070	-0.212	1.000	0.079	0.325
H.V.	0.854	-0.898	-0.078	-0.609	0.901	-0.047	-0.921	0.571	0.079	1.000	-0.454
Density	-0.209	0.650	0.341	-0.318	-0.296	-0.736	0.362	-0.602	0.325	-0.454	1.000

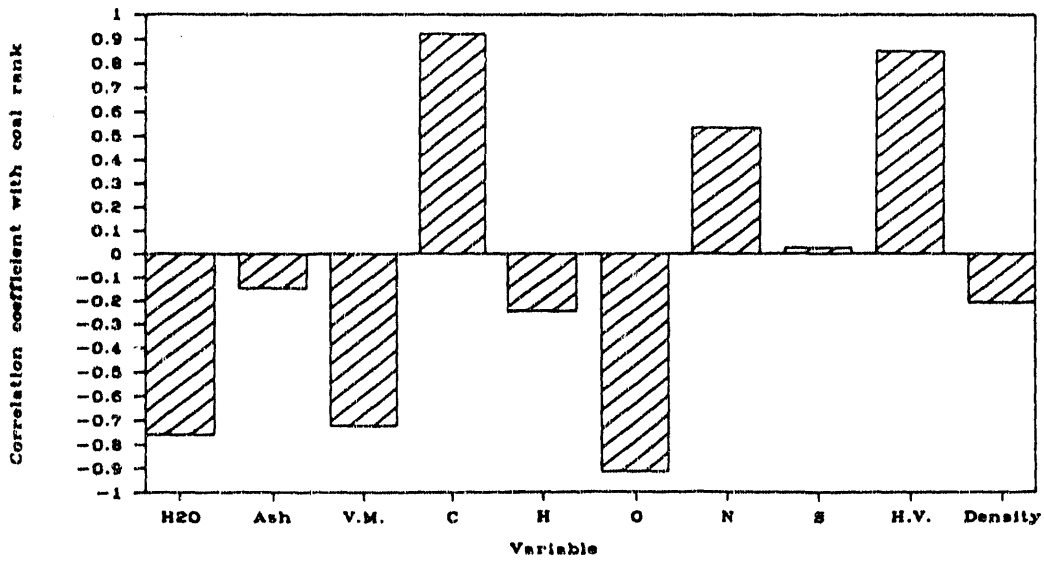

Figure 6.1 Correlation coefficients of analytical variables with coal rank.

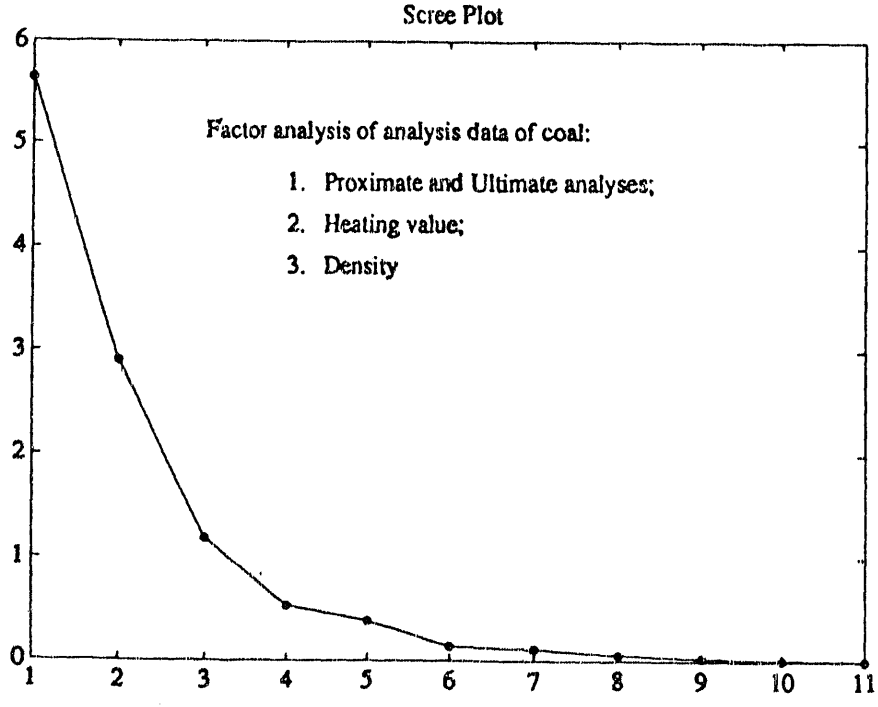

Figure 6.2 Scree plot for coal variables.

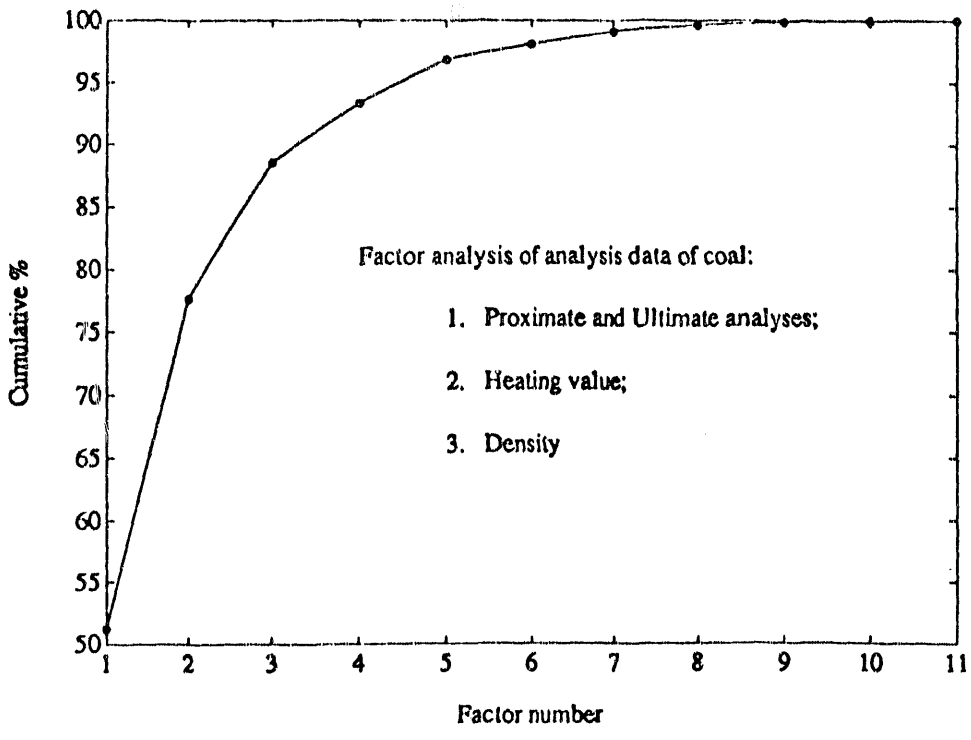

Figure 6.3 Cumulative percent versus factor number.

contributions from sulfur and ash. Factor pattern plots of coal analytical data are shown in Figure 6.5.

Based on the results of the analysis, carbon content will be used as the representative factor for coal rank in subsequent correlations.

6.3 Hardness and Grindability

Mechanical properties of coal vary significantly with rank. The relationship between mechanical properties and chemical structure and gas transport behavior is not completely understood. The Vicker's microhardness, Shore hardness, and Hardgrove grindability index for the Utah coals and the Colorado coal were measured. The results are found in Table 6.5.

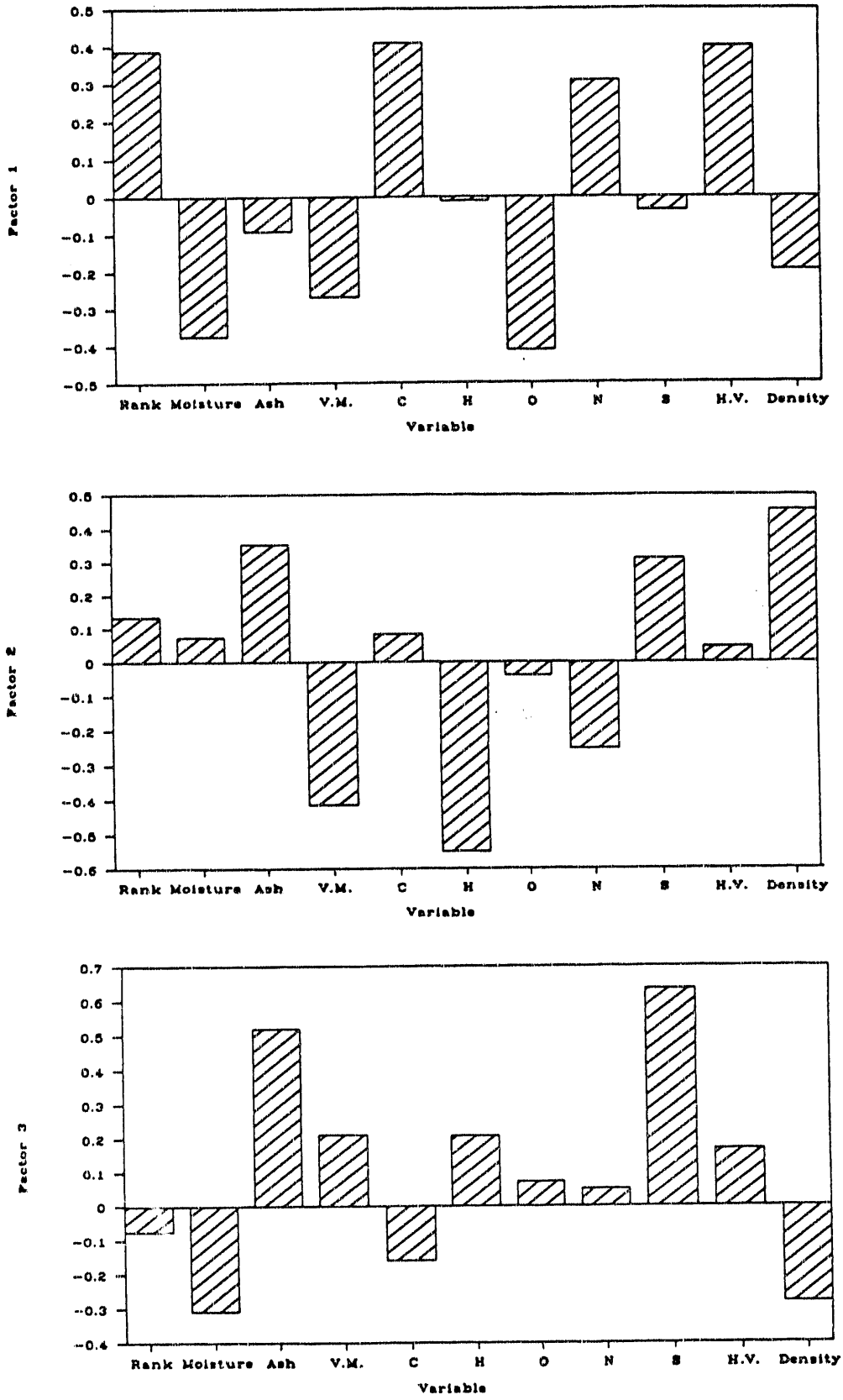

Figure 6.4 Factor loadings for coal variables.

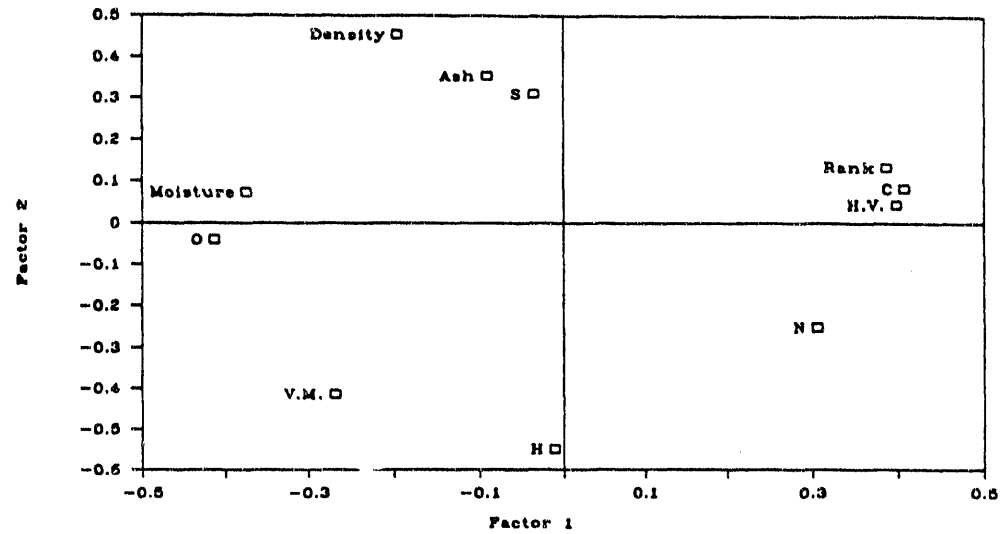

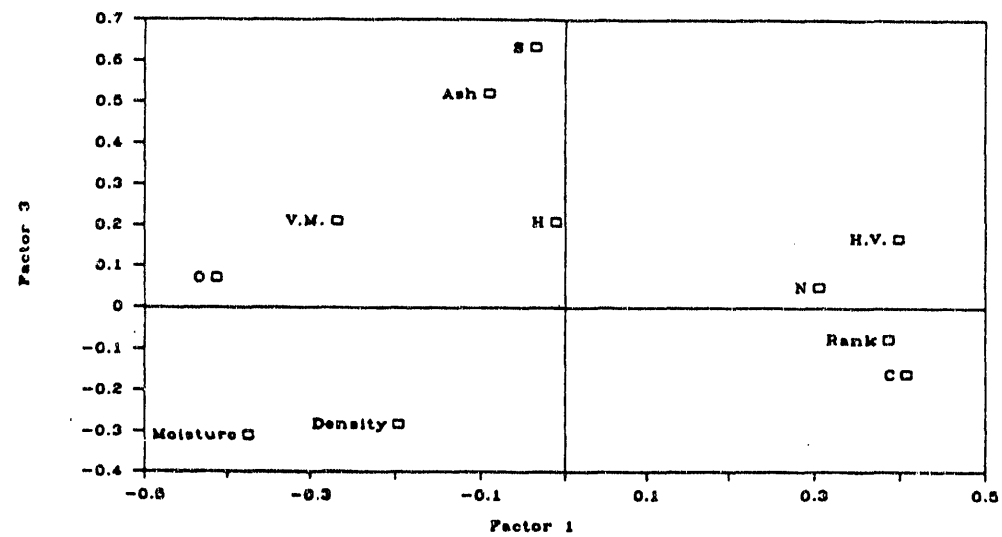

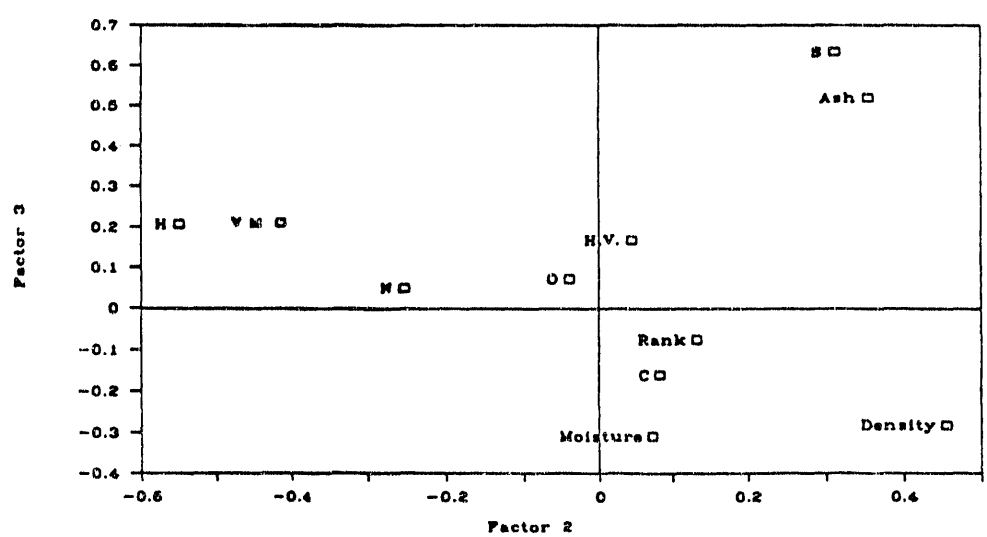

Figure 6.5 Factor pattern plots.

Table 6.5 Physical and mechanical properties of coal.

Mine	Seam	*Vickers Hardness V^h(kgf/mm²)	*Shore Hardness S^h	**Hardgrove Grindability Index
SUFCO	Upper Hiawatha	27.73	57.01	-
Skyline	Upper O'Connor	25.99	54.91	-
Beaver Creek #8	Castle-gate A	-	-	45
Castlegate	Sub-3	32.86	61.08	42
Pinnacle	Gilson	29.95	64.65	-
Aberdeen	Castle-gate A	-	-	-
Apex	Lower Sunnyside	-	-	-
Soldier Creek	Rock Canyon	32.30	60.24	36
Soldier Creek	Sunnyside	25.22	58.13	41
Sunnyside	Sunnyside	24.13	58.39	54
Dutch Creek	B Seam	25.34	27.68	101

* Hucka, 1990

**Karr, 1978, describes the grindability "as an index of the relative ease with which a coal may be pulverized in comparison with coals chosen as a standard". According to ASTM D409, "grindability of coal by the Hardgrove machine method is a standard method in which a prepared sample receives a definite amount of grinding energy in a miniature pulverizer, and the change in particle size consist determined by sieving".

7. RESULTS OF LABORATORY AND FIELD INVESTIGATIONS

Natural conditions of the coalbeds were evaluated during the in situ measurements. Table 7.1 shows some of the principal technical parameters.

7.1 Natural Conditions of Coalbeds in the Wasatch Field

The Wasatch Plateau coal field is oriented nearly north-south and is contiguous to the Book Cliff's coal field. The Wasatch Plateau is mountainous and deep canyons cut into the plateau from the east. Coal was here discovered in 1875. The coal-bearing strata in this field is concentrated in the lower Blackhawk Formation. There are several fault zones in the field such as the North Gordon, Pleasant Valley, and Joes Valley fault. According to Doelling (1972), folds of this zone have diverse trends and displacements up to 800 feet. The faulting and folding may have contributed to the past migration of the methane gas since shearing and crushing along the fault plane reduce the volume of mineable coal but increases the methane migration. However, as mining goes to greater depth the presence of methane pockets might increase. Coal production is coming from the north half of the field.

7.1.1 Castlegate A Seam at the Beaver Creek Mine No. 7

The Beaver Creek No. 8 mine is located 16 miles from Higway No. 6. about 24 mines from the town of Price, Carbon County Utah (Figure 4.1).

Figure 7.1 shows a section of the mine map where the field tests were performed. Eight boreholes were drilled into a freshly exposed coal face but only four of them provided valuable samples. Coal samples were evaluated in situ for methane content by use of the bubble desorbometer. Average values of 1.57 m^3 of methane per metric ton were determined. Results are shown in Tables 7.1 and 7.2. Further, samples were collected into three containers for the Bureau of Mines direct method estimation. However, no measurable values were obtained.

7.2 Natural Conditions of Coalbeds in the Book Cliff Field

Mines have been opened in the Book Cliffs field are since 1889 mostly located in the Castlegate and Sunnyside areas (Figure 4.2). Coal bearing strata in the Book Cliff field is again in the Blackhawk Formation. The coal has steam quality and is used also for domestic purposes. Faults are of small displacement. However, in the area of the Sunnyside mines two steeply dipping faults are reported by Doelling, 1972.

Table 7.1 Technical parameters of coal seams under investigation.

(All Utah coalbeds are of Upper Cretaceous age and are located in the Blackhawk Formation, while the B-seam is located in the Williams Formation.)

	Mine	Seam	Coalfield	Depth (ft.)	Seam Thickness (ft.)	Dip Degree
1.	SUFCO	Upper Hiawatha	Wasatch Plateau	886	12.5	2
2.	SKYLINE NO. 1	Upper O'Connor	Wasatch Plateau	1380	6.3	4
3.	BEAVER CREEK	Castlegate A	Wasatch Plateau	200	6-8	2
4.	CASTLE GATE (PRICE RIVER)	Sub-3	Book Cliffs	1800	5.9	5
5.	PINNACLE	Gilson	Book Cliffs	1130	5.6	2
6.	ABERDEEN	Castlegate A	Book Cliffs	1200	5.5	2
7.	APEX	Lower Sunnyside	Book Cliffs	1200	4.2	2
8.	SOLDIER CREEK	Lower Sunnyside	Book Cliffs	1300	7.85	6-7
9.	SOLDIER CREEK	Rock Canyon	Book Cliffs	1500	9.2	6-7
10.	SUNNYSIDE	Lower Sunnyside	Book Cliffs	2500	6.0	6-12
11.	DUTCH CREEK COLORADO	B Seam	Carbondale Coal Basin	2500	11.3	9

Table 7.1 (Cont.). Technical parameters of coal seams under investigation.

(All Utah coalbeds are of Upper Cretaceous age and are located in the Blackhawk Formation, while the B-seam is located in the Williams Formation.)

Mine	Seam	Rank	Roof Rocks	Floor Rocks
1. SUFCO	Upper Hiawatha	HvBc	Mudstone, Sandstone	Sandstone, Siltstone
2. SKYLINE NO. 1	Upper O'Connor	HvBc	Carbonaceous Siltstone	Mudstone, Siltstone
3. BEAVER CREEK	Castlegate A	HvBc	Carbonaceous Shale	Mudstone
4. CASTLE GATE (PRICE RIVER)	Sub-3	HvBb	Carbonaceous Shale	Massive Sandstone
5. PINNACLE	Gilson	HvBb	Sandstone	Sandstone
6. ABERDEEN	Castlegate A	HvBc	Shale	Sandstone
7. APEX	Sunnyside	HbBb	Sandstone	Sandstone
8. SOLDIER CREEK	Sunnyside	HvB	Carbonaceous Shale	Carbonaceous Shale
9. SOLDIER CREEK	Rock Canyon	HvBb	Carbonaceous Shale	Carbonaceous Shale
10. SUNNYSIDE	Lower Sunnyside	HvBa	Carbonaceous Siltstone	Siltstone
11. DUTCH CREEK COLORADO	B Seam	MvB	Carbonaceous Shale	Carbonaceous Siltstone

Table 7.1 (Cont.). Technical parameters of coal seams under investigation.

(All Utah coalbeds are of Upper Cretaceous age and are located in the Blackhawk Formation, while the B-seam is located in the Williams Formation.)

Mine	Seam	Methane Content cf/st	Methane Content m^3/tonne	Number of Samples n	Standard Deviation σ_{n-1}
1. SUFCO	Upper Hiawatha	3	*0.1	1	--
2. SKYLINE NO. 1	Upper O'Connor	3	*0.1	2	--
3. BEAVER CREEK	Castlegate A	50	1.57	8	0.08
4. CASTLE GATE (PRICE RIVER)	Sub-3	285	8.95	3	2.26
5. PINNACLE	Gilson	--	--	--	--
6. ABERDEEN	Castlegate A	--	--	--	--
7. APEX	Sunnyside	--	--	--	--
8. SOLDIER CREEK	Sunnyside	64	2.9	--	N/A
9. SOLDIER CREEK	Rock Canyon	180	5.63	6	2.01
10. SUNNYSIDE	Lower Sunnyside	118	3.7	17	0.54
11. DUTCH CREEK COLORADO	B Seam	123	3.85	12	2.63

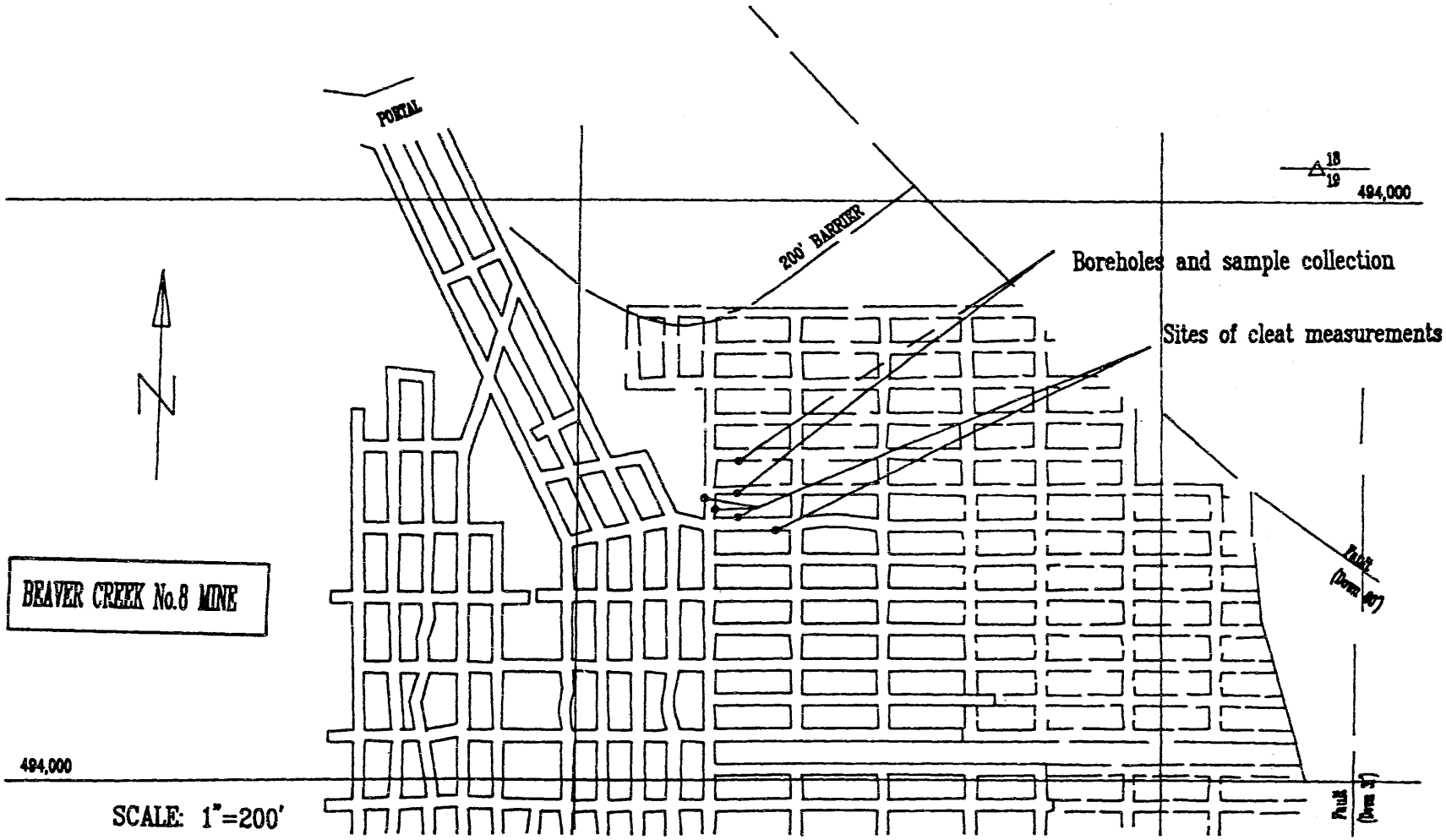

Figure 7.1. Section map of the Castlegate A seam at the Beaver Creek Mine (Central Utah).

7.2.1 Sub 3 Seam at the Castle Gate Coal Mine

The Castle Gate mine was opened in 1889. Two seams were mined: the Sub 3 seam in Mine No. 3, and the D seam in the mine No. 5. Both seams are known as gassy with low permeability coal.

The Sub 3 seam is the basal seam of the Spring Canyon Group in the Blackhawk Formation of the upper Cretaceous age (Figure 7.2). As part of the Wasatch Plateau, the seam is located between the book Cliffs and Wasatch Plateau seams where the methane content determination tests were conducted. The thickness of the seams is about 6 to 6.6 feet (1.8 to 2.00 meters). The roof is of carbonaceous shale and the floor consists of massive sandstone. The average dip of all cleats is 82 degrees and cleat planes are filled by calcite and resin.

An average direction of the main (face) cleat in the Sub 3 seam was N55W and N35E for the butt cleat with spacing averaging about 7 cleat per linear foot. The orientation of the main joint system measured in outcrops on the surface was N65W, while the minor system was N35E. Nine boreholes were drilled into coal faces as it is indicated on the section map (Figure 7.3). An methane content of average value of 8.95 m^3/tonne was determined for this seam. A summary of results of gas content for the Sub 3 seam is given in Table 7.2. Appendix B gives the detailed results.

7.2.2 Rock Canyon Seam at the Soldier Creek Canyon Coal Mine

The Soldier Creek Canyon Coal Mine is located about 30 miles (50 km) northeast from the town of Price, Central Utah. Besides the Rock Canyon seams there are two more coalbeds present in the property. At present, only the Rock Canyon seams is mined while the Lower Sunnyside seam is under development. Both seams belong to the upper part of the coal-bearing Blackhawk Formation of the Book Cliffs coal field. The formation is approximately 230 ft (70 meters) thick and contains as many as 6 mineable seams, three of them located outside of the mine property.

The thickness of the Rock Canyon seams is about 2.5 meters in the area of field tests (Figure 7.4). The roof rock consists of carbonaceous shale and the floor is formed of sandstone. The cleat measurements show two principal cleat orientations with the face cleat striking N63W and butt cleat striking N26E. Both systems are well developed with spacing about 0.4 to 0.8 inch (15 to 20 mm). The surface plane of the cleats are mostly uneven or striated. Six boreholes were

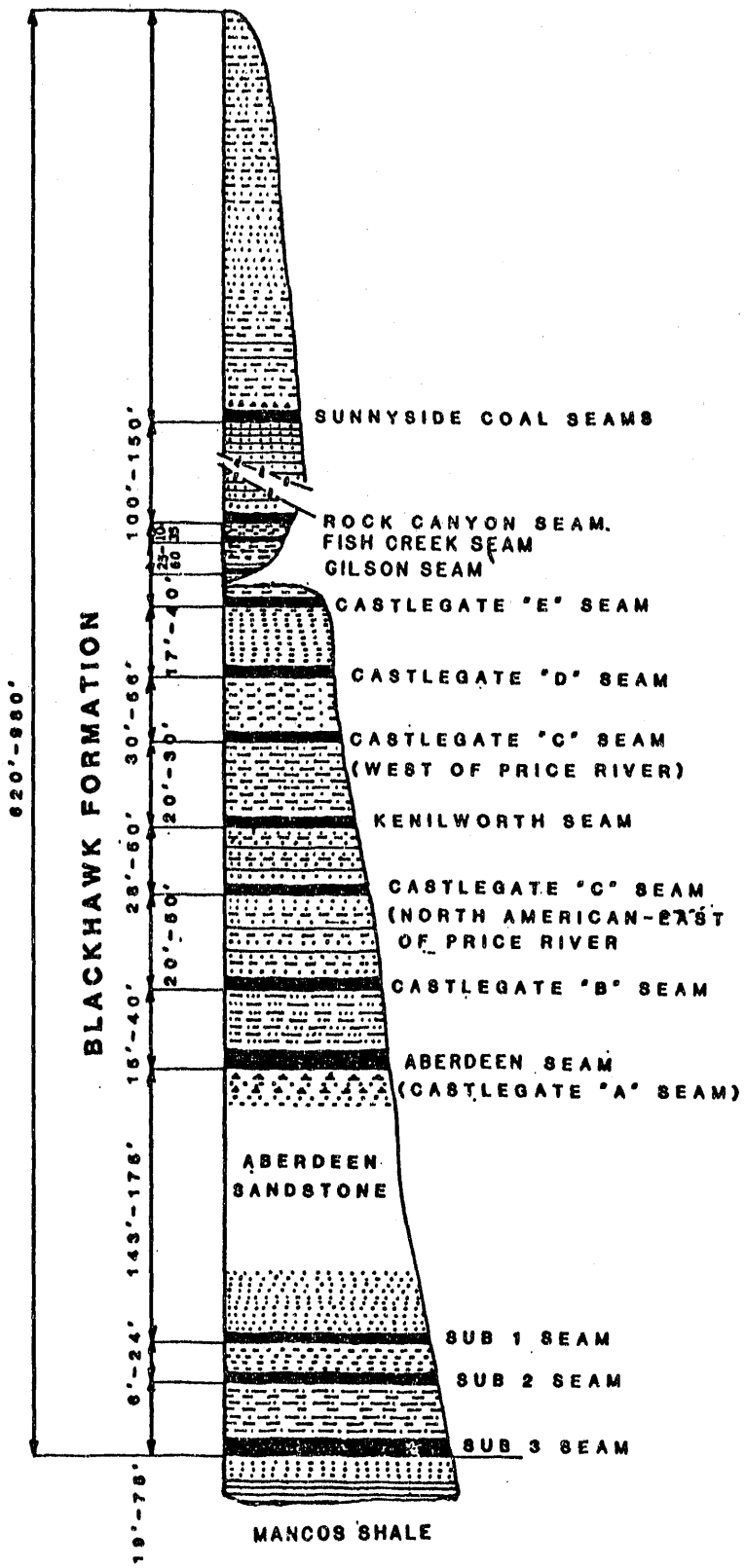

Figure 7.2. Geologic profile of the strata through the Sub 3 seam (after Hucka, 1990).

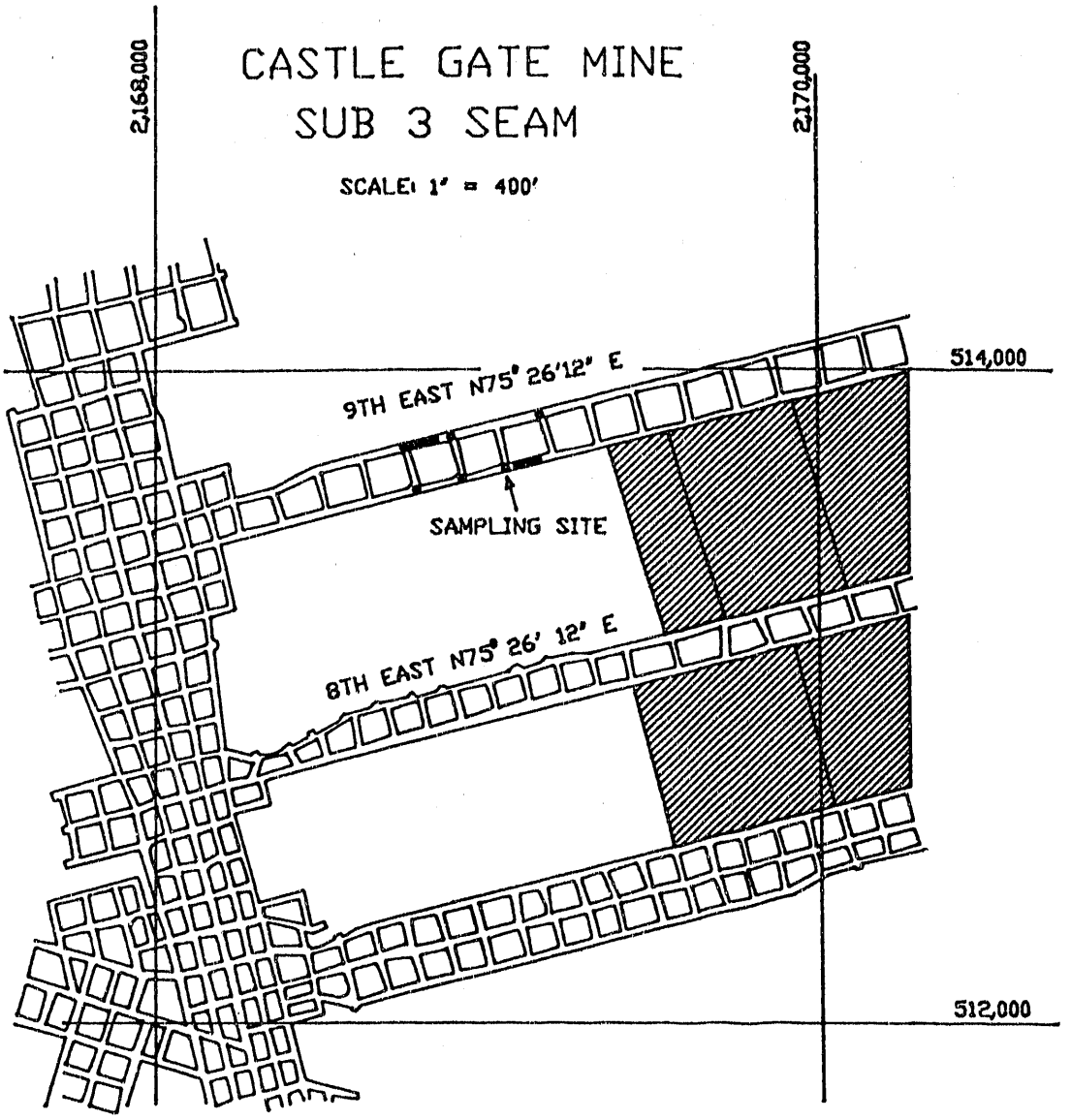

Figure 7.3. Section map of the Sub 3 seam.

drilled in the coal face as indicated in Figure 7.4 showing the particular section map. A methane content of 5.63 m^3/tonne was determined (see also Tables 7.1 and 7.2 and Appendix B).

7.2.3 Sunnyside Seam at the Soldier Creek Canyon Coal Mine

The Sunnyside seam is a part of Book Cliffs coal field and is mined by the Soldier Creek Canyon Mine as well as by the Sunnyside Coal Mine Company. Figure 7.5 shows the section map of the seam with the location of sample collection and the borehole location. The overlying unit is the Castlegate Sandstone while the floor rocks are made by sandstone of Mancos Shale unit. The units strike northwest and dip northeastly at 6 to 7 degrees. Faults occasionally cut the coal seam but are of small displacement. The thickness of the seam in the place of sample collection was about 7.8 ft. (2.37 m). The overburden thickness attained approximately 1,300 ft (395 m).

Several boreholes were drilled into the coal faces but only one provided samples with presence of methane in an amount of 2.9 m^3/tonne of coal (Table 7.2). The natural conditions of the seam at the site were not favorable for gas measurement. The coal was highly fractured inside the pillar. Unfortunately, for mine operational reasons there was no other place where the gas measurements could be repeated.

7.2.4 Lower Sunnyside Seam at the Sunnyside Coal Mine

The mine is located about 45 miles (70 km) south from the town of Price, Central Utah (Figure 4.2). There are two coalbeds: the Upper and Lower Sunnyside. The measurements took place in the Lower Sunnyside seam. The thickness of the seam was about 6.6 feet (2 meters - Figure 7.6). The rock composing the roof is a carbonaceous shale while the rock in the floor is siltstone. Altogether 17 boreholes were drilled into the Sunnyside seam. The average methane content of 3.7 m^3/tonne was measured (Table 7.2).

Some cleats transverse the entire thickness of the seam and sometimes extend into the roof rocks. The surface planes of cleats are smooth with traces of slickensides, some are striated and densely distributed in the coal. In the upper part of the seam, the cleat planes are coated with calcite and have spacing of about 0.24 in. (6 mm). The most prominent cleats have an uneven surface with quite regular distribution in the coal with spacing about 0.3 to 0.5 in. (10 to 13 mm). However, the permeability tests show quite low values of 0.011 to 0.016 mD. This is attributed to a small size of specimens (2.125 in. or 53 mm in diameter and height of 4.3 in. or 110 mm). In 1978, the U.S. Bureau of Mines conducted tests on methane drainage in the 18 dips longwall face of this seam

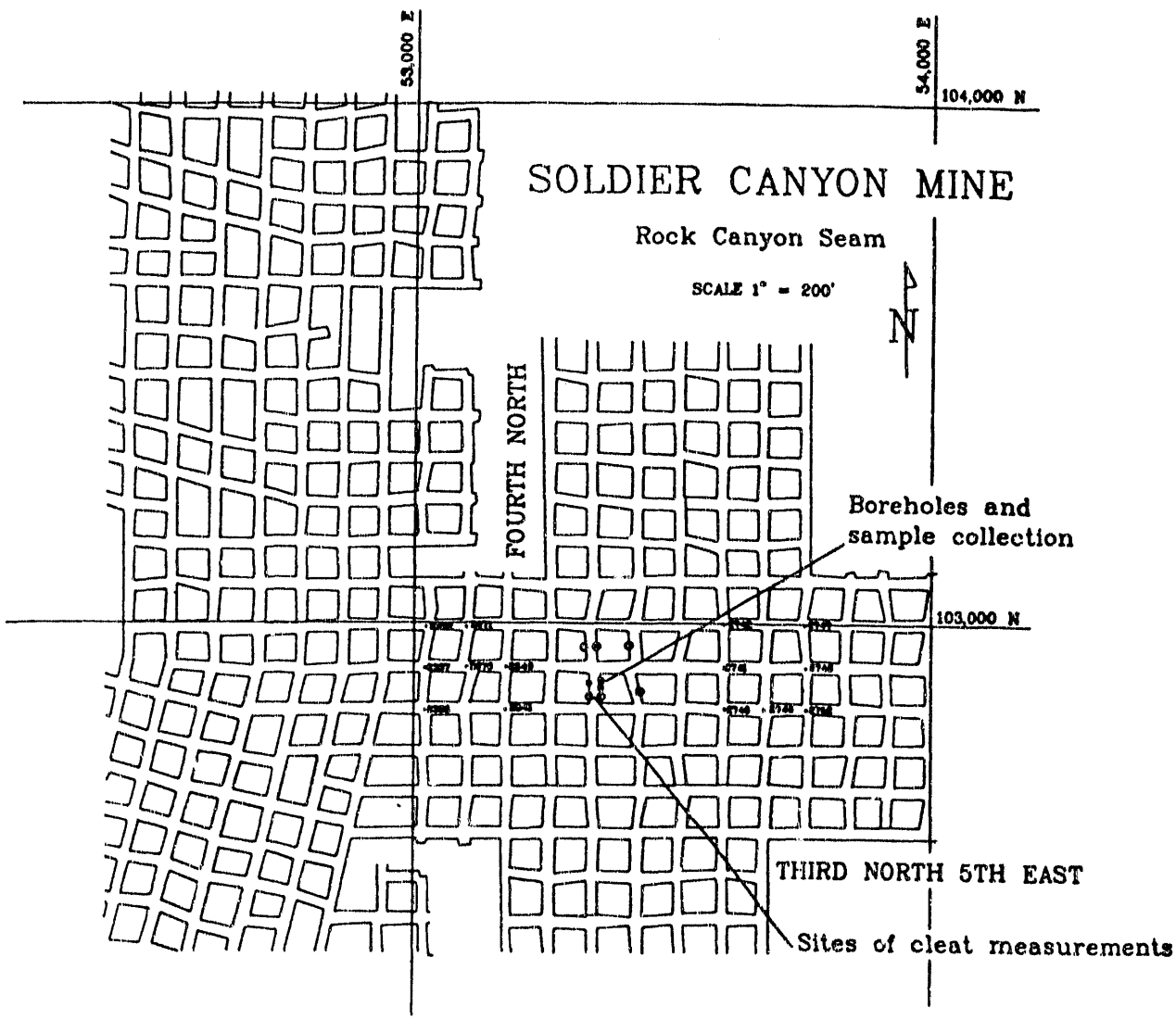

Figure 7.4. Section map of the Rock Canyon seam.

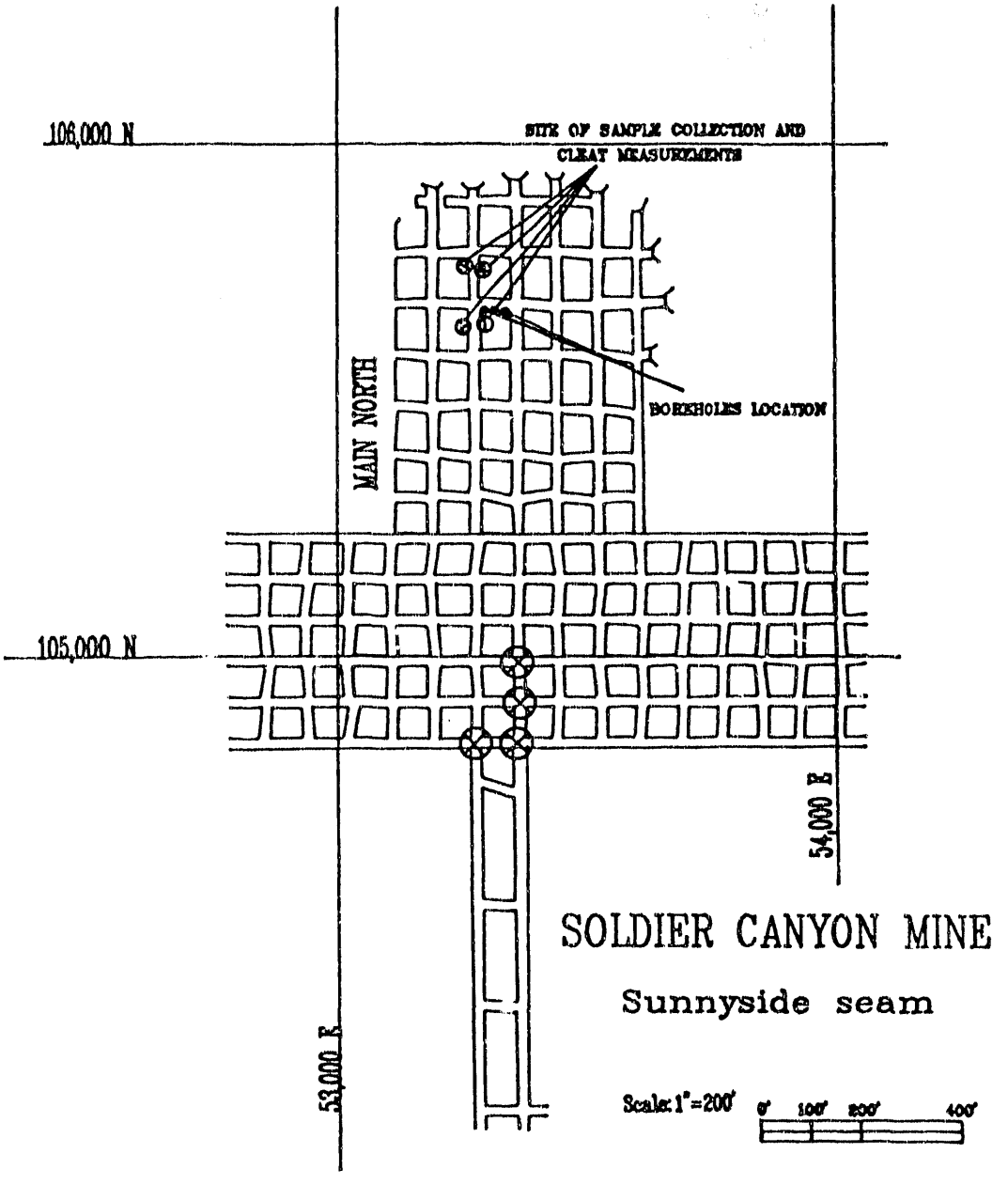

Figure 7.5. Section map of the Sunnyside seam at the Soldier Creek Canyon mine.

LOWER SUNNYSIDE SEAM AT THE SUNNYSIDE COAL MINE

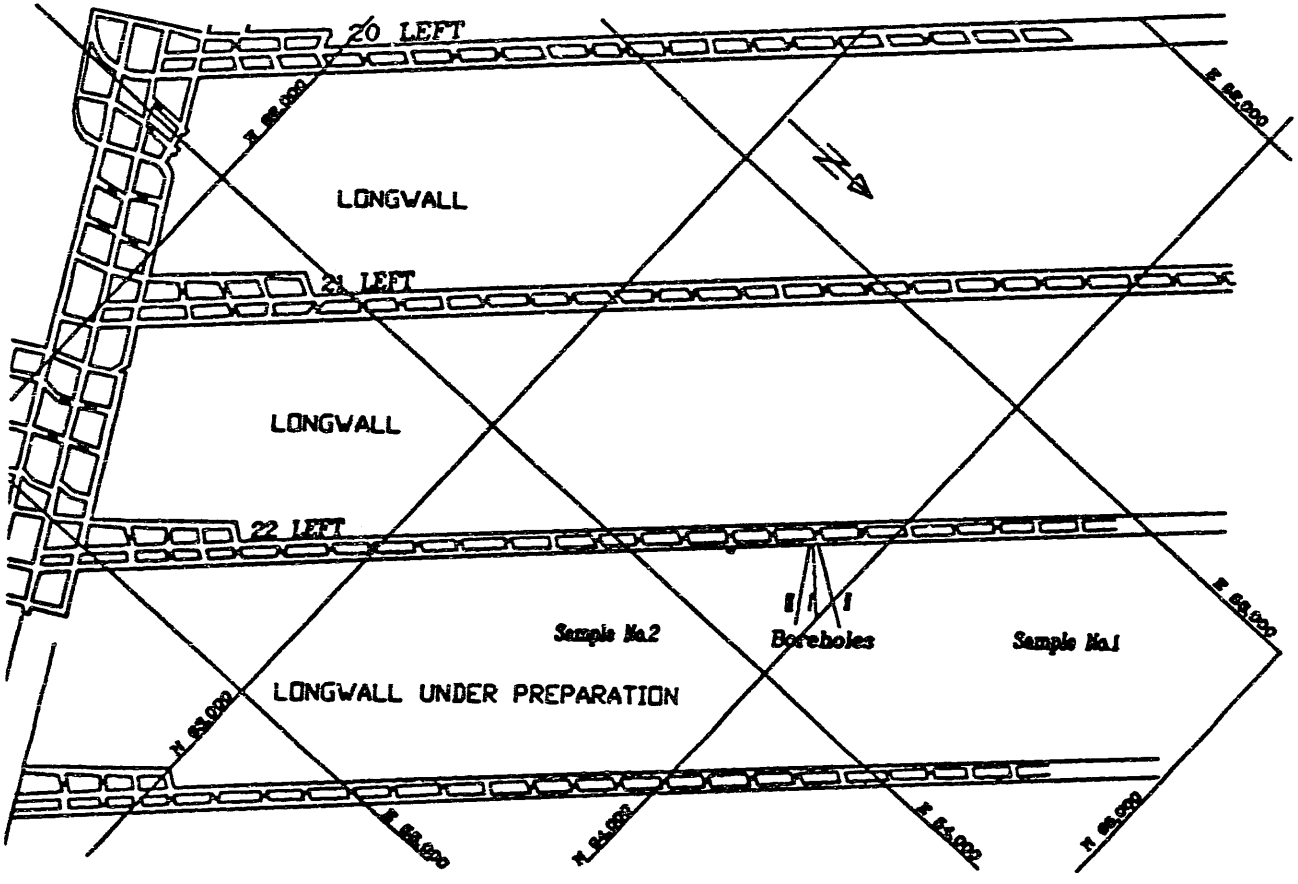

Figure 7.6 Section map of the Lower Sunnyside seam at the Sunnyside mine.

(Perry et al., 1978). The tests proved effective in draining commercial-quality methane. During 9 months of tests about 35 MMcf (0.98 x 10^6 m^3) of methane with an average heat value of 1,007 Btu has been drained.

7.3 Natural Conditions of Coalbeds at the Mid-Continent Resources Mines in Colorado

The Dutch Creek Coal mine of the Mid-Continent Resources, Inc., is located near the town of Redstone, Colorado. The portals of the mine are situated at an elevation of about 10,000 feet (3,100 m). Longwall face technology is used to mine two seams: M seam, and B seam. The seams are separated by a distance of about 500 feet (150 m). The tests were performed in the B seam having a dip from 9 to 15 degree to northwest. The overburden depth varies from 2,000 to 3,500 feet (610 to 1,600 m). The coal from the B seam is of high metallurgical quality. The seam is also quite gassy with a history of mine accidents.

7.3.1 B Seam at the Dutch Creek Coal Mine

Figure 7.7 shows a section of the mine map of the B seam. The overburden in the site of the tests was about 3000 feet. A block sample was collected from the seam for directional permeability tests. Twelve horizontal boreholes were drilled into a longwall face. Methane content of 3.85 m^3/tonne was measured. The results are also shown in Appendix B. Besides the in situ tests on methane content, samples were collected in 3 containers for evaluation on the residual gas (Appendix B).

7.4 Permeability Tests

The permeability tests were performed on coal samples from the gassy coalbeds under investigation. Table 7.2 gives the summary on permeability tests while detailed description of tests is presented in the Appendix D.

7.5 Field and Laboratory Coalbed Methane Content Determination Tests

Desorbable methane content was determined in situ from coal samples collected from horizontal boreholes drilled from a coal face at a depth of 6.6 feet (2 m) gradually increasing to 40 feet (12 m). The samples in a form of fine cuttings were collected by use of a special device (Appendix A). The samples were immediately screened to a particle size of 0.016 to 0.023 in. (0.425 to 0.6 mm) and inserted into a measuring cell of the isobaric bubble desorbometer. The emitted methane flow was measured and the total of released gas was determined. The procedure is described at length in Appendix A. The testing sites were selected with the cooperation of

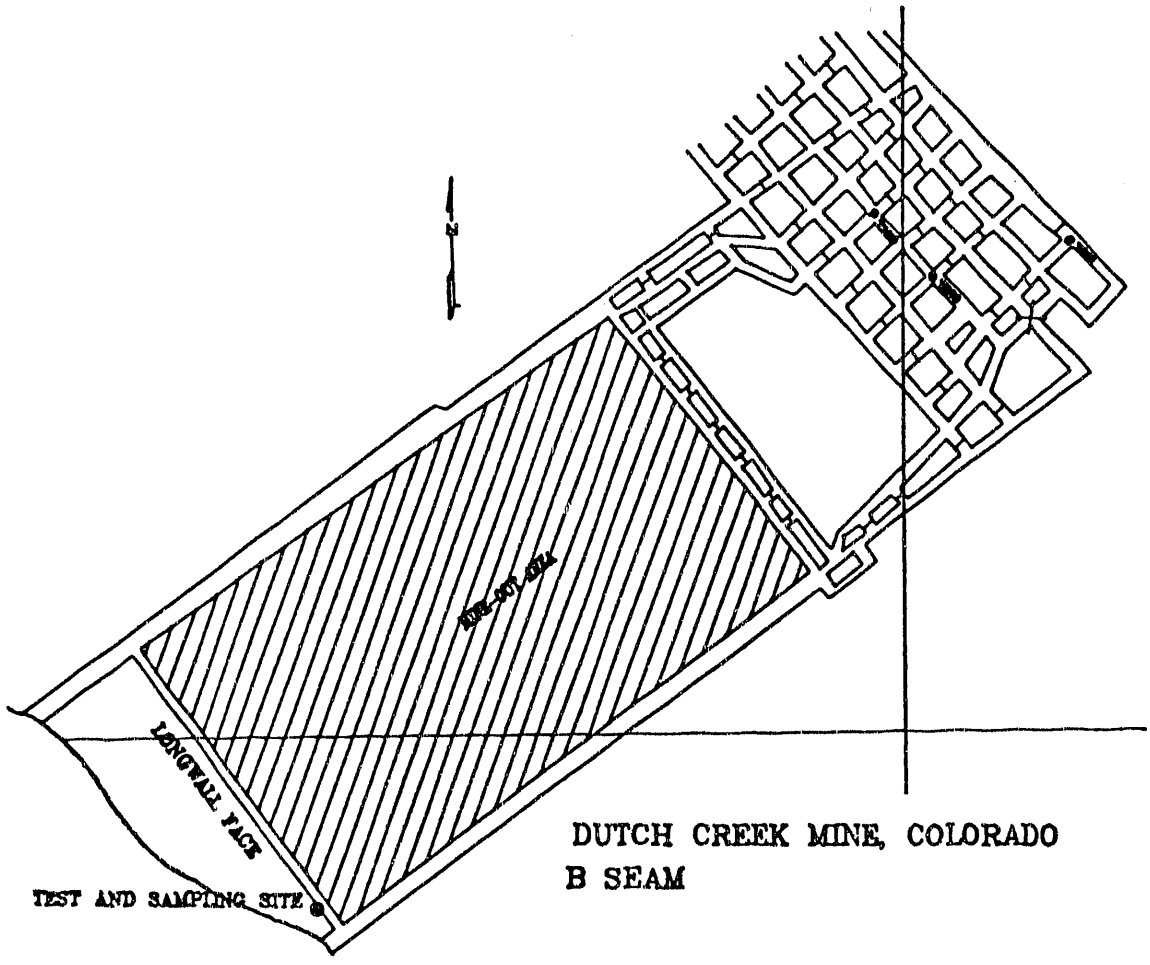

Figure 7.7 B seam at the Dutch Creek mine (after Hucka, B., 1989).

Table 7.2. Summary of results on methane content determination and permeability.

Mine	Seam	Methane Content Cu.M/T (Average Value)	No. of Bore-holes	Standard Deviation	Permeability Perpendicular to Bedding (mD)	Permeability Parallel to Bedding (mD)
Beaver No. 8	Castlegate A	1.57	4	0.08	0.395	--
Castle Gate	Sub 3	8.95	9	2.26	0.039	0.041
Soldier Creek	Rock Canyon	5.63	6	2.01	0.014	0.005
Soldier Creek	Sunnyside	2.9	1	N/A	0.096	0.063
Sunnyside	Lwr Sunnyside	3.7	17	0.54	0.011	0.016
Mid-Continent	B	3.85	12	2.63	0.035	0.319

each mining company and are indicated in section maps of the particular coalbeds.

A computer program was prepared for three types of methane content calculation using the so-called "power decay" function. The detailed results on methane content are given in Appendix B. Table 7.2 is a summary of all results on methane content including the results on permeability of selected Utah and Colorado gassy coalbeds. Figures 7.8 and 7.9 present average values on the methane content and a permeability measured perpendiculary to the bedding plane. Methane content increase was observed when comparing results from the Castlegate A seam (1.57 m^3/tonne) to the Sub 3 seam (Castle Gate mine) 8.95 m^3/tonne.

The high value of methane content in the Sub 3 seam is attributed to the depth of this seam as the Sub 3 seam is the lowest coalbed mined in the area (Figure 7.2). A decreasing trend was however found in the methane content measured in the Sub 3 seam compared with the Rock Canyon seam (5.63 m^3/tonne). This trend then continues towards the Sunnyside mines Sunnyside coalbed with 3.7 m^3/tonne. When the Geneva Coal mine was still in operation about 12 years ago, little methane gas occurrence was found there. The Geneva Coal mine was located south of the Sunnyside mine. Again, this phenomenon could be attributed to the presence of faults in the area.

Figures 7.8 and 7.9 and Table 7.2 do not show any correlation of the values of permeability with methane content.

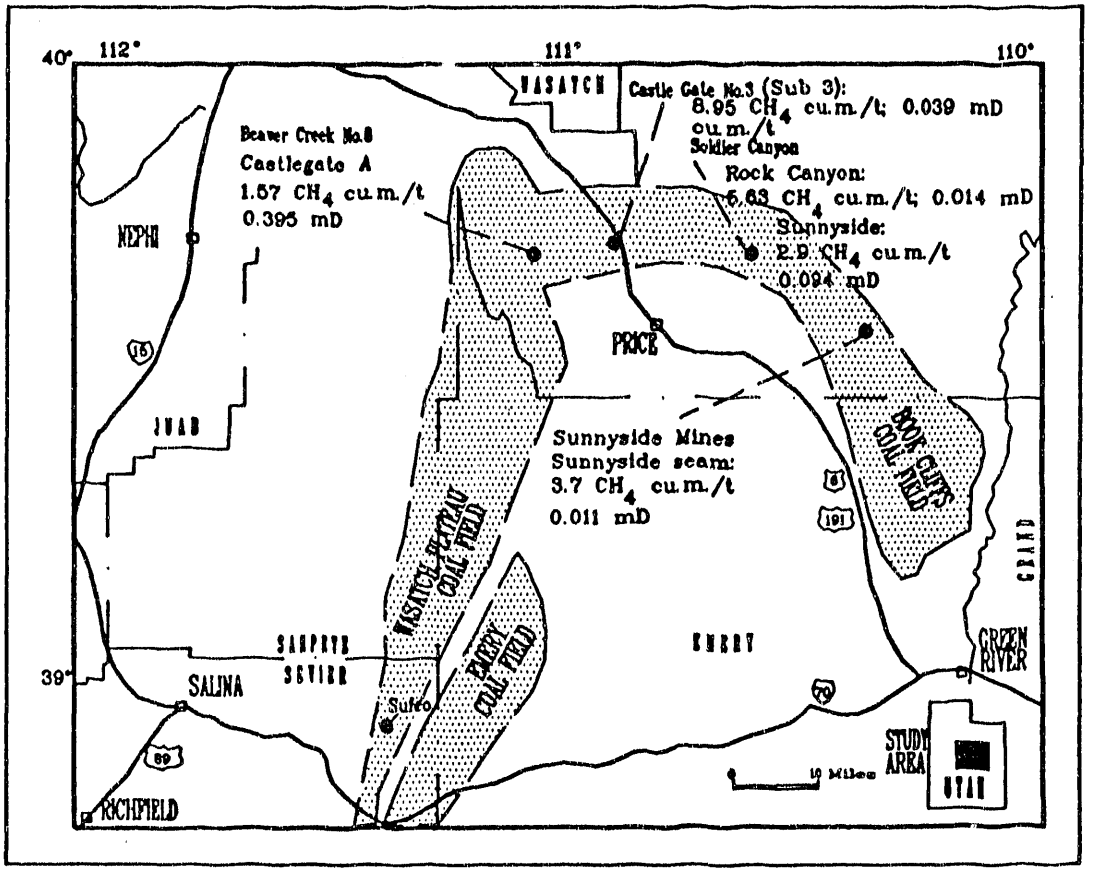

Figure 7.8 Methane content in Utah gassy mines (modified after Hucka, B., 1989).

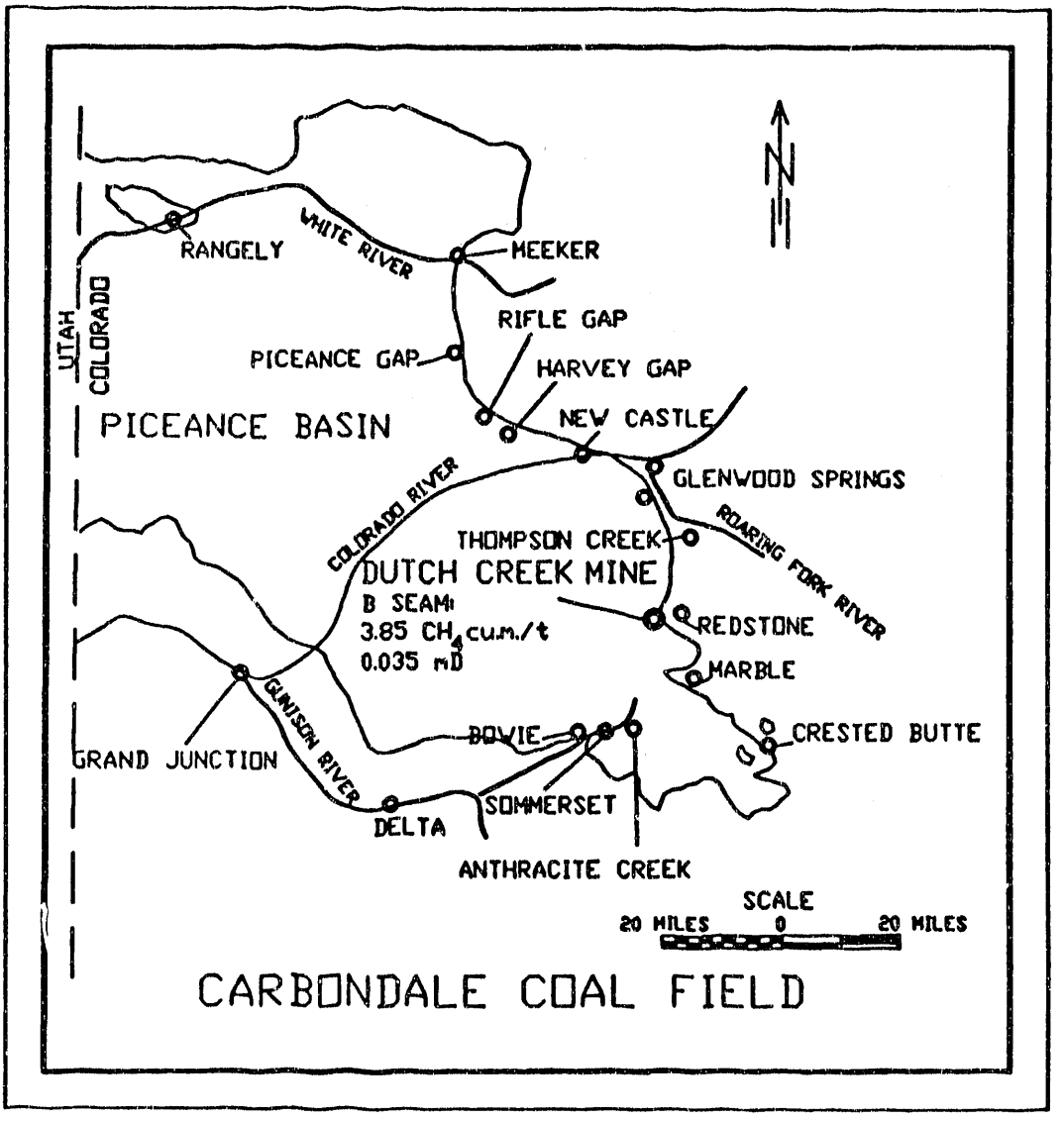

Figure 7.9 Methane content in the B seam (Carbondale coal field).

8. CHARACTERIZATION OF THE COAL SURFACES BY GAS CHROMATOGRAPHY

8.1 Introduction

Properties of coal surfaces are very important for gas retention in coal. Surface properties are primary factors in determining methane content and gas composition in a coalbed. In addition, a knowledge of the chemistry and physics of the coal surface is essential for explaining the mechanisms of coal conversion processes, such as coal gasification, liquefaction, and combustion. Therefore, it is necessary to develop simpler, quicker, and more accurate methods to characterize the chemistry and physics of coal surfaces. Gas chromatography (GC) provides a good approach to achieving these goals.

A gas adsorption isotherm, $V_{ads} = f(p)_T$, is the relationship between pressure and volume of a gas adsorbed on the coal surface. Its measurement is made at constant temperature, and the volume of gas adsorbed is normally corrected to STP. The gas adsorption isotherm is one of the most important functions used in the characterization of a coal surface. From it, the gas adsorption capacity, heat of gas adsorption, specific surface area and other properties of the coal surface can be determined. Using gases with diverse physical and chemical characteristics as molecular probes, we can interpret the types of gas-coal interactions involved in adsorption and infer the chemistry and physics of the coal surface.

There are several techniques to be used in determining the coefficients, isotherms, and thermodynamic and kinetic constants of gas adsorption on a solid (Brunauer, 1945; Young and Crowell, 1962; De Boer, 1953; Conder and Purnell, 1968; Davis, 1952). To date, static volumetric and gravimetric methods have most often been applied. Measurements made using these techniques require long times and fairly complicated vacuum apparatus. Static vacuum apparatus is acceptable for work with clean solid surfaces at low or moderate temperatures. It is not designed to be used in studying adsorption under conditions of most practical sorption processes, especially at high temperatures and pressures. When the adsorption capacity of a gas on a coal is low, the readings include considerable relative error. These shortcomings can generally be avoided by using dynamic methods, among which gas-solid chromatography is an important technique.

The primary advantages of the GC method over static methods in investigating the properties of coal surfaces are as follows:

1. The apparatus is easy to construct and operate, allowing various investigations to be performed with one system. Standard apparatus, which can be easily adapted for coal surface studies, is inexpensive.

2. GC is mainly used for examining very small samples at infinite dilution. Such concentrations can be directly applied to investigations of thermodynamic equilibrium.

3. Accuracy of measurement of different gas adsorption properties and phenomena by GC is at least as high as that of other methods, and the rate of measurement is much higher.

4. Analysis of the chromatogram from GC will provide data on the kinetics of gas adsorption and desorption.

In this research, the thermodynamics of a variety of gas molecules adsorbed on coal has been studied by GC. Three groups of gases have been used in this research. They include 1. hydrocarbon gases: methane (CH_4), ethane (C_2H_6), propane (C_3H_8), and propylene (C_3H_6); 2. elementary gases: argon (Ar), nitrogen (N_2), and oxygen (O_2); and 3. carbon oxides: carbon monoxide (CO), and carbon dioxide (CO_2). The relationship between the gas adsorption coefficients and gas retention variables has been derived by mass conservation. A novel gas retention variable, weighted mean retention time, has been defined and used in this study. When the retention variable was used to calculate gas adsorption coefficients, the results agreed with those obtained by a static method. Since the use of the GC method to obtain the thermodynamic data of gas adsorption on coal is not widespread, the technique will be briefly discussed. The theoretical basis and details are found in Appendix C. Multivariate analysis was applied in this study to understand the complex correlation of the gas adsorption capacities and coal surface properties with the analytical data of coal, e.g. proximate analyses, ultimate analyses, NMR data, and helium densities.

8.2 Theoretical Basis

8.2.1 Techniques

Various methods are used in determining the coefficients and/or isotherms of gas adsorption on a solid by GC methods. The most important techniques include the Peak Maximum (PM) method with a pulse technique (Kipping and Winter, 1965; Sewell and Stock, 1970), Elution by Characteristic Point (ECP) with a pulse technique (Knozinger and Spannheimer, 1964; Kisevel et al., 1964; Owens et al., 1964; Dollimore et al., 1970; Volf et al., 1973), and Frontal Analysis by Characteristic Point (FACP) with a pulse or continuous technique (Conder and Purnell, 1969; Glueckauf, 1947, 1949;

Stock, 1961; Eberly, 1961; Beebe et al., 1966; Conder et al., 1969).

In the peak maximum method, a series of adsorbate samples of varying size are injected into the column to obtain an isotherm. Although the experimental apparatus and the data treatment are quite simple for this method, many experiments must be performed to obtain only one isotherm.

The Elution by Characteristic Point with a pulse technique to determine adsorption isotherms is frequently used because of its rapidity and simplicity. This method is similar to the peak maximum method but the path of the isotherm (within a limited range) can be determined from a single chromatogram. Its restriction is that the front or rear profiles of the peaks must overlap for various sample sizes. Often one has to select suitable chromatographic conditions so that the extended chromatogram curves for various sample sizes overlap, or to make appropriate corrections to the peaks.

The frontal analysis by characteristic point with either a pulse or a continuous technique is one of the commonest methods to determine adsorption isotherms. Although the experimental principle is simple, the data treatment is quite complicated. Other disadvantages of this method are that it is time consuming and requires strict system design.

8.2.2 Relationship between Adsorption Coefficient and Retention Variables

The relationship between gas adsorption coefficients and gas retention variables in an ideal chromatographic column can be derived by mass conservation. The change in the concentration of gaseous species A across a chromatographic column is shown in Figure 8.1. The gas concentration, C_A, in the mobile phase is a complex function of the time, t, and the distance, x, of the layer under investigation from the column inlet

$$C_A = f(t,x) . \qquad (1)$$

If the accumulation of the gaseous species A in the column increment dx is dn_A (Figure 8.1),

$$\begin{aligned} dn_A &= inlet_A - outlet_A \\ &= -F_c dC_A , \end{aligned} \qquad (2)$$

i.e.,

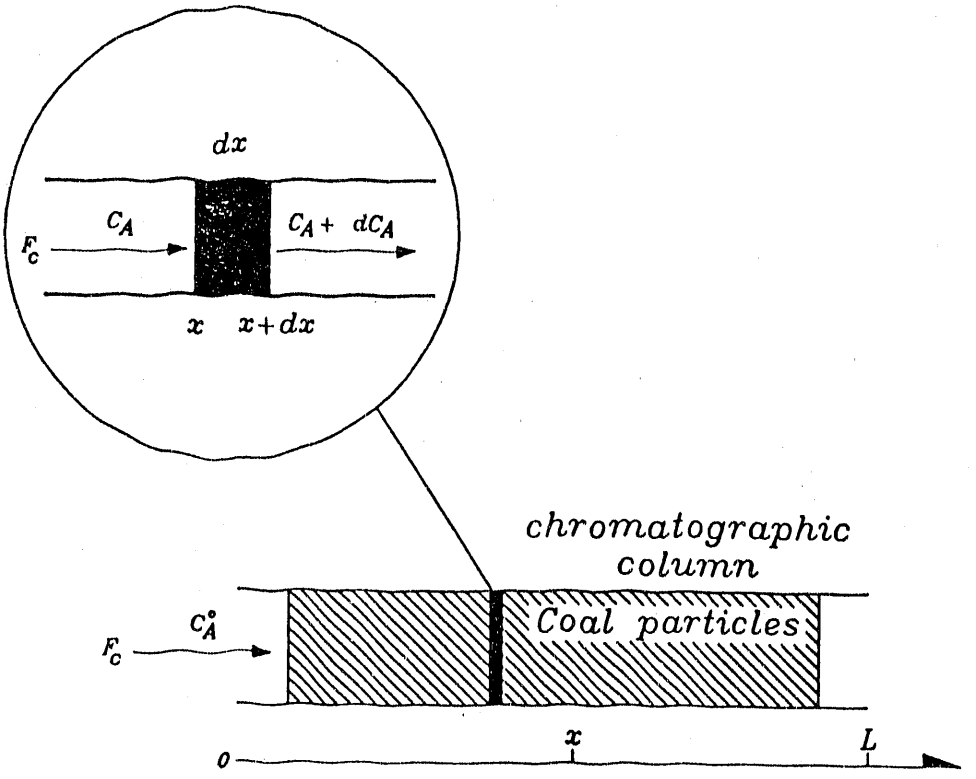

Figure 8.1 Concentration of species A across a chromatographic column.

$$(dn_A)_{x,t} = -F_c\left(\frac{\partial C_A}{\partial x}\right)_t dx. \qquad (3)$$

The accumulated quantity of species A in the column increment, dx, is distributed in the mobile phase and the stationary phase. Thus, the quantity of the adsorbate A in a unit length of the column is

$$V_L C_A + m_L a_A \ . \qquad (4)$$

According to the mass conservation law,

$$-F_c\left(\frac{\partial C_A}{\partial x}\right)_t = \left[\frac{\partial}{\partial t}\left(V_L C_A + m_L a_A\right)\right]_x dx. \qquad (5)$$

Rearranging Equation 5, we obtain the mass conservation equation of a chromatographic column,

$$F_c\left(\frac{\partial C_A}{\partial x}\right)_t + V_L\left(\frac{\partial C_A}{\partial t}\right)_x + m_L\left(\frac{\partial a_A}{\partial t}\right)_x = 0. \qquad (6)$$

Assuming that in each part of the column gas adsorption equilibrium is eventually established, we can combine the mass conservation equation with a gas adsorption isotherm to derive

the relationship between gas adsorption coefficient and gas retention variables. When infinite dilution of a gas sample is used, all of the proposed types (Brunauer et al., 1940) of gas adsorption isotherms become linear, i.e.,

$$\lim_{C_A \to 0} \left[\frac{da_A}{dC_A}\right] = K_{c,A} \ . \tag{7}$$

The range of infinite dilution of a sample size is normally less than 0.5 ml, which depends not only on the properties of adsorbate and adsorbent, but also on the chromatographic conditions. Substituting Equation 7 into Equation 6 and making necessary mathematical derivations (the details are illustrated in Appendix C), we obtain

$$K_{c,A} = \frac{F_c}{m}(t_r - t_M) \tag{8}$$

for an ideal packed-column (no pressure drop along the column). For a real parked column, there is a significant pressure drop along the column. The pressure gradient (James and Martin, 1952) of the carrier gas depends on

$$\frac{dp}{dx} = -\frac{\eta}{\kappa A_{column}} F_c \ , \tag{9}$$

where η is the gas viscosity, κ the column permeability, and A_{column}, the cross-sectional area of the column. If it is assumed that the carrier gas is an ideal gas under the experimental conditions, a pressure and temperature correction factor, $J_{p,T}$, can be derived mathematically (the details are shown in Appendix C), and the final form is

$$J_{p,T} = \frac{3}{2}\frac{T_c}{T_o}\frac{1-(\frac{P_i}{P_o})^2}{1-(\frac{P_i}{P_o})^3}, \tag{10}$$

where '$_o$' refers to measuring conditions, and T_c is the column temperature.

In summary, the most important equations used in this paper are summarized as follows:

$$V_n = \frac{1}{W_c} J_{p,T} F_{c,o} (t_R - t_M) \quad , \tag{11}$$

$$K_c = V_n \quad , \tag{12}$$

and

$$K_p = \frac{V_n}{RT_c} \, . \tag{13}$$

8.2.3 Determination of the Retention Time

The relationship between gas adsorption coefficient and gas retention variables, as shown in Equations 11-13, is fairly simple. However, determination of the retention time (t_r), and measurement of the gas hold-up time or the carrier gas retention time (t_M) is crucial in a real GC elution process. Conventionally, t_r is determined by a peak retention time, $t_{r,p}$, defined as the retention time at the peak height, h_p, where the detector response reaches the highest point. The peak retention time is a good representation of gas retention in an ideal elution process. However, it cannot describe gas retention in a non-ideal elution process. In a non-ideal elution process, it is better to use an average retention time, rather than the peak retention time.

There are two types of average retention times in a non-ideal elution process. One is a weighted mean retention time, $t_{r,m}$, defined as an arithmetic mean retention time weighted by GC detector response (h), i.e.,

$$t_{r,m} = \frac{\int_0^\infty h t dt}{\int_0^\infty h dt} = \frac{S_{p,r}}{S_p} \tag{14}$$

where S_p is the peak area, and $S_{p,r}$ the peak retention area. A second average is a half elution retention time, $t_{r,1/2}$, defined as a retention time at which one half of the injected amount of species A is eluted, i.e.,

$$t_{r,1/2} = n_a^{-1}\left(\frac{n_{a,o}}{2}\right) \tag{15}$$

where $n_{a,o}$ is the total injected amount of species A, and n_a^{-1} the inverse function of

$$n_a(t_r) = \int_0^{t_r} khdt. \qquad (16)$$

The relationships between the peak retention time, $t_{r,p}$, and the average retention times, $t_{r,m}$ and $t_{r,1/2}$ are shown in Figure 8.2. For a symmetric peak, $t_{r,p} = t_{r,1/2} = t_{r,m}$; for an asymmetric peak distorted with tailing, $t_{r,p} < t_{r,1/2} < t_{r,m}$; and for an asymmetric peak distorted with front profile spreading, $t_{r,p} > t_{r,1/2} > t_{r,m}$. From a statistics viewpoint, the best characteristic retention time for a non-ideal elution process is the weighted mean retention time, $t_{r,m}$.

8.2.4 Measurement of the Gas Hold-up Time

The gas hold-up time or the carrier gas retention time (t_M) can be either calculated from the dead volume of the GC system or measured by an injection of the carrier gas. In order to calculate the gas hold-up time precisely from the dead volume of the GC system, both the pressure profile and temperature profile alone the line from sample injection to GC detector has to be known. It is very difficult, sometimes even impossible, to determine these profiles. However, the measurement of the retention time of the carrier gas provides a simple way to obtain the gas hold-up time. In this method, the retention time of the carrier gas must be measured under the same conditions at which the investigated gas was evaluated.

8.2.5 Symmetry of GC Peaks

The symmetry of a GC peak can be quantitatively described by a symmetric factor, F_{sym}, defined as the ratio of the rear area to the front area of the peak. For a symmetric peak, $F_{sym} = 1$; for an asymmetric peak distorted with tailing, $F_{sym} > 1$; and for an asymmetric peak distorted with front profile spread, $F_{sym} < 1$. As an example, the symmetry of methane eluted from Upper Freeport coal is illustrated in Figure 8.3. The symmetric factor of this elution is equal to 3.53.

8.2.6 Thermodynamic Relationships

Thermodynamic constants can be estimated by gas adsorption coefficients measured at several temperatures. The most important thermodynamic constants of gas adsorption are ΔH and ΔS. The heat of gas adsorption, ΔH, can be determined by either application of the Clausius-Clapeyron equation or basic thermodynamic relationships. From the basic thermodynamic relationships

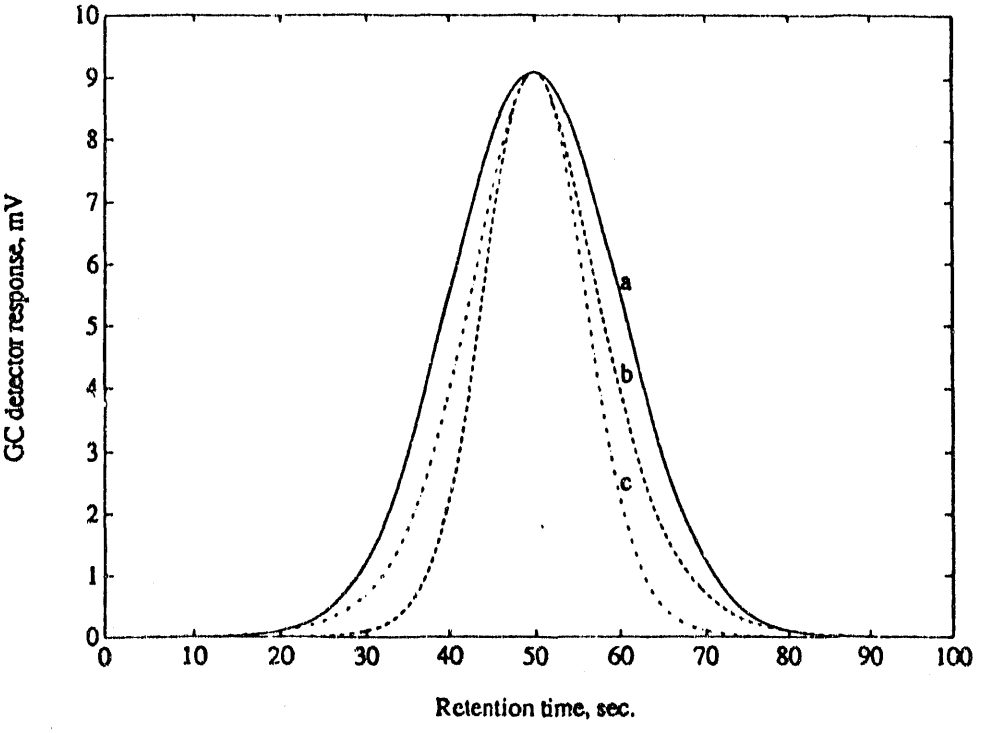

Figure 8.2 Three types of symmetry of elution curves. a: symmetric peak with $t_{r,p} = t_{r,1/2} = t_{r,m} = 50.00$ s. b: Asymmetric peak with tailing, $t_{r,p} = 50.00$ s, $t_{r,1/2} = 50.30$ s, $t_{r,m} = 50.92$ s. c: asymmetric peak with frontal spreading, $t_{r,p} = 50.00$ s, $t_{r,1/2} = 48.70$ s, $t_{r,m} = 48.08$ s.

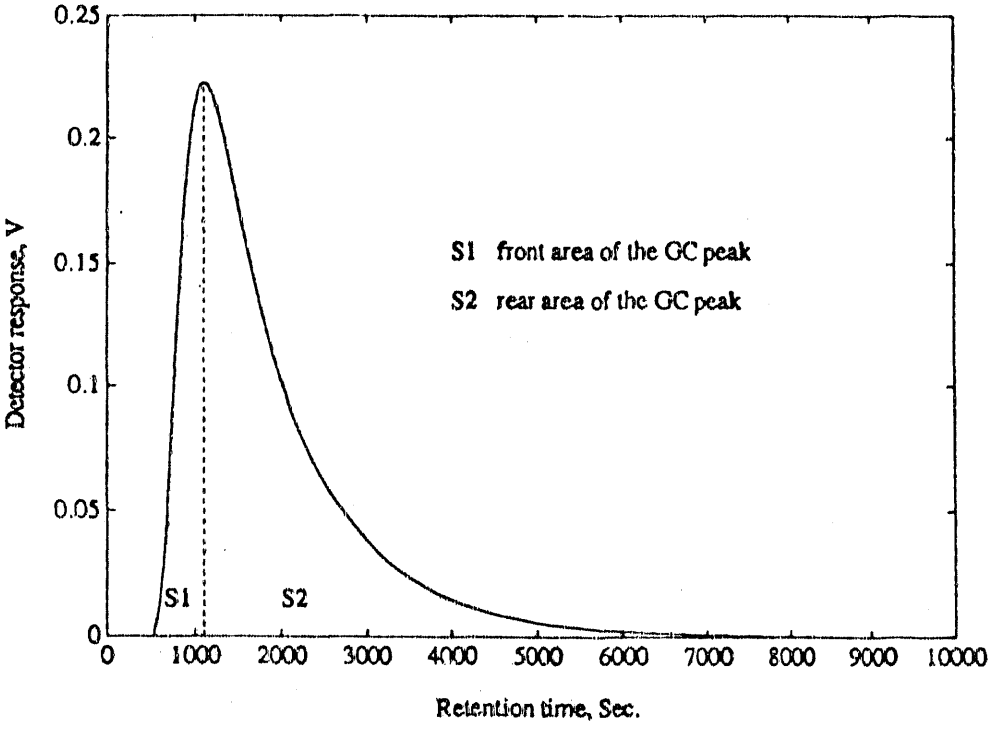

Figure 8.3 Symmetry of methane elution peak.

$$\Delta G = \Delta H - T\Delta S \qquad (17)$$

and

$$\Delta G = -RT\ln K_p \,, \qquad (18)$$

we have

$$\ln K_p = -\frac{\Delta H}{RT} + \frac{\Delta S}{R}. \qquad (19)$$

If ΔH is independent of temperature in the range of measurements,

$$\Delta H = f(\theta_A) \,, \text{ or } \Delta H = f(a_A) \qquad (20)$$

where θ_A is a ratio of a_A to the saturated adsorption of A, $a_A^{sat.}$. Therefore, the slope and intercept of a plot of $\ln K_p$ at $\theta_A \rightarrow 0$ against 1/T can be used to estimate ΔH and ΔS respectively. For the determination of ΔS a standard state is defined as $\theta_A \rightarrow 0$ when the reference state of K_p is taken as K_p°, 1 mol/(psia)(g).

It is worthy to mention that, while a real chromatographic column is in operation, the conditions of ideality are not entirely fulfilled because complete thermodynamic equilibrium is not likely to be established. However, it is possible to furnish conditions in a real column which approach the requirements of an ideal GC. To accomplish this, the optimum carrier gas flow rate should be used, the size and shape of the coal particles should be as uniform as possible, the whole column should be packed evenly, and a sufficiently high temperature should be applied. By adhering to these conditions, diffusional and kinetic broadening of the chromatogram can be reduced. Therefore, the following factors were considered when the experimental system was designed:

1. curvature in the distribution isotherm;
2. gas compressibility;
3. dependence of the isotherm on total pressure;
4. gas imperfection;
5. thermal effect and temperature control;
6. sorption of carrier gas;
7. non-ideality.

8.3 Experimental

8.3.1 Apparatus

A schematic diagram of the apparatus for GC adsorption studies is shown in Figure 8.4. The chromatograms were obtained using a dual column gas chromatograph (Series 580,

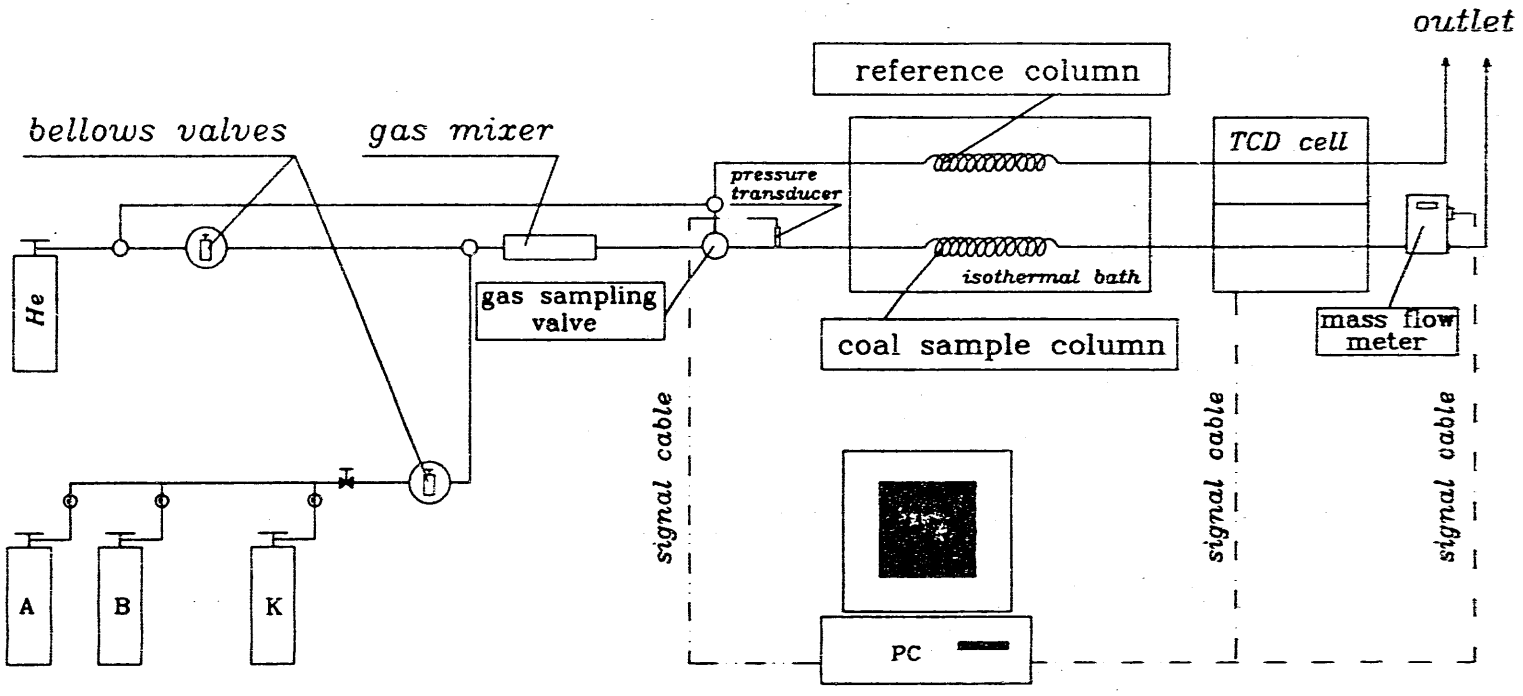

Figure 8.4 Apparatus for coal surface studies by GC.

GOW-MAC Instrument Co.) fitted with a thermal conductivity detector (TCD). The response signals from the TCD were first amplified by a PC isolated signal conditioning module (Wahl Instruments, Inc.) with an input of ±25 mV and output of ±5 V, and the amplified signals were collected by a PC equipped with a data acquisition and control board (DT 2001, ADT Research, Inc.) at 10 Hz sampling rate.

The chromatographic column was packed with the coal, and -80/+100 mesh glass beads were used as the reference column material. The sample column inlet pressure was measured by a pressure transducer in the range, 0 - 150 psig (OMEGA Engineering, Inc.). The signal from the pressure transducer was first amplified by a module with an input of ±100 mV and output of ±5 V, and collected at 1 Hz. The outlet pressure was measured by a barometer. At Salt Lake City, the atmospheric pressure is about 650 mmHg or 12.6 psia. The isothermal bath was controlled by a temperature controller (CN2042K, OMEGA Engineering, Inc.), and the column temperature was measured with a thermocouple. The signal from the thermocouple was first amplified by a K-type thermocouple module, and collected at 1 Hz. The column temperature was maintained within ±0.05 °C for 0 °C, and ±0.2 °C for the other temperatures. The carrier gas flow rate was measured by a mass flow monitor in the range of 0 - 20 ml(STP)/min (Sierra Instruments, Inc.) at the sample column outlet.

The signal from the mass flow monitor was collected at 1 Hz. Helium was used as carrier gas, except in cases where the gas hold-up retention times were measured. In the case of the measurements of the gas hold-up retention time, i.e., helium retention time, argon was used as carrier gas. A gas sample was introduced into the chromatographic column by a gas sampling loop of 0.25 ml. As shown in Figure 8.4, different concentrations of a gas can be injected into the column by adjusting the ratio of the gas to helium. Each chromatographic column was initially purged by the carrier gas at the experimental flow rate (about 18 ml/min) for at least 48 hours to thoroughly clean the coal surface.

The detector temperature was set at 40 °C. The bridge current was set at 220 mA for helium as carrier gas and 150 mA for argon as carrier gas.

Each weighted mean retention time is the average of at least three independent determinations. Precision of weighted mean retention times was always greater than 5% of the reported values for 0 °C, and 10% for other temperatures.

8.3.2 Coal Samples

Proximate and ultimate analyses of the eight Argonne Premium Coal Bank samples (Vorres, 1989) and one Utah coal

sample (Castlegate mine, Sub 3 seam) are given in Table 6.1. The helium densities of each of the coal samples were measured using a pycnometer (AccuPyc 1330 Pycnometer, Micromeritics, Inc.). The results are listed in Table 6.3. The samples were corrected to a mineral matter-free basis using a formula:

$$\frac{x}{\rho_m} + \frac{1-x}{\rho_c} = \frac{1}{\rho} \qquad (8.1)$$

where x is the weight fraction of the mineral matter, ρ_m the density of the mineral matter, assumed to be 2.85 g/ml, ρ_c the density of the coal, and ρ the measured density. The measured ash content is used for mineral matter. The calculated coal densities are given in Table 6.3. The 13 carbon structural parameters from the ^{13}C NMR tests for the coals are given in Table 6.2, where the NMR data of the 8 Argonne Premium Coals are from Solum et al. (1989).

The eight Argonne Coal Bank samples are carefully collected and preserved. They represent a range of coal rank from lignite to low volatile bituminous. Except for the Utah coal sample, Castlegate Sub 3, which was first ground, all samples were air dried under a vacuum (about -415 mmHg or -8 psig) at 80 °C for 48 hours and sieved before packing into stainless steel tubing (350 - 375 mm long and 4.0 mm i.d.). The characteristic data of the chromatographic columns is given in Table 8.1.

Table 8.1 Characteristic data of chromatographic columns

Sample No.	Coal	Particle size mesh	Wo* g	Length mm	Void %
1	Upper Freeport	-150/+200	4.7559	360	0.253
2	Wyodak-Anderson	-150/+200	5.0236	375	0.244
3	Illinois #6	-150/+200	4.5769	360	0.303
4	Pittsburgh (#8)	-150/+200	4.4489	360	0.276
5	Pocahontas #3	-150/+200	4.4357	360	0.284
6	Blind Canyon	-150/+200	4.6482	375	0.241
7	Lewiston-Stockton	-150/+200	4.7093	365	0.296
8	Beulah-Zap	-150/+200	4.5735	360	0.304
9	Sub 3	-200/+400	4.0126	350	0.301

* *Coal sample in the column on a dry basis*

8.3.3 Gas Samples

High purity of the carrier gas is essential, since even trace amounts of contaminants will adsorb on the coal surface and accumulate to the extent that they can disturb the results. The helium carrier gas was supplied from Liquid Air Co. with the guaranteed minimum purity of 99.99%. The major impurities were H_2, O_2, and Ar which were reversibly adsorbed on the coal surface without accumulation. Nitrogen, oxygen, argon, carbon monoxide, carbon dioxide, methane, ethane, propane, and propylene gases have been used as molecular probes. The gases were supplied from Air Liquid Co. with the following guaranteed minimum purities: N_2 99.99%; O_2 99.99%; Ar 99.99%; CO 99.97%; CO_2 99.9%; CH_4 99.99%; C_2H_6 99.0%; C_3H_8 99.0%; and C_3H_6 99.0%.

8.4 Results and Discussion

8.4.1 Determination of the Thermodynamic Constants

Several concentrations of methane from 3.88 to 100%, which are equivalent to 7.6 µl to 0.196 ml at STP, were used in examining the hypothesis of linearity of the gas adsorption isotherm in the low pressure range. The chromatograms of the tests on Upper Freeport coal at 0 °C are shown in Figure 8.5. Experimental conditions and primary results for the different methane injection concentrations are listed in Table 8.2. The adsorption coefficients, K_0 and K_p, and other pertinent experimental parameters, such as, the ratio of the column inlet pressure (P_i) to outlet pressure (P_o), the temperature and pressure correction factor ($J_{p,T}$), the partial pressure of methane (P_{CH_4}) during the adsorption, and the adsorption capacity (V_{ads}) are given in Table 8.2. A plot of the adsorption capacities (V_{ads}) against the partial pressures of methane is shown in Figure 8.6. This figure verifies the assumption of the linearity of gas adsorption isotherm within a sample size up to 0.196 ml(STP). The symmetric factors of the methane elution peaks are plotted versus the injected volumes in Figure 8.7. The symmetric factor approaches a constant value at larger injection volumes. It is about 3.6 for extrapolation to zero injection volume. The large asymmetry of the elution peak at zero injection volume indicates that the influence of methane diffusion in the micropores of coal is important.

To determine whether the gas chromatographic measurements have been made at thermodynamic equilibrium or whether they are limited by the kinetics of adsorption on coal, the dependence of net unit retention volume on flow rate was measured for two gases, methane and carbon dioxide, on Upper Freeport coal at 0 °C. The results are shown in Table 8.3. The data indicate that the net unit retention volumes are

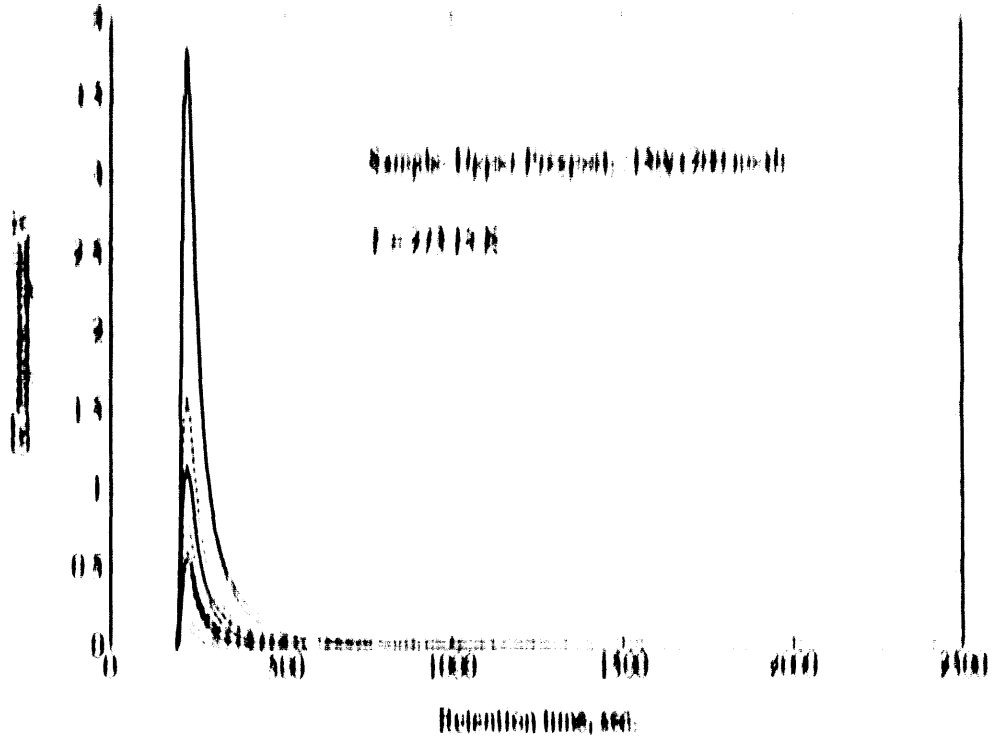

Figure 8.5 Methane elution peaks for various injection volumes.

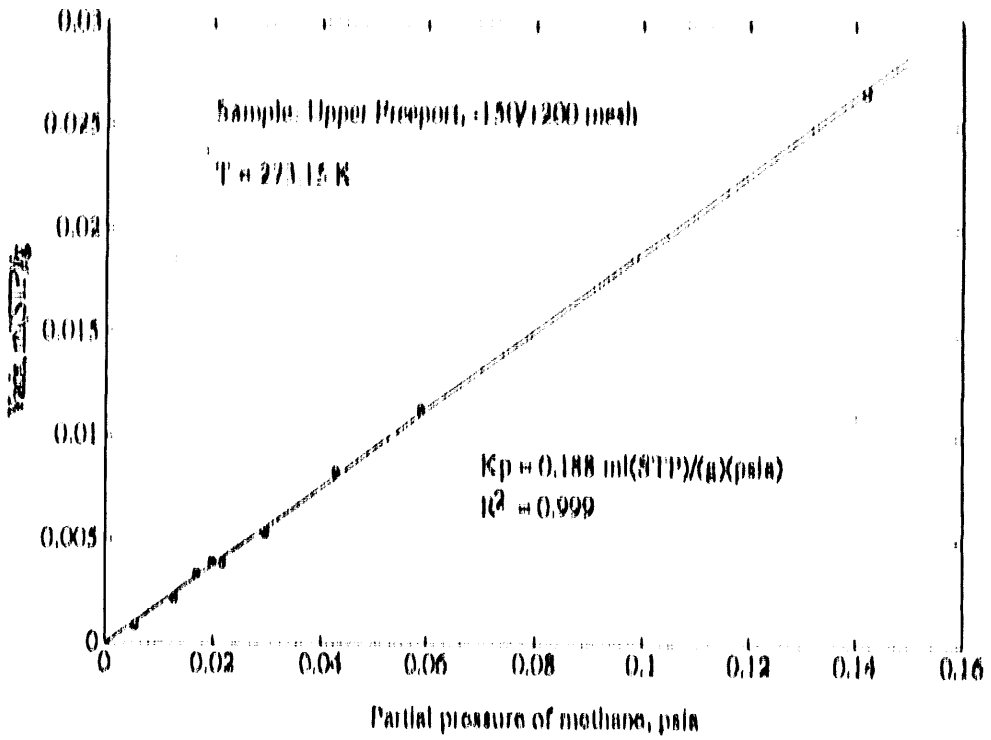

Figure 8.6 Methane adsorption isotherm at low pressures.

Table 3.5a [illegible]

Species	[illegible]	[illegible]	[illegible]	[illegible]	[illegible]	[illegible]	[illegible]	[illegible]	[illegible]	[illegible]
	[illegible]	[illegible]		[illegible]	[illegible]	[illegible]	[illegible]	[illegible]	[illegible]	[illegible]
He	[illegible]	-	[illegible]	[illegible]	[illegible]	[illegible]	[illegible]	[illegible]	[illegible]	[illegible]
CH4-He	[illegible]	[illegible]	[illegible]	[illegible]	[illegible]	[illegible]	[illegible]	[illegible]	[illegible]	[illegible]
CH4-He	[illegible]	[illegible]	[illegible]	[illegible]	[illegible]	[illegible]	[illegible]	[illegible]	[illegible]	[illegible]
CH4-He	[illegible]	[illegible]	[illegible]	[illegible]	[illegible]	[illegible]	[illegible]	[illegible]	[illegible]	[illegible]
CH4-He	[illegible]	[illegible]	[illegible]	[illegible]	[illegible]	[illegible]	[illegible]	[illegible]	[illegible]	[illegible]
CH4-He	[illegible]	[illegible]	[illegible]	[illegible]	[illegible]	[illegible]	[illegible]	[illegible]	[illegible]	[illegible]
CH4-He	[illegible]	[illegible]	[illegible]	[illegible]	[illegible]	[illegible]	[illegible]	[illegible]	[illegible]	[illegible]
CH4-He	[illegible]	[illegible]	[illegible]	[illegible]	[illegible]	[illegible]	[illegible]	[illegible]	[illegible]	[illegible]
CH4-He	[illegible]	[illegible]	[illegible]	[illegible]	[illegible]	[illegible]	[illegible]	[illegible]	[illegible]	[illegible]
CH4	[illegible]	[illegible]	[illegible]	[illegible]	[illegible]	[illegible]	[illegible]	[illegible]	[illegible]	[illegible]

[redacted]

[redacted]										
[redacted]										
[redacted]										
[redacted]										
[redacted]										
[redacted]										
[redacted]										
[redacted]										
[redacted]										
[redacted]										
[redacted]										

Table 8.4 Heats of gas adsorption on Upper Freeport coal (-150/+200 mesh)

Gas	Number of electrons	$-\Delta H_a$ kJ/mol	$-\Delta S_a$ kJ/(mol)(K)	r^2	Temperature range, °C	ΔH_{vap}* kJ/mol
Ar	18	9.3	138	0.999	0 - 80	6.65
N_2	14	9.3	140	0.999	0 - 80	5.59
O_2	16	9.9	140	0.999	0 - 80	6.82
CO	14	15.8	158	0.999	0 - 80	6.04
CO_2	22	28.6	178	0.992	0 - 90	25.23
CH_4	10	17.9	156	0.991	0 - 90	8.16
C_2H_6	18	21.4	148	0.998	0 - 90	14.70
C_3H_8	26	24.7	154	0.981	50 - 90	18.78
C_3H_6	24	25.1	145	0.998	0 - 80	18.42
H_2O**	10	29.9	-	-	25 - 150	40.71

* *Data from reference 26.*

** *Determined by differential scanning calorimetry.*

The gas adsorption studies are an important source of information about molecular interactions. In physical adsorption there is no transfer or sharing of electrons between atoms of the gas and the coal surface. The interactions in the physical adsorption are the sum of intermolecular forces

$$f = f_D + f_R + f_i + f_\mu + f_q + f_H \qquad (22)$$

where f_D is the dispersion force, f_R the short-range repulsive force, f_i the induced dipole interaction force (caused by polar atoms or π-electrons in the molecule), f_μ the permanent dipole interaction force, f_q the quadrapole moment force (examples are CO, CO_2 and N_2), and f_H the hydrogen bond. According to the type of the molecular interaction, gas adsorption can be classified into two groups. One is non-specific adsorption. In this group, the gas adsorption is caused by the dispersion and repulsive forces only, i.e., the universal intermolecular interaction or the van der Waals interaction. The second group is specific adsorption. In this group, gas adsorption is caused by additional specific electrical interactions, such as induced dipole interaction forces provoked by polar atoms or π-electrons in the molecule, and/or permanent dipole interaction forces. A diagram of the interactions between coal surfaces and gas molecules is shown in Figure 8.9.

As expected, the heats of gas adsorption are in the order of water > carbon dioxide > propene > propane > ethane >

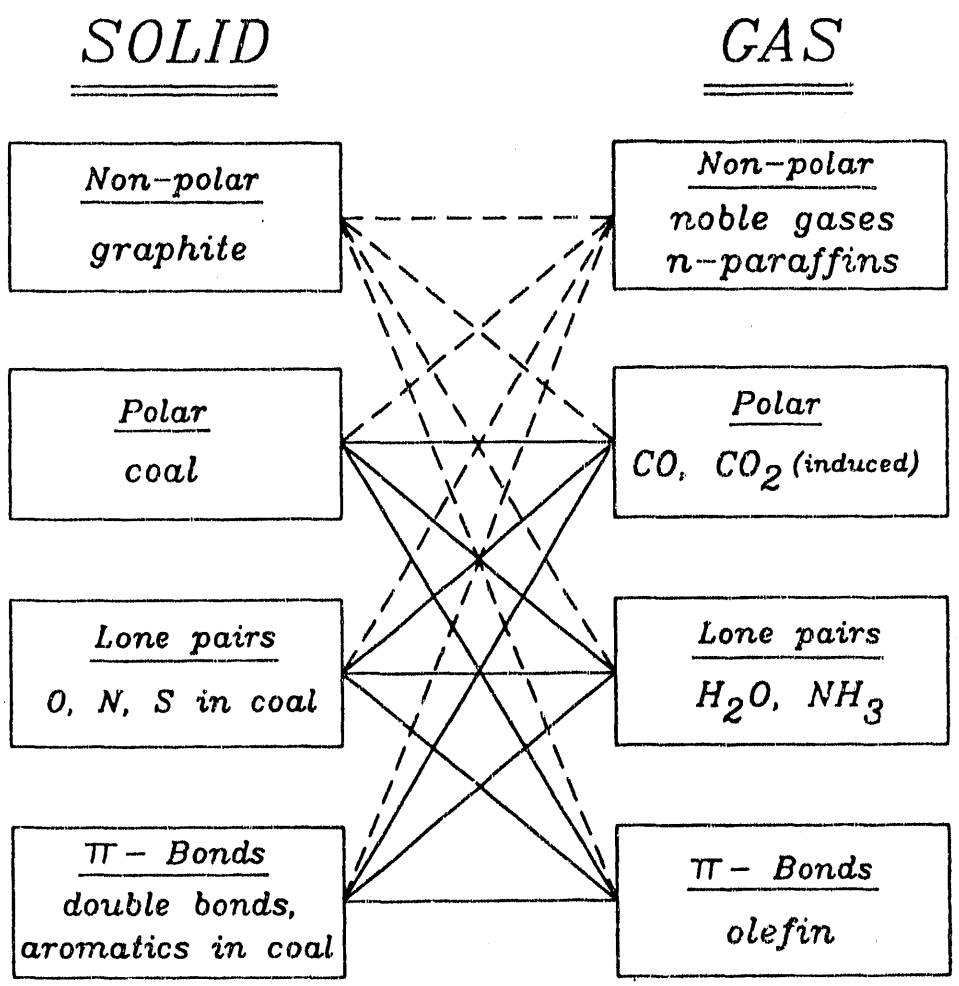

dispersion forces shown by – – – –

specific electronic interactions shown by ———

Figure 8.9 Interactions between coal surfaces and gas molecules.

methane > carbon monoxide > oxygen > nitrogen and argon. It is noted that the heat of adsorption of carbon monoxide with a permanent dipole interaction force is less than those of the n-paraffins, such as methane, ethane and propane. A possible explanation for this low adsorption heat of carbon monoxide on Upper Freeport coal is that the permanent dipole interaction force of this small molecule, carbon monoxide, plays a trivial role in the adsorption process. In research on the thermodynamics of adsorption of organic compounds on the surface of Bruceton coal, Larsen et al. (1978) pointed out that coal interacts strongly with non-polar molecules and weakly with both acidic and basic polar molecules. From their results, they also suggested that the coal surface is capable of undergoing strong, generalized van der Waals interactions with most molecules, and strong highly specific interactions with a few polar molecules.

The correlation of gas adsorption coefficients with heats of gas adsorption is shown in Figure 8.10. As expected, the capacities and heats of gas adsorption for specific adsorption are higher than those for non-specific adsorption, except in the case of the adsorption of carbon monoxide. Although the interactions between a gas molecule and a coal surface play an important role in determining the gas adsorption capacity, other factors, such as surface area, solubility of the gas in coal, coal pore structures and gas molecule structure must be included and considered. In fact, the high adsorption coefficient of propene on Upper Freeport coal, which is not shown in Figure 8.10, is due to its high solubility in the coal.

Data on the vaporization heats of the molecules used in the adsorption studies are listed in Table 8.4 (Perry and Green, 1984). A plot of the heats of vaporization versus the heats of adsorption is shown in Figure 8.11. All molecules, except water, have higher heats of adsorption than heats of vaporization. This indicates that the molecule-coal surface interactions are stronger than molecule-molecule interactions, and these gases have an additional affinity for the coal surface. As shown in Figure 8.11, methane gas has the largest difference in the heat of adsorption from the heat of vaporization. This shows that methane has a very strong affinity for the coal surface. This phenomenon may be the main reason that methane is the major component in a coalbed gas. The next gas having a large difference between heat of adsorption and heat of vaporization is carbon monoxide, which has a permanent dipole interaction force. This indicates that the coal surface is polar. Elemental gases (oxygen, nitrogen and argon) have slight differences in the heats of adsorption and the heats of vaporization. This may be due to the fact of that only van der Waals interactions exist between these molecules and the coal surface. However, in the case of water adsorbed on the coal surface, the heat of adsorption is much

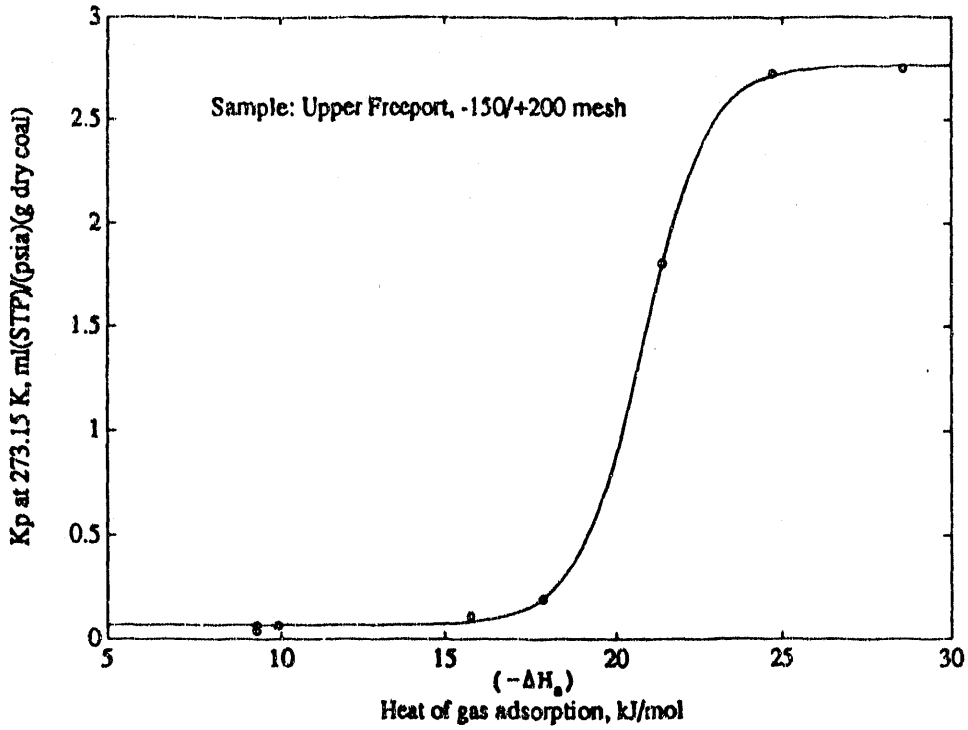

Figure 8.10 Correlation of K_p with heats of adsorption.

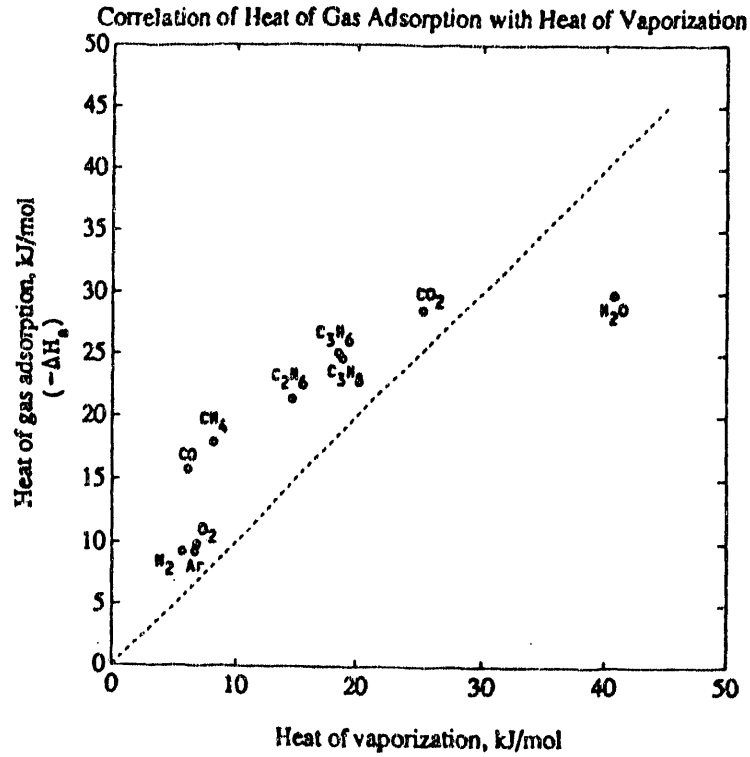

Figure 8.11 Correlation of heats of vaporization with heats of adsorption.

less than the heat of vaporization. This shows that the intramolecular interactions of water molecules must be greater than their interactions with the less polar coal surface. A detail explanation and discussion about the behavior between water adsorption on a coal surface and water in a liquid is given in Chapter 12.

The magnitude of the van der Waals interaction increases with an increase in the number of electrons in the molecule. Since the correlation of the heats of vaporization and the number of electrons in the molecule is linear (Figure 8.12), the strength of the van der Waals interaction increases linearly with the number of electrons in the molecule. A plot of the heats of gas adsorption versus the number of electrons in the molecules is shown in Figure 8.13. The dashed line through nitrogen and oxygen in the plot represents the van der Waals interactions between the gas molecules and the coal surface. As expected, water, carbon monoxide, and carbon dioxide have stronger interactions with the coal surface than nitrogen and oxygen, and give higher heats of adsorption, while the noble gas, argon, has a weaker van der Waals interaction, and gives a lower heat of adsorption. Water and carbon monoxide molecules have permanent dipole moments. In addition, water can form hydrogen bonds with oxygen-, nitrogen-, and sulfur-containing groups on the coal surface. Carbon dioxide has a strong induced dipole moment. The n-paraffins, methane, ethane, and propane, which have only van der Waals interactions, have higher heats of adsorption on coal than they should. This may be explained as the additional interactions of the hydrocarbon gases with the coal surface caused by affinity due to similarities in the gas and coal structures.

In Figure 8.13, there is good linearity among the n-paraffins. The adsorption heats of the other higher n-paraffine gases may be estimated by the empirical equation

$$-\Delta H_a\ (kJ/mol) = 0.425N_e + 13.68 \qquad (23)$$

where ΔH_a is the heat of n-paraffin gas adsorption, and N_e the number of electrons in the n-paraffin molecule. As shown in Figure 8.13, the heat of propene adsorption is above the n-paraffin line. This is due to the contribution from the interactions of the double bond in the propene molecule with the π-electrons on the coal surface.

8.4.2 Measurement of the Coefficients of Gas Adsorption

The coefficient of gas adsorption at zero coverage of the coal surface, K_c or K_p, is a physical constant used in characterizing the properties of the coal surface and determining the gas adsorption capacity at very low pressures. Since the relative gas adsorption capacities of coals at

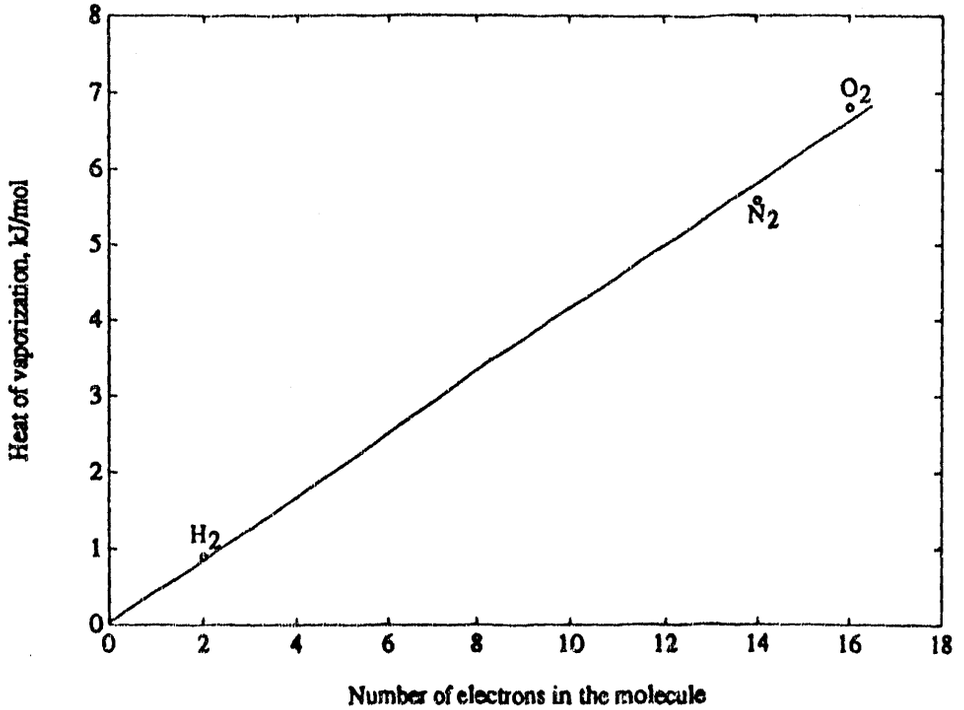

Figure 8.12 Correlation of heats of vaporization with number of electrons.

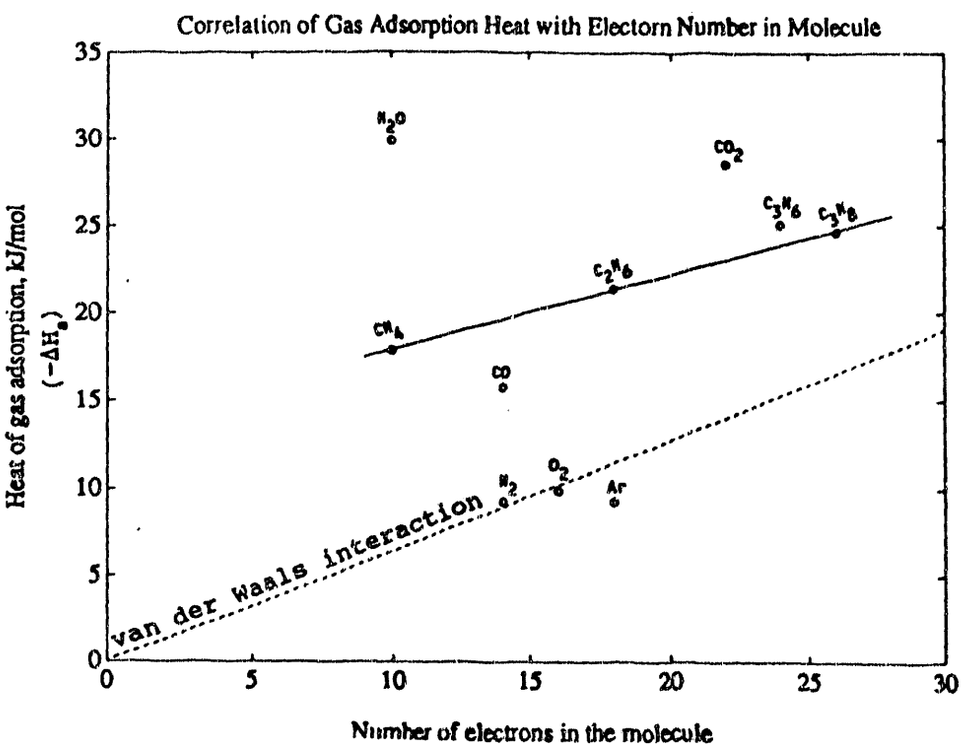

Figure 8.13 Correlation of heats of adsorption with number of electrons.

different pressures are similar (Joubert et al., 1973, 1974; Kim, 1977; Ruppel et al., 1972; Yang and Saunders, 1985; Choi et al., 1989), the gas adsorption coefficient measured at very low pressure can be used in estimating the relative adsorption capacities at higher pressures. Therefore, measurements of the gas adsorption coefficients on various coal samples are useful not only in theoretical studies of the coal surfaces, but also in practical estimation of the relative gas adsorption capacities of coals.

Those gases (Table 8.5) whose critical temperatures (T_c) are lower than 0°C, such as, Ar, N_2, O_2, CO, and CH_4, are neither condensed in coal pores nor adsorbed in multilayers on the coal surface above 0 °C. When these gases adsorb on a porous coal, they follow a pseudo-Langmuir isotherm (type I) (Smith and Van Ness, 1987; Gregg and Sing, 1982)

$$\frac{V}{V_m} = \frac{bp}{1 + bp} \tag{24}$$

where b is a fitting constant, V the volume (normally corrected to STP) of adsorbate, and V_m the volume adsorbate equivalent to a monolayer. The term pseudo-Langmuir isotherm used here is due to the fact that the gas adsorption on the coal surface is not physically consistent with the requirements of the Langmuir isotherm model but mathematically matches the Langmuir isotherm equation. In fact, the adsorption sites on the coal surface are not energetically uniform since the adsorption heats are functions of coverage; the interactions of adsorbate-adsorbate can not be ignored under high pressures.

The correlation of the gas adsorption coefficient with the parameters in the pseudo-Langmuir isotherm can be derived by taking $p \to 0$ in Equation 24, i.e.,

$$\begin{aligned} K_p &= \lim_{p \to 0} \left(\frac{V}{p}\right) \\ &= \lim_{p \to 0} \left(\frac{bV_m}{1+bp}\right) \\ &= bV_m \, . \end{aligned} \tag{25}$$

Therefore, the relationship of K_p with (bV_m) can be used as one of the equations to estimate the constants in the pseudo-Langmuir isotherm.

The adsorption coefficients for the gases Ar, N_2, O_2, CO, CO_2, CH_4, C_2H_6, C_3H_8, and C_3H_6 on the 9 coals are listed in Table 8.6a-c. Comparison of the values of K_p with those of (bV_m) from the static method (Ruppel et al., 1974) (Table 8.7) confirms the relationship between K_p and (bV_m).

Table 8.5 Properties of the gases used in the adsorption studies

Gas	T_c* K	P_c* psia	V_c* ml/mol	T_b** K
Ar	150.8	706.3	74.9	87.35
N2	126.2	491.7	89.5	77.35
O2	154.6	732.4	73.4	90.15
CO	132.9	507.6	93.1	81.65
CO2	304.2	1070.4	94.0	194.75
CH4	190.6	667.2	99.0	109.15
C2H6	305.4	707.8	148	184.55
C3H8	369.8	616.4	203	231.05
C3H6	365.0	670.1	181	225.75

* *Data from reference 34.*

** *Data from reference 26.*

To evaluate the effects of the specific interactions between the various gases and the different coals, a specific adsorption ratio, α_s, is defined as

$$\alpha_s = \frac{\frac{K_{p,i}}{N_{e,i}}}{\frac{K_{p,N_2}}{N_{e,N_2}}} \qquad (26)$$

where K_p is the adsorption coefficient in ml(STP)/(psia)(g daf coal), N_e the number of electrons in molecule, i represents Ar, N_2, O_2, CO, CO_2, CH_4, C_2H_6, C_3H_8, and C_3H_6. Nitrogen is taken as a reference gas in the adsorption studies. This is due to the fact that only van der Waals interactions are involved in N_2 adsorption. Since the calculation of these ratios are based on the same coal, the influence of the coal surface properties on the gas adsorption is minimized. In this way, the effects of the specific adsorption on different coals for each individual gas and the effects of the specific adsorption of different gases for each individual coal are compared. The calculated specific adsorption ratios using the data in Table 8.6c are given in Table 8.8. The mean of each individual gas characterizes the magnitude of the specific adsorption effect of this gas. The standard deviation (std) of each individual gas illustrates the dependence of the specific adsorption effect of this gas on the coals.

Argon and oxygen gas adsorption show no specific adsorption effects. This conclusion agrees with that of the previous discussion on the heats of adsorption. The mean and

Table 8.6a Gas adsorption coefficients (Kc) or net gas retention volumes (Vn) at 273.15 K

Sample No.	Seam	State	Rank	Kc (Vn), ml/g								
				Ar	N2	O2	CO	CO2	CH4	C2H6	C3H8	C3H6
1	Upper Freeport	PA	Med. Vol. Bit.	0.98	0.60	0.99	1.61	40.4	2.87	26.6	40.1	451.4
2	Wyodak-Anderson	WY	Subbituminous	0.50	0.39	0.83	0.74	17.0	0.43	4.2	4.6	31.5
3	Illinois #6	IL	High Vol. Bit.	1.21	0.98	1.58	1.91	42.5	2.35	42.8	211.7	903.8
4	Pittsburgh (#8)	PA	High Vol. Bit.	0.85	0.68	0.74	1.13	33.1	1.58	11.1	11.2	93.5
5	Pocahontas #3	VA	Low Vol. Bit.	1.25	0.91	1.41	2.05	64.9	3.47	48.6	85.7	631.4
6	Blind Canyon	UT	High Vol. Bit.	0.76	0.52	0.72	0.93	33.5	1.54	17.0	31.4	248.7
7	Lewiston-Stockton	WY	High Vol. Bit.	0.65	0.49	0.79	0.98	34.2	1.48	18.4	25.0	264.3
8	Beulah-Zap	ND	Lignite	0.37	0.28	0.44	0.66	16.0	0.37	1.5	0.9	10.1
9	Sub 3	UT	High Vol. Bit.	0.79	0.50	0.73	0.89	29.9	1.32	10.5	8.7	83.7

Table 8.6b Gas adsorption coefficients (Kp in ml(STP)/(psia)(g dry coal)) at 273.15 K

Sample No.	Seam	State	Rank	Kp, ml(STP)/(psia)(g dry coal)								
				Ar	N2	O2	CO	CO2	CH4	C2H6	C3H8	C3H6
1	Upper Freeport	PA	Med. Vol. Bit.	0.067	0.041	0.067	0.110	2.75	0.195	1.81	2.73	30.7
2	Wyodak-Anderson	WY	Subbituminous	0.034	0.027	0.056	0.050	1.16	0.029	0.28	0.32	2.1
3	Illinois #6	IL	High Vol. Bit.	0.082	0.067	0.107	0.130	2.89	0.160	2.91	14.40	61.5
4	Pittsburgh (#8)	PA	High Vol. Bit.	0.058	0.046	0.050	0.077	2.25	0.108	0.75	0.76	6.4
5	Pocahontas #3	VA	Low Vol. Bit.	0.085	0.062	0.096	0.139	4.41	0.236	3.31	5.83	43.0
6	Blind Canyon	UT	High Vol. Bit.	0.052	0.035	0.049	0.063	2.28	0.105	1.16	2.13	16.9
7	Lewiston-Stockton	WY	High Vol. Bit.	0.044	0.033	0.053	0.067	2.33	0.101	1.25	1.70	18.0
8	Beulah-Zap	ND	Lignite	0.025	0.019	0.030	0.045	1.09	0.025	0.10	0.06	0.69
9	Sub 3	UT	High Vol. Bit.	0.054	0.034	0.049	0.061	2.03	0.090	0.71	0.59	5.7

Table 8.6c Gas adsorption coefficients (Kp in ml(STP)/(psia)(g daf coal)) at 273.15 K

Sample No.	Seam	State	Rank	Kp, ml(STP)/(psia)(g d.a.f. coal)								
				Ar	N2	O2	CO	CO2	CH4	C2H6	C3H8	C3H6
1	Upper Freeport	PA	Med. Vol. Bit.	0.077	0.047	0.077	0.126	3.17	0.225	2.98	3.14	35.4
2	Wyodak-Anderson	WY	Subbituminous	0.037	0.029	0.062	0.055	1.27	0.052	0.31	0.35	2.4
3	Illinois #6	IL	High Vol. Bit.	0.097	0.079	0.127	0.154	3.42	0.180	3.45	17.94	72.8
4	Pittsburgh (#8)	PA	High Vol. Bit.	0.064	0.051	0.055	0.085	2.48	0.118	0.83	0.84	7.9
5	Pocahontas #3	VA	Low Vol. Bit.	0.089	0.065	0.101	0.147	4.64	0.248	3.47	6.13	45.1
6	Blind Canyon	UT	High Vol. Bit.	0.054	0.037	0.052	0.066	2.39	0.110	1.32	2.24	17.8
7	Lewiston-Stockton	WY	High Vol. Bit.	0.055	0.042	0.067	0.083	2.90	0.126	1.56	2.12	22.4
8	Beulah-Zap	ND	Lignite	0.028	0.021	0.033	0.059	1.21	0.028	0.11	0.57	0.8
9	Sub 3	UT	High Vol. Bit.	0.057	0.036	0.052	0.064	2.16	0.095	0.76	0.93	6.9

Table 8.7 Relationship between Kp and (bVm) of methane adsorption at 273.15 K

Coal	b* 1/atm	Vm* ml/g	bVm ml/((atm)(g)	bVm ml/((psia)(g)	Kp ml/((psia)(g)
Pittsburgh (#8), PA	0.080	18.8	1.504	0.102	0.108
Pocahontas #3, VA	0.139	24.8	3.447	0.235	0.236

* *Data from reference 37; Vm in ml(STP)/(g dry coal).*

standard deviation of the specific adsorption ratios for these two gases are very close to 1 and 0 respectively. Carbon monoxide has a mean of 2, indicating that there is a specific adsorption effect for this gas. However, there is no specific adsorption effect on the coals because it has a standard deviation of 0.31. Methane shows specific adsorption effects on both gas and coals. It has a mean of 3.79 and a standard deviation of 1.51.

The correlation of the specific adsorption ratio with carbon content, which is used as a parameter for coal rank, for Ar, O_2, CO, and CH_4 is shown in Figure 8.14. It is obvious that the specific adsorption effects of methane adsorption increase with increasing carbon content or rank of coal. The correlation of the specific adsorption effects with various gases is in the order propene > carbon dioxide > propane > ethane > methane > monoxide. The correlation of the specific adsorption effects with coal properties, such as, carbon content (or rank of coal), is in the order of propene > propane > ethane > carbon dioxide > methane > monoxide. These two orders are not exactly parallel. However, in the hydrocarbon gas series, they are not only parallel with each other but also parallel with the order of the heats of adsorption. This indicates that the interaction of gas molecules with coal surfaces increase with increasing rank of coal and size of molecule.

8.4.3 Multivariate Analysis

In order to understand the complex correlation of gas adsorption capacities and coal surface properties with the analytical data of coal, multivariate analysis, which determines interactions between the variables, was applied. Analytical data, e.g. proximate analyses, ultimate analyses, NMR data, nitrogen surface areas and coal densities, were correlated with the gas adsorption coefficients.

To eliminate the dependent variables, the translation of

Table 11 [illegible]

Sample No.	[illegible]	[illegible]	[illegible]	[illegible]	[illegible]	[illegible]	[illegible]	[illegible]	[illegible]	[illegible]	[illegible]
1	[illegible]	[illegible]	[illegible]	[illegible]	[illegible]	[illegible]	[illegible]	[illegible]	[illegible]	[illegible]	[illegible]
2	[illegible]	[illegible]	[illegible]	[illegible]	[illegible]	[illegible]	[illegible]	[illegible]	[illegible]	[illegible]	[illegible]
3	[illegible]	[illegible]	[illegible]	[illegible]	[illegible]	[illegible]	[illegible]	[illegible]	[illegible]	[illegible]	[illegible]
4	[illegible]	[illegible]	[illegible]	[illegible]	[illegible]	[illegible]	[illegible]	[illegible]	[illegible]	[illegible]	[illegible]
5	[illegible]	[illegible]	[illegible]	[illegible]	[illegible]	[illegible]	[illegible]	[illegible]	[illegible]	[illegible]	[illegible]
6	[illegible]	[illegible]	[illegible]	[illegible]	[illegible]	[illegible]	[illegible]	[illegible]	[illegible]	[illegible]	[illegible]
7	[illegible]	[illegible]	[illegible]	[illegible]	[illegible]	[illegible]	[illegible]	[illegible]	[illegible]	[illegible]	[illegible]
8	[illegible]	[illegible]	[illegible]	[illegible]	[illegible]	[illegible]	[illegible]	[illegible]	[illegible]	[illegible]	[illegible]
9	[illegible]	[illegible]	[illegible]	[illegible]	[illegible]	[illegible]	[illegible]	[illegible]	[illegible]	[illegible]	[illegible]
				[illegible]	[illegible]	[illegible]	[illegible]	[illegible]	[illegible]	[illegible]	[illegible]	[illegible]
				[illegible]	[illegible]	[illegible]	[illegible]	[illegible]	[illegible]	[illegible]	[illegible]	[illegible]

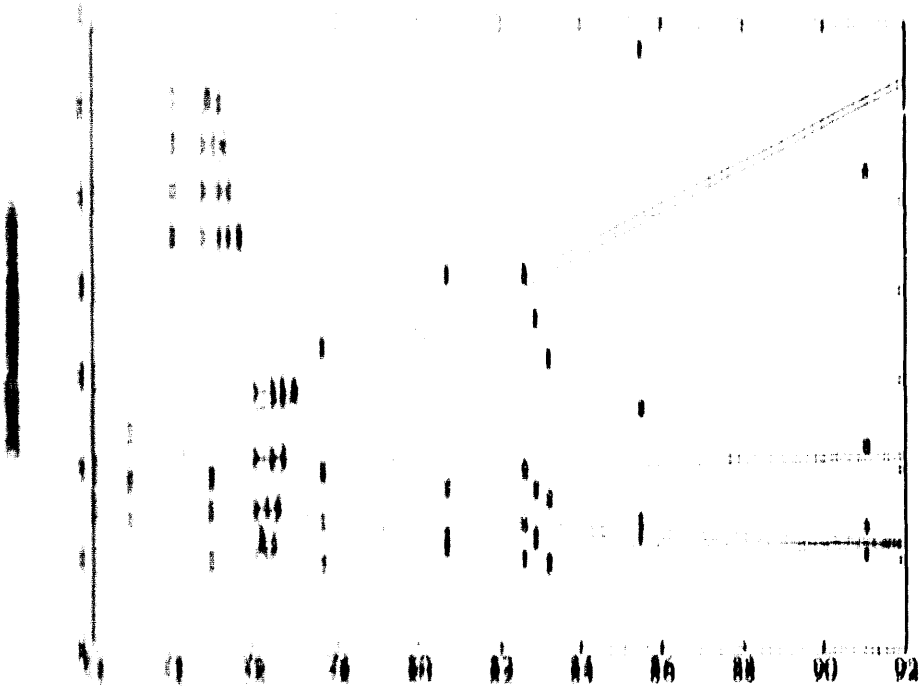

[illegible]

[illegible] correlation of specific adsorption ratio with [illegible] content.

[illegible] parameter with another was first examined by [illegible] analysis (Chapter 6). For example, [illegible] is used as a coal rank parameter. It is also [illegible] with oxygen content, heating value and [illegible] from the previous statistical analysis [illegible] consideration of the accuracy of measurements, [illegible] of these independent variables were carefully [illegible] multivariate analysis.

[illegible] Regression Analysis

[illegible] of the gas adsorption coefficient with [illegible], aliphatic aromatic carbon fraction, [illegible] (H, wt%), sulfur [illegible], ash content, nitrogen surface area, and coal [illegible] were examined using multiregression analysis. [illegible] coefficients of the variables used in the [illegible] analysis are given in Table 8.9. Correlation [illegible] between the adsorption coefficients at 0 °C and [illegible] parameters are listed in Table 8.10. [illegible] the adsorption coefficient of C_2H_6, which shows a [illegible] on the N_2 surface area, the adsorption [illegible] are strongly correlated with coal rank [illegible], such as carbon content, and aromaticity. The [illegible] between the correlation coefficients of K_p and

Table 8.9 Correlation coefficients of the variables used in the multivariate analysis

	C, wt%	H, wt%	S, wt%	d, g/ml	Ash	Aromaticity	Alk-Ar	Area
C, wt%	1	-0.227	-0.107	-0.433	-0.174	0.837	0.511	-0.296
H, wt%	-0.227	1	-0.274	-0.727	-0.243	-0.575	-0.373	-0.143
S, wt%	-0.107	-0.274	1	0.137	0.480	0.301	0.405	0.856
d, g/ml	-0.433	-0.727	0.137	1	0.199	-0.111	-0.152	0.251
Ash	-0.174	-0.243	0.480	0.199	1	0.242	0.724	0.361
Aromaticity	0.837	-0.575	0.301	-0.111	0.242	1	0.804	0.057
Alk-Ar	0.511	-0.373	0.405	-0.152	0.724	0.804	1	0.145
Area	-0.296	-0.143	0.856	0.251	0.361	0.057	0.145	1

Table 8.10 Correlation coefficients of Kp at T = 273.15 K for various gases

Gas	C, wt%	H, wt%	S, wt%	d, g/ml	Ash	Aromaticity	Alk-Ar	Area
Ar	0.697	-0.343	0.547	-0.202	-0.034	0.791	0.475	0.447
N2	0.541	-0.376	0.651	-0.059	0.055	0.720	0.442	0.606
O2	0.413	-0.461	0.627	0.131	0.144	0.646	0.428	0.702
CO	0.622	-0.608	0.580	0.086	0.103	0.835	0.537	0.479
CO2	0.852	-0.466	0.228	-0.142	-0.077	0.892	0.516	0.151
CH4	0.833	-0.511	0.356	-0.151	0.008	0.925	0.605	0.178
C2H6	0.616	-0.533	0.485	0.040	0.100	0.809	0.525	0.480
C3H8	0.087	-0.346	0.816	0.174	0.289	0.422	0.342	0.895
C3H6	0.375	-0.496	0.701	0.109	0.275	0.684	0.534	0.700

the most important coal analytical parameters, e.g. aromaticity, carbon content, and N_2 surface area, is plotted in Figure 8.15. The adsorption coefficients of methane and carbon dioxide show strong dependence on coal rank, and very weak correlation with the N_2 surface area. On the other hand, the adsorption coefficients of propane is strongly determined by the N_2 surface area rather than the coal rank.

In the hydrocarbon gas series, as molecule size increases, the dependence of the adsorption coefficients on coal rank decreases, but the dependence on N_2 surface area increases. These results indicate that larger molecules can not reach the internal surface of the small pores in the coal, and the controlling factor of the adsorption capacity for this larger molecule is the available surface area.

8.4.5 Factor Analysis

Factor analysis was performed to reduce matrices of data to their lowest dimensionality by the use of orthogonal factor space and transformations that yield predictions and/or recognizable factors. The number of significant factors is determined by either a Scree plot or a Cumulative plot. From the Scree plots (Figures 8.16a-c), all gases used in the adsorption studies show the same pattern and the slope levels

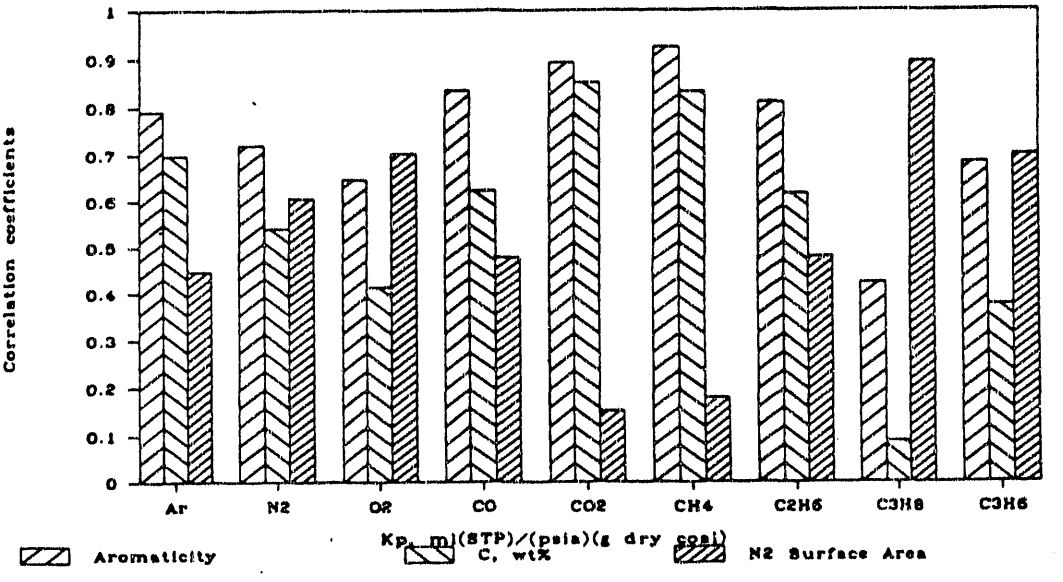

Figure 8.15 Correlation coefficients for K_p with aromaticity, carbon content, and N_2 surface area.

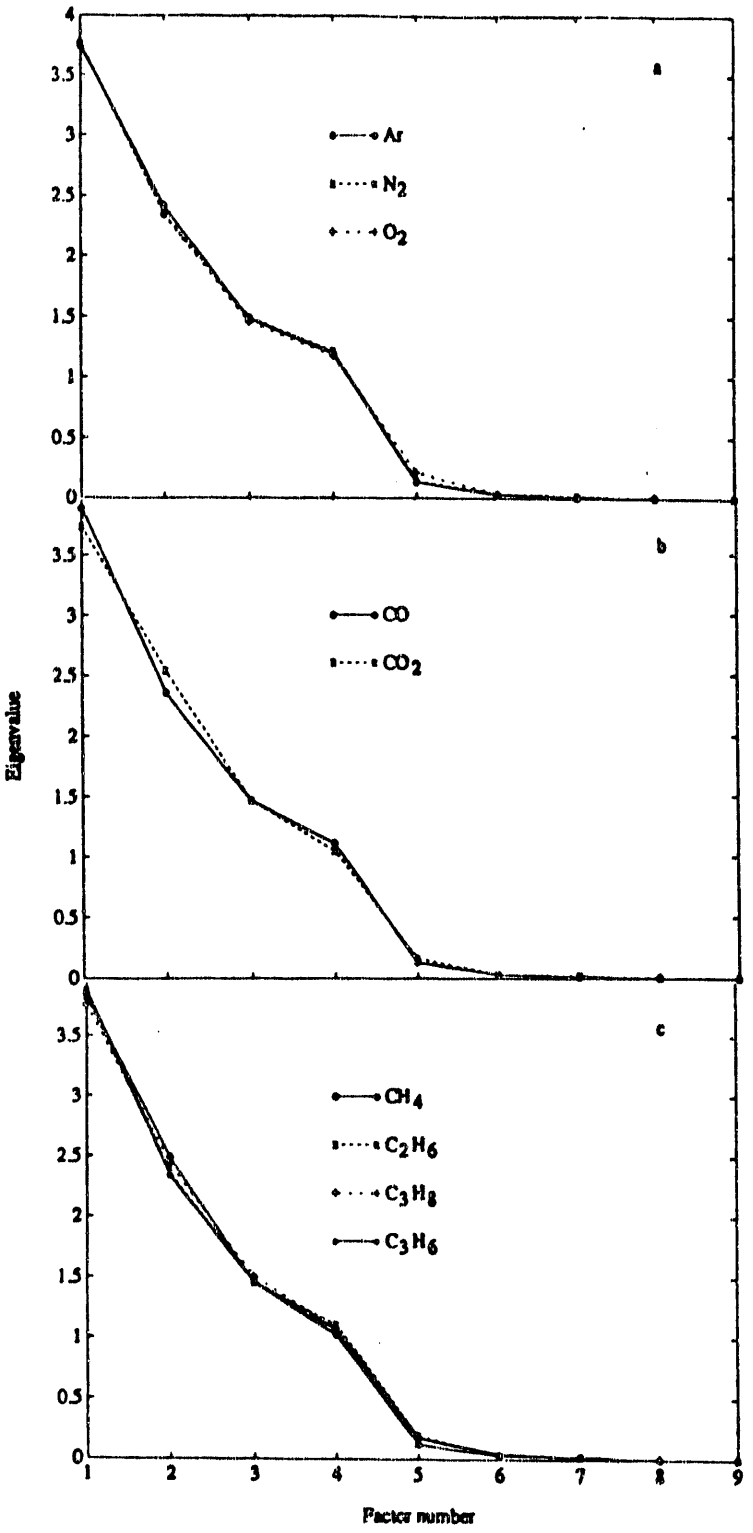

Figure 8.16 Scree plots.

off after factor 5, indicating that the first four factors are most important. The eigenvalues of the four retained factors are greater than one, and those of the remaining factors are much less than one, further supporting this determination. From the plot (Figure 8.17) of cumulative percent vs. factor number of representative gases, e.g. Ar, CO_2, and CH_4, the retained four factors account for above 95% of the variation.

To explore the physical meaning of the factors, the four retained factor loadings are plotted against the variables for methane adsorption in Figure 8.18. Factor 1 has positive correlation with carbon content, and aromaticity, and negative correlation with hydrogen content. These variables all are coal rank dependent, indicating that the physical interpretation of factor 1 is coal rank. The adsorption coefficient of methane has a high positive loading value for this factor, indicating that the methane adsorption capacity is mainly determined by coal rank. This conclusion is in agreement with the results obtained by other researchers (Creedy, 1988; Kim, 1977; Harpalani and Schraufnagel, 1990). Factor 2 has strong contributions from carbon content and sulfur content. This factor may be interpreted as the chemical composition of coal. The adsorption coefficient of methane has weak correlation with this factor. Factor 3 shows strong correlation with hydrogen content and coal density. The adsorption coefficient of methane is very weakly correlated with this factor. Factor 4 is positively correlated with the N_2 surface area and negatively correlated with the ash content. As expected, the adsorption coefficient of methane is positively correlated with this factor. This indicates that methane adsorbs on organic coal surface rather than on inorganic matter. Factor pattern plots of methane adsorption are shown in Figure 8.19.

Correlation coefficients of variables with factor 1, 2, 3, and 4 for all gases used in the adsorption studies are shown in Figures 8.20, 8.21, 8.22, and 8.23 respectively. Except for the gas of C_3H_8, which is mainly determined by the N_2 surface area, the correlation of the gas adsorption coefficients with analytical variables for coal are similar to that of methane as discussed in above.

Plots of the gas adsorption coefficients for representative gases, e.g. Ar, CO_2, and CH_4, versus aromaticity and carbon content (C, wt%) are given in Figures 8.24-8.26. As expected, they show very good agreement with the previous regression and factor analyses. As seen from these plots, Sample No. 3 (Illinois #6 coal) is far from the correlation for all cases and has an unusual behavior. This may be due to the fact that the sample has a very high N_2 surface area (about 4 to 11 times higher than those of other samples).

The strong correlation of the adsorption coefficients of

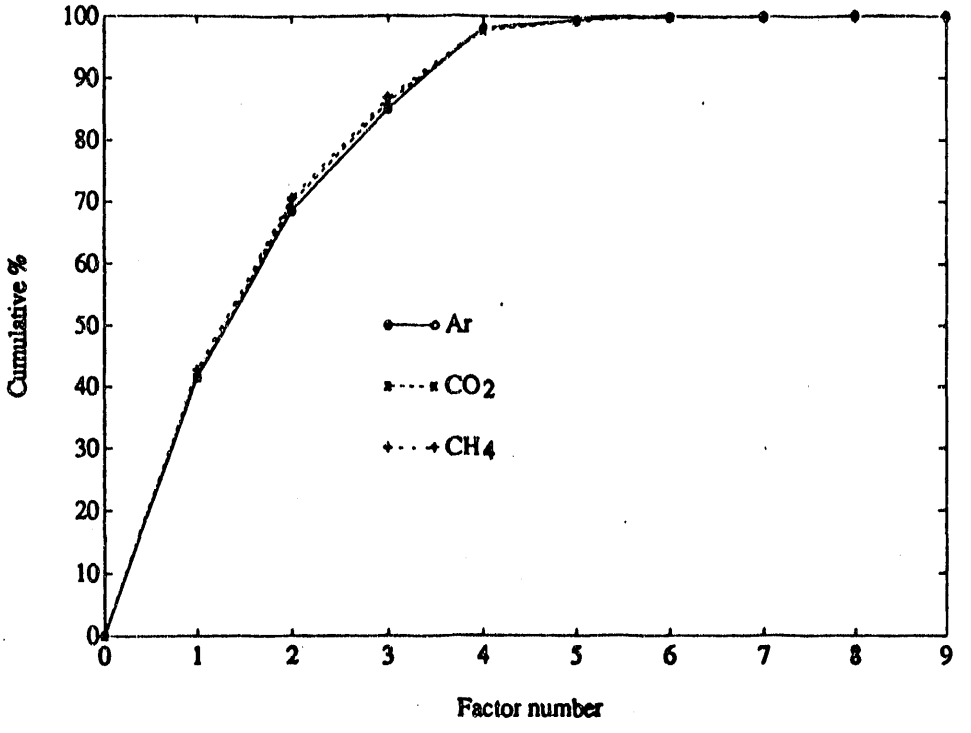

Figure 8.17 Cumulative percent versus factor number.

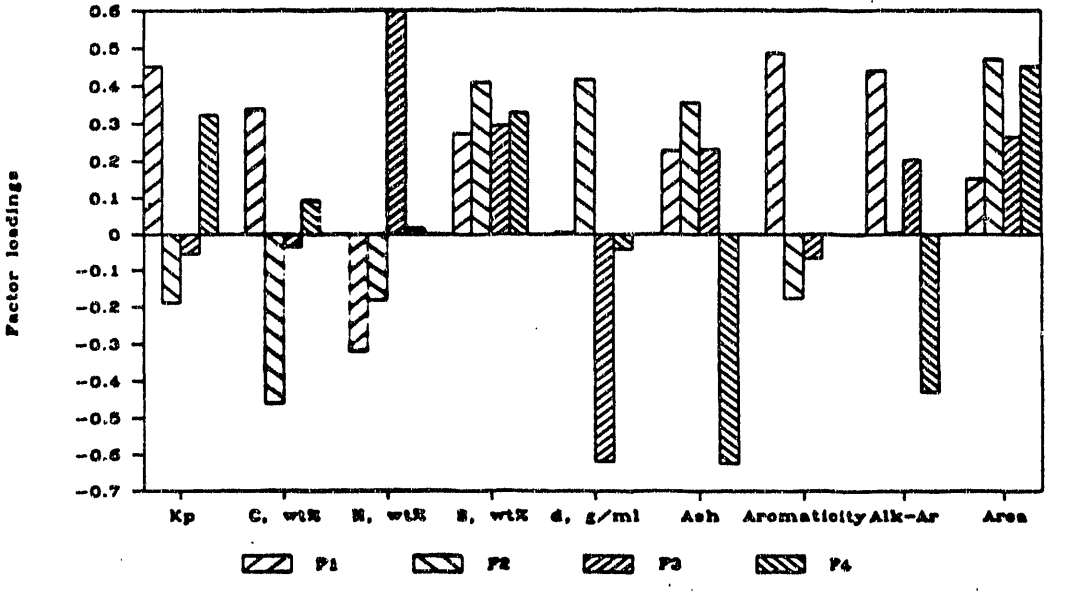

Figure 8.18 Factor loadings versus variables for methane adsorption.

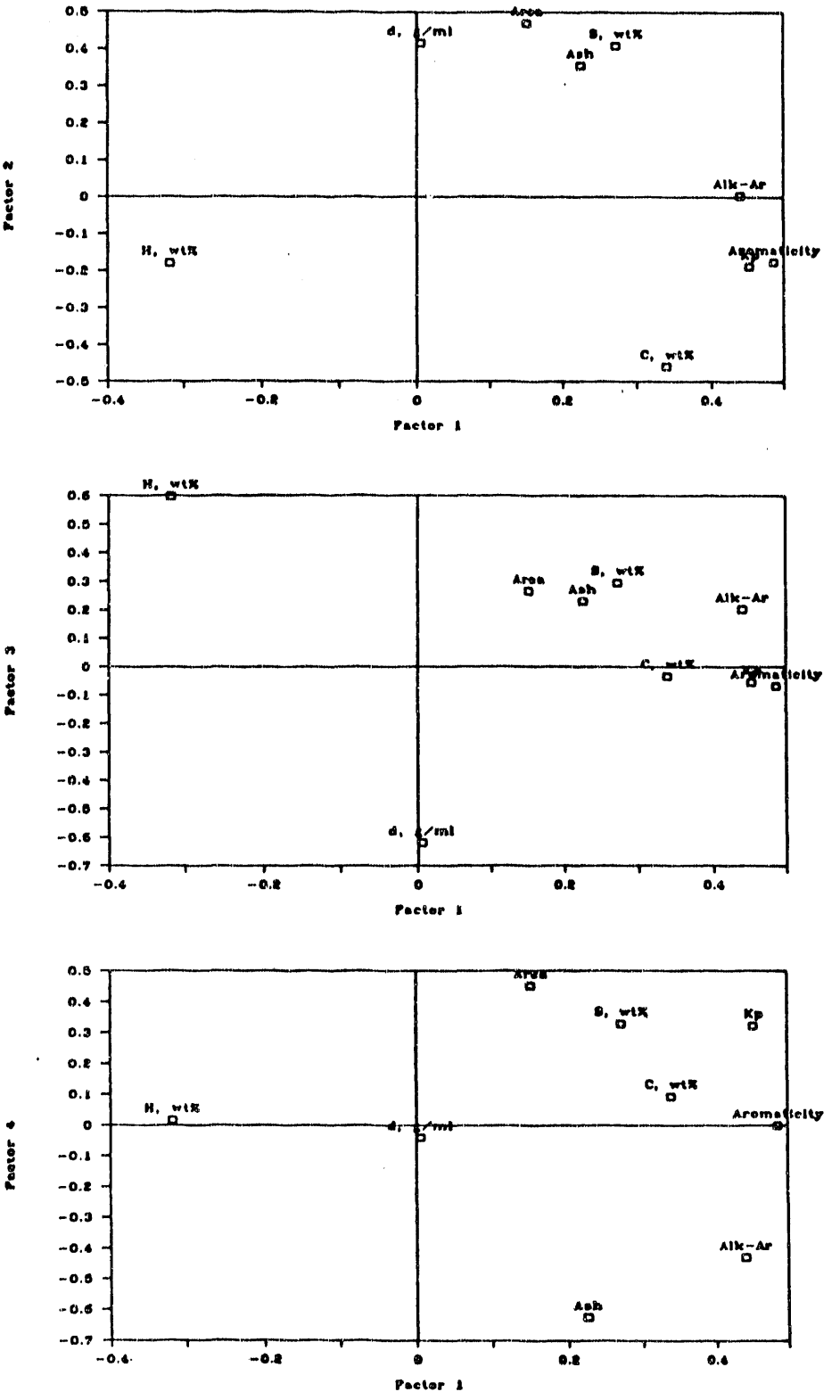

Figure 8.19 Factor pattern plots.

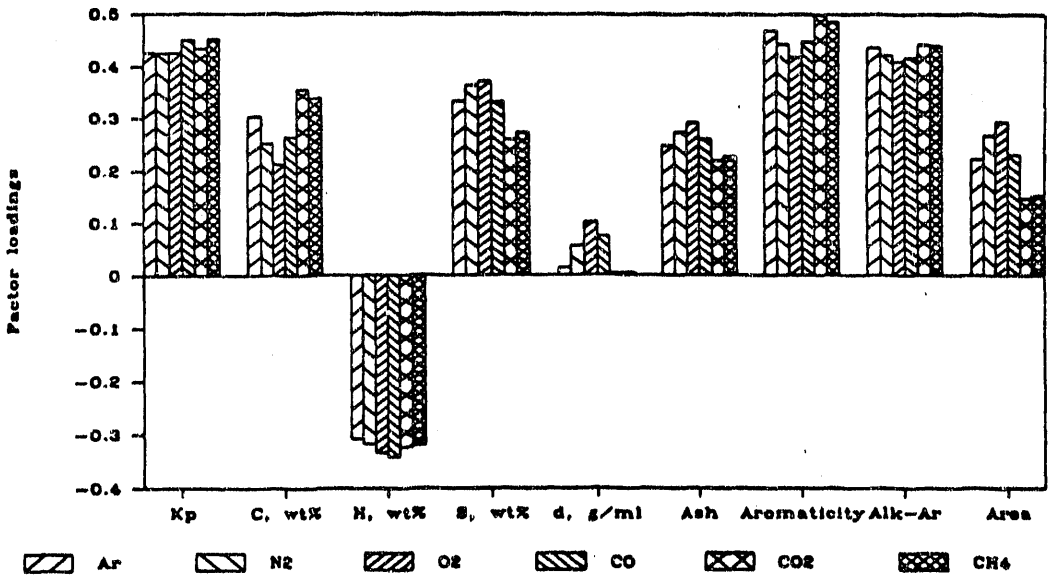

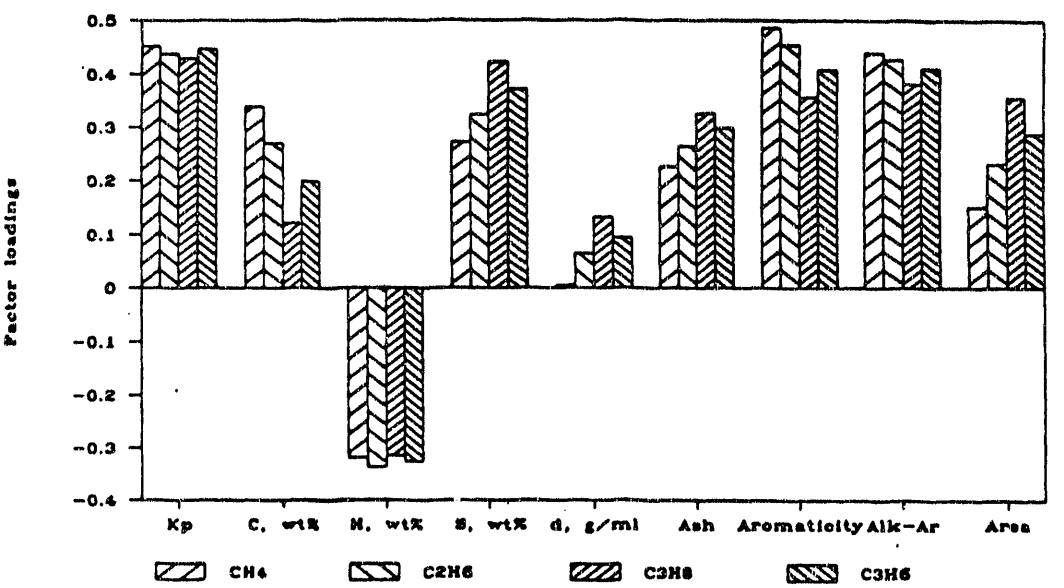

Figure 8.20 First factor loadings versus sample variables.

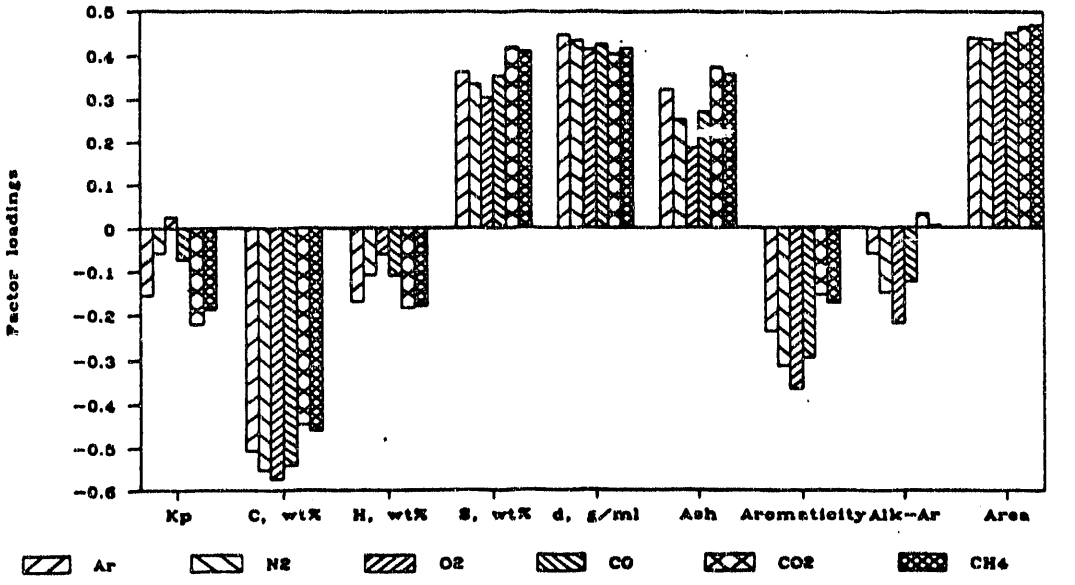

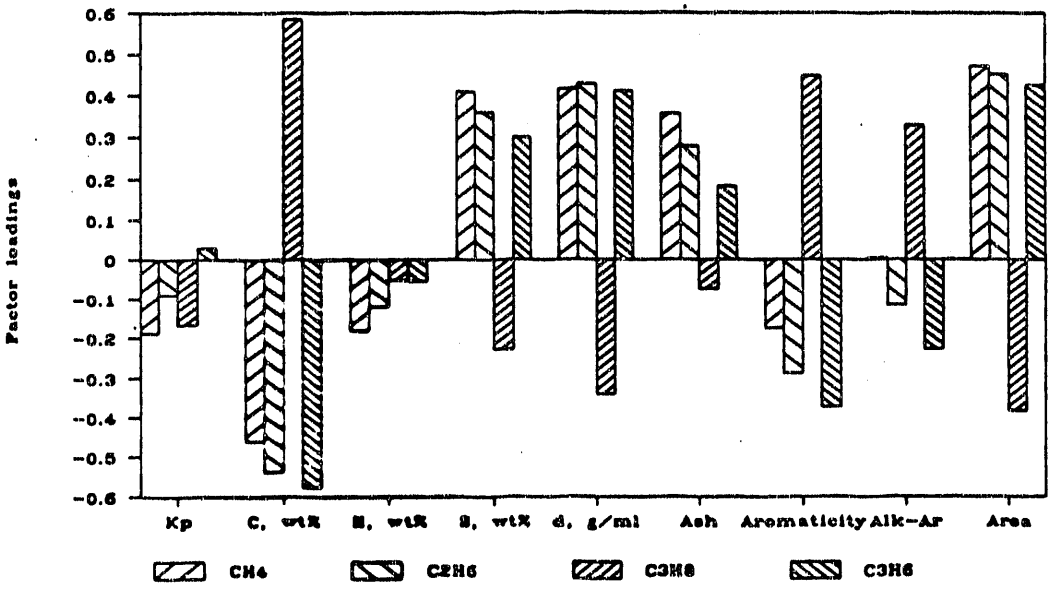

Figure 8.21 Second factor loadings versus sample variables.

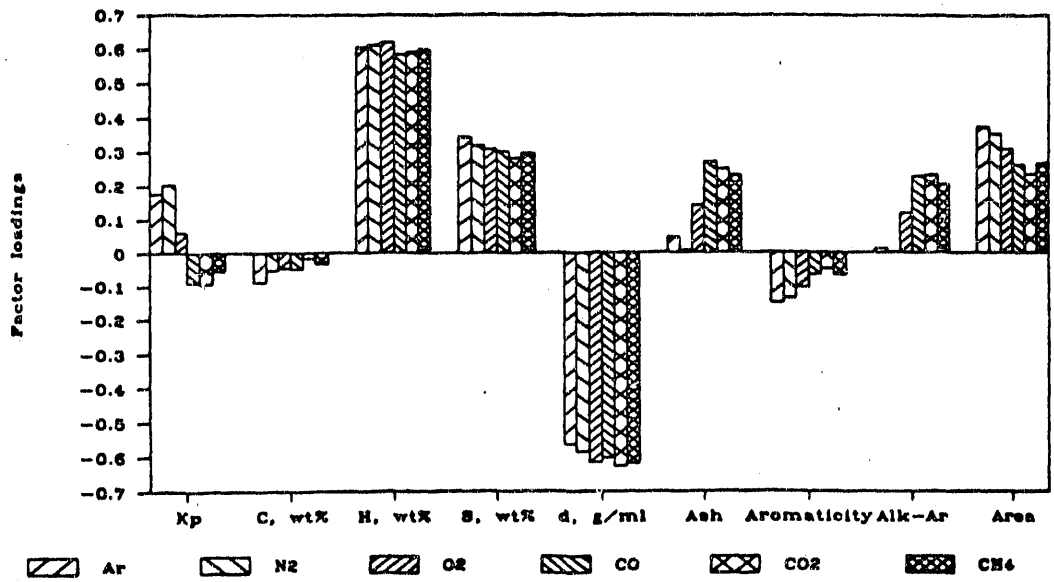

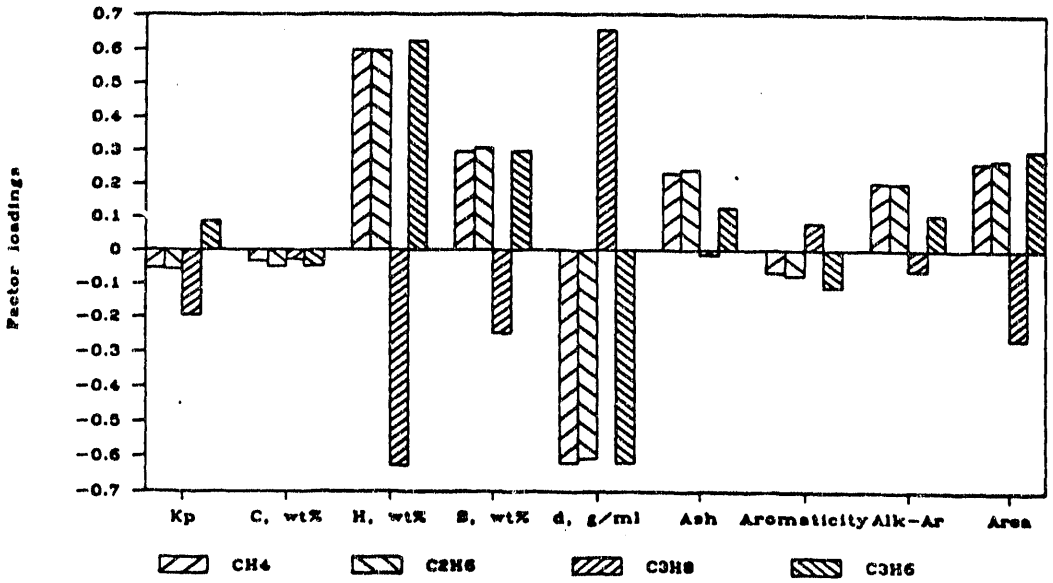

Figure 8.22 Third factor loadings versus sample variables.

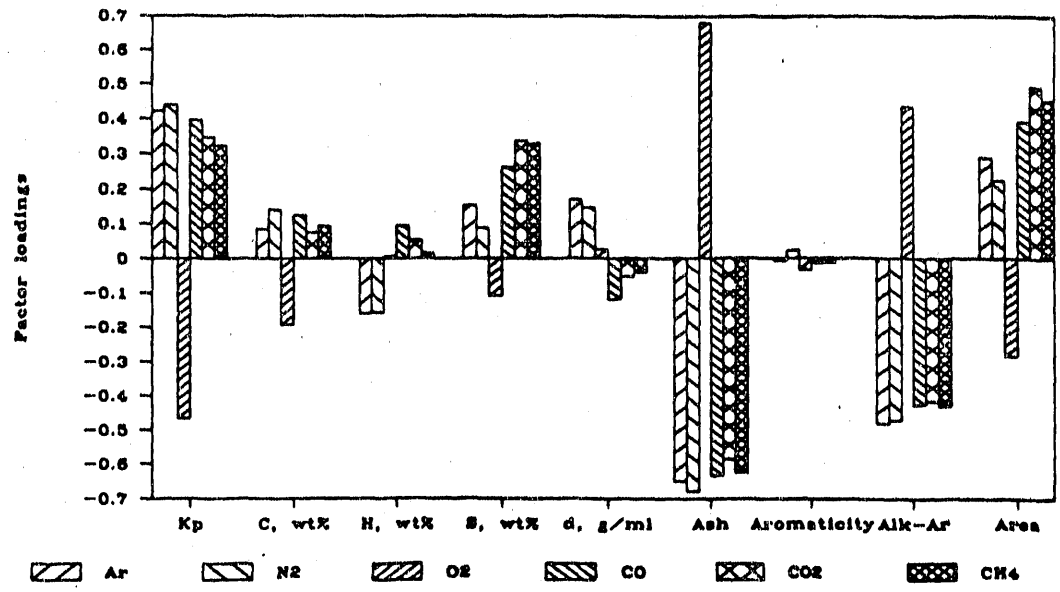

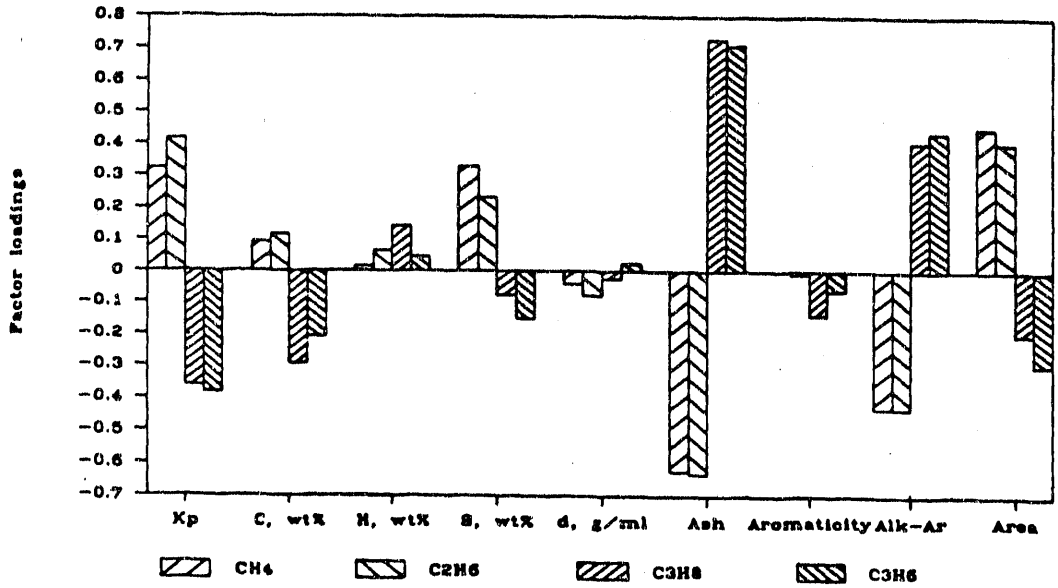

Figure 8.23 Fourth factor loading versus sample variables.

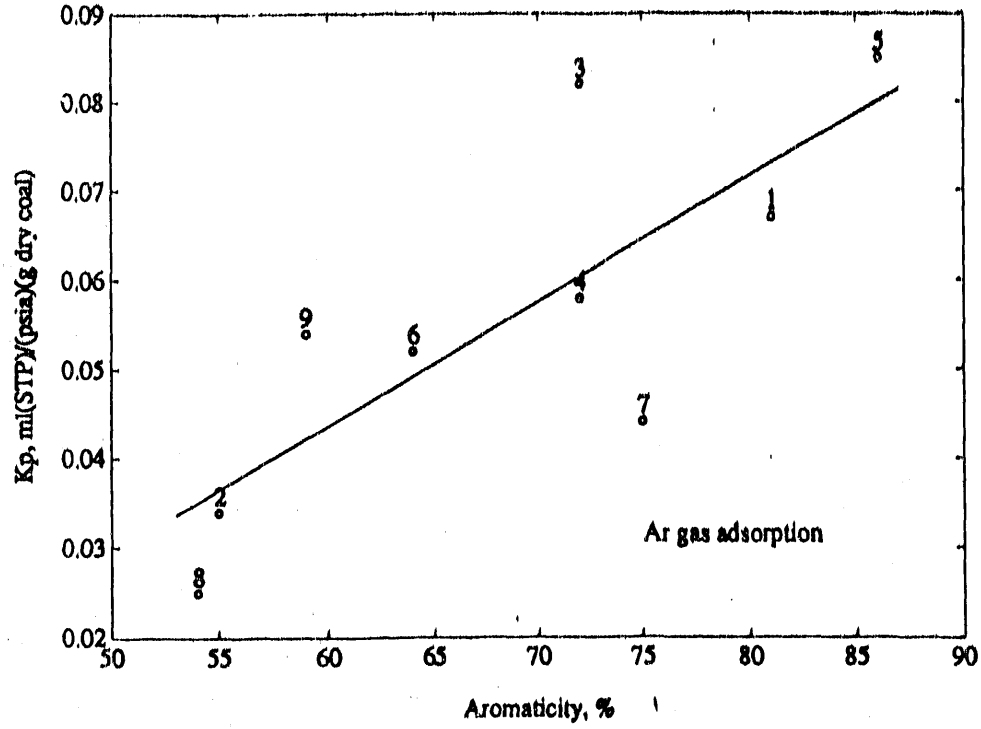

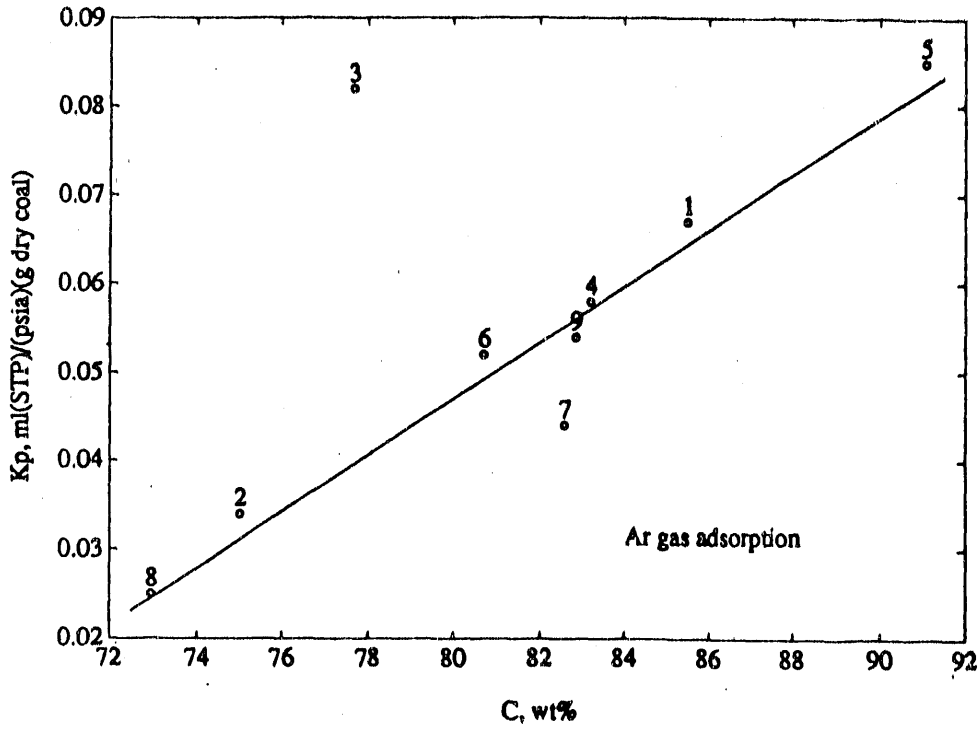

Figure 8.24 Correlation of K_p for argon with aromaticity and carbon content.

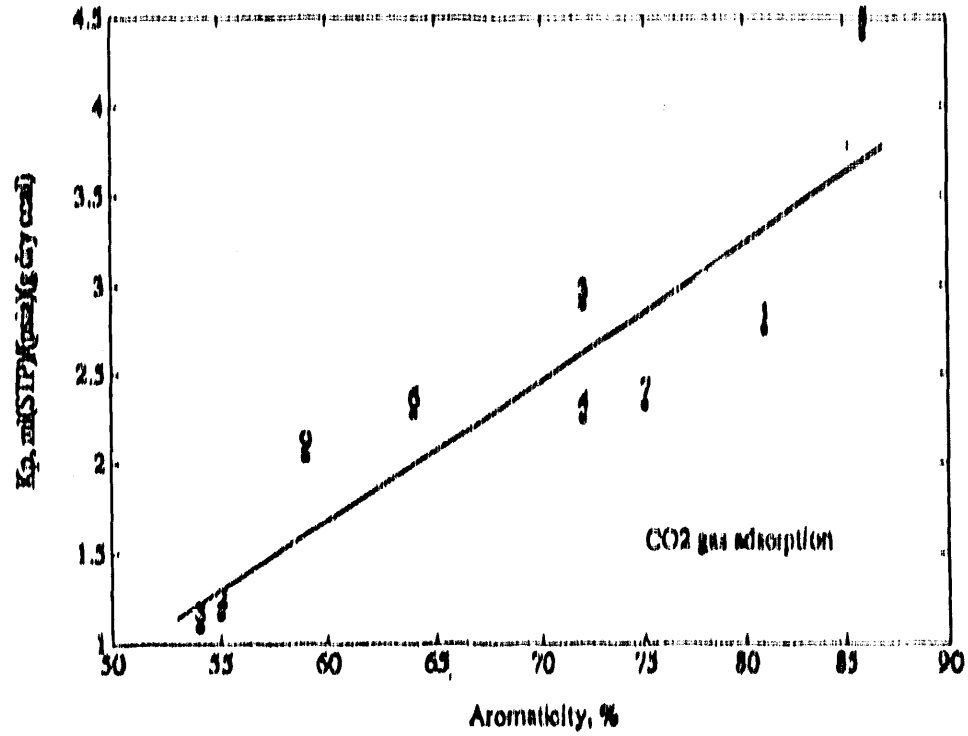

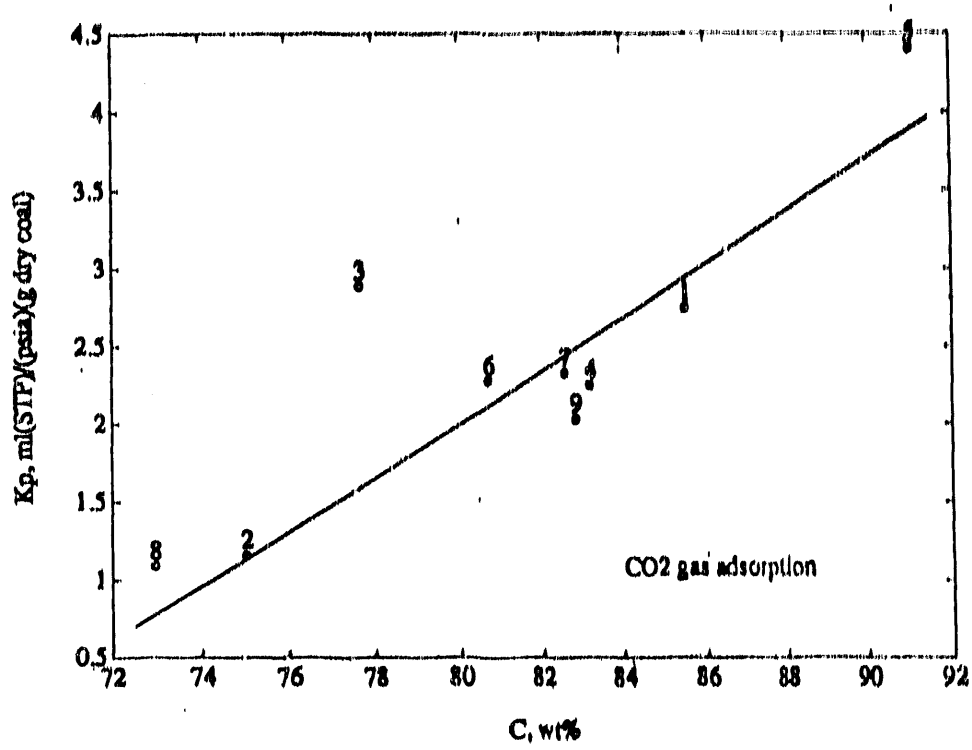

Figure 8.25 Correlation of K_p for carbon dioxide with aromaticity and carbon content.

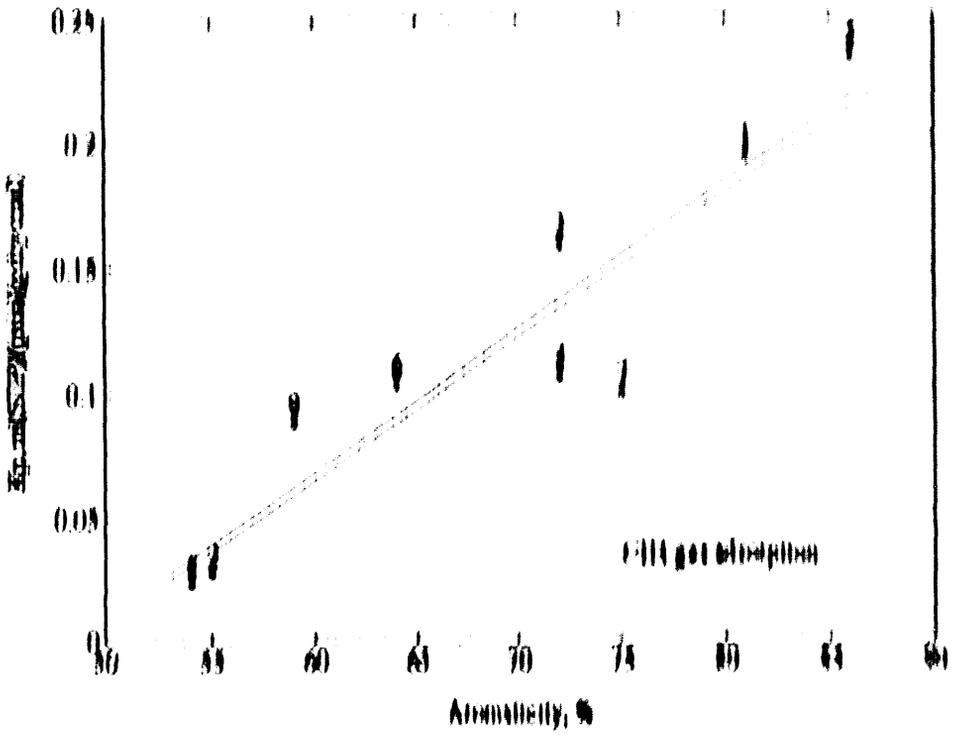

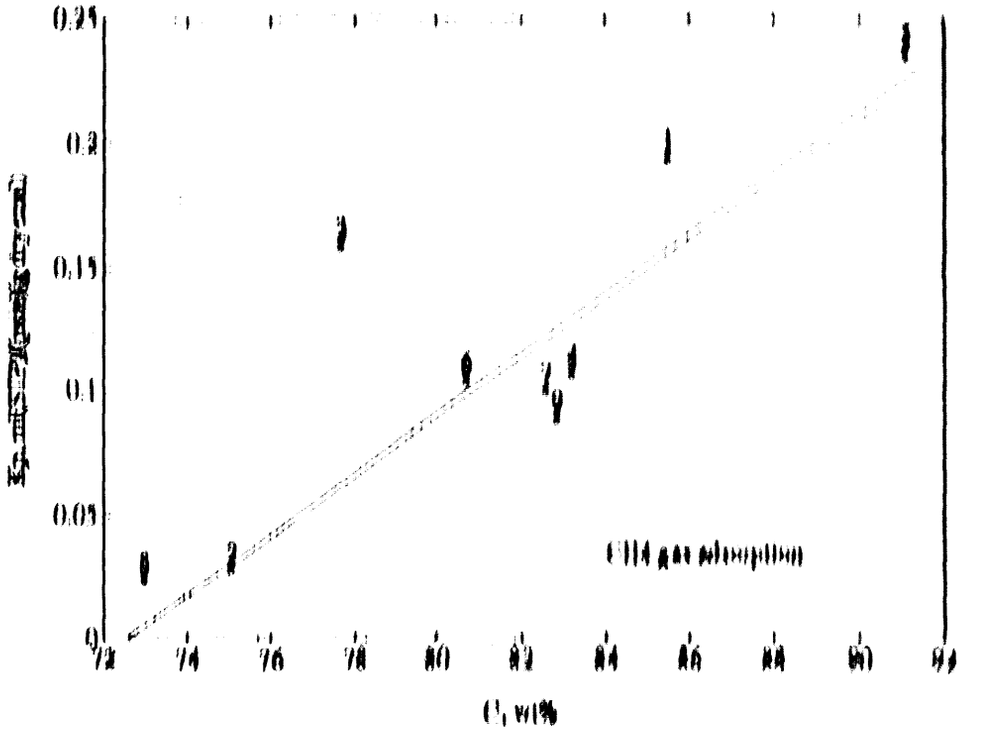

Figure 8.26 Correlation of K_D for methane with aromaticity and carbon content.

[illegible] and carbon dioxide with coal rank and the weak [illegible] with the H_2 surface area requires further [illegible]. It may be an indication that some absorption [illegible] (Rouquerol and Patel, 1983, 1986; [illegible] and Guthmann, 1987; Stacy and Jones, 1986).

[illegible]

[illegible] chromatography provides a simple, quick, and accurate [illegible] thermodynamic constants of gas adsorption on [illegible]. The weighted mean retention time is proven [illegible] a characteristic gas retention variable for the non-[illegible] elution process. Gas adsorption coefficients calculated [illegible] this weighted mean retention time agree with those [illegible] by a static method.

According to the types of the molecular interaction, gas [illegible] is classified into two groups, non-specific [illegible] and specific adsorption. The non-specific [illegible], such as for Ar, N_2, and O_2, is caused by dispersion [illegible] forces only, i.e., the universal intermolecular [illegible] of the van der Waals interaction. Specific [illegible], e.g. CO, CO_2, and C_3H_8, is caused by additional [illegible] intermolecular interactions, such as induced dipole [illegible] forces produced by the polar atoms or π-electrons [illegible] molecule, and/or permanent dipole interaction forces. [illegible] and coefficients of specific gas adsorption are [illegible] than those of the non-specific gas adsorption. [illegible] n-paraffin gases (e.g. methane, ethane, and [illegible]) have no specific electrical interactions with the [illegible] surface, they show unusually high heats and coefficients [illegible] adsorption. This is explained by a very strong affinity [illegible] the coal surface.

[illegible] heats of vaporization with heats of gas [illegible], all molecules except water, have higher heats of [illegible] than the heats of vaporization. This indicates [illegible] molecule-coal surface interactions are stronger than [illegible] intermolecular interactions. In the case of water adsorbed [illegible] medium volatile bituminous Upper Freeport coal, the heat [illegible] is much less than the heat of [illegible]. This shows that the interaction between water [illegible] must be greater than the interactions with the less [illegible] coal surface.

[illegible] strength of the van der Waals interaction increases [illegible] with the number of electrons in the molecule. Water, [illegible], carbon dioxide, and hydrocarbon gases have [illegible] interactions with the coal surface than nitrogen and [illegible], while the noble gas, argon, has a weaker interaction. [illegible] of the n-paraffin gas adsorption on Upper Freeport [illegible] follows an empirical equation

$$-\Delta H_a\ (kJ/mol) = 0.425N_e + 13.68.$$

The effects of specific interactions between the various gases and the different coals are characterized by a specific adsorption ratio (α_s)

$$\alpha_s = \frac{\frac{K_{p,i}}{N_{e,i}}}{\frac{K_{p,N_2}}{N_{e,N_2}}}$$

where N_2, which only involves van der Waals interactions, is taken as a reference gas. Argon and oxygen gas adsorption show no specific adsorption effects. Carbon monoxide has a specific adsorption effect, but no effects from coal rank. Methane shows both of specific adsorption effects on gas and coals, and the effects increases with increasing carbon content, e.g. coal rank. The correlation of the specific adsorption effects with various gases is in the order propene > carbon dioxide > propane > ethane > methane > monoxide. The correlation of the specific adsorption effects with coal properties, such as, carbon content (e.g. coal rank), is in the order propene > propane > ethane > carbon dioxide > methane > monoxide. These two orders are not exactly parallel. However, in the hydrocarbon gas series, they are not only parallel with each other but also parallel with the order of the heats of adsorption. This indicates that the interactions of gas molecules with coal surfaces increases with increasing rank of coal and size of molecule.

The relationship between the parameters in the pseudo-Langmuir isotherm, $(V/V_m) = (bp)/(1+bp)$, and the gas adsorption coefficient is shown to be $(bV_m) = K_p$, and confirmed experimentally.

The correlation of the gas adsorption coefficients with the analytical data of coal, e.g. proximate analyses, ultimate analyses, NMR data, nitrogen surface areas and coal densities was determined by the multivariate analysis. Except for the adsorption coefficient of C_3H_8, which shows a strong dependence on the N_2 surface area, the adsorption coefficients are strongly correlated with the coal rank parameters, such as, carbon content, and aromaticity.

9. A STUDY OF GAS ADSORPTION ON COAL

9.1 Introduction

Gas adsorption capacity of coal at room temperature is one of the most important factors which dominate gas retention in coal. Methane, carbon dioxide, carbon monoxide, and water, together with traces of higher hydrocarbons, are the major gaseous products during coalification (Speight, 1983; Melton and Giardini, 1975; Ruyter, 1982; Monthioux and Landais, 1987). Nitrogen and oxygen comprise 99% of the atmosphere. They may penetrate into a coal seam and become gas components in the coal seam. Therefore, the study of the adsorption of these gases, e.g. methane, carbon dioxide, carbon monoxide, water, nitrogen, and oxygen on coals will provide basic information on both gas content and gas composition in a coal seam. It will also aid in understanding the coal surface chemistry and physics.

Coals contain significant porosity, ranging in size from large cracks of micrometer dimensions to apertures which are even smaller than helium at room temperature. Understanding gas diffusion, especially methane diffusion, in coals during gas adsorption is of importance for a number of reasons. First, it leads to a better understanding of the phenomenon of gas release, especially methane release, from coal during underground mining and methane recovery through drilling a borehole into a coal seam. Second, knowledge of gas diffusion and its temperature dependence further clarifies the nature of porosity in the structure of coal.

Moisture is associated with coal as adsorbed water on coal surfaces and as liquid water in larger cracks and fissures. The adsorbed water retained in the coal can be expected to compete with methane for adsorption sites. All coals contain a certain amount of moisture. Its influence on methane adsorption should therefore be considered in any quantitative estimate of coalbed methane content.

A static adsorption system has been designed and used in the study of the gas adsorption on coals. The dependence of gas diffusion rate on temperatures, particle size effects, the water effect on methane adsorption and the correlation of gas adsorption capacity with coal rank has been investigated in the present study.

9.2 Experimental

9.2.1 Adsorption Apparatus

The low-pressure gas adsorption apparatus shown in Figure 9.1 consists of mass flow monitor, pressure transducer (up to 150 psig), and coal container (e.g. adsorption chamber). The

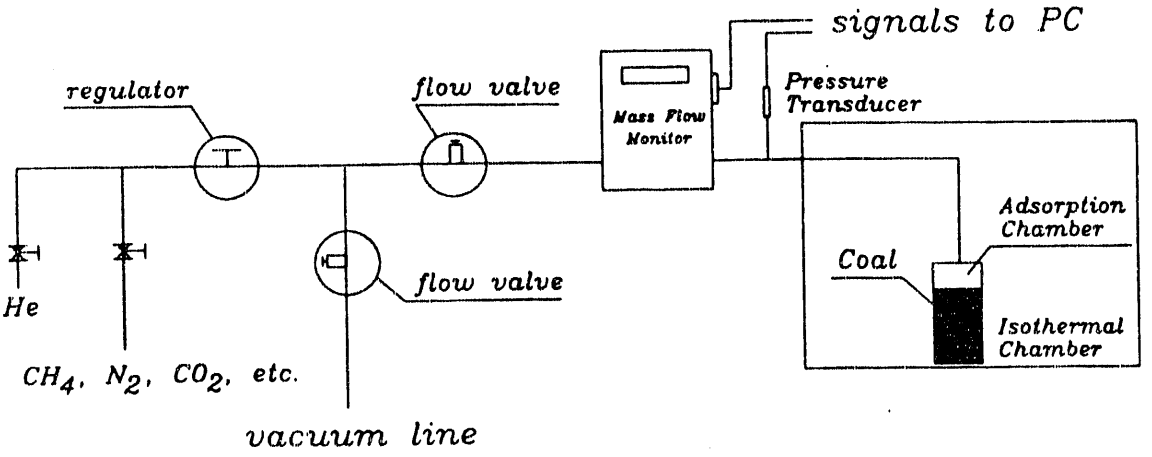

Figure 9.1 Apparatus for low pressure gas adsorption.

gas flow rate and the corresponding pressure in the adsorption chamber are continuously recorded by a PC at 10 Hz. The ranges and sensitivities of the gas flow rate measurements for different gases by the mass flow meter are given in Table 9.1. The details of their connections to the PC data acquisition board are described in Chapter 8. A standard laboratory vacuum line was connected with the system and was capable of evacuating the unit to approximately -8 psig. This vacuum, combined with helium purge, was used to freshen the coal surface. A turbo-air isotherm chamber was used as an isothermal bath. The temperature was maintained within ±0.5 °C.

9.2.2 Sample Preparation and Characteristics

The coals used in this investigation were one high volatile bituminous Utah coal (Sub 3 seam from Castlegate mine) and two Argonne Premium coals, which are Pocahontas #3 low volatile bituminous and Beulah-Zap lignite. The Utah coal was first ground in air. Previous work of Ruppel et al. (1974) has indicated that the effect of room-temperature oxidation on the methane adsorption characteristics of crushed coal is negligible. All samples used in this study were air dried under a vacuum (about -8 psig) at 80 °C for 48 hours and sieved before the tests. About 8 g samples were used for

Table 9.1 Ranges and sensitivities of the mass flow meter*

Gas	Fc ml/(sec)(V)	Range ml/sec	Sensitivity ml/sec
He	0.312	0 - 1.562	0.0122
Ar	0.312	0 - 1.558	0.0122
N2	0.215	0 - 1.074	0.0084
O2	0.215	0 - 1.074	0.0084
CO	0.215	0 - 1.074	0.0084
CO2	0.159	0 - 0.795	0.0062
CH4	0.155	0 - 0.773	0.0061

** ml in the table is converted to STP*

adsorption measurements. After the adsorption chamber was filled with coal sample, the system was purged by helium three times to clean the coal surface. In each purge, the adsorption chamber was pressurized up to about 100 psig. It was maintained at this pressure for about 1 h before evacuation.

Analytical data of the coals, which include proximate analyses, ultimate analyses, NMR parameters, maceral analyses, and densities, are given in Tables 6.1-6.3.

9.2.3 Theory of Measurements

As shown in Figure 9.1, the pressure and flow rate were continuously recorded during the gas adsorption process. Therefore, the moles of an adsorbate gas in the adsorption chamber was determined by accumulation of the gas flow rate

$$n_{in}(t) = \int_0^t f dt \qquad (1)$$

where n_{in} is the moles of adsorbate gas in the adsorption system and f the gas flow rate. The gas entering the system occupies the free space in the adsorption system (including free volume in both the coal container and the tubing line) and adsorbs on the coal surfaces. If the adsorption on the stainless steel wall is negligible, mathematically,

$$n_{in}(t) = n_{free}(t) + W_c n_{ads}(t) \qquad (2)$$

where n_{free} is the moles of the adsorbate gas in the free space of the adsorption system, W_c the mass of coal in the adsorption chamber, and n_{ads} the moles adsorbed on an unit mass

of coal. The P-V-T relationship of the gas in the free volume of the adsorption system is described by the equation (Reid et al., 1987; Smith and Van Ness, 1987)

$$n_{free} = \frac{p(t)\,V_{free}}{z(p,T)\,RT} \tag{3}$$

where V_{free} is the free volume in the adsorption system and z is calculated by

$$z = z^{(0)}(T_r,\ P_r) + \omega z^{(1)}(T_r,\ P_r)\,. \tag{4}$$

where

$$z^{(0)} = 1 + \left(0.083 - \frac{0.422}{T_r^{1.6}}\right)\frac{P_r}{T_r}$$

$$z^{(1)} = \left(0.139 - \frac{0.172}{T_r^{4.2}}\right)\frac{P_r}{T_r} \tag{5}$$

and ω is the acentric factor; T_r is the reduced temperature, the ratio of temperature to the critical temperature (T/T_c); and P_r is the reduced pressure, the ratio of pressure to the critical pressure (P/P_c).

Calibration of the dead volume (or free space) in the adsorption system, V_{free}, was performed using helium gas. If it is assumed that helium gas does not adsorb on the coal surface, n_{ads} is equal to zero in Equation 2 for a calibration run. Therefore,

$$V_{free} = \frac{z(p,T)\,RT}{p(t)}\int_0^t f\,dt \tag{6}$$

$$= Constant$$

at constant temperature. The standard derivation of the measurements of V_{free} is less than 1%.

Substituting the constant V_{free} (obtained by Equation 6) and Equation 1 into Equation 2, we have:

$$n_{ads}(t)\,(mol/g) = \frac{\int_0^t f\,dt - \dfrac{p(t)\,V_{free}}{z(p,T)\,RT}}{W_c}, \tag{7}$$

or

$$V_{ads}(ml(STP)/g) = 22,415n_{ads}. \quad (8)$$

where V_{ads} is the volume of adsorbate at STP per gram of coal.

Theoretically, the equilibrium adsorption volume, $V_{ads,e}$, can be obtained taking $t \rightarrow \infty$. Since the measurement of the flow rate is restricted by the sensitivity of the mass flow monitor (Table 9.1), less than 0.366 ml(STP)/min of the methane gas flow is impossible to detect. In other words, methane adsorption rates less than 0.366 ml(STP)/min were not correctly recorded and had a zero reading. Therefore, the equilibrium adsorption volume, $V_{ads,e}$, obtained by this experimental method is a detected equilibrium adsorption and the value might be much less than a true equilibrium adsorption volume if gas diffusion was the controlling-step at the experimental conditions.

The experimental measurements are schematically shown in Figure 9.2. The lower curve represents the STP gas volume at which the gas flows in to fill the free volume in the adsorption system (calculated by Equation 3 and converted to volume at STP). If the gas is adsorbed by the coal, additional gas will flow in as shown by the upper curve (calculated by Equation 1 and converted to volume at STP). The differences in the two curves gives the total gas volume at STP adsorbed by the coal.

9.3 Results and Discussion

The methane adsorption on Sub 3 coal at four different temperatures is shown in Figure 9.3. The adsorption at long times was taken as the detected equilibrium adsorption, where the flow meter gave zero readings. The higher the temperature, the shorter the time required to approach the detected equilibrium. This indicates that the gas diffusion rate is higher at higher temperatures. The amount of methane adsorbed decreases with increasing temperature for the range 299 K to 352 K. Figure 9.4 gives a clear picture of the dependence of gas diffusion rate on temperature. The points represent the detected equilibrium adsorption values for selected pressures and the curves illustrate the continuous adsorption where the pressure increases continuously. If the adsorption rate (including the gas diffusion process) is much faster than the gas flow rate, the adsorption curve at any time or any pressure gives an equilibrium adsorption. Therefore, the points should be on the curves in this case. However, if the adsorption rate is much slower than the gas flow rate, a diffusion time is required for gas adsorption to approach equilibrium. In this case, the equilibrium adsorption points are far from the continuous adsorption curves.

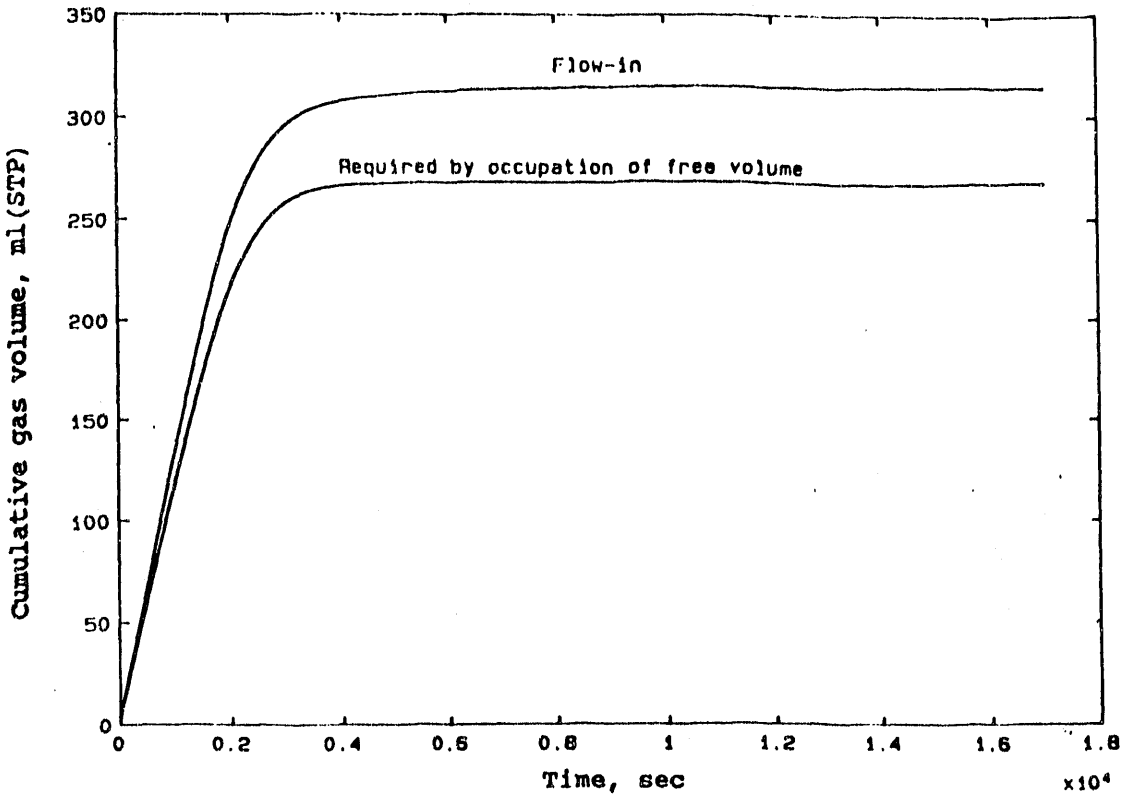

Figure 9.2 Schematic example of gas adsorption curves.

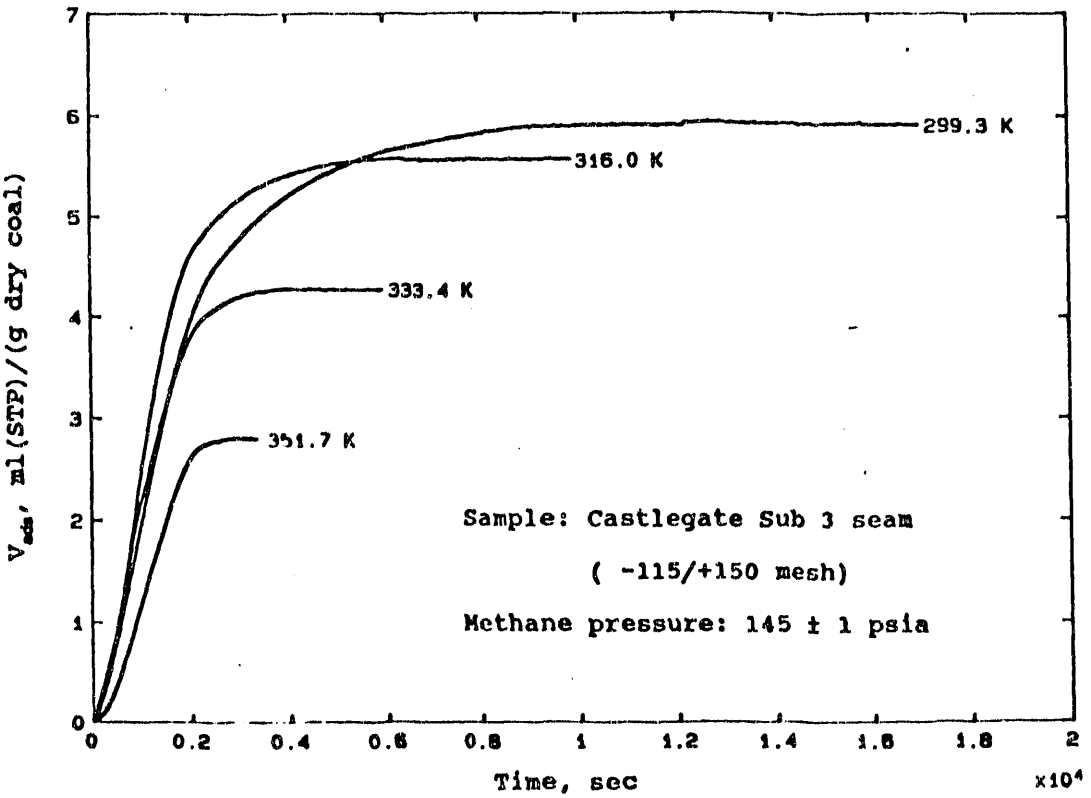

Figure 9.3 Methane adsorption at four temperatures.

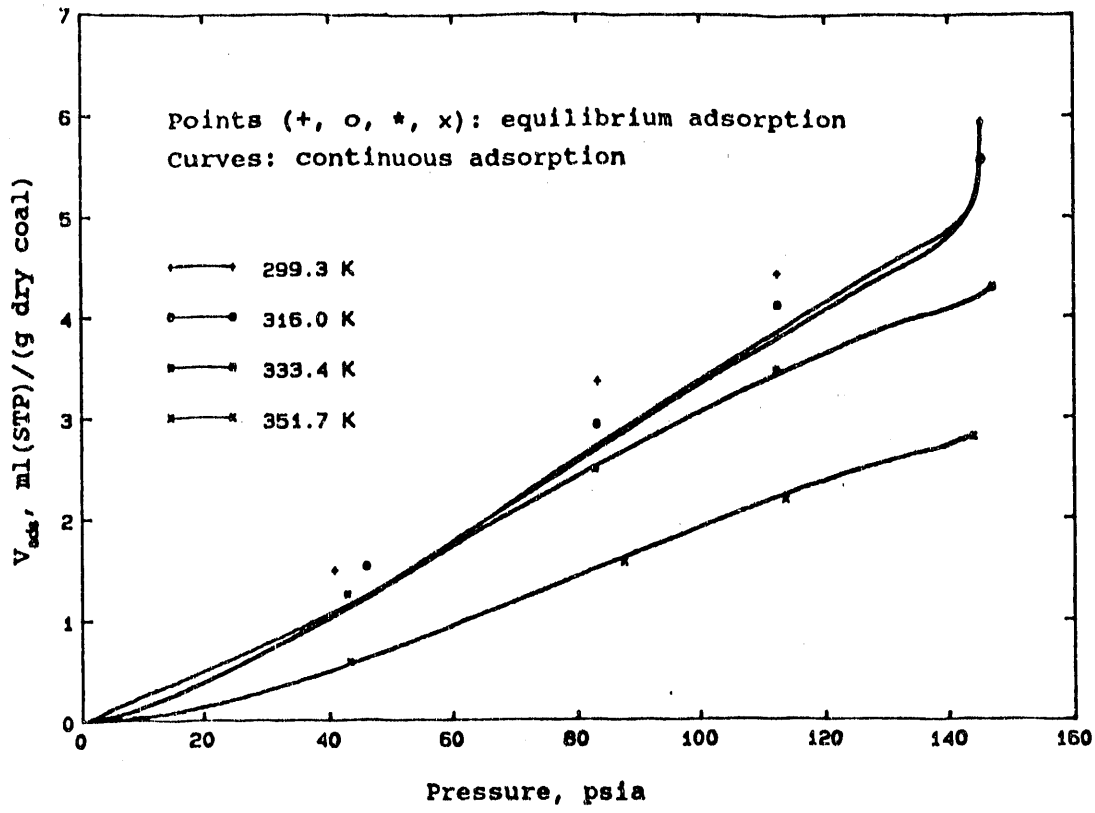

Figure 9.4 Comparison of equilibrium methane adsorption with continuous adsorption.

As observed in the experiments (Figure 9.4), the methane adsorption at high temperatures, 333.4 K (60.3 °C) and 351.7 K (78.6 °C), shows that no diffusion time is required for reaching equilibrium. However, the continuous methane adsorption curves at temperatures 299.3 K (26.2 °C) and 316.0 K (42.9 °C) are far from the equilibrium adsorption points and a long time is required for the gas adsorption to approach equilibrium at a constant pressure. The comparison of the relative methane adsorption rates at two different temperatures for Sub 3 coal is shown in Figure 9.5, further supporting the results on the dependence of gas diffusion on temperature during the gas adsorption.

The gas adsorption at different temperatures for different particle sizes of Sub 3 coal was determined to further evaluate the gas diffusion effect on gas adsorption. The effect of particle size on methane adsorption, together with those of other gases (argon, nitrogen, and carbon dioxide), at room temperature (26.2 °C) and 145 psia is shown in Figure 9.6. The magnitude of the particle size effect at room temperature observed for this system is too high compared to those obtained by other researchers (Ruppel et al., 1974). The reason for this unusually large effect of particle size at this temperature is that the detected equilibrium of this system for larger particle size samples is far from its true

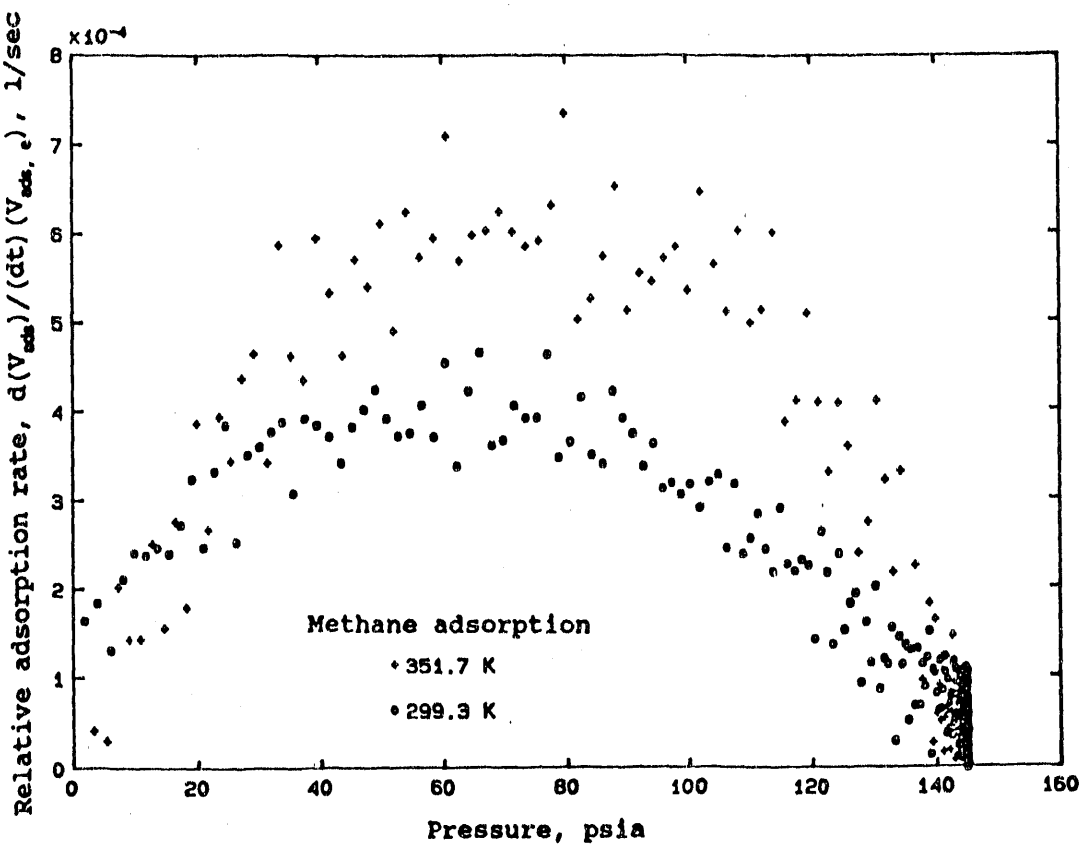

Figure 9.5 Relative rates of methane adsorption at two temperatures.

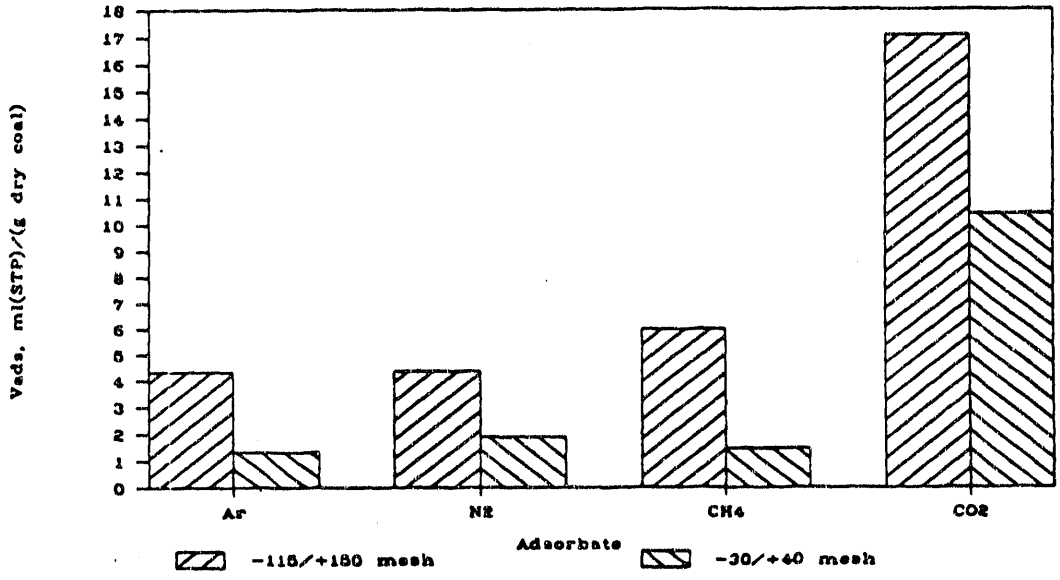

Figure 9.6 Particle size effects on gas adsorption at 299 K.

equilibrium due to very low gas diffusion rates.

As expected, particle size effect decreases with increasing temperature (Figure 9.7). To quantify the particle size effect, a ratio, α_{size}, is defined as

$$\alpha_{size} = \frac{V_{ads\ (-115/+150\ mesh)}}{V_{ads\ (-30/+40\ mesh)}}. \qquad (9)$$

The experimental results and calculated particle size effect ratio are listed in Table 9.2. If it is assumed that the coal particle is spherical and its distribution is normal, i.e., the diameters of particles can be represented by the mean of two openings of sieves, the relationship between external surface area and diameter of particle size can be derived as follows:

$$V\rho = W. \qquad (10)$$

Taking 1 gram coal as the basis for calculation,

$$N_1 V_1 \rho_1 = N_2 V_2 \rho_2 = 1 \qquad (11)$$

where N_i is the number of coal particles for particle size i, V_i the volume of each coal particle for particle size i, ρ_i the coal density of particle size i. Since the densities for different particle sizes are the same (Table 9.3) and

$$V_i = \frac{1}{6}\pi d_i^3, \qquad (12)$$

Equation 11 becomes

$$N_1 d_1^3 = N_2 d_2^3. \qquad (13)$$

For N_i spherical particles,

$$S_{e,i} = N_i \pi d_i^2. \qquad (14)$$

where $S_{e,i}$ is the external surface area per gram of coal for particle size i. Substituting Equation 14 into Equation 13, we have

$$\frac{S_{e,1}}{S_{e,2}} = \frac{d_2}{d_1}. \qquad (15)$$

The mean diameters of -115/+150 mesh and -30/+40 mesh are 0.115 and 0.505 mm respectively. Therefore, the maximum particle size effect ratio for these two samples is 4.39, where the adsorbate gas occupies only external surfaces. The

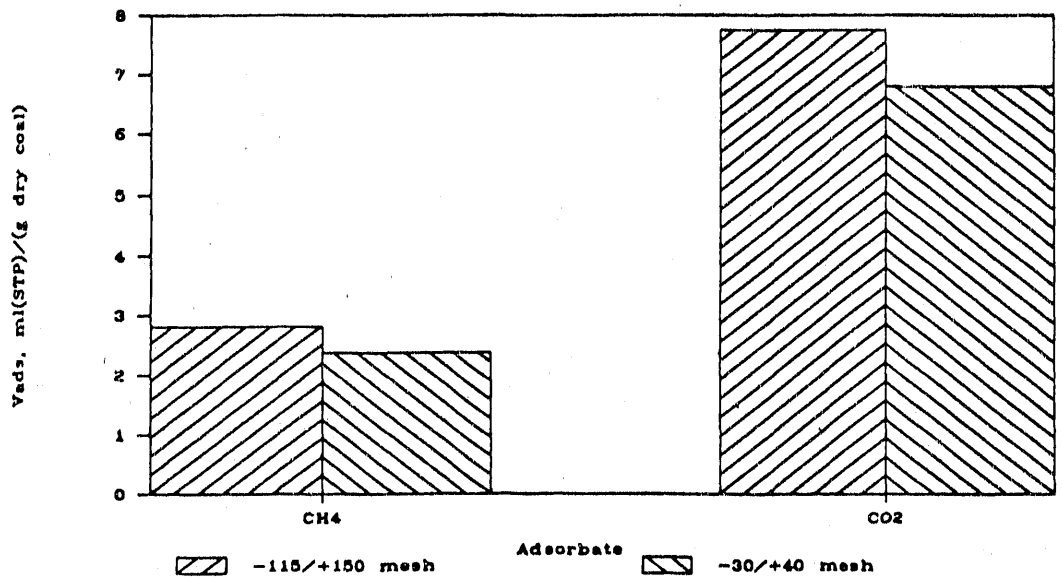

Figure 9.7 Particle size effects on gas adsorption at 352 K.

Table 9.2 Particle size effect on gas adsorption
Sample: Castlegate Sub 3 seam coal, p = 145 psia

	Vads, ml(STD)/(g dry coal)		Particle size effect ratio*
	-115/+150 mesh	-30/+40 mesh	
T = 299.3 K			
Ar	4.33	1.32	3.27
N2	4.34	1.88	2.30
CH4	5.95	1.47	4.05
CO2	17.06	10.37	1.64
T = 351.7 K			
CH4	2.81	2.37	1.18
CO2	7.75	6.79	1.14

** Vads(-115/+150)/Vads(-30/+40)*

Table 9.3 Helium densities of different particle sizes
Sample: Castlegate Sub 3 seam coal

Particle size mesh	He density g/cc
-20/+30	1.3043
-30/+40	1.3049
-80/+100	1.3053
-115/+150	1.3048
-150/+200	1.3051

detected particle size effect ratio of methane adsorption for these two samples is 4.05, which is very close to the theoretically calculated external surface area ratio of 4.39. This indicates that the diffusion rate of methane into coal pores at room temperature is very low. Since CO_2 is a cylindrical molecule and the diameter of the CO_2 molecular cylinder is about half of the diameter of methane (Nebergall et al., 1976), the particle size effect is much smaller than that of methane (Table 9.2), as expected. This indicates that the diffusion rate of molecules at low temperature is strongly dependent on molecular size.

Based on theoretical consideration, the adsorption rate (including the gas diffusion process) is also a function of interaction strength between gas molecules and coal surface. The magnitude of the van der Waals interaction increases with an increase in the number of electrons in the molecule. Therefore, the ratio of the molecule diameter to the number of electrons in the molecule, $\alpha_{d/Ne}$, gives a quantitative estimation of particle size effects on the molecular size and interaction. The smallest diameter of the molecules was estimated by data on atomic radii, bond distances, and bond angles. A plot of the particle size effect ratio versus $\alpha_{d/Ne}$ is shown in Figure 9.8. As expected,

$$\lim_{\alpha_{d/Ne}\to 0} \alpha_{size} = 1$$
$$\lim_{\alpha_{d/Ne}\to \infty} \alpha_{size} = 4.39 \qquad (16)$$

At high temperature (78.6 °C), the particle size effect ratios for both methane and carbon dioxide are very close to 1, i.e., no effect of particle size. This indicates that gas diffusion is very fast at high temperature and the contribution of the

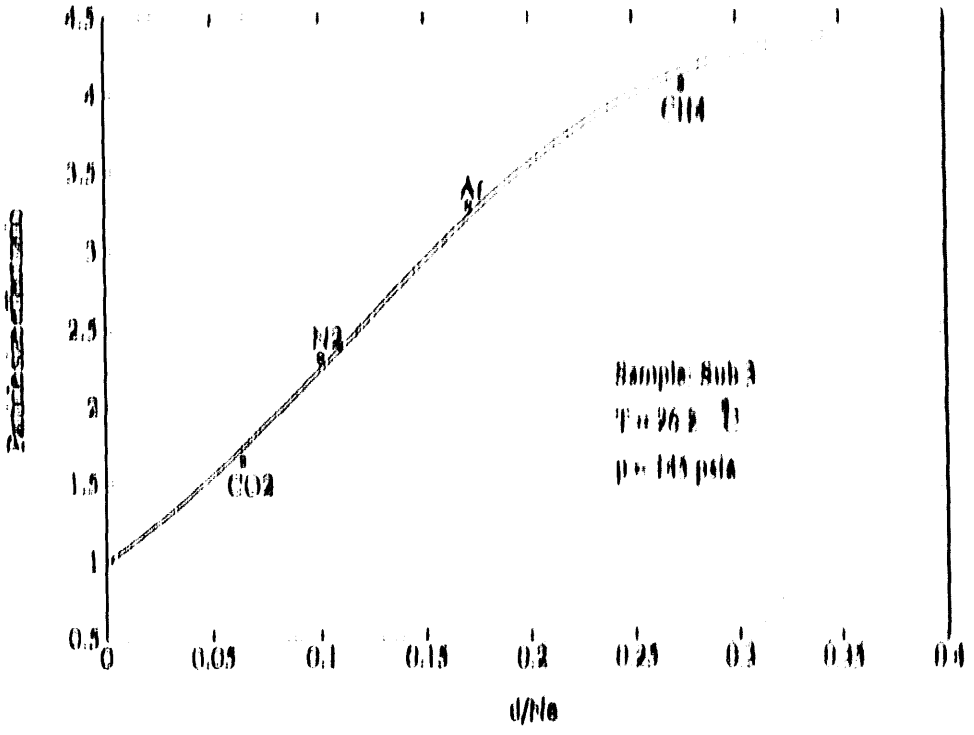

Figure 9.8 Correlation of particle size effect ratio with molecular parameters.

coal surface is mainly from the internal surface of pores.

Since the critical temperature (T_c) of methane is 190.6 K (= 82.6 °C)[8], methane gas is neither condensed in coal pores nor adsorbed in multilayers on coal surfaces at coalbed temperatures (a coal seam temperature is normally above 0 °C). Therefore, most of the methane remains in a coalbed as a monomolecular layer adsorbed on the internal surfaces of the coal matrix with a small amount of methane as free gas stored in large pores and cleats under pressure. When methane adsorbs on a porous coal, it follows a pseudo-Langmuir isotherm (type 1)

$$\frac{V_{ads}}{V_m} = \frac{bp}{1 + bp} \qquad (17)$$

where b is a fitting constant, V_{ads} the volume (normally corrected to STP) of adsorbate, and V_m the volume of adsorbate equivalent to a monolayer (Gregg and Sing, 1982; Grundy, 1988). The term pseudo-Langmuir isotherm used here is due to the fact that the gas adsorption on the coal surface does not physically fit the requirements of the Langmuir isotherm model but is mathematically matched with the Langmuir isotherm equation. In fact, the adsorption sites on the coal surface

are not energetically uniform and the interactions of adsorbate-adsorbate cannot be ignored at high pressures.

If 1 >> bp for the low pressure range of methane adsorption, i.e., 1 + bp ≈ 1, Equation 17 becomes

$$V_{ads} = (bV_m)p \qquad (18)$$

where (bV_m) is a constant. If K_p, the gas adsorption equilibrium constant (V_{ads}/p), is used to represent the constant (bV_m), we have

$$V_{ads} = K_p p. \qquad (19)$$

Methane adsorption isotherms of Sub 3 coal at different temperatures are shown in Figure 9.8. A linear relationship between V_{ads} and p was found to be the best fit.

Based on the adsorption isotherms at different temperatures, the isosteric heat of methane adsorption on Sub 3 coal can be estimated by application of the Clausius-Clapeyron equation:

$$\left(\frac{\partial \ln p}{\partial T}\right)_{V_{ads}} = -\frac{\Delta H}{RT^2}. \qquad (20)$$

Taking the logarithm of each side in Equation 19, we have

$$\ln V_{ads} = \ln K_p + \ln p. \qquad (21)$$

By partial differentiation of Equation 21 with respect to temperature at constant V_{ads}:

$$\left(\frac{\partial \ln K_p}{\partial T}\right)_{V_{ads}} = -\left(\frac{\partial \ln p}{\partial T}\right)_{V_{ads}} \qquad (22)$$

since

$$\left(\frac{\partial \ln V_{ads}}{\partial T}\right)_{V_{ads}} = 0. \qquad (23)$$

Substituting Equation 20 into Equation 22 gives

$$\left(\frac{\partial \ln K_p}{\partial T}\right)_{V_{ads}} = \frac{\Delta H}{RT^2}. \qquad (24)$$

If it is assumed that the isosteric heat Q_{ads} (ΔH_a) is independent of temperature in the range of measurements, integration of Equation 24 gives

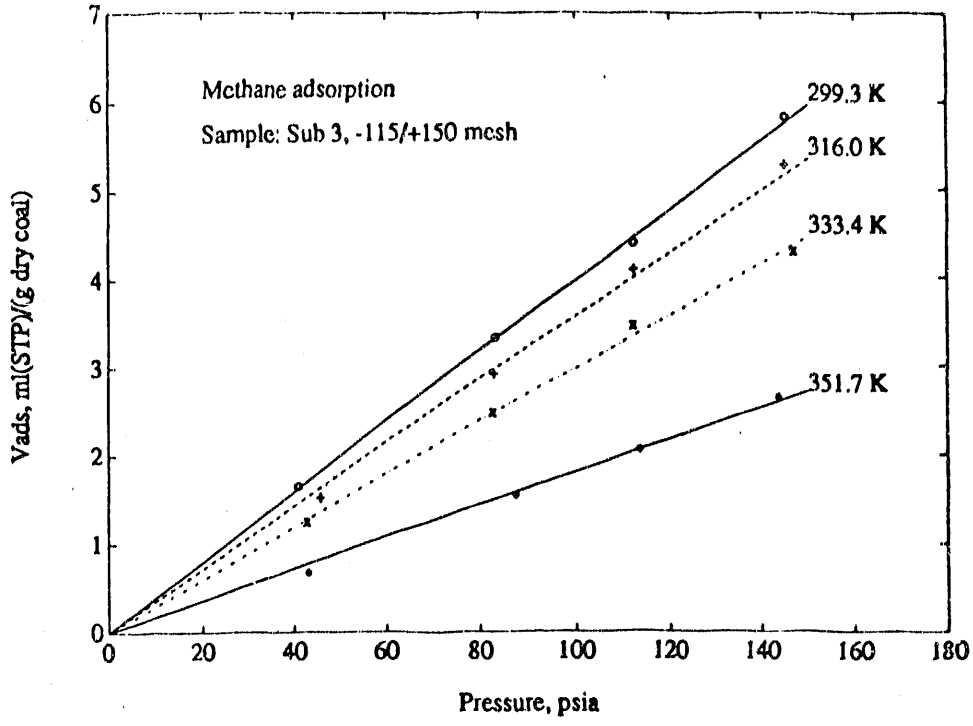

Figure 9.9 Methane adsorption isotherms.

$$lnK_p = -\frac{\Delta H}{RT} + Constant. \qquad (25)$$

A plot of lnK_p versus 1/T is shown in Figure 9.10. The point at 0 °C was measured by gas chromatography. Except for K_p at 26.2 °C, which is considerably lower than expected, the plot gives very good linearity with a correlation coefficient of 0.998. The reason for the low value of K_p at 26.2 °C is that the detected equilibrium is far from the true equilibrium due to the gas diffusion effect at this temperature. The average isosteric heat of methane adsorption in the coverage range of 0 to 3 ml(STP)/(g dry coal) is 14.9 kJ/mol. If the pseudo-Langmuir isotherm is used to fit (p, V_{ads}) data mathematically, the isosteric heat of methane adsorption was found to be a function of coverage. The correlation of the isosteric heat of methane adsorption with the coverage is shown in Figure 9.11. The average isosteric heat from the pseudo-Langmuir isotherm model is 13.5 kJ/mol, which is quite close to that obtained by the linear isotherm model. Obviously, the estimation of isosteric heat of gas adsorption depends on the use of the gas adsorption isotherm models.

Water adsorbed on coal was observed to be a prohibitor

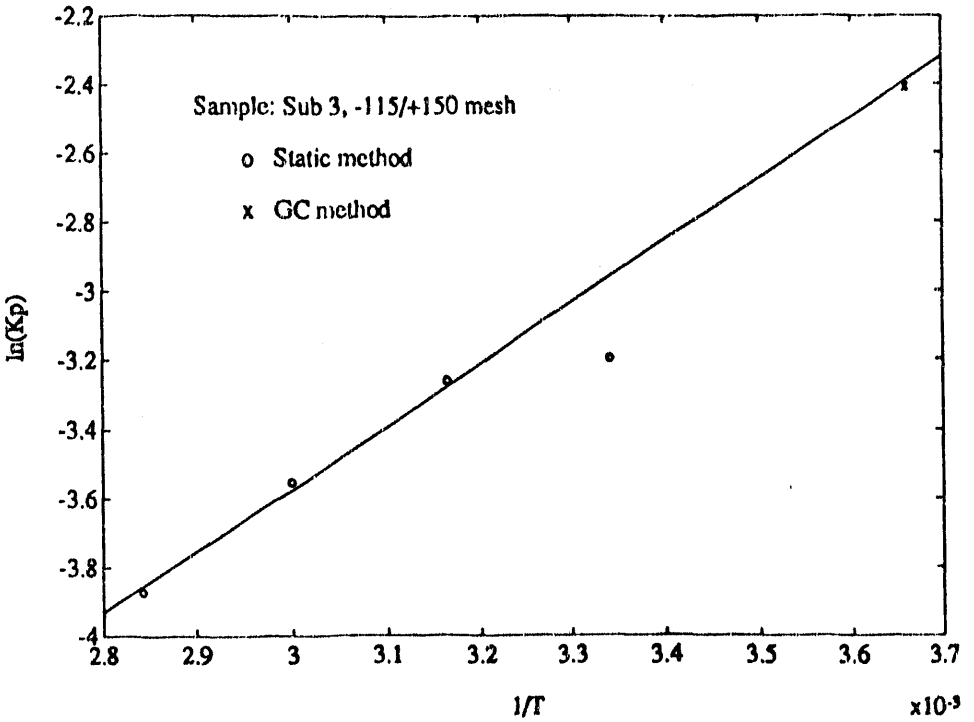

Figure 9.10 Plot of $\ln(K_p)$ versus 1/T.

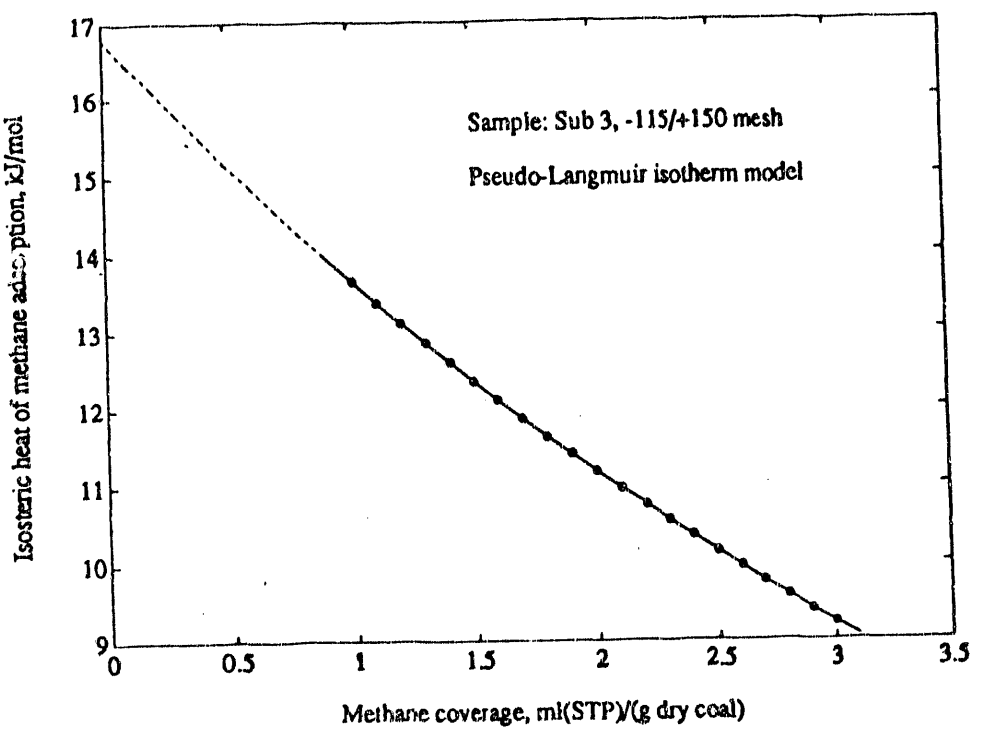

Figure 9.11 Isosteric heat of adsorption of methane versus surface coverage.

for methane adsorption (Creedy, 1988; Joubert, 1974, 1973). Sub 3 coal with moisture content 2.53 wt% was used to evaluate the water effect on methane adsorption. The results are given in Table 9.4. The data indicate that there is a strong water effect on methane adsorption. For 2.53 wt% water content, methane adsorption capacity of the coal is reduced by almost half. The water effect on methane adsorption will be discussed in detail in Chapter 12.

Different gases adsorbed on Sub 3 coal were tested and the results are shown in Figure 9.12. The adsorption capacities of the different gases are in the order of CO_2 > CH_4 > CO ~ N_2 ~ Ar ~ O_2. The results are in agreement with those obtained by the GC method (Chapter 8).

Adsorption of representative gases, Ar (elementary gas), CH_4 (hydrocarbon gas), and CO_2, on three coals with different rank (low volatile bituminous Pocahontas #3, high volatile bituminous Sub 3, and lignite Beulah-Zap) were tested and the results are shown in Figure 9.13. The correlation of the adsorption capacities with the carbon content, a parameter for rank of coal, is shown in Figure 9.14. The results suggest that methane adsorption has a strong correlation with the rank of coal while argon adsorption shows a weak correlation. These conclusions agree with those obtained using the GC method (Chapter 8).

9.4 Conclusions

Diffusion of gas components is important for gas adsorption at lower temperatures (< 50 °C). This was concluded by examining the correlation of continuous adsorption with the detected equilibrium adsorption and the adsorption characteristics of coal of different particle sizes.

Smaller molecules such as argon, nitrogen, and carbon dioxide have access to the internal surface of coal in diffusion-dominated regimes, while methane does not access the most internal surfaces of coal. Affinity of gas molecules for coal affects both the adsorption capacities and diffusion characteristics. The adsorption capacities of the different gases are in the order of CO_2 > CH_4 > CO ~ N_2 ~ Ar ~ O_2.

In the low pressure range, the methane adsorption isotherm becomes linear since $1 >> bp$, i.e., $(1+bp) \approx 1$ in the pseudo-Langmuir isotherm. The isosteric heat of methane adsorption on Castlegate Sub 3 seam coal was 14.9 kJ/mol.

Water adsorbed on coal inhibits methane adsorption. The methane adsorption capacity of Castlegate Sub 3 seam coal with 2.53 wt% moisture was only 59% of that of the dry coal.

Table 9.4 Water effect on methane adsorption
Sample: Castlegate Sub 3 seam coal

Water content, wt%		Vads, ml(STP)/g*
0.00		5.89
0.00		6.01
	Mean:	*5.95*
	Std:	*0.06*
2.53		3.42
2.53		3.58
	Mean:	*3.50*
	Std:	*0.08*
	*Ratio**:*	*0.59*

** Dry basis*
*** (Vads with 2.53 wt% water)/(Vads with 0.00 wt% water)*

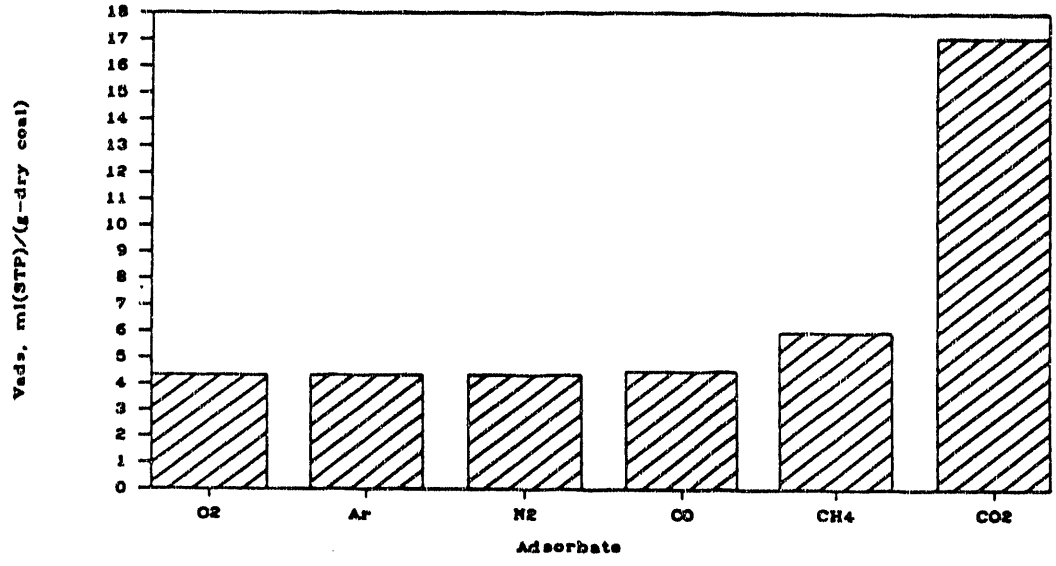

Figure 9.12 Adsorption of gases on Castlegate Sub 3 seam coal.

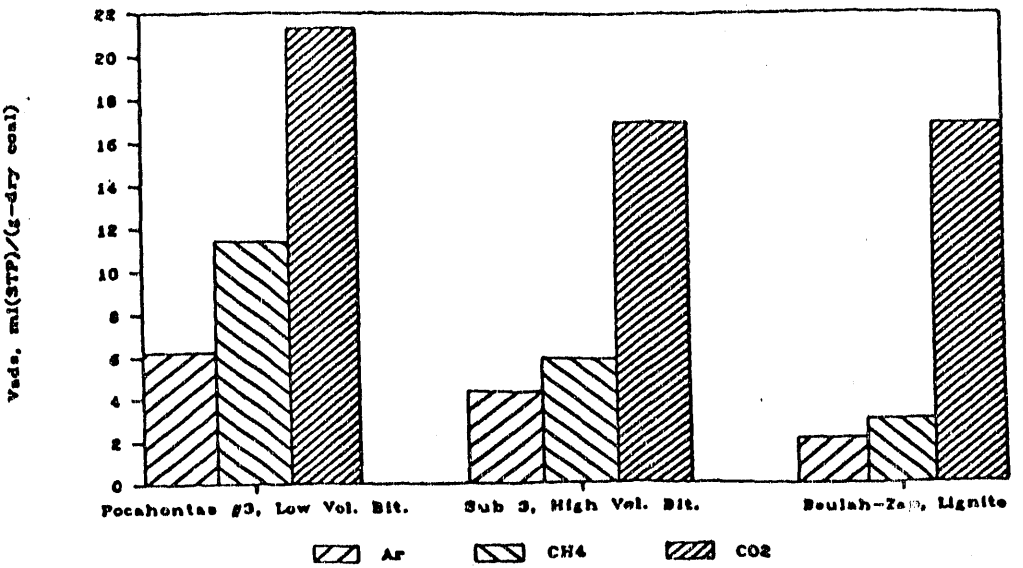

Figure 9.13 Effect of coal rank on gas adsorption.

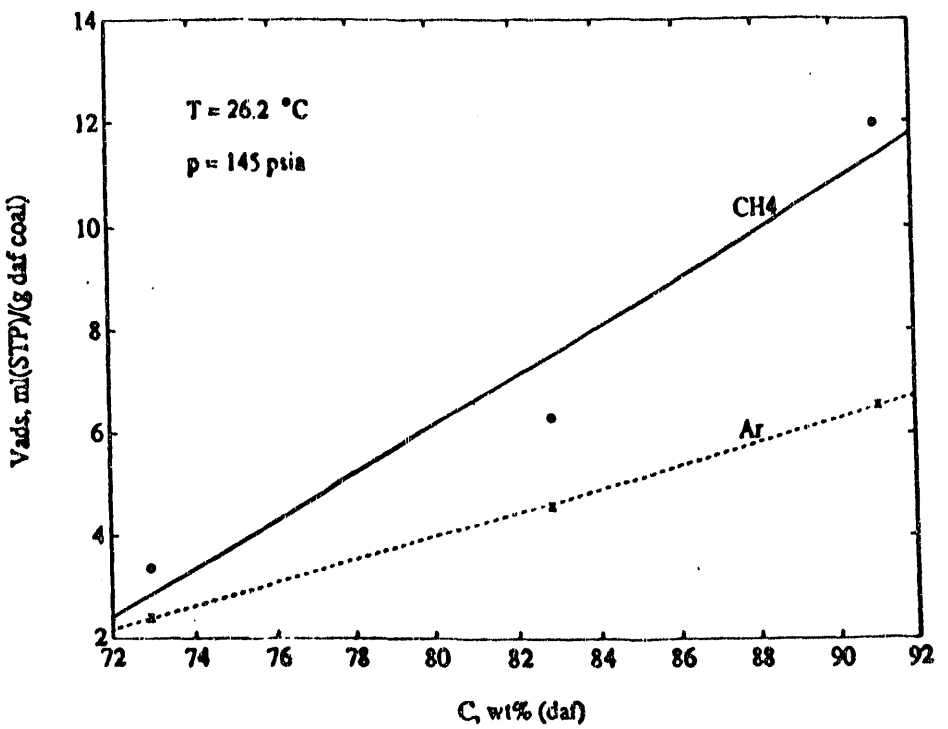

Figure 9.14 Correlation of gas adsorption with carbon content.

10. DETERMINATION OF THE SURFACE AREA OF SUB 3 UTAH COAL BY CONTINUOUS CO_2 DESORPTION AT 298 K

10.1 Introduction

To determine the surface area of coal by gas and vapor adsorption, one must find the monolayer capacity, i.e., the number of probe molecules which cover the surface with a complete monolayer. The value of the monolayer capacity is conventionally determined by one of three equations, which are widely used in surface area measurements, e.g., 1. Brunauer-Emmett-Teller (BET) equation (Brunauer et al., 1938); 2. Dubinin-Polanyi (DP) equation (Dubinin, 1966, 1958, 1960; Polanyi, 1932; Marsh and Siemieniewska, 1965); and 3. Langmuir equation (Gregg and Sing, 1982). The equation to use in determining the value of complete monolayer adsorption is dependent on the molecular probe used and the adsorption measurement conditions. The surface area is then calculated from the monolayer adsorption value multiplied by the area occupied by a single adsorbed molecule.

Coal is a porous material and contains significant porosity, ranging in size from large cracks of micrometer dimensions to apertures which are close to and even less than helium at room temperature. A schematic representation of the coal surface is shown in Figure 10.1. It is obvious that the

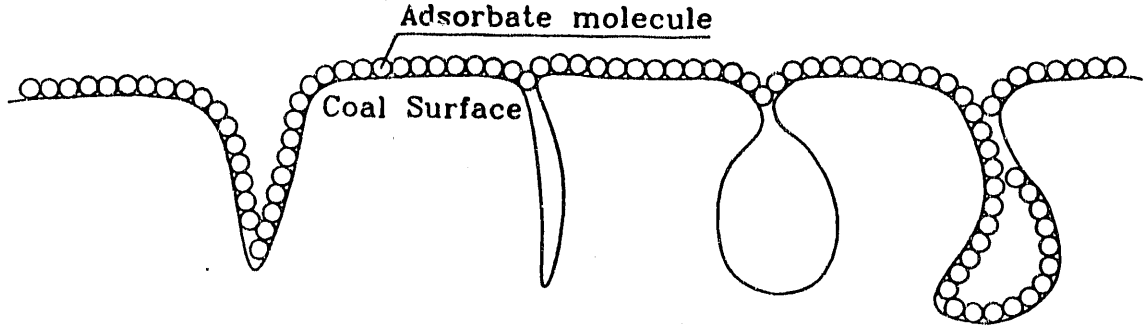

Figure 10.1 Schematic of coal surface.

coal surface area estimated by gas and vapor adsorption is not an absolute measurement. In fact, whether the surface area is close to the true value depends on several factors. One of the most important factors is the accessibility of the adsorbate molecule to all pores of the coal under the experimental conditions. This factor is mainly dependent on the size and shape of the molecular probe used in the gas adsorption and the adsorption temperature which governs activated diffusion of the adsorbate molecule. Secondly, it is difficult to evaluate experimentally the condensation in very small pores of coal and/or multilayer adsorption on coal

prior to complete coverage with a monolayer. As reported (Gan et al., 1972; Nandi and Walker, 1971; Mahajan and Walker, 1971; Walker and Kini, 1965; Walker and Patel, 1970; Anderson et al., 1965; Walker and Geller, 1956), the magnitude of the surface area of coal depends on the dimension of the molecular probe used and the experimental conditions, especially the adsorption temperature. Therefore, it is concluded that the surface area of a coal determined by gas and vapor adsorption is not a unique property.

Nitrogen surface areas measured by nitrogen adsorption at 77 K are considerably lower than expected. This has been explained as due to the micropore system in coal not being completely accessible to N_2 molecules at 77 K because an activated diffusion process is required and/or shrinkage of pores occurs (Anderson et al., 1965; Walker and Geller, 1956). Surface areas determined by CO_2 adsorption are generally much higher and it has been assumed that this molecular probe measures the total surface area associated with the micropore system (Walker and Kini, 1965; Walker and Patel, 1970). The swelling effect of CO_2 on the determination of the coal surface area by CO_2 adsorption is not completely understood (Stacey and Jones, 1986; Reucroft and Patel, 1986, 1983; Reucroft and Sethuraman, 1987). It is noted that the surface areas measured by xenon adsorption are in approximate agreement with CO_2 surface areas, and this has been taken as an evidence that there is no significant specific interaction of the CO_2 molecule with coal surfaces (Walker and Kini, 1965; Dietz et al:, 1964).

Since CO_2 gas adsorption near room temperature is widely used in the coal industry as the standard for coal surface area measurements (Linge, 1989), a novel technique using continuous desorption of CO_2 at 298 K has been applied to determine the BET surface area of high volatile bituminous Castlegate Sub 3 Utah coal. The surface areas of different particle sizes of the coal have been investigated by this technique.

10.2 Experimental

10.2.1 Adsorption Apparatus

The high-pressure gas adsorption apparatus shown in Figure 10.2 consists of mass flow meter, pressure transducer (up to 2000 psig) and coal container (adsorption chamber). Gas flow rates and the corresponding pressures in the adsorption chamber during CO_2 gas desorption are continuously recorded by a PC at 10 Hz. The flow valve 2 was used to reduce the pressure at the mass flow meter entrance and control the gas flow rate during depressurization. The range and sensitivity of the gas flow rate measurements for He and CO_2 by the mass flow meter are given in Table 10.1. The

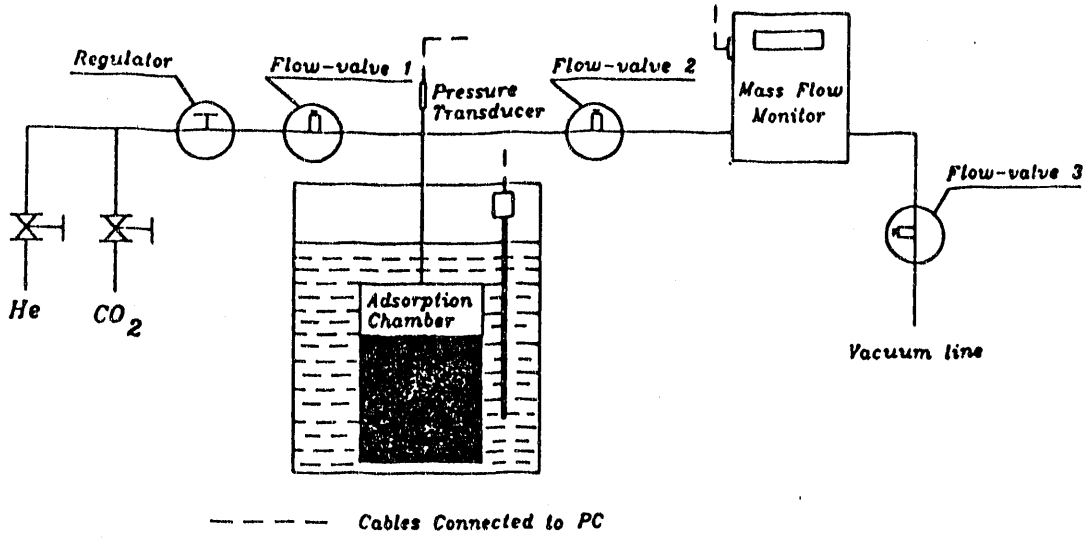

Figure 10.2 High-pressure gas adsorption apparatus.

Table 10.1 Ranges and sensitivities of the mass flow meter*

Gas	Fc ml/(sec)(V)	Range ml/sec	Sensitivity ml/sec
He	0.0625	0 - 0.312	0.002
CO2	0.0318	0 - 0.159	0.001

** ml in the table is converted to STP*

details of the connections of the instruments to a PC data acquisition board are described in Chapter 8. A standard laboratory vacuum line was connected with the system and was capable of evacuating the unit to approximately -8 psig. This vacuum, combined with helium purge, was used to clean the coal surface. A water bath was used as an isothermal chamber. The temperature of the water bath was controlled by a temperature controller (CN2042, OMEGA Engineering, Inc.), and set at 25 °C (298 K). The temperature fluctuation was within 25 ± 0.3 °C.

10.2.2 Sample Preparation and Characteristics

The coal used in this investigation was high volatile bituminous Utah coal, Sub 3 seam from the Castlegate mine. It was first ground in air, then air dried under a vacuum (about -8 psig) at 80 °C for 48 hours and sieved before the tests.

Approximately 17 g samples were used for the CO_2 adsorption/desorption measurements. After the adsorption chamber was filled with the coal sample, the system was purged by helium at about 500 psig three times. It was maintained at this pressure for 1 hour before evacuation.

Proximate analysis, ultimate analysis, NMR parameters, maceral analysis, and density of the coal are given in Tables 6.1-6.3.

10.2.3 Principle of Measurement

The CO_2 adsorption takes place by setting the pressure regulator in Figure 10.2 at an intermediate pressure (normally < 1000 psig), opening flow valve 1 and closing flow valve 2. After the CO_2 adsorption reaches equilibrium, CO2 desorption was measured by first closing flow valve 1, and opening flow valve 2. During the CO_2 desorption process, pressure in the adsorption chamber and gas flow rate were continuously recorded. Therefore, the moles of the adsorbate gas which flowed out of the adsorption chamber (n_{out}) are determined by accumulation of the gas flow rate (f)

$$n_{out}(t) = \int_0^t f dt. \qquad (1)$$

Taking t → ∞, we can get the total moles of the gas entering the adsorption chamber during the gas adsorption period. In other words, we can obtain the initial total moles of the gas in the adsorption chamber (n_{total}) before desorption takes place, i.e.,

$$n_{total} = \int_0^\infty f dt. \qquad (2)$$

Therefore, at any time t, the moles of the gas left in the adsorption chamber (n_{left}) are calculated by a mass conservation equation:

$$n_{left}(t) = n_{total} - n_{out}(t). \qquad (3)$$

The gas in the adsorption chamber occupies the free space in the adsorption system (including free volume in both the coal container and the tubing line) and adsorbs on the coal surfaces. If adsorption on the stainless steel wall is negligible, mathematically,

$$n_{ads}(t) = \frac{n_{left}(t) - n_{free}(t)}{W_c} \tag{4}$$

where $n_{ads}(t)$ is the moles of adsorbate on a unit mass of coal at time t and W_c the mass of coal in the adsorption chamber. The P-V-T relationship of the gas in the free volume of the adsorption system is described by the equation

$$n_{free}(t) = \frac{p(t)\,V_{free}}{z(p,T)\,RT} \tag{5}$$

where V_{free} is the free volume in the adsorption system and z is calculated by

$$z = z^{(0)}(T_r,\ P_r) + \omega z^{(1)}(T_r,\ P_r)\,. \tag{6}$$

where

$$z^{(0)} = 1 + (0.083 - \frac{0.422}{T_r^{1.6}})\frac{P_r}{T_r}$$
$$z^{(1)} = (0.139 - \frac{0.172}{T_r^{4.2}})\frac{P_r}{T_r} \tag{7}$$

and ω is the acentric factor; T_r is the reduced temperature, the ratio of temperature to the critical temperature (T/T_c); P_r is the reduced pressure, the ratio of pressure to the critical pressure (P/P_c) (Reid et al., 1987; Smith and Van Ness, 1987).

The dead volume (or free space) in the adsorption system, V_{free}, was calibrated using helium gas, which is assumed to not adsorb on the coal. For a calibration run, n_{ads} is equal to zero in Equation 4, i.e.,

$$V_{free} = \frac{z(p,T)\,RT}{p(t)}\left(\int_0^{\infty} f\,dt - \int_0^{t} f\,dt\right) \tag{8}$$
$$= Constant$$

at a constant temperature. The standard deviation of the measurements of V_{free} is less than 1%.

Substituting the constant V_{free} (obtained by Equation 8) and Equations 1-3 into Equation 4, we have:

$$n_{ads}(t)\,(mol/g) = \frac{\int_0^{\infty} f\,dt - \int_0^{t} f\,dt - \frac{p(t)\,V_{free}}{z(p,T)\,RT}}{W_c}, \qquad (9)$$

or

$$V_{ads}(t),\ ml(STP)/g = 22{,}415\,n_{ads}(t) \qquad (10)$$

where $V_{ads}(t)$ is the volume of adsorbate at STP per gram of coal at time t.

Theoretically, the equilibrium adsorption volume at any time t, $V_{ads,\,e}(t)$, can be obtained by taking $f \rightarrow 0$, i.e., allowing enough time for the system to approach equilibrium. Experimentally, if the gas flow rate during the gas desorption process is controlled at a very low value (for example, < 2 ml(STP)/min), the system follows an equilibrium path and $V_{ads}(t)$ measured at any time is equal to $V_{ads,\,e}(t)$. Therefore, we can obtain a continuous equilibrium adsorption isotherm in one run.

10.3 Results and Discussion

The results of continuous CO_2 depressurization for Sub 3 seam coal (-100/+115 mesh) are shown in Figure 10.3. The solid line is the total CO_2 in the adsorption system and the dashed line represents the free gaseous CO_2. The difference gives the adsorbed CO_2 is shown in Figure 10.4, plotted versus cell pressure.

To understand the time required for equilibrium adsorption of CO_2, the cell was exposed to a pressure of 231 ± 1 psia at 25 °C for different periods of time. At each exposure time, the depressurization experiment, i.e., CO_2 gas desorption test, was performed to determine the volume of CO_2 adsorbed, V_{ads}. The results are shown in Figure 10.5 and expanded for short times in Figure 10.6. It is clear that over 30 minutes is required for equilibrium under these conditions.

As discussed previously, if the gas flow rates of CO_2 are much lower than the gas desorption rates, the volumes of CO_2 adsorbed at any time, $V_{ads}(t)$, or pressure, $V_{ads}(p)$, are the equilibrium adsorption. Results of CO_2 adsorption data from the continuous desorption experiment, i.e., slow depressurization test, and those from several individual equilibrium adsorption experiments are plotted versus the relative saturation pressure in Figure 10.7. The solid line represents the data determined from continuous slow depressurization. The open circles represent equilibrium adsorption points determined by several individual equilibrium

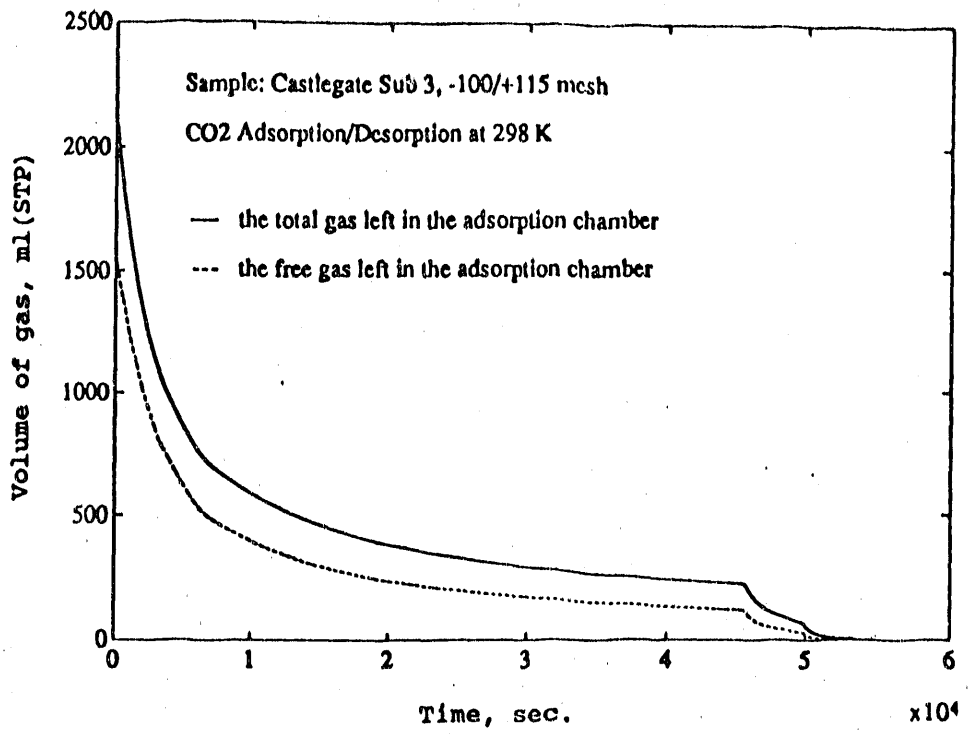

Figure 10.3 Carbon dioxide in high-pressure cell during slow depressurization.

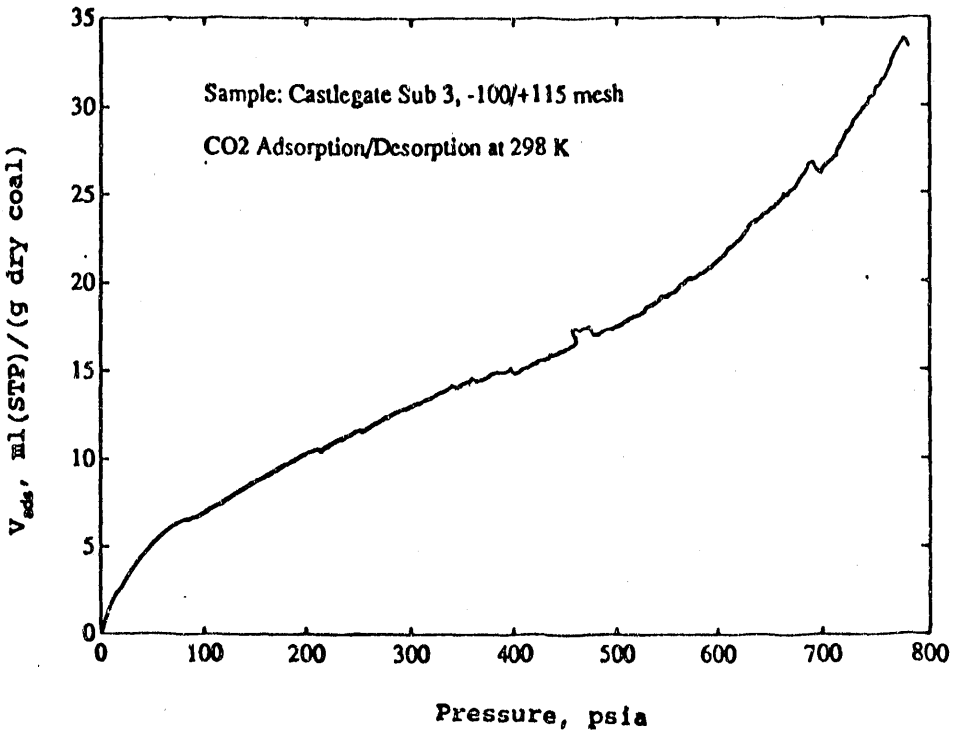

Figure 10.4 Carbon dioxide adsorbed versus pressure.

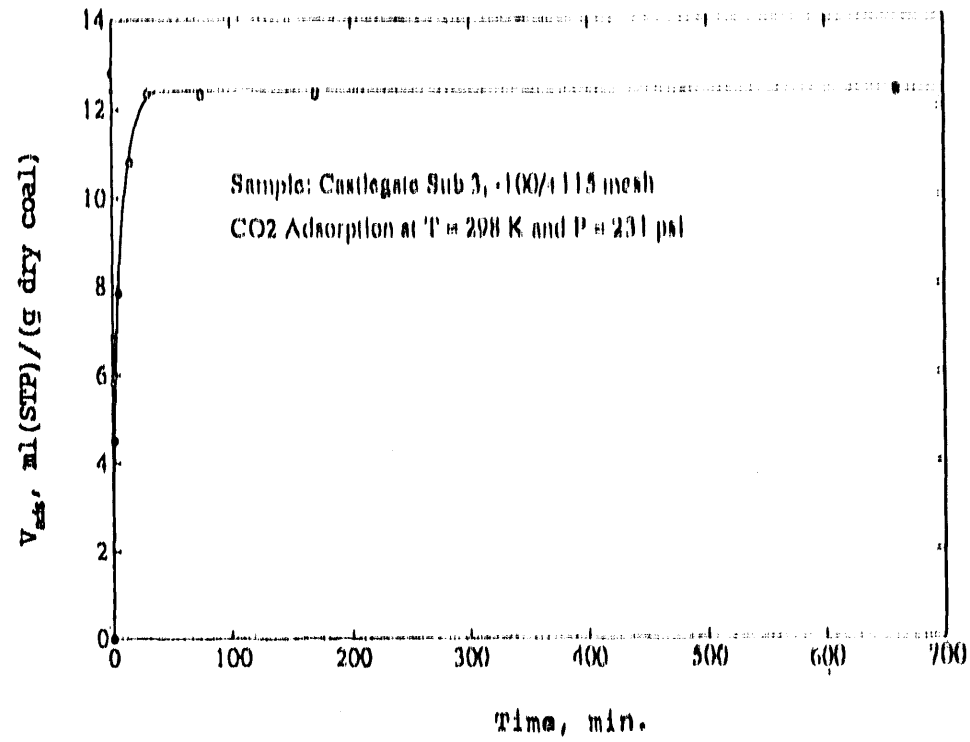

Figure 10.5 Carbon dioxide adsorbed versus time.

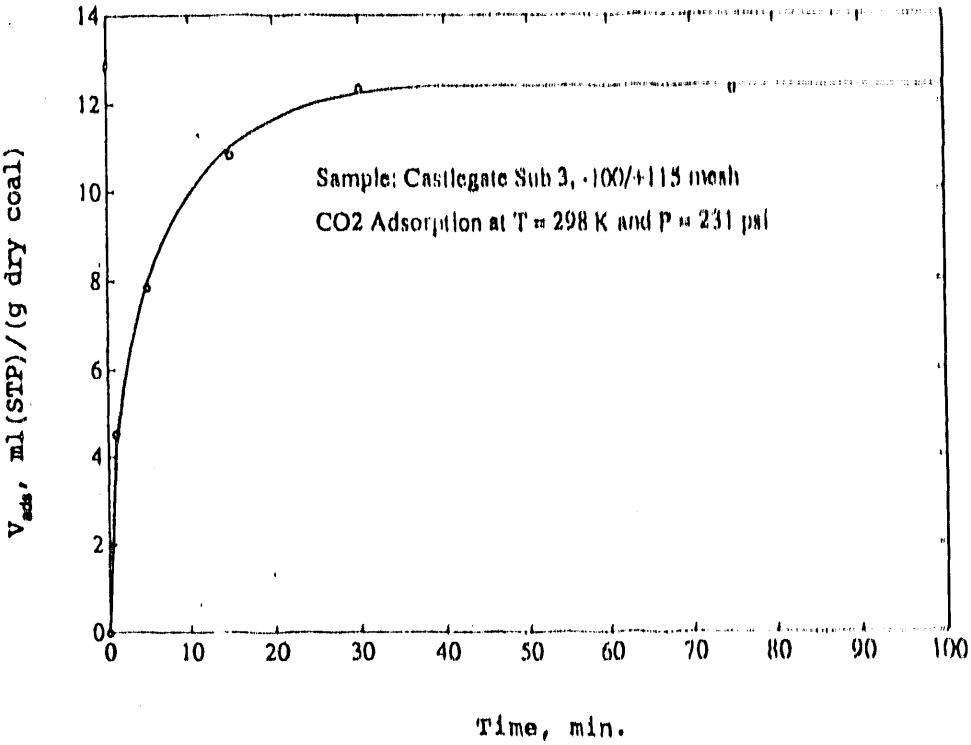

Figure 10.6 Carbon dioxide adsorbed at short times.

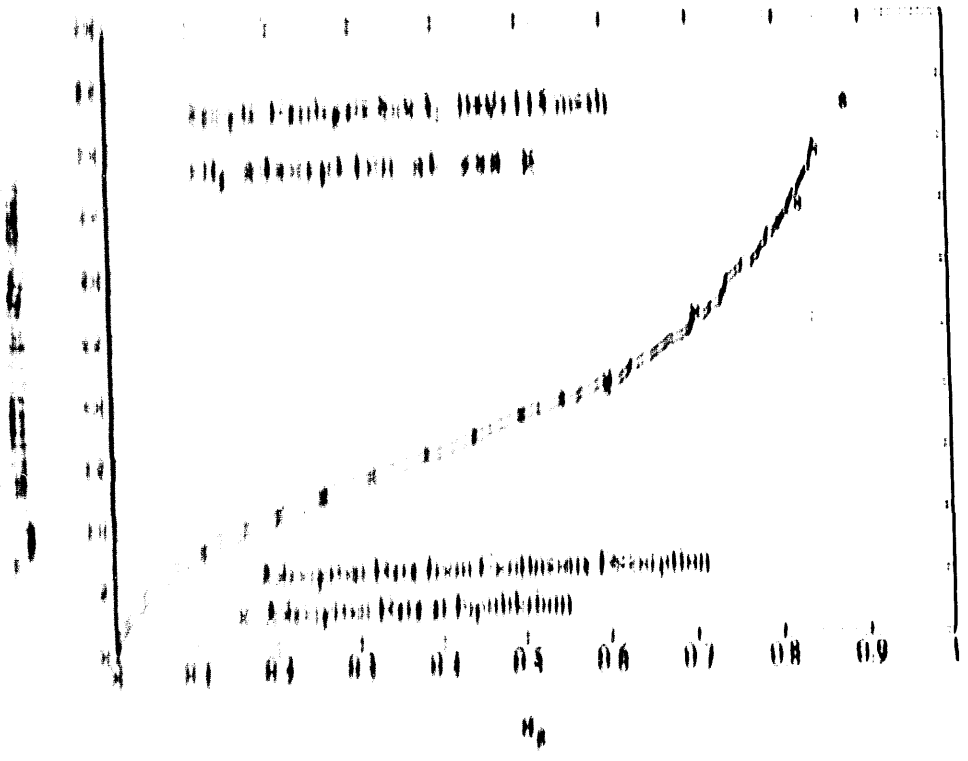

Figure 10.1 Comparison of continuous desorption and equilibrium desorption.

It is evident that the continuous data agree with the equilibrium adsorption points measured by discrete measurements using the slow adsorption technique have very high reproducibility.

From the p_a equilibrium adsorption data at 298 K, the surface area of coal can be determined by the BET equation. The probability of CO_2 covering the coal surface with a thickness of one layer is given by:

$$V_{ads}(T, p_a) = \frac{1}{V_m C} + \frac{C-1}{V_m C} p_a \qquad (11)$$

where p_a is the relative saturation pressure defined as a ratio of the adsorption equilibrium pressure of CO_2 to the saturated CO_2 vapor pressure at the adsorption temperature 25 °C, V_{ads} is the volume of CO_2 needed to cover completely the coal surface with a monolayer ($ml(STP)/g$), and C a constant depending on the adsorption energy and temperature. The slope and intercept of the relative saturation pressure, p_a, is used to calculate the determination of surface area by the BET equation. Since the saturated vapor pressure of CO_2 at 25 °C is relatively high (about 1000 psia), it is necessary to measure the CO_2 equilibrium adsorption at 25 °C (298 K) in the range

of 50 - 330 psia for determining the CO_2 surface area by the BET equation. The constants C and V_m are estimated by plotting $\alpha_p/[V_{ads}(1-\alpha_p)]$ against α_p. If the magnitude of V_m at STP and the area occupied by a molecule of adsorbate in the monolayer, σ, are known, the specific surface area of the coal, S (m^2/g), can be calculated by

$$S = 22,415 V_m N_A \sigma \qquad (12)$$

where N_A is the Avogadro number, σ = 0.235 nm^2/molecule for CO_2 at 25 °C (298 K) (Walker et al, 1959).

The equilibrium adsorption points obtained from individual measurements on Sub 3 seam coal (-100/+115 mesh) plotted in the linearized BET adsorption isotherm format, i.e., $\alpha_p/[V_{ads}(1-\alpha_p)]$ against α_p, are shown in Figure 10.8. A good linear fit with correlation coefficient of 1.000 is obtained using relative saturation pressures of from 0.1 to 0.3. The CO_2 surface area of the coal was estimated to be 69.9 m^2/(g dry coal). A similar plot using the data from the slow depressurization or the continuous desorption technique is shown in Figure 10.9. The fit gives very satisfactory results with 69.8 m^2/(g dry coal) for the CO_2 surface area and 0.998 for the correlation coefficient. As expected, it is in good agreement with that obtained from individual equilibrium adsorption measurement.

To evaluate particle size effect on the CO_2 surface area, two particle sizes, -80/+100 and -150/+200 mesh, were studied using the slow depressurization technique for the continuous determination of the CO_2 equilibrium adsorption. The results of these measurements and the reproducibility are given in Table 10.2. The coal surface areas of the different particle sizes are all about 70 m^2/g with a small standard deviation. Within experimental error, no effect of particle size on the CO_2 surface area was observed. R-squared values for all experimental data are larger than 0.99 for the BET plots and demonstrate that the fit of the BET model is quite good for this method.

In discussions of the surface properties of porous coals having a large specific surface, it is meaningful to distinguish between the external and internal surfaces. In many cases, however, such distinction is not so clear and the line of discrimination between the two kinds of surfaces may be drawn in an arbitrary manner. The surfaces of primary particles themselves suffer from imperfections in the form of cracks and fissures. Based on the characteristics of gas diffusion into coals, those gases that penetrate deeply into the interior will be considered as measuring the internal surfaces. Therefore, the external surface may perhaps be taken to include all cracks which are wider than they are deep

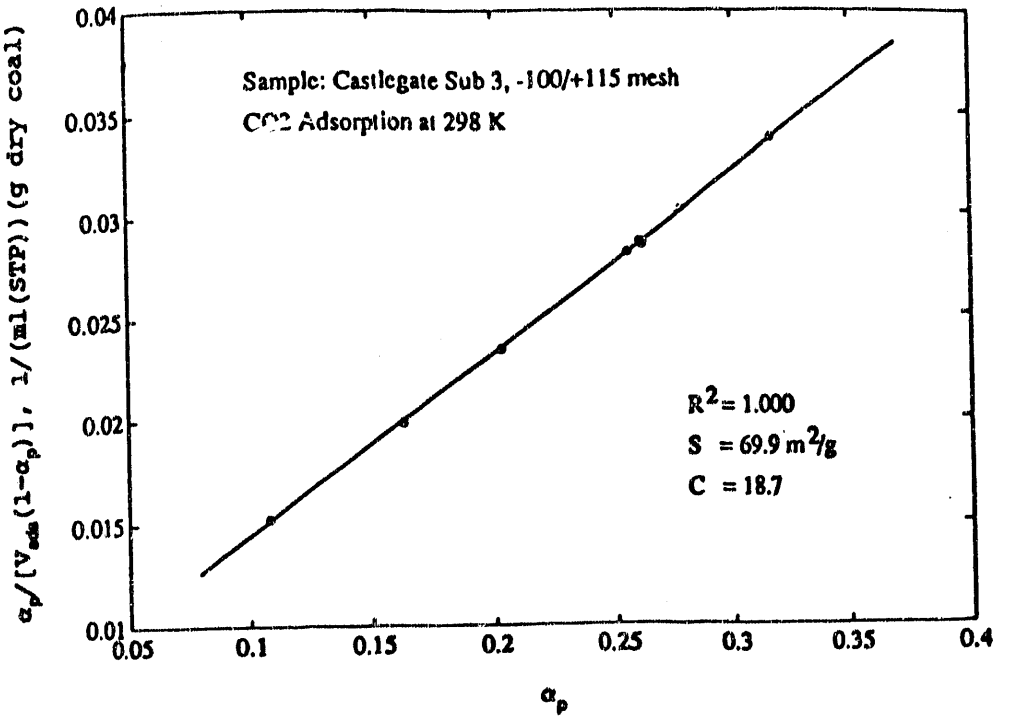

Figure 10.8 BET plot of CO_2 adsorption.

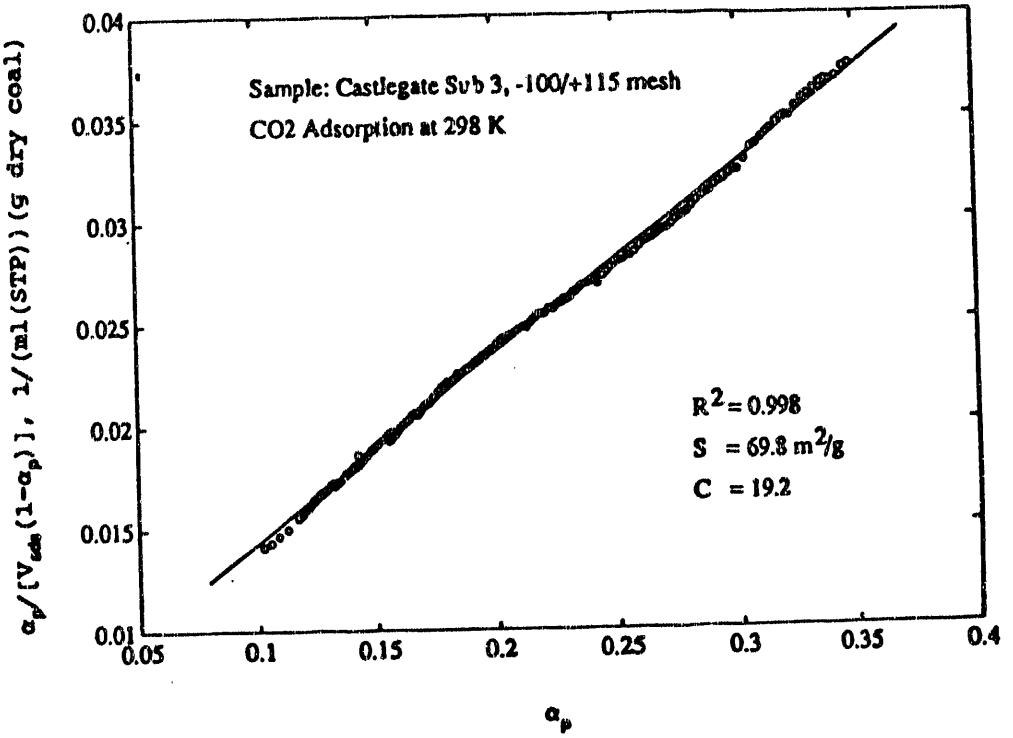

Figure 10.9 BET plot of continuous depressurization data.

Table 10.2 Surface areas of Castlegate Sub 3 Coal by CO2 adsorption at 298 K

	Particle size mesh	Surface area m^2/g	r^2
Method			
Multi-points	-100/+115	69.9	1.000
Continuous desorption technique	-100/+115	69.8	0.998
Reproducibility by the method of continuous desorption	-100/+115	69.8	0.998
	-100/+115	68.6	0.993
	-100/+115	70.2	0.991
	Mean	*69.5*	*0.994*
	Std	*0.7*	*0.003*
	-150/+200	70.3	0.992
	-150/+200	71.0	0.999
	-150/+200	71.5	0.997
	Mean	*70.9*	*0.996*
	Std	*0.5*	*0.003*
Particle size effect	-80/+100	68.5	0.998
	-100/+115	69.6	0.994
	-150/+200	70.9	0.996

and the internal surface will then comprise the walls of all cracks, pores and cavities which are deeper than they are wide.

To simplify calculations, a spherical particle model is proposed for the evaluation of the particle size effect on the external surface area of coal. In this model, the coal particle is assumed to be spherical. The relationship between the specific external surface area and the coal particle diameter has been derived in Chapter 9. The main results are summarized here as follows:

$$S_e = N\pi d^2 \qquad (13)$$

where S_e is the specific external surface area (m^2/g), d the diameter of coal particle, and N the number of the particles per gram of coal,

$$N = \frac{6}{\rho \pi d^3} \qquad (14)$$

where ρ is the density of the coal. Substituting Equation 14 into 13, we have

$$S_e = \frac{6}{\rho d}. \qquad (15)$$

If it is assumed that the particle size distribution of coal samples is normal, i.e., the diameters of the coal particles between two specific sieves can be represented by the mean openings of the sieves, the specific external surface area can be calculated by Equation 15. The specific external surface areas estimated for different particle sizes of Sub 3 seam coal are shown in Table 10.3. Comparison of the specific

Table 10.3 External surface areas of different particle sizes calculated by spherical particle model

Particle size mesh	Mean diameter mm	Se* m^2/g	CO2 Surface area m^2/g
-80/+100	0.165	0.028	68.5
-100/+115	0.137	0.034	69.6
-150/+200	0.090	0.051	70.9

** 1.3050 g/cc used as the density of Sub 3 seam coal which is independent on particle size (Table 9.3)*

external surface areas with the measured CO_2 surface areas indicates that the coal has mostly internal surface area. The results provide a good explanation for why no effect of particle size on the CO_2 surface area was observed.

The slow depressurization technique or continuous gas desorption method offers a relatively simple and quick technique for obtaining the surface area at higher pressures. One measurement of the CO_2 surface area with thousands of data points required only 8 hours by this method. However, the equilibrium time for each adsorption point measured at low pressure and -78 °C (195 K) was 12-24 hours (Walker et al., 1959; Wann, 1990). Therefore, one determination of the CO_2 surface area with 5 points to fit the BET equation requires at least 60-120 hours by the low pressure and low temperature method.

10.4 Conclusions

A novel technique using slow depressurization or continuous gas desorption has proven to be a simple and rapid method for determining the CO_2 surface area of coal at 298 K. The specific surface areas for the different particle sizes of a high volatile subbituminous Sub 3 Utah coal, which include -80/+100, -100/+115, and -150/+200 mesh, are about 70 m^2/(g dry coal). Particle size effects on the CO_2 surface area were not observed within experimental error. A spherical particle model was proposed to estimate the specific external surface area. The results indicate that the coal has mostly internal surface area. It also provides a good explanation for why no effect of particle size on the CO_2 surface area was observed.

11. GAS EVOLUTION IN THE PROGRAMMED-TEMPERATURE PYROLYSIS OF COAL

11.1 Introduction

Simulation of the natural evolution of gases during coalification is an important topic in coalbed methane studies. The methane content in a coal seam depends on the accumulation of methane during formation in the coal seam by coalification and methane loss by diffusion (Bodily et al., 1991; Haung et al., 1991). Some methane could flow into upper seams from lower seams, but this would be a small contribution in most cases. Although the large differences in temperature/pressure/time conditions between natural and artificial maturations cause errors in the simulation of maturation from laboratory coal pyrolysis experiments, methane production in coal pyrolysis can be used as a measure of the propensity to form methane during further coalification. This information is also useful in estimating the relative rate of methane formation in a coal seam at current times.

The pyrolysis of coal is generally defined as the thermal decomposition of coal in an inert atmosphere. Other terms may be applied, such as thermal decomposition, devolatilization, and carbonization (Speight, 1983; Gavalas, 1982). The products of coal pyrolysis are gas, carbonaceous residue (char or coke) and liquids (including tar, oil and water).

Coal pyrolysis is the initial step in most coal conversion processes, especially important in liquefaction and gasification processes. It accounts for up to 70% of the weight loss of coal. To study thermal decomposition, investigators have focused on how various parameters change with extent of decomposition. These parameters include effect of coal rank (Weimer and Ngan, 1979; Suuberg et al., 1978; Arendt and van Heck, 1981; Tyler, 1979), heating rate (Ciuryla et al., 1979; Strangeby and Sears, 1981), temperature profile (Wang and Shou, 1980; Lester et al., 1982), pressure (Morris and Keairns, 1979; Suuberg et al, 1980), particle size (Freihaut et al., 1977), surrounding gas (Morris and Keairns, 1979; Suuberg et al., 1980), weight loss (Speight, 1983; Gavalas, 1982; Howard, 1981), volatile evolution (Serio et al., 1987; Juntgen and van Heek, 1979; Campbell, 1978; Solomon et al., 1986), functional groups, (Serio et al., 1987; Niknis et al., 1988) and other factors (Howard, 1981; Lowry, 1963). However, few of the researchers have focused their studies on gas evolution during coal pyrolysis. In this study, a programmed-temperature pyrolysis system was used to investigate gas evolution during coal pyrolysis at a slow heating rate. The characteristic parameters of gas evolution during coal pyrolysis, such as production of selected gases and total gas and liquid yield are correlated with coal analytical data including proximate analyses, ultimate

analyses and carbon structural data from ^{13}C NMR.

11.2 Experimental

11.2.1 Pyrolysis

A programmed-temperature pyrolysis system running at atmospheric pressure is shown in Figure 11.1a. The details of the pyrolysis reactor, which has been designed to avoid plugging of the coal during pyrolysis, is illustrated in Figure 11.1b. A thermocouple extending to the center of the coal was used to record the pyrolysis temperature. The signal was first amplified by a K-type thermocouple module (Wahl Instruments, Inc.) and collected by a PC at 1 Hz. The temperature of the reactor was controlled by a temperature controller (CN2042K, OMEGA Engineering, Inc.). Linear heating was possible up to 12.5 °C/min, at which heating rate the furnace was operating at about 90% of capacity. To minimize the dead volume of the pyrolysis system, small diameter tubing with 4 mm i.d. and short lengths was used to connect all the instruments. Pyrolysis products including gases and liquids were swept from the reactor by flowing helium or argon and carried through a cold trap (at 0 °C) where tars, heavy hydrocarbons and water were precipitated.

Methane in the liquid-free gas stream was analyzed by an on-line Methane I.R. Analyzer (UNOR 6N Infra-Red Methane Gas Analyzer, H. Maihak AG, Ltd.) and the gas was then passed through a gas chromatograph (Series 580, GOW-MAC Instrument Co.) where the gas composition was analyzed. Total flow was detected by a mass flow monitor (Sierra Instruments, Inc.). Signals from the methane analyzer, gas chromatograph and mass flow monitor were all recorded by a PC computer.

The flow rate of the inert carrier gas (helium or argon) was set at about 30 ml(STP)/min during the coal pyrolysis. About 2 g of coal sample was used for each pyrolysis run. The system was first purged using the carrier gas at the experimental flow rate (about 30 ml/min) and room temperature for at least 2 hours to replace the air in the reactor and tubing. The delay of the gas stream in the dead volume of the system was accounted for by a correction to the delay time. After each pyrolysis experiment, all tubing including reactor tubing and tar-trap column were thoroughly washed using THF solvent to avoid plugging and accumulation of tars.

11.2.2 Gas Chromatograph

The chromatograms of the pyrolysis gases were obtained using the dual column gas chromatograph fitted with a thermal conductivity detector (TCD). The response signals from the TCD were first amplified by a PC isolated signal conditioning module (Wahl Instruments, Inc.) with an input of ±25 mV and

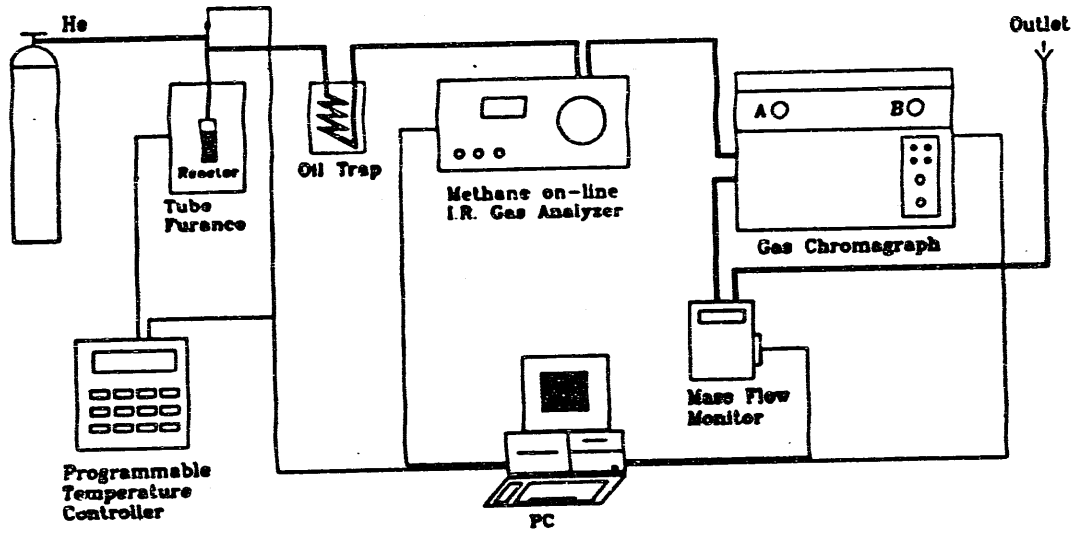

a. Pyrolysis apparatus

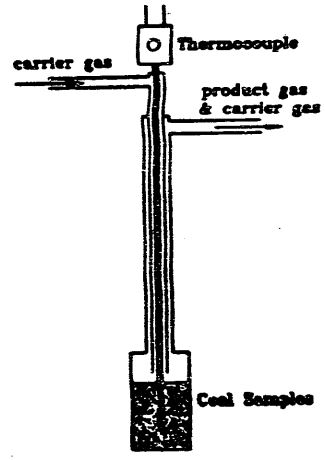

b. Pyrolysis reactor

Figure 11.1 Pyrolysis apparatus.

output of ±5 V, and the amplified signals were collected by a PC equipped with a data acquisition and control board (DT 2801, AST Research, Inc.) at a sampling rate 10 Hz. A gas sample valve with a sample loop of 0.25 ml was used to introduce a gas sample from the pyrolysis gas steam into the chromatograph for reproducibility and convenience. A Haysep Q column supplied by GOW-MAC Co. was used to separate the pyrolysis gases. The column temperature was set at 50 °C and the detector temperature at 60 °C. The flow rate of the GC carrier gas was 20 ml(STP)/min. Carbon monoxide, carbon dioxide and light hydrocarbon gases, such as methane, ethylene, and ethane were detected with the detector current at 180 mA and helium as carrier gas. Hydrogen was detected using argon as carrier gas and the detector current was set at 100 mA.

A gas mixture from Air Products Co. with the composition of methane 0.947 Vol.%, ethane 0.501 Vol.%, ethylene 0.107 Vol.%, propane 0.095 Vol.%, carbon monoxide 0.967 Vol.%, carbon dioxide 2.05 Vol.% and the rest balanced by helium was used to calibrate the TCD under gas chromatograph operating conditions. Pure gases which were analyzed during coal pyrolysis were also used for GC calibration. The calibration results show very good linearity of concentrations versus detector response within the range of the gas composition observed in coal pyrolysis. One gas analysis required about 10 minutes for helium as carrier gas and 2 minutes for argon as carrier gas.

11.2.3 Coal Preparation and Characteristics

Ten Utah coals, one Colorado coal and eight Argonne Premium Coal Bank samples (Vorres, 1989) were used in the study of coal pyrolysis. The proximate and ultimate analyses of the coals are given in Table 6.1. The 12 carbon structural parameters from the ^{13}C NMR tests for the 19 coals are given in Table 6.2, where the NMR data for the 8 Argonne Premium Coals are from Solum et al. (1989). The maceral analyses (Solum et al., 1989; Sommer et al., 1991) and other analytical data are listed in Table 6.3.

The Utah coal samples and one Colorado coal were first ground and then sieved into three fractions, i.e., +60 mesh, -60/+100 mesh and -100 mesh. The eight Argonne Premium Coal Bank samples were used as-received. They are carefully collected and preserved.

11.3 Results and Discussion

11.3.1 Primary Experimental Results on Coal Pyrolysis

The heating profile during the programmed-temperature pyrolysis of Sunnyside coal at -60/+100 mesh is shown in

Figure 11.2. There was a slight deviation from linearity at the temperature of initial rapid devolatilization for some coal samples. About 4,500 temperature measurements (sampling rate of 1 Hz) were taken in the range of gas evolution, e.g., from 100 to 900 °C, and the heating was found to be linear with a correlation coefficient greater than 0.9999. The heating rate was controlled at 12.2 °C/min.

Methane and total gas evolution were measured in each pyrolysis run by the methane I.R. analyzer and mass flow monitor. Methane, carbon dioxide, carbon monoxide, ethlyene and ethane gases were analyzed using the GC with helium as the carrier gas, and hydrogen and methane were measured in an additional experiment using argon as the carrier gas. The methane concentrations as determined by the methane I.R. analyzer from triplicate experiments for the Sunnyside coal at -60/+100 mesh are shown in Figure 11.3. The results are typical of the reproducibility obtained for other samples. The yield of methane, initial evolution temperature and temperature of maximum evolution (e.g., methane peak temperature) for the three runs are very close. The methane concentrations determined by gas chromatography in the runs with helium and argon as the carrier gas are identical to each other and also similar to those obtained with the methane I.R. analyzer.

The gas chromatograms obtained at different temperatures using helium as carrier gas are shown in Figure 11.4a. A similar plot for argon as carrier gas is shown in Figure 11.4b. The concentrations of each individual gas species obtained from the gas chromatograms are shown in Figure 11.5. The solid lines were drawn by a curve-fitting program using the Polynomial Fitting (PF) technique. Principles of the PF technique and source code of the program are given in Appendix E.

The rate of the gas evolution can be determined from the gas compositions and the total flow rate during coal pyrolysis. The results for Sunnyside coal at -60/+100 mesh are illustrated in Figure 11.6. The cumulative gas production from integration of Figure 11.6 with respect to time is shown in Figure 11.7. The pyrolysis temperature was held at 910 °C for about 10 min until gas evolution approached completion. Hence the cumulative gas production includes contributions from the both the linear heating period and the isothermal period. The sum of the gas yields agree with the total gas evolution. As expected, the coal pyrolysis results obtained in this study agree with those reported in the literature (Weimer and Ngan, 1979; Suuberg et al., 1978; Howard, 1981).

11.3.2 Effect of Particle Size

The effect of particle size on coal pyrolysis reactions

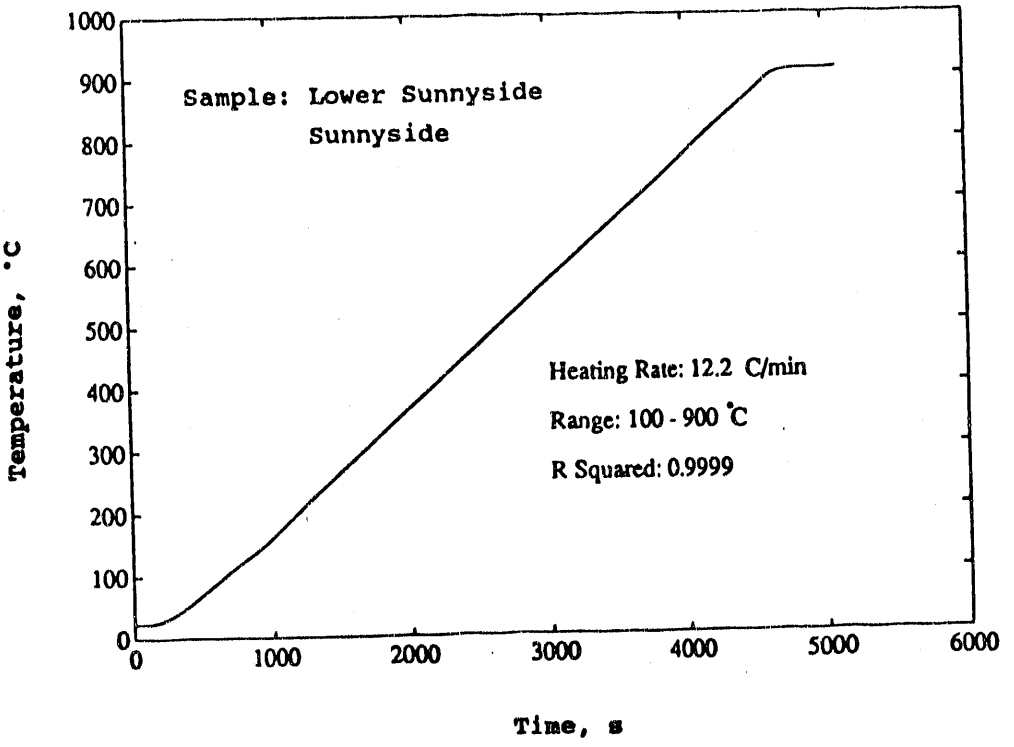

Figure 11.2 Heating profile for programmed-temperature pyrolysis of coal.

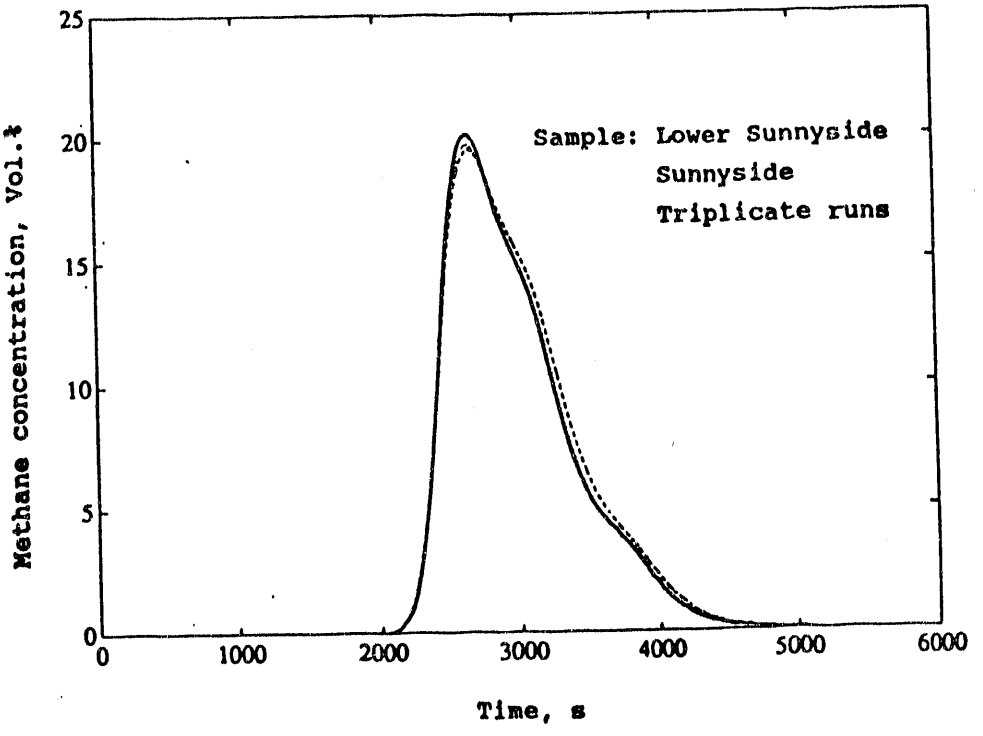

Figure 11.3 Reproducibility of methane formation for triplicate experiments.

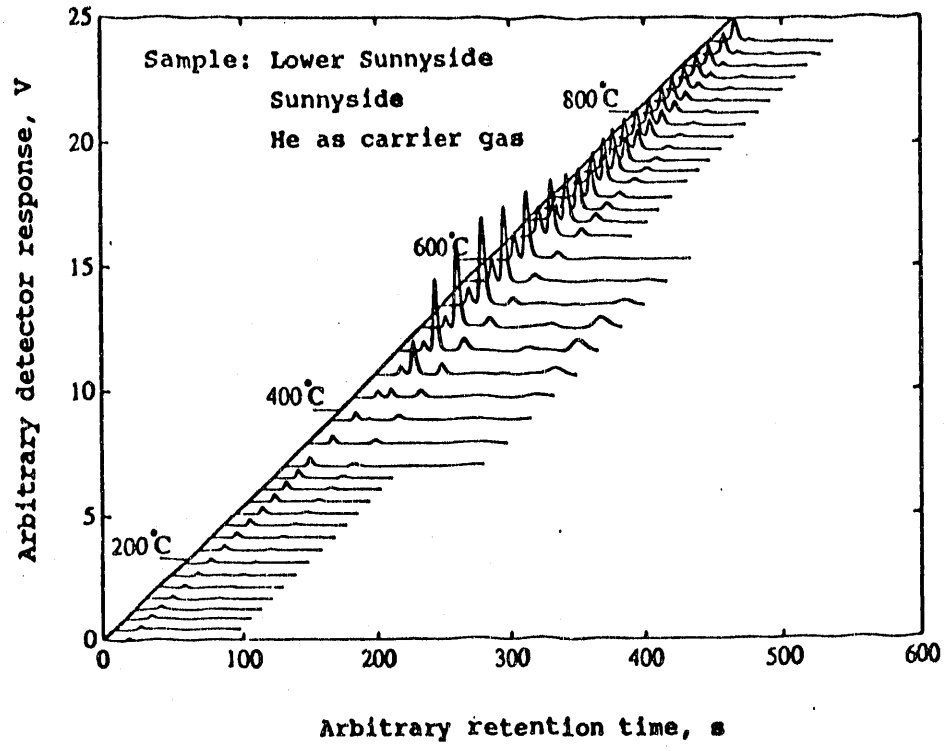

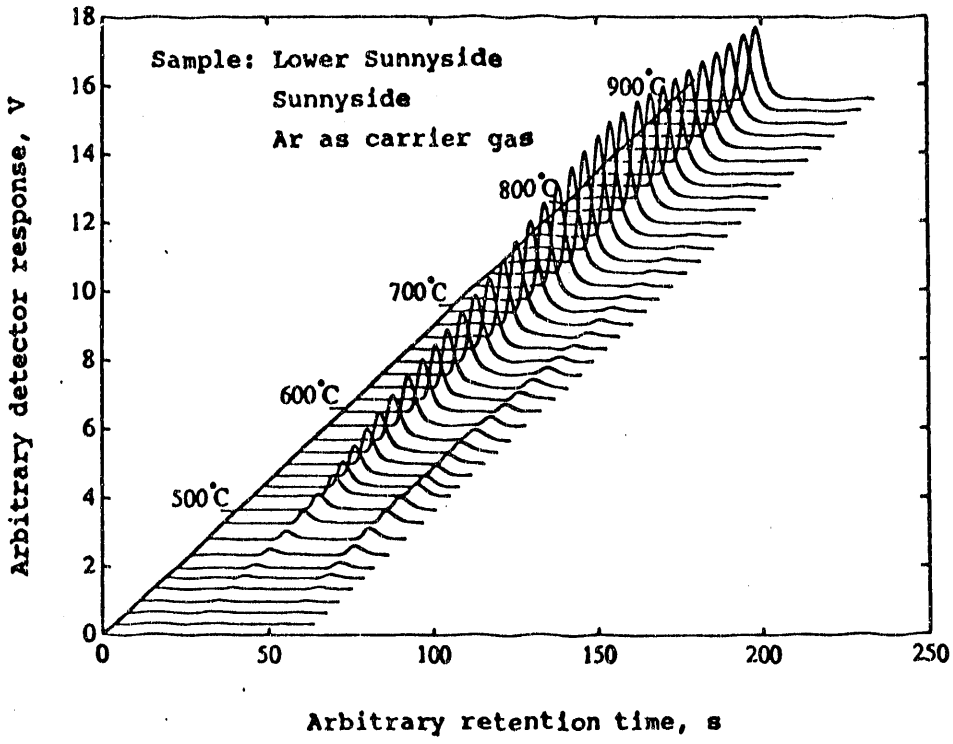

Figure 11.4 Gas chromatograms: a, helium carrier gas; b, argon carrier gas

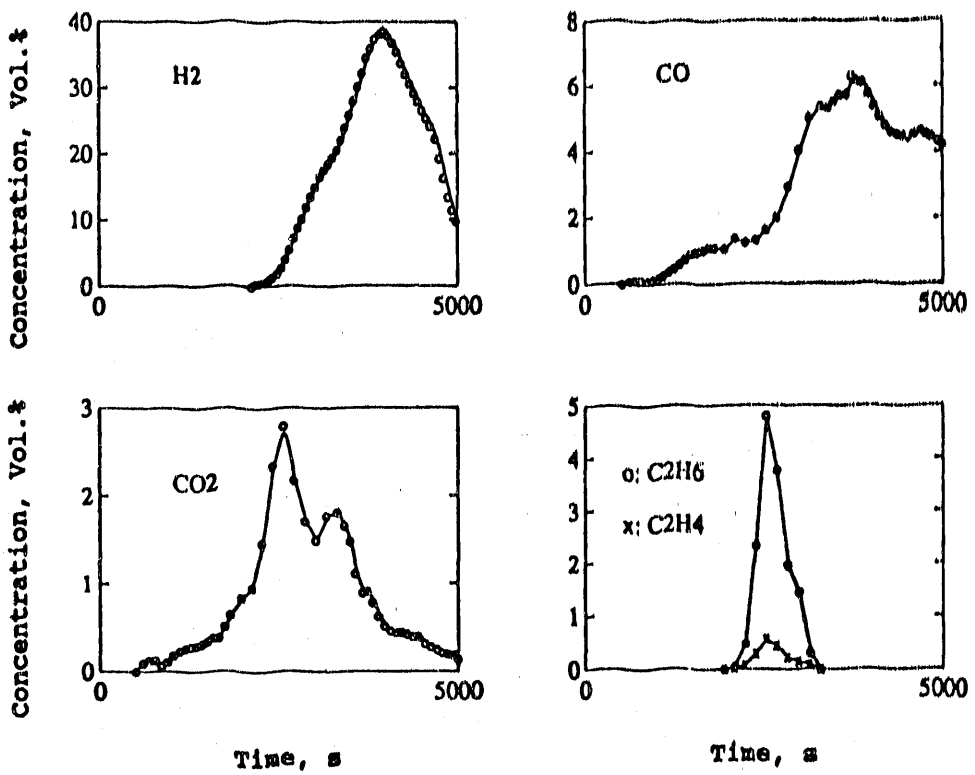

Figure 11.5 Pyrolysis gas yields.

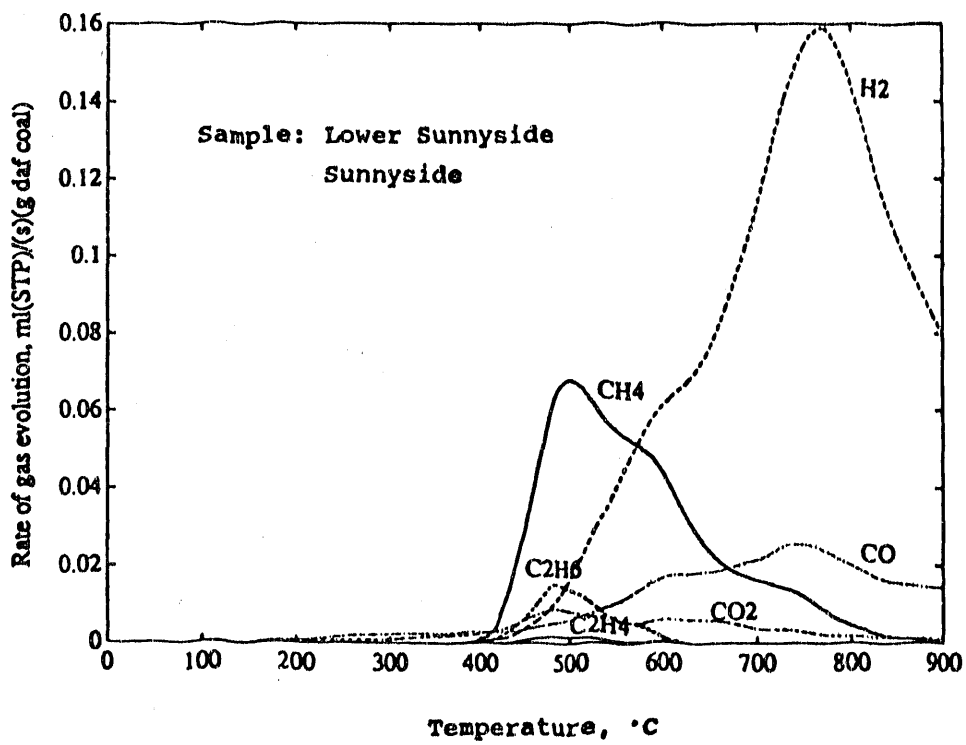

Figure 11.6 Gas evolution for Lower Sunnyside coal.

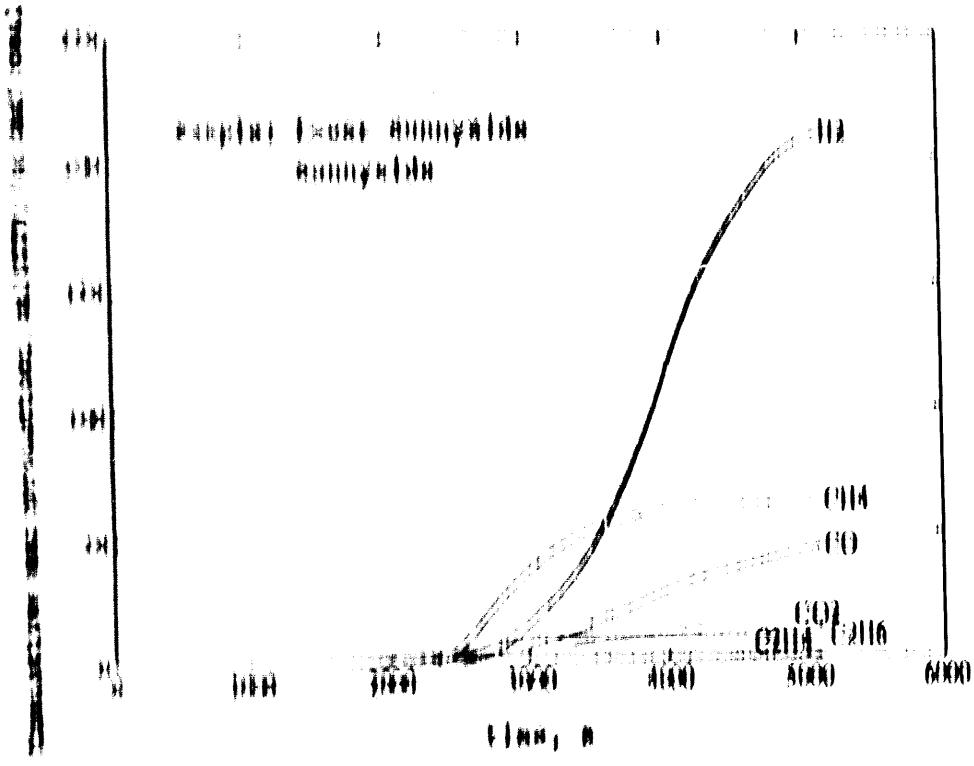

Figure 11.7 Cumulative gas production for Lower Sunnyside coal.

become significant when a combination of the physical and chemical parameters result in a set of experimental conditions in which the pyrolysis process is non-isothermal and non-uniform within the particle. This will generally occur at some critical particle size when heat and/or mass transfer control the pyrolysis reactions. If chemical reaction rates control the devolatilization of a coal particle, the rate would be independent of the particle size.

The effect of particle size on coal pyrolysis was determined for three different coals, i.e., the medium volatile Dutch Creek (U seam) coal, the high volatile and gassy Sunnyside (Upper Sunnyside seam) coal and the high volatile and gassy Hayden (Upper O'Connor seam). A -100 mesh fraction, a 40/100 mesh fraction and a +40 mesh fraction were used for this study. The results of methane evolution for different particle size fractions using Dutch Creek, Sunnyside and Hayden coals are shown in Figures 11.8-11.10. A comparison of the results in Figures 11.8-11.10 with those in Figure 11.7 indicates that no effect of particle size on coal pyrolysis is observed under the current pyrolysis conditions within experimental error.

The characteristic parameters of the programmed-temperature pyrolysis, such as initial temperatures, peak

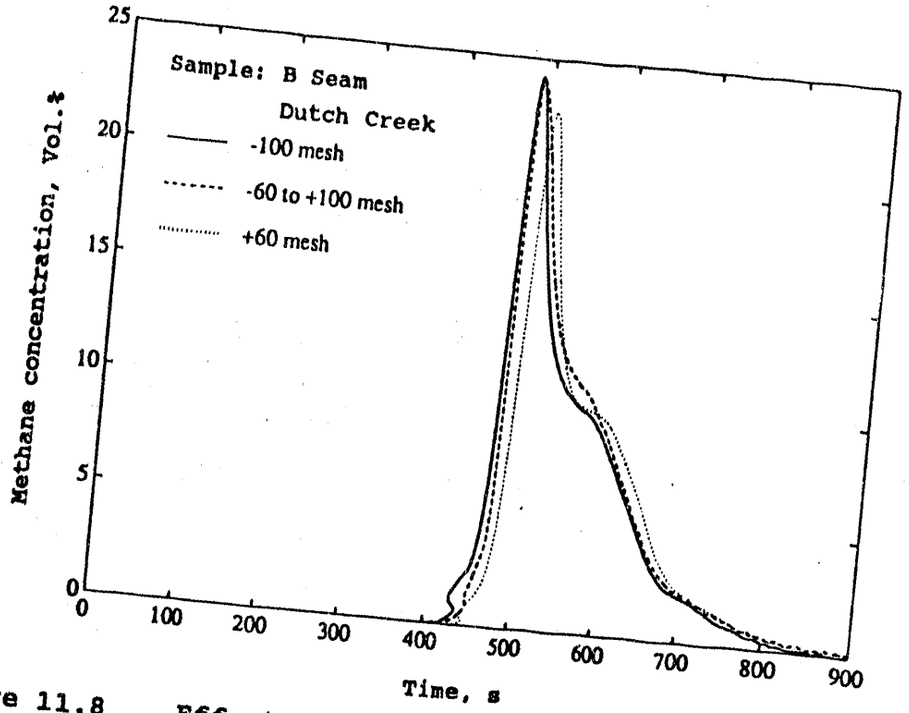

Figure 11.8 Effect of particle size on methane evolution for Dutch Creek coal.

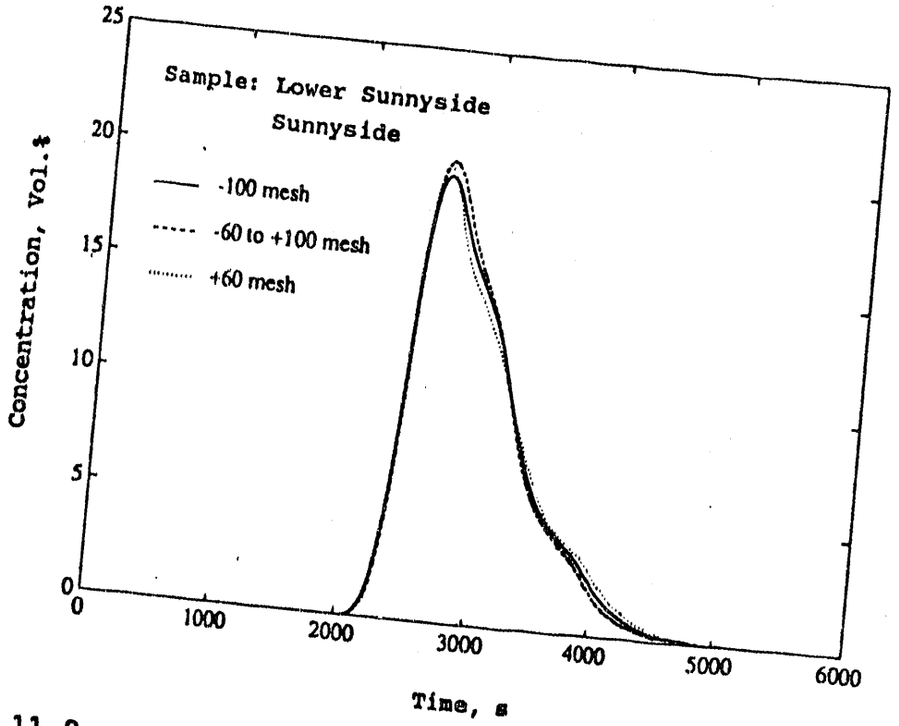

Figure 11.9 Effect of particle size on methane evolution for Lower Sunnyside coal.

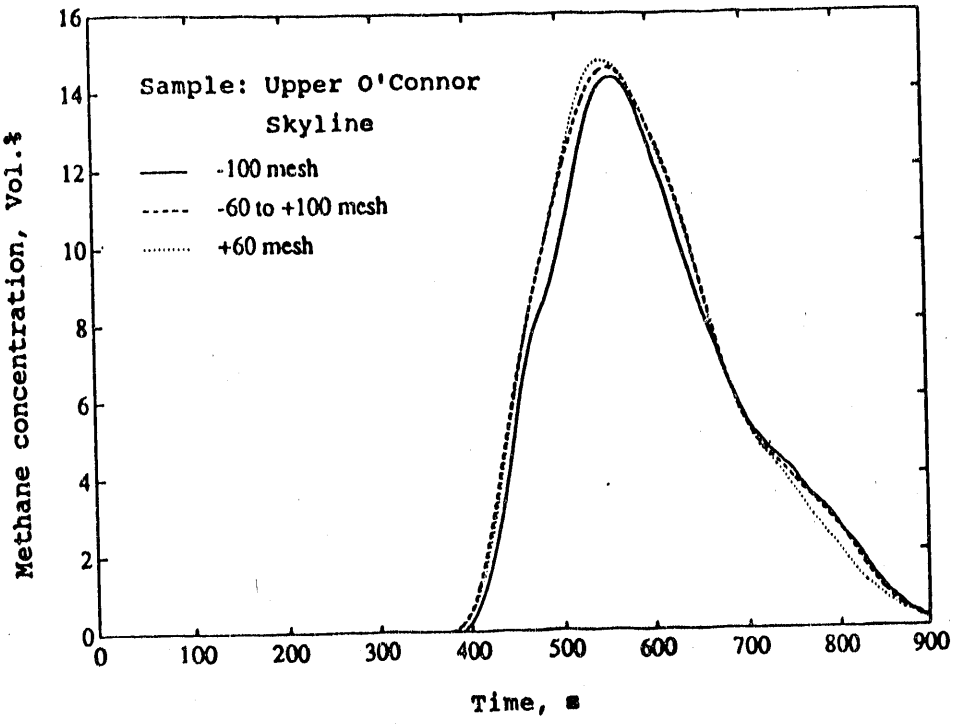

Figure 11.10 Effect of particle size on methane evolution for Skyline coal.

temperatures, and cumulative yields of different gas species are identical for different particle sizes of each coal within the experimental error. This further supports the above conclusion regarding the effect of particle size on coal pyrolysis under the pyrolysis conditions used. Therefore, the remaining Utah coals were studied using only the -60/+100 mesh fraction and the eight Argonne Premium Coal Bank samples using an as-received -20 mesh fraction.

It is noted that the particle size effect might be expected at higher heating rates, under which conditions the particle size may become important due to heat and mass transfer.

11.3.3 Gas Evolution in Coal Pyrolysis

The plots shown in a previous section (11.3.1) for the pyrolysis of -60/+100 mesh Sunnyside coal were used as an example to demonstrate the details of the experimental results. Among those results shown in Figures 11.3-11.7, the most important and characteristic pyrolysis curve is the rate of gas evolution as a function of temperature, where the rate has been corrected to 0 °C and 1 atm (STP) on a daf coal basis. From this curve, several characteristic parameters of the programmed-temperature coal pyrolysis for each gaseous

species, such as initial temperature, peak temperature, maximum rate (the rate at the peak temperature) and total gas yield are obtained. Secondary results, for instance total gas evolution rate and cumulative gaseous product yield as a function of temperature, may also be obtained from these data. For the remaining coals only the plots of the gas evolution rate as a function of temperature are shown. The rates of gas evolution plotted against temperatures for the remaining nine Utah coals are shown in Figures 11.11-11.19. Similar pyrolysis behavior is observed for all Utah coals. This may be due to the fact that the Utah coals are all ranked as high volatile bituminous.

A similar plot for a medium volatile Colorado coal (Dutch Creek B seam) is shown in Figure 11.20. Compared with the high volatile Utah coals, the medium volatile Colorado coal shows higher initial temperatures for gas evolution. The characteristic parameters of coal pyrolysis for these western coals are given in Table 11.1.

The western coals cover a relatively narrow range of rank, with only the Dutch Creek, Colorado coal outside of the high volatile bituminous range. Thus, the Argonne National Laboratory Coal Bank samples covering the range from lignite to low volatile bituminous were used to examine the effect of coal rank on the gas evolution during coal pyrolysis. Plots of the gas evolution rate versus temperature for each of the eight samples are shown in Figures 11.21-11.28. The characteristic pyrolysis parameters of the coals are listed in Table 11.2.

From the cumulative gas production data and char yields, liquid yields including tar, oil and water can be estimated by difference. The gas, char and liquid yields for the coals used in this study are given in Table 11.3.

11.3.4 Coal Pyrolysis and Coalification

The gas yields from coal pyrolysis have been used as a measure of gas formation in coal maturation. Oxygen-containing gases are evolved during the early stages of coalification. At a later stage, methane is evolved as the aliphatic groups in the coal react. At the stage where anthracites are formed, hydrogen is evolved. Comparison of the gas evolution stages in coalification with the temperature dependence of the gas evolution during programmed-temperature coal pyrolysis indicates that coal pyrolysis parallels the coal maturation process, but higher temperature are required for coal pyrolysis to make up for the much shorter time involved in the experiments. In fact, as shown in the plots of gas evolution rate versus temperature, CO_2 and CO gases were first evolved during the low-temperature stage of coal pyrolysis. At a higher-temperature, methane including other

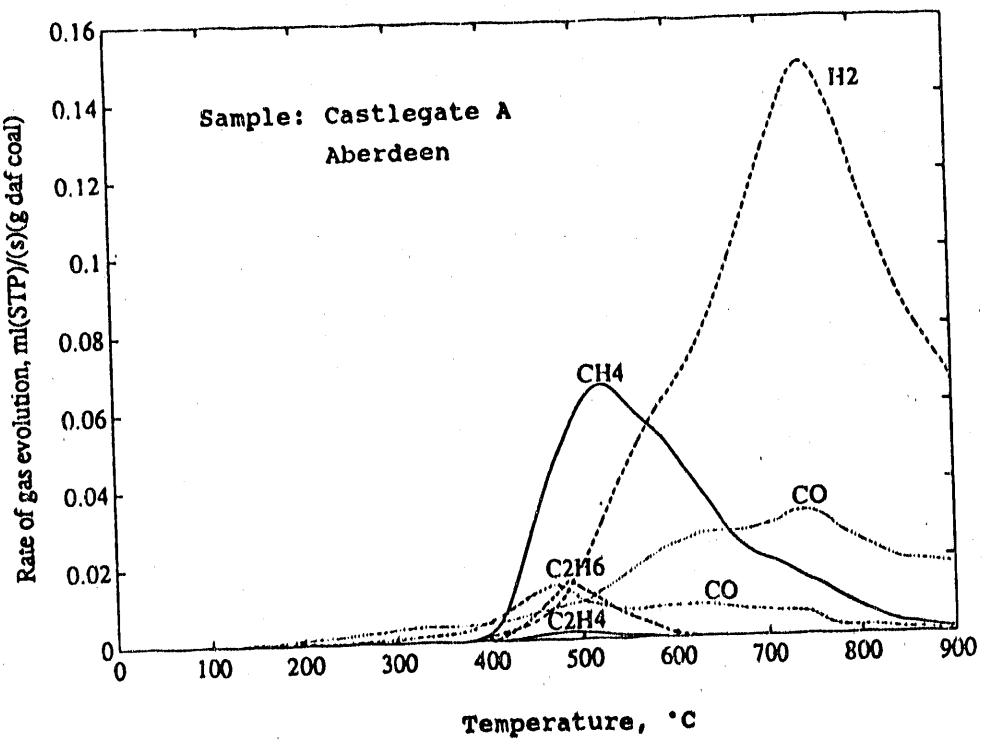

Figure 11.11 Pyrolysis gas yields for Castlegate A seam coal, Aberdeen mine.

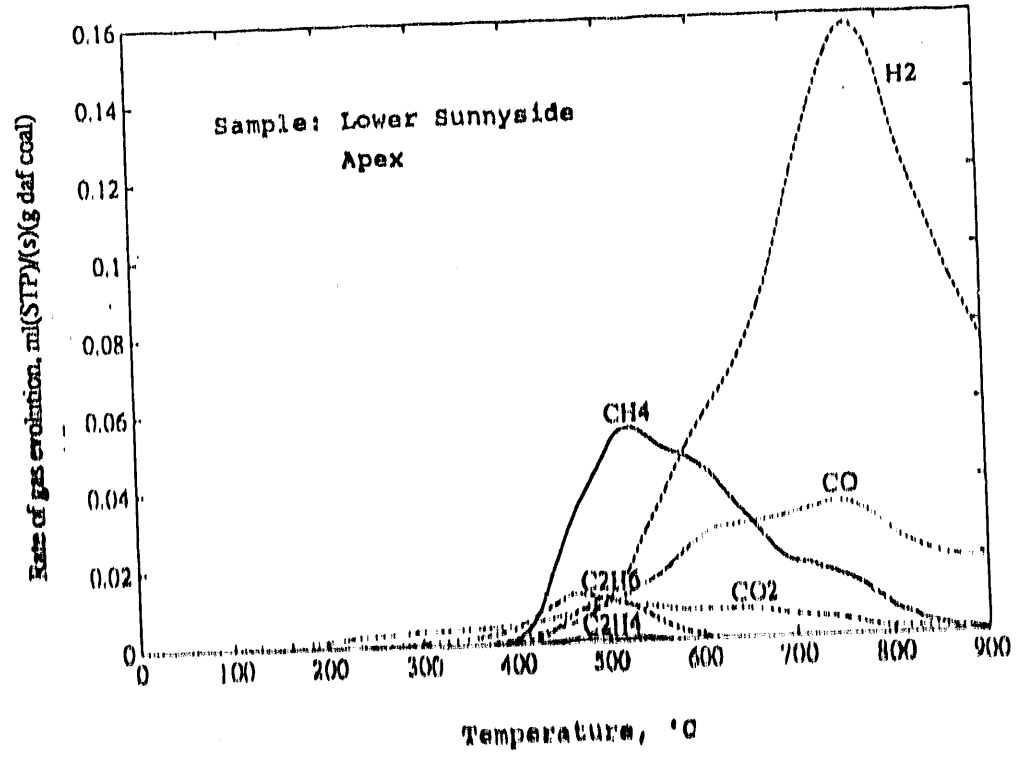

Figure 11.12 Pyrolysis gas yields for Lower Sunnyside seam coal, Apex mine.

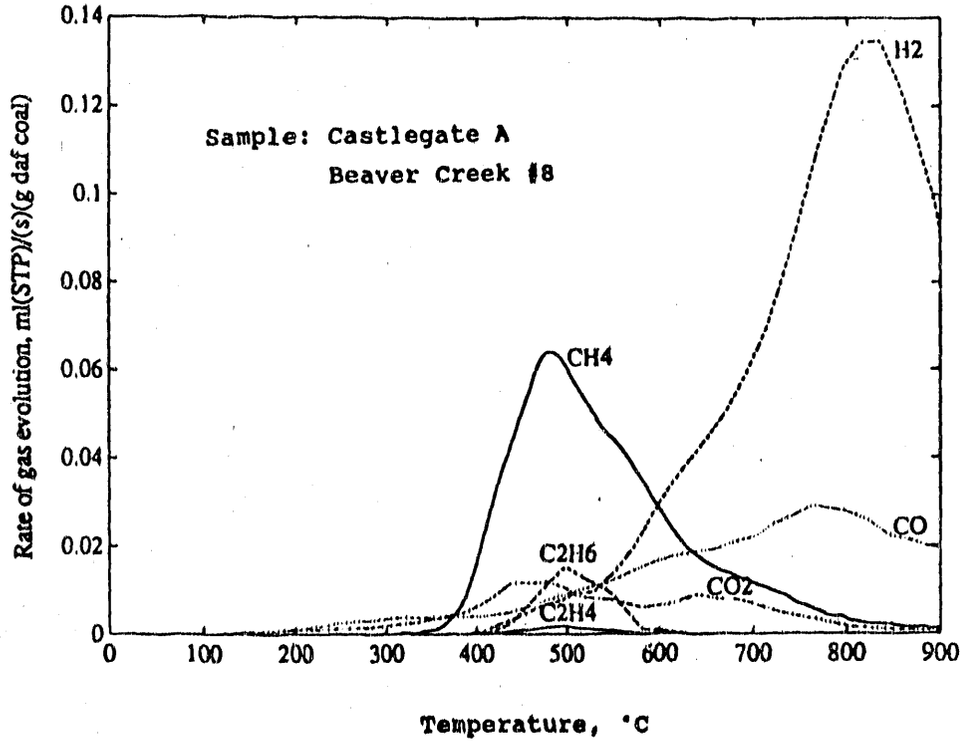

Figure 11.13 Pyrolysis gas yields for Lower Sunnyside seam coal, Beaver Creek #8 mine.

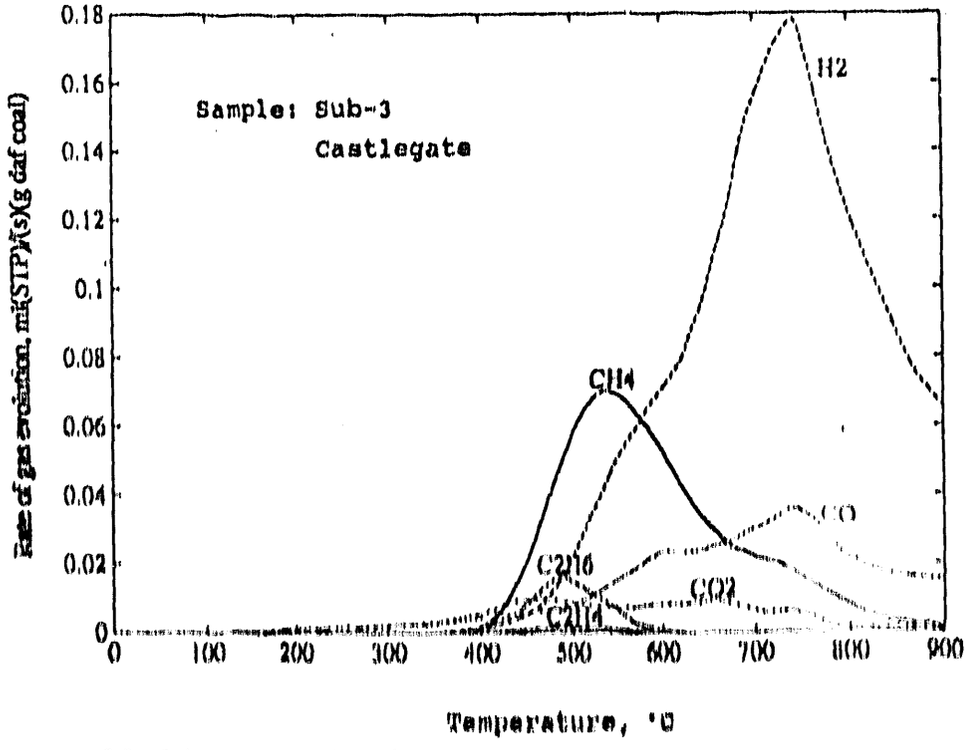

Figure 11.14 Pyrolysis gas yields for Sub 3 seam coal, Castlegate mine.

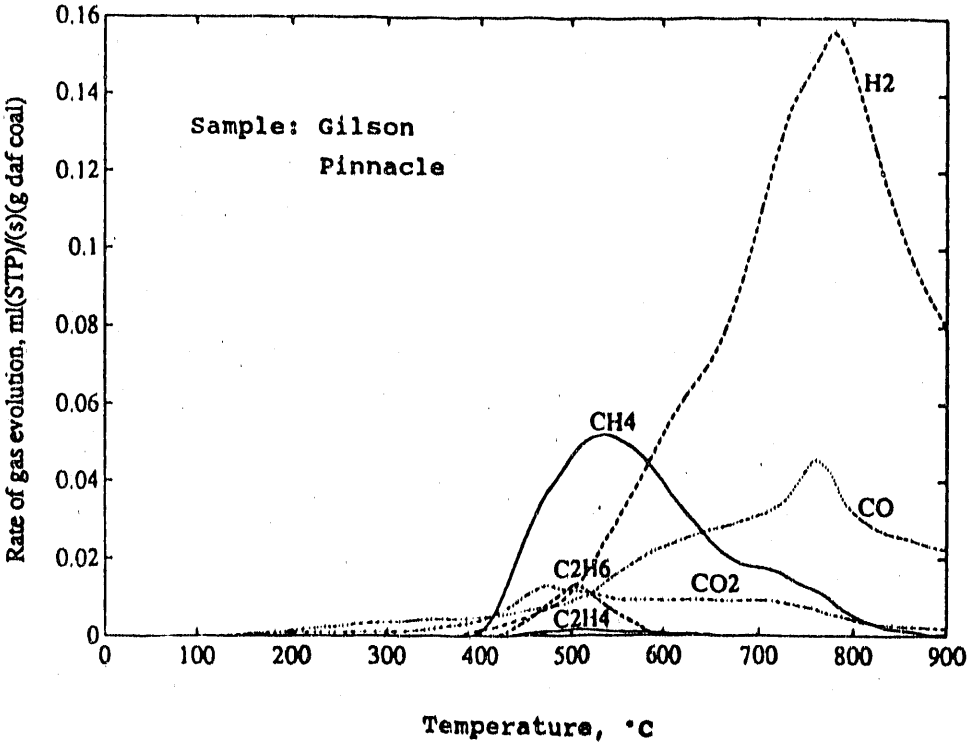

Figure 11.15 Pyrolysis gas yields for Gilson seam coal, Pinnacle mine.

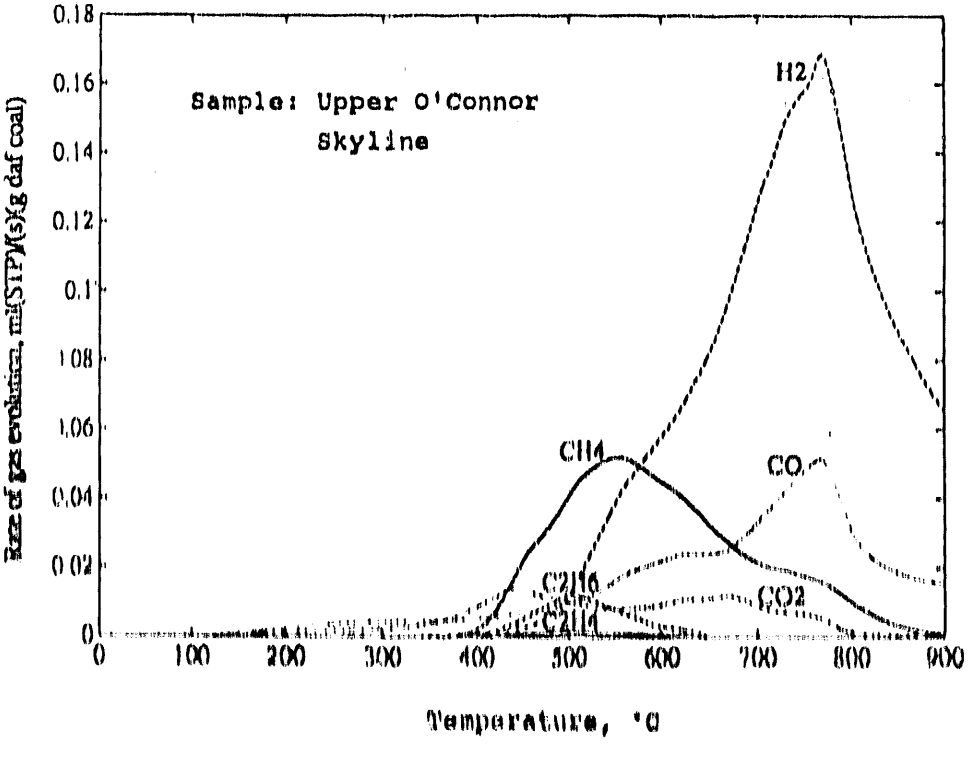

Figure 11.16 Pyrolysis gas yields for Upper O'Connor seam coal, Skyline mine.

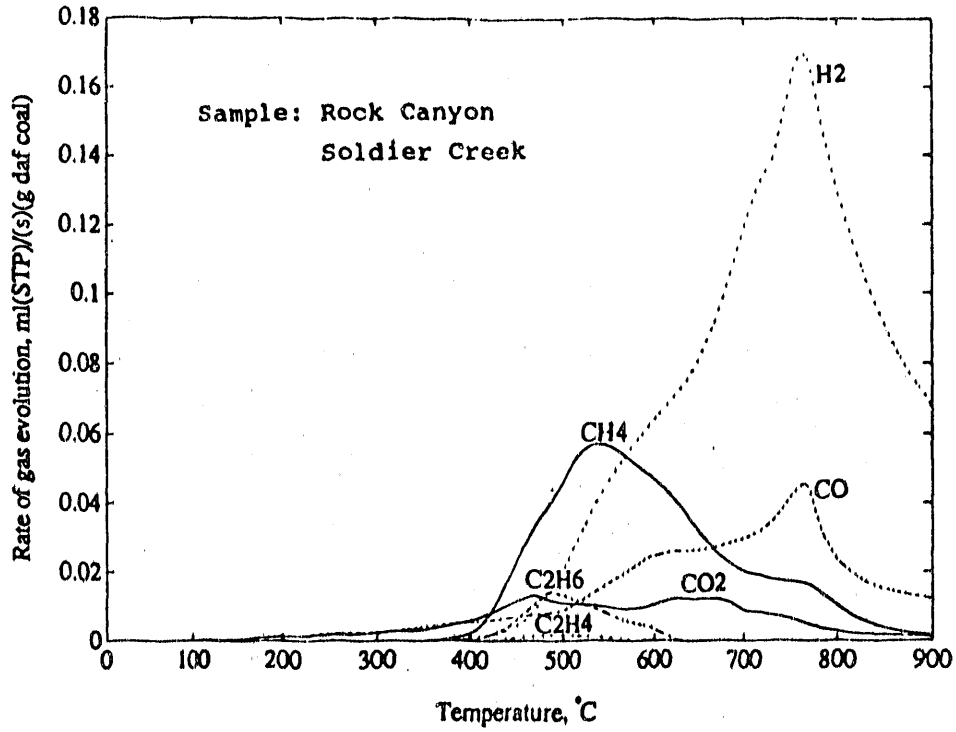

Figure 11.17 Pyrolysis gas yields for Rock Canyon seam coal, Soldier Creek mine.

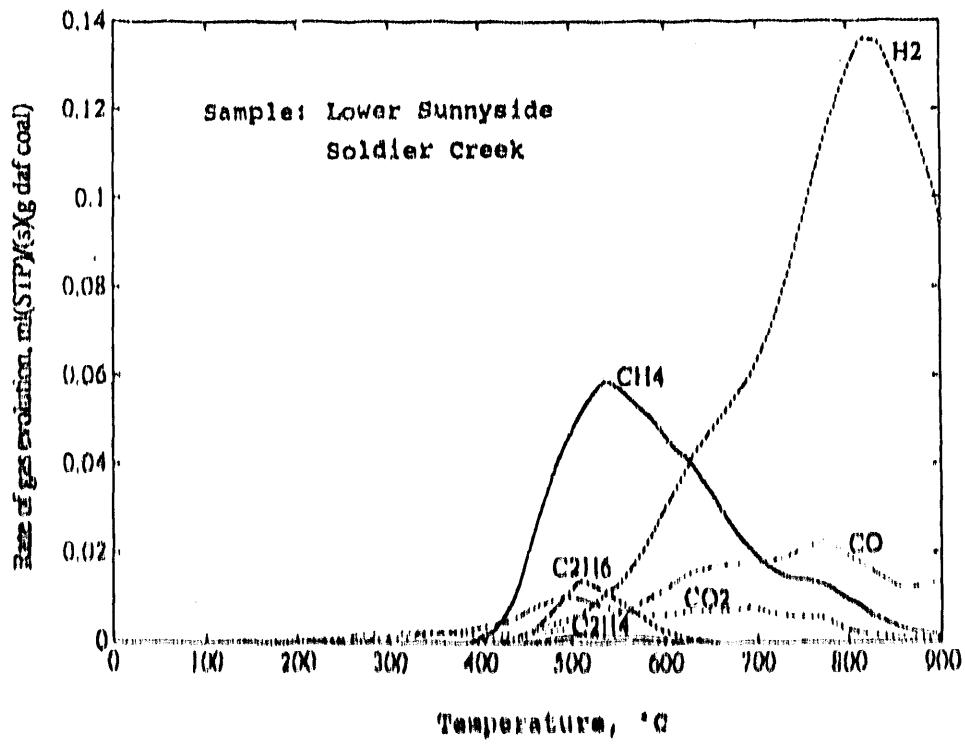

Figure 11.18 Pyrolysis gas yields for Lower Sunnyside seam coal, Soldier Creek mine.

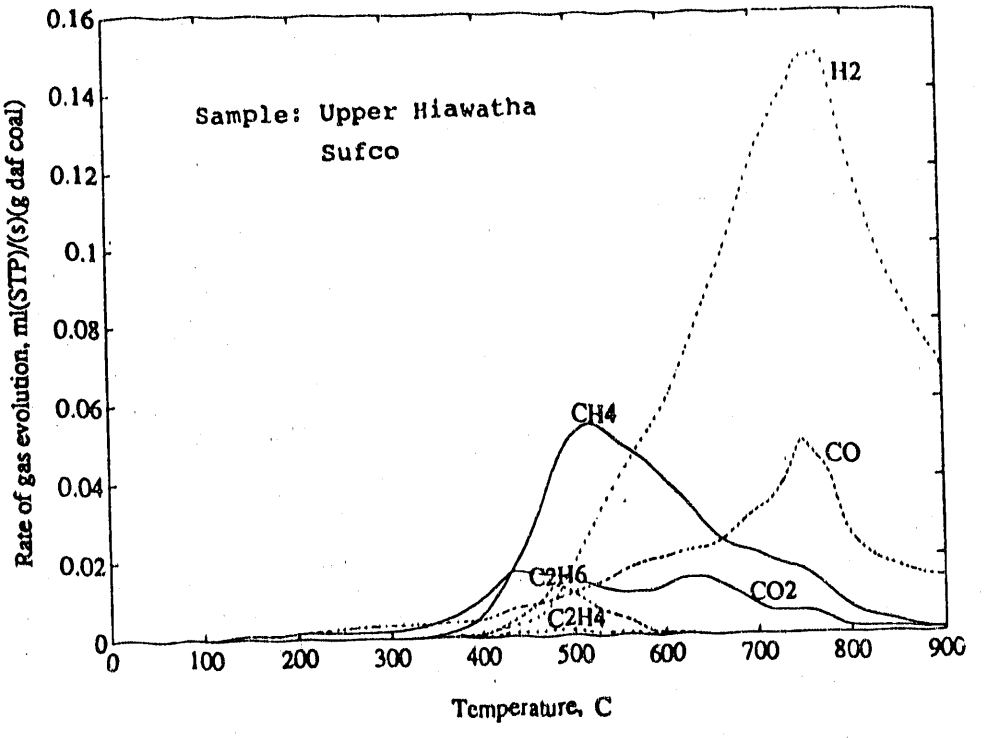

Figure 11.19 Pyrolysis gas yields for Upper Hiawatha seam coal, SUfCO mine.

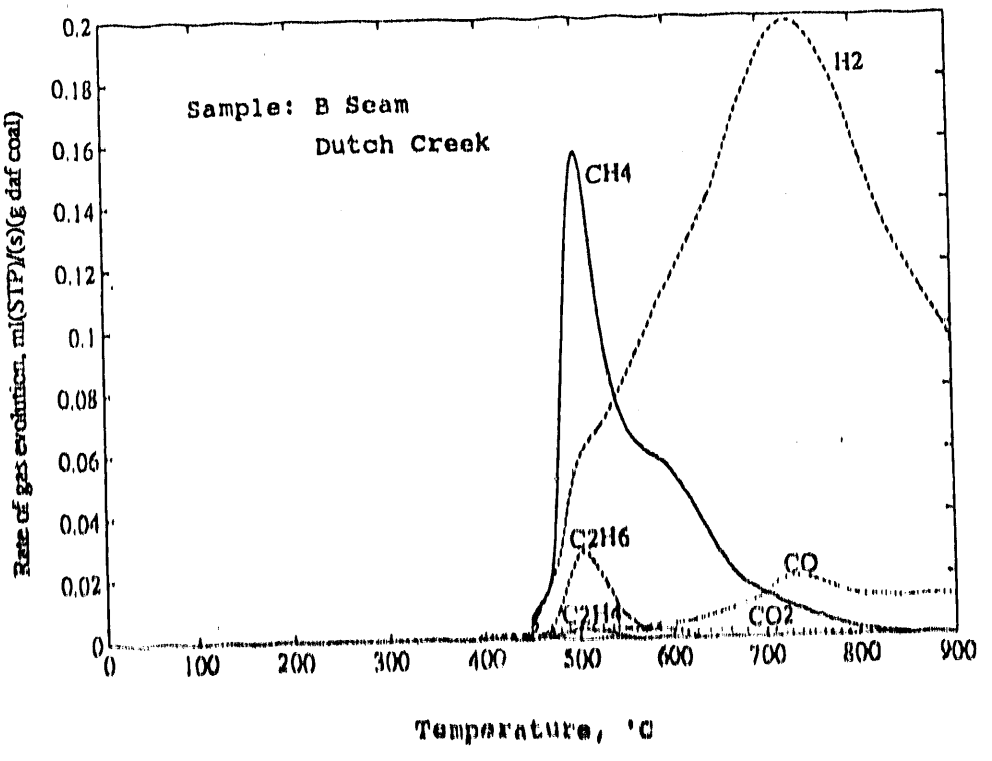

Figure 11.20 Pyrolysis gas yields for B seam, Dutch Creek mine.

Table 11.1 Characteristic parameters of the programmed-temperature pyrolysis of the ten Utah coals and one Colorado coal.

	Characteristic temperature, C		Max. rate*	Yield*	Percent
	Initial	Peak	ml/(sec.)(g)	ml/g	
Castlegate A (Aberdeen)					
CH4	348	524	0.066	67.6	19.3%
C2H4	410	487	0.0020	0.9	0.3%
C2H6	410	487	0.0151	6.9	2.0%
H2	391	749	0.148	199	56.7%
CO	176	744	0.0319	59.2	16.9%
CO2	119	471	0.0141	17.2	4.9%
			Total:	*351*	*99.9%*
Lower Sunnyside (Apex)					
CH4	335	527	0.055	60.4	17.4%
C2H4	400	504	0.0036	0.7	0.2%
C2H6	400	504	0.0286	5.7	1.6%
H2	378	730	0.198	200	57.6%
CO	168	732	0.0192	64.2	18.5%
CO2	97	504	0.0044	16.5	4.8%
			Total:	*348*	*100.1%*
Castlegate A (Beaver Creek #8)					
CH4	340	482	0.0642	59.1	19.5%
C2H4	410	498	0.0018	0.8	0.3%
C2H6	410	498	0.0151	6.9	2.3%
H2	408	820	0.134	164	54.1%
CO	172	765	0.0291	54.2	17.9%
CO2	108	473	0.0118	18.1	6.0%
			Total:	*303*	*100.0%*
Sub-3 (Castlegate)					
CH4	298	492	0.157	69.3	18.7%
C2H4	376	504	0.0036	1.0	0.3%
C2H6	376	504	0.0286	7.9	2.1%
H2	365	729	0.198	219	59.0%
CO	164	731	0.0456	55.5	15.0%
CO2	108	504	0.0131	18.1	4.9%
			Total:	*371*	*100.0%*

Table 11.1 *(Continued)*

	Characteristic temperature, C		Max. rate*	Yield*	Percent
	Initial	Peak	ml/(sec.)(g)	ml/g	
Gilson (Pinnacle)					
CH4	347	541	0.052	55.1	15.8%
C2H4	425	505	0.0016	1.0	0.3%
C2H6	425	505	0.0133	5.6	1.6%
H2	391	782	0.156	198	56.7%
CO	167	760	0.0453	68.5	19.6%
CO2	99	473	0.013	21.1	6.0%
			Total:	*349*	*100.1%*
Upper O'Connor (Skyline)					
CH4	269	554	0.052	60.5	17.0%
C2H4	378	502	0.0016	1.1	0.3%
C2H6	378	502	0.0122	7.2	2.0%
H2	352	769	0.169	199	56.1%
CO	154	768	0.0516	65.1	18.3%
CO2	90	442	0.0138	22.2	6.3%
			Total:	*355*	*100.0%*
Rock Canyon (Soldier Creek)					
CH4	300	539	0.057	64.1	17.9%
C2H4	346	487	0.0016	0.8	0.2%
C2H6	346	487	0.0142	7.5	2.1%
H2	384	762	0.170	205	57.2%
CO	151	765	0.0456	58.1	16.2%
CO2	88	470	0.0131	22.6	6.3%
			Total:	*358*	*99.9%*
Lower Sunnyside (Soldier Creek)					
CH4	368	538	0.0594	61.9	21.6%
C2H4	428	512	0.0017	1.0	0.3%
C2H6	428	512	0.0147	6.5	2.3%
H2	398	818	0.136	164	57.3%
CO	183	774	0.0231	36.5	12.8%
CO2	123	495	0.0107	15.9	5.6%
			Total:	*286*	*99.9%*

Table 11.1 *(Continued)*

	Characteristic temperature, C		Max. rate*	Yield*	Percent
	Initial	Peak	ml/(sec.)(g)	ml/g	
Upper Hiawatha (Sufco)					
CH4	294	517	0.0538	60.4	17.1%
C2H4	369	483	0.0016	0.8	0.2%
C2H6	369	483	0.0130	5.9	1.7%
H2	368	771	0.149	199	56.4%
CO	152	748	0.0490	60.8	17.2%
CO2	86	437	0.0168	26.2	7.4%
			Total:	*353*	*100.0%*
Lower Sunnyside (Sunnyside)					
CH4	309	500	0.0683	62.4	18.6%
C2H4	387	482	0.0018	0.9	0.3%
C2H6	387	482	0.0153	7.3	2.2%
H2	383	764	0.160	208	61.9%
CO	160	741	0.0257	44.7	13.3%
CO2	91	481	0.0089	12.4	3.7%
			Total:	*336*	*99.9%*
B seam (Dutch Creek, Colorado)					
CH4	419	502	0.157	73.5	18.3%
C2H4	450	505	0.0036	0.8	0.2%
C2H6	450	505	0.0286	7.5	1.9%
H2	444	731	0.198	298	74.2%
CO	181	732	0.0192	17.0	4.2%
CO2	129	505	0.0044	5.0	1.2%
			Total:	*402*	*100.0%*

** On a daf basis; ml at STP*

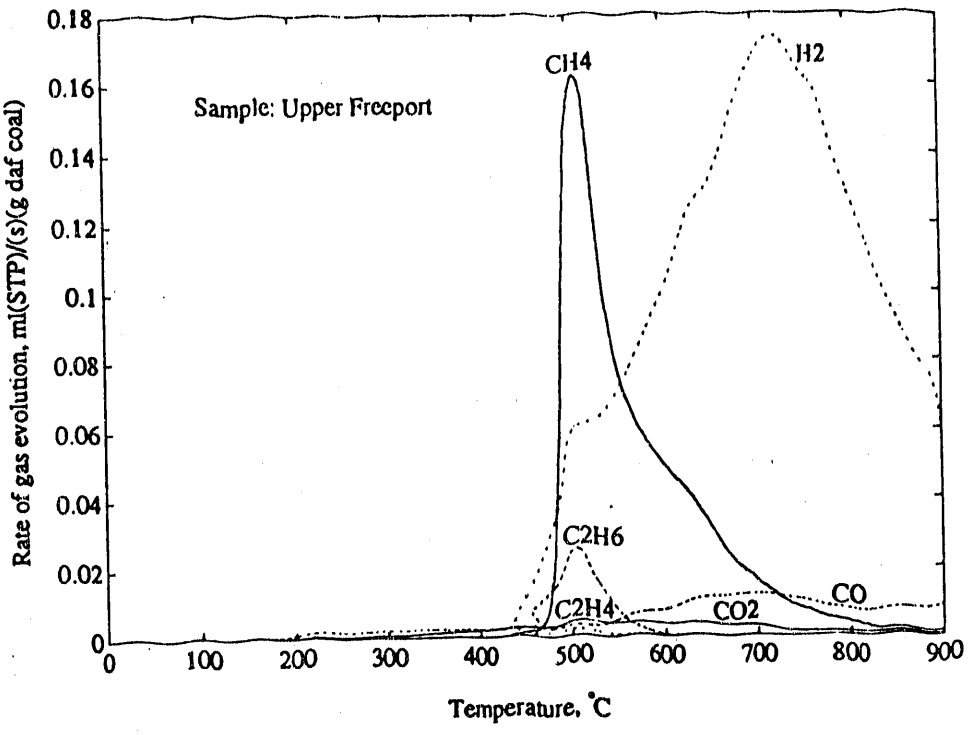

Figure 11.21 Pyrolysis gas yields for Upper Freeport coal.

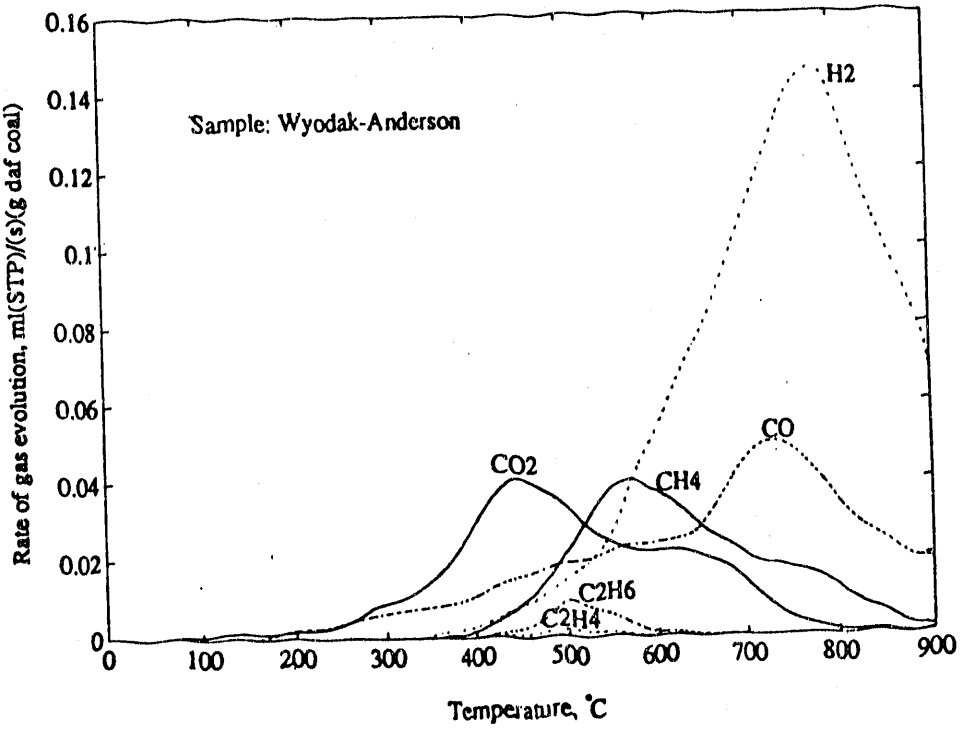

Figure 11.22 Pyrolysis gas yields for Wyodak-Anderson coal.

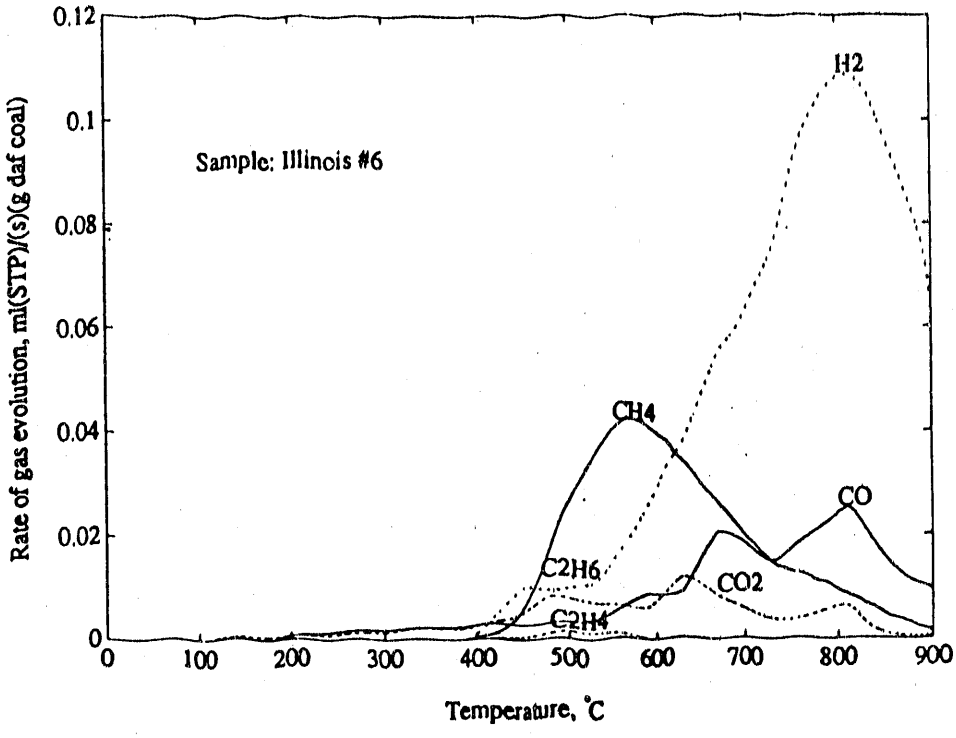

Figure 11.23 Pyrolysis gas yields for Illinois #6 coal.

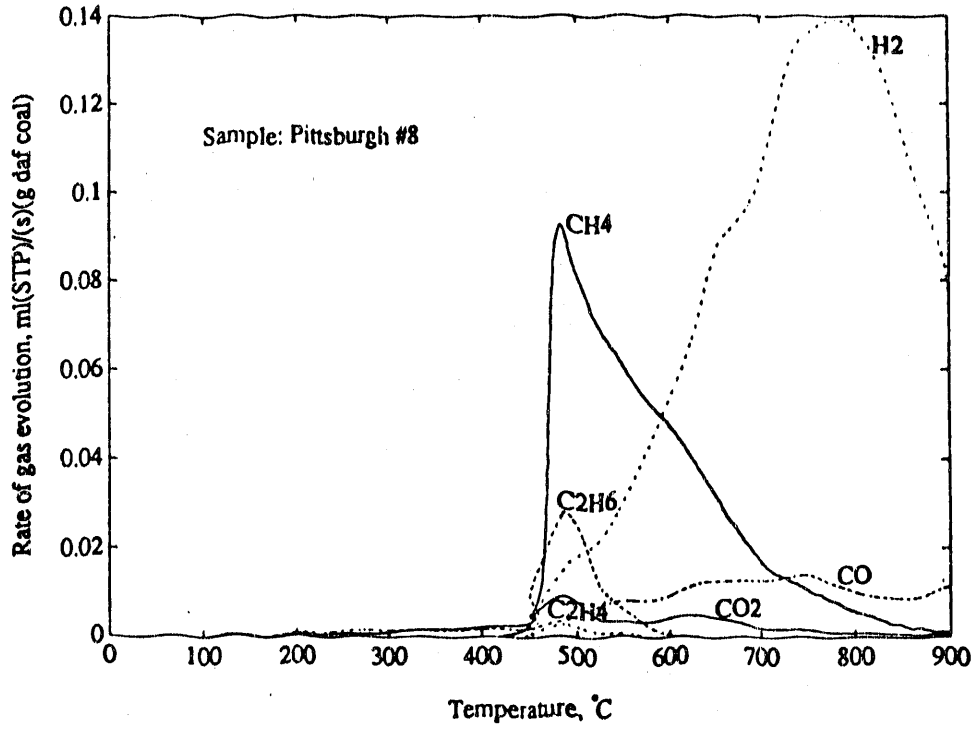

Figure 11.24 Pyrolysis gas yields for Pittsburgh #8 coal.

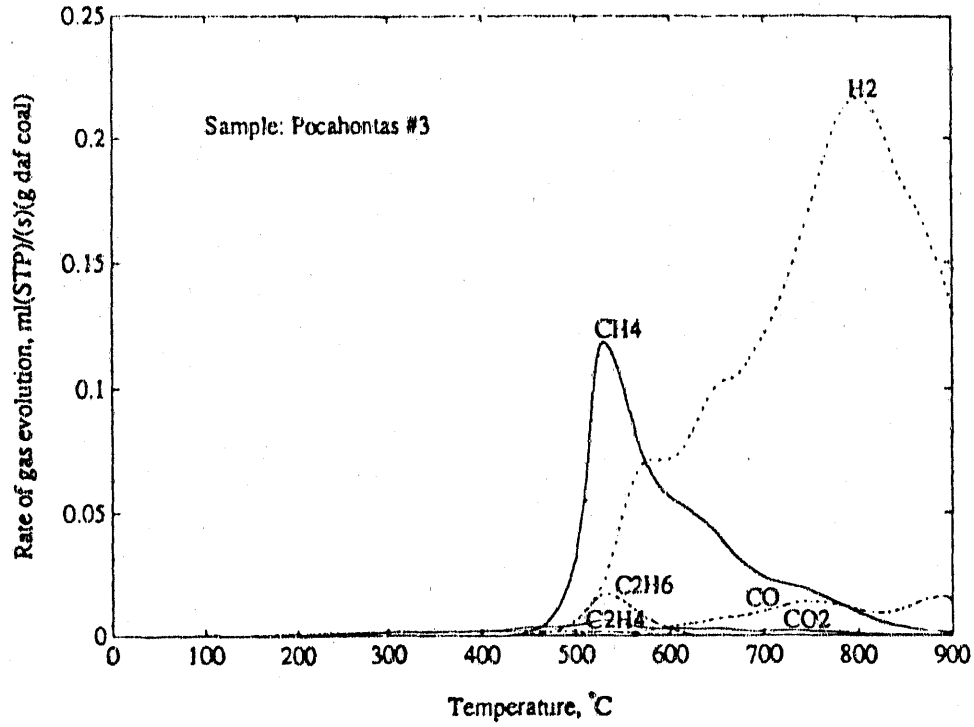

Figure 11.25 Pyrolysis gas yields for Pocahontas #3 coal.

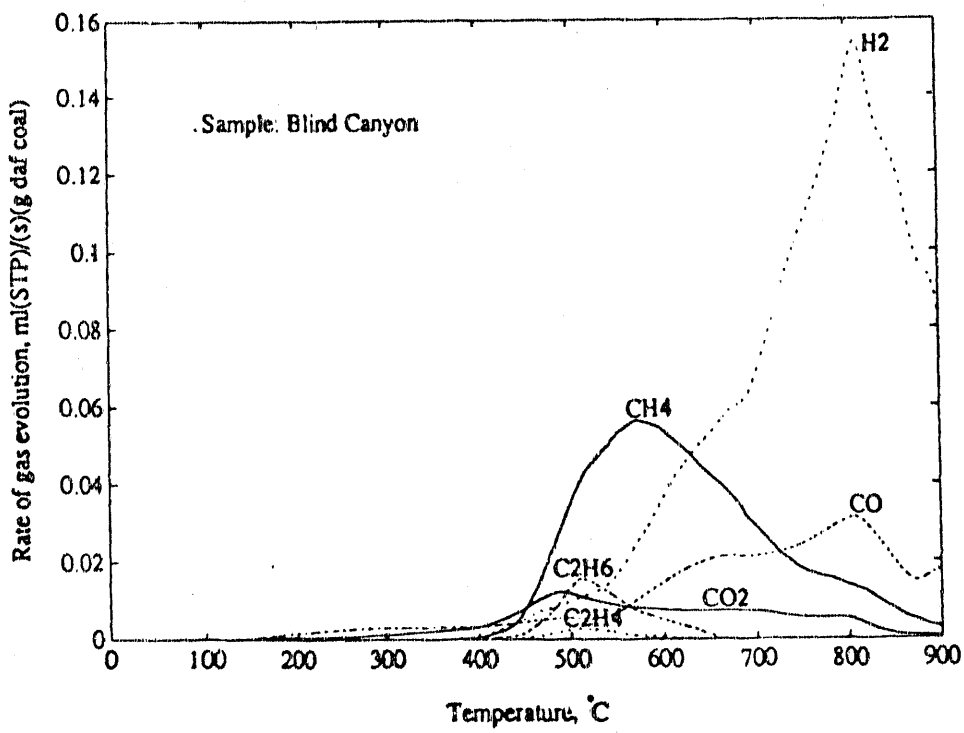

Figure 11.26 Pyrolysis gas yields for Blind Canyon coal.

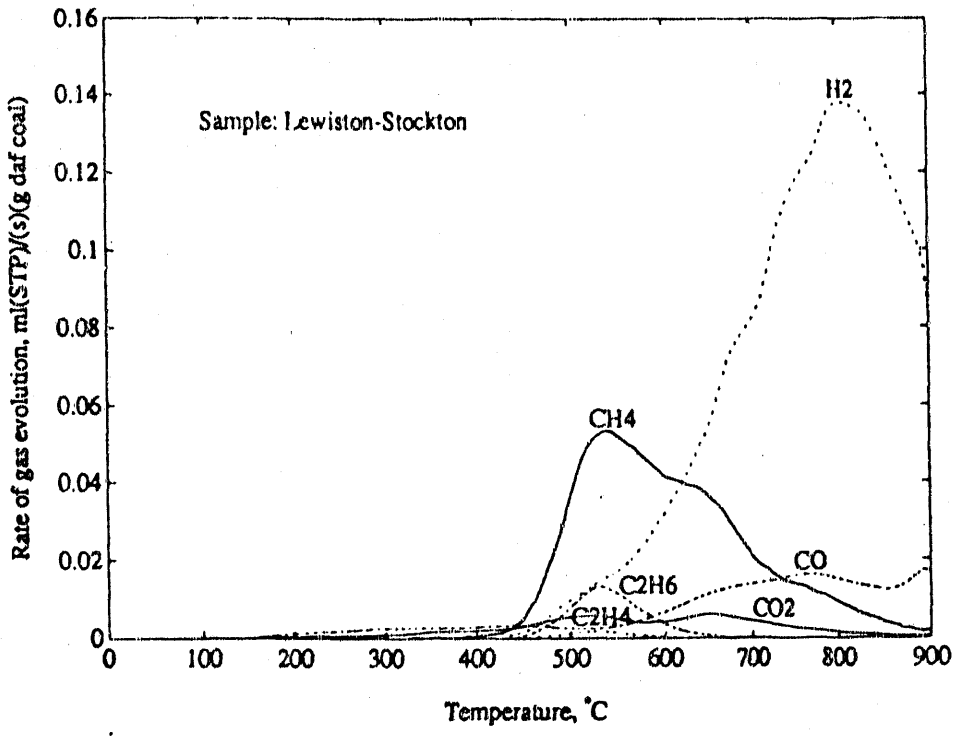

Figure 11.27 Pyrolysis gas yields for Lewiston-Stockton coal.

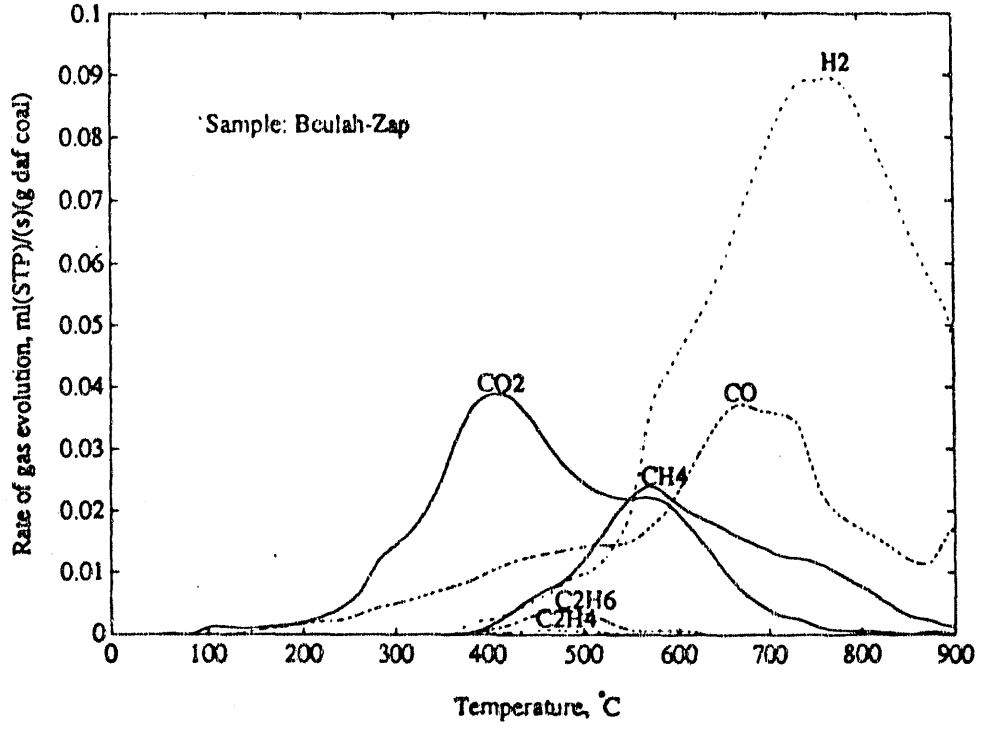

Figure 11.28 Pyrolysis gas yields for Beulah-Zap coal.

Table 11.2 Characteristic parameters of the programmed-temperature pyrolysis of the Argonne Premium Coal Bank samples

	Characteristic temperature, C		Max. rate*	Yield*	Percent
	Initial	Peak	ml/(sec.)(g)	ml/g	
Upper Freeport (PA), Med. Vol. Bit.					
CH4	405	508	0.162	71.5	19.7%
C2H4	416	504	0.0018	0.5	0.1%
C2H6	416	504	0.0252	7.2	2.0%
H2	445	724	0.173	254	70.0%
CO	166	691	0.0118	22.9	6.3%
CO2	79	512	0.0043	6.7	1.8%
			Total:	*363*	*100.0%*
Wyodak-Anderson (WY), Subbituminous					
CH4	362	575	0.0401	47.8	12.5%
C2H4	385	508	0.0017	0.8	0.2%
C2H6	385	508	0.0092	4.2	1.1%
H2	365	780	0.146	193	50.4%
CO	163	732	0.0498	82.8	21.6%
CO2	71	447	0.0409	54.3	14.2%
			Total:	*383*	*100.0%*
Illinois #6 (IL), High Vol. Bit.					
CH4	384	573	0.0421	47.7	19.4%
C2H4	388	504	0.0014	0.7	0.3%
C2H6	388	504	0.0116	6.1	2.5%
H2	387	807	0.109	143	58.1%
CO	183	812	0.0251	33.3	13.5%
CO2	106	483	0.0081	15.5	6.3%
			Total:	*246*	*100.0%*
Pittsburgh #8 (PA), High Vol. Bit.					
CH4	419	485	0.0926	65.3	21.1%
C2H4	445	487	0.0026	0.8	0.3%
C2H6	445	487	0.0281	8.4	2.7%
H2	429	782	0.139	200	64.5%
CO	162	749	0.0139	27.1	8.7%
CO2	106	486	0.0091	8.5	2.7%
			Total:	*310*	*100.0%*

Table 11.2 *(Continued)*

	Characteristic temperature, C		Max. rate*	Yield*	Percent
	Initial	Peak	ml/(sec.)(g)	ml/g	
Pocahontas #3 (VA), Low Vol. Bit.					
CH4	420	529	0.118	72.2	19.2%
C2H4	428	529	0.0016	0.5	0.1%
C2H6	428	529	0.0171	5.9	1.6%
H2	447	799	0.216	277	73.7%
CO	141	750	0.0136	13.2	3.5%
CO2	87	529	0.0061	7.0	1.9%
			Total:	*376*	*100.0%*
Blind Canyon (UT), High Vol. Bit.					
CH4	369	572	0.0564	65.2	20.9%
C2H4	387	512	0.0026	1.2	0.4%
C2H6	387	512	0.0156	7.7	2.5%
H2	395	811	0.154	173	55.3%
CO	139	807	0.0313	48.1	15.4%
CO2	68	488	0.0122	17.4	5.6%
			Total:	*313*	*100.0%*
Lewiston-Stockton (WV), High Vol. Bit.					
CH4	352	543	0.0532	54.7	19.5%
C2H4	440	529	0.0018	0.7	0.2%
C2H6	440	529	0.0132	6.0	2.1%
H2	426	804	0.138	179	63.7%
CO	140	768	0.0160	31.3	11.1%
CO2	99	521	0.0057	9.5	3.4%
			Total:	*281*	*100.0%*
Beulah-Zap (ND), Lignite					
CH4	355	570	0.0240	29.0	10.4%
C2H4	356	465	0.0007	0.4	0.1%
C2H6	356	465	0.0039	2.1	0.8%
H2	364	769	0.0900	135	48.3%
CO	115	668	0.0372	62.5	22.4%
CO2	52	412	0.0389	50.3	18.0%
			Total:	*279*	*100.0%*

** On a daf basis; ml at STP*

Table 11.3 Gas, char and tar yields* in coal pyrolysis

No.	Seam	State	Rank	Gas yield wt%	Char yield wt%	Liquid yield** wt%
Aronne Premium Coal Back samples						
1	Upper Freeport	PA	Med. Vol. Bit.	12.6	72.3	15.1
2	Wyodak-Anderson	WY	Subbituminous	26.8	46.2	27.0
3	Illinois #6	IL	High Vol. Bit.	12.8	57.7	29.5
4	Pittsburgh (#8)	PA	High Vol. Bit.	12.7	61.9	25.4
5	Pocahontas #3	VA	Low Vol. Bit.	11.5	84.6	3.9
6	Blind Canyon	UT	High Vol. Bit.	16.8	56.8	26.4
7	Lewiston-Stockton	WY	High Vol. Bit.	12.2	65.3	22.5
8	Beulah-Zap	ND	Lignite	21.3	49.8	28.9
Utah coals						
9	Castlegate A, AB	UT	High Vol. Bit.	18.4	60.1	21.5
10	L. Sunnyside, Apex	UT	High Vol. Bit.	18.2	67.7	14.1
11	Castlegate A, BC	UT	High Vol. Bit.	17.0	61.9	21.1
12	Sub-3	UT	High Vol. Bit.	18.6	66.5	14.9
13	Gilson	UT	High Vol. Bit.	19.3	72.2	8.5
14	Upper O'Connor	UT	High Vol. Bit.	19.7	63.2	17.1
15	Rock Canyon	UT	High Vol. Bit.	19.2	71.0	9.8
16	L. Sunnyside, SC	UT	High Vol. Bit.	14.6	65.9	19.5
17	Upper Hiawatha	UT	High Vol. Bit.	19.7	68.5	11.8
18	L. Sunnyside, SY	UT	High Vol. Bit.	15.4	67.2	17.4
Colorado coal						
19	B Seam	CO	Med. Vol. Bit.	12.1	84.1	3.8

Abbreviations: AB, Aberdeen; BC, Beaver Creek #8; SC, Soldier Creek; SY, Sunnyside
** On a daf basis; ** Liquid including tar, oil and water calculated by difference*

hydrocarbon gases was produced from the decomposition of aliphatic groups in the coal and/or the methanation of coal. At the stage where chars were formed, hydrogen gas was evolved as a major component.

The ultimate and proximate analyses of the pyrolysis chars from ten Utah coals and one Colorado coal are given in Table 11.4. All chars show similar properties with approximately 0.6 wt% H and 97 wt% C. About 60 - 80 percent of the nitrogen and sulfur are retained in the char. A van Krevelen plot (van Krevelen, 1961), e.g., H/C versus O/C, for the coals, chars and typical materials (Speight, 1983) (i.e., wood, peat, lignite, subbituminous, bituminous and anthracite) is shown in Figure 11.29a. The same plot expanded for the range of the coals and chars is shown in Figure 11.29b. As expected, coal pyrolysis follows the natural coalification trend. To convert the coals to chars, both hydrogen-containing and oxygen-containing species must be liberated from the coal during pyrolysis. The same gas evolution behavior has been found in the coalification process. This indicates that coal pyrolysis can be used to simulate the coalification process to some degree and the propensity of the coal to form additional methane can therefore be estimated by the methane production during coal pyrolysis.

11.3.5 Correlations

The dependence of production of different gases in coal pyrolysis on coal a rank parameter, carbon content, is shown in Figures 11.30-11.34. Both hydrogen and methane production increase with an increase of carbon content. However, methane production shows an approach to a constant level at carbon contents larger than 95 wt%. The production of the C_2 hydrocarbon gas fraction (including ethane and ethylene) increases with increasing carbon content initially. After reaching a maximum at about 85 wt%, it decreases with increasing carbon content. Both carbon monoxide and carbon dioxide productions decrease with increasing carbon content. However, the carbon dioxide production shows an approach to a constant value at carbon contents larger than 95 wt%. The correlation of the gas, liquid, and conversion (gas + liquid) yields of coal pyrolysis with carbon content is shown in Figure 11.35. As expected, the yields of gas, liquid and conversion decrease with increasing carbon content. Liquid yield shows more sensitivity to carbon content than gas yield.

To evaluate the contribution of aliphatic groups in coal to methane formation during coal pyrolysis, a plot of pyrolysis methane production versus the total fraction of aliphatic carbon for the eight Argonne Premium Coal Bank samples is shown in Figure 11.36. Obviously, there exists an unexpected negative correlation, although there is scatter in the results. This indicates that methane formation from the

Table 11.4 Proximate and ultimate analyses of chars

Seam	Mine	Proximate analysis (wt%)			Ultimate analysis (wt%, daf)				
		Moisture	Ash*	V.M.*	C	H	N	S	O**
Castlegate A	Aberdeen	1.03	4.23	3.89	96.91	0.58	2.27	0.61	0.00
Lower Sunnyside	Apex	1.20	8.61	3.98	96.69	0.60	2.04	0.43	0.24
Castlegate A	Beaver Creek #8	1.05	5.20	4.44	96.61	0.66	1.81	0.58	0.34
Sub-3	Castlegate	0.79	7.80	4.50	96.62	0.59	1.90	0.55	0.35
Gilson	Pinnacle	0.98	11.18	4.21	97.55	0.57	1.87	0.38	0.00
Upper O'Connor	Skyline	1.02	9.06	4.19	96.94	0.63	1.53	0.53	0.37
Rock Canyon	Soldier Creek	1.22	9.22	4.74	97.39	0.58	1.82	0.39	0.00
Lower Sunnyside	Soldier Creek	1.44	9.56	4.71	96.99	0.60	1.44	0.54	0.43
Upper Hiawatha	Sufco	0.94	10.65	4.48	97.40	0.62	1.34	0.35	0.30
Lower Sunnyside	Sunnyside	0.71	7.76	3.62	96.15	0.57	1.94	0.48	0.86
B Seam	Dutch Creek	0.13	8.52	4.57	97.19	0.60	1.99	0.55	0.00
			Mean:	*4.30*	*96.95*	*0.60*	*1.81*	*0.49*	*0.26*
			Std:	*0.34*	*0.40*	*0.03*	*0.26*	*0.08*	*0.25*

Abbreviations: V.M., volatile matter; daf, dry ash free basis
** dry basis; ** by difference*

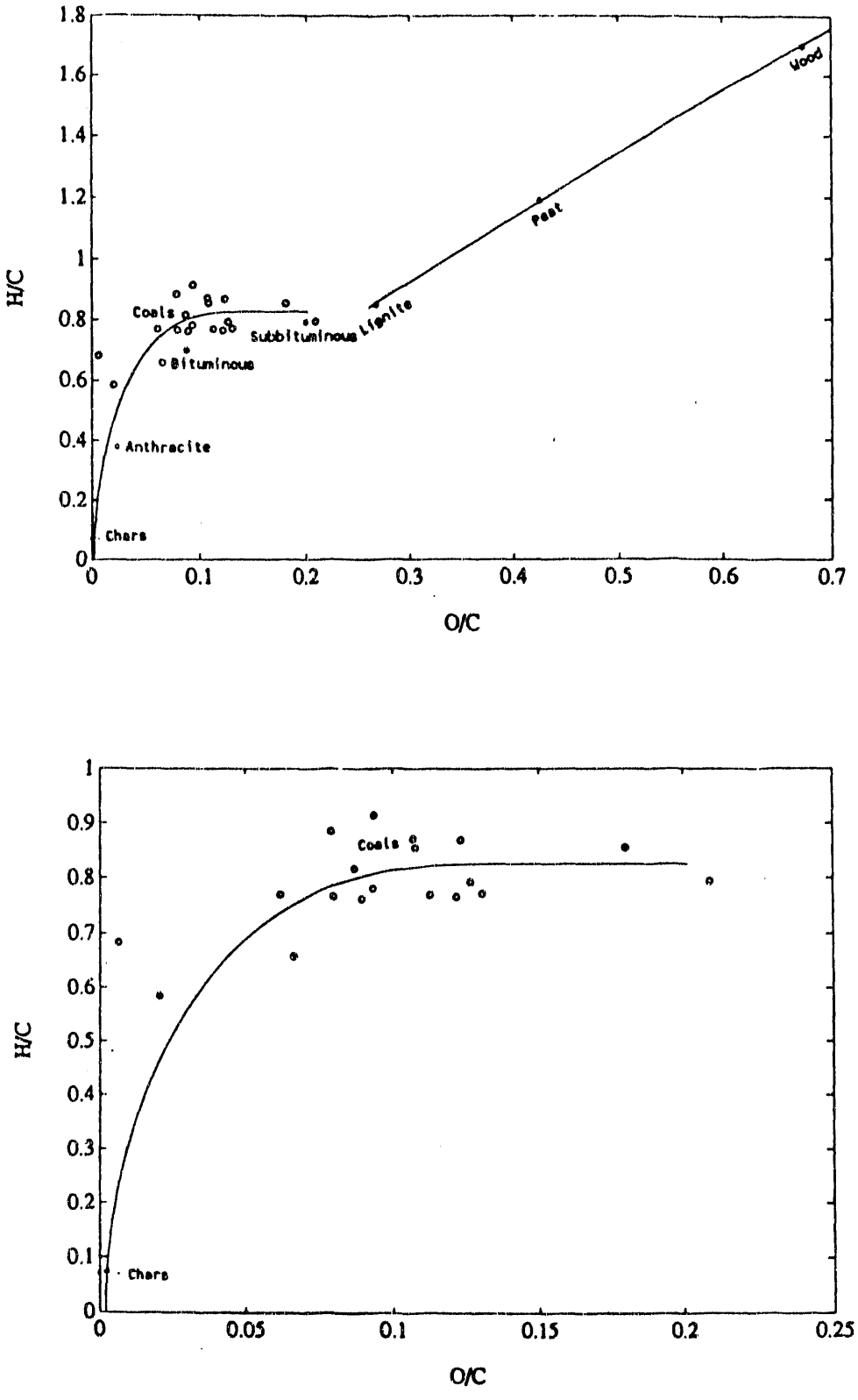

Figure 11.29 van Krevelen plots.

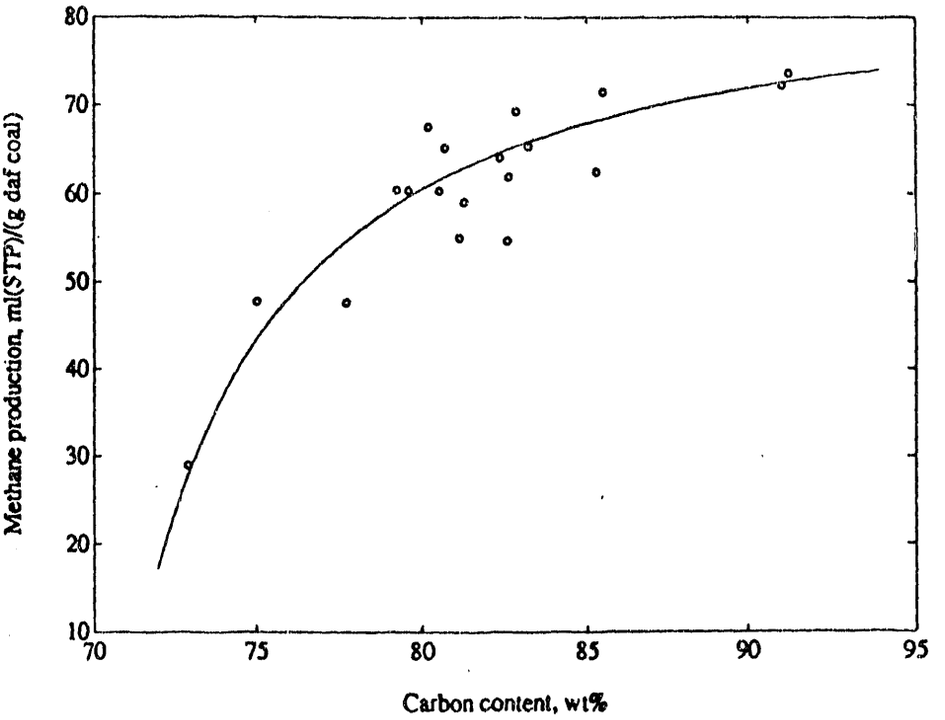

Figure 11.30 Pyrolysis methane yield versus carbon content.

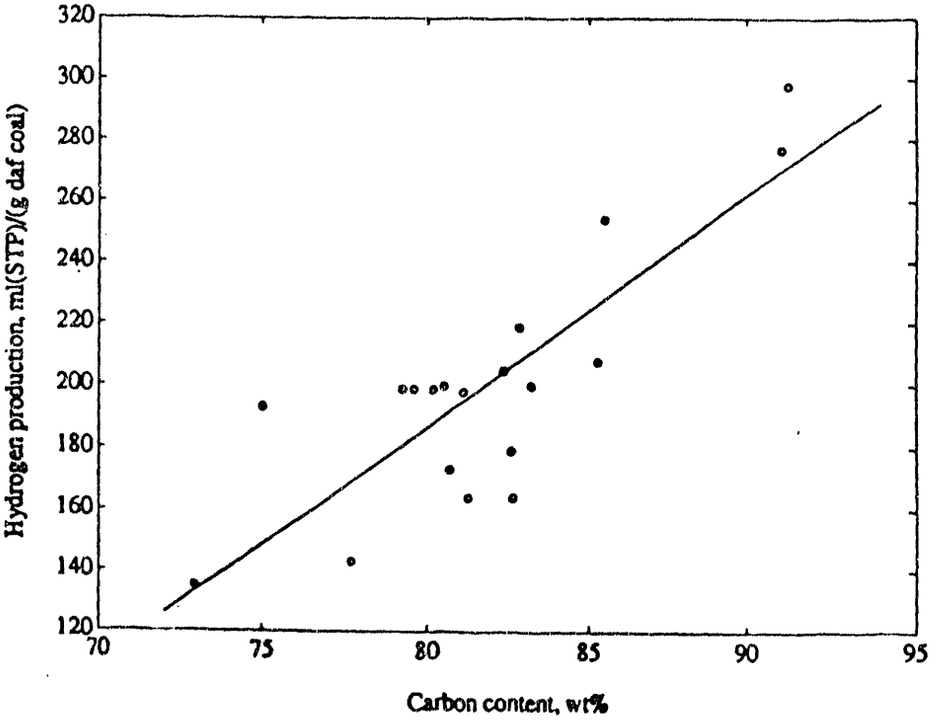

Figure 11.31 Pyrolysis hydrogen yield versus carbon content.

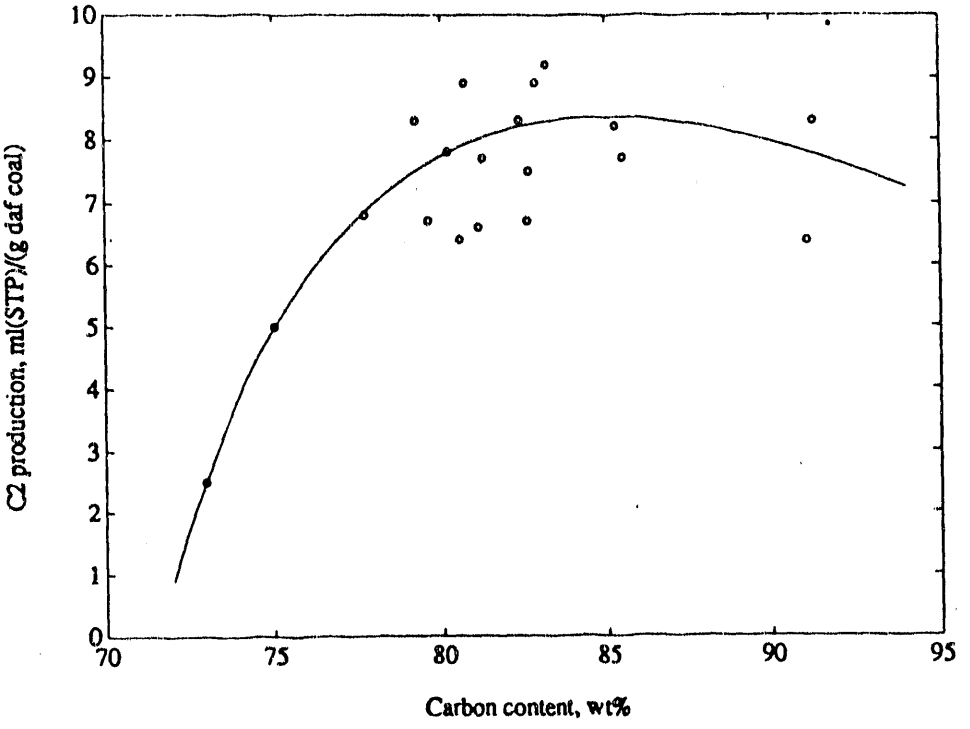

Figure 11.32 Pyrolysis ethane and ethylene yield versus carbon content.

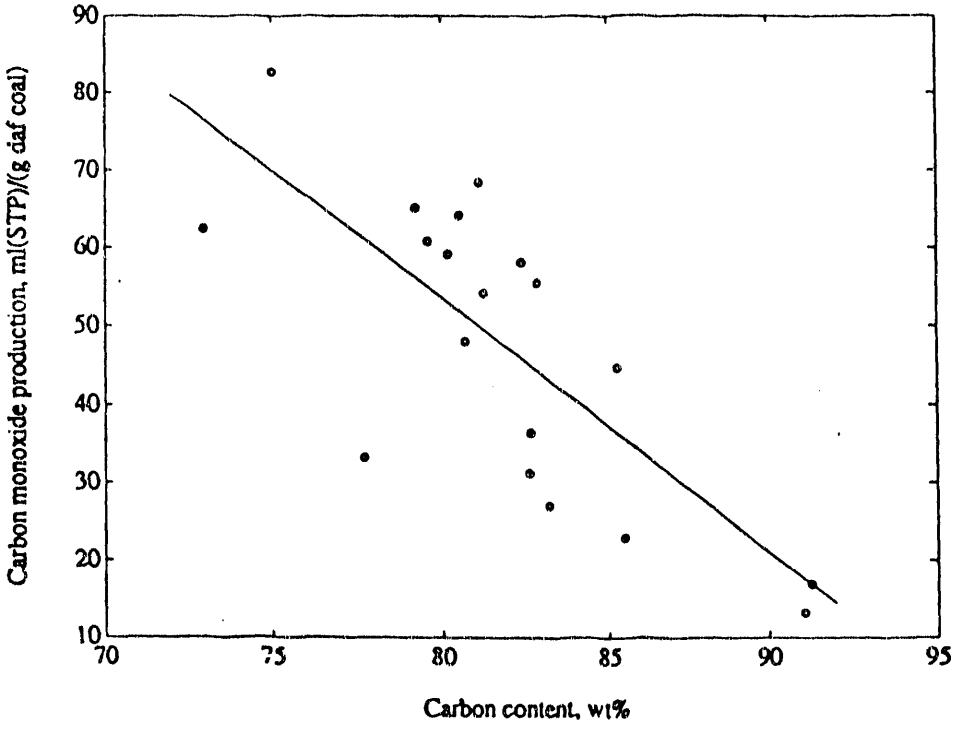

Figure 11.33 Pyrolysis carbon monoxide yield versus carbon content.

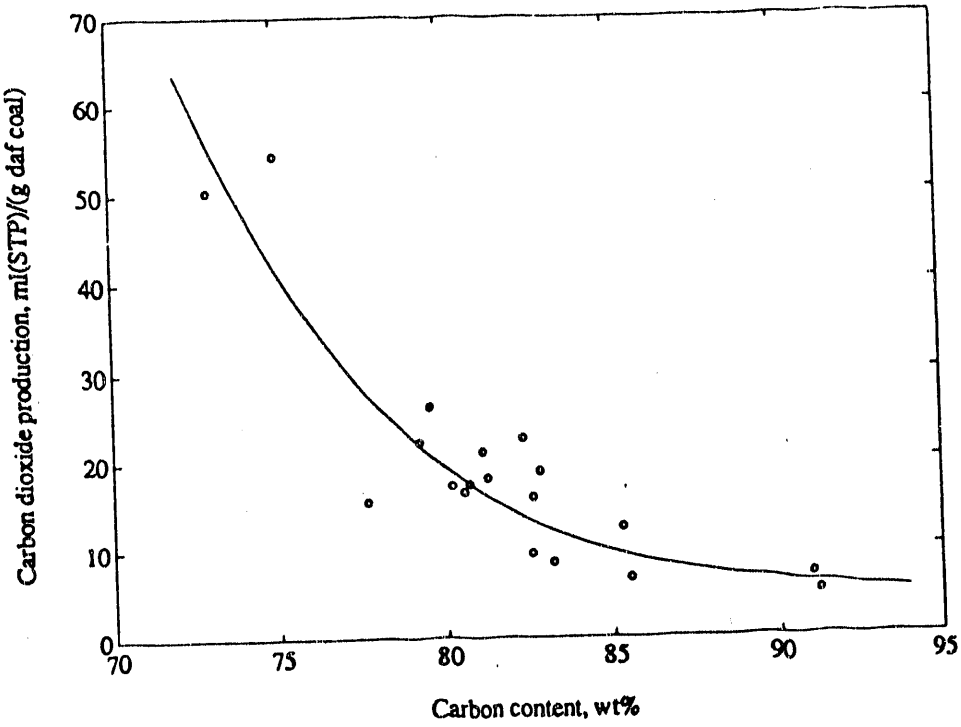

Figure 11.34 Pyrolysis carbon dioxide yield versus carbon content.

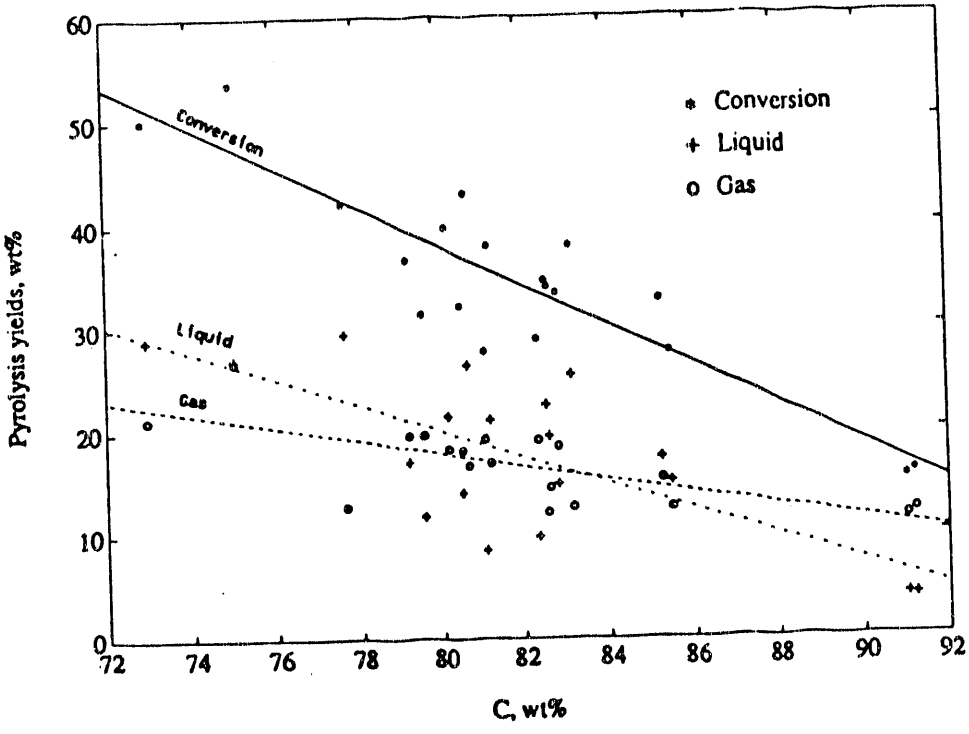

Figure 11.35 Pyrolysis yields versus carbon content.

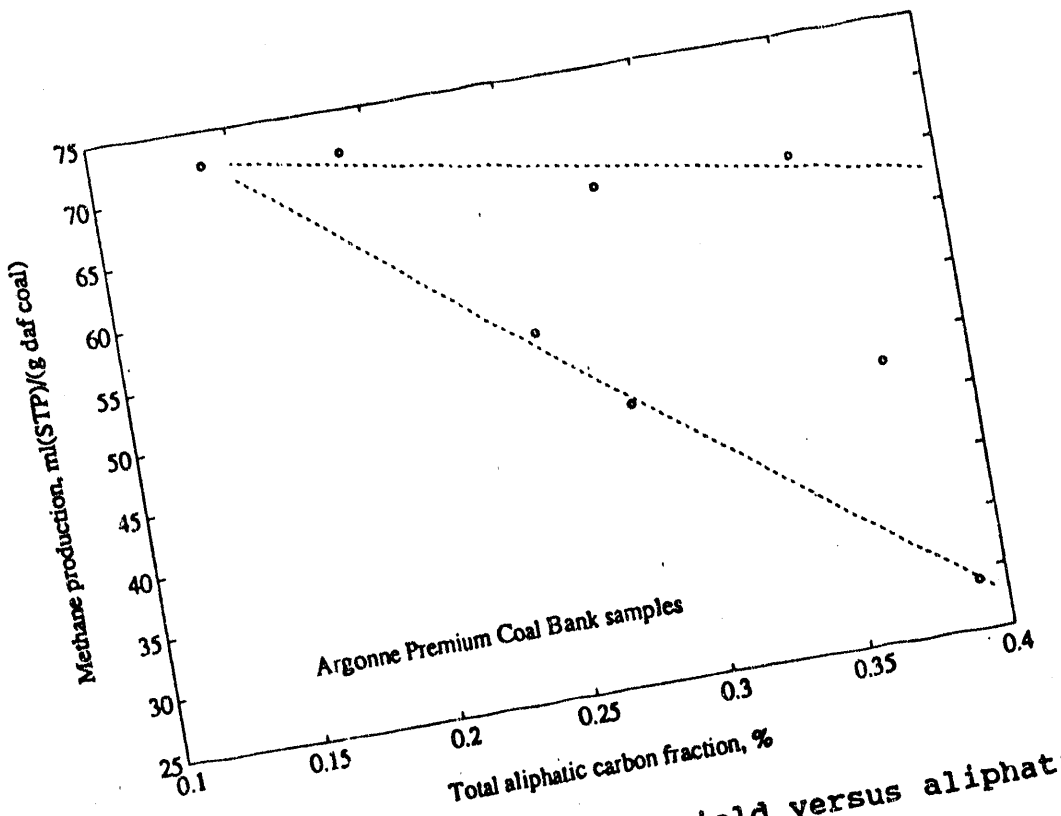

Figure 11.36 Pyrolysis methane yield versus aliphatic carbon.

decomposition of aliphatic groups in coal is not the dominant factor in coal pyrolysis.

The possible reactions to form methane during coal pyrolysis are:

1. Decomposition of aliphatic groups in coal (Graber and Huettinger. 1982a, 1982b, 1982c);

2. Coal-CH_x (x = 0 to 3) structural species produced during coal pyrolysis reacting with activated hydrogen ($H^\bullet$) which is generated in coal pyrolysis, i.e.,

$$Coal\text{-}CH_x + H^\bullet \rightarrow Coal\text{-}CH_{x+1} ;$$

for the final step (x = 3),

$$Coal\text{-}CH_3 + H^\bullet \rightarrow Coal + CH_4 .$$

3. Hydrogenation (Makino and Toda (1979a, 1979b), a secondary pyrolysis reaction,

$$C + 2H_2 \rightarrow CH_4.$$

There is a significant amount of methane produced by the hydrogenation reaction under high pressure of hydrogen (Morris and Keairns, 1979; Suuberg et al., 1980; Sundaram et al., 1982). A comparison of gas yields from pyrolysis using a helium atmosphere and a hydrogen atmosphere at 69 atm pressure is given in Table 11.5 (adapted from Suuberg et al., 1980). Methane yields during coal pyrolysis in a hydrogen atmosphere are four to seven times higher than those in a helium atmosphere. It is obvious that the main contribution to methane formation in hydropyrolysis is the hydrogenation reaction. It is interesting to compare total CO, CO_2 and H_2O formation in the two atmospheres. Apparently, the hydrogen atmosphere depresses CO and CO_2 formation, but favors water formation. This can be explained by a proposed hypothesis that the consumption of oxygen groups in coal during hydropyrolysis is by competitive reactions:

1. Formation of CO and CO_2:

$$Coal\text{-}O \rightarrow CO + Coal,$$

$$Coal\text{-}OO \rightarrow CO_2 + Coal;$$

2. Formation of H_2O

$$Coal\text{-}OO + 2H_2 \rightarrow 2H_2O + Coal,$$

$$Coal\text{-}O + H_2 \rightarrow H_2O + Coal.$$

When an H_2 atmosphere is used in coal pyrolysis, the oxygen-containing groups in coal can partially react with H_2 to form H_2O. Therefore, compared with coal pyrolysis in a He atmosphere, the hydropyrolysis of coal produces more water, and less CO and CO_2.

Since the decomposition of aliphatic groups in coal is not a main contributing factor for methane formation during coal pyrolysis, the methanation of carbon in coal by Coal-CH_x ($x = 0$ to 3) reacting with H^* and/or by hydrogenation becomes important. A plot (Figure 11.37) of methane production versus hydrogen production during coal pyrolysis shows a positive correlation. This supports this hypothesis. Since these pyrolysis experiments were performed at atmospheric pressure and the pyrolysis products including both gas and liquid were swept from the reactor using inert helium or argon as carrier gas, the contribution from the hydrogenation reaction to methane formation was negligible. Therefore, the concentration of activated hydrogen (H^*) determines both

Table 11.5 Comparion of yields from pyrolysis and hydropyrolysis at 69 atm pressure
(Adapted from Suuberg et al, 1978)

Gas product	Yield, wt% of lignite as-received*		Yield, wt% of coal as-received**	
	69 atm He	69 atm H2	69 atm He	69 atm H2
CO	9.0	7.1	2.5	N.M.
CO2	10.6	8.5	1.7	1.3
H2O	12.9	16.0	[illegible]	N.M.
CH4	2.5	9.5	[illegible]	23.2
C2H4	0.6	0.2	[illegible]	0.4
C2h6	0.2	[illegible]	[illegible]	2.3
Other hydrocarbons	1.7	[illegible]	[illegible]	8.0
Tar	3.0	8.0	[illegible]	12.0
Char	59.8	[illegible]	[illegible]	40.2

Abbreviation: N.M., not measured

* *Sample: Montana lignite; heating rate: 1000 C/s; average particle diameter, 74 m; holding time and temperature: pyrolysis under 69 atm He, 10 s at 850–1070 C; Hydorpyrolysis under 69 atm H2, 10 s at 850–1000 C;*

** *Sample: Pittsburgh seam bituminous coal; heating rate: 1000 C/s; average particle diameter, 74 m; holding time and temperature: pyrolysis under 69 atm He, 2–10 s at 850–1070 C; hydorpyrolysis under 69 atm H2, 14–20 s at 870–930 C*

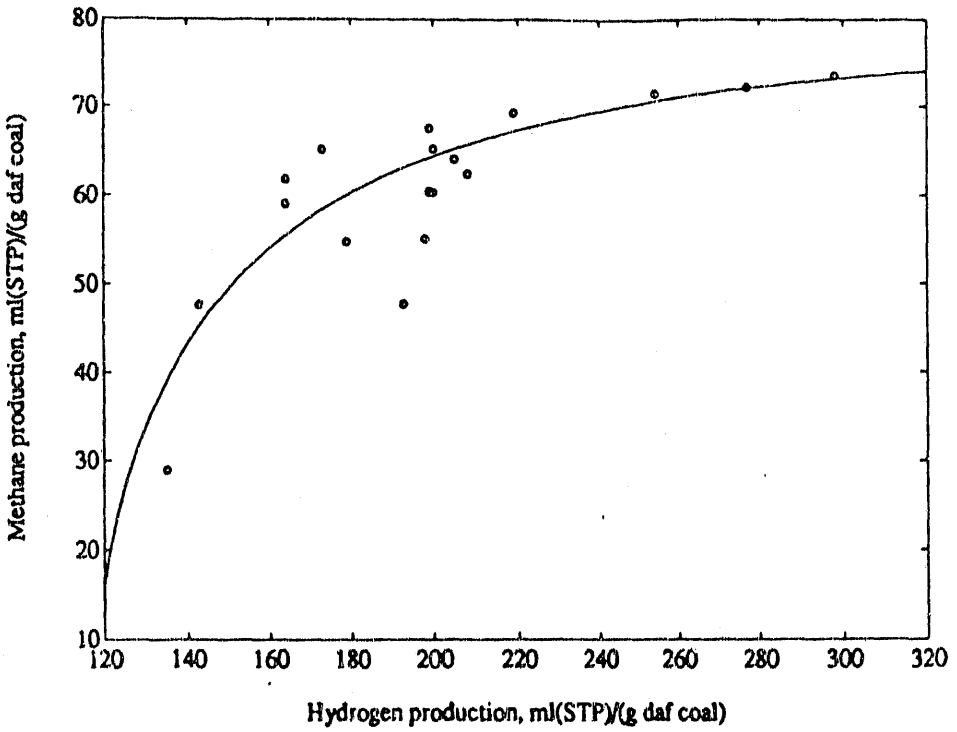

Figure 11.37 Pyrolysis methane yield versus pyrolysis hydrogen yield.

methane and hydrogen production. The activated hydrogen, H^*, which is generated during coal pyrolysis, may undergoes three types of reactions to form three kinds of product. They are

1. Methane production:

$$Coal\text{-}CH_x + H^* \rightarrow Coal\text{-}CH_{x+1} \qquad (x = 0 - 2)$$

$$Coal\text{-}CH_3 + H^* \rightarrow CH_4 + Coal.$$

For other hydrocarbon gases, such as ethane formation, the mechanisms are:

$$Coal\text{-}CH_2\text{-}CH_x + H^* \rightarrow Coal\text{-}CH_2\text{-}CH_{x+1} \qquad (x = 0 - 3)$$

$$Coal\text{-}CH_2\text{-}CH_3 + H^* \rightarrow C_2H_6 + Coal.$$

2. Hydrogen production:

$$H^* + H^* \rightarrow H_2.$$

3. Water production:

$$Coal\text{-}O + H^{*} \rightarrow Coal\text{-}OH$$

$$Coal\text{-}OH + H^{*} \rightarrow H_2O + Coal$$

H^{*} may also react with S and N groups in coal to form H_2S and NH_3. Since most of S and N in coal is either retained in the char or goes to form tar, the formation of H_2S and NH_3 is negligible.

If the proposed mechanisms for methane, hydrogen and water formation are true, there should exist a competitive effect of H^{*} consumption during coal pyrolysis. The correlation of pyrolysis methane production and hydrogen production with oxygen content in coal are shown in Figures 11.38 and 11.39. As expected, negative correlations were observed. The higher the oxygen content in coal, the more the activated hydrogen will be consumed by reacting with the oxygen-containing groups in coal. Since both methane and hydrogen production depend on the concentration of H^{*}, as shown in Figure 11.37, they have positive correlations with each other. To combine the effects of the hydrogen content, a promoting factor, and oxygen content, an inhibiting factor, on methane and hydrogen productions during coal pyrolysis, the ratio of H to O, H/O, is correlated with methane and hydrogen production. The results are shown in Figure 11.40 and 11.41. As expected, strong positive correlations of methane and hydrogen production with the H/O ratio are observed in the plots. Both methane and hydrogen production increase rapidly with an initial increase of H/O. Above a value of H/O of 3, both the methane and hydrogen production approach constant values.

Pyrolysis methane yields are plotted versus coalbed methane content in coal seams in Figure 11.42. The Utah coals show increasing coalbed methane with increasing pyrolysis methane. The colorado coal, shown by the star, lies off the trend. All of the gassy seams have shale roof rock, which is impermeable to gas transport. However, the geologic history of the Utah and Colorado coals is different and the natural fracture and cleat patterns in coal seams might be quite different. Pyrolysis methane can be used to evaluate the relative rate of formation of methane by coalification processes at the present time. It is found to be a function of both rank and maceral composition. The correlation indicates that the methane content appears to depend on the recent evolution of methane through coalification processes and not on the total gases produced during the coalification process. In other words, the results show that the present rate of methane formation is important in determining methane content for coals of similar rank in the same formation. The major fracture systems would be similar for all beds in the field and the rate of methane formation by pyrolysis generally

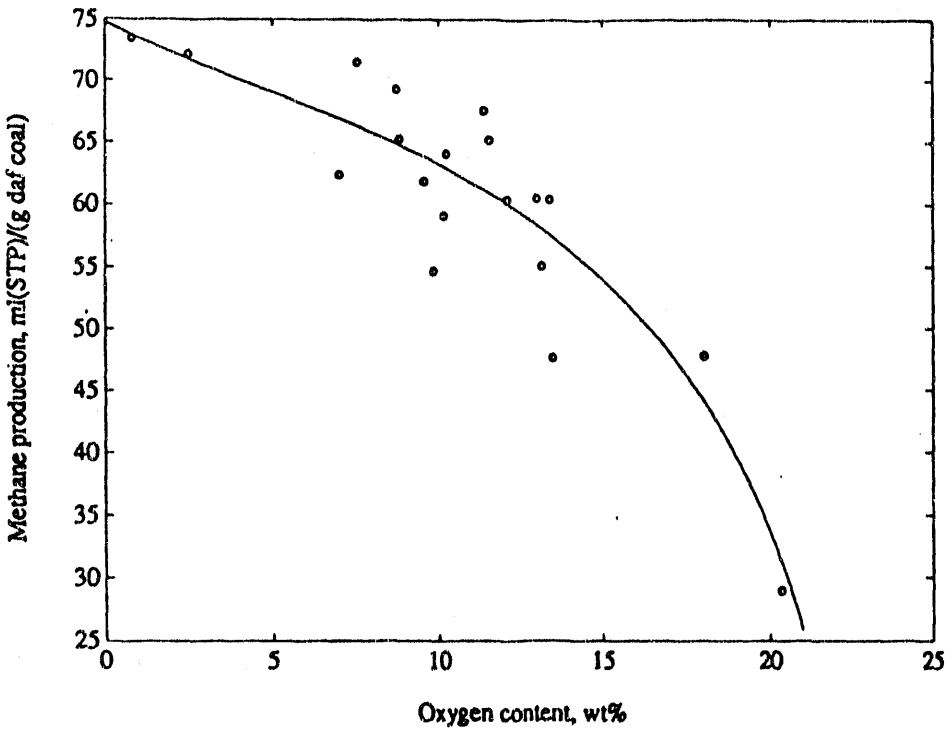

Figure 11.38 Pyrolysis methane yield versus oxygen content.

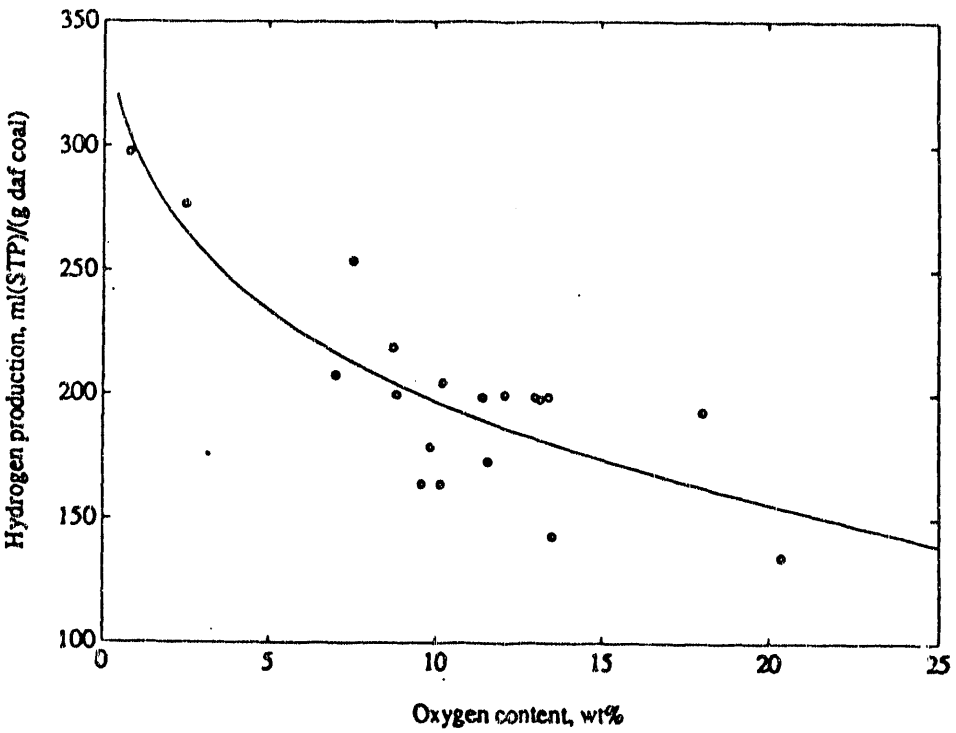

Figure 11.39 Pyrolysis hydrogen yield versus oxygen content.

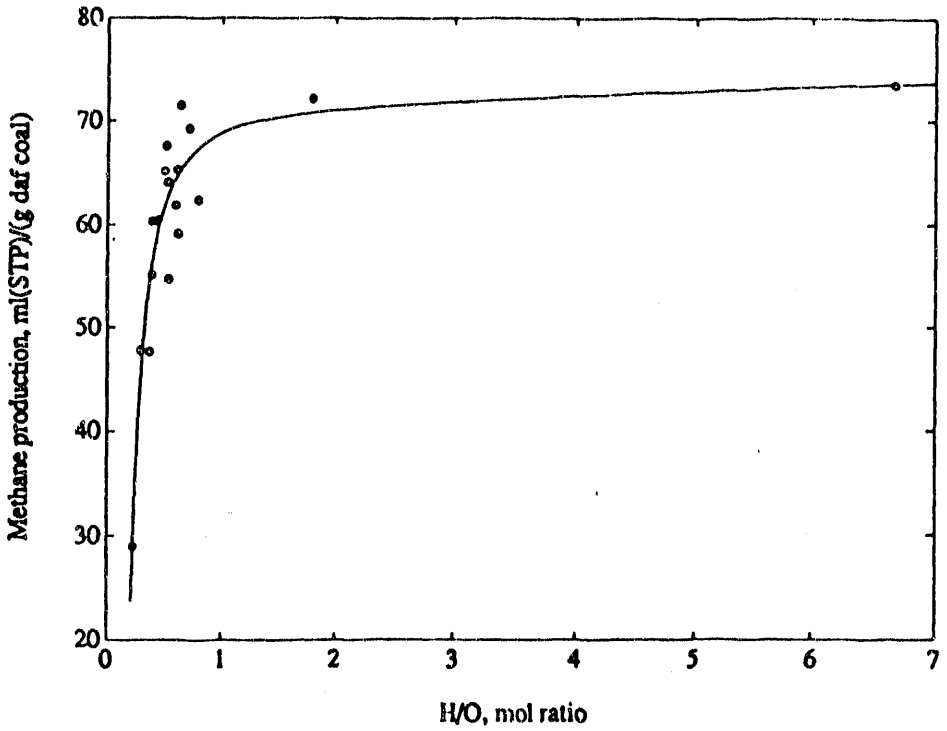

Figure 11.40 Pyrolysis methane yield versus hydrogen to oxygen ratio.

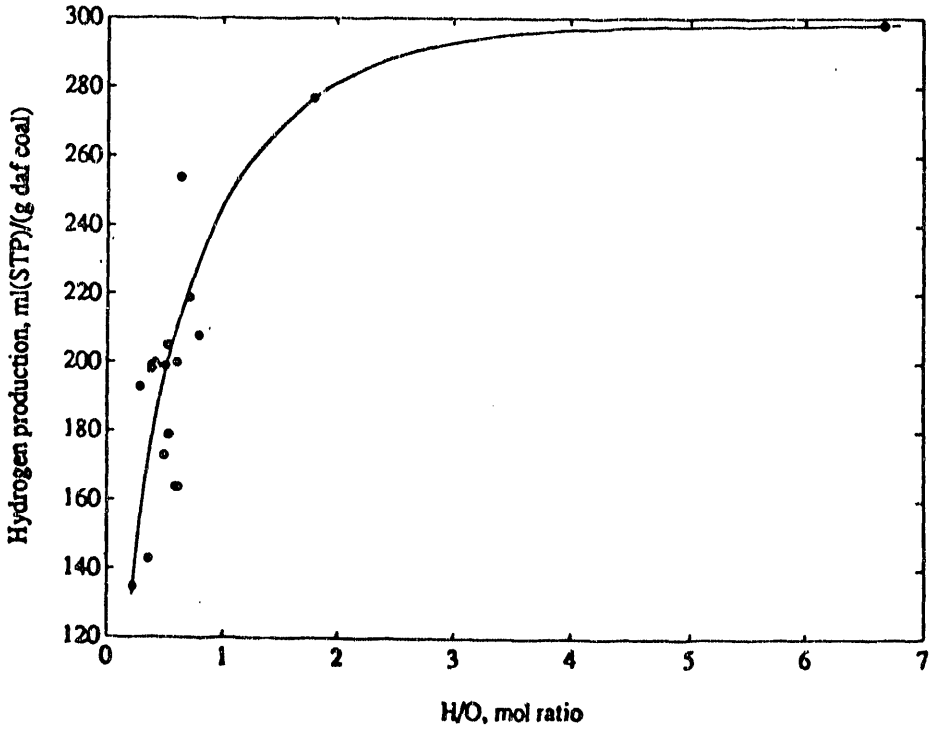

Figure 11.41 Pyrolysis hydrogen yield versus hydrogen to oxygen ratio.

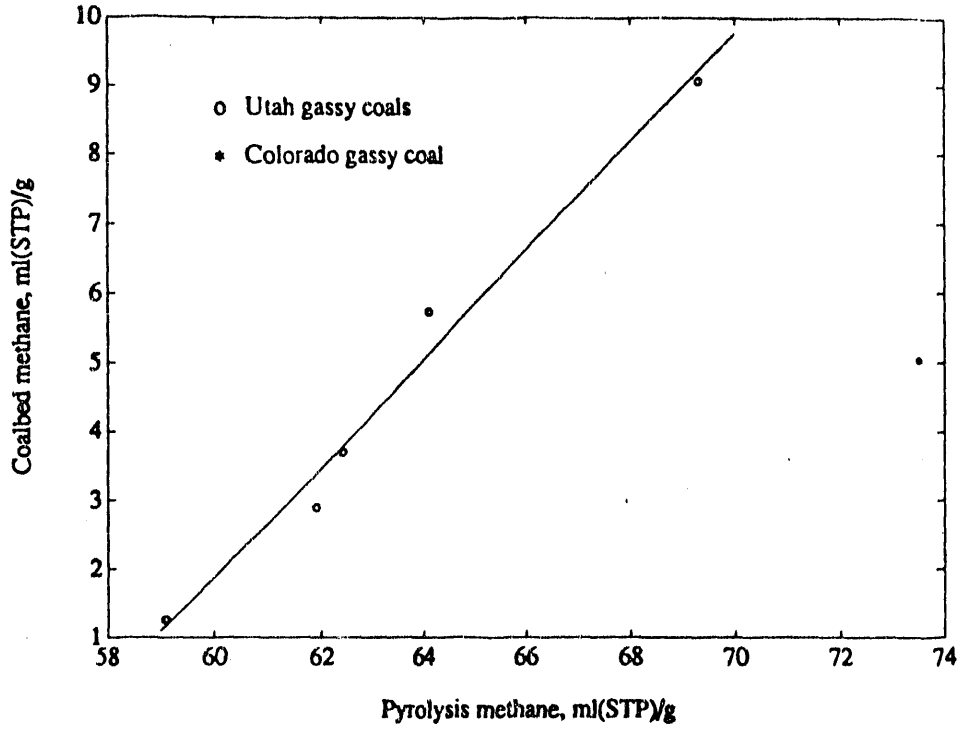

Figure 11.42 Pyrolysis methane yield versus coalbed methane content.

would increase with depth of burial of the seam or the temperature to which the coal has been exposed. In less mature coals, hydrogen in coal is evolved as water, while in higher rank coals, the hydrogen tends to be evolved as methane and hydrogen.

11.3.6 Redistribution of H, O and C in Coal Pyrolysis Products

It is interested to investigate the redistribution of H, O and C in coal pyrolysis products. As shown in Table 11.4, all chars show similar properties with approximately 0.6 wt% H, up to 0.9 wt% O and 97 wt% C. About 60 - 80 percent of the nitrogen and sulfur are retained in the char. From the data of proximate and ultimate analyses of coals (Table 6.1) and gas productions (Tables 11.1 and 11.2), the correlation of hydrogen content in gas products with the hydrogen content in coal is shown in Figure 11.43. The dashed line in the plot represents the maximum hydrogen content in gas products, assuming that all hydrogen in the coal goes to the gaseous products. It is obvious that, based on percent of hydrogen in coal, more hydrogen transfers to gaseous products after coal pyrolysis for higher rank coals. This effect becomes clearer when the percent hydrogen in gas products after coal pyrolysis is plotted against carbon content, a coal rank parameter, as

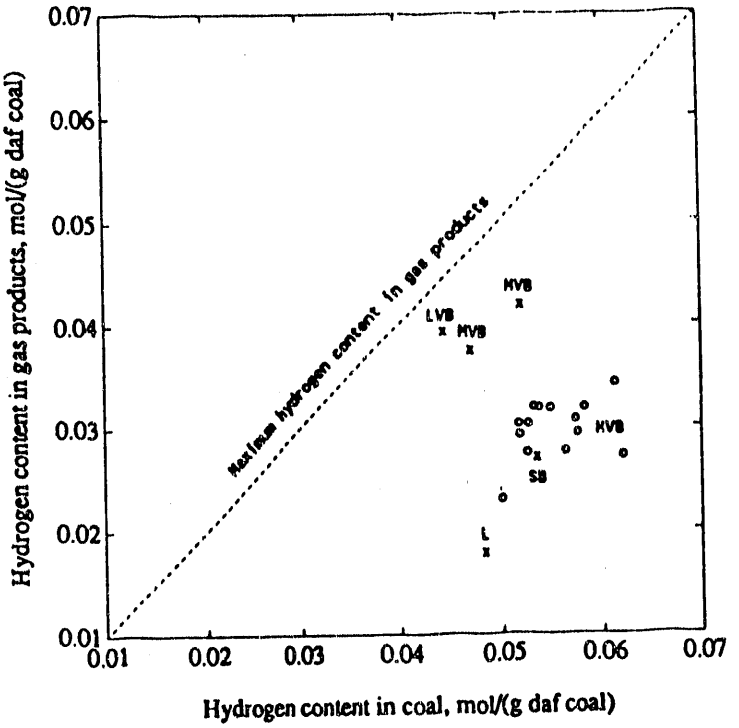

Figure 11.43 Hydrogen content in gaseous products.

shown in Figure 11.44. The correlation of oxygen content in gas products with the oxygen content in coal is shown in Figure 11.45. The higher the oxygen content in coal, the more the oxygen in the gaseous products. The effect of coal rank on the percent oxygen in the gaseous products after coal pyrolysis is shown in Figure 11.46. The data shows a great deal of scatter. This indicates that the percent oxygen in gas products after coal pyrolysis is independent of the coal rank parameter. The effect of coal rank on the percent carbon in gas products after coal pyrolysis is shown in Figure 11.47. As expected, carbon in gaseous products after coal pyrolysis decreases with an increase of coal rank and most of the carbon is retained in the char.

11.4 Conclusions

Gas evolution in programmed-temperature pyrolysis of coal with a slow heating rate is a good approach to understanding gas production in the coal maturation process. Carbon dioxide and carbon monoxide gases are first evolved at low-temperature stages of coal pyrolysis. At a higher-temperature stage, methane including other hydrocarbon gases was produced from decomposition of aliphatic groups in the coal and the methanation of carbon in coal. At the stage where chars were formed, hydrogen gas was evolved as a major component. This

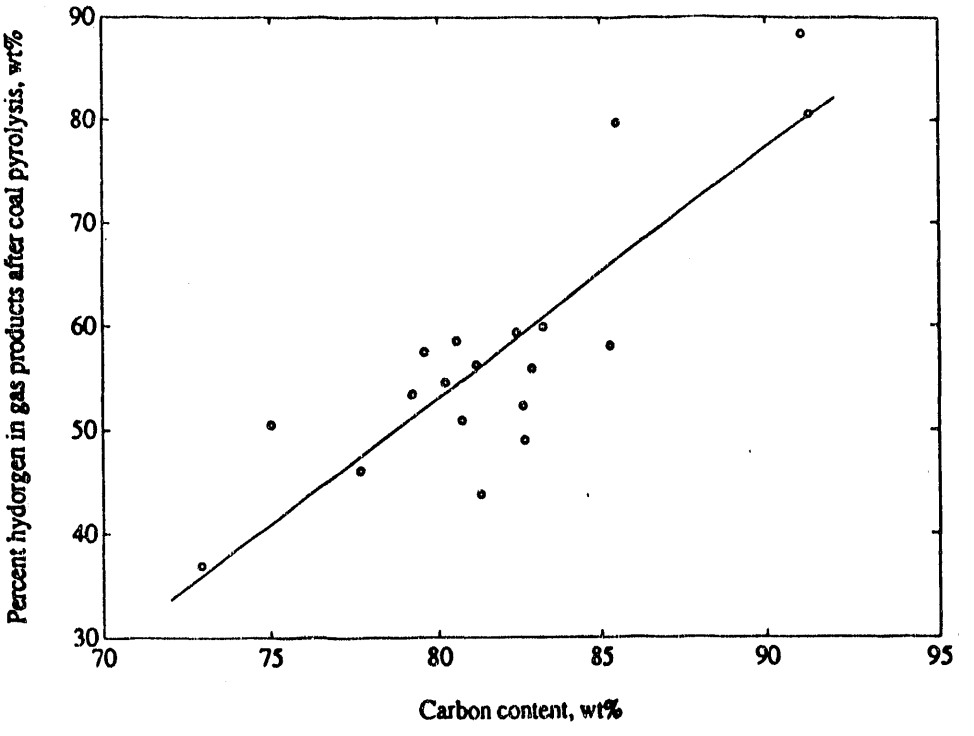

Figure 11.44 Percent hydrogen content of gaseous products versus carbon content.

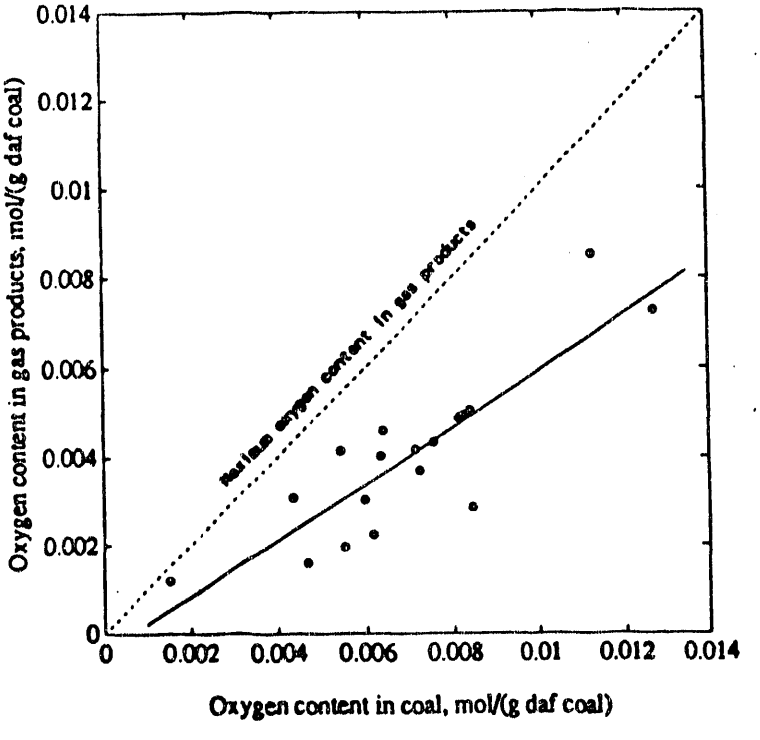

Figure 11.45 Oxygen content in gaseous products and coals.

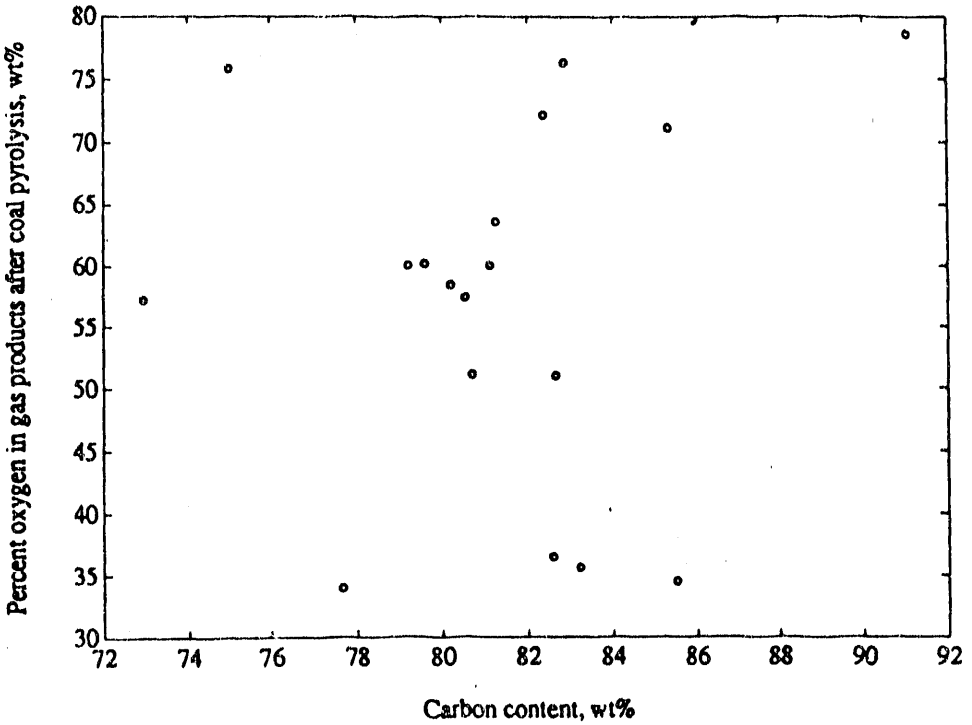

Figure 11.46 Percent oxygen content of gaseous products versus carbon content.

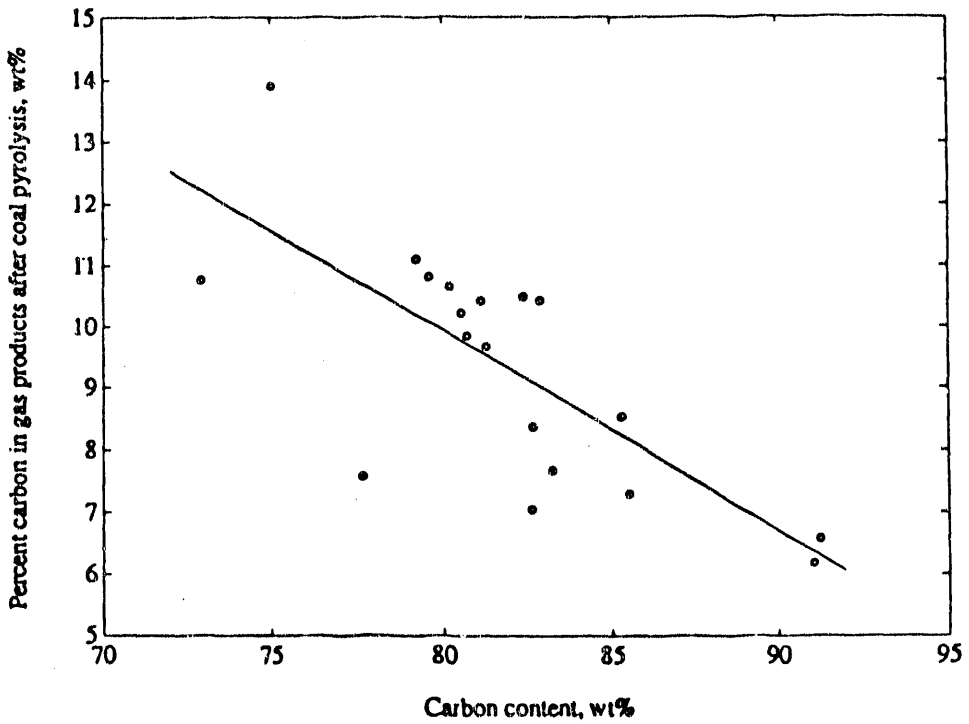

Figure 11.47 Percent carbon content of gaseous products versus carbon content.

temperature dependence of gas evolution during the coal pyrolysis parallels gas evolution stages in coalification. Based on the data of the ultimate and proximate analyses of the pyrolysis chars, coal pyrolysis follows the natural coalification trend in a van Krevelen plot.

The rate of gas evolution during coal pyrolysis has been found to be independent of particle size for the three selected coals, i.e., medium volatile Dutch Creek (B seam) coal, high volatile and gassy Sunnyside (Low Sunnyside seam) coal, and high volatile and non-gassy (Upper O'Connor seam) Skyline coal. This indicates that chemical reaction rates control the thermal devolatilization of a coal particle under the coal pyrolysis conditions used in this study.

Both hydrogen and methane production increase with an increase of carbon content. The production of C_2 hydrocarbon gases (including ethane and ethene) increases with increasing carbon content initially, reaches a maximum at about 85 wt% carbon, and then decreases. Both carbon monoxide and carbon dioxide production decrease with an increase of carbon content.

The correlation of the pyrolysis methane yield with the total fraction of aliphatic carbon in coal has been found to be negative. This indicates that the contribution of aliphatic groups in coal to methane formation in coal pyrolysis is not dominant. Methane production is positively correlated with hydrogen production and negatively correlated with oxygen content in coal. A mechanism for the methane production, hydrogen production and water formation during coal pyrolysis via an activated hydrogen H^*, which is generated during coal pyrolysis, has been proposed and the correlations explain the experimental results very well. The competitive effect of H^* consumption is confirmed by the correlation of methane production with the ratio of H/O in coal.

Coalbed methane content increases with an increase of pyrolysis methane yield for Utah gassy coals. This indicates that the methane content in a coalbed appears to depend on the recent evolution of methane through coalification processes and not on the total gases produced during the coalification process. The pyrolysis methane can be used to evaluate the relative rate of formation of methane by coalification processes at the current time.

The pyrolysis chars have similar properties with approximately 0.6 wt% H, up to 0.9 wt% O and 97 wt% C. About 60 - 80 percent of the nitrogen and sulfur are retained in the char. On a percent basis, more hydrogen transfers into gaseous products after coal pyrolysis for higher ranks of coal. The higher the oxygen content in coal, the more the

oxygen in the gaseous products. No effect of coal rank on the percent oxygen in gaseous products after coal pyrolysis was observed. Carbons in gas products after pyrolysis decrease with an increase of coal rank.

12. KINETICS AND THERMODYNAMICS OF WATER DESORPTION FROM COAL

12.1 Introduction

Moisture is associated with coal as adsorbed water on the coal surface and as liquid water in the larger cracks, fissures, and pores (Bond et al., 1950; Kreulen and Selms, 1950; Schafer, 1972; Murray and Evans, 1972). Prior to methane drainage, coal seams are commonly dewatered to remove water from the cracks. Adsorbed water retained in coal can be expected to compete with methane for adsorption sites and to reduce the capacity of methane adsorption (Joubert et al., 1973, 1974; and Kim, 1977). It can also have an influence on the transport of methane through the coal due to swelling and decreased permeability effects (Evans, 1973; Harpalani and Schraufnagel, 1990). Therefore, the desorption of water from coal plays an important role in coal-bed drainage and methane recovery.

To minimize transport costs, moist coals must be converted into high-grade forms of energy on an unit mass basis, and the first step in such conversion is always the evaporation of water. This drying process is also necessary for most coal utilization processes, such as, coal combustion, pyrolysis, gasification, and liquefaction. In order to estimate how much energy has to be input and the rate of the drying process, it is essential to study the kinetics and thermodynamics of water desorption from coal.

In this study, the eight Argonne Premium Coal Bank samples were investigated by thermal gravimetric analysis (TGA) and differential scanning calorimetry (DSC). Although the present work on the kinetics and thermodynamics of water desorption is confined to these eight samples, the proposed kinetic model and the heats of water desorption from these coals should be generally applicable to most other coals.

12.2 Experimental

A DuPont 951 TGA (Thermogravimetric Analyzer) and 910 DSC (Differential Scanning Calorimeter) connected with a TA 2000 module were used in this study. The proximate and ultimate analyses of the Argonne Premium Coal Bank samples are given in Table 6.1. The eight samples in this bank are carefully collected and preserved. They represent a range of coal rank from lignite to low volatile bituminous.

About 50 mg of coal sample was used for the TGA runs. Around 20 mg of coal sample was sealed in aluminum sample pans and used for the DSC tests. The experimental conditions for both TGA and DSC tests were initial temperature of 25 °C and isothermal control for 1 minute, followed by heating at a rate of 5 °C/min up to 150 °C and isothermal control for 10

minutes. Thirty ml/min of helium was used as carrier gas in the TGA tests. Under these conditions, the coal samples were completely dried after the tests.

12.3 Results and Discussion

12.3.1 Interaction of Coal and Water

Considering the properties of water and coal structure, we can classify the interactions between adsorbed water and the coal surface into three categories:

1. Water adsorbed on coal by normal interactions, such as dispersion forces, induced dipole interactions (polar or π-electrons), and/or permanent dipole interactions. These types of interactions are dominant factors only in coals of low oxygen, nitrogen, and sulfur content (i.e., high rank coals).

2. Water adsorbed on coal by "primary" hydrogen bonds with oxygen, nitrogen, and sulfur functional groups on the coal surface. This type of interaction is a governing factor only in high oxygen, nitrogen, and sulfur content coals (i.e., low and middle rank coals).

3. Water condensed on coal by "secondary" hydrogen bonds, i.e., the hydrogen in water interacting with adsorbed water rather than the polar sites of the coal surface. This happens only in the coals which have either very high oxygen, nitrogen, and sulfur content or very large pore volume.

Since the interaction of the hydrogen bonds between adsorbed water and the coal surface is much stronger than the other types of interaction, the equilibrium water content or coal-bed moisture is determined by its oxygen, nitrogen, and sulfur content. A plot of equilibrium moisture against total oxygen, nitrogen, and sulfur content for the eight Argonne Coal Bank samples, ten Utah coal samples and one Colorado coal sample is shown in Figure 12.1. As expected, the moisture increases with increasing total oxygen, nitrogen, and sulfur content. The empirical equation to estimate the equilibrium moisture by total oxygen, nitrogen, and sulfur is given by

$$Equilibrium\ moisture = (0.659 + 0.00187\,(O+N+S)^3)^2 \quad (1)$$

with a correlation coefficient of 0.97.

The relative oxygen, nitrogen, and sulfur contents in the eight Argonne Coal Bank samples are shown in Figure 12.2. It is obvious that the nitrogen content in these eight samples is

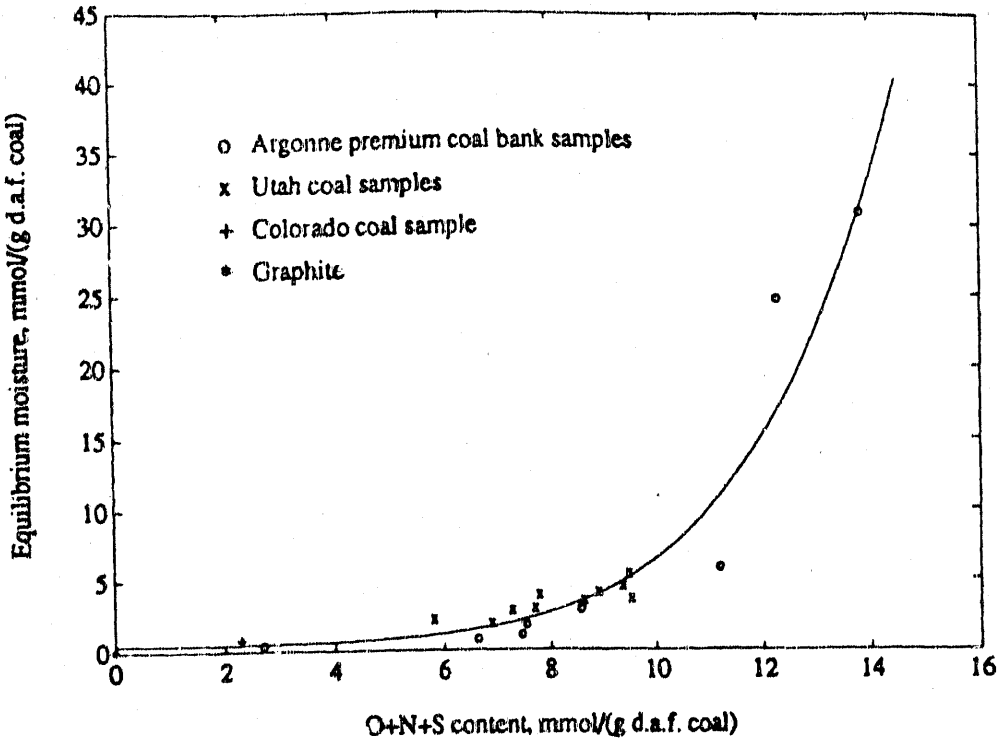

Figure 12.1 Correlation of equilibrium moisture with oxygen, nitrogen and sulfur.

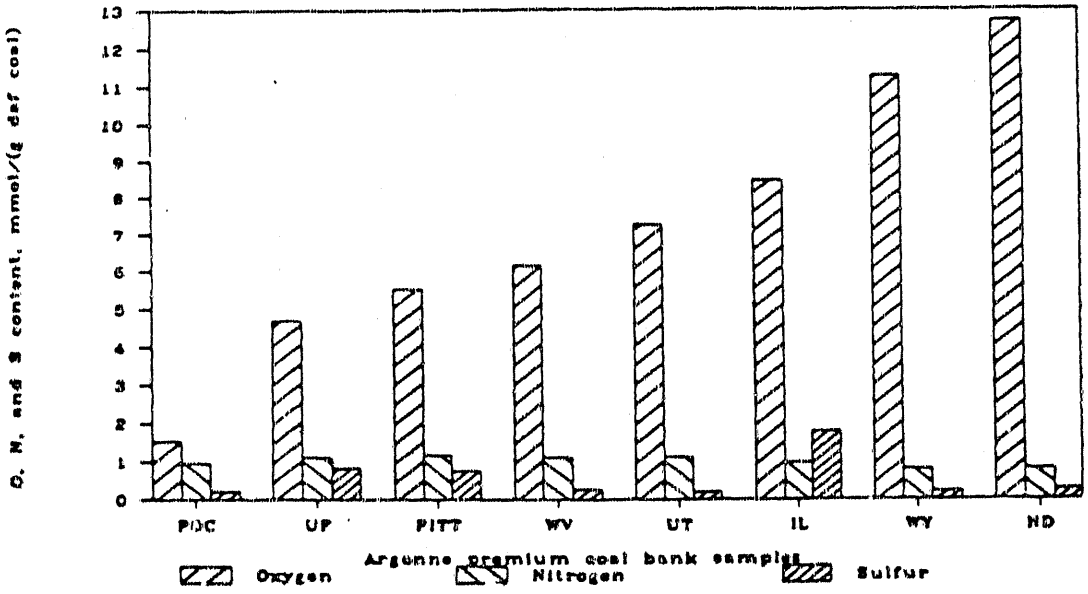

Figure 12.2 Oxygen, nitrogen and sulfur content of Argonne coal samples. POC=Pocahontas, UP=Upper Freeport, PITT=Pittsburgh, WV=Lewiston-Stockton, UT=Blind Canyon, IL=Illinois #6, WY=Wyodak Anderson, ND=Beulah-Zap.

nearly constant at 1.0 ± 0.1 mmol/(g d.a.f. coal). Except for Illinois #6, the sulfur content changes little with different samples. More importantly, the Pauling electronegativity (Pauling, 1960; Pauling, 1970) for oxygen, nitrogen and sulfur are 3.5, 3.0, and 2.5 respectively. Therefore, the oxygen-containing functional groups on the coal surface have a much stronger hydrogen bond with water than those of nitrogen- or sulfur-containing groups. The oxygen content is a dominant factor for the equilibrium moisture. This inference is coincident with the results of the effect of surface oxygen on water adsorption reported by Kaji et al. (1986). A plot of the equilibrium moisture against the oxygen content as shown in Figure 12.3 gives the same pattern as Figure 12.1.

The empirical equation to estimate the equilibrium moisture by the oxygen content alone is given by

$$Equilibrium\ moisture = (0.896 + 0.00244(Oxygen)^3)^2 \quad (2)$$

with a correlation coefficient of 0.98. This equation gives a little better correlation than that of Equation 1.

12.3.2 Heats of Desorption

To quantify the interaction between water molecules and the coal surface, the heats of desorption of moisture were measured by DSC. The results for the eight Argonne Coal Bank samples are shown in Figure 12.4. In order to calculate the heats of water desorption, it is crucial to determine the baseline properly. As shown in Figure 12.5, there obviously is no easily identifiable baseline point for water desorption in the high temperature range. Since the samples were sealed in aluminum pans, desorbed water was retained in the pans when the cell was heated. This was confirmed by weighing the sample before and after tests. If, compared with the heat effect of water desorption, the difference between the heat capacity of gaseous water and that of adsorbed water can be ignored, the heat capacity of the sample cell remains constant. Therefore, the baseline for water desorption can be determined from the low temperature range.

The suitability of this method was confirmed by a test of water desorption from a 900 °C coal char, which was produced by temperature-programmed pyrolysis of Blind Canyon coal in a helium stream with a low heating rate of 12 °C/min. The results are shown in Figure 12.6. As expected, a straight baseline in the high temperature range was obtained. It is coincident with that from the low temperature range. Since water can fill the pores in char (Toda and Toyoda, 1974), the equilibrium moisture of this char is 6.15 wt%, and its heat of water desorption is 40.4 kJ/mol, which is almost equal to the heat of vaporization of water, 40.6 kJ/mol. The baseline corrected DSC curves for the samples are shown in Figure 12.7.

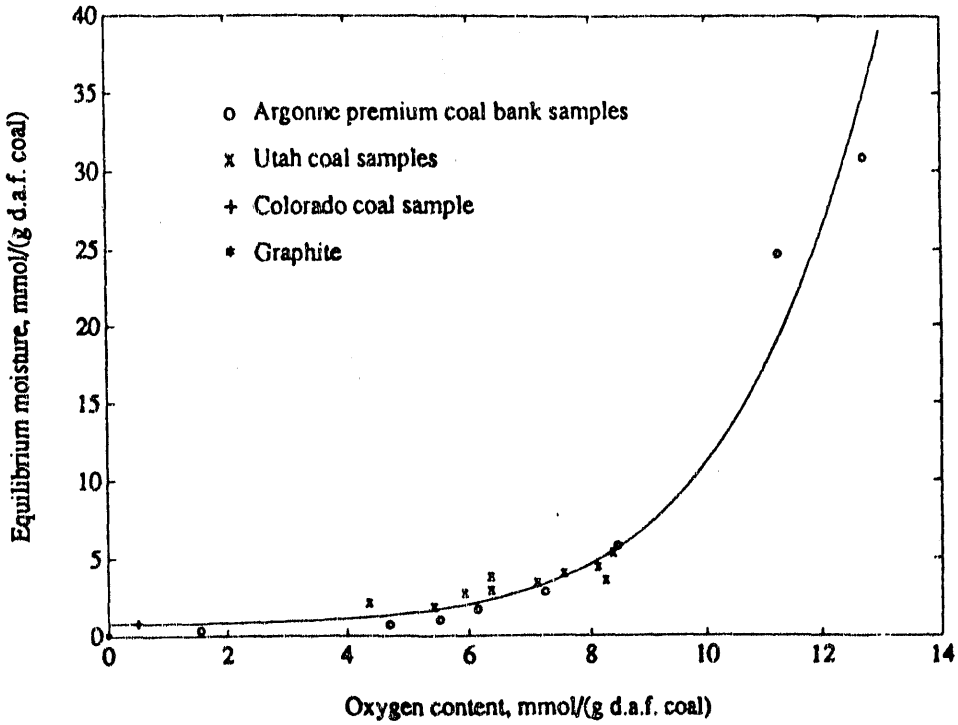

Figure 12.3. Correlation of equilibrium moisture with oxygen content.

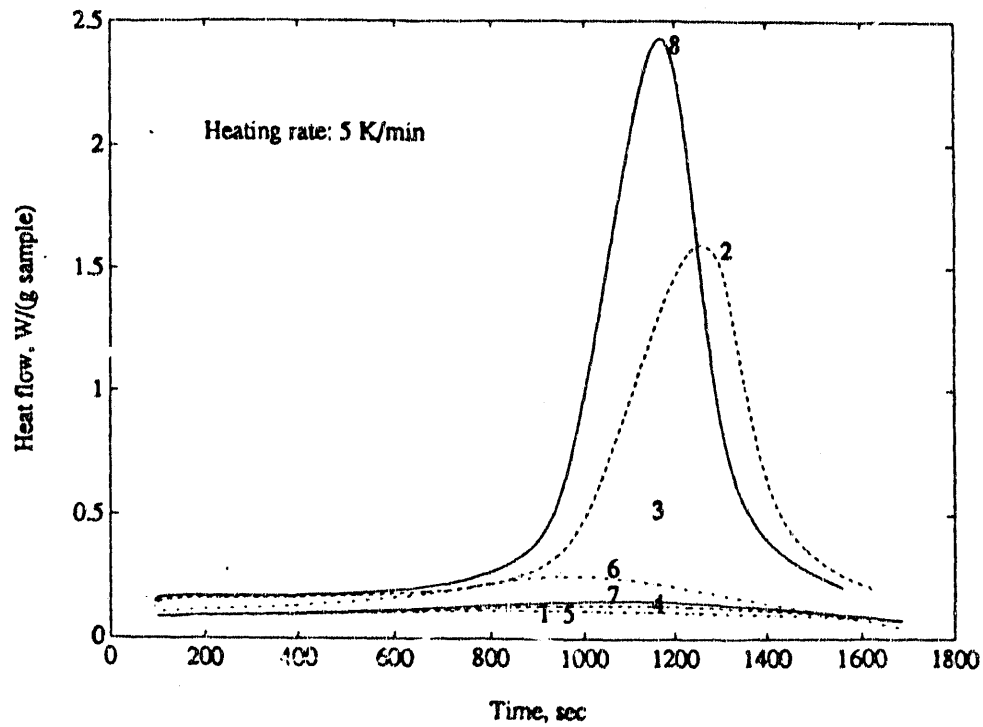

Figure 12.4 DSC curves of water desorption for Argonne coal samples. Numbers refer to samples in Table 1.

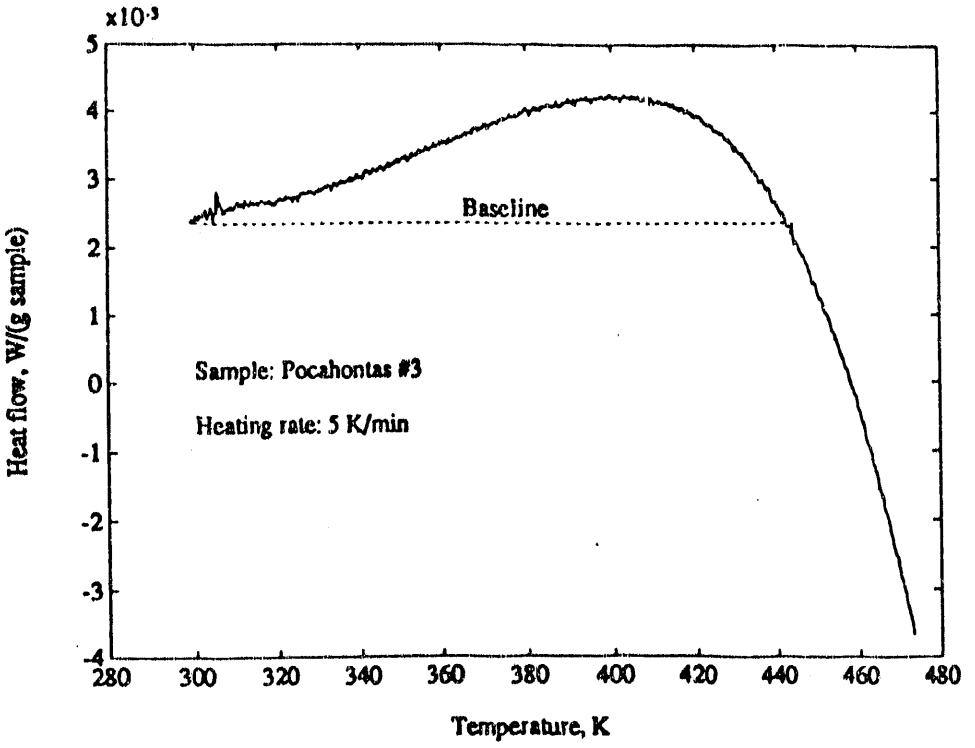

Figure 12.5 DSC baseline for water desorption.

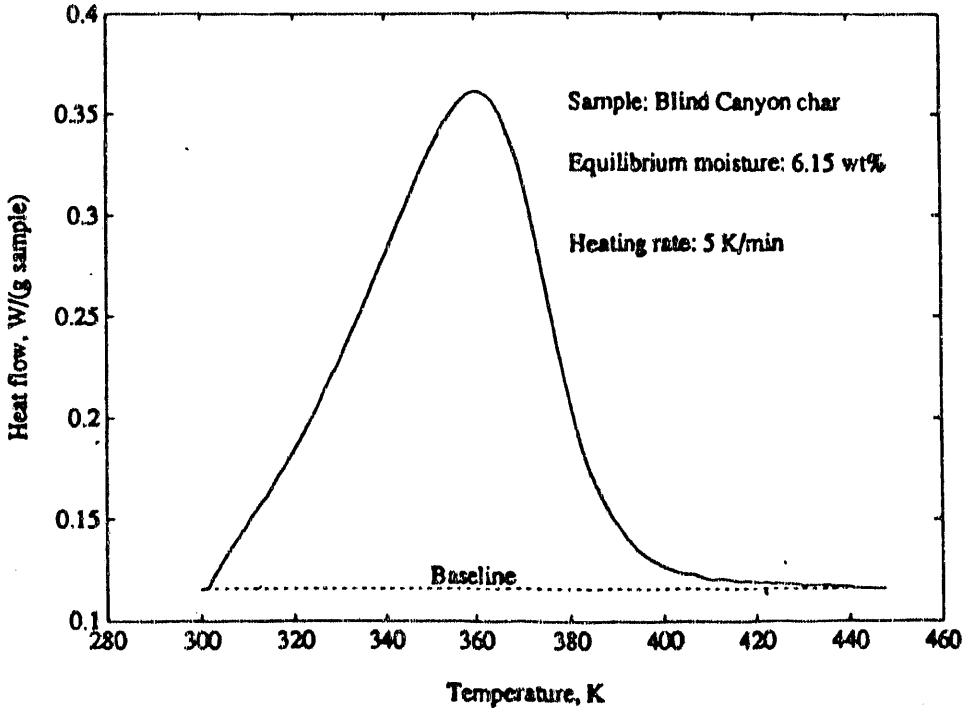

Figure 12.6 DSC curves of water desorption on Blind Canyon coal char.

It is obvious that the peak temperatures for various samples are different. Figure 12.8 shows the results of the heat flow normalized by moisture content. As observed in this figure, the same pattern of desorption was followed for the coals of low moisture content, from 0.6 to 5 wt%. The heat of desorption of moisture varies from 25 to 35 kJ/mol depending on the moisture content, and has an average value of 30 kJ/mol. The results are summarized in Table 12.1.

The correlation of the heats of water desorption with oxygen content is shown in Figure 12.9. The heat of water desorption increases with increasing oxygen content up to about 4 mmol/(g d.a.f. coal), and then it remains nearly constant from 4 to 10 mmol/(g d.a.f. coal). Above oxygen contents of 10 mmol/(g d.a.f. coal), it increases again with increasing oxygen, and approaches 40 kJ/mol, the heat of vaporization of water. This phenomenon can be explained by the behavior of hydrogen bonds of the adsorbed water molecules on coal surfaces with different oxygen content. The hydrogen bonds of water molecules in pure water (a), on a coal surface with low oxygen content (b), and with high oxygen content (c) are illustrated in Figure 12.10. For each water molecule, four hydrogen bonds are formed in pure water, two hydrogen bonds on the low surface oxygen of a coal, and three hydrogen bonds on the high surface oxygen of a coal. If we assume that the strength of hydrogen bonds in these instances is similar, the order of heat effects for water desorption should be $-\Delta H_{vap} > -\Delta H_{d\ (high\ oxygen)} > -\Delta H_{d\ (low\ oxygen)}$. The same order of the heats of water desorption has been observed in these experiments. These results suggest that the contribution from the hydrogen bonds of case (b) in Figure 12.10 to the heat of water desorption becomes significant as oxygen content increases. Therefore, the heat of water desorption increases with increasing oxygen content. For a range of oxygen content, this type of hydrogen bonds becomes dominant, and determines the heat of water desorption. Thus, the heat of water desorption remains nearly constant in this range. As oxygen content further increases, the hydrogen bonds of case (c) in Figure 12.10 become important, and the heat of water desorption increases again with increasing oxygen content. It approaches the heat of vaporization of water where multilayers of water adsorption take place.

It should be pointed out that the strength of hydrogen bonds for various functional groups on the coal surfaces is different. Carboxylic acid (-COOH), carboxylate ion ($-COO^-$), carboxylate, carbonyl, dialkyl ether (R-O-R'), diaryl ether (Ar-O-Ar'), aralkyl ether (R-O-Ar), alcoholic hydroxyl (R-OH) and phenolic hydroxyl (Ar-OH) are the most important oxygen-containing functional groups on the coal surfaces. Carboxylic acid, carboxylic ion, and carboxylate can form very strong hydrogen bonds with water molecules, even much stronger than those in pure water. A very high heat of water desorption,

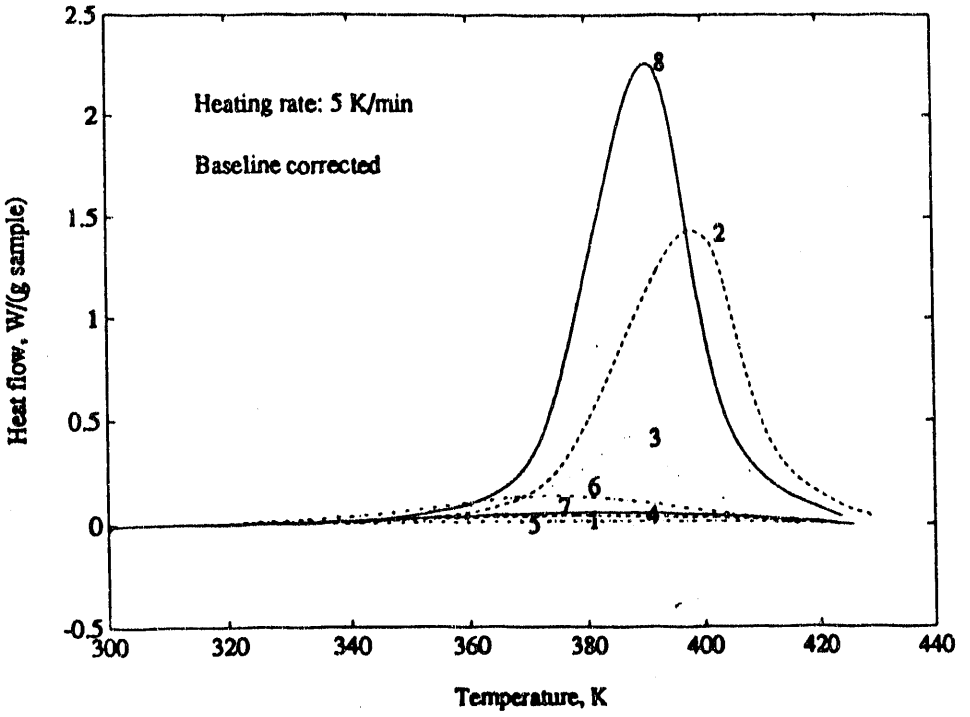

Figure 12.7 Baseline corrected DSC curves for water desorption of Argonne coal samples. Numbers refer to Table 12.1.

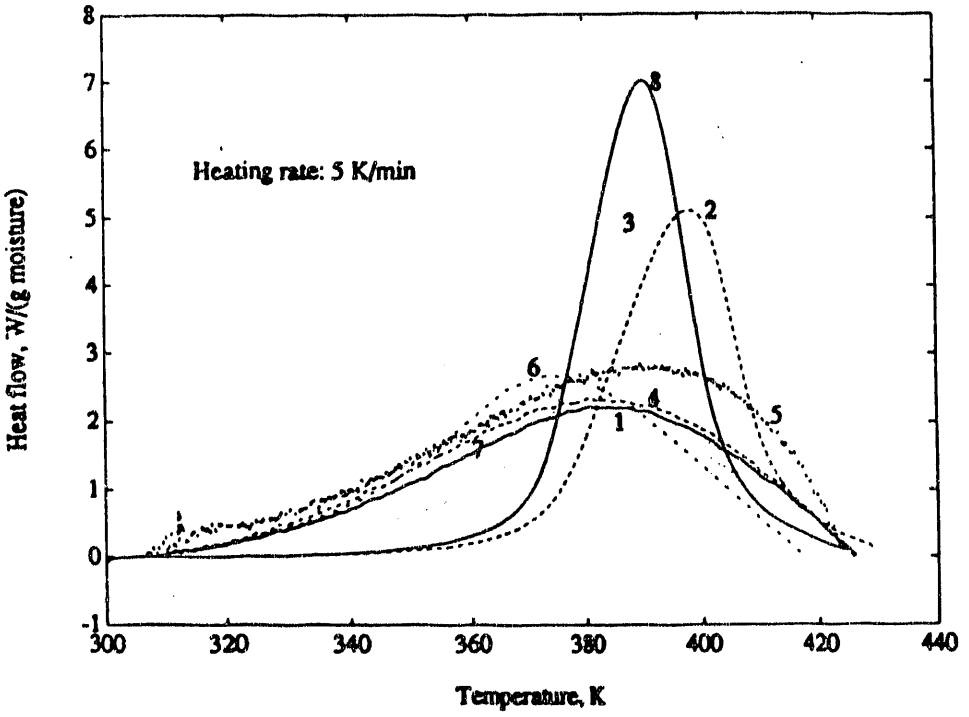

Figure 12.8 Heat flow normalized by moisture content for Argonne coals. Numbers refer to Table 12.1.

Table 12.1 Analysis data of the Argonne Premium Coal Bank samples (daf basis)

Sample No.	Seam	State	Rank	Moisture (as received)	Ash*	C	H	S	N	O
1	Upper Freeport	PA	Med. Vol. Bit.	1.13	13.18	85.50	4.70	2.32	1.55	7.51
2	Wyodak-Anderson	WY	Subbituuminous	28.09	8.77	75.00	5.35	0.63	1.12	18.02
3	Illinois #6	IL	High Vol. Bit.	7.97	15.48	77.70	5.00	4.83	1.37	13.51
4	Pittsburgh (#8)	PA	High Vol. Bit.	1.65	9.25	83.20	5.32	2.19	1.64	8.83
5	Pocahontas #3	VA	Low Vol. Bit.	0.65	4.77	91.10	4.44	0.66	1.33	2.47
6	Blind Canyon	UT	High Vol. Bit.	4.63	4.71	80.70	5.76	0.62	1.57	11.58
7	Lewiston-Stockton	WY	High Vol. Bit.	2.42	19.84	82.60	5.25	0.71	1.56	9.83
8	Beulah-Zap	ND	Lignite	32.24	9.72	72.90	4.83	0.80	1.15	20.34

* *dry basis*

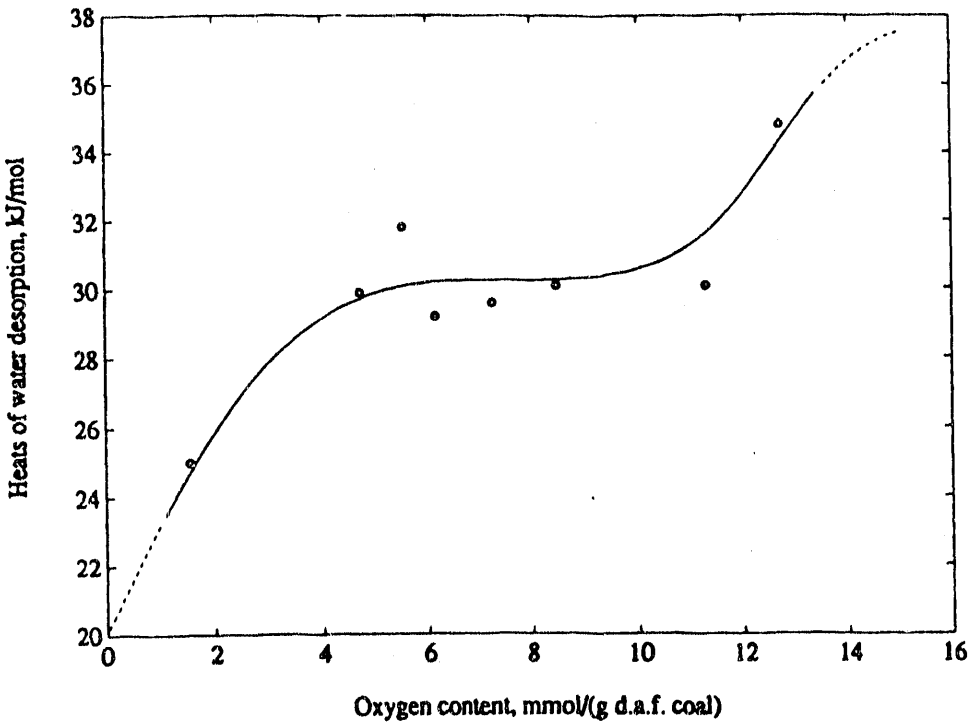

Figure 12.9 Correlation of heats of water desorption with oxygen content.

58.7 kJ/mol, on the Yallourn Brown lignite coal has been observed by Allardice and Evans (1978) at a low moisture loading, equivalent to about 0.6% of its equilibrium moisture. The analysis of this lignite coal shows that it has a quite high oxygen content, 25.8 wt%, and 19% of the oxygen is in the form of free carboxylic acid, 3.5% as carboxylate, 30% as phenolic hydroxyl, and 11% as carbonyl (Murray and Evans, 1972). Therefore, the high heat of water desorption on this lignite is expected to correlate with the very strong hydrogen bonds that are formed between water molecules and carboxylic acid, carboxylate, and carboxylic ion on the coal surfaces.

12.3.3 Kinetics of Desorption

The kinetic behavior of water desorption on the eight Argonne coal bank samples has been investigated by TGA. The rate of percent weight loss during water desorption for these samples is shown in Figure 12.11. A kinetic rate expression,

$$r_d = -\frac{1}{W_c}\frac{dW_{H_2O}}{dt} = k\left(\frac{W_{H_2O}}{W_c}\right)^n , \qquad (3)$$

was used to model the rate of moisture loss. In this expression, r_d is the water desorption rate, k the rate

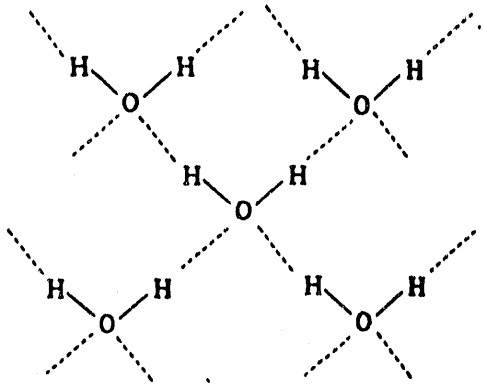

a. Hydrogen bonds in water

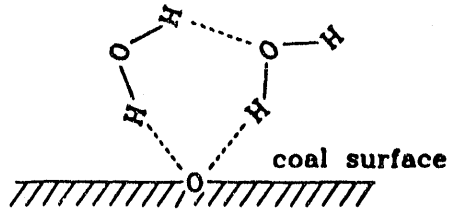

b. Hydrogen bonds of the adsorbed water on a coal surface of low oxygen content

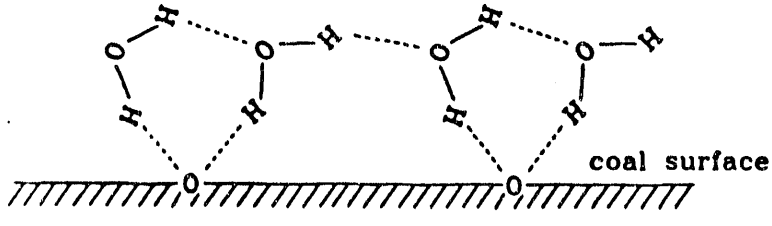

c. Hydrogen bonds of the adsorbed water on a coal surface of high oxygen content

Figure 12.10 Hydrogen Bonds in Water Molecules.

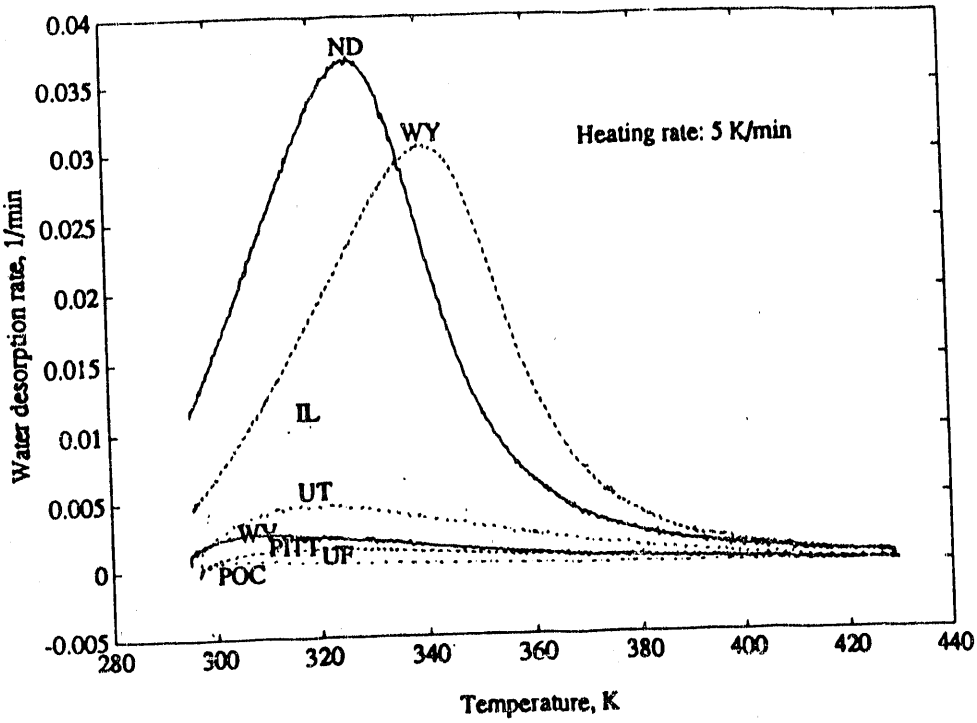

Figure 12.11 Water desorption rates of Argonne coal samples.

constant, W_c the sample size, W_{H2O} the moisture content, and n the kinetic order of water desorption. If an Arrhenius temperature dependence is assumed for water desorption and

$$X_{H_2O} = \frac{W_{H_2O}}{W_c} , \tag{4}$$

we have

$$r_d = -\frac{dX_{H_2O}}{dt} = A\exp(-\frac{E_d}{RT}) X_{H_2O}^n , \tag{5}$$

where A is the pre-exponential factor, E_d the activation energy for desorption, and R the gas constant. Equation 5 can be linearized as follows:

$$\ln(r_d) = \ln(A) - \frac{E_d}{RT} + n\ln(X_{H_2O}) . \tag{6}$$

A least squares method was used to calculate the kinetic parameters. The comparison of the desorption rates against temperature of TGA data with modelling results for two typical samples are illustrated in Figure 12.12. The moisture loss

from TGA data and the modelling curves for these samples are shown in Figure 12.13. From these figures, it is apparent that the kinetic modelling gives a good description of water desorption. The estimated kinetic parameters and corresponding correlation coefficients are tabulated in Table 12.2. The activation energy for water desorption varies from 27 to 78 kJ/mol, with an average value of 49.2 kJ/mol. The activation energy of water desorption and pre-exponential factor increases with increasing moisture. These correlations are shown in Figures 12.14 and 15.15 respectively. As expected, the more moisture in the coal, the higher the pre-exponential factor. This reflects that the pre-exponential factor, A, is somehow representative of the available sites for water desorption. The greatest difference is shown between the Pocahontas coal which has very little moisture and oxygen content and the Wyodak-Anderson and Beulah-Zap coals which have large amounts of water and high oxygen contents. For most samples, the activation energy of water desorption is very close to the heat of vaporization of water, 40.63 kJ/mol, indicating that the adsorbed water is in a state similar to the liquid state as far as hydrogen bonding is concerned.

Except for the Beulah-Zap lignite coal (32 wt% equilibrium moisture) with a kinetic order of 2.7, the kinetic order of water desorption is around 2 and independent of moisture content. There are several possibilities for the hydrogen bonded water molecules to be desorbed from the coal surfaces. Each mechanism may give a particular molecularity. If only water-water hydrogen bonds are broken in Figure 12.10(b) or (c), they cause no desorption, and the water-water hydrogen bonds can be formed again. If water-water hydrogen bonds are broken first, followed by breakage of hydrogen bonds between water molecules and oxygen-containing groups on the coal surfaces, it will give a molecularity of 1. In this case, the kinetic order of water desorption should be 1. If water-water hydrogen bonds are stronger than those between water molecules and oxygen-containing groups on the coal surfaces, the hydrogen bonds between water molecules and oxygen-containing groups on the coal surfaces will be broken first, and associated water desorption takes place. Thus, it will give a molecularity of 2 for a coal surface with low oxygen content, and 3 for a coal surface with very high oxygen content. The kinetic orders of water desorption should be 2 and 3 respectively. Comparing the molecularity of water desorption in different cases with the kinetic order obtained from the experiments, the water desorption agrees with an associated water desorption mechanism, i.e., the kinetic order of water desorption is 2 for a coal surface with low oxygen content and 3 for a coal surface with very high oxygen content. When the oxygen content is in the range between these two extremes, the contribution of the water desorption with a kinetic order of 3 increases with oxygen content. Therefore, the experimental kinetic order for Beulah-Zap

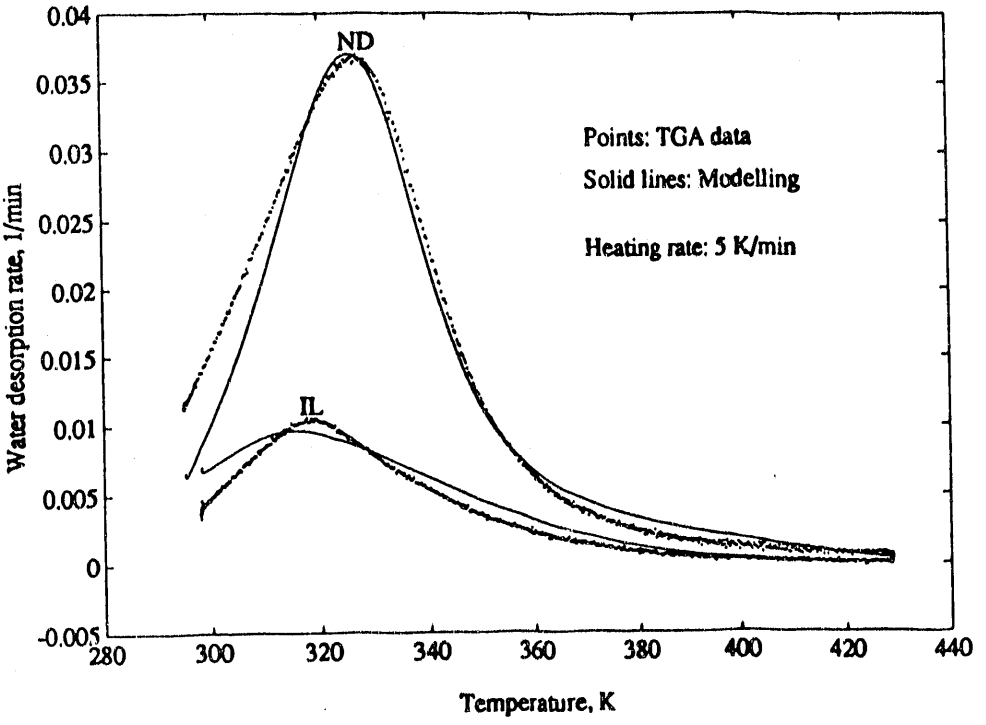

Figure 12.12 Comparison of water desorption rates from TGA data with modelling results for two samples.

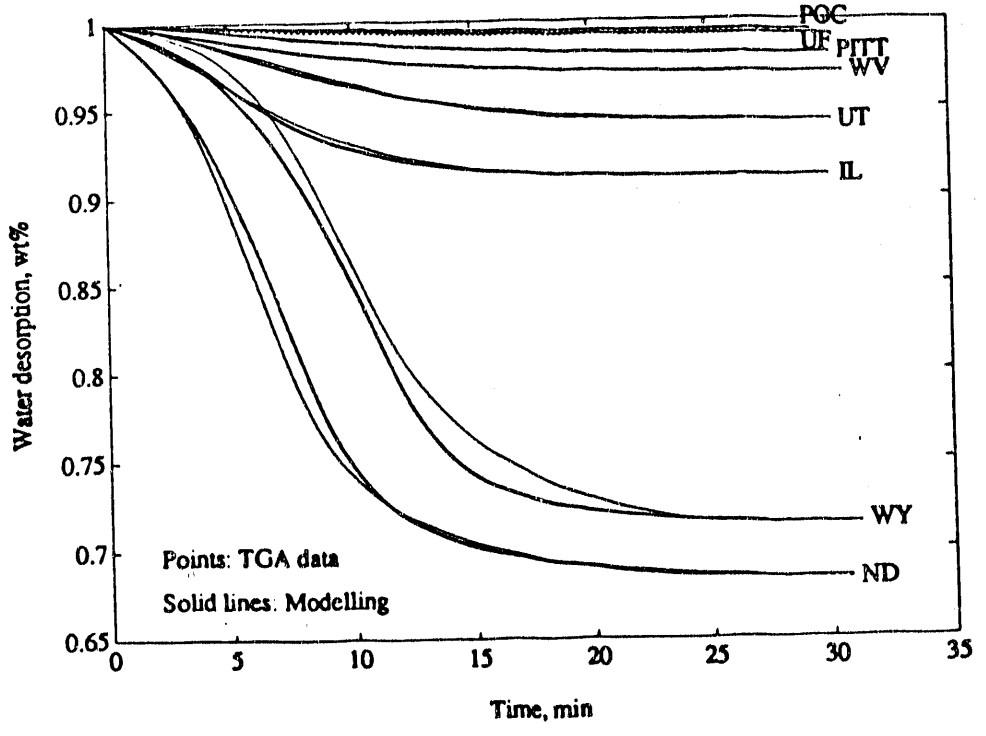

Figure 12.13 Comparison of TGA weight loss with modelling results for Argonne coal samples.

Table 12.2 Kinetic and thermodynamic data of water desorption on the Argonne Premium Coal Bank samples.

Sample No.	Seam	State	Water, wt%		Qd (DSC)	Kinetic parameters from TGA modelling				Peak temperature
			Literature*	TGA	kJ/mol	Ed, kJ/mol	n	lnA	r	K
1	Upper Freeport	PA	1.13%	0.80%	29.9	43.0	2.1	19.65	0.891	310
2	Wyodak-Anderson	WY	28.09%	28.50%	30.1	77.9	2.1	28.43	0.952	340
3	Illinois #6	IL	7.97%	8.84%	30.1	44.1	1.7	16.77	0.986	318
4	Pittsburgh (#8)	PA	1.65%	1.89%	31.8	41.3	2.0	17.58	0.897	320
5	Pocahontas #3	VA	0.65%	0.61%	25.0	26.9	1.8	12.59	0.925	307
6	Blind Canyon	UT	4.63%	5.72%	29.6	44.5	2.0	17.61	0.920	318
7	Lewiston-Stockton	WV	2.42%	2.96%	29.2	37.9	2.0	16.21	0.943	308
8	Beulah-Zap	ND	32.24%	31.61%	34.8	78.2	2.7	30.45	0.984	328
			Average heat of water desorption:		30.1					
			Heat of vaporization of water:		40.6					

* Karl S. Vorres, "Users Handbook for the Argonne Premium Coal Sample Program", Argonne National Laboratory, 1989.

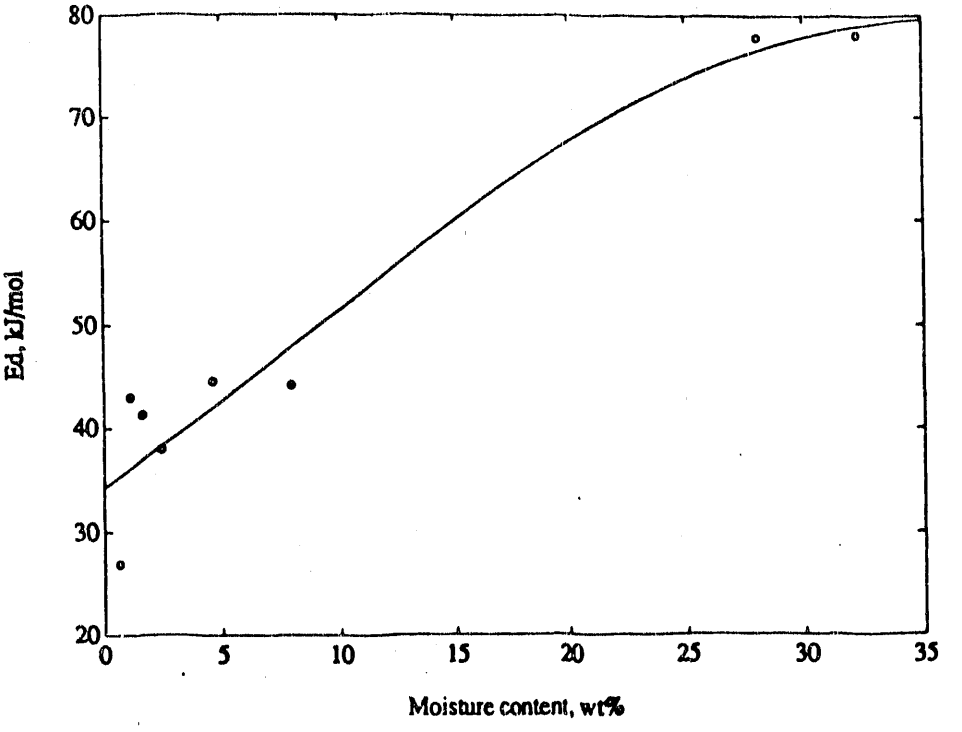

Figure 12.14 Correlation of activation energy for water desorption with moisture content.

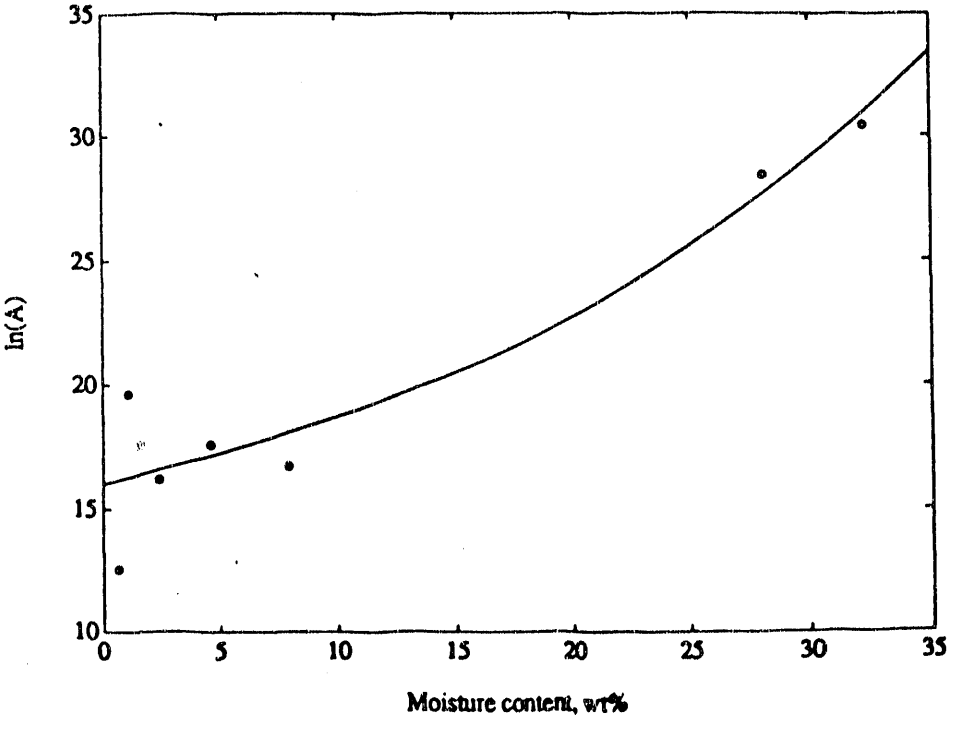

Figure 12.15 Correlation of pre-exponential factor with moisture content.

lignite is 2.7, which is between 2 and 3.

12.4 Conclusions

Moisture in coal is positively correlated with oxygen content. This is due to the formation of hydrogen bonds between water and oxygen functional groups on the coal surface. The rate of moisture desorption can be described by

$$r_d = kX_{H_2O}^n = Aexp(-\frac{E_d}{RT}) X_{H_2O}^n \qquad (7)$$

and the activation energy of moisture desorption, E_d, varies from 27 to 78 kJ/mol depending on the moisture content, with an average value of 49.2 kJ/mol. Except for the Beulah-Zap lignite coal (32 wt% equilibrium moisture) with a kinetic order of 2.7, the kinetic order of water desorption is about 2 and independent of moisture content. These results show that there exist hydrogen bonds between water molecules and O, N, S groups on the coal surface, and the desorption of water follows an associated water desorption mechanism.

13. CONCLUSIONS

Coalification of biomass involves biochemical and geochemical reactions that convert plant material to carbonaceous solids. The major products of the coalification process are methane, carbon dioxide, water, and traces of other components such as low-molecular-weight hydrocarbons, nitrogen, and hydrogen. Oxygen-containing gaseous species are produced in the early stages of coalification, while hydrogen-containing gaseous species predominate at the later stages. Coal rank is a measure of the progress along the coalification pathway. Water, methane, carbon dioxide, and other hydrocarbons adsorb on the coal micropore surfaces and might be expected to be retained in the coal seams. Other gases would remain as gases in the pore space and would not be expected to be retained in large volumes. Only traces of carbon dioxide are found in higher-rank coal seams, which might be explained by the solubility of carbon dioxide in water. Methane is the predominant gas recovered from coal seams.

The gas content of a coal seam will depend on the gas formed in the seam, transport of gas from the seam, and gas transport into the seam. Transport into the seam is usually not significant. The rank of coal, the maceral content, and the degree of maturation will determine the amount and type of gases formed in the seam. Adsorption coefficients, temperature history, pressure, permeability of coal, and permeability of roof rock will determine the transport of gases from the seam.

The Wasatch Plateau and Book Cliffs coal fields are of similar chemical and physical structure and were formed under similar geological conditions. The Book Cliffs coal field contains gassy coal seams, while only isolated pockets of methane are found in the Wasatch Plateau coal field. Methane content measured in the Book Cliffs field varied from about 3 to 9 cm^3/g. The methane content decreased with increasing moisture content and with present bed depth. Methane content showed a decrease with increased coal permeability.

The influence of tectonics (geological structures) such as folding and faulting on coalbed gas content has been considered. It is understood that the gas content of a seam changes smoothly over an area which may vary uniformly in rank (Creedy, 1988). However, folding may disrupt this by providing a pathway for incropping seams to lose some gas. Over geological time, faults have provided channels for gas migration. Figure 4.1 shows the Joes Valley, Pleasant Valley, and North Gordon fault zones oriented from north to south in the Wasatch Plateau and Emery coal fields. Their presence contributed to the low gas content in coal mines in these fields. On the other hand, the Book Cliffs field contains

high gas volumes as there are no faults (with the exception of the region of the Sunnyside mines where only a minor faults occur).

The Sub 3 seam of the Castlegate mine is the lowest minable seam in the Book Cliffs coal field. The largest methane content of 8.95 m^3/tonne was measured in this seam. Methane content shows a decreasing trend towards the Sunnyside mine with 3.7 m^3/tonne of methane measured for this location. Figure 4.3 shows a cross-section of the Sunnyside coal mines area. The strata may contain permeable disturbances as described by Alpern (1970). The dip of the strata is evidently favorable for the migration of gas from the Sunnyside seam, accounting for the lower methane content. Unfortunately, the Sunnyside Coal mines closed in 1990 and it was not possible to further investigation this possible explanation for differences in methane content.

Gas chromatography was used to measure thermodynamic constants of gas adsorption on the coal surfaces. The weighted mean retention time proved to be a characteristic gas retention variable for the non-ideal elution process. Gas adsorption coefficients calculated from this weighted mean retention time agree with those obtained by a static method.

Molecular interactions for gas adsorption are classified into two groups, non-specific adsorption and specific adsorption. Non-specific adsorption, such as for Ar, N_2, and O_2, is caused by dispersion and repulsive forces or van der Waals interactions. Specific adsorption, e.g. CO, CO_2, and C_3H_6, is caused by additional specific electrical interactions, such as induced dipole interaction forces provoked by the polar atoms or π-electrons in the molecule, and/or permanent dipole interaction forces. The heats and coefficients of specific gas adsorption are higher than those for non-specific gas adsorption. The n-paraffin gases (e.g. methane, ethane, and propane) have no specific electrical interactions with the coal surface, but they show unusually high heats and coefficients of adsorption. This is explained by a very strong affinity for the coal surface.

All molecules except water, have higher heats of gas adsorption than heats of vaporization. This indicates that the molecule-coal surface interactions are stronger than molecule-molecule interactions. In the case of water adsorbed on medium volatile bituminous Upper Freeport coal, the heat of water adsorption is much less than the heat of vaporization. This shows that the interaction between water molecules must be greater than the interactions with the less polar coal surface.

The strength of the van der Waals interaction increases linearly with the number of electrons in the molecule. Water,

carbon monoxide, carbon dioxide, and hydrocarbon gases have stronger interactions with the coal surface than nitrogen and oxygen, while the noble gas, argon, has a weaker interaction. Argon and oxygen gas adsorption show no specific adsorption effects. Carbon monoxide has a specific adsorption effect, but no effects from coal rank. Methane shows specific adsorption effects on coals, and the effects increase with increasing carbon content. The correlation of the specific adsorption effects with various gases is in the order propylene > carbon dioxide > propane > ethane > methane > monoxide. The correlation of the specific adsorption effects with coal carbon content is in the order propylene > propane > ethane > carbon dioxide > methane > carbon monoxide. These two orders are not exactly parallel. However, in the hydrocarbon gas series, they are not only parallel with each other but also parallel with the order of the heats of adsorption. This indicates that the interactions of gas molecules with coal surfaces increase with increasing rank of coal and size of molecule. The adsorption coefficient of C_3H_8 shows a strong dependence on the N_2 surface area, while the adsorption coefficients of other gases are strongly correlated with coal rank parameters.

Diffusion of gas components is important for gas adsorption at lower temperatures (< 50 °C). The correlation of continuous adsorption with the detected equilibrium adsorption and the adsorption characteristics of coal of different particle sizes lead to this conclusion.

Smaller molecules such as argon, nitrogen, and carbon dioxide have access to the internal surface of coal in diffusion-dominated regimes, while methane does not access the most internal surfaces of coal. Affinity of gas molecules for coal affects both the adsorption capacities and diffusion characteristics. The adsorption capacities of the different gases are in the order of $CO_2 > CH_4 > CO \sim N_2 \sim Ar \sim O_2$.

In the low pressure range, the methane adsorption isotherm becomes linear with pressure. The isosteric heat of methane adsorption on Castlegate Sub 3 seam coal was 14.9 kJ/mol.

Water adsorbed on coal inhibits methane adsorption. The methane adsorption capacity of Castlegate Sub 3 seam coal with 2.53 wt% moisture was only 59% of that of the dry coal.

Continuous gas desorption at slow rates was used to determine the CO_2 surface area of coal at 298 K. The specific surface areas for the different particle sizes of a high volatile subbituminous Sub 3 Utah coal are about 70 m^2/g (dry coal). This is lower than expected and is probably due to errors in the total adsorbed carbon dioxide determination from slow evolution at low pressures, below the detection limits of

the mass flow meter. The measurements were reproducible. Particle size effects on the CO_2 surface area were not observed within experimental error. A spherical particle model was used to calculate the specific external surface area. The coal has mostly internal surface area and hence, no effect of particle size on the CO_2 surface area was observed.

Gas evolution in programmed-temperature pyrolysis of coal with was used to understand gas production during the coal maturation process. Carbon dioxide and carbon monoxide gases are evolved at low-temperature stages of coal pyrolysis. At a higher-temperature stage, methane and other hydrocarbon gases were produced from decomposition of aliphatic groups in the coal and the methanation of carbon in coal. At the stage where chars were formed, hydrogen gas was evolved as a major component. The temperature dependence of gas evolution during coal pyrolysis parallels gas evolution stages in coalification. The rate of gas evolution during coal pyrolysis was found to be independent of particle size for the three selected coals, i.e., medium volatile Dutch Creek (B seam) coal, high volatile and gassy Sunnyside (Low Sunnyside seam) coal, and high volatile and non-gassy (Upper O'Connor seam) Skyline coal. This indicates that chemical reaction rates control the thermal devolatilization of a coal particle under the coal pyrolysis conditions used in this study.

Both hydrogen and methane production increase with an increase of carbon content. The production of C_2 hydrocarbon gases increases with increasing carbon content initially, reaches a maximum at about 85 wt% carbon, and then decreases. Both carbon monoxide and carbon dioxide production decrease with an increase of carbon content.

The correlation of the pyrolysis methane yield with the total fraction of aliphatic carbon in coal has been found to be negative. This indicates that the contribution of aliphatic groups in coal to methane formation in coal pyrolysis is not dominant. Methane production is positively correlated with hydrogen production and negatively correlated with oxygen content in coal. A mechanism for methane production, hydrogen production and water formation during coal pyrolysis via an activated hydrogen H^*, which is generated during coal pyrolysis, has been proposed. The correlations explain the experimental results well. The competitive effect of H^* consumption is confirmed by the correlation of methane production with the ratio of H/O in coal.

Coalbed methane content increases with an increase of pyrolysis methane yield for Utah gassy coals. This indicates that the methane content in a coalbed appears to depend on the recent evolution of methane through coalification processes and not on the total gases produced during the entire

coalification process. The methane content for the Colorado coal is less than would be expected based on the behavior of the Utah coals.

Moisture in coal is positively correlated with oxygen content. This is due to the formation of hydrogen bonds between water and oxygen functional groups on the coal surface. The rate of moisture desorption can be described by

$$r_d = kX_{H_2O}^n = A\exp(-\frac{E_d}{RT})X_{H_2O}^n \qquad (7)$$

and the activation energy of moisture desorption, E_d, varies from 27 to 78 kJ/mol depending on the moisture content, with an average value of 49.2 kJ/mol. Except for the Beulah-Zap lignite coal (32 wt% equilibrium moisture) with a kinetic order of 2.7, the kinetic order of water desorption is about 2 and independent of moisture content. These results show that there exist hydrogen bonds between water molecules and O, N, S groups on the coal surface, and the desorption of water follows an associated water desorption mechanism.

The strength and amount of water adsorption on the surface of coals depends on the number and polarity of heteroatom functional groups on the coal surface. For highly polar groups such as carboxyl groups, the heat of water adsorption is greater than the heat of vaporization. A model is proposed to explain water adsorption processes.

14. REFERENCES

Airey, E. M., 1968, Gas Emissions from Broken Coal, Int. J. Rock Mech. and Min. Sci., Pergamon Press, Vol. 5, pp. 475-494.

Allardice, D. J. and Evans, D. G., 1978, In Analytical Methods for Coal and Coal Products, Karr, C., Jr., Ed.; Academic Press, New York, Vol. 1, Chapter 7.

Alpern, B., 1970, Tectonics and Gas Deposit in Coalbeds: A Bibliographic Study and Examples of Application, Int. J. Rock Mech. Sci. Vol. 7, Pergamon Press, pp. 76-76.

Anderson, R. B., Bayer, J. and Hofer, L. J. E., 1965, Fuel 44, 443.

Arendt, F. and Van Heck, K. H., 1981, Fuel 60, 779.

Aul, G., 1983, Methane Drainage Study at the Price River Mine No. 3 (presently: Castle Gate Coal Mine near the town Helper, Utah), Occidental Research Corp., P. O. Box 196, Irvine, CA 92713, April, 16 p.

Averitt, P., 1975, "Coal Resources of the United States", January 1, 1974, USGS Bull. 1412, 131 p.

Ayres, W. B., and Kelso, B. C., 1989, Knowledge of Methane Potential for Coalbed Resources Grows, But Needs More Study, Oil and Gas Journal, Oct. 23, 1989 (Technology), also Special Pub. (Week of October 9, 1989), A Penwell Publication" Coalbed Methane), pp. 9-12.

Baker, E. C., Oyler, D. C., Perry, J. H., and Finfinger, G. L., 1984, Economic Evaluation of Directional Drilling for Methane Drainage from Coalbeds, U.S. Bureau of Mines, Rep. of Invest. RI 8842, 11 p.

Beebe, R. A., Evans, P. L., Kleinsteuber, T. C. and Richards, L. W., 1966, J. Phys. Chem. 70, 1009.

Bertard, C, Bruyet, B., and Gunther, J., 1970, Determination of Desorbable Gas Concentration of Coal (Direct Method), Int. J. Rock Mech. and Min. Sci., Pergamon Press, January, Vol. 7, pp. 43-65.

Bertard, C., Bruyet, B., and Gunther, J., Determination of Desorbable Gas Concentration of Coal (Direct Method), Int. J. Rock Mech. and Min. Sci., Pergamon Press, Vol. 7., pp. 43-65.

Bodily, D. M., Hucka, V. J. and Huang, H., 1991, Correlation of Chemical Structure of Coals in the Book Cliffs and Wasatch Plateau Fields with Methane Formation and Retention, in Geology of East-Central Utah - Utah, Chidsey, T. C. Jr., Ed., Utah Geol. Assoc., p. 211.

Bodily, D. M., Wann, J. -P., Kopp, V. R., 1989, "The Effect of Solvent Swelling on Coal Structure", Proc. Inter. Conf. Coal Science., 1, 201.

Bond, R. L., Griffith, M. and Maggs, F. A. P., 1958, Fuel 29, 83.

Brenner, 1983, Fuel 62, 1347.

Brenner, 1984, Fuel 63, 1324.

Brenner, 1985, Fuel 64, 167.

Brandenburg, C. F. (Editor), 1988, "Quarterly Review of Methane from Coal Seams Technology", Gas Research Institute, Colorado School of Mines, Volume 6, No. 2, November, 54 p.

Brunauer, S., 1945, Sorption of Gases and Vapours, Princeton Univ. Press, Princeton, New Jersey.

Brunauer, S., Deming, L. S., Deming, W. S. and Teller, E., 1940, J. Amer. Chem. Soc. 62, 1723.

Brunauer, S., Emmett, P. H. and Teller, E., 1938, J. Am. Chem. Soc. 60, 309.

Bunnell, 1982, Roof Geology and Stability of Underground Coal Mines in Carbon County, Utah, Proc. 5th Symp. on the the Geology of Rockey Mountain Coal, Bull. 118, May, Utah Geol. and Min. Surv., pp. 121-128.

Campbell, J. H., 1978, Fuel 57, 217.

Cervik, J., 1967, An Investigation of the Behavior and Control of Methane Gas, Min. Congr. J., Vol. 53, July, 52 p.

Choi, C., Bloomquist, C. A. A. and Dyrkacz, G. R., 1989, Energy Fuels 3, 38.

Ciuryla, V. T., Weimer, R. F. and Motika, S. A., 1979, Fuel 58, 748.

Clark, F. R., 1928, Economic Geology of the Castlegate, Wellington, and Sunnyside Quadrangles, Carbon County, Utah, U.S. Geol. Survey Bull. 793, 165 p.

Claypool, G. E., Threlkeld, C. N., Magoon, L. B., 1980, Bull. Am. Assoc. Pet. Geologists 64, 1131.

Cody, G. D., Jr., Larsen, J. W., Siskin, M., 1988, Energy Fuels 2, 340.

Collins, B. A., 1976, Coal Deposits of the Carbondale, Grand Hogback, and Southern Danforth Hills Coal Fields, Eastern Piceance Basin, Colorado: Quarterly of the Colorado School of Mines, Vol. 71, No. 1, 138 p.

Collins, B. A., 1985, Generalized Stratigraphic Section, Mesaverde Group, Coal Basin Area, Mid-Continent Resources Ltd., Carbondale, CO.

Conder, J. R., Locke, D. C. and Purnell, J. H., 1969, J. Phys. Chem. 73, 700.

Conder, J. R. and Purnell, J. H., 1968, Trans. Faraday Soc. 64, 3100.

Conder, J. R. and Purnell, J. H., 1969, Trans. Faraday Soc. 65, 824.

Creedy, D. P., 1988, Geological Controls on the Strata Formation and Distribution of Gas in British Coal Measure Strata, International Journal of Coal Geology 1988, 10, 1-31.

Curl, S. J., 1978, "Methane Prediction in Coal Mines", Report No. ICTIS/TR 04, London, IEA Coal Research, p. 9.

Davis, R., 1952, Chem. Ind. 8, 160.

De Boer, J. H., 1953, The Dynamic Character of Adsorption, The Clarendon Press, Oxford.

Deul, M, and Kim, A, G., 1975, Methane in Coal: From Liability to Asset, Mining Congress Journal, November, pp. 28-32.

Deul, M., and Kim, A. G., 1986, Methane Control Research: Summary of Results, 1964-1980, Bureau of Mines Bull. No. 687, 112 p.

Diamond, W. P., 1984, Site-Specific and Regional Geologic Considerations for Coalbed Gas Drainage, Bureau of Mines RI 8898, 23 p.

Dietz, V. R., Carpenter, F. G. and Arnold, F. G., 1964, Carbon 1, 245.

Doelling, H.H., 1972, Central Utah Coal Fields: Sevier-Sanpete, Wasatch Plateau, Book Clifs, andEmery, Utah Geol. and Miner. Surv. Monograph No. 3, 572 p.

Doelling, H.H., Smith, A.D., and Davis, F.D., 1979, Methane Content of Utah Coals, Special Studies 49, Utah Geological and Mineral Survey, 43 p.

Dollimore, D., Heal, G. R. and Martin, D. R., 1978, J. Chromatogr. **50**, 209.

Donnell, J. R., 1959, Mesaverde Stratigraphy in the Carbondale Area, Northwestern Colorado, in: Symp. on Cretaceous Rocks of Colorado and Adjacent Areas, Rocky Mnt. Assoc. Geologists, 11th Field Conf. Guidebook, pp. 76-77.

Dubinin, M. M., 1958, Industrial Carbon and Graphite, Society of Chemical Industry, London.

Dubinin, M. M., 1966, Chemistry and Physics of Carbon, Vol. II, (Ed. P. L. Walker Jr.), Marcel Dekker, Inc., New York, p 51.

Dubinin, M. M., 1960, Chem. Rev., **60**, 235.

Eberly, P. E. Jr., 1961, J. Phys. Chem. **65**, 1261.

Evans, D. G., 1973, Fuel **52**, 186.

Fisekci, M. Y., and Barron, K., 1975, Methane Pressure and Flow Measurements in Coal and Surrounding Strata, CIM Bull. October, pp. 98.

Francis, W., 1961, Coal: Its Formation and Composition, Edward Arnold Pub., London, 806 p.

Freihaut, J. D., Leff, A. A. and Vastola, F. J., 1977, Am. Chem. Soc. Div. Fuel Chem. Prepr. **22**, 1, 149.

Fuex, A. N., 1977, J. Geochem. Explor. **7**, 155.

Gan, H., Nandi, S. P. and Walker, P. L., Jr., 1972, Fuel **51**, 272.

Gavalas, G. R., 1982, Coal Pyrolysis, Elsevier Scientific Publishing Co., New York.

Gethner, J. S., 1986, J. Appl. Phys. **59**, 1068.

Given, P. H., 1984, An Essay on the Organic Geochemistry of Coal in Coal Science, Gorbaty, M. L., Larsen, J. W., and Wender, I., Eds., Vol. 3, Academic Press, Orlando, Florida.

Glueckauf, E., 1947, Nature 160, 301.

Glueckauf, E., 1949, J. Chem. Soc. 3280.

Goslar, J., Corray, L. S., Kispert, L. D., 1989, Fuel 68, 1402.

Graber, W. D. and Huettinger, K. J., 1982a, Fuel 61, 499.

Graber, W. D. and Huettinger, K. J., 1982b, Fuel 61, 505.

Graber, W. D. and Huettinger, K. J., 1982c, Fuel 61, 510.

Gray, R. J., Patalski, R. M., and Shapiro, N., 1966, Correlation of Coal Deposits from Central Utah, Utah Geol. Survey, Bull. 80, pp. 81-86.

Gregg, S. J. and Sing, K. S. W., 1982, Adsorption, Surface Area and Porosity, 2nd Ed., Academic Press, New York.

Gunther, J., 1965, Investigation of the Relationship between Coal and Gas Contained, in Proc. Int. Conf. of Directors of Safety in Mines Research, Sheffield, U.K., Safety of Mines Research Establishment, Transl. No. 5134.

Hargraves, A. J., 1962, Gas in Face Coal, Reprint No. 203, Proc. Aus. Inst. Min. Met. Australasian Inst. of Min. Met., 399 Little Collins Str., Melbourne, Australia, pp. 7-44.

Harpalani, S. and Schraufnagel, R. A., 1990, Fuel 69, 551.

Hileman, B., 1989, Chem. Eng. News, March 13, 25.

Howard, J. B., 1981, Fundamentals of Coal Pyrolysis and Hydropyrolysis, in Chemistry of Coal Utilization, 2nd Supplementary Volume, Ed. Elliott, M. A., Wiley-Interscience, New York, pp. 340-394.

Huang, H., Bodily, D. M. and Hucka, V. J., 1991, Formation of Methane during Coalification and Pyrolysis, in 1991 International Conference on Coal Science Proceedings,IEA Coal Research, Ed., Butterworth-Heinemann Ltd, Oxford, p. 640.

Hucka, B., 1990, Cleat and Joint System Evaluation and Coal Characterization of the Lower Sunnyside Seam, Sunnyside Mines, Carbon County, Utah, Open File Rep. No. 190, Utah Geol. Survey, Salt Lake City, Utah, 25 p.

Hucka, B., 1991a, Analysis and Regional Implication of Cleat and Joint Systems in Selected Coal Seams, Carbon, Emery, Sanpete, Sevier, and Summit Counties, Utah, Spec. Studies 74, Utah Geol. Survey, Salt Lake City , Utah, 47 p.

Hucka, B., 1991b, Cleat and Joint System Evaluation and Coal Characterization of the Castlegate "A" Coal, Beaver Creek Mine No. 8, Carbon County, Utah, Open-File Rep. 202, January, Utah Geol. Surv., Salt Lake City, Utah, 29 p.

Hucka, B., 1991c, Cleat and Joint System Evaluation and Coal Characterization of the Sunnyside Coal, Soldier Creek Canyon Mine, Carbon County, Utah, Open-File Rep. 203, January, Utah Geol. Surv., Salt Lake City, Utah, 30 p.

Hucka, B., Sommer, S. N., and Keith, A. C., 1989, Cleat and Joint System Evaluation and Coal Characterization of the B-seam, Dutch Creek Mine, Pitkin County, Colorado, Open-File Rep. 171, Utah Geolog. Survey, Salt Lake City, UT, 36 p.

Hucka, B., Sommer, S. N., and Keith, A. C., 1990, Cleat and Joint System Evaluation and Coal Characterization of the Sub 3 seam, Castle Gate No. 3 Mine, Carbon County, Utah, Open File Rep. No. 170, Utah Geol. Survey, Salt Lake City, Utah, 34 p.

Hucka, V. J., and Bodily, D. M., 1989, Methane Drainage From Gassy Western U.S. Coal seams, Proc. Intern. Symp., Today's Technology for the Min. and Met. Ind., Kyoto, Japan, Pub. Min. Mat. Processing Inst., pp. 453-460.

James, A. T. and Martin, A. J. P., 1952, J. Biochem. **50**, 679.

Jones, A. H., Ahmed, U., Abou-Sayed, A. S., Mahyera, A. and Sakashita, B., 1982, Fractured Vertical Wells Versus Horizontal Boreholes for Methane Drainage in Advance of Mining U.S. Coals, The Australian Inst. Min. Met., Illawarra Branch Symp.,May, pp. 1-28.

Joubert, J. I., Grein, C. T. and Bienstock, D., 1973, Fuel **52**, 181.

Joubert, J. I., Grein, C. T. and Bienstock, D., 1974, Fuel **53**, 186.

Juntgen, H. and van Heek, K. H., 1979, Fuel Process. Technol. **2**, 261.

Kaji, R., Muranaka, Y., Otsuka, K. and Hishinuma, Y., 1986, Fuel **65**, 288.

Karr, C., Jr., Ed., 1978, Analytical Methods for Coal and Coal Products, Vol. 1, Academic Press, New York, 569 p.

Kim, A. G., 1973, The Composition of Coalbed Gas, U.S. Bureau of Mines, Rep. of Invest., RI 7762, 9 p.

Kim, A. G., 1977, Estimating Methane Content of Bituminous Coalbeds from Adsorption Data, U.S. Dept. of the Interior, Bureau of Mines.

Kim, A. G., and Douglas, L. J., 1973, Gases Desorbed from Five Coals of Low Gas Content, U.S. Bureau of Mines, Rep. of Invest., RI 7768, 9 p.

Kipping, P. J. and Winter, D. G., 1965, Nature **205**, 1002.

Kiselev, A. V., Nikitin, Y. S., Petrova, R. S., Scherbakova, K. D. and Yashin, Y., 1964, Anal. Chem. **36**, 1526.

Kissell, F. N., McCulloch, C. M., and Elder, E. H., 1973, The Direct Method of Determining Methane Content of Coalbeds for Ventilation Design, Bureau of Mines Rep. of Invest., RI 7677, pp. 17.

Kissell, F. N., 1976, Two-Phase Flow in Coalbeds, U.S. Bureau of Mines Rep. of Invest. RI 8066, 16 p.

Knözinger, H. and Spannheimer, H., 1964, J. Chromatogr. **16**, 1.

Kreulen, F. G. and Selms, V., 1950, Fuel **29**, 196.

Kuuskraaa, V. A., and Branderburg, C. F., 1989, Coalbed Methane Sparks a New Energy Industry, Special Pub. (Week of October 9), A Penwell Publication" Coalbed Methane), pp. 3-8.

Lama, R. D., and Bartosiewicz, H., 1982, Determination of Gas Content of Coal Seams, Proc. "Seam Gas Drainage with Particular Reference to the Working Seam, Illawara Branch of the Australasian Inst. Min. Met., Univ. of Wollongong, May 11-14, pp. 36-52.

Langmuir, I., 1916, The Constitution and Fundamental Properties of Solids and Liquids, Jour. Am. Chem Soc., Vol 38, pp. 2,221-2,295.

Larson, J. W., Green, T. K., Kovac, J., 1985, J. Org. Chem., 50, 4729.

Larsen, J. W., Kennard, L. and Kuemmerle, E. W., 1978, Fuel **57**, 309.

Lester, T. W., Polavarapu, J. and Merklin, J. F., 1982, Fuel **61**, 493.

Levine, J. R., 1987, Influence of Coal Composition on the Generation and Retention of Coalbed Natural Gas, Proc. 1987 Coalbed Methane Symp., Tuscaloosa, Alabama, Nov. 16-19, pp. 15-18.

Linge, H. G., 1989, Fuel 68, 111.

Littlewood, A. B., 1962, Gas Chromatography, Academic Press, New York.

Lowry, H. H., 1963, Chemistry of Coal Utilization, supplementary volume, John Wiley and Sons, New York.

Lucht, L. M., Larsen, J. M., and Peppas, N. A., 1987, Energy Fuels 1, 56.

Mahajan, O. P., 1982, "Coal Porosity,", Coal Structure, R. A. Meyers, Ed., Academic Press, New York, Chap.3.

Mahajan, O. P. and Walker, P. L., Jr., 1971, Fuel 50, 308.

Mahajan, O. P., and Walker, P. L., Jr., 1978, "Porosity of Coals and Coal Products," Analytical Methods for Coal and Coal Products, C. Karr, Jr., Ed., Vol. 1, Academic Press, New York, Chap. 4.

Makino, M. and Toda, Y., 1979a, Fuel 58, 231.

Makino, M. and Toda, Y., 1979b, Fuel 58, 573.

Maksimovic, S. D., and Kissell, F. N., 1980, Three Coal Mine Gob Degasification Studies Using Surface Boreholes and a Bleeder System, U.S. Bureau of Mines Rep. of Invest., RI 8459, 10 p.

Mallory, W. W., (Editor-in-Chief), 1972, Geologic Atlas of the Rocky Mountain Region, Denver, Rocky Mountain Association of Geologists, 331 p.

Marsh, H. and Siemieniewska, T., 1965, Fuel 44, 355.

Maurer, W. C., and Wise, R. L., 1979, Methane Drainage Turbodrills, Proc., Methane Recovery from Coalbeds Symp., Pittsburgh, PA, April 18-20, 7 p.

Melton, C. E. and Giardini, A. A., 1975, Fuel 54, 162.

Monthioux, M. and Landais, P., 1987, Fuel 66, 1703.

Morris, J. P. and Keairns, D. L., 1979, Fuel 58, 445.

Mroz, T. H., Ryan, J. G., and Byrer, C. W., 1983, Methane Recovery from Coalbeds: A Potential Energy Source, U.S. Dept. of Energy, Report DOE/METC/83-76.

Murray, D. K., and Haun, J. D., 1974, Introduction to the Geology of the Piceance Creek Basin and Vicinity, Northwestern Colorado, in: Guidebook to the Energy Resources of the Piceance Creek Basin, Colorado, Rocky Mnt. Assoc. Geologists, 25th Field Conf. pp. 29-39.

Murray, D. K., Fender, H. B., and Jones, D. C., 1977, Coal Methane Gas in the Southeastern Part of the Piceance Creek Basin, Colorado, in: Rocky Mnt. Assoc. Geologists, 1977 Symp., Denver, Colorado, pp. 379-405.

Murray, J. B. and Evans, D. G., 1972, Fuel **51**, 290.

McCulloch, C. M., Deul, M., and Jeran, P. W., 1974, Cleat in Bituminous Coalbeds, Bureau of Mines RI 7910, 25 p.

McCulloch, C. M., Diamond, W. P., Bench, B. M., and Deul, M., 1975, Selected Geologic Factors Affecting Mining of the Pittsburgh Coalbed, Bureau of Mines RI 8093, 72 p.

McCulloch, C. M., and Diamond, W. P., 1976, An Inexpensive Method Helps Predict Methane Content of Coal Beds, Coal Age, June, pp. 102-106.

McCulloch, C. M., 1975, Measuring Methane Content of Bituminous Coalbeds: U.S. Bureau of Mines RI 8043, 22 p.

Nandi, S. P., and Walker, P. L., Jr., 1964, Fuel **43**, 385.

Nandi, S. P. and Walker, P. L., Jr., 1971, Fuel **50**, 345.

Neavel, R. C., 1981, in Chemistry of Coal Utilization, 2nd Supplementary Volume, Ed. Elliott, M. A., Wiley-Interscience, New York, Chap. 3.

Nebergall, W. H., Schmidt, F. C. and Holtzclaw, H. F., Jr., 1976, College Chemistry, 5th Ed., D. C. Heath and Co., Lexington.

Niknis, F. P., Turner, T. F., Ennen, L. W. and Netzel, D. A., 1988, Fuel **67**, 1568.

Owens, D. R., Hamlin, A. C. and Phillips, T. R., 1964, Nature **20**, 901.

Patching, T. H., 1970, "The Retention and Release of Gas in Coal - A Review", The Canadian and Metallurgical (CIM) Bulletin, November, pp. 1302-1308.

Pauling, L., 1960, The Nature of the Chemical Bond, Cornell University Press, Ithaca, New York.

Pauling, L., 1970, General Chemistry, Freeman, San Francisco.

Perry, J. H., Aul, G. N., and Cervik, J., 1978, Methane Drainage Study in the Sunnyside Coalbed, Utah, Bureau of Mines RI 8323, 11 p.

Perry, R. H. and Green, D., 1984, Perry's Chemical Engineers' Handbook, 6th Ed., McGraw-Hill, Inc.

Plaizier, R. R., 1990, Methane Desorption Modelling and Analysis for Selected Western Coal Fields: M. Sc. Thesis, University of Utah, 207 p.

Polanyi, M., 1932, Trans. Faraday Soc. **28**, 316.

Raistrick, A., and Marshall, C. A., 1939, The Nature and Origin of Coal and Coal Seams, The English University Press, Ltd., London. pp. 92-99.

Reid, R. C., Prausnitz, J. M., and Poling, B. E., 1987, The Properties of Gases & Liquids, 4th Edition, McGraw-Hill Book Co.

Reucroft, P. J. and Patel, K. B., 1983, Fuel **62**, 279.

Reucroft, P. J. and Patel, H., 1986, Fuel **65**, 816.

Reucroft, P. J. and Sethuraman, A. R., 1987, Energy Fuels **1**, 72.

Ruppel, T. C., Grein, C. T. and Beinstock, D., 1972, Fuel **51**, 297.

Ruppel, T. C., Grein, C. T. and Beinstock, D., 1974, Fuel **53**, 152.

Ruyter, H. P., 1982, Fuel **61**, 1182.

Schafer, H. N. S., 1972, Fuel **51**, 4.

Schwoebel, J. J., 1987, Coalbed methane: Conversion of a Liability to an Asset, Mining Engineering, April, pp. 270-274.

Scott, F. E., 1981, Degasification for Safety and Profit, Coal Mining and Processing J., March, pp. 62-66.

Serio, M. A., Hamblen, D. G., Markham, J. R. and Solomon, P. R., 1987, Energy Fuels **1**, 138.

Sewell, P. A. and Stock R., 1970, J. Chromatogr. **50**, 10.

Smith, A. D., 1985, Methane and Coal Mining: Methane Resources, Survey Notes, Vol. 19, No. 2., Utah Geol. Surv., pp. 3-6.

Smith, A. D., and Keith, A. C., 1989, Methane Content, Residual Gas and Maceral Comparisons of Two Central Utah Coal Fields, Proc. 28th Int. Geol. Congr.: Tertiary and Cretaceous Coals in the Rocky Mountain Region - Field Trip Guidebook T132, Casper, Wyoming to Salt Lake City, Utah, June 29-July 8, 48-56.

Smith, J. M. and Van Ness, H. C., 1987, Introduction to Chemical Engineering Thermodynamics, 4th Ed., McGraw-Hill Book Co., New York.

Solomon, P. R., Serio, M. A., Carangelo, R. M. and Markham, J. R., 1986, Fuel **65**, 182.

Solum, M. S., Pugmire, R. J. and Grant, D. M., 1989, Energy Fuels **3**, 187.

Sommer, S. N., Bodily, D. M. and Whitney, E. M., 1991, Characteristics of Utah Coals in the University of Utah's Coal Sample Bank, in Geology of East-Central Utah - Utah Geological Association Publication 19, Chidsey, T. C. Jr., Ed., Utah Geological Association, Salt Lake City, p. 199.

Speight, J. G., 1983, The Chemistry and Technology of Coal, Marcel Dekker, Inc., New York.

Stacy, W. O. and Jones, J. C., 1986, Fuel **65**, 1171.

Steele, D. J., and McCulloch, C. M., 1980, Methane Drainage: Safety and Energy Benefits, Dames and Moore Engineering Bull. 54, 445 South Figueroa, Suite 3500, Los Angeles, CA 90017, December, pp. 21-32.

Stephenson, H. G., 1977, A Study of Methane Drainage Practices in Coal Mines and Their Potential Application to Canadian Conditions, Dames & Moore, prepared for CANMET, 193 p.

Stock R., 1961, Anal. Chem. **33**, 966.

Strangeby, P. C. and Sears, P. L., 1981, Fuel **60**, 131.

Sundaram, M. S., Steinberg, M. and Fallon P. T., 1982, Flash Hydropyrolysis of Coal for Conversion to Liquid and Gaseous Fuels, Summary Report No. DOE/METC/82-84.

Suuberg, E. M., Peters, W. A. and Howard, J. B., 1978, Am. Chem. Soc. Div. Pet. Chem. Prepr. **23**, 1, 175.

Suuberg, E. M., Peters, W. A. and Howard, J. B., 1980, Fuel **59**, 405.

Teichmüller, M., and Teichmüller, R., 1982, Fundamentals of Coal Petrology in Stack's Textbook of Coal Petrology, Gebrüder Borntraeger, Berlin, Chap. 2.

Thrush, P. W., Editor, 1968, "A Dictionary of Mining, Mineral, and Related Terms", U.S. Department of the Interior, Bureau of Mines, The U.S. Government Printing Office, Washington, D.C. 20402, 1269 p.

Toda, Y. and Toyoda, S., 1974, Fuel **53**, 60.

Tyler, R. J., 1979, Fuel **58**, 680.

Uhrin, D. D., du Breuil, F., and Saltsman, R. D., 1980, Survey of Coal Industry Programs for Utilization of Methane from Coal Seams, Bituminous Coal Research, Inc., Fin. Rep. No. L-1068, to Gas Research Inst., Contr. No. 5010-380-0164, Feb., 30 p.

Van Krevelen, D. W., 1961, Coal, Elsevier Publishing Co., Amsterdam.

Volf, J., Koubek, J. and Pasek, J., 1973, J. Chromatogr. **81**, 9.

Vorres, K. S., 1989, Users Handbook for the Argonne Premium Coal Samples Program, ANL/PCSP-89/1, Argonne National Laboratory, Argonne, Illinois.

Vorres, 1990, Energy Fuels **4**, 420.

Walker, P. L., Jr. and Geller, J., 1956, Nature **178**, 1001.

Walker, P. L., Jr. and Kini, K. A., 1965, Fuel **44**, 453.

Walker, P. L., Jr. and Patel, R. L., 1970, Fuel **49**, 91.

Walker, P. L. Jr., Rusinco, F., and Austin, L. G., 1959, Adv. Catal. **11**, 60.

Walker, P. L., Jr., Verma, S. K., Rivera-Utrilla, J. Davis, A., 1988, Fuel **67**, 1615.

Wang, Z. and Shou, J. K., 1980, Am. Chem. Soc. Div. Fuel Chem. Prepr. **25**, 4, 171.

Wann, J.-P., 1990, Coal Comminution with Induced Swelling by Organic Solvents, Ph. D. Thesis, University of Utah, Salt Lake City.

Warneck, P., 1988, Chemistry of the Natural Atmosphere, Academic Press, New York.

Weimer, R. F. and Ngan, D. Y., 1979, Am. Chem. Soc. Div. Fuel Chem. Prepr. 24, 3, 129.

Winans, R. E., Thiyagarajan, 1988, Energy Fuels 2, 356.

Yang, R. T. and Saunders, J. T., 1985, Fuel 64, 616.

Young, D. M. and Crowell, A. D., 1962, Physical Adsorption of Gases, Butterworths, London.

Young, R. G., 1955, Sedimentalry Facies and Intertonguing in the Upper Cretaceous of the Book Cliffs, Utah, Colorado, in Geolocial Society of America Bulletin, Vol. 66, pp. 177-202.

Young, R. G., 1959, Cretaceous Deposits of the Grand Junction Area, Garfield, Mesa and Delta Counties, Colorado, in: Sym. on Cretaceous Rock of Colrado and Adajacent Areas, Rock Mnt. Assoc. Geologists, 11th Field Conf. Guidebook, pp. 17-25.

Young, R. G., 1966, Stratigraphy of Coal-bearing Rocks of Book Cliffs, Utah, Cororado, in Central Utah Coals, Utah Geological and Mineral Survey, Bulletin 80, pp. 7-21.

APPENDIX A

AN ASSESSMENT OF METHANE CONTENT BY ITS DETERMINATION IN SITU

UNIVERSITY OF UTAH
COLLEGE OF MINES AND EARTH SCIENCES
DEPARTMENT OF MINING ENGINEERING

IN SITU DETERMINATION OF DESORBABLE METHANE CONTENT BY USE OF THREE DIFFERENT DECAY FUNCTIONS

by

R. R. Plaizier and V. J. Hucka

Prepared for
1991 RMAG Guidebook,
Coalbed Methane of Western North America

Colorado School of Mines

October 1990

IN SITU DETERMINATION OF DESORBOBABLE METHANE CONTENT BY USE OF THREE DIFFERENT DECAY FUNCTIONS(1)

R. R. Plaizier (2)
V. J. Hucka (3)

(1) Received
(2) Westech Engineering, Inc., Salt Lake City, Utah
(3) Professor of Mining Engineering, University of Utah

ABSTRACT

The desorptive properties of methane in selected western coal seams were studied through actual field measurements using a manual bubble 'desorbometer' and later verified through laboratory modelling. Data were reduced using a power decay function, a quadratic function, and an exponential function. Methane desorption characteristics from individual coal seams were shown theoretically to be a good estimator of a seam's total methane content to within ±20%.

A laboratory was set up and equipped to properly analyze and reduce field data, in addition to providing a controlled model for studying methane adsorption properties on coal. The results of the field tests indicate that all three theoretical desorption functions provide a satisfactory model of the desorption process based on estimated and actual gas contents, and on superior coefficient of regression.

The estimated gas content for four western coal mines are presented based on computer reduction of data obtained from field and laboratory tests. One of the investigated coal seams is located in Colorado (B seam of the Dutch Creek Mine in Carbondale) and three are located in Central Utah (Rock Canyon seam of the Soldier Creek Mine), Lower Sunnyside (Sunnyside Coal Mines) and Sub 3 (Castle Gate Mine) seam). Their average methane content ranges from 1.8 cc/g to 5.5 cc/g. Graphic results from laboratory tests indicated the power function may provide a more accurate model of the desorption process than the other two theories discussed.

INTRODUCTION

Coalbed methane creates potential hazards in underground mines. Consequently, the methane content of a coal seam is an essential parameter for mine ventilation designs and for feasibility studies of methane drainage systems. This parameter is important as well in assessing gas outburst potential. However, coalbed methane is also a valuable source of clean energy. Presently, the most utilized method for gas content determination in U.S. gassy coal mines is the direct method developed by the U.S. Bureau of Mines (McCulloch, 1975).

Testing methods used in Germany and France for determining in situ gas content have been studied and modified for use in western coal seams. The so-called "bubble desorbometer method" was used in this research work. The method is described and the results are compared with results obtained from the direct method.

BACKGROUND AND TEST PROCEDURE FOR DETERMINING COALBED GAS CONTENT

The gas content is measured in volumes of gas in a given unit weight of coal. The methane gas in coal is found as a free gas in actual void spaces, and the gas adsorbed to the internal surface of coal. The volume of free gas is directly related to the porosity of coal, and in most coals makes up only 3 - 5% of the total gas content (Firedamp Drainage Handbook, 1980).

Residual gas content is measured as the total gas (methane) volume per unit weight of coal reatained in the coal at 0.145 psi (1 kPa) atmospheric pressure and in a pure methane environment.

French and German Influences

Researchers at France's National Coal Institut (CERCHAR) studied methane properties in coal, gas content testing procedures and development of drainage systems.

They proposed a method in which long boreholes are drilled from an entry horizontally into the seam, or a vertical borehole intersecting the seam. Coal samples are taken every one to two meters from a horizontal borehole depth until a relatively constant gas content is reached. When using vertical boreholes, many boreholes at various intersections of the seam must be drilled. Samples consist of 0.35 ounce (10 grams) of core or

cuttings screened to include only particles above 0.079 inch (2 mm) which are immediately sealed into a transportable container.

Researchers at the German Mine Ventilation Institute in Bochum, Germany developed a similar procedure for testing the gas content in coal seams in situ. Coal samples collected from bottom of horizontal boreholes are tested at the face. A bubble desorbometer (Fig. 1) is used directly at the face to estimate the methane content within minutes of the sample removal. The method is similar to the French method in the sampling procedure and determination of the quantity of residual gas and gas desorbed after the sample is sealed in a container, but differs in the theory and determination of the lost gas given off before the sample is tested and sealed. The coal sample, in a form of fine cuttings, is collected from every 1 to 2 meters of the borehole depth until a relatively constant gas content value is reached.

The collection of samples is facilitated by using a special sample collection device. After the collection, the sample is screened to a size of 0.015 to 0.025 inch (0.4 to 0.63 mm). An amount of 0.14 to 0.17 ounce (4 to 5 g) are placed into the cell of the desorbometer. The desorbometer is manually operated, but an automatic electronic desorbometer is also available.

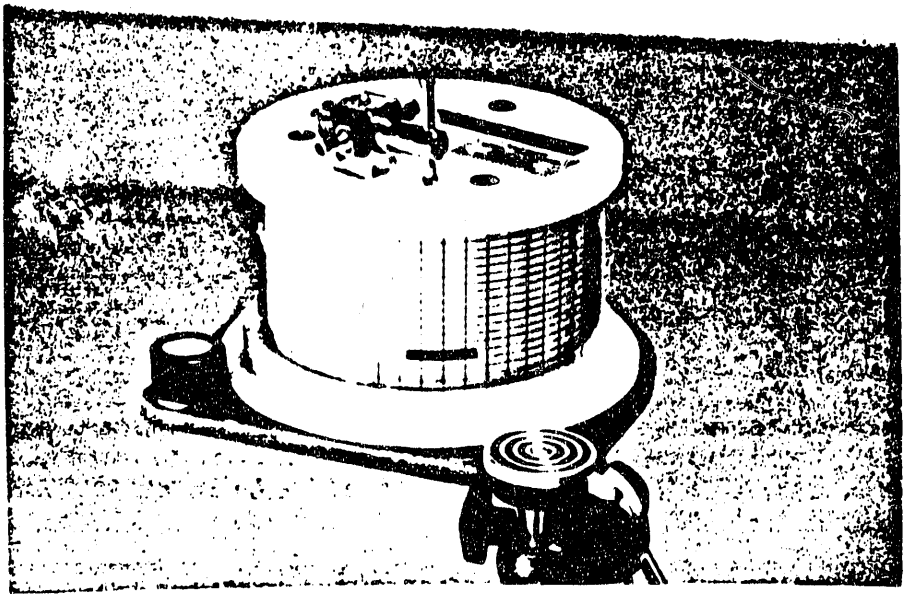

Figure 1. Manual bubble desorbometer.

Modified Method for Determining the Gas Content in Coal Seams

Both the French and German methods were modified to arrive at a procedure best suited for the conditions and equipment available for Western Coal bed evaluation. The respective theories for estimating the lost gas used by the French and Germans were used for a comparative basis in this study. The modified procedure is herein presented:

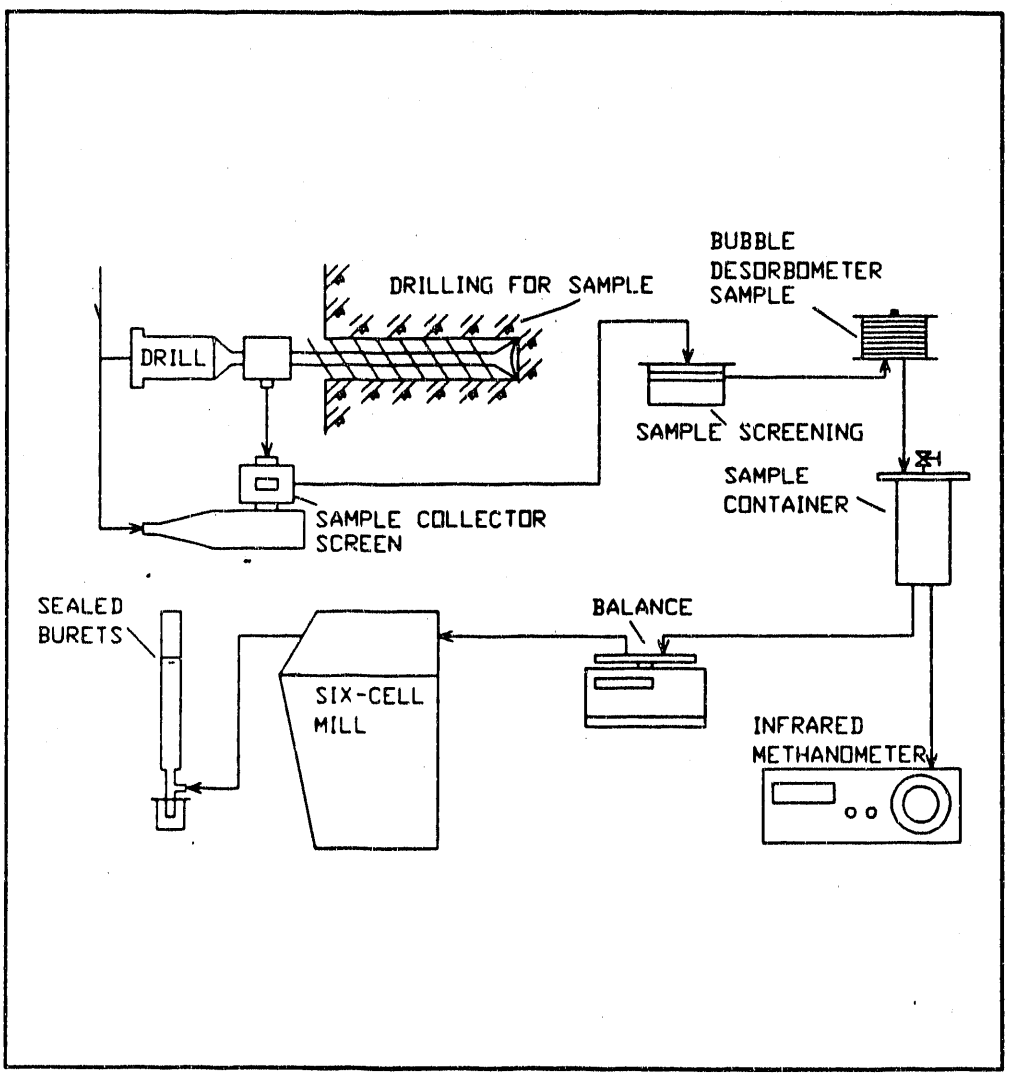

Figure 2. Flow chart of methane content determination.

Determination of Q1

Q1 is defined as the quantity of gas given off and lost from the time the sample is originally disturbed to the time it is sealed in a transportable container. Drill cuttings from horizontal boreholes are collected

and sieved to a size of 0.0078 to 0.015 inch (0.20 to 0.40 mm). The sample is then placed and sealed in the bubble desorbometer cell. The desorbed gas from the sample pushes a slug of colored glycol through a small diameter nylon tubing. A movement of the slug (bubble) of one full circle around the desorbometer corresponds to a volume of 7.5×10^{-2} cu.in (1.233×10^{-3} m3) of gas. This value is referred to as the Kd factor of the desorbometer. The tubing of the desorbometer is graduated volumetrically, enabling recording of the amount of the released gas at periodic time imtervals (i.e., every 30 seconds). A maximum of 18 circles can be read on the desorbometer, but normally only 3-6 are required for the test. Figure 2 shows the flow chart for the test procedure.

The theory and function descriping the desorption process with respect to time is one of the main parameters tested in this study. The French use a quadratic expression, the Germans a decaying power function and the modified test uses a decaying exponential function. These functions are summarized in Equations (1), (2) and (3) for the French, German and Modified methods, respectively:

$$Q1 = k\ t_1 - k\ t_0 \qquad (1)$$

$$Q1 = [V_1/(1-K_t)] \times t_b^{(1-K_t)} \qquad (2)$$

$$Q_1 = (r_0/-k_t) \cdot (e^{(-k_t \cdot t_1)} - 1) \qquad (3)$$

where,

t_0 = the time elapsed from sample disturbance to insertion of the sample into the desorbometer;

t_1 = the elapsed time to the end of the testing period in the desorbometer (for the French method, $t_1 = 2t_0$);

V1 = the specific desorption rate at 1 minute after initial sample disturbance;

Kt = the desorption constant specific for the coal seam; t_b is the elapsed time to the end of the tests in the desorbometer;

r_0 = the initial desorption rate when the sample is initially disturbed;

kt = the desorption constant specific for the coal seam as outlined in the exponential method.

The constants V_1, r_0, K_t and kt are determined from data obtained from the desorbometer. The volumetric desorption rate against the cumulative desorption time since initial drilling on a log-log paper for the German method (power decay function), and on semi-log paper for the modified method (exponential decay function), a straight line results with a slope of K_t or k_t, respectively (Fig. 3a and Fig. 3b).

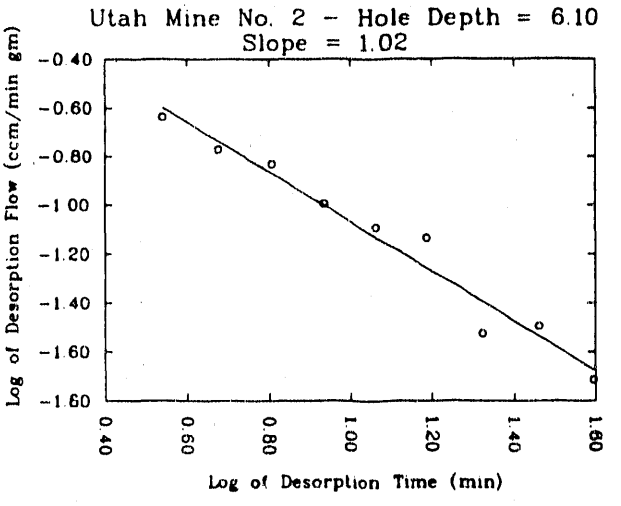

Figure 3a. Slope K_t plotted on log-log paper (power decay function).

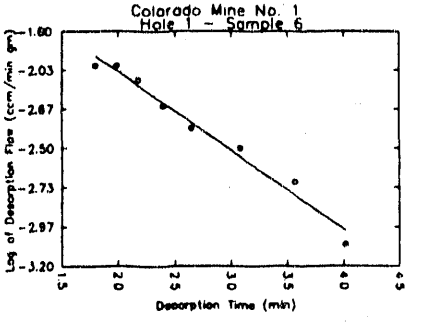

Figure 3b. Slope k_t plotted on semi-log paper (exponential decay function).

Determination of Q2

The volume Q2 is defined as gas desorbed after the sample is sealed in the transportable container and before the container is opened in the lab for further tests. This volume is determined from the gas pressure and methane content in the transportable containers. Upon arrival at the laboratory facilities, the container pressure, lab temperature, ambient temperature and methane concentration in the container are measured. The volumetric percent of methane gas in the container is calculated by the following formula in

which the volume displaced by the coal sample itself is taken into account.

$$V_f = V_b \times (P/P_b) - MR/p \qquad (4)$$

where,

V_f = the free (increased) volume in the transportable container (cu.in or cm^3);

V_b = normal volume of the transport container (cu.in or cm^3);

P = gas pressure in the container (psi or pascals) adjusted for temperature and pressure changes;

P_b = ambient pressure (in psi or kPa = 1000 mbar);

MR = mass of the sample (ounces or grams);

p = density of the coal (lbs/cu.ft or g/cm^3).

The specific volume q2 is then found by:

$$q2 = (V_f \times c)/(Mk \times 100) \qquad (5)$$

where,

q2 = specific volume of released methane in transportable container (m^3/t) or (cm^3/gm)

c = concentration on methane in container (% volume)

Mk = ash-free mass of the coal sample

The ash content of the coal is determined immediately after milling the sample, and the ash free mass is calculated.

$$M^k = M^r \times (100 - 1.1A)/100 \qquad (6)$$

where,

A = the ash content (% weight).

Determination of Q3

Q3 is defined as the volume of the gas released from the sample after it was removed from the transportable container and crushed in the testing mill. The specific volume of the released gas, q3 is measured by use of liquid-filled burets (Fig. 4).

The specific volume q3 is composed of the sum:

$$q3 = q'3 + \blacktriangle q'3 \qquad (7)$$

where,

q3 = gas remaining in coal sample after q2 measurement (cu.ft/ short ton or m^3/t),

q'3 = gas released by milling the sample (cu.ft/st or m^3/t), and

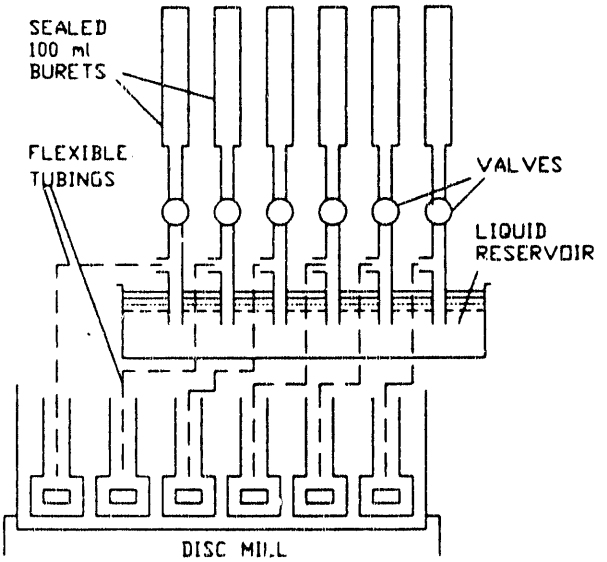

Figure 4. Milled gas collection system.

▲q'3 = amount of methane remaining in the coal after milling due to the partial pressure of methane in the mill (cu.ft/st or m^3/t).

After the q2 measurement is completed, the coal sample is placed in a disc mill, where it is milled in ten minute intervals. The gas released from this crushing is collected in liquid-filled burets. Milling is continued until no more bubbles of gas are released in a two minute interval. The value of q'3 is then simply:

$$\Delta q'3 = \text{sum}(Q'3)/Mk \qquad (8)$$

where, the sum(Q'3) is the total gas measured in the burette.

The partial pressure of methane in the mill, which is directly proportional to the methane content in the mill and also influences the amount yet desorbed from the crushed coal. Consequently, the concentration of methane in the mill must be measured for a precise measurement. If the mill was purged with pure methane before milling begins, then the amount of gas remaining in the coal after milling corresponds to the value of q1bar, since the partial pressure of methane in the mill will be 0.145 psi (1 kPa or 1 bar). Therefore, the methane concentration in the mill is calculated after each milling time interval according to the following equation:

$$C_n = [V_f \times C_{(n-1)} + Q'3_{(n)}]/[V_f + Q'3_{(n)}] \times 100 \qquad (9)$$

where,

C_n = methane content in milling cell after the nth milling interval (% CH_4);

$C_{(n-1)}$ = methane content in mill cell after n-1 milling interval (% CH_4);

$Q'3_{(n)}$ = gas released during the nth milling interval (cm_3);

V_f = free volume of the mill cell (cu.in or cm^3).

$\Delta q'3$ can then be found by:

$$\Delta q'3 = q1bar \times Cn/100 \qquad (10)$$

where,

q1bar = the residual gas content of the coal determined in the laboratory.

Laboratory Determination of Methane Gas Content

To verify the accuracy of the field tests, six sample cells are filled with coal cuttings from the same borehole sample and screened to a particle size from 0.0078 to 0.015 inch (0.20 to 0.40 mm). These cells are inter-connected by copper tubing and the total six cell system is initially placed in a pure methane environment under increased pressures to approximate in situ adsorption conditions. These samples are then measured for their q1 and q3 values, which represents the total gas content adsorbed on the sample.

Gas Content Transformed to In Situ Conditions

In order to relate the desorbed gas measured under laboratory conditions to those of in situ conditions, factors for temperature and moisture content must be considered. This particular formula is described at length in Plaizier (1990).

Determination of Free Gas

The free gas is defined as the gas present in coal samples in the void spaces, but not desorbed on the coal. This value is normally less than 5% of the total gas content, and can be found after the following formula (Firedamp Drainage Handbook, 1980):

$$q_f = V_n \times P/(k \times P_a) \qquad (11)$$

where,

q_f = in situ free gas content (m^3 gas/m^3 non-disturbed coal);

V_n = effective porosity for methane in the coal (m^3/m^3);

P = methane gas pressure in pores;

K = compressibility coefficient of methane (for technical calculations, K=1);

P_a = atmospheric pressure in psi (kilopascals or bars).

The volumetric effective porosity is determined by the equation:

$$V_n = 3.84\times10^{-2} - 1.81\times10^{-3} \times F + 9.38\times10^{-7} \times F^3 \times p(k) \quad (12)$$

where,

F = volatile matter content of the coal in % weight (waf); and

p(k) = coal density (g/cm^3).

TOTAL GAS CONTENT DETERMINATION

The total specific gas content of the coal is then:

$$qtot = q1 + q2 + q3 + qf. \quad (13)$$

The desorbable gas content is, however:

$$qd = qtot - q1bar. \quad (14)$$

RESULTS OF FIELD IN SITU TESTS

Field tests were performed in gassy coal mines in Colorado and in Utah. In Colorado, the B seam of the Dutch Creek Coal Mine in Redstone, was tested. The mine is located about 6 miles south from the town of Redstone, Colorado. The seam is situated in the lower part of the Mesaverde Group of Cretaceous age. Overlying unit is the Bowie Shale Member of the Williams Fork Formation. The underlying unit is the Rollins Sandstone Member of the Iles Formation (Hucka et al., 1989). Rank of the coal is medium volatile bituminous. The samples were collected from the operating longwall face (Figure 5).

The Sub 3 seam of the Castle Gate Coal Mine (Utah Mine 1) is located in the vicinity of the town of Helper, Central Utah. The Sub 3 seam is basal coal bed of the Spring Canyon Member. The Spring Canyon Member is situated in the Blackhawk Formation of Upper Cretaceous age.

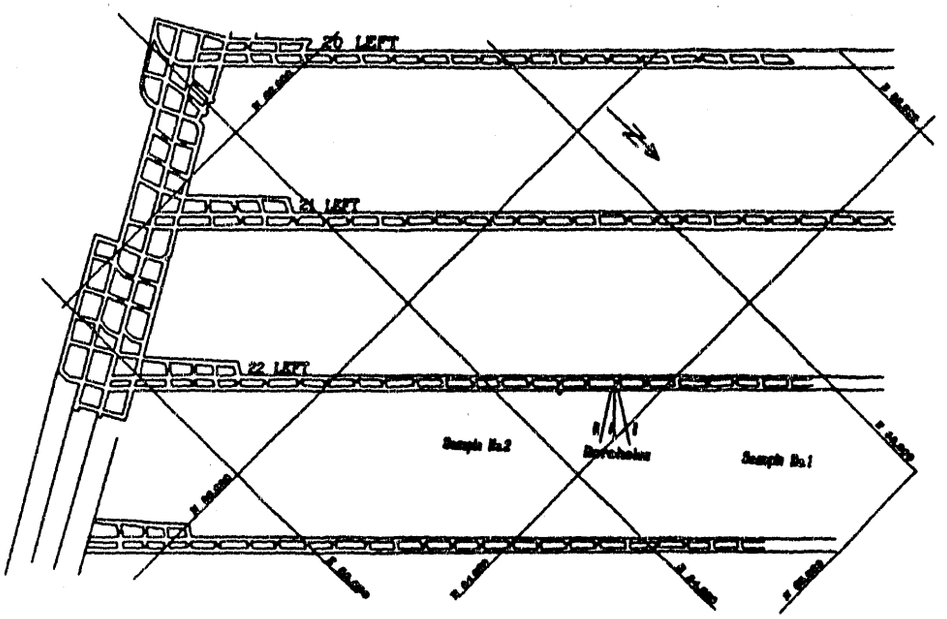

Figure 5. Regional map of the sampling site in Sunnyside Mine, Utah.

In Utah, the tests were executed in the Rock Canyon seam of the Soldier Creek Mine (Utah Mine No. 2). The Rock Canyon seam is part of the Book Cliffs of East-Central Utah Formation developed during the Triassic and Jurassic periods. The Rock Canyon seam is part of the Mesaverde Group (Cretaceous age). The rank of coal is high volatile bituminous B.

The Sunnyside seam of the Sunnyside Coal Mines was tested, as well. The Sunnyside coal zone lies immediately above the Sunnyside Sandstone Member of the Blackhawk Formation. A gassy 2 foot (0.6 m) thick rider seam exists above the seam. The coal rank is high volatile bituminous A. The mine is located south of the town of Price, Central Utah. The Sunnyside seam belongs to the Blackhawk Formation of the Upper Cretaceous age.

A complete tabulation of field test results are given at length in Plaizier (1990). The results are categorized by the three desorption theories (i.e., German power decay function theory, French quadratic decay function theory and Plaizier's exponential decay function theory). A sample output sheet from the field study analysis is provided in Table 1.

Upon compilation of field results and desorption characteristics of treated samples, a German desorption constant (K_t constant) was discovered to be greater than 1

for many samples. As Equation (15) suggests, a value of K_t greater than 1 yields a negative desorbed gas volume, which is obviously impossible.

$$q(0\text{-}b) = [V1/(1-K_t)] \times t_b^{(1-K_t)}. \quad (15)$$

Table 1 - Sample Field Test Results

NAME OF MINE (TEST SITE):	Colorado No. 1
LOCATION WITHIN MINE:	Panel 102 Head Gate - B seam #5
DATE OF TESTS:	7/15/86
ADSORPTION CONSTANT:	16.7
MINE TEMPERATURE (C):	24.0
MINE ATMOS. PRESSURE (Pa):	70897

BOREHOLE NO. 1

SAMPLE NO. 3

ASH CONTENT (%):	5.64	BOREHOLE DEPTH (M):	5.03
SAMPLE WEIGHT (G):	3.40	DRILL TIME (SEC):	32
DESORBOMETER CONSTANT:	1.233		

DATA REDUCTION FUNCTION

	POWER	QUAD.	EXP.
TOTAL GAS CONTENT (CU.M/T):	1.8	1.5	1.0
TOTAL ESTIMATED CONTENT (CU.M/T):	2.8	1.4	1.4
PERCENT ERROR (%):	-54.2	11.8	-45.1
GAS LOST WHILE DRILLING (%):	52.4	42.8	8.1
DESORBED VOLUME IN SITU Q1 (%):	54.9	45.8	12.9
DESORBED VOLUME IN CONTAINER Q2 (%):	31.3	37.6	60.4
DESORBED VOLUME AFTER MILLING Q3 (ml):	13.8	16.6	26.7
COEFFICIENT OF REGRESSION (r2):	0.947	0.988	0.939
SLOPE OR KT CONSTANT:	1.36	0.13	0.28
ESTIMATED TIME CONSTANT:	10.83	37.89	7.17
DESORPTION CONSTANT (Non comparable):	170.43	-0.19	37.74

Time of Read (Minute)	Desorbed Time (Minute)	Gas Volume (ccm)	Desorption Rate (ml/min/g)

2.783	0.0	0.0	—
3.267	0.483	0.025	15.903
3.733	0.467	0.025	16.471
4.467	0.733	0.025	10.482
5.400	0.933	0.025	8.235
6.400	1.000	0.025	7.686
7.917	1.517	0.025	5.068

This deviation from physically possible results using Equation (15) is due to the integral being considered an improper integral because the logarithmic function is undefined at t = 0. The desorbed gas can be approximated using computer numerical integration algorithms as long as the lower limit of the integration is slightly more than zero. The German power decay function representing the methane desorption rate [Equation (2)] implies that the desorption rate at the instant the coal sample is disturbed (i.e., t = 0) is infinite.

Because of the difficulties in modelling methane desorption using the power function with some samples, a theory that methane desorption from coal can be modelled by an exponentially decaying function was thus incorporated into testing procedures and calculations for this work and tests were carried out to verify its authenticity and physical accuracy.

Figure 6 represents a plot of the desorption rate versus time based on this exponential relationship. This curve can be represented by the general equation:

$$r = r_0 \cdot e^{(-k \cdot t)} \tag{16}$$

The amount of gas desorbed between t_0 and t_1 can be found by the integral:

$$q_1 = \int_{t_0}^{t_1} r\,dt \tag{17}$$

Using Equations (16) and (17) and assuming $t_0 = 0$, the volume q_1 is found to be:

$$q_1 = (r_0/-k_t) \cdot [e^{(-k_t \cdot t_1)} - 1] \tag{18}$$

where,

r_0 = the initial desorption rate;

To = Time at which drill bit cuts sample;

T1 = Time to insertion of sample into desorbometer;

T2 = Time to removal of sample from desorbometer and enclosure in a sealed flask;

T3 = time to concentration measurement in a sealed flask and subsequent milling.

The only unknowns in Equation (18) are the curve constant k and the initial desorption rate r_0. The constant k_t can be found with data points measured by the desorbometer between t_1 and t_2 and the rate r_0 extrapolated from t_1 using this curve constant k. No change in testing procedures are required for this desorption theory, only in the data reduction.

The BASIC computer code of the program was prepared to reduce the field data. Upon compilation of the field data from the three mines, an average Time Constant was calculated for each mine and inserted into the program to calculate the estimated total gas content based on initial desorption data.

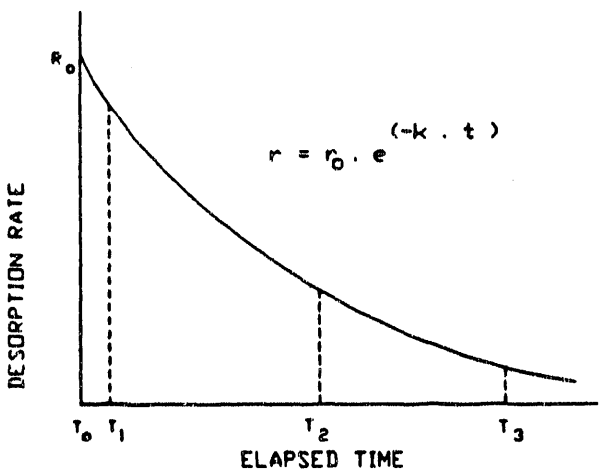

Figure 6. Desorption rate versus time.

t_0 = time at which drill bit cuts sample;

t_1 = time to insertion of sample into desorbometer;

t_2 = time to removal of sample from desorbometer and enclosure in a sealed flask;

t_3 = time to concentration measurement in a sealed flask and subsequent milling.

Time Constants

A coal's 'Time Constant' is a characteristic of a particular coal which reflects the rate of gas desorption for the coal. This constant is used in this testing procedure to quickly estimate the total gas content with data available from tests at the face. The definition and testing of this constant is treated in detail in Plaizier (1990).

DISCUSSION OF RESULTS

Table 2 summarizes the results of the total gas content measurements for the three seams. The heading 'GC' means 'Gas Content'; 'EC' means 'Estimated Content In Situ' using the estimated time constant and the desorbometer readings and '%' signifies the percent error of the in situ estimate based on actual lab results.

The results for Utah No. 1 seam yield some in situ estimates deviating from the actual gas content by as much as 50% of the actual content for all methods. However when summing the total gas content measured versus the total estimated, the percent error decreases significantly. This might be expected from using an estimating time constant derived by averaging all samples, however for practical use in situ, the estimating constant should be verified through many more samples and locations in the mine.

Results from the Utah No. 2 seam yielded estimates consistently within 25% of actual measured contents using the quadratic and exponential theories. Using cumulative totals and percent error, the exponential decay function theory reflects the most consistency in estimated results, with error percentages falling within the 3 - 6% range.

Figures 7 through 9 show the relationship between actual measured gas content and estimated content for the three desorption theories. The estimated content values for the Colorado No. 1 Seam and the Utah No. 2 seam showed relatively close approximations to the actual measured values. The estimated values for Utah No. 1 seam did not correlate well. This can perhaps be attributed to the difficulty in collecting the sample and properly performing

the tests in the Utah No. 1 seam. Due to the hardness of the coal in this seam, drilling time and sample collection time in the first test took double or triple the drill time achieved on subsequent tests. The unexpected difficulty in drilling in the harder coal and difficulties encountered with the drilling equipment prevented an adequate number of samples to be collected for a more complete analysis.

Table 2 - Summary of Field Results

Gas Content Summary

Mine and Sample No.	Theory of Desorption: Power GC	Power EC	Power %	Quadratic GC	Quadratic EC	Quadratic %	Exponential GC	Exponential EC	Exponential %
Utah No. 1									
1	8.1	7.9	2	6.6	2.9	56	7.0	5.3	25
2	5.5	4.1	25	4.6	4.6	0	4.7	4.7	0
3	4.8	7.4	-54	4.0	5.4	-35	4.4	6.8	-53
Total	18.4	19.4	-5%	15.2	12.9	15%	16.1	16.8	-4%
Utah No. 2									
1	5.0	6.4	-28	4.5	5.0	-12	4.7	5.5	-19
2	4.2	3.6	14	3.8	2.6	33	3.8	2.9	23
3	5.4	5.3	.9	5.0	4.2	16	5.1	4.6	10
4	4.6	6.0	-31	4.0	4.9	-22	4.4	5.3	-22
5	4.7	6.9	-46	4.0	5.0	-24	4.4	4.7	-7
6	4.9	6.2	-27	4.3	5.2	-21	4.6	4.7	-1
Total	28.8	34.4	-19%	25.6	26.9	-5%	27	27.7	-3%
Colorado No.1									
1	1.0	1.3	-31	1.0	0.6	44	0.5	0.6	-6
2	3.0	3.1	-4	2.4	2.4	-1	2.3	2.2	3
3	1.8	2.8	-54	1.5	1.4	12	1.0	1.4	-45
4	2.4	2.3	7	2.3	2.0	13	1.9	1.7	11
5	2.0	2.1	-4	1.9	1.6	14	1.6	1.6	0
6	3.4	2.5	25	3.0	2.5	16	2.8	1.8	35
7	3.5	2.9	19	3.3	5.2	-60	3.2	4.7	-47
8	2.7	2.6	5	2.4	3.1	-32	2.2	2.5	-13
Total	19.8	19.6	1%	17.8	18.8	-6%	15.5	16.5	-6%

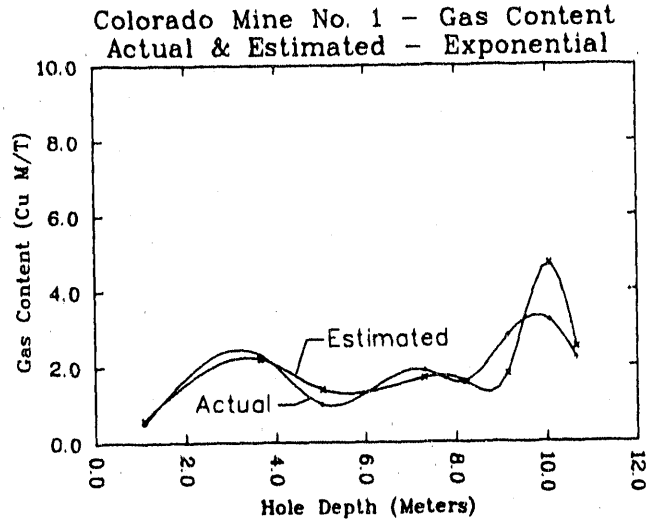

Figure 7. Relationship between actual measured and estimated gas content determined by use of the exponential decay function theory.

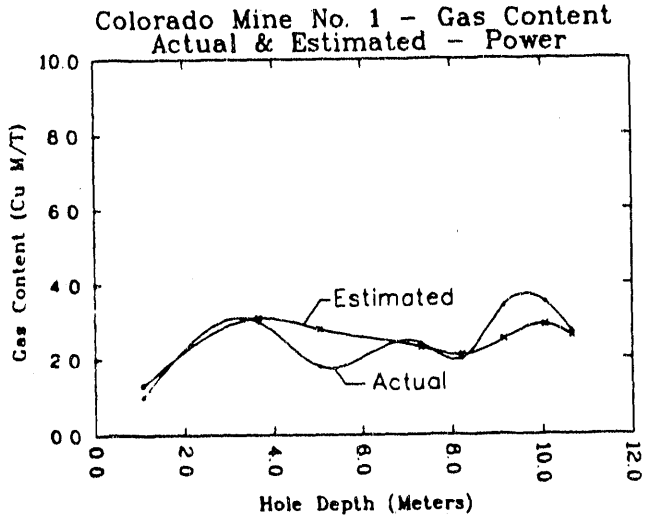

Figure 8. Relationship between actual measured and estimated gas content determined by use of the power decay function theory.

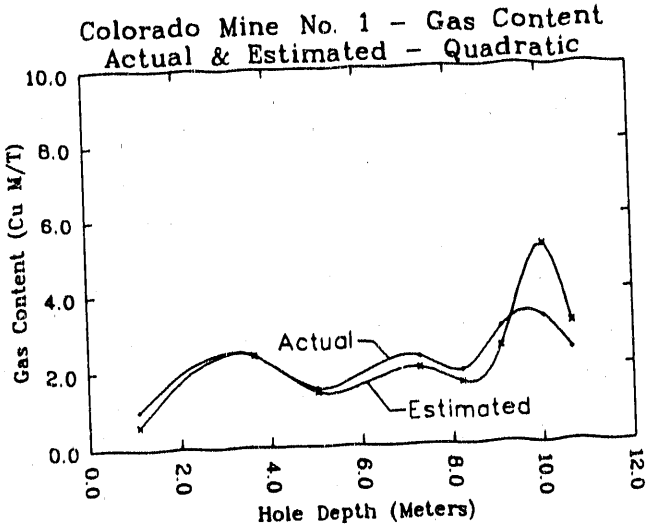

Figure 9. Relationship between actual and estimated gas content determined by use of the quadratic decay function theory.

From Figures 10 through 12 there is not sufficient evidence to determine a preference in the accuracy or reliability of any of the three desorption theories over the other two. However, if graphical plots of the individual sample data is observed, a 'best fit' line would indicate a more accurate representation of the actual physical process of desorption.

Figures 10 through 12 show identical field sample data plotted to the respective desorption theory requirements. That is, for the power function theory the sample readings are plotted on log-log axes, with the X-Axis representing the log of the desorption time, and the Y-Axis representing the log of the specific desorption rate. For the exponential function, the sample readings are plotted on semi-log axes, the X-Axis representing actual desorption time, and the Y-Axis representing the log of the specific desorption rate. For the quadratic function, the readings are plotted on an X-Axis representing the square root of the desorption time, and the Y-Axis representing the cumulative desorbed gas volume.

When the data points are run through a regression analysis as an indication of best fit to the expected theoretical curves, all theories perform equally well.

Table 3 summarizes the results of the regression analysis by indicating the coefficients of regression and the desorption or 'slope' constant for the various field tests. 94% of the coefficients of regression are calculated to be above 0.90.

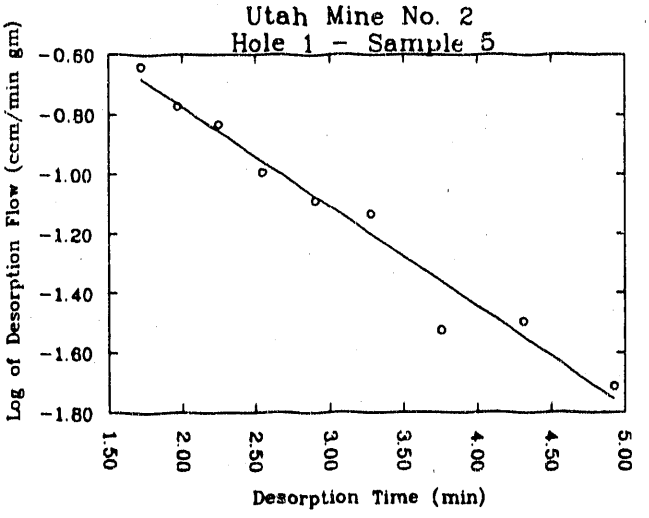

Figure 10. Results on desorption flow versus desorption time plotted on semi-log paper using exponential decay function (Rock Canyon seam).

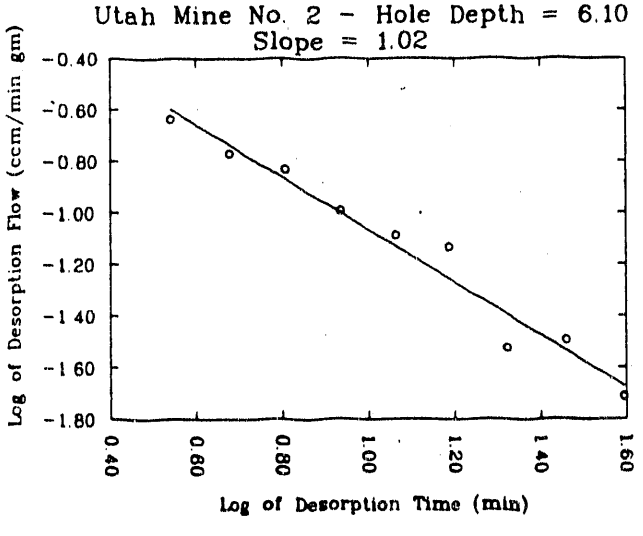

Figure 11. Results on desorption flow versus desorption time plotted on log-log paper using power decay function (Rock Canyon seam).

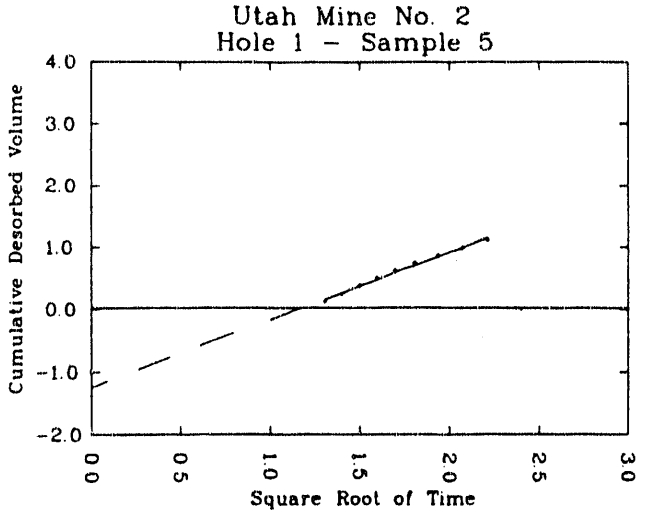

Figure 12. Results on cumulative desorbed volume of gas versus square root of time using quadratic decay function.

The analysis using the quadratic theory generally yielded the highest coefficient of regression, but only in the tests taken at the Colorado No. 1 seam was this coefficient signifi-cantly higher than the other two methods. The results of these regression coefficients indicate that any of the three methods discussed could be used to model the desorption process.

The K_t value is used as a measure of the rate at which the total gas volume of the sample desorbs. The higher the Kt value, the faster the total gas volume will desorb from the sample. The K_t value obtained from the power function analysis is commonly used in European coal mines to determine the risk of gas outbursts in local areas of a working seam or for an entire seam.[16] From the K_t values of the three seams listed in Table 4, it is apparent that each coal seam can and will have its own desorption characteristics.

The area of the K_t value determination is the area in which the three proposed methods differ most. Using the two logarithmic theories (power and exponential), the K_t values indicate a high gas outburst potential for the Utah No. 1 seam, with a lesser potential for the Colorado No. 1 seam, and a very small potential for the Utah No. 2 seam. The K_t values derived from the quadratic theory indicate the Utah No. 2 seam to have the greatest gas outburst risk.

The Standard Deviations of the K_t values listed in Table 3 have been normalized by dividing the numerical value of the standard deviation by the average value to give a standard means of comparison.

Table 3 - Regression Analysis Summary

REGRESSION ANALYSIS SUMMARY

Mine and Sample No.	Theory of Desorption: Power r^2	Power K_t	Quadratic r^2	Quadratic K_t	Exponential r^2	Exponential K_t
Utah No. 1						
1	0.945	2.11	0.948	0.36	0.984	0.71
2	0.996	1.42	0.987	0.56	0.992	0.63
3	0.881	1.71	0.970	0.86	0.947	0.62
Ave.:	0.941	1.75	0.968	0.59	0.974	0.65
N Std Dev:	0.062	0.20	0.021	0.42	0.025	0.08
Utah No. 2						
1	0.998	0.59	0.971	0.99	0.981	0.24
2	0.983	0.69	0.999	0.82	0.989	0.17
3	0.993	0.82	0.996	1.11	0.964	0.21
4	0.994	0.94	0.991	1.37	0.981	0.22
5	0.963	1.02	0.993	1.09	0.964	0.34
6	0.992	0.87	0.978	1.21	0.993	0.33
Ave:	0.987	0.82	0.988	1.10	0.979	0.25
N Std Dev:	0.013	0.20	0.011	0.17	0.012	0.28
Colorado No.1						
1	1.000	1.07	0.998	0.08	0.993	0.33
2	0.976	1.42	0.981	0.27	0.988	0.46
3	0.947	1.36	0.988	0.13	0.939	0.28
4	0.971	0.94	0.999	0.22	0.952	0.31
5	0.956	1.09	0.993	0.22	0.943	0.27
6	0.949	1.29	0.987	0.30	0.977	0.47
7	0.912	0.74	0.992	0.65	0.937	0.23
8	0.776	0.97	0.989	0.38	0.723	0.32
Ave:	0.936	1.11	0.991	0.28	0.932	0.33
N Std Dev:	0.075	0.21	0.006	0.64	0.093	0.27

SUMMARY

The total gas contents measured and calculated using the three methods were generally within 20% of each other. The quadratic theory fits the field data slightly better than the other two theories, but not significantly. The power function theory resulted in consistently higher gas content values than the other two. The exponential theory resulted in an overall better estimating accuracy using measurements taken at the face.

ACKNOWLEDGEMENTS

Thanks are due to the University of Utah Research Grant Committee for sponsoring the research work. Thanks belong also to the Department of Energy for financial support necessary for preparation and writing this paper.

REFERENCES

Plaizier, R.R., 1990, Methane Desorption Modelling and Analysis for Selected Western Coal Fields: M. Sc. thesis, University of Utah, 207 p.

McCulloch, C.M., 1975, Measuring Methane Content of Bituminous Coalbeds: U.S. Bureau of Mines RI 8043, 22 p.

Handbook for the Coalmining Industry in the European Community, 1980, Firedamp Drainage: Verlag Glueckauf GmbH, Essen, 415 p.

Hucka, B., Sommer, S.N., and Heith, A.C., 1989, Cleat and Joint System Evaluation and Coal Characterization of the B-seam, Dutch Creek Mine, Pitkin County, Colorado: Unpubl. Techn. Rep., Utah Geological and Mineral Survey, Salt Lake City, UT, 36 p.

APPENDIX B

RESULTS ON FIELD AND LABORATORY TESTS ON METHANE CONTENT

TABLE B-1

METHANE CONTENT OF UTAH AND COLORADO GASSY COALBEDS

MINE SEAM (DATE)	BORE-HOLE NO.	SAMPLE NO.	METHANE CONTENT (CH4) IN CU.M/T — DECAY FUNCTION POWER	QUADRAT	EXPONENT
BEAVER NO. 8	B	1	1.5	0.9	0.1
CASTLEGATE A	B	3	1.7	0.8	0
	C	1	1.6	0.7	0
	D	1	1.5	0.7	0.2
AVERAGE			1.57	0.77	0.07
ST DEV			0.08	0.08	0.08
CASTLE GATE	A	1	8.1	6.6	7
SUB 3	A	2	5.5	4.6	4.7
LONGWALL	A	3	4.8	4	4.4
	B	1	9.6	7.5	7.8
	B	2	10.6	9.1	9.5
	B	3	11.3	8.6	9.2
	B	4	10.2	7.5	8.1
	B	5	9.1	7.6	8
	B	6	11.4	3.3	3.8
AVERAGE			8.95	6.53	6.94
ST DEV			2.26	1.95	2.01
SOLDIER CREEK	A	1	5.9	5.4	5.5
ROCK CANYON	A	2	5	4.5	4.5
	A	3	6.3	5.9	6.1
	A	4	5.4	4.8	5.2
	A	5	5.5	4.8	5.2
	A	6	5.7	5.1	5.5
AVERAGE			5.63	5.08	5.33
ST DEV			2.01	1.82	1.91
SOLDIER CREEK SUNNYSIDE MIDDLE BOREHOLE	B	1	2.9	1.5	0.7

TABLE B-1

METHANE CONTENT OF UTAH AND COLORADO GASSY COALBEDS (CONT.)

MINE SEAM (DATE)	BORE-HOLE NO.	SAMPLE NO.	METHANE CONTENT (CH4) IN CU.M/T		
			DECAY FUNCTION		
			POWER	QUADRAT	EXPONENT
SUNNYSIDE	A	1	4.1	4	3.8
LWR SUNNYSIDE	A	2	4.2	4.2	3.9
	A	3	3.8	3.7	3.6
	B	1	4	3.1	2.6
	B	2	2.5	4	1.9
	B	3	3.3	3.4	2.8
	B	4	3.5	3.3	3.1
	B	5	3.5	3.4	3.2
	B	6	3.5	3.6	3.2
	B	7	3.6	3.6	3.3
	C	1	2.9	3.1	2.6
	C	2	5	5	4.8
	C	3	3.9	3.9	3.7
	C	4	3.7	3.6	3.5
	C	5	4	3.9	3.8
	C	6	3.3	3.2	3
	C	7	4.1	4.2	3.8
AVERAGE			3.7	3.71	3.32
ST DEV			0.54	0.47	0.64
MID-CONTINENT	A	1	1	1	0.5
B SEAM	A	2	3	2.4	2.3
(COLORADO)	A	3	1.8	1.5	1
# 5 DOOR	A	4	2.4	2.3	1.9
	A	5	2	1.9	1.6
	A	6	3.4	3	2.8
	A	7	3.5	3.3	3.2
	A	8	2.7	2.4	2.2
	B	1	4	4.8	4.8
	B	2	4.7	5.7	5.5
LONGWALL	B	3	11.3	9.6	9.6
	B	4	6.5	9.4	9.7
AVERAGE			3.85	7.37	3.75
ST DEV			2.63	2.78	2.96

BEAVER CREEK COAL MINE

NAME OF MINE (TEST SITE):	Beaver Creek #8 Mine
LOCATION WITHIN MINE:	Castlegate A seam, borehole B
DATE OF TESTS: 6/27/90	ADSORPTION CONSTANT: 21.3
Mine Temperature (C): 14.5	Mine Atmos. Pressure (Pa): 77931

BOREHOLE NO. B

SAMPLE NO. 1

ASH CONTENT (%):	5.64	BOREHOLE DEPTH (M):	4.02
SAMPLE WEIGHT (G):	4.00	DRILL TIME (SEC):	9
DESORBOMETER CONSTANT:	1.233		

	POWER	QUADRATIC	EXPONENT
TOTAL GAS CONTENT (CU.M/T):	1.5	0.9	0.1
TOTAL ESTIMATED CONTENT (CU.M/T):	1.1	0.1	0.1
PERCENT ERROR (%):	27.6	92.4	-17.8
GAS LOST WHILE DRILLING (%):	95.9	92.7	11.6
DESORBED VOLUME INSITU Q1 (%):	96.4	93.5	20.9
DESORBED VOLUME IN CONTAINER Q2 (%):	0.0	0.0	0.0
DESORBED VOLUME AFTER MILLING Q3 (ml)	3.6	6.5	79.1
COEFFICIENT OF REGRESSION (r2):	1.000	1.000	1.000
SLOPE OR KT CONSTANT:	1.62	0.02	0.82
ESTIMATED TIME CONSTANT:	29.40	182.90	4.50
DESORPTION CONSTANT (Non comparable):	52.26	-0.01	12.96

Time of Read (min)	Desorbed Time (min)	Gas Volume (ccm)	Desorption Rate (ml/min/g)
0.825	0.0	0.0	--
1.475	0.650	0.012	5.026
4.758	3.283	0.012	0.995

BEAVER CREEK COAL MINE (CONT.)

BOREHOLE B

SAMPLE NO. 3

ASH CONTENT (%):	5.64	BOREHOLE DEPTH (M):	8.02
SAMPLE WEIGHT (G):	4.40	DRILL TIME (SEC):	16
DESORBOMETER CONSTANT:	1.233		

	POWER	QUADRATIC	EXPONENT
TOTAL GAS CONTENT (CU.M/T):	1.7	0.8	0.0
TOTAL ESTIMATED CONTENT (CU.M/T):	0.9	0.1	0.1
PERCENT ERROR (%):	45.5	92.1	-78.5
GAS LOST WHILE DRILLING (%):	98.1	96.0	16.7
DESORBED VOLUME INSITU Q1 (%):	98.5	96.7	32.5
DESORBED VOLUME IN CONTAINER Q2 (%):	0.0	0.0	0.0
DESORBED VOLUME AFTER MILLING Q3 (ml)	1.5	3.3	67.5
COEFFICIENT OF REGRESSION (r2):	1.000	1.000	1.000
SLOPE OR KT CONSTANT:	1.48	0.02	0.86
ESTIMATED TIME CONSTANT:	39.09	176.34	2.97
DESORPTION CONSTANT (Non comparable):	43.06	-0.01	10.91

Time of Read (min)	Desorbed Time (min)	Gas Volume (ccm)	Desorption Rate (ml/min/g)
0.667	0.0	0.0	--
1.300	0.633	0.012	4.689
4.250	2.950	0.012	1.007

BEAVER CREEK COAL MINE (CONT.)

NAME OF MINE (TEST SITE): Beaver Creek #8 Mine
LOCATION WITHIN MINE: Castlegate A seam, borehole C
DATE OF TESTS: 6/28/90 ADSORPTION CONSTANT: 21.3
Mine Temperature (C): 13.5 Mine Atmos. Pressure (Pa): 77828

BOREHOLE NO. C

SAMPLE NO. 1

ASH CONTENT (%): 5.64 BOREHOLE DEPTH (M): 12.01
SAMPLE WEIGHT (G): 5.00 DRILL TIME (SEC): 14
DESORBOMETER CONSTANT: 1.233

	POWER	QUADRATIC	EXPONENT
TOTAL GAS CONTENT (CU.M/T):	1.6	0.7	0.0
TOTAL ESTIMATED CONTENT (CU.M/T):	0.8	0.1	0.1
PERCENT ERROR (%):	46.5	89.1	-84.0
GAS LOST WHILE DRILLING (%):	98.2	95.9	17.8
DESORBED VOLUME INSITU Q1 (%):	98.6	96.7	33.4
DESORBED VOLUME IN CONTAINER Q2 (%):	0.0	0.0	0.0
DESORBED VOLUME AFTER MILLING Q3 (ml)	1.4	3.3	66.6
COEFFICIENT OF REGRESSION (r2):	1.00	1.00	1.00
SLOPE OR KT CONSTANT:	1.36	0.02	0.86
ESTIMATED TIME CONSTANT:	39.84	127.37	2.88
DESORPTION CONSTANT (Non comparable):	39.06	-0.01	10.08

Time of Read (min)	Desorbed Time (min)	Gas Volume (ccm)	Desorption Rate (ml/min/g)
0.717	0.0	0.0	--
1.350	0.633	0.012	4.126
3.217	1.867	0.012	1.400

BEAVER CREEK COAL MINE (CONT.)

NAME OF MINE (TEST SITE):	Beaver Creek #8 Mine
LOCATION WITHIN MINE:	Castlegate A seam, borehole D
DATE OF TESTS: 6/28/90	ADSORPTION CONSTANT: 21.3
Mine Temperature (C): 15.0	Mine Atmos. Pressure (Pa): 77828

BOREHOLE NO. D

SAMPLE NO. 1

ASH CONTENT (%):	5.64	BOREHOLE DEPTH (M):	4.02
SAMPLE WEIGHT (G):	4.80	DRILL TIME (SEC):	17
DESORBOMETER CONSTANT:	1.233		

	POWER	QUADRATIC	EXPONENT
TOTAL GAS CONTENT (CU.M/T):	1.5	0.7	0.2
TOTAL ESTIMATED CONTENT (CU.M/T):	1.0	0.1	0.1
PERCENT ERROR (%):	31.7	82.1	39.8
GAS LOST WHILE DRILLING (%):	89.9	80.0	5.6
DESORBED VOLUME INSITU Q1 (%):	90.4	81.1	10.7
DESORBED VOLUME IN CONTAINER Q2 (%):	0.0	0.0	0.0
DESORBED VOLUME AFTER MILLING Q3 (ml)	9.6	18.9	89.3
COEFFICIENT OF REGRESSION (r2):	0.511	0.981	0.631
SLOPE OR KT CONSTANT:	1.18	0.04	0.84
ESTIMATED TIME CONSTANT:	31.18	77.81	8.81
DESORPTION CONSTANT (Non comparable):	47.13	-0.03	14.99

Time of Read (min)	Desorbed Time (min)	Gas Volume (ccm)	Desorption Rate (ml/min/g)
0.658	0.0	0.0	--
1.225	0.567	0.012	4.804
1.575	0.350	0.012	7.778
3.108	1.533	0.012	1.775

CASTLE GATE COAL MINE
(FORMER: PRICE RIVER COAL COMPANY)
(Tests made by Plaizier, 1990)

NAME OF MINE (TEST SITE):	Price River Coal Co.
LOCATION WITHIN MINE:	#5 - 11th West - Longwall Panel Borehole A
DATE OF TESTS: 4/18/86	ADSORPTION CONSTANT: 21.1
Mine Temperature (C): 14.4	Mine Atmos. Pressure (Pa): 79897

BOREHOLE NO. A

SAMPLE NO. 1

ASH CONTENT (%):	5.56	BOREHOLE DEPTH (M):	2.44
SAMPLE WEIGHT (G):	3.20	DRILL TIME (SEC):	52
DESORBOMETER CONSTANT:	1.233		

	POWER	QUADRATIC	EXPONENT
TOTAL GAS CONTENT (CU.M/T):	8.1	6.6	7.0
TOTAL ESTIMATED CONTENT (CU.M/T):	7.9	2.9	5.3
PERCENT ERROR (%):	2.3	56.0	25.2
GAS LOST WHILE DRILLING (%):	17.5	-0.1	5.3
DESORBED VOLUME INSITU Q1 (%):	19.1	1.8	7.1
DESORBED VOLUME IN CONTAINER Q2 (%):	63.9	77.5	73.4
DESORBED VOLUME AFTER MILLING Q3 (ml):	17.0	20.6	19.5
COEFFICIENT OF REGRESSION (r2):	0.945	0.948	0.984
SLOPE OR KT CONSTANT:	2.11	0.36	0.71
ESTIMATED TIME CONSTANT:	21.60	56.30	14.68
DESORPTION CONSTANT (Non comparable)	373.34	-0.34	339.16

Time of Read (min)	Desorbed Time (min)	Gas Volume (ccm)	Desorption Rate (ml/min/g)
1.667	0.0	0.0	--
2.183	0.517	0.123	78.967
2.867	0.683	0.123	59.707
3.483	0.617	0.074	39.697
3.817	0.333	0.025	24.479
4.200	0.383	0.025	21.287
4.850	0.650	0.025	12.553

CASTLE GATE COAL MINE (CONT.)
(FORMER: PRICE RIVER COAL COMPANY)

BOREHOLE A

SAMPLE NO. 2

ASH CONTENT (%):	5.56	BOREHOLE DEPTH (M):	5.79
SAMPLE WEIGHT (G):	3.20	DRILL TIME (SEC):	15
DESORBOMETER CONSTANT:	1.233		

	POWER	QUADRATIC	EXPONENT
TOTAL GAS CONTENT (CU.M/T):	5.5	4.6	4.7
TOTAL ESTIMATED CONTENT (CU.M/T):	4.1	4.6	4.7
PERCENT ERROR (%):	24.6	-0.0	0.8
GAS LOST WHILE DRILLING (%):	18.4	1.5	5.3
DESORBED VOLUME INSITU Q1 (%):	21.2	4.9	8.6
DESORBED VOLUME IN CONTAINER Q2 (%):	50.1	60.5	58.1
DESORBED VOLUME AFTER MILLING Q3 (ml):	28.7	34.6	33.3
COEFFICIENT OF REGRESSION (r2):	0.996	0.987	0.992
SLOPE OR KT CONSTANT:	1.42	0.56	0.63
ESTIMATED TIME CONSTANT:	27.99	24.80	11.06
DESORPTION CONSTANT (Non comparable):	196.32	-0.55	268.46

Time of Read (min)	Desorbed Time (min)	Gas Volume (ccm)	Desorption Rate (ml/min/g)
1.292	0.0	0.0	--
1.575	0.283	0.099	115.199
2.058	0.483	0.123	84.414
2.308	0.250	0.049	65.279
2.592	0.283	0.049	57.600
2.758	0.167	0.025	48.958
3.958	1.200	0.123	34.000

CASTLE GATE COAL MINE (CONT.)
(FORMER: PRICE RIVER COAL COMPANY)

BOREHOLE A

SAMPLE NO. 3

ASH CONTENT (%): 5.56 BOREHOLE DEPTH (M): 7.62
SAMPLE WEIGHT (G): 4.20 DRILL TIME (SEC): 19
DESORBOMETER CONSTANT: 1.233

	POWER	QUADRATIC	EXPONENT
TOTAL GAS CONTENT (CU.M/T):	4.8	4.0	4.4
TOTAL ESTIMATED CONTENT (CU.M/T):	7.4	5.4	6.8
PERCENT ERROR (%):	-53.6	-35.3	-52.6
GAS LOST WHILE DRILLING (%):	15.9	-2.7	8.3
DESORBED VOLUME INSITU Q1 (%):	21.1	3.7	14.0
DESORBED VOLUME IN CONTAINER Q2 (%):	32.5	39.7	35.5
DESORBED VOLUME AFTER MILLING Q3 (ml):	46.3	56.6	50.5
COEFFICIENT OF REGRESSION (r2):	0.881	0.970	0.947
SLOPE OR KT CONSTANT:	1.71	0.86	0.62
ESTIMATED TIME CONSTANT:	13.74	18.34	7.20
DESORPTION CONSTANT (Non comparable):	352.77	-0.78	384.94

Time of Read (min)	Desorbed Time (min)	Gas Volume (ccm)	Desorption Rate (ml/min/g)
1.292	0.0	0.0	--
1.692	0.400	0.222	139.884
1.925	0.233	0.123	133.224
2.242	0.317	0.123	98.164
2.408	0.167	0.049	74.605
2.642	0.233	0.074	79.935
3.042	0.400	0.123	77.714
3.575	0.533	0.123	58.285
4.392	0.817	0.123	38.064
5.208	0.817	0.049	15.226

CASTLE GATE COAL MINE
(FORMER: PRICE RIVER COAL COMPANY)

NAME OF MINE (TEST SITE): CASTLE GATE MINE
LOCATION WITHIN MINE: SUB-3, Borehole B
DATE OF TESTS: 9/14/89 ADSORPTION CONSTANT: 6.41
Mine Temperature (C): 19.0 Mine Atmos. Pressure (Pa): 73716

BOREHOLE NO. B
SAMPLE NO. 1

ASH CONTENT (%): 7.13 BOREHOLE DEPTH (M): 3.00
SAMPLE WEIGHT (G): 3.30 DRILL TIME (SEC): 15.7
DESORBOMETER CONSTANT: 1.233

	POWER	QUAD.	EXPONENT
TOTAL GAS CONTENT (CU.M/T):	9.6	7.5	7.8
TOTAL ESTIMATED CONTENT (CU.M/T):	12.3	6.9	9.3
PERCENT ERROR (%):	-28.2	8.4	-19.2
GAS LOST WHILE DRILLING (%):	22.9	1.4	5.2
DESORBED VOLUME INSITU Q1 (%):	32.5	13.7	17.0
DESORBED VOLUME IN CONTAINER Q2 (%):	50.9	65.1	62.5
DESORBED VOLUME AFTER MILLING Q3 (ml):	16.6	21.3	20.4
COEFFICIENT OF REGRESSION (r2):	0.996	0.997	0.960
SLOPE OR KT CONSTANT:	0.80	1.40	0.15
ESTIMATED TIME CONSTANT:	5.00	72.73	35.36
DESORPTION CONSTANT (Non comparable):	381.49	-1.67	237.73

BOREHOLE B
SAMPLE NO. 2

ASH CONTENT (%): 7.13 BOREHOLE DEPTH (M): 4.00
SAMPLE WEIGHT (G): 3.00 DRILL TIME (SEC): 21.3
DESORBOMETER CONSTANT: 1.233

	EXPONENT	POWER	QUAD.
TOTAL GAS CONTENT (CU.M/T):	10.6	9.1	9.5
TOTAL ESTIMATED CONTENT (CU.M/T):	8.0	10.2	9.3
PERCENT ERROR (%):	25.2	-11.5	2.3
GAS LOST WHILE DRILLING (%):	15.4	1.7	5.4
DESORBED VOLUME INSITU Q1 (%):	24.1	11.8	15.1
DESORBED VOLUME IN CONTAINER Q2 (%):	57.3	66.6	64.1
DESORBED VOLUME AFTER MILLING Q3 (ml):	18.5	21.6	20.7
COEFFICIENT OF REGRESSION (r2):	0.985	0.998	0.959
SLOPE OR KT CONSTANT:	0.70	1.46	0.12
ESTIMATED TIME CONSTANT:	8.57	59.77	43.12
DESORPTION CONSTANT (Non comparable):	369.39	-2.11	234.30

CASTLE GATE COAL MINE (CONT.)
(FORMER: PRICE RIVER COAL COMPANY)

BOREHOLE B

SAMPLE NO. 3

ASH CONTENT (%): 16.03 BOREHOLE DEPTH (M): 5.00
SAMPLE WEIGHT (G): 3.20 DRILL TIME (SEC): 60.0
DESORBOMETER CONSTANT: 1.233

	POWER	QUAD.	EXPONENT
TOTAL GAS CONTENT (CU.M/T):	11.3	8.6	9.2
TOTAL ESTIMATED CONTENT (CU.M/T):	13.9	11.2	9.4
PERCENT ERROR (%):	-23.0	-29.9	-2.8
GAS LOST WHILE DRILLING (%):	25.0	1.9	7.5
DESORBED VOLUME INSITU Q1 (%):	33.5	13.1	18.0
DESORBED VOLUME IN CONTAINER Q2 (%):	52.6	68.8	65.0
DESORBED VOLUME AFTER MILLING Q3 (ml):	13.8	18.1	17.1
COEFFICIENT OF REGRESSION (r2):	0.996	0.997	0.969
SLOPE OR KT CONSTANT:	0.79	1.42	0.12
ESTIMATED TIME CONSTANT:	5.21	51.30	40.98
DESORPTION CONSTANT (Non comparable):	456.91	-2.32	236.67

BOREHOLE B
SAMPLE NO. 4

ASH CONTENT (%): 16.03 BOREHOLE DEPTH (M): 6.00
SAMPLE WEIGHT (G): 4.30 DRILL TIME (SEC): 18.4
DESORBOMETER CONSTANT: 1.233

	POWER	QUAD.	EXPONENT
TOTAL GAS CONTENT (CU.M/T):	10.2	7.5	8.1
TOTAL ESTIMATED CONTENT (CU.M/T):	13.6	4.9	8.5
PERCENT ERROR (%):	-33.3	35.3	-4.5
GAS LOST WHILE DRILLING (%):	26.9	1.0	7.8
DESORBED VOLUME INSITU Q1 (%):	34.3	10.9	17.1
DESORBED VOLUME IN CONTAINER Q2 (%):	54.2	73.4	68.4
DESORBED VOLUME AFTER MILLING Q3 (ml):	11.5	15.6	14.5
COEFFICIENT OF REGRESSION (r2):	0.996	0.998	0.970
SLOPE OR KT CONSTANT:	0.80	1.73	0.12
ESTIMATED TIME CONSTANT:	4.81	102.98	40.30
DESORPTION CONSTANT (Non comparable):	425.07	-3.09	212.66

CASTLE GATE COAL MINE (CONT.)
(FORMER: PRICE RIVER COAL COMPANY)

BOREHOLE B

SAMPLE NO. 5

ASH CONTENT (%): 16.03 BOREHOLE DEPTH (M): 7.00
SAMPLE WEIGHT (G): 4.40 DRILL TIME (SEC): 33.0
DESORBOMETER CONSTANT: 1.233

	POWER	QUAD.	EXPONENT
TOTAL GAS CONTENT (CU.M/T):	9.1	7.6	8.0
TOTAL ESTIMATED CONTENT (CU.M/T):	7.9	2.4	9.4
PERCENT ERROR (%):	12.8	69.0	-17.7
GAS LOST WHILE DRILLING (%):	16.7	0.5	5.3
DESORBED VOLUME INSITU Q1 (%):	28.9	15.0	19.1
DESORBED VOLUME IN CONTAINER Q2 (%):	65.5	78.3	74.5
DESORBED VOLUME AFTER MILLING Q3 (ml):	5.7	6.8	6.4
COEFFICIENT OF REGRESSION (r2):	0.995	0.998	0.954
SLOPE OR KT CONSTANT:	0.71	1.88	0.13
ESTIMATED TIME CONSTANT:	7.35	214.66	35.80
DESORPTION CONSTANT (Non comparable):	360.93	-2.27	237.48

BOREHOLE B

SAMPLE NO. 6

ASH CONTENT (%): 16.03 BOREHOLE DEPTH (M): 9.00
SAMPLE WEIGHT (G): 6.60 DRILL TIME (SEC): 42.0
DESORBOMETER CONSTANT: 1.233

	POWER	QUAD.	EXPONENT
TOTAL GAS CONTENT (CU.M/T):	11.4	3.3	3.8
TOTAL ESTIMATED CONTENT (CU.M/T):	48.7	-2.0	8.4
PERCENT ERROR (%):	-326.0	161.2	-118.8
GAS LOST WHILE DRILLING (%):	70.8	-0.9	13.1
DESORBED VOLUME INSITU Q1 (%):	78.4	25.3	35.7
DESORBED VOLUME IN CONTAINER Q2 (%):	20.5	70.9	61.0
DESORBED VOLUME AFTER MILLING Q3 (ml)	1.1	3.8	3.3
COEFFICIENT OF REGRESSION (r2):	0.997	0.992	0.967
SLOPE OR KT CONSTANT:	0.94	2.24	0.14
ESTIMATED TIME CONSTANT:	1.50	-108.83	19.25
DESORPTION CONSTANT (Non comparable):	460.42	-3.12	213.53

SOLDIER CREEK CANYON COAL MINE

NAME OF MINE (TEST SITE): Soldier Creek Coal Co.
LOCATION WITHIN MINE: 1400 South 3rd West-Rock Canyon
DATE OF TESTS: 4/20/86 ADSORPTION CONSTANT: 21.1
Mine Temperature (C): 17.0 Mine Atmos. Pressure (Pa): 78745

BOREHOLE NO. A

SAMPLE NO. 1

ASH CONTENT (%): 5.02 BOREHOLE DEPTH (M): 2.00
SAMPLE WEIGHT (G): 2.90 DRILL TIME (SEC): 20
DESORBOMETER CONSTANT: 1.233

	POWER	QUADRATIC	EXPONENT
TOTAL GAS CONTENT (CU.M/T):	5.9	5.4	5.5
TOTAL ESTIMATED CONTENT (CU.M/T):	4.9	8.9	11.5
PERCENT ERROR (%):	16.6	-67.2	-107.1
GAS LOST WHILE DRILLING (%):	11.1	2.4	5.8
DESORBED VOLUME INSITU Q1 (%):	16.3	8.1	11.3
DESORBED VOLUME IN CONTAINER Q2 (%):	78.3	86.0	83.0
DESORBED VOLUME AFTER MILLING Q3 (ml)	5.4	5.9	5.7
COEFFICIENT OF REGRESSION (r2):	0.998	0.971	0.981
SLOPE OR KT CONSTANT:	0.59	0.99	0.24
ESTIMATED TIME CONSTANT:	25.31	14.84	5.30
DESORPTION CONSTANT (Non comparable):	232.26	-0.93	255.30

Time of Read (min)	Desorbed Time (min)	Gas Volume (ccm)	Desorption Rate (ml/min/g)
1.333	0.0	0.0	--
2.067	0.733	0.345	170.918
3.083	1.017	0.370	132.092
3.467	0.383	0.123	116.776

SOLDIER CREEK CANYON COAL MINE (CONT.)

BOREHOLE NO. A

SAMPLE NO. 2

ASH CONTENT (%):	5.02	BOREHOLE DEPTH (M):	4.00
SAMPLE WEIGHT (G):	4.70	DRILL TIME (SEC):	15
DESORBOMETER CONSTANT:	1.233		

	POWER	QUADRATIC	EXPONENT
TOTAL GAS CONTENT (CU.M/T):	5.0	4.5	4.5
TOTAL ESTIMATED CONTENT (CU.M/T):	2.5	4.6	6.1
PERCENT ERROR (%):	48.7	-0.6	-33.4
GAS LOST WHILE DRILLING (%):	12.4	4.4	4.4
DESORBED VOLUME INSITU Q1 (%):	15.7	8.1	8.0
DESORBED VOLUME IN CONTAINER Q2 (%):	79.8	87.0	87.1
DESORBED VOLUME AFTER MILLING Q3 (ml)	4.5	4.9	4.9
COEFFICIENT OF REGRESSION (r2):	0.983	0.999	0.989
SLOPE OR KT CONSTANT:	0.69	0.82	0.17
ESTIMATED TIME CONSTANT:	41.16	24.65	8.23
DESORPTION CONSTANT (Non comparable):	120.50	-1.25	91.67

Time of Read (min)	Desorbed Time (min)	Gas Volume (ccm)	Desorption Rate (ml/min/g)
2.575	0.0	0.0	--
3.058	0.483	0.123	57.146
3.575	0.517	0.123	53.459
4.142	0.567	0.123	48.742
4.775	0.633	0.123	43.611
5.508	0.733	0.123	37.665
6.292	0.783	0.123	35.260

SOLDIER CREEK CANYON COAL MINE (CONT.)

BOREHOLE NO. A

SAMPLE NO. 3

ASH CONTENT (%):	5.02	BOREHOLE DEPTH (M):	5.00
SAMPLE WEIGHT (G):	3.90	DRILL TIME (SEC):	17
DESORBOMETER CONSTANT:	1.233		

	POWER	QUADRATIC	EXPONENT
TOTAL GAS CONTENT (CU.M/T):	6.3	5.9	6.1
TOTAL ESTIMATED CONTENT (CU.M/T):	4.8	7.5	9.5
PERCENT ERROR (%):	24.2	-26.3	-56.7
GAS LOST WHILE DRILLING (%):	8.4	1.7	4.5
DESORBED VOLUME INSITU Q1 (%):	15.2	9.0	11.6
DESORBED VOLUME IN CONTAINER Q2 (%):	80.5	86.4	84.0
DESORBED VOLUME AFTER MILLING Q3 (ml):	4.2	4.5	4.4
COEFFICIENT OF REGRESSION (r2):	0.993	0.996	0.964
SLOPE OR KT CONSTANT:	0.82	1.11	0.21
ESTIMATED TIME CONSTANT:	27.85	19.63	7.01
DESORPTION CONSTANT (Non comparable):	227.59	-1.29	185.98

Time of Read (min)	Desorbed Time (min)	Gas Volume (ccm)	Desorption Rate (ml/min/g)
1.608	0.0	0.0	--
1.842	0.233	0.123	142.656
2.092	0.250	0.123	133.145
2.375	0.283	0.123	117.482
2.692	0.317	0.123	105.115
3.025	0.333	0.123	99.859
3.425	0.400	0.123	83.216
3.842	0.417	0.123	79.887
4.275	0.433	0.123	76.815
4.775	0.500	0.123	66.573
5.325	0.550	0.123	60.521
5.958	0.633	0.123	52.557
6.608	0.650	0.123	51.210
7.325	0.717	0.123	46.446

SOLDIER CREEK CANYON COAL MINE (CONT.)

BOREHOLE NO. A

SAMPLE NO. 4

ASH CONTENT (%):	5.02	BOREHOLE DEPTH (M):	6.00
SAMPLE WEIGHT (G):	4.10	DRILL TIME (SEC):	20
DESORBOMETER CONSTANT:	1.233		

	POWER	QUADRATIC	EXPONENT
TOTAL GAS CONTENT (CU.M/T):	5.4	4.8	5.2
TOTAL ESTIMATED CONTENT (CU.M/T):	6.8	8.7	11.1
PERCENT ERROR (%):	-26.5	-82.2	-114.9
GAS LOST WHILE DRILLING (%):	11.6	0.7	7.8
DESORBED VOLUME INSITU Q1 (%):	19.8	10.0	16.4
DESORBED VOLUME IN CONTAINER Q2 (%):	78.4	88.0	81.8
DESORBED VOLUME AFTER MILLING Q3 (ml)	1.8	2.0	1.9
COEFFICIENT OF REGRESSION (r2):	0.994	0.991	0.981
SLOPE OR KT CONSTANT:	0.94	1.37	0.22
ESTIMATED TIME CONSTANT:	16.68	13.61	5.11
DESORPTION CONSTANT (Non comparable):	322.38	-1.84	224.94

Time of Read (min)	Desorbed Time (min)	Gas Volume (ccm)	Desorption Rate (ml/min/g)
2.100	0.0	0.0	--
2.317	0.217	0.123	146.135
2.783	0.467	0.247	135.697
3.050	0.267	0.123	118.735
3.350	0.300	0.123	105.542
3.667	0.317	0.123	99.987
4.000	0.333	0.123	94.988
4.383	0.383	0.123	82.598
4.783	0.400	0.123	79.156
5.233	0.450	0.123	70.362
6.833	1.600	0.370	59.367
7.483	0.650	0.123	48.712

SOLDIER CREEK CANYON COAL MINE (CONT.)

BOREHOLE NO. A

SAMPLE NO. 5

ASH CONTENT (%):	5.02	BOREHOLE DEPTH (M):	7.00
SAMPLE WEIGHT (G):	3.20	DRILL TIME (SEC):	20
DESORBOMETER CONSTANT:	1.233		

	POWER	QUADRATIC	EXPONENT
TOTAL GAS CONTENT (CU.M/T):	5.5	4.8	5.2
TOTAL ESTIMATED CONTENT (CU.M/T):	6.6	8.9	9.7
PERCENT ERROR (%):	-20.3	-84.4	-87.6
GAS LOST WHILE DRILLING (%):	13.1	0.7	7.6
DESORBED VOLUME INSITU Q1 (%):	19.8	8.3	14.7
DESORBED VOLUME IN CONTAINER Q2 (%):	75.8	86.6	80.6
DESORBED VOLUME AFTER MILLING Q3 (ml)	4.5	5.1	4.7
COEFFICIENT OF REGRESSION (r2):	0.963	0.993	0.964
SLOPE OR KT CONSTANT:	1.02	1.09	0.34
ESTIMATED TIME CONSTANT:	17.53	13.45	5.85
DESORPTION CONSTANT (Non comparable):	314.06	-1.27	296.64

Time of Read (min)	Desorbed Time (min)	Gas Volume (ccm)	Desorption Rate (ml/min/g)
1.600	0.0	0.0	--
1.833	0.233	0.123	173.861
2.100	0.267	0.123	152.130
2.383	0.283	0.123	143.180
2.717	0.333	0.123	121.704
3.083	0.367	0.123	110.640
3.467	0.383	0.123	105.828
4.033	0.567	0.123	71.590
4.583	0.550	0.123	73.759
5.267	0.683	0.123	59.368

SOLDIER CREEK CANYON COAL MINE (CONT.)

BOREHOLE NO. A

SAMPLE NO. 6

ASH CONTENT (%):	5.02	BOREHOLE DEPTH (M):	8.00
SAMPLE WEIGHT (G):	3.40	DRILL TIME (SEC):	15
DESORBOMETER CONSTANT:	1.233		

	POWER	QUADRATIC	EXPONENT
TOTAL GAS CONTENT (CU.M/T):	5.7	5.1	5.5
TOTAL ESTIMATED CONTENT (CU.M/T):	5.7	9.3	9.7
PERCENT ERROR (%):	1.0	-80.5	-76.9
GAS LOST WHILE DRILLING (%):	10.6	0.4	6.3
DESORBED VOLUME INSITU Q1 (%):	16.6	7.1	12.5
DESORBED VOLUME IN CONTAINER Q2 (%):	82.1	91.4	86.0
DESORBED VOLUME AFTER MILLING Q3 (ml)	1.3	1.5	1.4
COEFFICIENT OF REGRESSION (r2):	0.992	0.978	0.993
SLOPE OR KT CONSTANT:	0.87	1.21	0.33
ESTIMATED TIME CONSTANT:	21.31	13.74	6.21
DESORPTION CONSTANT (Non comparable):	268.57	-1.28	287.93

Time of Read (min)	Desorbed Time (min)	Gas Volume (ccm)	Desorption Rate (ml/min/g)
1.375	0.0	0.0	--
1.808	0.433	0.247	176.222
2.058	0.250	0.123	152.726
2.342	0.283	0.123	134.757
3.342	1.000	0.370	114.544
3.775	0.433	0.123	88.111
4.258	0.483	0.123	78.996

SOLDIER CREEK CANYON COAL MINE

NAME OF MINE (TEST SITE): Soldier Creek Mine
LOCATION WITHIN MINE: Sunnyside Seam, middle borehole (B)
DATE OF TESTS: 9/13/90 ADSORPTION CONSTANT: 21.3
Mine Temperature (C): 14.0 Mine Atmos. Pressure (Pa): 83810

BOREHOLE NO. B

SAMPLE NO. 1

ASH CONTENT (%): 5.64 BOREHOLE DEPTH (M): 1.01
SAMPLE WEIGHT (G): 2.10 DRILL TIME (SEC): 142
DESORBOMETER CONSTANT: 1.233

	POWER	QUADRATIC	EXPONENT
TOTAL GAS CONTENT (CU.M/T):	2.9	1.5	0.7
TOTAL ESTIMATED CONTENT (CU.M/T):	4.1	0.7	0.6
PERCENT ERROR (%):	-40.4	54.4	9.8
GAS LOST WHILE DRILLING (%):	80.5	62.1	14.5
DESORBED VOLUME INSITU Q1 (%):	81.4	63.8	18.3
DESORBED VOLUME IN CONTAINER Q2 (%):	-17.4	-33.8	-76.3
DESORBED VOLUME AFTER MILLING Q3 (ml):	36.0	70.0	158.0
COEFFICIENT OF REGRESSION (r2):	1.000	1.000	1.000
SLOPE OR KT CONSTANT:	1.51	0.10	0.71
ESTIMATED TIME CONSTANT:	15.17	30.50	5.88
DESORPTION CONSTANT (Non comparable):	191.13	-0.10	80.22

Time of Read (min)	Desorbed Time (min)	Gas Volume (ccm)	Desorption Rate (ml/min/g)
1.500	0.0	0.0	--
2.050	0.550	0.025	22.627
2.983	0.933	0.025	13.334

SUNNYSIDE COAL MINES

NAME OF MINE (TEST SITE): Sunnyside Mine
LOCATION WITHIN MINE: Upper left 22 & crosscut 17, hole A
DATE OF TESTS: 3/21/90 ADSORPTION CONSTANT: 21.3
Mine Temperature (C): 10.3 Mine Atmos. Pressure (Pa): 85138

BOREHOLE NO. A

SAMPLE NO. 1

ASH CONTENT (%): 5.64 BOREHOLE DEPTH (M): 1.52
SAMPLE WEIGHT (G): 4.90 DRILL TIME (SEC): 42
DESORBOMETER CONSTANT: 1.233

	POWER	QUADRATIC	EXPONENT
TOTAL GAS CONTENT (CU.M/T):	4.1	4.0	3.8
TOTAL ESTIMATED CONTENT (CU.M/T):	2.5	1.2	1.2
PERCENT ERROR (%):	39.7	70.0	69.0
GAS LOST WHILE DRILLING (%):	9.8	7.7	1.8
DESORBED VOLUME INSITU Q1 (%):	12.4	10.3	4.6
DESORBED VOLUME IN CONTAINER Q2 (%):	78.9	80.8	85.9
DESORBED VOLUME AFTER MILLING Q3 (ml):	8.6	8.9	9.4
COEFFICIENT OF REGRESSION (r2):	0.914	0.998	0.948
SLOPE OR KT CONSTANT:	0.68	0.40	0.23
ESTIMATED TIME CONSTANT:	35.35	46.28	17.11
DESORPTION CONSTANT (Non comparable):	116.50	-0.42	51.81

Time of Read (min)	Desorbed Time (min)	Gas Volume (ccm)	Desorption Rate (ml/min/g)
1.250	0.0	0.0	--
1.667	0.417	0.074	38.401
2.017	0.350	0.049	30.477
2.350	0.333	0.049	32.001
2.533	0.183	0.025	29.092
2.717	0.183	0.025	29.092
2.900	0.183	0.025	29.092
3.133	0.233	0.025	22.858
3.567	0.433	0.049	24.616
4.067	0.500	0.049	21.334
4.667	0.600	0.049	17.778
5.683	1.017	0.074	15.738

SUNNYSIDE COAL MINES (CONT.)

BOREHOLE NO. A

SAMPLE NO. 2

ASH CONTENT (%):	5.64	BOREHOLE DEPTH (M):	2.44
SAMPLE WEIGHT (G):	4.90	DRILL TIME (SEC):	37
DESORBOMETER CONSTANT:	1.233		

	POWER	QUADRATIC	EXPONENT
TOTAL GAS CONTENT (CU.M/T):	4.2	4.2	3.9
TOTAL ESTIMATED CONTENT (CU.M/T):	2.5	1.4	1.4
PERCENT ERROR (%):	41.6	66.1	64.0
GAS LOST WHILE DRILLING (%):	7.7	7.1	1.5
DESORBED VOLUME INSITU Q1 (%):	11.6	10.9	5.6
DESORBED VOLUME IN CONTAINER Q2 (%):	77.3	77.9	82.5
DESORBED VOLUME AFTER MILLING Q3 (ml):	11.1	11.2	11.8
COEFFICIENT OF REGRESSION (r2):	0.654	0.996	0.736
SLOPE OR KT CONSTANT:	0.56	0.47	0.21
ESTIMATED TIME CONSTANT:	36.50	40.99	14.71
DESORPTION CONSTANT (Non comparable):	115.17	-0.43	55.39

Time of Read (min)	Desorbed Time (min)	Gas Volume (ccm)	Desorption Rate (ml/min/g)
0.942	0.0	0.0	--
1.042	0.100	0.025	53.335
1.275	0.233	0.025	22.858
1.575	0.300	0.074	53.335
1.825	0.250	0.049	42.668
2.208	0.383	0.074	41.740
2.475	0.267	0.049	40.001
3.008	0.533	0.074	30.001
3.358	0.350	0.049	30.477
3.575	0.217	0.025	24.616
4.008	0.433	0.049	24.616
4.492	0.483	0.049	22.070
5.308	0.817	0.074	19.592
5.942	0.633	0.049	16.842
7.008	1.067	0.074	15.000

SUNNYSIDE COAL MINES (CONT.)
BOREHOLE NO. A
SAMPLE NO. 3

ASH CONTENT (%): 5.64 BOREHOLE DEPTH (M): 3.05
SAMPLE WEIGHT (G): 5.00 DRILL TIME (SEC): 11
DESORBOMETER CONSTANT: 1.233

	POWER	QUADRATIC	EXPONENT
TOTAL GAS CONTENT (CU.M/T):	3.8	3.7	3.6
TOTAL ESTIMATED CONTENT (CU.M/T):	2.9	2.1	1.9
PERCENT ERROR (%):	22.0	44.1	46.7
GAS LOST WHILE DRILLING (%):	5.6	4.4	1.6
DESORBED VOLUME INSITU Q1 (%):	12.5	11.4	8.8
DESORBED VOLUME IN CONTAINER Q2 (%):	84.3	85.4	87.9
DESORBED VOLUME AFTER MILLING Q3 (ml):	3.2	3.2	3.3
COEFFICIENT OF REGRESSION (r2):	0.607	0.994	0.656
SLOPE OR KT CONSTANT:	0.63	0.71	0.27
ESTIMATED TIME CONSTANT:	27.32	24.86	9.95
DESORPTION CONSTANT (Non comparable):	138.36	-0.47	98.14

Time of Read (min)	Desorbed Time (min)	Gas Volume (ccm)	Desorption Rate (ml/min/g)
0.558	0.0	0.0	--
0.775	0.217	0.037	36.185
0.908	0.133	0.111	176.404
1.125	0.217	0.099	96.495
1.275	0.150	0.049	69.690
1.475	0.200	0.074	78.402
1.642	0.167	0.049	62.721
1.892	0.250	0.074	62.722
2.075	0.183	0.049	57.020
2.392	0.317	0.074	49.517
2.625	0.233	0.049	44.801
2.992	0.367	0.074	42.765
3.275	0.283	0.049	36.895
3.708	0.433	0.074	36.185
4.042	0.333	0.049	31.361
4.542	0.500	0.074	31.361
5.558	1.017	0.123	25.706
6.758	1.200	0.123	21.778

NAME OF MINE (TEST SITE): Sunnyside mine
LOCATION WITHIN MINE: Upper left 22, crosscut 17, hole B
DATE OF TESTS: 3/21/90 ADSORPTION CONSTANT: 21.1
Mine Temperature (C): 11.0 Mine Atmos. Pressure (Pa): 84724

BOREHOLE NO. B

SAMPLE NO. 1

ASH CONTENT (%): 5.64 BOREHOLE DEPTH (M): 3.00
SAMPLE WEIGHT (G): 4.60 DRILL TIME (SEC): 29
DESORBOMETER CONSTANT: 1.233

	POWER	QUADRATIC	EXPONENT
TOTAL GAS CONTENT (CU.M/T):	4.0	3.1	2.6
TOTAL ESTIMATED CONTENT (CU.M/T):	0.3	0.3	0.3
PERCENT ERROR (%):	93.7	90.5	88.4
GAS LOST WHILE DRILLING (%):	34.7	17.2	0.7
DESORBED VOLUME INSITU Q1 (%):	35.0	17.5	1.0
DESORBED VOLUME IN CONTAINER Q2 (%):	55.0	69.8	83.7
DESORBED VOLUME AFTER MILLING Q3 (ml):	10.0	12.7	15.2
COEFFICIENT OF REGRESSION (r2):	0.573	0.981	0.660
SLOPE OR KT CONSTANT:	1.53	0.05	0.82
ESTIMATED TIME CONSTANT:	332.57	260.29	94.97
DESORPTION CONSTANT (Non comparable):	11.88	-0.05	22.49

Time of Read (min)	Desorbed Time (min)	Gas Volume (ccm)	Desorption Rate (ml/min/g)
1.125	0.0	0.0	--
1.658	0.533	0.012	5.326
2.025	0.367	0.012	7.747
3.392	1.367	0.012	2.079

SUNNYSIDE COAL MINES (CONT.)

BOREHOLE NO. B

SAMPLE NO. 2

ASH CONTENT (%): 5.64 BOREHOLE DEPTH (M): 5.00
SAMPLE WEIGHT (G): 2.60 DRILL TIME (SEC): 10
DESORBOMETER CONSTANT: 1.233

	POWER	QUADRATIC	EXPONENT
TOTAL GAS CONTENT (CU.M/T):	2.5	4.0	1.9
TOTAL ESTIMATED CONTENT (CU.M/T):	0.1	0.3	-1.0
PERCENT ERROR (%):	97.6	93.4	150.2
GAS LOST WHILE DRILLING (%):	22.5	51.0	0.2
DESORBED VOLUME INSITU Q1 (%):	22.9	51.3	0.7
DESORBED VOLUME IN CONTAINER Q2 (%):	60.4	38.2	77.8
DESORBED VOLUME AFTER MILLING Q3 (ml):	16.7	10.6	21.5
COEFFICIENT OF REGRESSION (r2):	0.997	1.000	1.000
SLOPE OR KT CONSTANT:	-0.09	0.03	-0.03
ESTIMATED TIME CONSTANT:	894.01	375.71	-31.25
DESORPTION CONSTANT (Non comparable):	2.81	-0.03	2.82

Time of Read (min)	Desorbed Time (min)	Gas Volume (ccm)	Desorption Rate (ml/min/g)
1.333	0.0	0.0	--
3.000	1.667	0.012	3.015
4.583	1.583	0.012	3.374

SUNNYSIDE COAL MINES (CONT.)

BOREHOLE NO. B

SAMPLE NO. 3

ASH CONTENT (%): 5.64 BOREHOLE DEPTH (M): 6.00
SAMPLE WEIGHT (G): 4.10 DRILL TIME (SEC): 14
DESORBOMETER CONSTANT: 1.233

	POWER	QUADRATIC	EXPONENT
TOTAL GAS CONTENT (CU.M/T):	3.3	3.4	2.8
TOTAL ESTIMATED CONTENT (CU.M/T):	0.4	0.4	0.5
PERCENT ERROR (%):	87.3	86.8	81.2
GAS LOST WHILE DRILLING (%):	16.5	17.7	0.7
DESORBED VOLUME INSITU Q1 (%):	17.3	18.6	1.7
DESORBED VOLUME IN CONTAINER Q2 (%):	64.8	63.8	77.0
DESORBED VOLUME AFTER MILLING Q3 (ml):	17.9	17.6	21.2
COEFFICIENT OF REGRESSION (r2):	0.854	0.952	0.959
SLOPE OR KT CONSTANT:	1.37	0.07	0.54
ESTIMATED TIME CONSTANT:	166.25	187.90	58.32
DESORPTION CONSTANT (Non comparable):	19.90	-0.04	25.94

Time of Read (min)	Desorbed Time (min)	Gas Volume (ccm)	Desorption Rate (ml/min/g)
0.800	0.0	0.0	--
1.367	0.567	0.025	11.248
1.817	0.450	0.025	14.165
2.183	0.367	0.012	8.692
2.667	0.483	0.012	6.594
3.200	0.533	0.012	5.976
4.133	0.933	0.012	3.415
6.383	2.250	0.012	1.416

SUNNYSIDE COAL MINES (CONT.)

BOREHOLE NO. B

SAMPLE NO. 4

ASH CONTENT (%):	5.64	BOREHOLE DEPTH (M):	8.00
SAMPLE WEIGHT (G):	5.00	DRILL TIME (SEC):	16
DESORBOMETER CONSTANT:	1.233		

	POWER	QUADRATIC	EXPONENT
TOTAL GAS CONTENT (CU.M/T):	3.5	3.3	3.1
TOTAL ESTIMATED CONTENT (CU.M/T):	1.0	1.1	1.3
PERCENT ERROR (%):	71.0	66.5	59.4
GAS LOST WHILE DRILLING (%):	13.2	8.8	1.7
DESORBED VOLUME INSITU Q1 (%):	14.7	10.3	3.4
DESORBED VOLUME IN CONTAINER Q2 (%):	70.8	74.4	80.2
DESORBED VOLUME AFTER MILLING Q3 (ml):	14.5	15.2	16.4
COEFFICIENT OF REGRESSION (r2):	0.610	0.986	0.564
SLOPE OR KT CONSTANT:	1.24	0.21	0.46
ESTIMATED TIME CONSTANT:	72.69	73.92	27.07
DESORPTION CONSTANT (Non comparable):	48.31	-0.19	53.22

Time of Read (min)	Desorbed Time (min)	Gas Volume (ccm)	Desorption Rate (ml/min/g)
1.217	0.0	0.0	--
1.400	0.183	0.037	42.765
1.667	0.267	0.025	19.600
1.900	0.233	0.037	33.601
2.117	0.217	0.012	12.062
2.183	0.067	0.012	39.201
2.333	0.150	0.012	17.423
2.600	0.267	0.012	9.800
3.050	0.450	0.025	11.615
3.233	0.183	0.012	14.255
3.500	0.267	0.012	9.800
4.183	0.683	0.025	7.649
4.733	0.550	0.025	9.503

SAMPLE NO. 5

ASH CONTENT (%): 5.64 BOREHOLE DEPTH (M): 10.00
SAMPLE WEIGHT (G): 4.90 DRILL TIME (SEC): 13
DESORBOMETER CONSTANT: 1.233

	POWER	QUADRATIC	EXPONENT
TOTAL GAS CONTENT (CU.M/T):	3.5	3.4	3.2
TOTAL ESTIMATED CONTENT (CU.M/T):	1.7	2.1	2.4
PERCENT ERROR (%):	51.9	36.6	27.1
GAS LOST WHILE DRILLING (%):	11.3	6.1	2.5
DESORBED VOLUME INSITU Q1 (%):	14.6	9.6	6.2
DESORBED VOLUME IN CONTAINER Q2 (%):	71.4	75.7	78.5
DESORBED VOLUME AFTER MILLING Q3 (ml):	13.9	14.8	15.3
COEFFICIENT OF REGRESSION (r2):	0.683	0.984	0.684
SLOPE OR KT CONSTANT:	1.13	0.40	0.39
ESTIMATED TIME CONSTANT:	43.90	39.11	15.05
DESORPTION CONSTANT (Non comparable):	80.86	-0.35	84.41

Time of Read (min)	Desorbed Time (min)	Gas Volume (ccm)	Desorption Rate (ml/min/g)
1.108	0.0	0.0	--
1.392	0.283	0.086	65.884
1.525	0.133	0.012	20.000
1.575	0.050	0.025	106.669
1.725	0.150	0.025	35.556
1.808	0.083	0.025	64.002
1.975	0.167	0.025	32.001
2.108	0.133	0.025	40.001
2.258	0.150	0.025	35.556
2.442	0.183	0.025	29.092
2.575	0.133	0.025	40.001
2.775	0.200	0.025	26.667
3.008	0.233	0.025	22.858
3.242	0.233	0.025	22.858
3.525	0.283	0.025	18.824
3.775	0.250	0.025	21.334
4.092	0.317	0.025	16.842
4.808	0.717	0.049	14.884
5.275	0.467	0.025	11.429
5.742	0.467	0.025	11.429

BOREHOLE NO. B

SAMPLE NO. 6

ASH CONTENT (%): 5.64 BOREHOLE DEPTH (M): 14.00
SAMPLE WEIGHT (G): 4.90 DRILL TIME (SEC): 10
DESORBOMETER CONSTANT: 1.233

	POWER	QUADRATIC	EXPONENT
TOTAL GAS CONTENT (CU.M/T):	3.5	3.6	3.2
TOTAL ESTIMATED CONTENT (CU.M/T):	0.6	1.3	1.2
PERCENT ERROR (%):	81.7	63.1	62.4
GAS LOST WHILE DRILLING (%):	8.5	9.8	0.9
DESORBED VOLUME INSITU Q1 (%):	10.3	11.6	2.8
DESORBED VOLUME IN CONTAINER Q2 (%):	72.1	71.1	78.1
DESORBED VOLUME AFTER MILLING Q3 (ml):	17.6	17.3	19.0
COEFFICIENT OF REGRESSION (r2):	0.786	0.991	0.861
SLOPE OR KT CONSTANT:	0.75	0.25	0.38
ESTIMATED TIME CONSTANT:	115.39	67.14	29.21
DESORPTION CONSTANT (Non comparable):	30.48	-0.19	42.74

Time of Read (min)	Desorbed Time (min)	Gas Volume (ccm)	Desorption Rate (ml/min/g)
0.683	0.0	0.0	--
0.933	0.250	0.025	21.334
1.100	0.167	0.025	32.001
1.250	0.150	0.025	35.556
1.433	0.183	0.025	29.092
1.633	0.200	0.025	26.667
1.900	0.267	0.025	20.000
2.183	0.283	0.025	18.824
2.500	0.317	0.025	16.843
2.883	0.383	0.025	13.913
3.300	0.417	0.025	12.800
3.833	0.533	0.025	10.000
4.383	0.550	0.025	9.697

SUNNYSIDE COAL MINES (CONT.)

BOREHOLE NO. B

SAMPLE NO. 7

ASH CONTENT (%):	5.64	BOREHOLE DEPTH (M):	15.00
SAMPLE WEIGHT (G):	4.70	DRILL TIME (SEC):	36
DESORBOMETER CONSTANT:	1.233		

	POWER	QUADRATIC	
EXPONENT			
TOTAL GAS CONTENT (CU.M/T):	3.6	3.6	3.3
TOTAL ESTIMATED CONTENT (CU.M/T):	0.8	1.7	1.6
PERCENT ERROR (%):	78.1	51.5	51.0
GAS LOST WHILE DRILLING (%):	10.8	9.7	1.5
DESORBED VOLUME INSITU Q1 (%):	12.6	11.5	3.5
DESORBED VOLUME IN CONTAINER Q2 (%):	73.1	74.0	80.7
DESORBED VOLUME AFTER MILLING Q3 (ml):	14.3	14.4	15.7
COEFFICIENT OF REGRESSION (r2):	0.628	0.997	0.728
SLOPE OR KT CONSTANT:	0.66	0.31	0.33
ESTIMATED TIME CONSTANT:	96.35	51.09	22.39
DESORPTION CONSTANT (Non comparable):	37.52	-0.29	48.68

Time of Read (min)	Desorbed Time (min)	Gas Volume (ccm)	Desorption Rate (ml/min/g)
0.933	0.0	0.0	--
1.183	0.250	0.025	22.242
1.333	0.150	0.025	37.070
1.500	0.167	0.025	33.362
1.650	0.150	0.025	37.069
1.850	0.200	0.025	27.802
2.083	0.233	0.025	23.830
2.317	0.233	0.025	23.830
2.583	0.267	0.025	20.852
2.850	0.267	0.025	20.852
3.150	0.300	0.025	18.535
3.467	0.317	0.025	17.559
3.933	0.467	0.025	11.915

NAME OF MINE (TEST SITE): Sunnyside mine
LOCATION WITHIN MINE: Upper left 22, crosscut 17,hole C
DATE OF TESTS: 3/21/90 ADSORPTION CONSTANT: 21.1
Mine Temperature (C): 10.5 Mine Atmos. Pressure (Pa): 84724

BOREHOLE NO. C

SAMPLE NO. 1

ASH CONTENT (%): 5.64 BOREHOLE DEPTH (M): 2.00
SAMPLE WEIGHT (G): 4.80 DRILL TIME (SEC): 24
DESORBOMETER CONSTANT: 1.233

	POWER	QUADRATIC	EXPONENT
TOTAL GAS CONTENT (CU.M/T):	2.9	3.1	2.6
TOTAL ESTIMATED CONTENT (CU.M/T):	0.5	1.0	1.1
PERCENT ERROR (%):	81.9	68.0	59.7
GAS LOST WHILE DRILLING (%):	10.8	14.7	1.0
DESORBED VOLUME INSITU Q1 (%):	12.7	16.5	3.0
DESORBED VOLUME IN CONTAINER Q2 (%):	71.0	67.9	78.8
DESORBED VOLUME AFTER MILLING Q3 (ml)	16.3	15.6	18.2
COEFFICIENT OF REGRESSION (r2):	0.871	0.996	0.931
SLOPE OR KT CONSTANT:	0.74	0.18	0.30
ESTIMATED TIME CONSTANT:	116.74	77.62	27.22
DESORPTION CONSTANT (Non comparable):	25.10	-0.14	28.68

Time of Read (min)	Desorbed Time (min)	Gas Volume (ccm)	Desorption Rate (ml/min/g)
0.817	0.0	0.0	--
1.433	0.617	0.049	17.658
1.683	0.250	0.025	21.778
1.983	0.300	0.025	18.149
2.383	0.400	0.025	13.611
2.783	0.400	0.025	13.612
3.250	0.467	0.025	11.667
3.800	0.550	0.025	9.899
4.483	0.683	0.025	7.968
5.250	0.767	0.025	7.102

BOREHOLE NO. C
SAMPLE NO. 2

SH CONTENT (%): 5.64 BOREHOLE DEPTH (M): 4.00
SAMPLE WEIGHT (G): 4.70 DRILL TIME (SEC): 10
DESORBOMETER CONSTANT: 1.233

	POWER	QUADRATIC	EXPONENT
TOTAL GAS CONTENT (CU.M/T):	5.0	5.0	4.8
TOTAL ESTIMATED CONTENT (CU.M/T):	1.5	3.6	3.7
PERCENT ERROR (%):	70.6	27.9	24.1
GAS LOST WHILE DRILLING (%):	5.5	4.3	1.4
DESORBED VOLUME INSITU Q1 (%):	9.1	8.0	5.2
DESORBED VOLUME IN CONTAINER Q2 (%):	72.8	73.7	75.9
DESORBED VOLUME AFTER MILLING Q3 (ml):	18.1	18.4	18.9
COEFFICIENT OF REGRESSION (r2):	0.281	0.990	0.389
SLOPE OR KT CONSTANT:	0.53	0.64	0.26
ESTIMATED TIME CONSTANT:	71.73	34.40	14.46
DESORPTION CONSTANT (Non comparable):	70.28	-0.58	87.80

Time of Read (min)	Desorbed Time (min)	Gas Volume (ccm)	Desorption Rate (ml/min/g)
0.783	0.0	0.0	--
0.950	0.167	0.025	33.362
1.083	0.133	0.025	41.704
1.217	0.133	0.025	41.703
1.300	0.083	0.025	66.725
1.417	0.117	0.049	95.321
1.517	0.100	0.025	55.604
1.550	0.033	0.025	166.812
1.650	0.100	0.049	111.208
1.750	0.100	0.025	55.604
1.850	0.100	0.025	55.604
1.933	0.083	0.025	66.725
2.067	0.133	0.025	41.704
2.183	0.117	0.025	47.661
2.550	0.367	0.074	45.494
2.817	0.267	0.049	41.703
3.300	0.483	0.074	34.513
3.633	0.333	0.049	33.362
4.217	0.583	0.074	28.596
4.633	0.417	0.049	26.690
5.367	0.733	0.074	22.747

BOREHOLE NO. C

SAMPLE NO. 3

ASH CONTENT (%): 5.64 BOREHOLE DEPTH (M): 6.00
SAMPLE WEIGHT (G): 4.90 DRILL TIME (SEC): 10
DESORBOMETER CONSTANT: 1.233

	POWER	QUADRATIC	EXPONENT
TOTAL GAS CONTENT (CU.M/T):	3.9	3.9	3.7
TOTAL ESTIMATED CONTENT (CU.M/T):	1.2	2.5	2.5
PERCENT ERROR (%):	68.8	35.2	33.4
GAS LOST WHILE DRILLING (%):	7.2	5.9	1.4
DESORBED VOLUME INSITU Q1 (%):	10.3	9.1	4.8
DESORBED VOLUME IN CONTAINER Q2 (%):	70.8	71.8	75.2
DESORBED VOLUME AFTER MILLING Q3 (ml):	18.9	19.1	20.1
COEFFICIENT OF REGRESSION (r2):	0.752	0.998	0.770
SLOPE OR KT CONSTANT:	0.70	0.47	0.34
ESTIMATED TIME CONSTANT:	67.54	38.28	16.50
DESORPTION CONSTANT (Non comparable):	58.08	-0.38	75.54

Time of Read (min)	Desorbed Time (min)	Gas Volume (ccm)	Desorption Rate (ml/min/g)
0.717	0.0	0.0	--
0.950	0.233	0.049	45.715
1.033	0.083	0.025	64.003
1.117	0.083	0.025	64.002
1.233	0.117	0.025	45.715
1.333	0.100	0.025	53.335
1.433	0.100	0.025	53.335
1.600	0.167	0.025	32.001
1.683	0.083	0.025	64.001
1.817	0.133	0.025	40.001
1.950	0.133	0.025	40.001
2.083	0.133	0.025	40.001
2.267	0.183	0.025	29.092
2.417	0.150	0.025	35.556
2.583	0.167	0.025	32.001
2.767	0.183	0.025	29.092
2.967	0.200	0.025	26.667
3.167	0.200	0.025	26.667
3.417	0.250	0.025	21.334
3.700	0.283	0.025	18.824
3.883	0.183	0.025	29.092
4.417	0.533	0.049	20.000

BOREHOLE NO. C
SAMPLE NO. 4

ASH CONTENT (%): 5.64 BOREHOLE DEPTH (M): 8.00
SAMPLE WEIGHT (G): 5.00 DRILL TIME (SEC): 14
DESORBOMETER CONSTANT: 1.233

	POWER	QUADRATIC	EXPONENT
TOTAL GAS CONTENT (CU.M/T):	3.7	3.6	3.5
TOTAL ESTIMATED CONTENT (CU.M/T):	1.4	2.6	2.5
PERCENT ERROR (%):	61.7	27.1	27.2
GAS LOST WHILE DRILLING (%):	8.7	5.1	1.9
DESORBED VOLUME INSITU Q1 (%):	12.2	8.7	5.7
DESORBED VOLUME IN CONTAINER Q2 (%):	79.7	82.8	85.6
DESORBED VOLUME AFTER MILLING Q3 (ml):	8.1	8.5	8.7
COEFFICIENT OF REGRESSION (r2):	0.698	0.991	0.717
SLOPE OR KT CONSTANT:	0.85	0.50	0.39
ESTIMATED TIME CONSTANT:	55.11	34.02	15.08
DESORPTION CONSTANT (Non comparable):	67.52	-0.40	90.11

Time of Read (min)	Desorbed Time (min)	Gas Volume (ccm)	Desorption Rate (ml/min/g)
0.767	0.0	0.0	--
0.933	0.167	0.025	31.361
0.983	0.050	0.025	104.536
1.133	0.150	0.049	69.690
1.217	0.083	0.025	62.721
1.267	0.050	0.025	104.536
1.400	0.133	0.025	39.201
1.517	0.117	0.025	44.802
1.617	0.100	0.025	52.268
1.717	0.100	0.025	52.268
1.850	0.133	0.025	39.201
1.967	0.117	0.025	44.801
2.100	0.133	0.025	39.201
2.250	0.150	0.025	34.845
2.400	0.150	0.025	34.845
2.583	0.183	0.025	28.510
2.767	0.183	0.025	28.510
2.950	0.183	0.025	28.510
3.133	0.183	0.025	28.510
3.383	0.250	0.025	20.907
3.617	0.233	0.025	22.401
3.850	0.233	0.025	22.401
4.400	0.550	0.049	19.006
4.700	0.300	0.025	17.423

SUNNYSIDE COAL MINES (CONT.)
BOREHOLE NO. C
SAMPLE NO. 5

ASH CONTENT (%): 5.64 BOREHOLE DEPTH (M): 10.00
SAMPLE WEIGHT (G): 4.70 DRILL TIME (SEC): 16
DESORBOMETER CONSTANT: 1.233

	POWER	QUADRATIC	EXPONENT
TOTAL GAS CONTENT (CU.M/T):	4.0	3.9	3.8
TOTAL ESTIMATED CONTENT (CU.M/T):	1.5	3.0	3.0
PERCENT ERROR (%):	61.7	22.5	20.4
GAS LOST WHILE DRILLING (%):	8.2	5.2	2.0
DESORBED VOLUME INSITU Q1 (%):	11.7	8.8	5.7
DESORBED VOLUME IN CONTAINER Q2 (%):	78.7	81.3	84.0
DESORBED VOLUME AFTER MILLING Q3 (ml):	9.6	10.0	10.3
COEFFICIENT OF REGRESSION (r2):	0.862	0.998	0.839
SLOPE OR KT CONSTANT:		0.73	0.54
0.34ESTIMATED TIME CONSTANT:	55.05	31.98	13.80
DESORPTION CONSTANT (Non comparable):	72.81	-0.45	92.37

Time of Read (min)	Desorbed Time (min)	Gas Volume (ccm)	Desorption Rate (ml/min/g)
0.817	0.0	0.0	--
0.983	0.167	0.049	66.725
1.050	0.067	0.025	83.406
1.150	0.100	0.025	55.604
1.217	0.067	0.025	83.406
1.317	0.100	0.025	55.604
1.400	0.083	0.025	66.725
1.500	0.100	0.025	55.605
1.600	0.100	0.025	55.604
1.733	0.133	0.025	41.703
1.850	0.117	0.025	47.661
1.967	0.117	0.025	47.661
2.083	0.117	0.025	47.661
2.217	0.133	0.025	41.703
2.383	0.167	0.025	33.363
2.517	0.133	0.025	41.703
2.683	0.167	0.025	33.362
2.833	0.150	0.025	37.069
3.017	0.183	0.025	30.330
3.167	0.150	0.025	37.069
3.350	0.183	0.025	30.330
3.533	0.183	0.025	30.330
3.733	0.200	0.025	27.802
4.000	0.267	0.025	20.852
4.183	0.183	0.025	30.330

SUNNYSIDE COAL MINES (CONT.)
BOREHOLE NO. C
SAMPLE NO. 6

ASH CONTENT (%): 5.64 BOREHOLE DEPTH (M): 12.00
SAMPLE WEIGHT (G): 5.00 DRILL TIME (SEC): 27
DESORBOMETER CONSTANT: 1.233

	POWER	QUADRATIC	EXPONENT
TOTAL GAS CONTENT (CU.M/T):	3.3	3.2	3.0
TOTAL ESTIMATED CONTENT (CU.M/T):	1.1	2.3	2.4
PERCENT ERROR (%):	67.0	28.4	20.9
GAS LOST WHILE DRILLING (%):	9.9	8.2	2.0
DESORBED VOLUME INSITU Q1 (%):	13.1	11.4	5.5
DESORBED VOLUME IN CONTAINER Q2 (%):	75.8	77.3	82.5
DESORBED VOLUME AFTER MILLING Q3 (ml):	11.1	11.3	12.1
COEFFICIENT OF REGRESSION (r2):	0.579	0.999	0.614
SLOPE OR KT CONSTANT:	0.63	0.44	0.28
ESTIMATED TIME CONSTANT:	63.97	34.64	13.88
DESORPTION CONSTANT (Non comparable):	51.13	-0.41	61.43

Time of Read (min)	Desorbed Time (min)	Gas Volume (ccm)	Desorption Rate (ml/min/g)
0.908	0.0	0.0	--
1.092	0.183	0.025	28.510
1.158	0.067	0.025	78.402
1.292	0.133	0.025	39.201
1.458	0.167	0.025	31.361
1.542	0.083	0.025	62.721
1.675	0.133	0.025	39.201
1.808	0.133	0.025	39.201
1.958	0.150	0.025	34.846
2.125	0.167	0.025	31.361
2.275	0.150	0.025	34.845
2.475	0.200	0.025	26.134
2.658	0.183	0.025	28.510
2.808	0.150	0.025	34.845
3.025	0.217	0.025	24.124
3.225	0.200	0.025	26.134
3.475	0.250	0.025	20.907
3.675	0.200	0.025	26.134
3.925	0.250	0.025	20.907
4.242	0.317	0.025	16.506
4.508	0.267	0.025	19.600

SUNNYSIDE COAL MINES (CONT.)

BOREHOLE NO. C

SAMPLE NO. 7

ASH CONTENT (%):	5.64	BOREHOLE DEPTH (M):	14.00
SAMPLE WEIGHT (G):	4.90	DRILL TIME (SEC):	12
DESORBOMETER CONSTANT:	1.233		

	POWER	QUADRATIC	EXPONENT
TOTAL GAS CONTENT (CU.M/T):	4.1	4.2	3.8
TOTAL ESTIMATED CONTENT (CU.M/T):	0.6	1.4	1.3
PERCENT ERROR (%):	84.4	67.5	65.6
GAS LOST WHILE DRILLING (%):	6.6	8.8	0.7
DESORBED VOLUME INSITU Q1 (%):	8.4	10.6	2.6
DESORBED VOLUME IN CONTAINER Q2 (%):	62.4	60.9	66.3
DESORBED VOLUME AFTER MILLING Q3 (ml):	29.2	28.5	31.1
COEFFICIENT OF REGRESSION (r2):	0.766	0.992	0.868
SLOPE OR KT CONSTANT:	0.70	0.25	0.33
ESTIMATED TIME CONSTANT:	134.90	76.23	31.90
DESORPTION CONSTANT (Non comparable)	30.08	-0.19	39.70

Time of Read (min)	Desorbed Time (min)	Gas Volume (ccm)	Desorption Rate (ml/min/g)
0.650	0.0	0.0	--
0.917	0.267	0.025	20.000
1.067	0.150	0.025	35.556
1.250	0.183	0.025	29.092
1.433	0.183	0.025	29.092
1.633	0.200	0.025	26.667
1.867	0.233	0.025	22.858
2.133	0.267	0.025	20.000
2.417	0.283	0.025	18.824
2.733	0.317	0.025	16.842
3.083	0.350	0.025	15.238
3.583	0.500	0.025	10.667
4.567	0.983	0.049	10.848
5.233	0.667	0.025	8.000

DUTCH CREEK COAL MINE

NAME OF MINE (TEST SITE): Mid Continent Resources
LOCATION WITHIN MINE: Panel 102 Head Gate, B seam #5 Door
DATE OF TESTS: 7/15/86 ADSORPTION CONSTANT: 36.7
Mine Temperature (C): 24.0 Mine Atmos. Pressure (Pa): 70897

BOREHOLE NO. A

SAMPLE NO. 1

ASH CONTENT (%): 5.64 BOREHOLE DEPTH (M): 1.07
SAMPLE WEIGHT (G): 4.90 DRILL TIME (SEC): 29
DESORBOMETER CONSTANT: 1.233

	POWER	QUAD.	EXPONENT
TOTAL GAS CONTENT (CU.M/T):	1.0	1.0	0.5
TOTAL ESTIMATED CONTENT (CU.M/T):	2.8	0.6	0.6
PERCENT ERROR (%):	-188.2	43.8	-6.5
GAS LOST WHILE DRILLING (%):	49.6	52.0	4.7
DESORBED VOLUME INSITU Q1 (%):	51.7	54.1	8.8
DESORBED VOLUME IN CONTAINER Q2 (%)	14.9	14.2	28.2
DESORBED VOLUME AFTER MILLING Q3 (m	33.3	31.7	63.0
COEFFICIENT OF REGRESSION (r2):	1.000	0.998	0.993
SLOPE OR KT CONSTANT:	1.07	0.08	0.33
ESTIMATED TIME CONSTANT:	12.74	59.41	9.77
DESORPTION CONSTANT (Non comparable	77.51	-0.07	17.88

Time of Read (min)	Desorbed Time (min)	Gas Volume (ccm)	Desorption Rate (ml/min/g)
1.608	0.0	0.0	--
2.842	1.233	0.049	8.649
3.775	0.933	0.025	5.714
5.058	1.283	0.025	4.156

DUTCH CREEK COAL MINE (CONT.)

BOREHOLE NO. A

SAMPLE NO. 2

ASH CONTENT (%):	5.64	BOREHOLE DEPTH (M):	3.66
SAMPLE WEIGHT (G):	3.90	DRILL TIME (SEC):	60
DESORBOMETER CONSTANT:	1.233		

	POWER	QUAD.	EXPONENT
TOTAL GAS CONTENT (CU.M/T):	3.0	2.4	2.3
TOTAL ESTIMATED CONTENT (CU.M/T):	6.9	2.4	2.2
PERCENT ERROR (%):	-128.1	-1.1	2.6
GAS LOST WHILE DRILLING (%):	29.6	11.5	6.9
DESORBED VOLUME INSITU Q1 (%):	30.7	12.9	8.4
DESORBED VOLUME IN CONTAINER Q2 (%):	58.7	73.9	77.7
DESORBED VOLUME AFTER MILLING Q3 (ml)	10.5	13.2	13.9
COEFFICIENT OF REGRESSION (r2):	0.976	0.981	0.988
SLOPE OR KT CONSTANT:	1.42	0.27	0.46
ESTIMATED TIME CONSTANT:	16.09	33.03	10.68
DESORPTION CONSTANT (Non comparable):	187.86	-0.38	98.04

Time of Read (min)	Desorbed Time (min)	Gas Volume (ccm)	Desorption Rate (ml/min/g)
2.417	0.0	0.0	--
2.883	0.467	0.049	28.719
3.450	0.567	0.049	23.651
3.817	0.367	0.025	18.275

DUTCH CREEK COAL MINE (CONT.)

BOREHOLE NO. A

SAMPLE NO. 3

ASH CONTENT (%):	5.64	BOREHOLE DEPTH (M):	5.03
SAMPLE WEIGHT (G):	3.40	DRILL TIME (SEC):	32
DESORBOMETER CONSTANT:	1.233		

	POWER	QUAD.	EXPONENT
TOTAL GAS CONTENT (CU.M/T):	1.8	1.5	1.0
TOTAL ESTIMATED CONTENT (CU.M/T):	6.3	1.4	1.4
PERCENT ERROR (%):	-238.9	11.8	-45.1
GAS LOST WHILE DRILLING (%):	52.4	42.8	8.1
DESORBED VOLUME INSITU Q1 (%):	54.9	45.8	12.9
DESORBED VOLUME IN CONTAINER Q2 (%):	31.3	37.6	60.4
DESORBED VOLUME AFTER MILLING Q3 (ml)	13.8	16.6	26.7
COEFFICIENT OF REGRESSION (r2):	0.947	0.988	0.939
SLOPE OR KT CONSTANT:	1.36	0.13	0.28
ESTIMATED TIME CONSTANT:	10.83	37.89	7.17
DESORPTION CONSTANT (Non comparable):	170.43	-0.19	37.74

Time of Read (min)	Desorbed Time (min)	Gas Volume (ccm)	Desorption Rate (ml/min/g)
2.783	0.0	0.0	--
3.267	0.483	0.025	15.903
3.733	0.467	0.025	16.471
4.467	0.733	0.025	10.482
5.400	0.933	0.025	8.235
6.400	1.000	0.025	7.686
7.917	1.517	0.025	5.068

DUTCH CREEK COAL MINE (CONT.)

BOREHOLE NO. A

SAMPLE NO. 4

ASH CONTENT (%):	5.64	BOREHOLE DEPTH (M):	7.32
SAMPLE WEIGHT (G):	3.90	DRILL TIME (SEC):	25
DESORBOMETER CONSTANT:	1.233		

	POWER	QUAD.	EXPONENT
TOTAL GAS CONTENT (CU.M/T):	2.4	2.3	1.9
TOTAL ESTIMATED CONTENT (CU.M/T):	5.0	2.0	1.7
PERCENT ERROR (%):	-104.1	12.9	10.9
GAS LOST WHILE DRILLING (%):	23.4	19.4	3.6
DESORBED VOLUME INSITU Q1 (%):	26.1	22.2	7.0
DESORBED VOLUME IN CONTAINER Q2 (%):	59.6	62.7	75.0
DESORBED VOLUME AFTER MILLING Q3 (ml	14.3	15.1	18.0
COEFFICIENT OF REGRESSION (r2):	0.971	0.999	0.952
SLOPE OR KT CONSTANT:	0.94	0.22	0.31
ESTIMATED TIME CONSTANT:	17.98	38.36	11.67
DESORPTION CONSTANT (Non comparable)	136.10	-0.23	51.91

Time of Read (min)	Desorbed Time (min)	Gas Volume (ccm)	Desorption Rate (ml/min/g)
1.508	0.0	0.0	--
2.158	0.650	0.074	30.928
2.708	0.550	0.049	24.367
3.042	0.333	0.025	20.103
3.408	0.367	0.025	18.276
3.792	0.383	0.025	17.481
4.292	0.500	0.025	13.402
4.775	0.483	0.025	13.864

DUTCH CREEK COAL MINE (CONT.)

BOREHOLE NO. A

SAMPLE NO. 5

ASH CONTENT (%):	5.64	BOREHOLE DEPTH (M):	8.23
SAMPLE WEIGHT (G):	4.80	DRILL TIME (SEC):	19
DESORBOMETER CONSTANT:	1.233		

	POWER	QUAD.	EXPONENT
TOTAL GAS CONTENT (CU.M/T):	2.0	1.9	1.6
TOTAL ESTIMATED CONTENT (CU.M/T):	4.6	1.6	1.6
PERCENT ERROR (%):	-128.7	13.5	0.2
GAS LOST WHILE DRILLING (%):	24.4	19.6	3.9
DESORBED VOLUME INSITU Q1 (%):	27.9	23.4	8.4
DESORBED VOLUME IN CONTAINER Q2 (%):	59.2	62.9	75.2
DESORBED VOLUME AFTER MILLING Q3 (ml	12.9	13.7	16.4
COEFFICIENT OF REGRESSION (r2):	0.956	0.993	0.943
SLOPE OR KT CONSTANT:	1.09	0.22	0.27
ESTIMATED TIME CONSTANT:	16.05	38.61	10.42
DESORPTION CONSTANT (Non comparable)	124.68	-0.23	41.47

Time of Read (min)	Desorbed Time (min)	Gas Volume (ccm)	Desorption Rate (ml/min/g)
1.758	0.0	0.0	--
2.608	0.850	0.099	25.621
2.892	0.283	0.025	19.216
3.208	0.317	0.025	17.193
3.958	0.750	0.049	14.519
4.442	0.483	0.025	11.265
4.842	0.400	0.025	13.611
5.408	0.567	0.025	9.608
6.025	0.617	0.025	8.829
6.758	0.733	0.025	7.424

DUTCH CREEK COAL MINE (CONT.)

BOREHOLE NO. A

SAMPLE NO. 6

ASH CONTENT (%): 5.64 BOREHOLE DEPTH (M): 9.14
SAMPLE WEIGHT (G): 4.30 DRILL TIME (SEC): 20
DESORBOMETER CONSTANT: 1.233

	POWER	QUAD.	EXPONENT
TOTAL GAS CONTENT (CU.M/T):	3.4	3.0	2.8
TOTAL ESTIMATED CONTENT (CU.M/T):	5.5	2.5	1.8
PERCENT ERROR (%):	-64.7	15.8	35.3
GAS LOST WHILE DRILLING (%):	19.4	9.1	3.7
DESORBED VOLUME INSITU Q1 (%):	21.1	10.9	5.6
DESORBED VOLUME IN CONTAINER Q2 (%):	48.0	54.2	57.4
DESORBED VOLUME AFTER MILLING Q3 (ml)	30.9	34.9	37.0
COEFFICIENT OF REGRESSION (r2):	0.949	0.987	0.977
SLOPE OR KT CONSTANT:	1.29	0.30	0.47
ESTIMATED TIME CONSTANT:	22.28	39.65	16.07
DESORPTION CONSTANT (Non comparable):	150.57	-0.38	82.38

Time of Read (min)	Desorbed Time (min)	Gas Volume (ccm)	Desorption Rate (ml/min/g)
1.717	0.0	0.0	--
1.900	0.183	0.025	33.151
2.083	0.183	0.025	33.151
2.283	0.200	0.025	30.388
2.517	0.233	0.025	26.047
2.783	0.267	0.025	22.791
3.383	0.600	0.049	20.259
3.750	0.367	0.025	16.575
4.283	0.533	0.025	11.396

DUTCH CREEK COAL MINE (CONT.)

BOREHOLE NO. A

SAMPLE NO. 7

ASH CONTENT (%):	5.64	BOREHOLE DEPTH (M):	10.06
SAMPLE WEIGHT (G):	4.40	DRILL TIME (SEC):	22
DESORBOMETER CONSTANT:	1.233		

	POWER	QUAD.	EXPONENT
TOTAL GAS CONTENT (CU.M/T):	3.5	3.3	3.2
TOTAL ESTIMATED CONTENT (CU.M/T):	6.3	5.2	4.7
PERCENT ERROR (%):	-78.8	-59.8	-47.2
GAS LOST WHILE DRILLING (%):	13.4	6.3	4.6
DESORBED VOLUME INSITU Q1 (%):	19.0	12.2	10.7
DESORBED VOLUME IN CONTAINER Q2 (%):	76.2	82.6	84.0
DESORBED VOLUME AFTER MILLING Q3 (ml)	4.8	5.2	5.3
COEFFICIENT OF REGRESSION (r2):	0.912	0.992	0.937
SLOPE OR KT CONSTANT:	0.74	0.65	0.23
ESTIMATED TIME CONSTANT:	20.52	20.90	7.07
DESORPTION CONSTANT (Non comparable):	172.63	-0.72	102.95

Time of Read (min)	Desorbed Time (min)	Gas Volume (ccm)	Desorption Rate (ml/min/g)
1.550	0.0	0.0	--
1.867	0.317	0.099	75.026
2.633	0.767	0.173	54.231
3.550	0.917	0.197	51.836
3.783	0.233	0.049	50.910
4.250	0.467	0.074	38.183
4.567	0.317	0.049	37.513
5.067	0.500	0.074	35.637
5.433	0.367	0.049	32.397
5.867	0.433	0.049	27.413

DUTCH CREEK COAL MINE (CONT.)

BOREHOLE NO. A

SAMPLE NO. 8

ASH CONTENT (%):	5.64	BOREHOLE DEPTH (M):	10.67
SAMPLE WEIGHT (G):	4.30	DRILL TIME (SEC):	17
DESORBOMETER CONSTANT:	1.233		

	POWER	QUAD.	EXPONENT
TOTAL GAS CONTENT (CU.M/T):	2.7	2.4	2.2
TOTAL ESTIMATED CONTENT (CU.M/T):	5.6	3.1	2.5
PERCENT ERROR (%):	-109.9	-32.1	-12.7
GAS LOST WHILE DRILLING (%):	22.3	12.1	5.3
DESORBED VOLUME INSITU Q1 (%):	24.8	15.0	8.3
DESORBED VOLUME IN CONTAINER Q2 (%):	70.9	80.2	86.4
DESORBED VOLUME AFTER MILLING Q3 (ml)	4.3	4.9	5.3
COEFFICIENT OF REGRESSION (r2):	0.776	0.989	0.723
SLOPE OR KT CONSTANT:	0.97	0.38	0.32
ESTIMATED TIME CONSTANT:	17.49	25.29	9.22
DESORPTION CONSTANT (Non comparable):	153.20	-0.50	76.83

Time of Read (min)	Desorbed Time (min)	Gas Volume (ccm)	Desorption Rate (ml/min/g)
1.942	0.0	0.0	--
2.075	0.133	0.025	45.582
2.358	0.283	0.049	42.901
2.858	0.500	0.049	24.311
3.325	0.467	0.049	26.047
3.558	0.233	0.025	26.047
3.808	0.250	0.025	24.311
4.358	0.550	0.049	22.101

DUTCH CREEK MINE - COLORADO

NAME OF MINE (TEST SITE): COLORADO DUTCH CREEK MINE
LOCATION WITHIN MINE: B-SEAM LONGWALL FACE
DATE OF TESTS: 3/23/89 ADSORPTION CONSTANT: 3.8
Mine Temperature (C): 17.0 Mine Atmos. Pressure (Pa): 66219

BOREHOLE NO. B

SAMPLE NO. 1

ASH CONTENT (%): 2.87 BOREHOLE DEPTH (M): 2.00
SAMPLE WEIGHT (G): 4.80 DRILL TIME (SEC): 10.9
DESORBOMETER CONSTANT: 1.233

	POWER	QUAD.	EXPONENT
TOTAL GAS CONTENT (CU.M/T):	4.0	4.8	4.8
TOTAL ESTIMATED CONTENT (CU.M/T):	-3.4	3.6	13.1
PERCENT ERROR (%):	183.9	24.9	-171.1
GAS LOST WHILE DRILLING (%):	-16.0	2.5	4.1
DESORBED VOLUME INSITU Q1 (%):	-5.1	11.7	13.2
DESORBED VOLUME IN CONTAINER Q2 (%):	105.1	88.3	86.8
DESORBED VOLUME AFTER MILLING Q3 (ml):	0.0	0.0	0.0
COEFFICIENT OF REGRESSION (r2):	0.985	0.916	0.958
SLOPE OR KT CONSTANT:	1.49	0.63	0.20
ESTIMATED TIME CONSTANT:	-4.53	40.72	42.93
DESORPTION CONSTANT (Non comparable):	431.70	-0.37	124.32

SAMPLE NO. 2

ASH CONTENT (%): 2.87 BOREHOLE DEPTH (M): 3.00
SAMPLE WEIGHT (G): 4.80 DRILL TIME (SEC): 8.8
DESORBOMETER CONSTANT: 1.233

	POWER	QUAD.	EXPONENT
TOTAL GAS CONTENT (CU.M/T):	4.7	5.7	5.5
TOTAL ESTIMATED CONTENT (CU.M/T):	-2.9	9.0	5.9
PERCENT ERROR (%):	162.0	-58.7	-6.5
GAS LOST WHILE DRILLING (%):	-13.9	5.2	1.8
DESORBED VOLUME INSITU Q1 (%):	-8.3	9.8	6.6
DESORBED VOLUME IN CONTAINER Q2 (%):	78.9	65.7	68.0
DESORBED VOLUME AFTER MILLING Q3 (ml)	29.4	24.5	25.4
COEFFICIENT OF REGRESSION (r2):	0.994	0.958	0.942
SLOPE OR KT CONSTANT:	1.22	0.36	0.14
ESTIMATED TIME CONSTANT:	-6.13	19.26	109.29
DESORPTION CONSTANT (Non comparable):	169.43	-0.28	54.00

DUTCH CREEK MINE - COLORADO (CONT.)

BOREHOLE NO. B

SAMPLE NO. 3

ASH CONTENT (%): 2.87 BOREHOLE DEPTH (M): 4.00
SAMPLE WEIGHT (G): 4.90 DRILL TIME (SEC): 11.0
DESORBOMETER CONSTANT: 1.233

	POWER	QUAD.	EXPONENT
TOTAL GAS CONTENT (CU.M/T):	11.3	9.6	9.6
TOTAL ESTIMATED CONTENT (CU.M/T):	6.0	4.2	12.4
PERCENT ERROR (%):	46.9	56.0	-28.2
GAS LOST WHILE DRILLING (%):	16.0	1.4	2.1
DESORBED VOLUME INSITU Q1 (%):	31.4	19.4	19.9
DESORBED VOLUME IN CONTAINER Q2 (%):	65.0	76.3	75.8
DESORBED VOLUME AFTER MILLING Q3 (ml	3.6	4.3	4.3
COEFFICIENT OF REGRESSION (r2):	0.996	0.989	0.910
SLOPE OR KT CONSTANT:	0.79	1.49	0.05
ESTIMATED TIME CONSTANT:	7.16	69.48	90.79
DESORPTION CONSTANT (Non comparable)	333.65	-1.20	108.95

SAMPLE NO. 4

ASH CONTENT: 2.87 BOREHOLE DEPTH (M): 7.00
SAMPLE WEIGHT (G): 5.40 DRILL TIME (SEC): 18.5
DESORBOMETER CONSTANT: 1.233

	POWER	QUAD.	EXPONENT
TOTAL GAS CONTENT (CU.M/T):	6.5	9.4	9.7
TOTAL ESTIMATED CONTENT (CU.M/T):	-15.7	4.0	10.9
PERCENT ERROR (%):	343.2	57.7	-12.4
GAS LOST WHILE DRILLING (%):	-42.9	1.4	4.7
DESORBED VOLUME INSITU Q1 (%):	-24.5	14.1	17.0
DESORBED VOLUME IN CONTAINER Q2 (%):	70.5	48.7	47.0
DESORBED VOLUME AFTER MILLING Q3 (ml):	54.0	37.3	36.0
COEFFICIENT OF REGRESSION (r2):	0.970	0.964	0.980
SLOPE OR KT CONSTANT:	1.23	1.18	0.06
ESTIMATED TIME CONSTANT:	-1.56	72.21	103.53
DESORPTION CONSTANT (Non comparable):	969.22	-1.86	96.44

APPENDIX C

CONSERVATION EQUATIONS OF ADSORPTIVE GAS IN A GAS CHROMATOGRAPHIC COLUMN

The relationship between gas adsorption coefficients and gas retention variables in an ideal chromatographic column can be derived by mass conservation. The change in the concentration of gaseous species A across a chromatographic column is shown in Figure 8.1. The gas concentration C_A in the mobile phase is a complex function of time t and distance x of the layer under investigation from the column inlet

$$C_A = f(t,x). \tag{1}$$

If the accumulation of the gaseous species A in the column increment dx is dn_A (Figure 8.1), based on mass conservation we have

$$\begin{aligned} dn_A &= inlet_A - outlet_A \\ &= -F_c dC_A \end{aligned} \tag{2}$$

i.e.,

$$(dn_A)_{x,t} = -F_c\left(\frac{\partial C_A}{\partial x}\right)_t dx \tag{3}$$

where F_c is the volumetric flow rate of carrier gas. This accumulated quantity of species A in the column increment dx is distributed in the mobile phase and the stationary phase. Thus, the quantity of the adsorbate A in a unit length of the column is

$$V_L C_A + m_L a_A \tag{4}$$

where V_L is the volume of the mobile phase in a unit length of the column, m_L the mass of coal in a unit length of the column, and a_A the mole of adsorbate A on a unit mass of coal. According to the mass conservation law,

$$-F_c\left(\frac{\partial C_A}{\partial x}\right)_t = \left[\frac{\partial}{\partial t}(V_L C_A + m_L a_A)\right]_x dx. \tag{5}$$

Rearranging Equation 5, we obtain the mass conservation equation of an adsorptive gas through a gas chromatographic column:

$$F_c\left(\frac{\partial C_A}{\partial x}\right)_t + V_L\left(\frac{\partial C_A}{\partial t}\right)_x + m_L\left(\frac{\partial a_A}{\partial t}\right)_x = 0. \tag{6}$$

Mathematically,

$$\left(\frac{\partial a_A}{\partial t}\right)_x \equiv \left(\frac{\partial a_A}{\partial C_A}\right)_x \left(\frac{\partial C_A}{\partial t}\right)_x . \tag{7}$$

The derivative term $(\partial a_A/\partial C_A)_x$ represents the dependence of the adsorbed quantity of species A on its concentration in the mobile phase C_A at a given temperature. It thus represents the adsorption isotherm, i.e.,

$$\left(\frac{\partial a_A}{\partial C_A}\right)_x = \frac{da_A}{dC_A}. \tag{8}$$

From Equation 1, we have

$$dC_A = \left(\frac{\partial C_A}{\partial t}\right)_x dt + \left(\frac{\partial C_A}{\partial x}\right)_t dx. \tag{9}$$

Therefore,

$$\left(\frac{\partial C_A}{\partial t}\right)_x = -\left(\frac{\partial C_A}{\partial x}\right)_t \left(\frac{\partial x}{\partial t}\right)_{C_A} . \tag{10}$$

Substituting Equations 7, 8, and 10 into Equation 6 gives:

$$F_c\left(\frac{\partial C_A}{\partial x}\right)_t + \left(V_L + m_L \frac{da_A}{dC_A}\right)\left(\frac{\partial C_A}{\partial t}\right)_x = 0$$

$$F_c\left(\frac{\partial C_A}{\partial x}\right)_t - \left(V_L + m_L \frac{da_A}{dC_A}\right)\left(\frac{\partial C_A}{\partial x}\right)_t \left(\frac{\partial x}{\partial t}\right)_{C_A} = 0 \tag{11}$$

$$F_c - \left(V_L + m_L \frac{da_A}{dC_A}\right)\left(\frac{\partial x}{\partial t}\right)_{C_A} = 0$$

or

$$F_c - \left(V_L + m_L \frac{da_A}{dC_A}\right) u_A = 0 \tag{12}$$

where u_A is the linear migration velocity of species A at concentration C_A moving along the column in the mobile phase.

Assuming that in each part of the column gas adsorption equilibrium is eventually established, we can combine the mass conservation equation with a gas adsorption isotherm to derive the relationship between gas adsorption coefficient and gas retention variables. When an infinite dilution of a gas sample is used (Brunauer et al., 1940), all of the proposed types of gas adsorption isotherms become linear, i.e.,

$$\lim_{C_A \to 0}\left[\frac{da_A}{dC_A}\right] = K_{c,A} \tag{13}$$

where $K_{c,A}$ is the concentration coefficient of gas adsorption of species A. The range of infinite dilution of a sample size is normally less than 0.5 ml, which depends not only on the properties of adsorbate and adsorbent, but also on the chromatographic conditions.

Based on the mass conservation equations (Equation 6, 10, or 12) and

$$u_A = \frac{L}{t_r} \tag{14}$$

where t_r is the gas retention time, for an ideal packed column (no pressure drop along the column, i.e., constant F_c), we have

$$V + W_c K_{c,A} = F_c t_r \tag{15}$$

and

$$\begin{aligned} K_{c,A} &= \frac{1}{W_c}(F_c t_r - V) \\ &= \frac{1}{W_c}(V_r - V) \end{aligned} \tag{16}$$

where W_c is the total mass of coal in the column.

To consider the dead volume in gas chromatography, the retention volume of unsorbed gas becomes

$$\begin{aligned} V_M &= V + V_{GC} \\ &= F_c t_M \end{aligned} \tag{17}$$

where t_M is the gas hold-up time or the retention time of the carrier gas. Finally, we have

$$\begin{aligned} K_{c,A} &= \frac{1}{W_c}(V_r - V_M) \\ &= \frac{F_c}{W_c}(t_r - t_M). \end{aligned} \tag{18}$$

For a real packed column, there is a significant pressure drop along the column. The pressure gradient of the carrier gas depends on (James and Martin, 1952):

$$\frac{dp}{dx} = -\frac{\eta}{\kappa} u_c$$
$$= -\frac{\eta}{\kappa A_{column}} F_c \qquad (19)$$
$$= c_1 F_c$$

where η is gas viscosity, κ the column permeability, A_{column} the cross-sectional area of the column, and u_c the linear velocity of the carrier gas, and constant c_1

If it is assumed that the carrier gas is an ideal gas

$$c_1 = -\frac{\eta}{\kappa A_{column}}. \qquad (20)$$

under the experimental conditions, we have:

$$\frac{pF_c}{T_c} = \frac{P_o F_{c,o}}{T_o}$$
$$F_c = \frac{T_c P_o F_{c,o}}{T_o} \frac{1}{p} \qquad (21)$$

where subscript 'o' refers to the value at measurement conditions, and 'c' the value under column conditions. Substituting Equation 21 into Equation 19 gives:

$$\frac{dp}{dx} = c_1 P_o F_{c,o} \frac{T_c}{T_o} \frac{1}{p}. \qquad (22)$$

Integrating Equation 22 gives:

$$\frac{1}{2} p^2 = c_1 P_o F_{c,o} \frac{T_c}{T_o} x + c_2. \qquad (23)$$

Constants c_1 and c_2 in Equation 23 are determined by the boundary conditions:

$$x = 0, \quad p = P_i;$$
$$x = L, \quad p = P_o. \qquad (24)$$

Substituting these boundary conditions into Equation 23 gives:

$$C_1 = \frac{T_o}{2T_c P_o F_{c,o} L} \frac{1}{P_o^2 - P_i^2}$$
$$C_2 = \frac{1}{2} P_i^2 \ . \qquad (25)$$

Substituting Equation 25 into Equation 23 gives:

$$x = \frac{p^2 - P_i^2}{P_o^2 - P_i^2} L. \qquad (26)$$

Plots of pressure and volumetric velocity gradient along the column are shown in Figures C.1a and C.1b.

Differentiating Equation 26 gives:

$$dx = \frac{2L}{P_o^2 - P_i^2} p dp. \qquad (27)$$

For an unsorbed carrier gas, $K_{c,A} = 0$. Therefore, Equation 12 for the carrier gas becomes:

$$F_c - V_L u_c = 0. \qquad (28)$$

Substituting Equations 21 and 27 into Equation 28 gives:

$$\frac{2L}{P_o^2 - P_i^2} p \frac{dp}{dt} = \frac{P_o F_{c,o}}{V_L} \frac{T_c}{T_o} \frac{1}{p}. \qquad (29)$$

The boundary conditions for Equation 29 are:

$$t = 0, \quad p = P_i;$$
$$t = t_M, \quad p = P_o. \qquad (30)$$

Thus,

$$\int_{P_i}^{P_o} \frac{2L}{P_o^2 - P_i^2} p^2 dp = \int_0^{t_M} \frac{P_o F_{c,o}}{V_L} \frac{T_c}{T_o} dt. \qquad (31)$$

Integrating, rearranging, and substituting V by V_M (to consider the dead volume in gas chromatography) in Equation 31 gives:

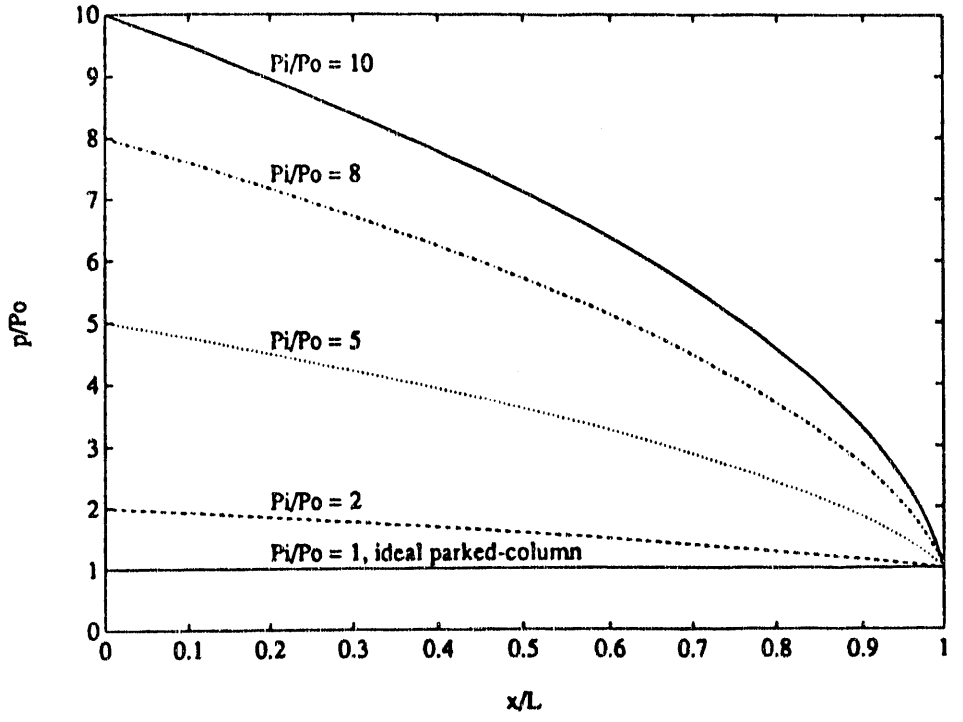

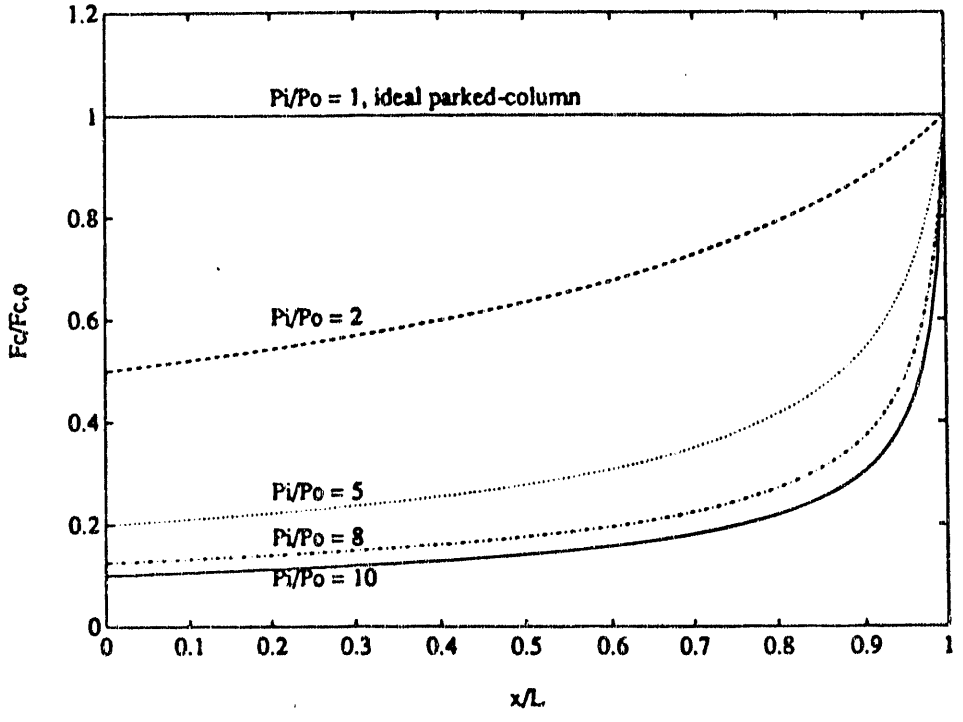

Figure C.1. Pressure gradient (a) and volumetric velocity gradient (b) along a gas chromatographic column.

$$V_M = \frac{3}{2}\frac{T_c}{T_o}\frac{1-\left(\frac{P_i}{P_o}\right)^2}{1-\left(\frac{P_i}{P_o}\right)^3}F_{c,o}t_M \qquad (32)$$

$$= J_{p,T}F_{c,o}t_M$$

where $J_{p,T}$ is a pressure and temperature correction factor, and

$$J_{p,T} \equiv \frac{3}{2}\frac{T_c}{T_o}\frac{1-\left(\frac{P_i}{P_o}\right)^2}{1-\left(\frac{P_i}{P_o}\right)^3}. \qquad (33)$$

Comparing Equation 32 with Equation 17 shows:

$$F_c = J_{p,T}F_{c,o}. \qquad (34)$$

Substituting Equation 34 into Equation 18 gives:

$$K_{c,A} = \frac{1}{W_c}J_{p,T}F_{c,o}(t_r - t_M). \qquad (35)$$

Net unit retention volume is defined as:

$$V_N = \frac{1}{W_c}J_{p,T}F_{c,o}(t_r - t_M). \qquad (36)$$

Thus,

$$K_{c,A} = V_N$$
$$K_{p,A} = \frac{V_N}{RT}. \qquad (37)$$

The most important equations and relationships are summarized as follows:

$$V_n = \frac{1}{W_c} J_{p,T} F_{c,o} (t_R - t_M) \tag{38}$$

$$K_c = V_n \tag{39}$$

$$K_p = \frac{V_n}{RT_c} \tag{40}$$

and

$$\begin{aligned} \varepsilon &= \frac{V}{V_{column}} \\ V &= L \times V_L \\ m &= L \times m_L \\ \rho_{coal} &= \frac{m}{(1-\varepsilon)\, V_{column}} \\ u_A &= \left(\frac{\partial x}{\partial t}\right)_{c_A} \\ V_M &= V_{GC} + V. \end{aligned} \tag{41}$$

APPENDIX D

RESULTS ON PERMEABILITY TESTS

Large coal lumps were retrieved from the seams under investigation, placed in containers and transported to the University of Utah. At the laboratory, each coal lump was cast in cement or grout. Each sampled seam was represented by one lump cast with the bedding plane in the horizontal direction and another lump cast with the bedding plane in avertical orientation. A coring drill bit with inside diameter of 2.125 inches was utilized to produce core samples from the cast coal lump. Each coal lump was drilled so as to provide as many good coal cores as possible.

As was expected, frequent fractures found in coal made it difficult to produce a continuous core longer than a couple of inches. However, with the exception of coal from the Beaver Creek Mine, each coal seam was represented with at least one core, in each bedding direction, long enough to use in the permeability experiments. Then the samples were trimmed to the 2.125 inches in diameter with height of about twice the diameter.

Before testing for permeability, the samples were allowed to climatize in the laboratory for a period of one week. The laboratory is air conditioned with the temperature maintained at around 23 degrees Celsius. This period allowed for a similar water content among the samples without any thermal damage which could have occurred if a more aggressive drying procedure was utilized. Water content may not be the same for different coals but would be equilibrated at the same relative humidity.

TerraTek Inc., University of Utah Research Park, Salt Lake City, Utah, performed permeability and porosity tests on samples shaped on specimens having 4 in. in diameter and 6 in. in height. Only coal samples collected from the Rock Canyon seam (Soldier Canyon Creek Coal Mine) and B seam (Dutch Creek Mine in Colorado) permitted shaping on such a large diameter. The porosity measurements were made by use of Boyle's Law Medium pore volume technique and the permeability tests were measured by Helium using a transient pulse decay method. The results are shown in Table D-1.

Consequently, a permeability testing apparatus was set up in the Methane Analysis Laboratory for smaller 2.125 in. diameter specimens. The tester consisted of a pressurized nitrogen container, triaxial cell with modified platens, hydraulic pump, compression machine, and a gas flow meter. Where necessary, the network was connected with pressure hoses. Figure D-1 shows the standard network setup.

TABLE D-1. Results on permeability performed on large diameter specimens.

(Seam), Mine	Orientation in the seam: N 18 E/87 SE	Porosity %	Permeability mD	
		Vertical	*N + 0	*N + 90
(Rock Canyon) Soldier Creek Mine, UT		1.21	0.033	0.065	0.032
(B seam) Dutch Creek Mine, CO		3.15	0.034	**0.319	0.26

*where N = 18 E (dip = 87 SE)
** N = 68 E (dip = 9 SE)

Nitrogen was chosen to supply the gas flow necessary for permeability testing. A 230 scf standard vessel served as the source of nitrogen for all experiments.

The vessel was connected to the bottom platen of the triaxial cell via a high pressure hose. Three pressure gauges with upper limits of 100 psi, 200 psi, and 400 psi, were attached to the pressure hose to accurately monitor the various inlet pressures.

A triaxial cell with modified platens (Figure D-2) at both the top and the bottom end was used to allow variable axial and confining forces to act upon the sample, and to allow the gas to flow through the sample.

The triaxial cell utilizes a urethane membrane to separate the confining hydraulic oil from the coal sample. Furthermore, the membrane created a seal between itself and the coal sample, thus preventing the oil from passing into the coal. The cell accommodates a coal sample 2.125 inches in diameter and up to 4.25 inches in height. This is consistent with ASTM standards for triaxial compressive strength measurements.

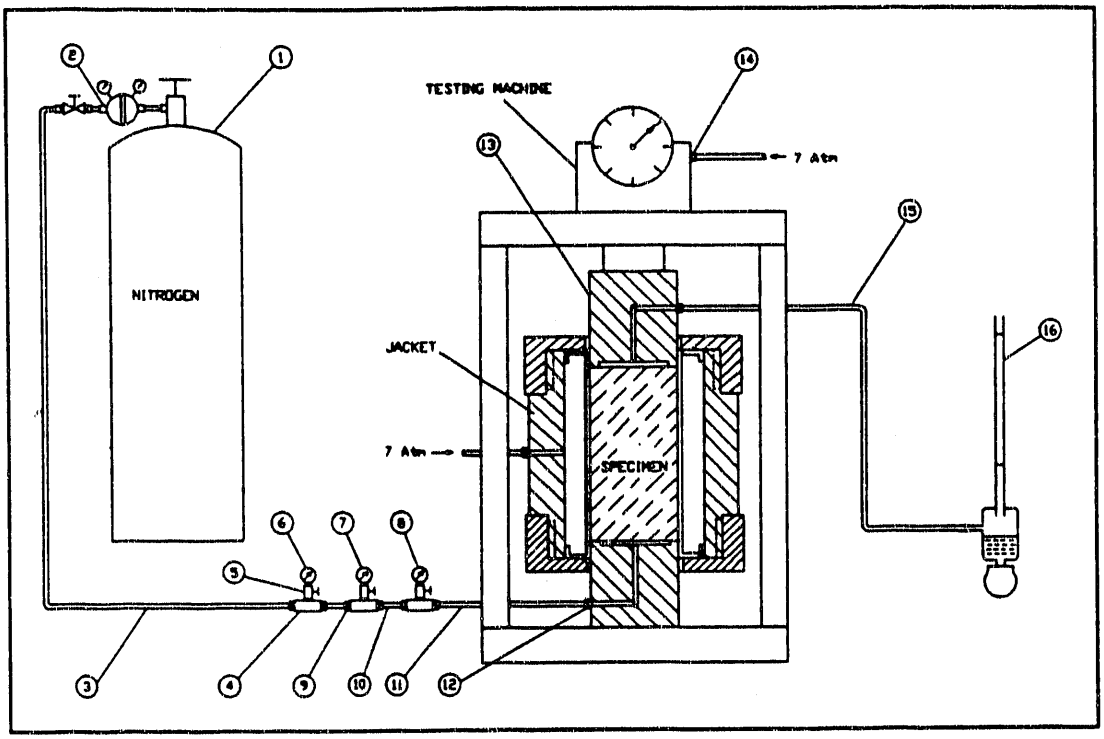

Figure D-1. Permeability tester.

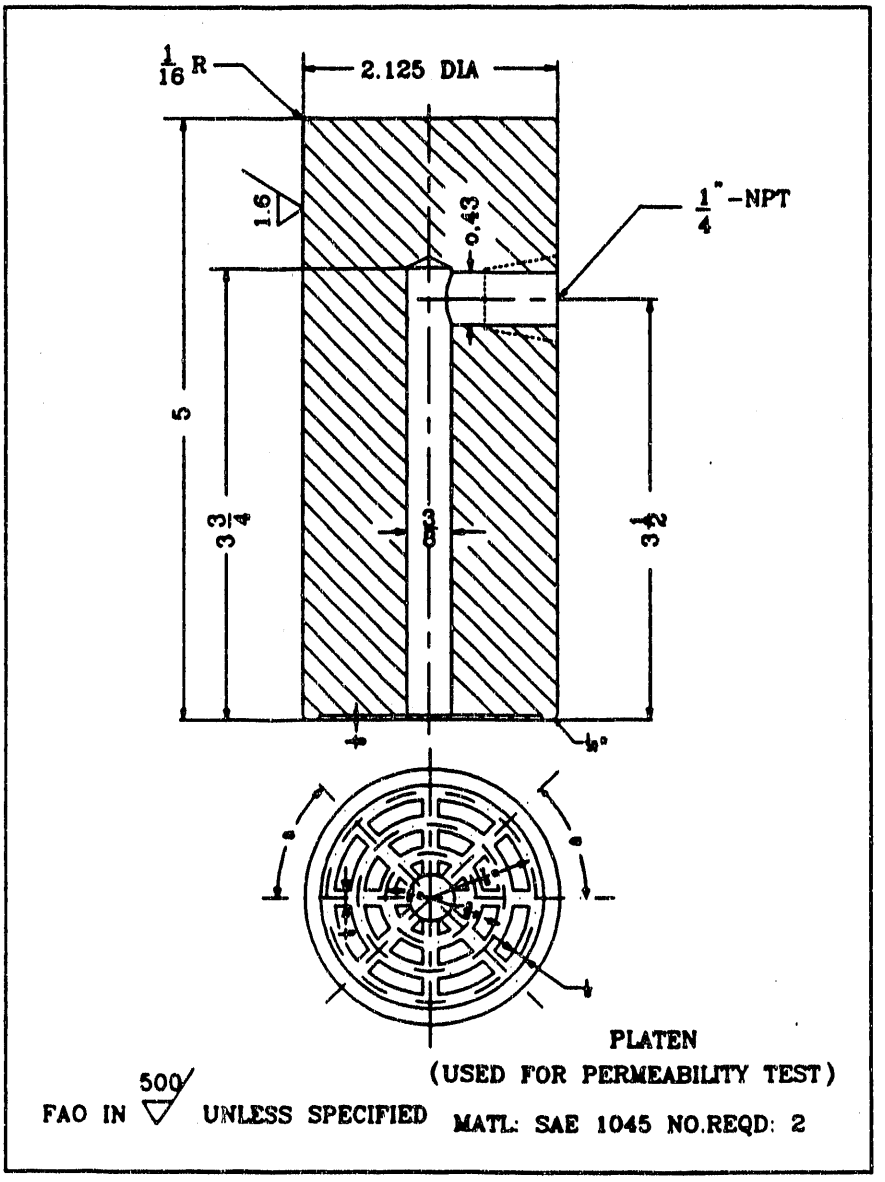

Figure D-2. Platens for the permeability tester.

A hand operated hydraulic pump was used to deliver a steady confining pressure to the coal sample, monitored via a pressure gauge. The oil pressure delivered by the hydraulic pump had a tendency to decrease with time. This was remedied by persistent pressure monitoring and timely adjustments by the operator.

A hand operated compression test machine was utilized to supply axial stress to the spherical platens. The compression machine was capable of generating up to 20,000 pounds of force, which was sufficient to carry out the gas flow analysis under axial stresses of up to 5,080 psi.

The compression machine allowed for variation of the axial stress upon demand without any network or sample disturbance. A simple soap bubble flowmeter was utilized to measure the outlet gas volume (Figure D-1). The soap flowmeter consisted of a calibrated vertical glass cylinder with a rubber bottom filled with a mixture of water and soap. The water and soap mixture was only contained at the rubber bottom of the cylinder to allow for convenient bubble making. The formed bubbles indicated the gas volume entering the cylinder per given time interval. By simple observation, the operator could easily select the most convenient time interval and measure the gas volume generated in that particular time interval. A number of readings were taken to assure that gas flow had reached steady state before flow rates were recorded for permeability calculations. This flow measuring technique proved very attractive because of its simplicity, accuracy, and reliability.

During the permeability testing procedure each coal sample was subjected to a total of nineteen combinations of axial stress, confining stress, and inlet gas pressure. This was necessary in order to identify the magnitude of the permeability and trends for each coal sample. Furthermore, this wide range of parameters allowed for better approximation of permeability under various subsurface conditions during mining operations.

Coal samples were was subjected to the same sequence of varying external stresses and inlet gas pressures. The test was design such that only one parameter was variable at a time, while keeping the other two constant. This allowed for examination of each parameter's effect on permeability.

The sequence was a battery of three tests, always in the same order. First was the "variable inlet gas pressure test or IGP test", followed by the "variable confining stress test (CS)", and the "variable axial stress test (AS)" concluded the battery. The sample remained in the urethane sheet within the cell at all times and only the variable parameters were changed during this series of tests. Moreover, precaution was taken to make sure that axial and confining stresses remained

balanced thus preventing a potential crushing or distortion of the sample.

In an attempt to eliminate other factors influencing permeability, the testing conditions were held as constant as possible for all samples. Moreover, to assure similar testing conditions for all samples, the temperature selected was 23 degrees Celsius with an allowed deviation of 1 degree Celsius. The outlet pressure selected was 22 inches of mercury with an allowed deviation of 10 percent. Both the temperature and the outlet pressure were constant during each experiment sequence.

Another reason for undertaking the permeability experiment was to analyze the relationship between bedding orientation with respect to medium flow and permeability. It was for this reason that each coal seam, with the exception of coal from the Beaver Creek Mine, was represented by two sets of samples. One with gas flow perpendicular to the bedding plane, and the other with flow parallel to the bedding plane. Unfortunately, the coal from Beaver Creek was very weak and repeatably disintegrated during the coring process.

During the tests the axial stress was raised to 2,750 psi while the confining stress was raised to 700 psi. The inlet gas pressure, IGP, was increased to 50 psi. The system was allowed to stabilize until the outlet gas flow reached a steady state, at which time the system was ready for the "variable inlet gas pressure test".

The first test in the sequence was the "variable inlet gas pressure test, IGP". During this test, axial stress and confining stress remained at 2,750 psi and 700 psi respectively. However, the inlet gas pressure, IGP, was incrementally increased from 50 psi to 300 psi. The increment was 50 psi each time. Before each increment's flow recording, the flow was examined to make sure it had reached steady state. In order to average out any human error, several readings were taken for each increment until the same flow was observed at least three times. After the completion of the first test, two adjustments were necessary before the second test could began. The inlet gas pressure was reduced from 300 psi to 100 psi, and the confining pressure was reduced to 500 psi. The network was allowed to stabilize until the flow reached steady state once again.

The second test in the sequence was the "variable confining stress or CS test". During this test, the axial stress and inlet gas pressure remained at 2,750 psi and 100 psi respectively. The confining stress was raised from 500 psi to 1,500 psi in 250 psi increments. Once again, flow was allowed to stabilize after each increase and then cautiously recorded. After the conclusion of this test, the confining stress was reduced from 1,500 psi to 700 psi, and the axial pressure was decreased from 2,700 psi to 1,410 psi. The

system was again allowed to stabilize. Upon the achievement of steady flow, the last test in the battery was ready to be performed.

The last test was the "variable axial stress (AS) test". During this test the confining stress and inlet gas pressure remained at 700 psi and 100 psi respectively. The axial stress was increased from 1,410 psi to 5,080 psi in the following sequence: 1,410; 1,690; 2,260; 2,820; 3,380; 3,950; 4,510; 5,080. At each interval, the sample was allow to stabilize and the flow rates were again carefully recorded.

Results of Permeability Tests

Multiple gas flow readings were taken for each described scenario. The number of readings depended on how quickly the flow stabilized. However, in each case the readings continued until similar reading was recorded at least three times. At that time the readings representing stable condition were averaged. It is these averaged recordings which were used in the permeability calculations.

Extreme caution was exercised to maintain the axial and confining stress, and gas (inlet) pressure constant during each test. At no time was a reading recorded when these parameters deviated from their designed setting. The results are shown in Table D-2. Figures D-3 to D-8 present the relationship between the permeability and axial, confining, and inlet stress.

Table D-2 Summary of results on permeability tests performed on 2.125 in. diameter specimens

MINE	COALBED	PERMEABILITY PARALLEL TO BEDDING PLANES (mD)	PERMEABILITY PERPENDICULAR (mD)
BEAVER CREEK	CASTLEGATE A	*	0.395
CASTLE GATE	SUB 3	0.041	0.039
SOLDIER CREEK	ROCK CANYON	0.005	0.014
SOLDIER CREEK	SUNNYSIDE	0.063	0.096
SUNNYSIDE COAL	LWR SUNNYSIDE	0.016	0.011
DUTCH CREEK	B	*	0.035

* SPECIMEN FAILED

TEST PARAMETERS:

AXIAL STRESS:	2750 psi	(18.98 MPa)
CONFINING STRESS:	700 psi	(4.83 MPa)
PORE PRESSURE:	200 psi	(1.38 MPa)

Table D-3 Results on permeability tests

PERMEABILITY TEST

Mine Name: ***Beaver Creek***
Seam Name: ***Castlegate A***

Specimen's	Bedding:	Horizontal	Temperature (C):	23.5
	Length (m):	0.107	Baromet. P. (Hg):	22.2
	Diameter(in):	2.125	Viscosity(Ns/m3):	1.775E-05
	X-Area(in2):	3.545	Specimen's I.D.:	22

Variable Gas Pressure:

	Stress			Pressure				Flow	Perme
Exp	Axial	Conf.	Mean	Inlet	Mean	Reciprocal		Rate	ability
ID#	(psi)	(psi)	(psi)	(psi)	(psi)	Mean (psi)		(m3/s)	(md)
194	2,750	700	1,383	50	30	0.0328		1.03E-07	0.113
195	2,750	700	1,383	100	55	0.0180		9.70E-07	0.258
196	2,750	700	1,383	150	80	0.0124		2.45E-06	0.288
197	2,750	700	1,383	200	105	0.0095		6.00E-06	0.395
198	2,750	700	1,383	250	130	0.0077		1.00E-05	0.421
199	2,750	700	1,383	300	155	0.0064		1.66E-05	0.485

Variable Confining Pressure:

	Stress			Pressure				Flow	Perme
Exp	Axial	Conf.	Mean	Inlet	Mean	Reciprocal		Rate	ability
ID#	(psi)	(psi)	(psi)	(psi)	(psi)	Mean (psi)		(m3/s)	(md)
200	2,750	500	1,250	100	55	0.0180			0.000
201	2,750	750	1,417	100	55	0.0180			0.000
202	2,750	1,000	1,583	100	55	0.0180			0.000
203	2,750	1,250	1,750	100	55	0.0180			0.000
204	2,750	1,500	1,917	100	55	0.0180			0.000

Variable Axial Pressure:

	Stress			Pressure				Flow	Perme
Exp	Axial	Conf.	Mean	Inlet	Mean	Reciprocal		Rate	ability
ID#	(psi)	(psi)	(psi)	(psi)	(psi)	Mean (psi)		(m3/s)	(md)
205	1,410	700	937	100	55	0.0180		1.67E-06	0.443
206	1,690	700	1,030	100	55	0.0180		1.43E-06	0.380
207	2,260	700	1,220	100	55	0.0180		1.25E-06	0.332
208	2,820	700	1,407	100	55	0.0180		1.26E-06	0.336
209	3,380	700	1,593	100	55	0.0180		1.20E-06	0.320
210	3,950	700	1,783	100	55	0.0180			0.000
211	4,510	700	1,970	100	55	0.0180			0.000
212	5,080	700	2,160	100	55	0.0180			0.000

Table D-3 Results on permeability tests (cont.)

PERMEABILITY TEST

Mine Name: *Castlegate*
Seam Name: *Sub 3*

Specimen's	Bedding:	Vertical	Temperature (C):	23.5
	Length (in):	0.108	Baromet. P. (Hg):	22.22
	Diameter(in):	2.125	Viscosity(Ns/m3):	1.775E-05
	X-Area(in2):	3.545	Specimen's I.D.:	20

Variable Gas Pressure:

	Stress			Pressure			Flow	Permeability
Exp ID#	Axial (psi)	Conf. (psi)	Mean (psi)	Inlet (psi)	Mean (psi)	Reciprocal Mean 1/(psi)	Rate (m3/s)	(md)
156	2,750	700	1,383	50	30	0.0328	3.90E-08	0.043
157	2,750	700	1,383	100	55	0.0180	1.21E-07	0.032
158	2,750	700	1,383	150	80	0.0124	2.79E-07	0.033
159	2,750	700	1,383	200	105	0.0095	6.10E-07	0.041
160	2,750	700	1,383	250	130	0.0077	1.52E-06	0.064
161	2,750	700	1,383	300	155	0.0064	3.10E-06	0.092

Variable Confining Pressure:

	Stress			Pressure			Flow	Permeability
Exp ID#	Axial (psi)	Conf. (psi)	Mean (psi)	Inlet (psi)	Mean (psi)	Reciprocal Mean 1/(psi)	Rate (m3/s)	(md)
162	2,750	500	1,250	100	55	0.0180	1.31E-06	0.352
163	2,750	750	1,417	100	55	0.0180	1.14E-07	0.031
164	2,750	1,000	1,583	100	55	0.0180	3.13E-08	0.008
165	2,750	1,250	1,750	100	55	0.0180	0.00E+00	0.000
166	2,750	1,500	1,917	100	55	0.0180	0.00E+00	0.000

Variable Axial Pressure:

	Stress			Pressure			Flow	Permeability
Exp ID#	Axial (psi)	Conf. (psi)	Mean (psi)	Inlet (psi)	Mean (psi)	Reciprocal Mean 1/(psi)	Rate (m3/s)	(md)
167	1,410	700	937	100	55	0.0180	8.00E-08	0.021
168	1,690	700	1,030	100	55	0.0180	7.80E-08	0.021
169	2,260	700	1,220	100	55	0.0180	7.90E-08	0.021
170	2,820	700	1,407	100	55	0.0180	7.41E-08	0.020
171	3,380	700	1,593	100	55	0.0180	7.53E-08	0.020
172	3,950	700	1,783	100	55	0.0180	7.69E-08	0.021
173	4,510	700	1,970	100	55	0.0180	7.19E-08	0.019
174	5,080	700	2,160	100	55	0.0180	7.69E-08	0.021

Table D-3 Results on permeability tests (cont.)

PERMEABILITY TEST

Mine Name: *Castle Gate*
Seam Name: *Sub 3*

Specimen's	Bedding:	Horizontal	Temperature (C):	23.5
	Length (m):	0.066	Baromet. P. (Hg):	22.15
	Diameter(in):	2.125	Viscosity(Ns/m3):	1.775E-05
	X-Area(in2):	3.545	Specimen's I.D.:	13

Variable Gas Pressure:

	Stress			Pressure			Flow	Perme
Exp	Axial	Conf.	Mean	Inlet	Mean	Reciprocal	Rate	ability
ID#	(psi)	(psi)	(psi)	(psi)	(psi)	Mean (psi)	(m3/s)	(md)
80	2,750	700	1,383	50	30	0.0329	6.90E-08	0.047
81	2,750	700	1,383	100	55	0.0180	2.17E-07	0.036
82	2,750	700	1,383	150	80	0.0124	5.05E-07	0.036
83	2,750	700	1,383	200	105	0.0095	9.64E-07	0.039
84	2,750	700	1,383	250	130	0.0077	1.84E-06	0.048
85	2,750	700	1,383	300	155	0.0064	3.33E-06	0.060

Variable Confining Pressure:

	Stress			Pressure			Flow	Perme
Exp	Axial	Conf.	Mean	Inlet	Mean	Reciprocal	Rate	ability
ID#	(psi)	(psi)	(psi)	(psi)	(psi)	Mean (psi)	(m3/s)	(md)
86	2,750	500	1,250	100	55	0.0180	6.48E-07	0.106
87	2,750	750	1,417	100	55	0.0180	1.89E-07	0.031
88	2,750	1,000	1,583	100	55	0.0180	7.01E-08	0.011
89	2,750	1,250	1,750	100	55	0.0180	2.72E-08	0.004
90	2,750	1,500	1,917	100	55	0.0180	1.50E-08	0.002

Variable Axial Pressure:

	Stress			Pressure			Flow	Perme
Exp	Axial	Conf.	Mean	Inlet	Mean	Reciprocal	Rate	ability
ID#	(psi)	(psi)	(psi)	(psi)	(psi)	Mean (psi)	(m3/s)	(md)
91	1,410	700	937	100	55	0.0180	9.54E-08	0.016
92	1,690	700	1,030	100	55	0.0180	8.51E-08	0.014
93	2,260	700	1,220	100	55	0.0180	7.55E-08	0.012
94	2,820	700	1,407	100	55	0.0180	7.09E-08	0.012
95	3,380	700	1,593	100	55	0.0180	6.73E-08	0.011
96	3,950	700	1,783	100	55	0.0180	6.68E-08	0.011
97	4,510	700	1,970	100	55	0.0180	7.02E-08	0.011
98	5,080	700	2,160	100	55	0.0180	6.95E-08	0.011

Table D-3 Results on permeability tests (cont.)

PERMEABILITY TEST

Mine Name: ***Soldier Creek***
Seam Name: ***Rock Canyon***

Specimen's	Bedding:	Vertical	Temperature (C):	23.5
	Length (m):	0.108	Baromet. P. (Hg):	22.2
	Diameter(in):	2.125	Viscosity(Ns/m3):	1.775E-05
	X-Area(in2):	3.545	Specimen's I.D.:	19

Variable Gas Pressure:

	Stress			Pressure			Flow	Permeability
Exp ID#	Axial (psi)	Conf. (psi)	Mean (psi)	Inlet (psi)	Mean (psi)	Reciprocal Mean 1/(psi)	Rate (m3/s)	(md)
137	2,750	700	1,383	50	30	0.0328	0.00E+00	0.000
138	2,750	700	1,383	100	55	0.0180	0.00E+00	0.000
139	2,750	700	1,383	150	80	0.0124	3.72E-08	0.004
140	2,750	700	1,383	200	105	0.0095	7.54E-08	0.005
141	2,750	700	1,383	250	130	0.0077	1.79E-07	0.008
142	2,750	700	1,383	300	155	0.0064	3.64E-07	0.011

Variable Confining Pressure:

	Stress			Pressure			Flow	Permeability
Exp ID#	Axial (psi)	Conf. (psi)	Mean (psi)	Inlet (psi)	Mean (psi)	Reciprocal Mean 1/(psi)	Rate (m3/s)	(md)
143	2,750	500	1,250	200	105	0.0095	7.55E-08	0.005
144	2,750	750	1,417	200	105	0.0095	6.93E-08	0.005
145	2,750	1,000	1,583	200	105	0.0095	2.51E-08	0.002
146	2,750	1,250	1,750	200	105	0.0095	1.15E-08	0.001
147	2,750	1,500	1,917	200	105	0.0095	5.75E-09	0.000

Variable Axial Pressure:

	Stress			Pressure			Flow	Permeability
Exp ID#	Axial (psi)	Conf. (psi)	Mean (psi)	Inlet (psi)	Mean (psi)	Reciprocal Mean 1/(psi)	Rate (m3/s)	(md)
148	1,410	700	937	200	105	0.0095	6.56E-08	0.004
149	1,690	700	1,030	200	105	0.0095	5.83E-08	0.004
150	2,260	700	1,220	200	105	0.0095	5.33E-08	0.004
151	2,920	700	1,407	200	105	0.0095	5.13E-08	0.003
152	3,380	700	1,593	200	105	0.0095	5.04E-08	0.003
153	3,950	700	1,783	200	105	0.0095	6.32E-08	0.004
154	4,510	700	1,970	200	105	0.0095	6.45E-08	0.004
155	5,080	700	2,160	200	105	0.0095	7.96E-08	0.005

Table D-3 Results on permeability tests (cont.)

PERMEABILITY TEST

Mine Name: *Soldier Creek*
Seam Name: *Rock Canyon*

Specimen's	Bedding:	Horizontal	Temperature (C):	23.5
	Length (m):	0.108	Baromet. P. (Hg):	21.92
	Diameter(in):	2.125	Viscosity(Ns/m3):	1.775E-05
	X-Area(in2):	3.545	Specimen's I.D.:	12

Variable Gas Pressure:

	Stress			Pressure			Flow	Perme
Exp	Axial	Conf.	Mean	Inlet	Mean	Reciprocal	Rate	ability
ID#	(psi)	(psi)	(psi)	(psi)	(psi)	Mean (psi)	(m3/s)	(md)
61	2,750	700	1,383	50	30	0.0329	1.84E-08	0.020
62	2,750	700	1,383	100	55	0.0181	5.28E-08	0.014
63	2,750	700	1,383	150	80	0.0124	1.06E-07	0.012
64	2,750	700	1,383	200	105	0.0095	2.10E-07	0.014
65	2,750	700	1,383	250	130	0.0077	4.25E-07	0.018
66	2,750	700	1,383	300	155	0.0064	6.67E-07	0.019

Variable Confining Pressure:

	Stress			Pressure			Flow	Perme
Exp	Axial	Conf.	Mean	Inlet	Mean	Reciprocal	Rate	ability
ID#	(psi)	(psi)	(psi)	(psi)	(psi)	Mean (psi)	(m3/s)	(md)
67	2,750	500	1,250	100	55	0.0181	1.41E-07	0.037
68	2,750	750	1,417	100	55	0.0181	3.54E-08	0.009
69	2,750	1,000	1,583	100	55	0.0181	1.50E-08	0.004
70	2,750	1,250	1,750	100	55	0.0181	6.30E-09	0.002
71	2,750	1,500	1,917	100	55	0.0181	3.70E-09	0.001

Variable Axial Pressure:

	Stress			Pressure			Flow	Perme
Exp	Axial	Conf.	Mean	Inlet	Mean	Reciprocal	Rate	ability
ID#	(psi)	(psi)	(psi)	(psi)	(psi)	Mean (psi)	(m3/s)	(md)
72	1,410	700	937	100	55	0.0181	2.36E-08	0.006
73	1,690	700	1,030	100	55	0.0181	2.72E-08	0.007
74	2,260	700	1,220	100	55	0.0181	2.26E-08	0.006
75	2,820	700	1,407	100	55	0.0181	2.00E-08	0.005
76	3,380	700	1,593	100	55	0.0181	2.10E-08	0.006
77	3,950	700	1,783	100	55	0.0181	1.90E-08	0.005
78	4,510	700	1,970	100	55	0.0181	1.85E-08	0.005
79	5,080	700	2,160	100	55	0.0181	1.80E-08	0.005

Table D-3 Results on permeability tests (cont.)

PERMEABILITY TEST

Mine Name: *Soldier Creek*
Seam Name: *Sunnyside*

Specimen's	Bedding:	Vertical	Temperature (C):	23.5
	Length (m):	0.107	Baromet. P. (Hg):	22.2
	Diameter(in):	2.125	Viscosity(Ns/m3):	1.775E-05
	X-Area(in2):	3.545	Specimen's I.D.:	21

Variable Gas Pressure:

	Stress			Pressure			Flow	Permeability
Exp ID#	Axial (psi)	Conf. (psi)	Mean (psi)	Inlet (psi)	Mean (psi)	Reciprocal Mean (psi)	Rate (m3/s)	(md)
175	2,750	700	1,383	50	30	0.0328	8.59E-08	0.095
176	2,750	700	1,383	100	55	0.0180	2.17E-07	0.058
177	2,750	700	1,383	150	80	0.0124	4.94E-07	0.058
178	2,750	700	1,383	200	105	0.0095	9.52E-07	0.063
179	2,750	700	1,383	250	130	0.0077	1.13E-06	0.048
180	2,750	700	1,383	300	155	0.0064	2.00E-06	0.058

Variable Confining Pressure:

	Stress			Pressure			Flow	Permeability
Exp ID#	Axial (psi)	Conf. (psi)	Mean (psi)	Inlet (psi)	Mean (psi)	Reciprocal Mean (psi)	Rate (m3/s)	(md)
181	2,750	500	1,250	100	55	0.0180	3.42E-07	0.091
182	2,750	750	1,417	100	55	0.0180	1.01E-07	0.027
183	2,750	1,000	1,583	100	55	0.0180	3.88E-08	0.010
184	2,750	1,250	1,750	100	55	0.0180	2.04E-08	0.005
185	2,750	1,500	1,917	100	55	0.0180	1.28E-08	0.003

Variable Axial Pressure:

	Stress			Pressure			Flow	Permeability
Exp ID#	Axial (psi)	Conf. (psi)	Mean (psi)	Inlet (psi)	Mean (psi)	Reciprocal Mean (psi)	Rate (m3/s)	(md)
186	1,410	700	937	100	55	0.0180	9.71E-08	0.026
187	1,690	700	1,030	100	55	0.0180	8.49E-08	0.023
188	2,260	700	1,220	100	55	0.0180	7.16E-08	0.019
189	2,820	700	1,407	100	55	0.0180	5.72E-08	0.015
190	3,380	700	1,593	100	55	0.0180	5.26E-08	0.014
191	3,950	700	1,783	100	55	0.0180	5.00E-08	0.013
192	4,510	700	1,970	100	55	0.0180	4.48E-08	0.012
193	5,080	700	2,160	100	55	0.0180	4.76E-08	0.013

Table D-3 Results on permeability tests (cont.)

PERMEABILITY TEST

Mine Name: *Soldier Creek*
Seam Name: *Sunnyside*

Specimen's	Bedding:	Horizontal	Temperature (C):	23.5
	Length (m):	0.107	Baromet. P. (Hg):	22.2
	Diameter(in):	2.125	Viscosity(Ns/m3):	1.775E-05
	X-Area(in2):	3.545	Specimen's I.D.:	18

Variable Gas Pressure:

	Stress			Pressure			Flow	Permeability
Exp ID#	Axial (psi)	Conf. (psi)	Mean (psi)	Inlet (psi)	Mean (psi)	Reciprocal Mean 1/(psi)	Rate (m3/s)	(md)
121	2,750	700	1,383	50	30	0.0326	2.75E-08	0.030
122	2,750	700	1,383	100	55	0.0180	5.60E-08	0.015
123	2,750	700	1,383	150	80	0.0124	1.25E-07	0.015
118	2,750	700	1,383	200	105	0.0095	2.78E-07	0.018
119	2,750	700	1,383	250	130	0.0077	4.79E-07	0.020
120	2,750	700	1,383	300	155	0.0064	7.58E-07	0.022

Variable Confining Pressure:

	Stress			Pressure			Flow	Permeability
Exp ID#	Axial (psi)	Conf. (psi)	Mean (psi)	Inlet (psi)	Mean (psi)	Reciprocal Mean 1/(psi)	Rate (m3/s)	(md)
124	2,750	500	1,250	100	55	0.0180	1.70E-07	0.045
125	2,750	750	1,417	100	55	0.0180	5.80E-08	0.015
126	2,750	1,000	1,583	100	55	0.0180	2.80E-08	0.007
127	2,750	1,250	1,750	100	55	0.0180	1.57E-08	0.004
128	2,750	1,500	1,917	100	55	0.0180	9.30E-09	0.002

Variable Axial Pressure:

	Stress			Pressure			Flow	Permeability
Exp ID#	Axial (psi)	Conf. (psi)	Mean (psi)	Inlet (psi)	Mean (psi)	Reciprocal Mean 1/(psi)	Rate (m3/s)	(md)
129	1,410	700	937	100	55	0.0180	5.51E-08	0.015
130	1,690	700	1,030	100	55	0.0180	4.84E-08	0.013
131	2,260	700	1,220	100	55	0.0180	4.47E-08	0.012
132	2,820	700	1,407	100	55	0.0180	4.21E-08	0.011
133	3,380	700	1,593	100	55	0.0180	3.95E-08	0.011
134	3,950	700	1,783	100	55	0.0180	3.71E-08	0.010
135	4,510	700	1,970	100	55	0.0180	3.41E-08	0.009
136	5,080	700	2,160	100	55	0.0180	3.53E-08	0.009

Table D-3 Results on permeability tests (cont.)

PERMEABILITY TEST

Mine Name: *Soldier Creek*
Seam Name: *Sunnyside*

Specimen's	Bedding:	Horizontal	Temperature (C):	23.5
	Length (m):	0.107	Baromet. P. (Hg):	22.14
	Diameter(in):	2.125	Viscosity(Ns/m3):	1.775E-05
	X-Area(in2):	3.545	Specimen's I.D.:	15

Variable Gas Pressure:

	Stress			Pressure			Flow	Perme
Exp ID#	Axial (psi)	Conf. (psi)	Mean (psi)	Inlet (psi)	Mean (psi)	Reciprocal Mean 1/(psi)	Rate (m3/s)	ability (md)
42	2,750	700	1,383	50	30	0.0329	1.14E-07	0.125
43	2,750	700	1,383	100	55	0.0180	3.63E-07	0.096
44	2,750	700	1,383	150	80	0.0124	7.34E-07	0.086
45	2,750	700	1,383	200	105	0.0095	1.47E-06	0.096
46	2,750	700	1,383	250	130	0.0077	2.47E-06	0.104
47	2,750	700	1,383	300	155	0.0064	3.85E-06	0.112

Variable Confining Pressure:

	Stress			Pressure			Flow	Perme
Exp ID#	Axial (psi)	Conf. (psi)	Mean (psi)	Inlet (psi)	Mean (psi)	Reciprocal Mean (psi)	Rate (m3/s)	ability (md)
48	2,750	500	1,250	100	55	0.0180	7.69E-07	0.204
49	2,750	750	1,417	100	55	0.0180	2.94E-07	0.078
50	2,750	1,000	1,583	100	55	0.0180	1.40E-07	0.037
51	2,750	1,250	1,750	100	55	0.0180	7.40E-08	0.020
52	2,750	1,500	1,917	100	55	0.0180	4.00E-08	0.011

Variable Axial Pressure:

	Stress			Pressure			Flow	Perme
Exp ID#	Axial (psi)	Conf. (psi)	Mean (psi)	Inlet (psi)	Mean (psi)	Reciprocal Mean (psi)	Rate (m3/s)	ability (md)
53	1,410	700	937	100	55	0.0180	2.37E-07	0.063
54	1,690	700	1,030	100	55	0.0180	2.16E-07	0.057
55	2,260	700	1,220	100	55	0.0180	2.00E-07	0.053
56	2,820	700	1,407	100	55	0.0180	1.98E-07	0.052
57	3,380	700	1,593	100	55	0.0180	1.92E-07	0.051
58	3,950	700	1,783	100	55	0.0180	1.84E-07	0.049
59	4,510	700	1,970	100	55	0.0180	1.87E-07	0.050
60	5,080	700	2,160	100	55	0.0180	2.05E-07	0.054

Table D-3 Results on permeability tests (cont.)

PERMEABILITY TEST

Mine Name: *Sunnyside*
Seam Name: *Sunnyside*

Specimen's	Bedding:	Vertical	Temperature (C):	22.5
	Length (m):	0.108	Baromet. P. (Hg):	22.05
	Diameter(in):	2.125	Viscosity(Ns/m3):	1.775E-05
	X-Area(in2):	3.545	Specimen's I.D.:	17

Variable Gas Pressure:

	Stress			Pressure			Flow	Perme
Exp	Axial	Conf.	Mean	Inlet	Mean	Reciprocal	Rate	ability
ID#	(psi)	(psi)	(psi)	(psi)	(psi)	Mean (psi)	(m3/s)	(md)
99	2,750	700	1,383	50	30	0.0329	2.29E-08	0.025
100	2,750	700	1,383	100	55	0.0180	6.33E-08	0.017
101	2,750	700	1,383	150	80	0.0124	1.32E-07	0.016
102	2,750	700	1,383	200	105	0.0095	2.45E-07	0.016
103	2,750	700	1,383	250	130	0.0077	4.84E-07	0.020
104	2,750	700	1,383	300	155	0.0064	3.82E-08	0.112

Variable Confining Pressure:

	Stress			Pressure			Flow	Perme
Exp	Axial	Conf.	Mean	Inlet	Mean	Reciprocal	Rate	ability
ID#	(psi)	(psi)	(psi)	(psi)	(psi)	Mean (psi)	(m3/s)	(md)
105	2,750	500	1,250	100	55	0.0180	2.06E-07	0.055
106	2,750	750	1,417	100	55	0.0180	5.33E-08	0.014
107	2,750	1,000	1,583	100	55	0.0180	2.39E-08	0.006
108	2,750	1,250	1,750	100	55	0.0180	1.11E-08	0.003
109	2,750	1,500	1,917	100	55	0.0180	8.90E-09	0.002

Variable Axial Pressure:

	Stress			Pressure			Flow	Perme
Exp	Axial	Conf.	Mean	Inlet	Mean	Reciprocal	Rate	ability
ID#	(psi)	(psi)	(psi)	(psi)	(psi)	Mean (psi)	(m3/s)	(md)
110	1,410	700	937	100	55	0.0180	4.05E-08	0.011
111	1,690	700	1,030	100	55	0.0180	4.16E-08	0.011
112	2,260	700	1,220	100	55	0.0180	4.05E-08	0.011
113	2,820	700	1,407	100	55	0.0180	3.65E-08	0.010
114	3,380	700	1,593	100	55	0.0180	3.75E-08	0.010
115	3,950	700	1,783	100	55	0.0180	3.68E-08	0.010
116	4,510	700	1,970	100	55	0.0180	3.61E-08	0.010
117	5,080	700	2,160	100	55	0.0180	3.48E-08	0.009

Table D-3 Results on permeability tests (cont.)

PERMEABILITY TEST

Mine Name: *Sunnyside*
Seam Name: *Sunnyside*

Specimen's	Bedding:	Horizontal	Temperature (C):	22.5
	Length (m):	0.092	Baromet. P. (Hg):	22.18
	Diameter(in):	2.125	Viscosity(Ns/m3):	1.775E-05
	X-Area(in2):	3.545	Specimen's I.D.:	14

Variable Gas Pressure:

	Stress			Pressure			Flow	Perme
Exp ID#	Axial (psi)	Conf. (psi)	Mean (psi)	Inlet (psi)	Mean (psi)	Reciprocal Mean (psi)	Rate (m3/s)	ability (md)
24	2,750	700	1,383	50	30	0.0328	1.64E-08	0.016
25	2,750	700	1,383	100	55	0.0180	4.22E-08	0.010
26	2,750	700	1,383	150	80	0.0124	1.01E-07	0.010
27	2,750	700	1,383	200	105	0.0095	1.94E-07	0.011
22	2,750	700	1,383	250	130	0.0077	4.79E-07	0.017
23	2,750	700	1,383	300	155	0.0064	8.89E-07	0.022

Variable Confining Pressure:

	Stress			Pressure			Flow	Perme
Exp ID#	Axial (psi)	Conf. (psi)	Mean (psi)	Inlet (psi)	Mean (psi)	Reciprocal Mean (psi)	Rate (m3/s)	ability (md)
28	2,750	500	1,250	100	55	0.0180	1.53E-07	0.035
29	2,750	750	1,417	100	55	0.0180	2.76E-08	0.006
30	2,750	1,000	1,583	100	55	0.0180	1.18E-08	0.003
31	2,750	1,250	1,750	100	55	0.0180	6.00E-09	0.001
32	2,750	1,500	1,917	100	55	0.0180	3.10E-09	0.001

Variable Axial Pressure:

	Stress			Pressure			Flow	Perme
Exp ID#	Axial (psi)	Conf. (psi)	Mean (psi)	Inlet (psi)	Mean (psi)	Reciprocal Mean (psi)	Rate (m3/s)	ability (md)
33	1,410	700	937	100	55	0.0180	1.91E-08	0.004
34	1,690	700	1,030	100	55	0.0180	1.92E-08	0.004
35	2,260	700	1,220	100	55	0.0180	1.90E-08	0.004
36	2,820	700	1,407	100	55	0.0180	1.84E-08	0.004
37	3,380	700	1,593	100	55	0.0180	1.76E-08	0.004
38	3,950	700	1,783	100	55	0.0180	1.63E-08	0.004
39	4,510	700	1,970	100	55	0.0180	1.97E-08	0.004
40	5,080	700	2,160	100	55	0.0180	2.00E-08	0.005

Table D-3 Results on permeability tests (cont.)

PERMEABILITY TEST

Mine Name: *Dutch Creek*
Seam Name: *B Seam*

Specimen's	Bedding:	Vertical	Temperature (C):	22.5
	Length (m):	0.087	Baromet. P. (Hg):	21.84
	Diameter(in):	2.125	Viscosity(Ns/m3):	1.775E-05
	X-Area(in2):	3.545	Specimen's I.D.:	11

Variable Gas Pressure:

	Stress			Pressure			Flow	Permeability
Exp ID#	Axial (psi)	Conf. (psi)	Mean (psi)	Inlet (psi)	Mean (psi)	Reciprocal Mean (psi)	Rate (m3/s)	(md)
194	2,750	700	1,383	50	30	0.0329		0.000
195	2,750	700	1,383	100	55	0.0181	1.76E-07	0.037
196	2,750	700	1,383	150	80	0.0124	3.27E-07	0.031
197	2,750	700	1,383	200	105	0.0095	6.82E-07	0.036
198	2,750	700	1,383	250	130	0.0077	1.14E-06	0.038
199	2,750	700	1,383	300	155	0.0064		

Variable Confining Pressure:

	Stress			Pressure			Flow	Permeability
Exp ID#	Axial (psi)	Conf. (psi)	Mean (psi)	Inlet (psi)	Mean (psi)	Reciprocal Mean (psi)	Rate (m3/s)	(md)
200	2,750	500	1,250	100	55	0.0181		0.000
201	2,750	750	1,417	100	55	0.0181		0.000
202	2,750	1,000	1,583	100	55	0.0181		0.000
203	2,750	1,250	1,750	100	55	0.0181		0.000
204	2,750	1,500	1,917	100	55	0.0181		0.000

Variable Axial Pressure:

	Stress			Pressure			Flow	Permeability
Exp ID#	Axial (psi)	Conf. (psi)	Mean (psi)	Inlet (psi)	Mean (psi)	Reciprocal Mean (psi)	Rate (m3/s)	(md)
205	1,410	700	937	100	55	0.0181		0.000
206	1,690	700	1,030	100	55	0.0181		0.000
207	2,260	700	1,220	100	55	0.0181		0.000
208	2,820	700	1,407	100	55	0.0181		0.000
209	3,380	700	1,593	100	55	0.0181		0.000
210	3,950	700	1,783	100	55	0.0181		0.000
211	4,510	700	1,970	100	55	0.0181		0.000
212	5,080	700	2,160	100	55	0.0181		0.000

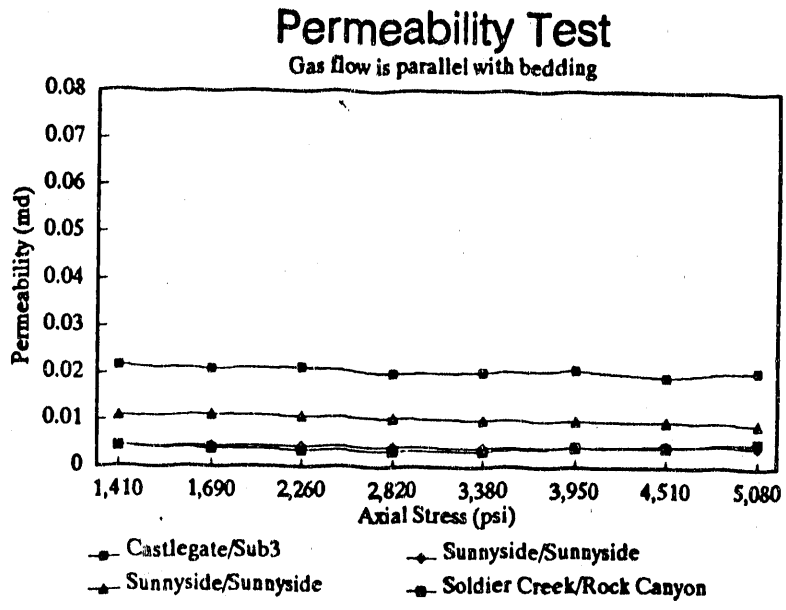

Figure D-3. Permeability versus axial stress for gas flow parallel and to bedding planes.

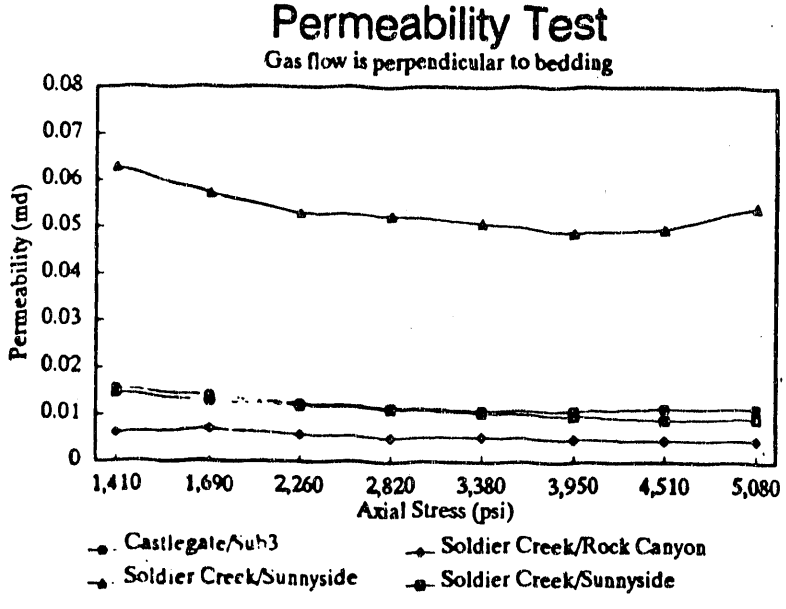

Figure D-4. Permeability versus axial stress for gas flow perpendicular to bedding planes.

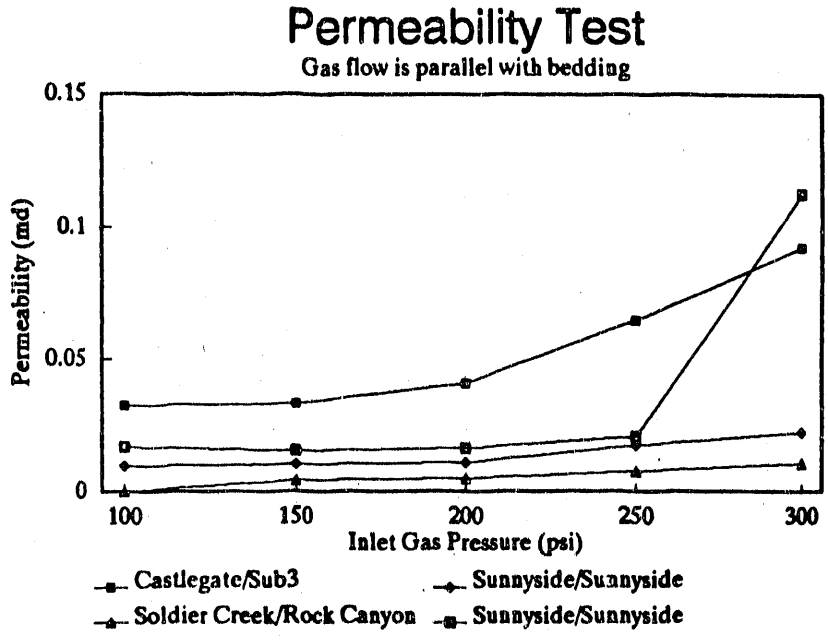

Figure D-5. Permeability versus inlet stress for gas flow parallel to bedding planes.

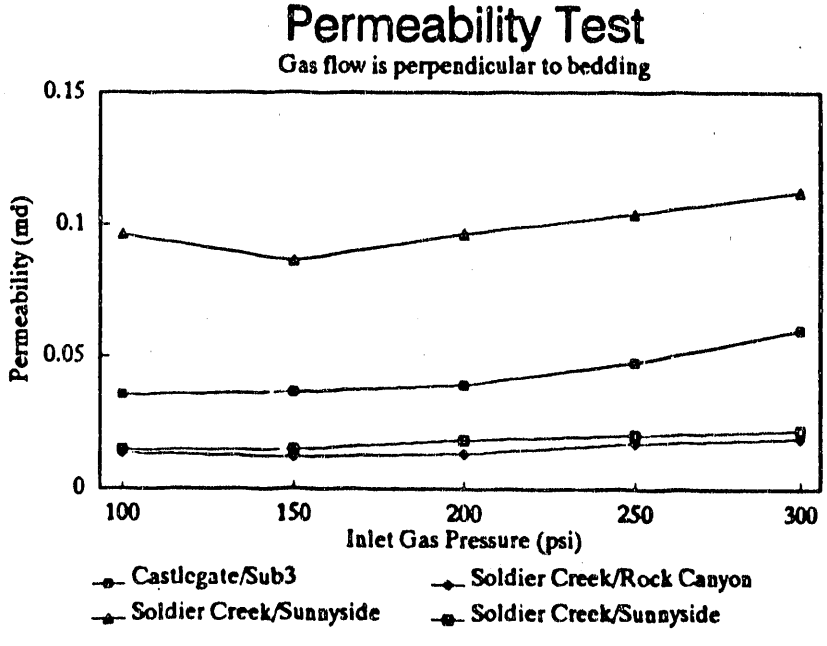

Figure D-6. Permeability versus inlet stress for gas flow perpendicular to bedding planes.

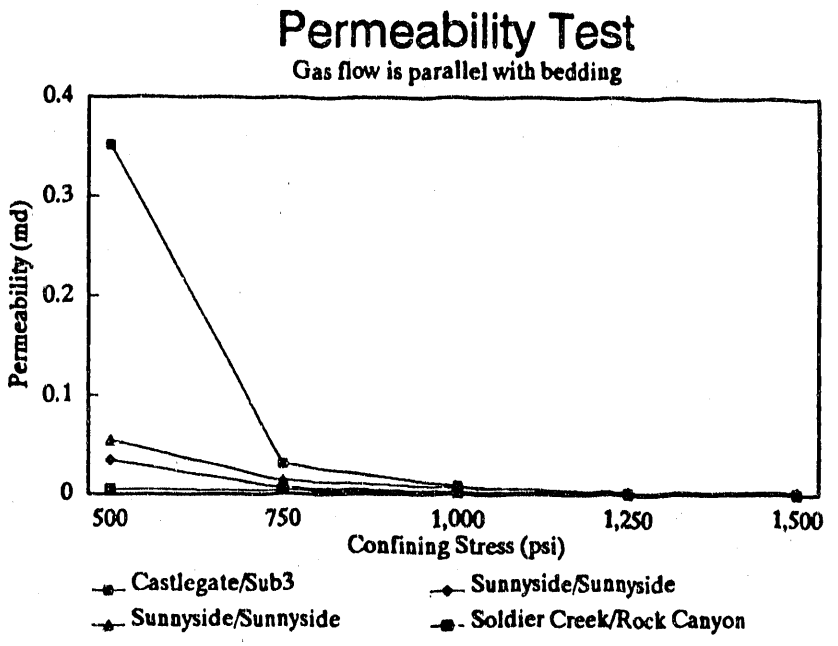

Figure D-7. Permeability versus confining stress for gas flow parallel to bedding planes.

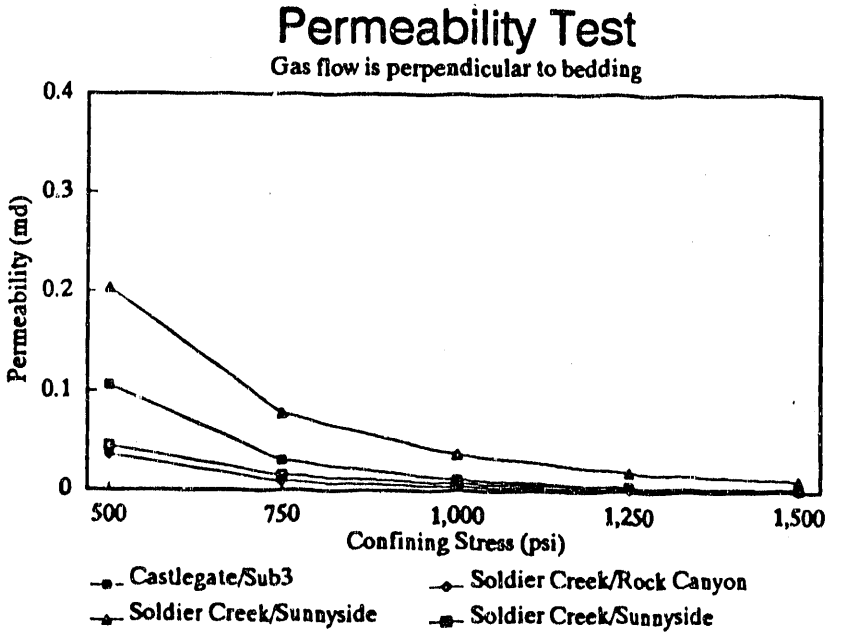

Figure D-8. Permeability versus confining stress for gas flow perpendicular to bedding planes.

APPENDIX E

COMPUTER CODE

E.1 Polynomial Fitting Technique

E.1.1 Principle

There are two methods to fit data with a polynomial technique: full range fitting using a high degree of polynomial, and group fitting using a set of low degree (normally n = 4, 6) of polynomial. Although the full range fitting method is quite simple, it is not stable and resulting curve is not expected in most cases. For these reasons, the group fitting method will be used for curve fitting. The principle of this method is as follows:

1. Take n points (n = 2m+2, m = 1, 2, 3, or ...) each time.

2. Use the nth degree polynomial, for example fourth degree polynomial, to fit the group data.

3. Calculate (x,y) in the range of points (1+m) to (n-m) using the nth degree polynomial.

4. The end points, (x,y), are calculated in the range of points 1 to (n-m) and (1+m) to n for the initial group and final groups, respectively.

5. Group the data as data(1,n), data(2,n+1), data(3,n+2), ..., data(n_t-n+1,n_t) where n_t is the total data points used in the fitting.

E.1.2 Program Source Code

This program must run in a MATLAB environment. It is ease to translate into C language simply writing a nth order polynomial fitting subroutine.

Beginning of the program code:

```
%     PFIT is a program using Polynomial Fitting Technique for
      universal curve-fitting purpose.
%
%     Variables explanation:
%
%     input variables: x, and y;
%     output variables: z;
%     n: polyfit degree;
%     p: point number for ploy fitting each time;
%     m: total points.
```

```
z=0;
wx=0;
wy=0;

s=1;
n=3;
p=4;

ans=size(x);
m=ans(1,1);

Nloop=m-p+1;

for i=1:x(1,1),
z(i,1)=0;
end

for i=1:p,
        wx(i,1)=x(i,1);
        wy(i,1)=y(i,1);
end

        polyfit(wx,wy,n);
        anst=ans';

b=wx(1,1);
e=wx(p/2+1,1);

for i=b+1:s:e-1,
     for l=1:n+1,
          sz(l)=anst(l)*i^(n+1-l);
        end
     sum=0;
        for l=1:n+1,
          sum=sum+sz(l);
        end
z(i,1)=sum;
end

for i=2:Nloop-1,
     label=0;
     for j=i:i+p-1,
          label=label+1;
          wx(label,1)=x(j,1);
          wy(label,1)=y(j,1);
     end

     polyfit(wx,wy,n);
        anst=ans';

b=wx(p/2,1);
e=wx(p/2+1,1);
```

```
for j=b:s:e-1,
        for l=1:n+1,
                sz(l)=anst(l)*j^(n+1-l);
        end
        sum=0;
        for l=1:n+1,
                sum=sum+sz(l);
        end
z(j,1)=sum;
end
end

i=Nloop;
label=0;
        for j=i:i+p-1,
     label=label+1;
                wx(label,1)=x(j,1);
                wy(label,1)=y(j,1);
        end

        polyfit(wx,wy,n);
        anst=ans';

b=wx(p/2,1);
e=5100;

for j=b:s:e,
        for l=1:n+1,
                sz(l)=anst(l)*j^(n+1-l);
        end
        sum=0;
        for l=1:n+1,
                sum=sum+sz(l);
        end
z(j,1)=sum;
end
```

E.2 Translation of Temperature Signals

E.2.1 Program code using Fortran language

```
      program  temp
c
      character     w*52, file(4)*12, TF(2)*1
      integer       n(10)
      real          x(600), l(60),y(10000),z(10000)
      real          a(9),b(9),c(9)
c
c     variables explanations:
c
c     n(1)      =     Sampling Rate
c     n(2)      =     Beginning Time
c     n(3)      =     End Time
```

```
c      n(4)      =    Smoothing Data Points
c      n(5)      =    n(3)-n(2)
c      n(6)      =    n(5)*60
c
c      x matrix =     1 min. raw data stored
c      y matrix =    1st order smoothed data stored, or others
(1
c                     Hz)
c       z matrix =     2nd order smoothed data stored, or 1st
order
c                     curve, 2nd order curve, etc.
c
c      *****
c
c      Input the Menu File & Parameters
c
       open(unit=11, file='tempmenu.prn',status='old')
c
       do 5 i=1,9
          read(11,10)w
          print*,w
5      continue
c
       read(11,15)w,file(1)
       print*,w,file(1)
       read(11,10)w
c
       read(11,15)w,file(2)
       print*,w,file(2)
       read(11,10)w
c
       read(11,20)w,n(1)
       print*,w,n(1)
       read(11,10)w
c
       read(11,20)w,n(2)
       print*,w,n(2)
       read(11,10)w
c
       read(11,20)w,n(3)
       print*,w,n(3)
       read(11,10)w
c
       read(11,20)w,n(4)
       print*,w,n(4)
       read(11,10)w
c
       read(11,25)w,tf(1)
       print*,w,tf(1)
       read(11,10)w
c
       read(11,15)w,file(3)
       print*,w,file(3)
```

```
      read(11,10)w
c
      read(11,25)w,tf(2)
      print*,w,tf(2)
      read(11,10)w
c
      read(11,15)w,file(4)
      print*,w,file(4)
c
10    format(a52)
15    format(a52,a12)
20    format(a52,i3)
25    format(a52,a1)
c
      close(unit=11)
c
      n(5)=n(3)-n(2)
      n(6)=n(5)*60
c
      print*,' '
      print*,' '
c     *****
c
c     Raw data input and the 1st order smoothing
      print*,'Part I.     Raw Data Input & the 1st Order
Smoothing'
      print*,' '
c
      open(unit=11,file=file(1),status='old')
      open(unit=12,file=file(2),status='new')
c
      print*,'      The total runs of the data input: ',n(5)
      print*,' '
c
      do 30 i=1,n(2)*n(1)*60
         read(11,*)x(1)
30    continue
c
      do 60 l=1,n(5)
c
      print*, '          DATA INPUT RANGE ',l
      do 35 i=1,n(1)*60
         read(11,*)x(i)
35    continue
c
      j=1
      do 50 i=1,60
         sum=0.0
         do 45 k=j,j+n(1)-1
            sum=sum+x(k)
45       continue
         j=k
         x1(i)=sum/(n(1)*1.0)
```

```
50    continue
c
      do 55 i=1,60
          y((l-1)*60+i)=x1(i)
55    continue
c
60    continue
c
      close(unit=11)
c
c     *****
c
c     The 2nd order smoothing, i.e., data points smoothing
c
      print*,' '
      print*,' '
      print*,'Part II.  The 2nd Order Smoothing'
c
      print*,' '
      print*,'       ',n(4),' data point(s) smoothing'
      print*,' '
      print*,' '
c
      if (n(4).eq.0) then
          do 65 i=1,n(6)
               z(i)=y(i)
65        continue
          goto 90
      endif
c
      do 70 i=1,(n(4)-1)/2
          z(i)=y(i)
70    continue
c
      do 75 i=n(6)+1-(n(4)-1)/2,n(6)
          z(i)=y(i)
75    continue
c
      do 85 i=(n(4)-1)/2+1,n(6)-(n(4)-1)/2
          sum=0.0
          do 80 j=i-(n(4)-1)/2,i+(n(4)-1)/2
               sum=sum+y(j)
80        continue
          z(i)=sum/(n(4)*1.0)
85    continue
c
c     *****
c
c     Transfer the signal to temperature.
c
90    print*,'Part III. Transfer the signal to temperature.'
      print*,' '
      print*,' '
```

```
c
c Range     Average     STD              Regression Output
c
c  °C                                Constant  Coefficient     r²
c
c < 100     0.00000   0.309019   24.55288     476.6994    0.999882
c 100-200  -0.00002   0.732628   22.20936     495.0368    0.999426
c 200-300  -0.00002   0.531382   22.98634     492.4859    0.999787
c 300-400  -0.00004   0.518817   30.18500     479.5892    0.999793
c 400-500  -0.00008   0.385489   37.57280     470.0709    0.999871
c 500-600  -0.00010   0.545482   37.09575     470.5710    0.999731
c 600-700  -0.00005   0.484075   34.68281     472.6496    0.999775
c 700-800  -0.00006   0.344412   18.47958     484.0608    0.999888
c 800-900   0.00000   0.460348   -2.49169     496.7637    0.999789
c
c max error (calc. value - expt. value)={ -1.54621, 1.106061}
c
c
c                    Y = a + b*X
c
c                    constant       coefficient
c
c
      a(1)      =    24.55288
      b(1)      =                   476.6994
      a(2)      =    22.20936
      b(2)      =                   495.0368
      a(3)      =    22.98634
      b(3)      =                   492.4859
      a(4)      =    30.18500
      b(4)      =                   479.5892
      a(5)      =    37.57280
      b(5)      =                   470.0709
      a(6)      =    37.09575
      b(6)      =                   470.5710
      a(7)      =    34.68281
      b(7)      =                   472.6496
      a(8)      =    18.47958
      b(8)      =                   484.0608
      a(9)      =    -2.49169
      b(9)      =                   496.7637
c
c     determined range parameters: C-value
c
      c(1)      =    0.15826981
      c(2)      =    0.35914630
      c(3)      =    0.56248039
      c(4)      =    0.77110785
      c(5)      =    0.98373926
      c(6)      =    1.19621527
      c(7)      =    1.40763307
      c(8)      =    1.61450887
      c(9)      =    1.81674242
```

```
c
      do 100 i=1,n(6)
          do 95 j=1,9
               if (z(i).le.c(j)) then
                    d1=a(j)
                    d2=b(j)
                    goto 96
               endif
95        continue
96        y(i)=d1+d2*z(i)
100   continue
c
c     *****
c
c     Generate the temperature data file
c
      print*,'Part VI.  Generate Temperature Data File'
      print*,' '
      print*,' '
c
      do 105 i=1,n(6)
          write(12,*)y(i)
105   continue
c
      close(unit=12)
c
c     *****
c
c     Generate First Derivative Data
c
      if (tf(1).eq.'Y'.or.tf(1).eq.'y') then
          print*,'Part V.   Generate First Derivative Data'
          print*,' '
          print*,' '
c
          do 110 i=2,n(6)-1
               z(i)=( y(i+1)-y(i-1) )/2.0
110       continue
          z(1)=z(2)
          z(n(6))=z(n(6)-1)
c
          open(unit=11,file=file(3),status='new')
c
          do 115 i=1,n(6)
               write(11,*)z(i)
115       continue
          close(unit=11)
      else
          goto 130
      endif
c
c      *****
c
```

```
c      Generate Second Derivative Data
c
       if (tf(2).eq.'Y'.or.tf(2).eq.'y') then
           print*,'Part VI.  Generate Second Derivative Data'
           print*,' '
           print*,' '
c
           do 120 i=2,n(6)-1
                y(i)=( (z(i)-z(i-1) ) + ( z(i+1)-z(i) ) )/2.0
120        continue
           y(1)=y(2)
           y(n(6))=y(n(6)-1)
c
           open(unit=11,file=file(4),status='new')
c
           do 125 i=1,n(6)
                write(11,*)y(i)
125        continue
           close(unit=11)
       endif
c
130    print*,'**********  END  **********'
       print*,' '
       print*,' '
       print*,'Thank you for your using this program. '
       print*,' '
       print*,'Appreciate your suggestion!'
       print*,' '
c
       stop
       end
```

E.2.2 Setup menu for the program

SETUP MENU

<<< Temperature Recording >>>

Input Data File Name (.PRN)	t001.prn
Output Data File Name (.PRN)	ot001.prn
Sampling Rate, Hz	1
Beginning of the Time, min	0
End of the Time, min	85
Smoothing Data Points (0, 3, 5, 7, 9)	5
First Derivative Curve (Y or N)	N
First Derivative Data File Name (.PRN)	FD.prn
Second Derivative Curve (Y or N)	N
Second Derivative Data File Name (.PRN)	SD.prn

APPENDIX F

DIRECTIONAL PERMEABILITY OF SELECTED COALBEDS IN UTAH

Methane drainage from gassy Western U.S. coal seams

V. J. Hucka
Department of Mining Engineering, University of Utah, Salt Lake City, Utah, U.S.A.
D. M. Bodily
Department of Fuels Engineering, University of Utah, Salt Lake City, Utah, U.S.A.

SYNOPSIS

Methane gas retained in gassy coal seams is a valuable source of clean energy. However, methane is also a potential safety hazard. Its removal prior to mining improves mine safety by reducing the potential for explosions as well as economics by decreasing ventilation costs. A method of field evaluation of methane content in some Western U. S. coal seams is presented. Results of pre-mining degasification in seams of similar methane content are described. The results indicate that degasification, or methane drainage, depends heavily on coal permeability. Since the permeability is affected by the presence of joints, fractures and cleats in coal and associated strata, their influence on the optimum direction of boreholes was studied. The results of methane drainage are discussed and recommendations as to the orientation of boreholes with respect to the main cleat systems in coal are suggested.

INTRODUCTION

The presence of methane in coal seams renders the underground working environment dangerous and the methane level must be maintained below the safe concentration limit. The methane must either be drained prior to mining operations or the mining plan must be adapted to accommodate methane emissions.

It has been estimated that about 7 Mm^3 of methane containing 252 MJ of heating value is wasted daily in the U.S.A. (Jones et al., 1982). Studies show that there is about 22.6 Tm^3 in place in the U.S.A. Provided that consumption of gas is 566 Gm^3 per year, it equates to a 40 year supply of gas. If only a quarter of it is recovered it would cover 10 year consumption (Rightmire, 1984). The methane gas coming from coal seams is considered as unconventional natural gas, and therefore, is not regulated by the U. S. Federal Energy Regulatory Commission, (Section 107 of the Natural Gas Policy Act).

From the mining point of view, this gas is a potential hazard and must be removed or diluted if the mining of coal is to be done. Methane drainage has been practiced in some mining countries for over 40 years and the gas is used mostly for heating purposes. This adds to mining costs, often in excess of the value of the recovered gas. The dilution of methane below the permissible level is mostly done by ventilation. In very gassy coalbeds, this is not effective enough and the removal of methane gas must be done by a separate removal system or by methane gas drainage. There are several options available. The coalbed can be accessed from the surface by drilling vertical boreholes and methane can be drained through the boreholes. Directional drilling helps to change the vertical direction into horizontal when the borehole reaches the seam level. Directional drilling allows access to larger volumes of the seam and thus the methane release is more efficient.

Horizontal boreholes can be drilled from the underground openings into virgin parts of coalbeds. This technique was used in Central Utah gassy coal seams, identified as Seams No. 1, 2, and 3 in this paper. The results of gas yields indicated that the coal permeability has a strong influence on the gas yield. In this paper the influence of coal cleats on the permeability in the three seams is discussed and the results on the methane drainage experiments are evaluated.

PHYSICAL PARAMETERS OF GAS FLOW

Properties of coal controlling the methane emission are porosity, permeability and the ability of coal to adsorb the gas. Coal may have a large voidage to bulk volume ratio, that is, a high porosity. If the pores are not interconnected, then the coal has a low permeability. However, the internal surface of pores is enormous and thus such a coal may contain a large volume of methane, as the methane molecule has a great affinity for the coal. Carbon dioxide, water and methane are products of the coalification process. Coal surfaces become increasingly hydrophobic as the rank increases. Water is expelled from the pores. Carbon dioxide has an affinity for coal, but is highly soluble in water. Thus, methane is retained in the pores. So the large area of the pores retains a tremendous quantity of methane in the adsorbed state. Temperature, which often correlates with depth of burial, and time are the important parameters in coalification. Retention of the methane depends on a number of geological and physical factors. Laboratory experiments on the adsorption of methane in coals indicate that adsorption follows a Langmuir isotherm while diffusion obeys Fick's second law (Walker and Mahajan, 1978).

COLLECTION OF SAMPLES FOR METHANE ANALYSIS

As U.S. coal mining has progressed to greater depths, new coal mines developed in virgin seams have the potential to be gassy. The U. S. Bureau of Mines developed a simple, inexpensive test, the so-called "direct method", to measure the methane content of coal samples obtained from exploratory drilling (Kissell et al., 1973). The core is placed in hermetically sealed containers and the pressure and gas emission are determined daily. The gas is bled off through a tube attached to the head of the sample container into a graduated cylinder filled with water (Figure 1). Gas emission is plotted versus the square root of time. The gas lost during the collection of the core can be estimated by back extrapolation of the correlation curve (McCulloch et al., 1976).

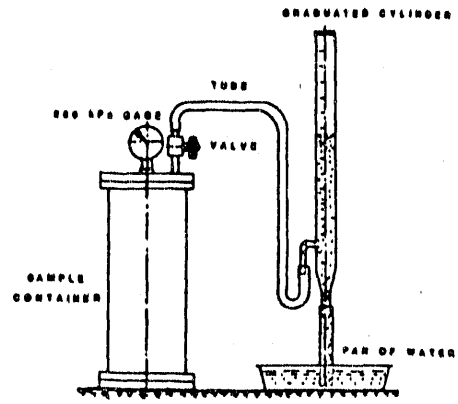

Figure 1. Laboratory direct method of methane gas content determination

Another method is the so-called "in-situ bubble desorbometer" method. It allows for the estimation of the methane gas directly at the coal face. This method was originally developed in European coal mining countries to predict coal and gas outbursts (Lisner, 1981, Plazier et al., 1987, Plazier, 1989). The method makes possible quite reliable estimates of methane content within minutes after collection of the sample. More accurate results can be obtained within hours of sample collection. Cuttings from a borehole are screened with a 0.6 mm sieve and about 10 grams of fine cuttings are inserted into the plastic cell of the bubble desorbometer (Figure 2). The

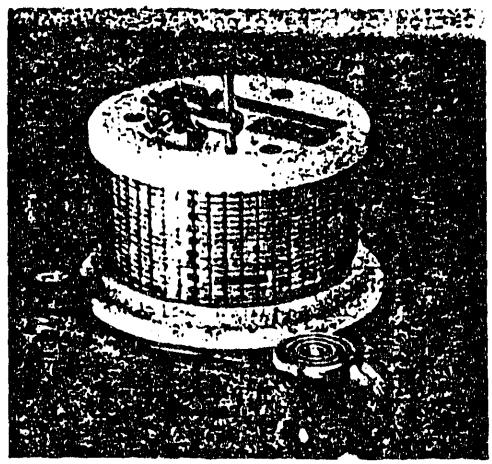

Figure 2. Bubble desorbometer for in-situ methane gas determination

gas from the sample pushes a slug of colored glycol in a graduated plastic tube. The time is measured and the content of methane gas released from the sample is determined (Hucka et al., 1984). Samples are collected from different depths of the borehole using a special collecting device (Figure 3). Compressed air hose is connected to the hose attachment 1 and passes through valve 2 into the barrel of the drill to purge out the bore hole. Valve 2 is then closed and fresh sample is sucked through the barrel and valves 4 and 5 into container 6 by the compressed air passing through valve 4 and exit 7. The methane content as a function of distance from the face is shown for typical experiments in two coal seams in Figure 4. As expected, methane is depleted near the face, but quickly approaches a steady-state concentration with depth.

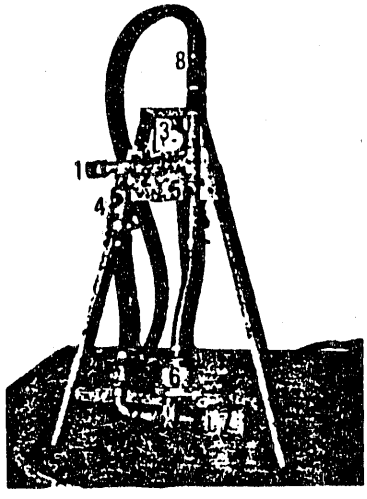

Figure 3. A special sampling device for collecting fine drill cuttings from the bottom of the borehole (1- compressed air inset valve; 2- valve; 3- pressure gauge; 4- valve; 5- purge valve; 6- container for sample collection; 7- exit; 8- drill hammer hose)

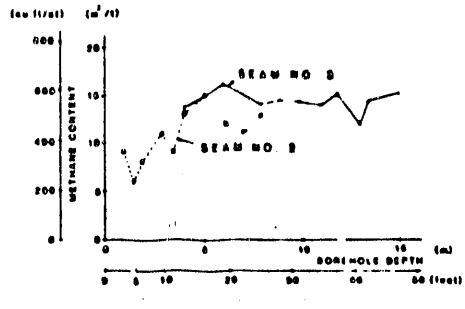

Figure 4. Relation between the depth of the borehole and the methane contant (Lisner, 1982)

INFLUENCE OF CLEATS ON THE PERMEABILITY OF COAL

Gas in excess of that which can be adsorbed on the coal surface is present as free gas in fractures and voids in the coal and surrounding strata. The fractures are called cleats in the mining industry. In western coal seams, a cleat is a joint or set of joints in coal generally almost perpendicular to the coalbed. There are usually two cleat sets developed nearly perpendicular to each other (Hucka, B., 1989).

Face cleats or the major cleats may extend to great distances. Butt cleats (also called end cleats or minor cleats) usually extend only from one face cleat fracture to the next. According to McCulloch et al., 1975, face cleats yield longer fractures and are often more prominent. Horizontal holes drilled perpendicular to the face cleats would be expected to drain a larger volume, and therefore, produce more methane than holes drilled parallel to the face cleats (Figure 5).

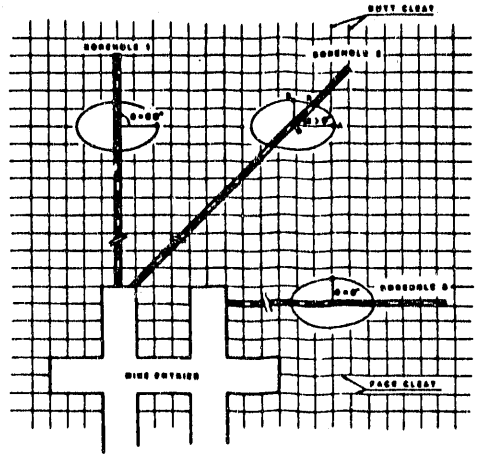

Figure 5. A plain view of directional permeability due to the cleat orientation (Boreholes with drainage ellipses)

In Seam No. 1, the Bureau of Mines performed a series of successful drainage tests using horizontal boreholes drilled from underground mine workings into coal beds (Figure 6). During nine months of drainage tests, almost one Mm^3 (991,000 m^3) of methane was removed from the seam, thus reducing by 40% the methane emission from the face. The average heating value of the methane gas was 37.52 MJ/m^3. Overall, the tests proved that commercial-quality methane can be recovered from this seam (Perry et al., 1978).

TABLE I. Proximate Analysis of Three Gassy Utah Coal Seams

Seam	Rank	Volatile Matter VM %	Fixed Carbon C %	Moisture M %	Ash A %	Sulfur S %	Heat Content Kj/Kg	Methane Content Lab Tests m^3/t	Methane Content Field Tests m^3/t
No. 1	A Bituminous	38.3	54.8	2	5	0.7	39936	4.76*	7.0
No. 2	B Bituminous	39	48.2	--	7.8	0.6	29147	2.87*	14.5
No. 3	A Bituminous	39	49.1	4.8	6.9	0.85	29679	2.30*	10.0

*Utah Geological and Mineral Survey

Table 1 contains a summary of results on methane content determined by this method and compares the results with the laboratory direct method performed by the U.S. Bureau of Mines and the Utah Geological and Mineral Survey (Doelling et al., 1979).

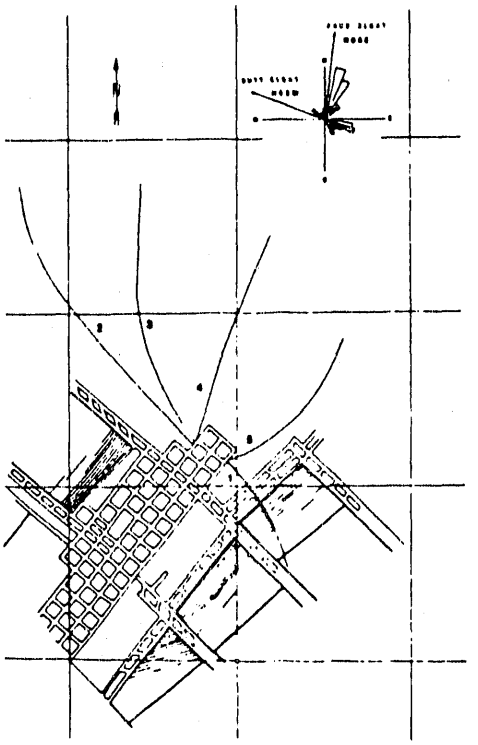

Figure 6. Location of horizontal boreholes at the Seam No. 1

The orientation of face and butt cleats are shown by the rose diagram in the upper right corner of Figure 6. Horizontal bore holes were drilled as shown by numbers 1-5. It was found that the orientation of coal cleats is important in determining the efficiency of drainage as the face and butt cleat provide a directional permeability for the flow of methane. The flow of methane was greater when the hole was drilled perpendicular to the direction of face cleats (Table 2). These holes intersect a larger number of face cleats thus yielding 2.5 to 10 times more gas than the holes drilled perpendicular to the butt cleats (Rightmire et al., 1984).

An attempt has been made to represent the directional permeability of coal by an ellipse drawn with the major axis parallel to the face cleat in a coalbed. Figure 5 shows a hypothetical case of three boreholes drilled perpendicular, parallel and at an angle to the face cleats. A relationship between the two extreme directions can be established by the ellipse with half axes $\overline{OA}$ and $\overline{OB}$, and an angle θ (Figure 5, borehole No. 2). A vector $\overline{OR}$ placed inside the ellipse and coinciding with the direction of the borehole is used to represent the orientation of the borehole with respect to the cleat system. The magnitude of the vector would represent the effective permeability. The equation for an ellipse:

$$\frac{x^2}{(\overline{OA})^2} + \frac{y^2}{(\overline{OB})^2} = 1; \quad (1)$$

$$x = \overline{OR} \cos\theta; \quad (2a)$$

$$y = \overline{OR} \sin\theta; \quad (2b)$$

Substituting Equations (2) into Eq. (1):

$$\frac{1}{(\overline{OA})^2} (\overline{OR})^2 \cos^2\theta + \frac{1}{(\overline{OB})^2} (\overline{OR})^2 \sin^2\theta = 1 \quad (3)$$

or

$$(\overline{OR})^2 = \frac{1}{\frac{\cos^2\theta}{(\overline{OA})^2} + \frac{\sin^2\theta}{(\overline{OB})^2}} \quad (4)$$

Therefore, if $(\overline{OA})$ and $(\overline{OB})$ are known, then $(\overline{OR})$ can be obtained for any corresponding value of θ. Borehole No. 1 in Figure 5 is drilled perpendicular and the borehole No. 3 is drilled parallel to the direction of face cleats. Borehole No. 2 is then drilled under an angle θ to the direction of face cleats.

TABLE II. Results on Drainage Tests

Coal Seam	Depth	Cleat		No.	Borehole Length	Angle θ	Peak Daily Prod.	Unit Prod.	Calculated Unit Prod. Min	Calculated Unit Prod. Max	Percentage Improvement for Optimum Orientation
		Face	Butt					OR	OB	OA	
	m	deg.	deg.		m	deg	$m^3/d/m$	$m^3/d/m$	$m^3/d/m$	$m^3/d/m$	%
Seam 1	450	N 5E	N65W	1	240	17	708	2.95	1.42	3.55	17
				2	510	35	3400	6.66	4.40	11.00	39
				3	487	25	963	1.97	1.10	2.74	28
				4	137	16	3596	26.24	12.41	31.03	15
				5	55	37	2180	39.64	27.00	67.52	41
Seam 2	450	N65W	N25E	2	343	27	42	0.12	0.07	0.17	29
	to			4	495	6	368	0.74	0.30	0.76	3
	530			5	615	2	396	0.64	0.25	0.64	0
				6	410	90	566	1.38	0.55	1.38	0
				7	396	90	424	1.07	0.42	1.07	0
				12	524	44	382	0.72	0.54	1.35	46
				13	485	90	396	0.81	0.32	0.81	0
				14	513	90	396	0.77	0.30	0.77	0
Seam 3	485	N55W	N35E	1	85	9	13	0.15	0.06	0.16	6
	to			2	182	40	76	0.41	0.29	1.72	76
	605			3	94	64	11	0.18	0.16	0.41	56

An ellipse with half-axes $\overline{OA}$ and $\overline{OB}$ represents the maximum and minimum values of drained gas if the borehole is drilled under an oblique angle θ to the direction of face cleats or butt cleats. Calculated production for boreholes drilled perpendicular and parallel to the face cleats are shown in Table 2. Minimum production is expected for the parallel orientation and maximum production for the perpendicular orientation. It is apparent that if the borehole is drilled under an angle θ = 17 degrees to the face cleat (see Seam No. 1, borehole No. 1) with the unit daily production of gas, $\overline{OR}$, equal 2.95 $m^3/d/m$ (cubic metre per day per metre of length of the borehole) then the maximum cubic unit production for this borehole (if drilled perpendicular to the face cleat), $\overline{OA}$ would equal 3.55 $m^3/d/m$. Assuming the length of the borehole is 240 m, then the borehole would yield a total of about 852 m^3/d of methane.

In this approach it is assumed that the quality and quantity (spacing) of cleats were approximately the same for the given natural conditions of Seams no. 1, 2, and 3.

RESULTS ON DRAINAGE TESTS

Seam No. 1

The seam is mined by a coal company located about 70 kilometers south from the town of Price, Central Utah. The thickness of the seam where the drainage tests took place is about 2 meters. The rock composing the roof is carbonaceous shale while the rock in the floor is siltstone. Very recently, the Utah Geological and Mineral Survey undertook an extensive study of cleat and joint systems in all working coal mines in Utah (Hucka, B., 1989). The results on face and butt cleats measured in the Seam No. 1 are presented in the form of a rose diagram (Figure 6.).

Some cleats transverse the entire thickness of the seam and sometimes extend into the roof rocks. The surface planes of cleats are smooth with traces of slickensides, some are striated and densely distributed in the coal. In the upper part of the seam, the cleat planes are coated with calcite and have spacing of about 6 millimeter. The most prominent cleats have uneven surface with quite regular distribution in the coal with spacing about 10 to 13 millimeters. Figure 6 shows the direction of boreholes and their relation to the direction of the face cleats.

The low production in borehole #1 is attributed to the location of the borehole near previous workings. The U.S. Bureau of Mines stopped the drilling of borehole #5 due to suspected inflow of methane from previously drilled boreholes. Boreholes #'s 2, 3 and 4 are in virgin areas and show similar drainage behavior.

Seam No. 2.

The location of the seam is about 50 kilometers northeast of the town of Price, Utah. There are two more seams in the property but, at present, only Seam No. 2 is mined. The seam belong to the upper part of the coal-bearing Blackhawk Formation of the Book Cliffs

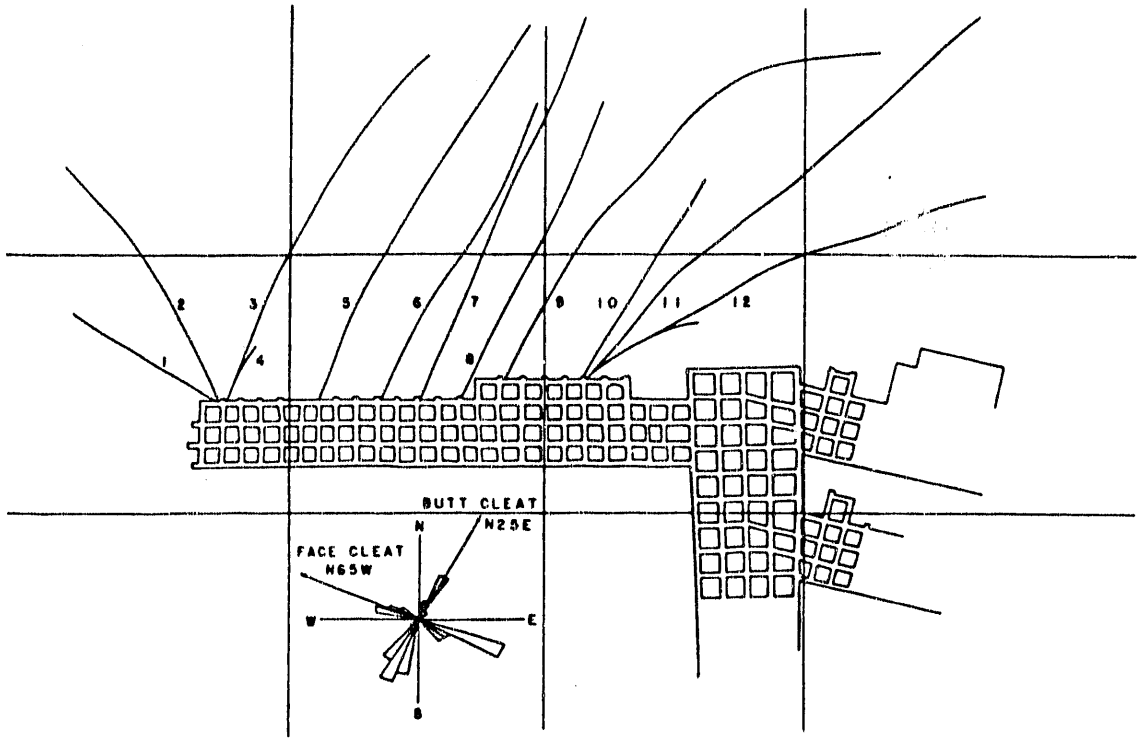

Figure 7. Location of horizontal boreholes drilled in the Seam No. 2

coal field. The formation is approximately 70 meters thick and contains as many as 6 mineable coal seams (Allen, 1989).

The thickness of the Seam No. 2 attains a value of about 2.5 meters. The roof rock consists of carbonaceous shale and the foor is formed of sandstone. The cleat measurements show two principal cleat orientations with the face cleat striking N 65 W and butt cleat striking N 25 E. Both cleat systems are well developed with spacing about 35 to 40 millimeters. The surface planes of the cleats are mostly uneven of striated.

Borehole #12 shows anonomously high methane yields (Table 2). No explaination is available for this behavior. The remaining boreholes show similar behavior.

Seam No. 3

The seam is the basal seam of the Spring Canyon group in the Blackhawk Formation of the upper Cretaceous age. The mine is located near the Wasatch Plateau Field where the drainage tests were conducted (Von Schoenfeldt, 1985).

The thickness of the seam is about 1.8 to 2.0 meters. The roof is built of carbonaceous shale and the foor consists of massive sandstone. The azimuth of the face and butt cleats in a form of a rose diagram is shown in Figure 8. There is a secondary set of cleats striking N 75 E. The average spacing is 20 to 35 millimeters and the dip is 82 degrees. The cleat planes are filled by calcite and resin.

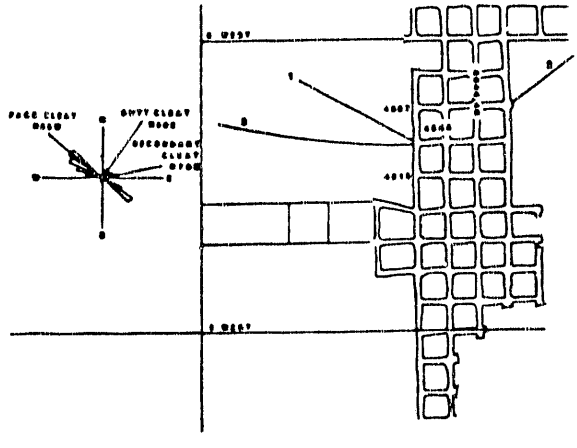

Figure 8. Location of boreholes drilled in the Seam No. 3

The permeability of Seam No. 3 appears to be lower than that of the other seams. This may be due in part to the greater lithostatic pressure of the overburden.

DISCUSSION OF RESULTS

Directional permeability in coal seams has been observed in all three tested seams. An extensive study of cleats shows that the majority of the boreholes drilled into Seam No. 2 were correctly oriented. In Seam No. 1, the boreholes were drilled under an angle of 16 and 37 degrees to the face cleats. Yet, the methane flow was higher than in the case of Seam No. 2, which underlies Seam No. 1 and should yield about the same content of methane (Table 1).

It is known that the rate at which gas flows through the coal depends on the porosity, permeability of coal, gas pressure and the presence of natural fissures. Thus, the controlling factor here is the permeability.

CONCLUSION

A detailed methane content estimation of Utah coal seams has been conducted by use of laboratory tests and also in three selected seams by use of an in situ technique. Results from the seams under investigation indicate that methane gas from those seams is of commercial significance.

During the laboratory tests on methane content it has been found that the gas content varied from 2.30 to 4.76 m^3/t in the three seams (Table 1). During the drainage tests over almost one Mm^3 of commercial quality gas was removed from Seam No. 1 in about nine months of degasification. From the Table 2 it is evident that the drainage tests in Seam No. 3 were not successful while some boreholes drilled into the Seam No. 2 released larger volumes of methane (Schwoebel, 1987). Since the same method of methane drainage was used in the three seams it is assumed that the permeability in Seam No. 1 is higher than in Seam No. 2. It is obvious that the permeability is much lower in Seam No. 3. As the permeability depends on the cleat in coals the choice of direction of drainage boreholes play a significant role.

The factors controlling methane drainage are not fully understood and require further study.

Knowledge of the permeability is indispensable also for proper design of methane drainage. A method for in situ permeability measurements needs to be developed. Longwall face technology is used in Seams No. 1 and 3, and the management of the mine operating Seam No. 2 plans to use longwall technology if the methane content in the seam can be lowered to a level enabling a smooth longwall operation. The present excessive amounts of methane (Table 2) may cause numerous stoppages in the longwall face as the emission of methane above one percent automatically disconnects the electrical power at the face.

REFERENCES

Allen, C., 1989, Personal Communication

Diamond, W. P., 1984, Site-Specific and Regional Geological Considerations for Coalbed Gas Drainage, Bureau of Mines RI 8898, 23 p.

Doelling, H. H., Smith, A. D., and Davis, F. D., 1979, Methane Content of Utah Coals, Special Studies 49, Utah Geological and Mineral Survey, August, 68 p.

Hucka, B. P., 1989, Analysis of Cleats in Utah Coal Seams, Preliminary Report, Utah Geological and Mineral Survey, Salt Lake City, Utah, 84108- 1280.

Hucka, V. J., and Lisner, U. W., 1984-85, In Situ Determination of Methane Gas in Utah Coal Mines, Trans. SME-AIME, Vol. 276, pp. 1959-63.

Jones, A. H., et al., 1982, Fractured Vertical Wells Versus Horizontal Boreholes for Methane Drainage in Advance of Mining U. S. Coals, The Australian I. M. M. Illawarra Branch Symp., May, pp. 1-28.

Kissell, F. N., McCulloch, C. M., and Elder, E., H., 1973, The Direct Method of Determining Methane Content of Coalbeds for Ventilation Design, Bureau of Mines RI 7677, pp. 17.

Lisner, U. W., 1981, Desorbable Methane Content Estimation of Utah Coal. M. S. Thesis, University of Utah, Department of Mining Engineering, 154 p.

McCulloch, C. M., Deul, M., and Jeran, P. W., 1974, Cleat in Bituminous Coalbeds, Bureau of Mines RI 7910, 25 p.

McCulloch, C. M., Diamond, W. P., Bench, B. M., and Eul, M., 1975, Selected Geologic Factors Affecting Mining of the Pittsburgh Coalbed, Bureau of Mines RI 8093, 72 p.

McCulloch, C. M., and Diamond, W. P., 1976, An Inexpensive Methods Help Predict Methane Content of Coal Beds, Coal Age, June, pp. 102-106.

Perry, J. M., Aul, G. N., and Cervik, J., 1978, Methane Drainage Study in the Sunnyside Coalbed, Utah, Bureau of Mines RI 8323, 11 p.

Plazier, R., 1989, Methane Desorption Modelling and Analysis for Selected Western Coal Fields, M. S. Thesis (under preparation).

Plazier, R., Tu, H. J., and Hucka, V. J., 1987, In Situ Method of Methane Das Content Determination, 22nd Intern. Conf. on Mines Safety Research Institutes, Beijing, PRC, Nov. 2-7, pp. 205-212.

Rightmire, C. T., Eddy, G. E. and Kirr, J. N., 1984, Coalbed Methane Resources of the United States, AAPG Studies in Geology Series #17, Published by The Amer. Assoc. of Petroleum Geologists, Tulsa, Oklahoma 74101, 378 p.

Schwoebel, J. J., 1987, Coalbed methane: Conversion of a Liability to an Asset, Mining Engineering, April, pp. 270-274.

von Schoenfeldt, H., 1985, Personal Communication.

Walker, P. L., Jr. and Mahajan, O. P., 1978, Methane Diffusion in Coals and Chars, Analytical Methods For Coal and Coal Products, Vol. I, Karr, C., Jr., Ed., Academic Press, New York.

END

DATE
FILMED
10/6/92